NUCLEAR DATA AND BENCHMARKS FOR REACTOR SHIELDING

DONNÉES NUCLÉAIRES ET EXPÉRIENCES REPÈRES EN MATIÈRE DE PROTECTION DES RÉACTEURS

Proceedings of a Specialists' Meeting
Compte rendu d'une réunion de spécialistes

PARIS
27 - 29 Octobre 1980

NUCLEAR ENERGY AGENCY
ORGANISATION FOR ECONOMIC CO-OPERATION AND DEVELOPMENT

AGENCE POUR L'ÉNERGIE NUCLÉAIRE
ORGANISATION DE COOPÉRATION ET DE DÉVELOPPEMENT ÉCONOMIQUES

Proceedings of a Specialists' Meeting on

NUCLEAR DATA AND BENCHMARKS FOR REACTOR SHIELDING

Paris, 27th-29th October 1980

Compte rendu d'une réunion de spécialistes sur

LES DONNÉES NUCLÉAIRES ET LES EXPÉRIENCES REPÈRES EN MATIÈRE DE PROTECTION DES RÉACTEURS

Paris, 27-29 octobre 1980

Sponsored by the
NEA COMMITTEE ON REACTOR PHYSICS
Organisé sous l'égide du
COMITÉ DE L'AEN DE LA PHYSIQUE DES RÉACTEURS

NUCLEAR ENERGY AGENCY
ORGANISATION FOR ECONOMIC CO-OPERATION AND DEVELOPMENT

AGENCE POUR L'ÉNERGIE NUCLÉAIRE
ORGANISATION DE COOPÉRATION ET DE DÉVELOPPEMENT ÉCONOMIQUES

The Organisation for Economic Co-operation and Development (OECD) was set up under a Convention signed in Paris on 14th December, 1960, which provides that the OECD shall promote policies designed:

- to achieve the highest sustainable economic growth and employment and a rising standard of living in Member countries, while maintaining financial stability, and thus to contribute to the development of the world economy;
- to contribute to sound economic expansion in Member as well as non-member countries in the process of economic development;
- to contribute to the expansion of world trade on a multilateral, non-discriminatory basis in accordance with international obligations.

The Members of OECD are Australia, Austria, Belgium, Canada, Denmark, Finland, France, the Federal Republic of Germany, Greece, Iceland, Ireland, Italy, Japan, Luxembourg, the Netherlands, New Zealand, Norway, Portugal, Spain, Sweden, Switzerland, Turkey, the United Kingdom and the United States.

The OECD Nuclear Energy Agency (NEA) was established on 20th April 1972, replacing OECD's European Nuclear Energy Agency (ENEA) on the adhesion of Japan as a full Member.

NEA now groups all the European Member countries of OECD and Australia, Canada, Japan, and the United States. The Commission of the European Communities takes part in the work of the Agency.

The primary objectives of NEA are to promote co-operation between its Member governments on the safety and regulatory aspects of nuclear development, and on assessing the future role of nuclear energy as a contributor to economic progress.

This is achieved by:

- *encouraging harmonisation of governments' regulatory policies and practices in the nuclear field, with particular reference to the safety of nuclear installations, protection of man against ionising radiation and preservation of the environment, radioactive waste management, and nuclear third party liability and insurance;*
- *keeping under review the technical and economic characteristics of nuclear power growth and of the nuclear fuel cycle, and assessing demand and supply for the different phases of the nuclear fuel cycle and the potential future contribution of nuclear power to overall energy demand;*
- *developing exchanges of scientific and technical information on nuclear energy, particularly through participation in common services;*
- *setting up international research and development programmes and undertakings jointly organised and operated by OECD countries.*

In these and related tasks, NEA works in close collaboration with the International Atomic Energy Agency in Vienna, with which it has concluded a Co-operation Agreement, as well as with other international organisations in the nuclear field.

L'Organisation de Coopération et de Développement Économiques (OCDE), qui a été instituée par une Convention signée le 14 décembre 1960, à Paris, a pour objectif de promouvoir des politiques visant :

— à réaliser la plus forte expansion possible de l'économie et de l'emploi et une progression du niveau de vie dans les pays Membres, tout en maintenant la stabilité financière, et contribuer ainsi au développement de l'économie mondiale;
— à contribuer à une saine expansion économique dans les pays Membres, ainsi que non membres, en voie de développement économique;
— à contribuer à l'expansion du commerce mondial sur une base multilatérale et non discriminatoire, conformément aux obligations internationales.

Les Membres de l'OCDE sont : la République Fédérale d'Allemagne, l'Australie, l'Autriche, la Belgique, le Canada, le Danemark, l'Espagne, les États-Unis, la Finlande, la France, la Grèce, l'Irlande, l'Islande, l'Italie, le Japon, le Luxembourg, la Norvège, la Nouvelle Zélande, les Pays-Bas, le Portugal, le Royaume-Uni, la Suède, la Suisse et la Turquie.

L'Agence de l'OCDE pour l'Énergie Nucléaire (AEN) a été créée le 20 avril 1972, en remplacement de l'Agence Européenne pour l'Énergie Nucléaire de l'OCDE (ENEA) lors de l'adhésion du Japon à titre de Membre de plein exercice.

L'AEN groupe désormais tous les pays Membres européens de l'OCDE ainsi que l'Australie, le Canada, les États-Unis et le Japon. La Commission des Communautés Européennes participe à ses travaux.

L'AEN a pour principaux objectifs de promouvoir, entre les gouvernements qui en sont Membres, la coopération dans le domaine de la sécurité et de la réglementation nucléaires, ainsi que l'évaluation de la contribution de l'énergie nucléaire au progrès économique.

Pour atteindre ces objectifs, l'AEN :

— *encourage l'harmonisation des politiques et pratiques réglementaires dans le domaine nucléaire, en ce qui concerne notamment la sûreté des installations nucléaires, la protection de l'homme contre les radiations ionisantes et la préservation de l'environnement, la gestion des déchets radioactifs, ainsi que la responsabilité civile et les assurances en matière nucléaire ;*
— *examine régulièrement les aspects économiques et techniques de la croissance de l'énergie nucléaire et du cycle du combustible nucléaire, et évalue la demande et les capacités disponibles pour les différentes phases du cycle du combustible nucléaire, ainsi que le rôle que l'énergie nucléaire jouera dans l'avenir pour satisfaire la demande énergétique totale ;*
— *développe les échanges d'informations scientifiques et techniques concernant l'énergie nucléaire, notamment par l'intermédiaire de services communs ;*
— *met sur pied des programmes internationaux de recherche et développement, ainsi que des activités organisées et gérées en commun par les pays de l'OCDE.*

Pour ces activités, ainsi que pour d'autres travaux connexes, l'AEN collabore étroitement avec l'Agence Internationale de l'Énergie Atomique de Vienne, avec laquelle elle a conclu un Accord de coopération, ainsi qu'avec d'autres organisations internationales opérant dans le domaine nucléaire.

THE NEA DATA BANK

An important aspect of the work of the NEA concerns the exchange of scientific data and computer programs needed for nuclear energy applications, and this work is carried out by the NEA Data Bank.

The Data Bank, which was set up in January 1978, took over the tasks of two previously separate centres, the Computer Program Library (CPL) at Ispra, Italy, and the Neutron Data Compilation Centre (CCDN) at Saclay, France. It is financed by seventeen of the NEA Member countries.

The Data Bank offers to scientists and technologists nuclear physics information and computer programs necessary for reactor design and other calculations over a wide range of nuclear energy applications. One characteristic of the Data Bank is that its services cover all stages from storing experimental data values to their use in reactor physics applications and span the continuing feedback processes necessary for the gradual refinement of these data. Such integration is achieved through continuing close contacts with the corresponding NEA scientific policy committees: the Committee on Reactor Physics (NEACRP) and the Nuclear Data Committee (NEANDC).

The involvement of the Data Bank in the chain of measurement and then refinement and end use of nuclear data is exceptionally close. The Data Bank's own contribution is twofold: it represents a central point at which nuclear data and computer program information is concentrated, from many sources and at different stages of refinement; and it presents these data and programs to users in a standard form and at a modest but useful level of validation.

LA BANQUE DE DONNEES DE L'AEN

Parmi les activités de l'AEN, l'échange des données scientifiques et des programmes de calcul nécessaires aux applications de l'énergie nucléaire occupe une place importante ; ces travaux sont effectués par la Banque de Données de l'AEN.

La Banque de Données a été créée en janvier 1978 pour reprendre les fonctions précédemment exercées sur une base distincte par deux centres, la Bibliothèque de programmes de calcul (CPL) située à Ispra, Italie, et le Centre de compilation de données neutroniques (CCDN) situé à Saclay, France. Son financement est assuré par dix-sept des pays Membres de l'AEN.

La Banque de Données offre aux spécialistes de la science et de la technologie nucléaires les informations et les programmes de calcul sur la physique nucléaire requis pour la conception des réacteurs et d'autres calculs portant sur toute une gamme d'applications de l'énergie nucléaire. La Banque de Données se caractérise notamment par le fait que ses services couvrent toutes les phases allant de l'enregistrement des éléments de données expérimentales à leur utilisation dans les applications de la physique des réacteurs, et prévoient le retour permanent de l'information nécessaire à l'affinement progressif de ces données. Pour parvenir à intégrer ces divers aspects, la Banque de Données maintient des relations étroites avec les comités de politique scientifique correspondants de l'AEN, tels que le Comité de la physique des réacteurs (NEACRP), et le Comité des constantes nucléaires (NEANDC).

La Banque de Données participe de très près aux opérations successives de mesure, d'affinement et d'utilisation finale des constantes nucléaires. Elle apporte une double contribution à cet égard : d'une part, elle constitue un organe de centralisation des constantes nucléaires et des informations sur les programmes de calcul émanant de nombreuses sources et ayant atteint divers degrés d'affinement ; de l'autre, elle présente ces données et programmes à l'utilisateur sous une forme normalisée et après leur avoir consacré un effort modeste, mais utile, de validation.

FOREWORD

In 1973, the NEA Committee on Reactor Physics initiated a collaborative programme on the application of sensitivity and uncertainty analyses to shielding calculations and on the execution of penetration benchmark experiments. This meeting appraised the current situation and considered developments for the future. It brought together a number of shielding specialists from the NEA Member countries participating in the programme and the papers presented highlighted the considerable developments that have occurred since the major meeting in this series in 1976.

The capabilities now exist for performing sensitivity analyses in complex geometries. Several papers reported the development, at different laboratories, of multi-dimensional Monte Carlo transport codes, incorporating techniques such as correlated tracking or differentiation of the scoring probabilities. These methods were illustrated by application to generic design problems. The meeting reviewed the multigroup data sets in general use and emphasised the importance of the covariance matrices which are currently available for only a limited number of materials. The major experimental shielding programs were presented and there is now general agreement on the conduct of benchmark exercises. Five papers reported the various approaches that have been adopted for data adjustment which is now widely accepted as essential in order to derive quantitative information from benchmark experiments.

AVANT-PROPOS

En 1973, le Comité de Physique des Réacteurs de l'A.E.N. a lancé un programme coopératif sur l'application des analyses d'incertitude d'expériences repères de pénétration. Lors de cette réunion la situation actuelle et les développements envisagés pour le futur ont été examinés et un nombre de spécialistes des pays de l'A.E.N. qui participent au programme, étaient présents. Les communications présentées ont mis en évidence les développements considérables qui se sont produits depuis la réunion principale dans cette série de 1976.

A l'heure actuelle il est devenu possible d'effectuer des analyses de sensibilité dans des domaines de géométrie complexe. Plusieurs contributions ont rendu compte du développement, dans différents laboratoires, de codes de transport Monte Carlo multidimensionnels, en utilisant des techniques telles que la méthode des échantillons correlés et la méthode de la différentiation des probabilités de score. Ces méthodes ont été illustrées par leur application à des problèmes actuels de conception. Au cours de la réunion on a présenté les ensembles de données multigroupes dont l'usage est largement répandu et souligné l'importance des matrices de covariance qui ne sont disponibles couramment que pour un nombre limité de matériaux. Les principaux programmes de protection expérimentaux ont été présentés et l'unanimité existe maintenant en ce qui concerne la conduite à suivre pour les exercices de problèmes repères. Cinq communications ont traité les différentes approches utilisées pour l'ajustement des données qui a été accepté unanimement comme étant essentiel pour la dérivation d'informations quantitatives des expériences repères.

CONTENTS

TABLE DES MATIERES

SUMMARY OF THE MEETING

Dr. J. Butler

The meeting was attended by forty representatives from the seven NEA member countries participating in the collaborative programme and also by ESIS staff from the JRC Laboratory at Ispra.

A total of twenty-seven papers was tabled and summaries of each session were presented by the chairmen. In the final session, the state-of-the-art was reviewed and a formal programme of further work was agreed with the aim of utilising the new analytical techniques which have been developed for the improvement of working data-sets.

In order to appreciate the major progress which has been made in this field, it is only necessary to recall the state-of-the-art revealed at the joint IAEA/NEA meeting held in Vienna in 1976. At that time, the only codes which were generally available for sensitivity analysis were early versions of ANISN/SWANLAKE in which there was no separation of the elastic and inelastic components of the scattering matrix with a consequence that these could not be treated separately in order to perform a proper calculation of the sensitivity profiles. Code modifications had to be made and additional routines written to process the available uncertainty information which was limited to the compilation of Schmidt intended for fast reactor physics. Whilst this document provided an estimate of the variances and enabled some allowance to be made for the correlation between partial cross-sections, no energy-dependent correlation data were available and it was necessary to make the assumption of full correlation between values of a given cross-section at different energies. Whilst this artifice provided an estimate of the accuracy of a shielding calculation, it did not enable the shielding practitioners to make specific requests for new evaluations or differential measurements which were properly supported by quantitative analyses of the available data.

These limitations were clearly evident in the comparison of calculations submitted by the participating laboratories for two theoretical benchmarks which had been established following the 1975 meeting to provide test-beds for the development of sensitivity analysis. The first of these, proposed by Barré, was a typical sodium-cooled FBR radial shield which could be modelled in one dimension; the second, due to Hehn, was a representation of a typical PWR design. Significant and unexplained discrepancies were observed between the solutions submitted by the participants using the same codes but different in-house data-sets and the results of this exercise were inconclusive. At this stage it was clear that the objectives of revising the WRENDA compilation of shielding requests would not be realised until adequate tools for sensitivity analysis had been developed, including a multi-dimensional capability, and covariance files became available to enable proper assessments to be made of the accuracies which could be achieved with existing data-sets.

The limitation of the available tools for sensitivity analysis had also precluded the development of adjusted multi-group sets although a number of so-called benchmark experiments had been conducted at the various laboratories using a range of different fission-plate and reactor-core sources. These were reported at the Vienna meeting. Only the fission-plate experiments were amenable to a nominally exact treatment using the ANISN/DOT discrete-ordinate codes and attention was accordingly focussed on the development of Monte Carlo techniques in order to utilise the wealth of integral measurements which had been published by attempting systematic adjustments of multi-group data in

the manner of fast reactor core physics. It was also clear that no useful exchange of benchmark information could be implemented until it had been shown that experiments conducted at one laboratory could be analysed independently by other laboratories; this objective called for greatly improved standards of documentation of benchmark measurements in accordance with an agreed format.

From the papers tabled at this meeting, it appears that the feasibility of performing uncertainty analysis in the complicated geometries of practical shields has been established and viable methods for adjusting multi-group data in single-material benchmark experiments have been developed. In view of the timescale on which these developments have been made by laboratories with major project commitments for which the adjustment of basic multi-group data was not feasible in the short term, there can be no doubt that the NEA Collaborative Programme has produced a major stimulus without which some of the developments reported would not have been achieved. It is convenient to review the progress under the separate headings of Uncertainty Analysis and Consistency Analysis (or data-adjustment) since the techniques of sensitivity analysis are required for both activities.

Uncertainty Analysis

The most important development in uncertainty analysis is the emergence of several codes for calculating sensitivity profiles in shields with complicated geometries. All of these are based on the Monte Carlo method. The French code TRIPOLI and the program TIMOC at Ispra both utilise the correlated tracking technique but DUCKPOND, a program developed at Winfrith, U.K., differentiates the scoring probabilities. Several papers presented at the meeting discussed these and other methods in detail and illustrated their application to practical reactor shielding problems.

The status of multi-group cross-section and covariance information has changed considerably since the 1976 meeting. Multi-group data-sets applicable to radiation shielding transport problems are now generally available. Multi-group covariance data exists only for a limited range of materials, but the situation has improved due to the compilation of Drischler and Weisbin, based on ENDF/B-IV supplemented by some in-house evaluations or ORNL. In the discussion on the availability of data, some change of emphasis was apparent from the original aim of the collaborative exercise, namely that of generating a revised Data Request List for shielding in WRENDA; it is clear that most laboratories now regard the improvement of working data-sets as the more important objective, at least in the short term. To this end, a formal proposal was made to recalculate the PWR and Fast Reactor benchmarks using the new methods and data-sets. Both benchmarks will be modified to be more representative of current reactor designs and the related work of the American Nuclear Society will be examined in updating the PWR specification. By the end of 1980 Dr. Hehn will distribute a revised specification of the PWR benchmark, in particular correcting some earlier material deficiencies. On this timescale Dr. Salvatores will re-issue the specification of the Fast Reactor benchmark including a volume-distributed source and some revision of the configuration and materials. The participating laboratories will submit their analyses by the end of 1981. Comparison of the PWR results will be co-ordinated by Dr. Rief of JRC/Ispra and Dr. Hehn of IKE/Stuttgart and those of the Fast Reactor will be reviewed jointly by the Cadarache and Winfrith Shielding groups. It is expected that this collation period will require about six months and so a further Specialists' Meeting in this series should be envisaged for mid-1982, to review the results of the programme.

It is hoped that in both the PWR and the Fast Reactor benchmarks, differences between the results due to the calculational method can be eliminated so that any remaining discrepancies can be attributed to the data-sets which have been employed. The forward calculation will be

accomplished with ANISN, the one-dimensional discrete-ordinates transport code, and the benchmark specifications will include guidance on parameters such as mesh size, convergence criteria, etc. Sensitivity analyses will then be performed with the programs available at the different laboratories. Each laboratory will use its in-house data-set for the calculations, but may also use the EURLIB set if resources permit.

Consistency Analysis (Data-Adjustment)

At the 1976 meeting the adjustment of data in shielding experiments was a contentious issue: there was little agreement about the role of this approach (which was well establishedin fast reactor physics) for shield design where transport methods were essential for deep-penetration calculations. From the papers presented at this meeting it appears that most laboratories have investigated data-adjustment in one form or another and it was generally agreed that this approach is essential in order to draw quantitative results from benchmark experiments. There were, however, two schools of thought on how the information obtained in this way should be utilised. On the one hand, it could be used as a pointer for the evaluators and differential measurers to identify cross-section data which did not meet the accuracy requirements. When a data file had been revised on the basis of the information derived from the adjustments, a new multi-group set could then be processed and tested against the original benchmark experiment(s). On the other hand, adjusted data-sets could be used directly in design calculations, and there were several papers tabled at the meeting describing this approach based on the ANISN code using relatively coarse energy-group schemes. In these circumstances, it is inevitable that the effects of some approximations in the methods (such as multi-group averaging) are being accommodated in the adjustment procedure. This practice is acceptable provided that the methods are not applied to situations outside the range bracketed by the benchmark validations. The possibility of applying coarse-group adjustment to bands of fine-group data used in codes such as TIMOC and McBEND was also suggested recognising that the unaltered angular distribution laws would be retained in such a hybrid scheme.

Six papers presented at the meeting reviewed the major experimental shielding programmes which are in progress at different laboratories. For benchmark experiments in general, there is now agreement on the techniques and standards that should be adopted. This represents considerable progress from the situation in 1976 when the principal difficulty was that of representing the complex source and detector geometries. These can now be treated by Monte Carlo codes. By using filters such as water tanks, layers of stainless steel or graphite, the sensitivity profiles can be changed to cover a wider range in order to cover the design requirements.

Notwithstanding these developments, there was a consensus at the meeting in favour of implementing a further collaborative exercise in which all laboratories will be invited to perform a forward calculation for one single benchmark. The winfrith ASPIS experiment was chosen for this purpose and the exercise will be conducted to the same schedule as that proposed above. The detailed specification has been issued by the Winfrith Radiation Physics and Shielding Group and the results of all calculations will be assessed by JRC Ispra with the assistance of Tokyo University. Calculations will be performed of the spectra and detector reaction-rates measured at different positions in the block of iron exposed to the disc fission source. No data-adjustment will be requested but any such contributions would be of considerable interest.

In the concluding discussion, consideration was given to the general direction of future work in this area. It is apparent that the techniques developed for fusion reactors, both experimental and

theoretical, can benefit fission reactor shielding and these should not be specifically excluded from the NEA Collaborative Programme. Of particular interest here are the techniques to discriminate against alpha pulses in scintillation spectrometers at high neutron energies reported by Birmingham University and the inclusion of secondary energy distributions (SED's) in sensitivity calculations by Los Alamos using the SENSIT package. With regard to the development of adjustment techniques, considerable interest was expressed in the so-called Consistent Method originally proposed by Professor Gandini and demonstrated by Gandini and Salvatores. In this method the parameters of nuclear cross-section models are adjusted instead of the magnitudes of the group-averaged cross-sections. The particular attraction for shielding is that relatively few parameters are involved in the energy regions of importance and this clearly simplifies the problem of deriving their covariance matrices. Such an approach would be the natural consequence of the increasing use of "point" cross-section Monte Carlo codes in data adjustment procedures which circumvent the problem of multi-group averaging in deep penetration calculations.

SESSION I

STATUS OF MULTIGROUP DATA SETS AND COVARIANCE INFORMATION

Chairman - Président

R.W. ROUSSIN

(United States)

SEANCE I

ETAT DES CONNAISSANCES SUR LES SERIES DE DONNEES MULTIGROUPES ET L'INFORMATION SUR LA COVARIANCE

SUMMARY OF THE SESSION I RESUME DE LA SEANCE I

Status of Multigroup Data Sets and Covariance Information

Dr. R.W. Roussin

It is evident that the status of multigroup cross section and covariance information is much improved from the situation which existed at the time of the last meeting.

Multigroup cross section libraries designed for studies of the types of radiation transport problems of interest to this body are generally available. Multigroup covariance data, though still sadly lacking in quality and in breadth of coverage for the materials of interest, have been given a significant impetus by the availability of the compilation of Drischler and Weisbin based on ENDF/B-IV and of informal evaluations at ORNL.

The paper by G. Hehn et al outlined the techniques used to verify the production of the (100n, 20g) EURLIB-IV cross section data and gave comparisons between calculations of benchmarks using other data libraries developed in the United States and Japan, namely DLC-41/VITAMIN-C and DLC-51/JSD-120, respectively. Concern was expressed with the treatment of iron inelastic scattering angular distributions (EURLIB) and with the use of the Bondarenko factor approach (VITAMIN-C) for deep-penetration problems. The effect of both of these features will be scrutinised in continuing studies at IKE/Stuttgart and at ORNL.

An interesting presentation was given by V. Herrnberger, EIR, on the automatic selection of group boundaries in a collapsing procedure, which considers sensitivity profiles and required target accuracies. The scheme, AGRUKO, produces sets which are recommended for further use in complex transport calculations and adjustment procedures.

The impact of the DLC-44/COVERX data library (the RSIC designation for the Drischler-Weisbin compilation), was seen in three of the presentations.

The paper by M. Hall on the preliminary version of the EURLIB variance-covariance matrices (presented by McCracken) outlined a prescription for expanding the 15 group Shielding Covariance Library of DLC-44 into the 100 group EURLIB structure. The Hehn paper suggested the use of the 26 group Fast Reactor Covariance Library of DLC-44 in conjunction with EURLIB.

Two review papers detailed the status of multigroup cross sections, sensitivity profiles and covariance matrices, which are available from the Radiation Shielding Information Center at Oak Ridge. These presentations emphasised the recent improvements to the RSIC Data Library Collection (DLC) which have had a positive impact on the sensitivity and uncertainty analysis field. Data libraries for multigroup cross sections such as DLC-41/VITAMIN-C, which contain all reactions and transfer matrices in fine-group form, offer the detail necessary for complete sensitivity analyses. The inclusion of DLC-45/SENPRO multigroup sensitivity profiles and DLC-44/COVERX covariance matrices now allow the possibility of complete sensitivity and uncertainty analyses. The review also summarised the current status of multigroup cross sections and covariance matrices based on ENDF/B-V. The meeting discussed the impact that the present limitations on the free distribution of ENDF/B-V will have on the availability of multigroup libraries derived from that file.

The session ended on an optimistic note with a paper by Hall (presented by McCracken). The comparison of two multigroup sets for iron was reported, one adjusted with the ASPIS iron benchmark measurements, and the other adjusted with measurements in the cores of fast criticals. The results appear complementary and suggest that "the possibility of producing a rationalised data set to embrace both shielding and core calculations cannot be ruled out".

CHECKING AND IMPROVEMENTS OF THE MULTIGROUP DATA LIBRARY EURLIB-4

G. Hehn, M. Mattes, K. Al Malah, G. Kicherer
IKE University of Stuttgart
Stuttgart (FRG)

ABSTRACT

Multigroup data libraries, which are widely distributed and used in many projects, must be checked properly before release. The zero version calculated with given flux weighting from evaluated nuclear data files is checked automatically by consistency tests in particle and energy transfer as far as possible. For EURLIB two data sets are produced with different processing codes independently at EURATOM/ Ispra and at IKE/Stuttgart, so that a good check is given. With the help of several generic shielding problems the differences to US and Japanese group data sets have been studied in detail showing the effect of other group structures or other concepts of resonance weighting. It is shown that an improved treatment of thermal neutrons is very important. Finally the cross section requirements for deep penetration in iron are discussed. The present status of the library is presented.

1. INTRODUCTION

For evaluating shielding benchmark experiments within the cooperative work of OECD/NEA countries it was decided, that as an important basis a common multigroup library should be applied [1]. For that purpose the library EURLIB was produced in a coordinated effort by EURATOM/Ispra and IKE/Stuttgart. This library was designed for coupled neutron and gamma calculations with 100 neutron and 20 gamma groups [2]. The choice of the group structure was a compromise between energy details needed and calculation effort justifiable for shielding applications. The neutron group structure was a subset for shielding of the 239 CSEWG fast neutron groups, representing important cross section minima for proper transport calculations as well as some requirements of threshold and resonance detectors including the effective Cadmium cut off energy. The final result is, that EURLIB represent today an excellent multigroup library for shielding problems of light water reactors. The most stringent data requirement in LWR shielding is needed for determining the neutron damage of the pressure vessel and for this field of application the group structure is most perfect as we can show.

In comparison with VITAMIN-C [3] and JSD120 from JAERI [4] the question was, in which form the treatment of resonances should be done best. The f-factor concept of Bondarenko [5] has large advantages for core physics of fast reactors, but its benefit has not been demonstrated for shielding calculations, so we had to study this effect to get the right arguments for further developing of the EURLIB library.

A further problem exists in the proper treatment of thermal neutrons, which can be shown best in comparing the thermal flux and its secondary gamma radiation in concrete shields [6]. Finally for calculating the transmission of neutrons through thick slabs of iron as measured in single material benchmark experiments and used for adjustment of group cross sections we need a relatively fine group structure with a good representation of the inelastic scatter process.

2. STATUS OF EURLIB-IV

The number of isotopes in the library had been steadily increased to describe the burn-up of fuel elements for thermal reactors more correctly. For light water reactors the Plutonium isotopes were completed as well as important fission products were added. The requirements for reactors with heavy water were satisfied and additions

had been made for the gas cooled high temperature reactor with Thorium fuel cycle. In the latter case eight thermal groups had been added with a full upscatter matrix and the number of gamma groups had been enlarged to 36 groups as used in VITAMIN-C. Details of the present status of EURLIB-IV are shown in Table I.

3. DATA CHECK AND INTERCOMPARISON WITH OTHER LIBRARIES

Multigroup data libraries, which are widely distributed and used in many projects, must be checked properly before release. The zero version calculated with given flux weighting from point data is checked automatically by consistency tests in particle and energy transfer as far as possible. Optical checks are performed with plots containing point and group data. In the next step the cross sections are directly compared with other independently generated group data originating from the same evaluated nuclear data library like ENDF/B-IV. For EURLIB always two data sets are produced independently at Ispra and at Stuttgart, so that a good check of the numerical results is possible including all details of the scattering matrices.

The comparison with other multigroup libraries can best be done with the help of generic shielding problems. We compared the libraries EURLIB-IV, VITAMIN-C and JSD120 in calculating the target quantities of interest in a radial shield of a modern BWR (KRB-II, 1300 MW_{el} [7]. The results are given in Table II. Inspite of the differences in the group structure and the application of the f-factor concept in the Japanese library we get a good agreement of the maximum damage rate in the pressure vessel. The heat production at the inner edge of the primary concrete shield as well as the gamma dose rate after 1 m of primary shield are underestimated by JSD120, which can be explained by the use of POPOP4-data for the gamma production. The influence of the f-factor concept has its maximum at the core surface coming from the Uranium resonances as can be seen in the neutron spectrum of Figure 1. But this effect is totally lost in the neutron spectrum shown in Figure 2 for the pressure vessel. We can therefore conclude that the f-factor concept has some minor advantages for proper description of the resonances of fissionable nuclides in the outer core regions but in the shielding layers it is more correct and easier to apply macroscopic $1/\Sigma_T$-weighting.

At RSIC an intercomparison between different libraries had been performed for a neutron transmission problem in a 1 m concrete slab. Since an old version of EURLIB had been used which didn't profit from the double check system, we repeated these calculations and the

Table I: Content of the coupled neutron-gamma multigroup library EURLIB-4 (IKE-version) with 100 neutron groups and 20 gamma groups in P_5-approximation

Z	Isotope	MAT*	Comments
1	H - 1	1261	covariance matrices from ENDF/B-V MAT=1301
	H - 2	1120	
2	He- 3	1146	γ-production data from ENDL-2 MAT=7104
	He- 4	1270	without gamma-production data
3	Li- 6	1271	
	Li- 7	1272	
4	Be- 9	1289	
5	B - 10	1273	
	B - 11	1160	γ-production data from ENDL-2 MAT=7111
6	C - 12	1274	covariance matrices given; additionally data set from ENDF/B-V MAT=1306 with covariance m.
7	N - 14	1275	covariance matrices given
8	O - 16	1276	covariance matrices given
9	F	1277	
11	Na- 23	1156	
12	Mg	1280	
13	Al- 27	1193	
14	Si	1194	
15	P - 31	7121**	
16	S - 32	7122**	
17	Cl	1149	
19	K	1150	
20	Ca	1195	
22	Ti	1286	
23	V	1196	
24	Cr	1191	
25	Mn-55	1197	
26	Fe	1192	additionally $1/\Sigma_T$-weighting
28	Ni	1190	
29	Cu	1295	
30	Sn	7850***	
40	Zr	7141**	
	Zirc-2	1284	without gamma-production
41	Nb-93	1189	
42	Mo	1287	
56	Ba-138	7151**	
62	Sm-149	1027	without gamma-production
64	Gd	1030	without gamma-production
74	W -182	1128	
	W -183	1129	
	W -184	1130	
	W -186	1131	
82	Pb	1288	
90	Th-232	1296	γ-production data from ENDL-2 MAT=7164
91	Pa-233	1297	without gamma-production
92	U -233	1260	γ-production data from ENDL-2 MAT=7166
	U -234	1043	γ-production data from ENDL-2 MAT=7167
	U -235	1261	
	U -236	1163	γ-production data from ENDL-2 MAT=7169
	U -238	1262	
93	Np-237	1263	without gamma-production
94	Pu-239	1264	
	Pu-240	1265	
	Pu-241	1266	without gamma-production
	Pu-242	1161	without gamma-production

* All data from ENDF/B-IV unless otherwise noted
** ENDL-2
*** ENDL-3

results are given in Table III. Comparing the dose rates of epithermal and fast neutrons of the VITAMIN-C results in 171 and in 100 neutron groups, we can conclude that one half of the difference to EURLIB-IV results from the reduced number of groups and the second half of the difference can be removed by proper weighting. Also shown are the results of few group libraries like BUGLE and EURLIB-LWR-45. The latter is a 45 group condensation of EURLIB-IV optimized for LWR calculations [8].

A special problem is the representation of thermal neutrons as shown in Table IV. The differences can be explained by different physical models of the scattering dynamics. The thermal data of EURLIB represent chemical binding as well as thermal motion. In the few group libraries the effect of changes in the thermal sources can be seen. Of course the increase of the thermal neutron flux density gives a higher gamma field. Figure 3 shows the details in the neutron spectrum leaking from the concrete slab.

A comparison of deep penetration in an iron slab is given in Table V. There is no problem for moderate penetration up to 20 cm as needed for reactor application. But for deeper penetrations a better description of the inelastic scatter process combined with a larger number of energy groups of VITAMIN-C results in a better transport of the neutrons. The differences in the neutron spectrum are shown in Figure 4. We are now implementing the higher angular moments of inelastic scattering into the EURLIB-IV library to see which is the dominating effect.

4. DATA FOR ERROR ANALYSIS

Together with the total cross section matrices for transport calculations the EURLIB data are also available in the form of nonelastic matrices seperately. In the case that more details can be made available concerning the covariance information also partial cross sections can be supplied in EURLIB structure. For the most important elements in shielding of thermal power reactors the covariance information had been collected from ENDF/B-IV and -V and the 26 group COVERX library [9]. Of these covariance matrices the diagonal rows are plotted in Figure 5 up to Figure 10 in the form of standard deviations.

Table II: Shield calculation of a BWR (KRB-II, 1300 MW_{el}) with EURLIB-IV, VITAMIN-C and JSD120

Multigroup Library	Damage DPA/s	Heat W/cm^3	N-Dose REM/H	G-Dose R/H
EURLIB-IV	3.41 -14*	2.47 -6	7.93 -3	4.09 -1
VITAMIN-C	+ 1 %	+ 5 %	+ 6 %	+ 1.5 %
JSD120	+ 3 %	- 9 %	+ 3 %	- 6.5 %

*read $3.41 \cdot 10^{-14}$

Table III: Percent of deviation from EURLIB-IKE-100 of neutron dose rates at the exit face of a 1 meter ordinary concrete slab calculated with various libraries

Library	Fission Source	Fission + Fusion Source
	epithermal and fast neutrons	epithermal and fast neutrons
VITAMIN-C-171	+12.4	-7.3
VITAMIN-C-100	+6.4	-3.5
BUGLE-45	+1.5	+14.6
EURLIB-LWR-45	-2.2	-5.3

Table IV: Dose of thermal neutrons in relation to the dose of fast and epithermal neutrons at the exit face of 1 m ordinary concrete slab calculated with various libraries

Library	Fission Source	Fission + Fusion Source
EURLIB-IV	.103	.036
VITAMIN-C	.168	.062
BUGLE-45	.211	.062
EURLIB-LWR-45	.094	.039

Table V: Percent of deviation from VITAMIN-C-171 ($1/\Sigma_T$-W.) of neutron dose rates at various locations of 1 m PV-steel slab calculated with EURLIB-IV

	Neutron dose rates (rem/h)		
slab-thickness cm	VITAMIN-C-171	EURLIB-IV	Deviation from VITAMIN-C-171 %
1	2.67 E-4	2.67 E-4	0.
20	1.45 E-4	1.41 E-4	- 2.7
40	5.60 E-5	4.80 E-5	-14.0
60	2.24 E-5	1.67 E-5	-25.0
80	8.49 E-6	5.51 E-6	-35.0
100	1.10 E-6	5.72 E-7	-48.0

5. REFERENCES

(1) Butler, J., Nicks, R.:
Sensitivity studies and shielding benchmark experiments
NEACRP-L-1 (1974)

(2) Cagliotti, E., Nicks, R., Penkuhn, H., Hehn, G., Mattes, M., Herrnberger, V.:
Generation and testing of the shielding data library EURLIB for fission and fusion technology
in Reactor Shielding, Science Press, Princeton (1977)

(3) Roussin, R.W., Weisbin, C.R., White, J.E., Greene, N.M., Wright, R.Q., Wright, J.B.:
The CTR Processed Multigroup Cross-Section Library for Neutronics Studies
ORNL/RSIC-37 (1978)
Available from RSIC (Radiation Shielding Information Center) as DLC-41/VITAMIN-C

(4) Koyama, K., Okumura, Y., Furuta, K., Miyasaka, S.:
Multigroup Cross Section Sets for Shielding Materials
- 100 neutron groups and 20 gamma-ray groups in P_5 approximation -
JAERI-M 6928 (1977)
Available from NEA Data Bank as ZZ-JSD-120

(5) Bondarenko, I.:
Group constants for nuclear reactor calculations
Constants Bureau, New York (1964)

(6) Methalchi, M., Roussin, R.W., West, J.T., Nakhai, B.:
A Comparison of the use of EURLIB-III and other multigroup cross-section libraries for a 1 meter concrete slab problem
ESIS Newletter 31, pp. 3 - 5 (1979)

(7) Hehn, G., Kicherer, G.:
Shielding data requirements for thermal power reactors of boiling water and gas cooled type
Specialists' Meeting on Nuclear Data and Benchmarks for Reactor Shielding, Paris, 27.-28. Oct. 1980

(8) Herrnberger, V., Padiyath, S.:
Examples of optimized broad energy group structures generated by the automatic collapsing scheme AGRUKO
Specialists' Meeting on Nuclear Data and Benchmarks for Reactor Shielding, Paris, 27.-28. Oct. 1980

(9) Drischler, J.D., Weisbin, C.R.:
Compilation of multigroup cross-section covariance matrices for several important reactor materials
ORNL-5318 (ENDF-235) (1977)
Available from RSIC as DLC-44/COVERX

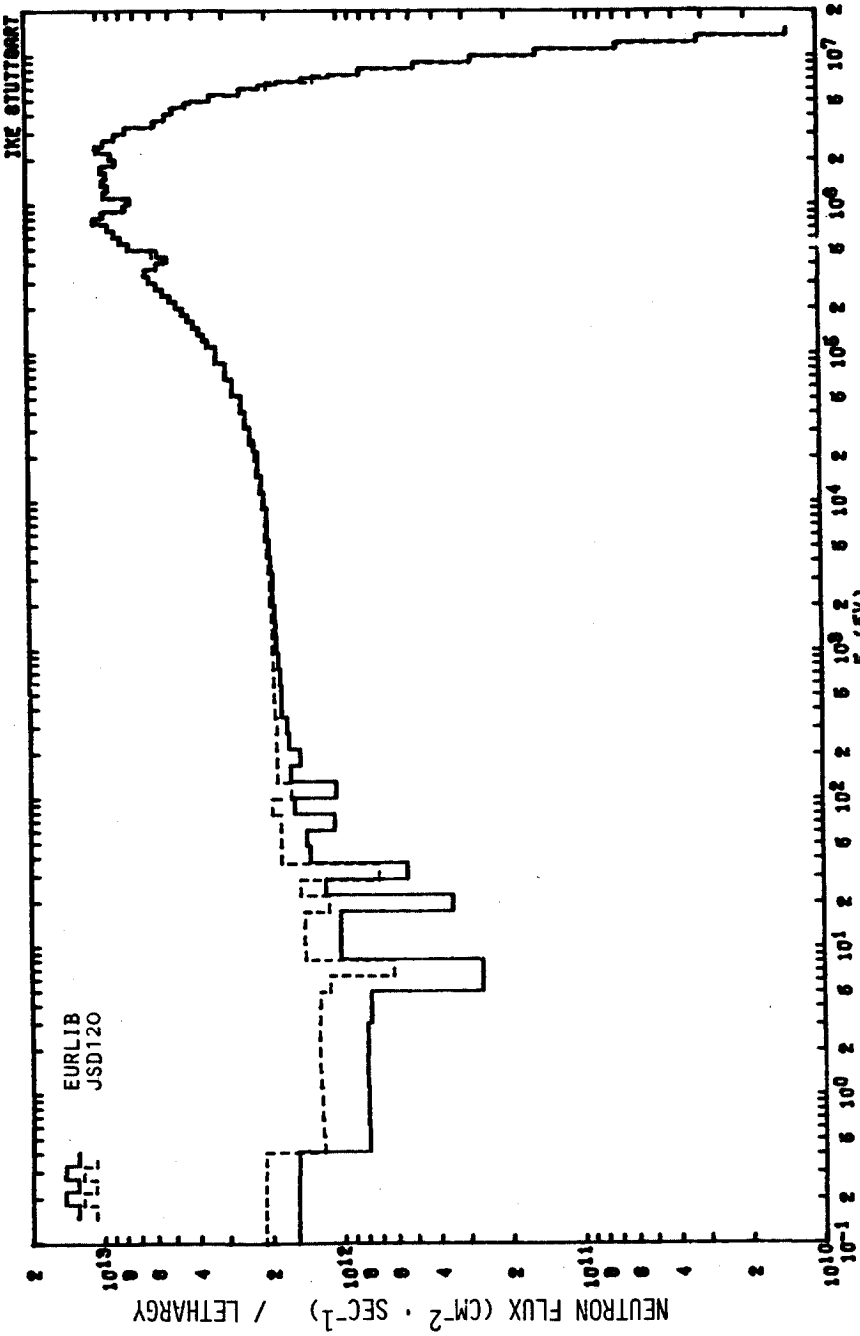

FIG. 1 NEUTRON SPECTRUM AT CORE SURFACE (BWR, KRB-II, 1300 MW_{EL})
EURLIB IV AND JSD120

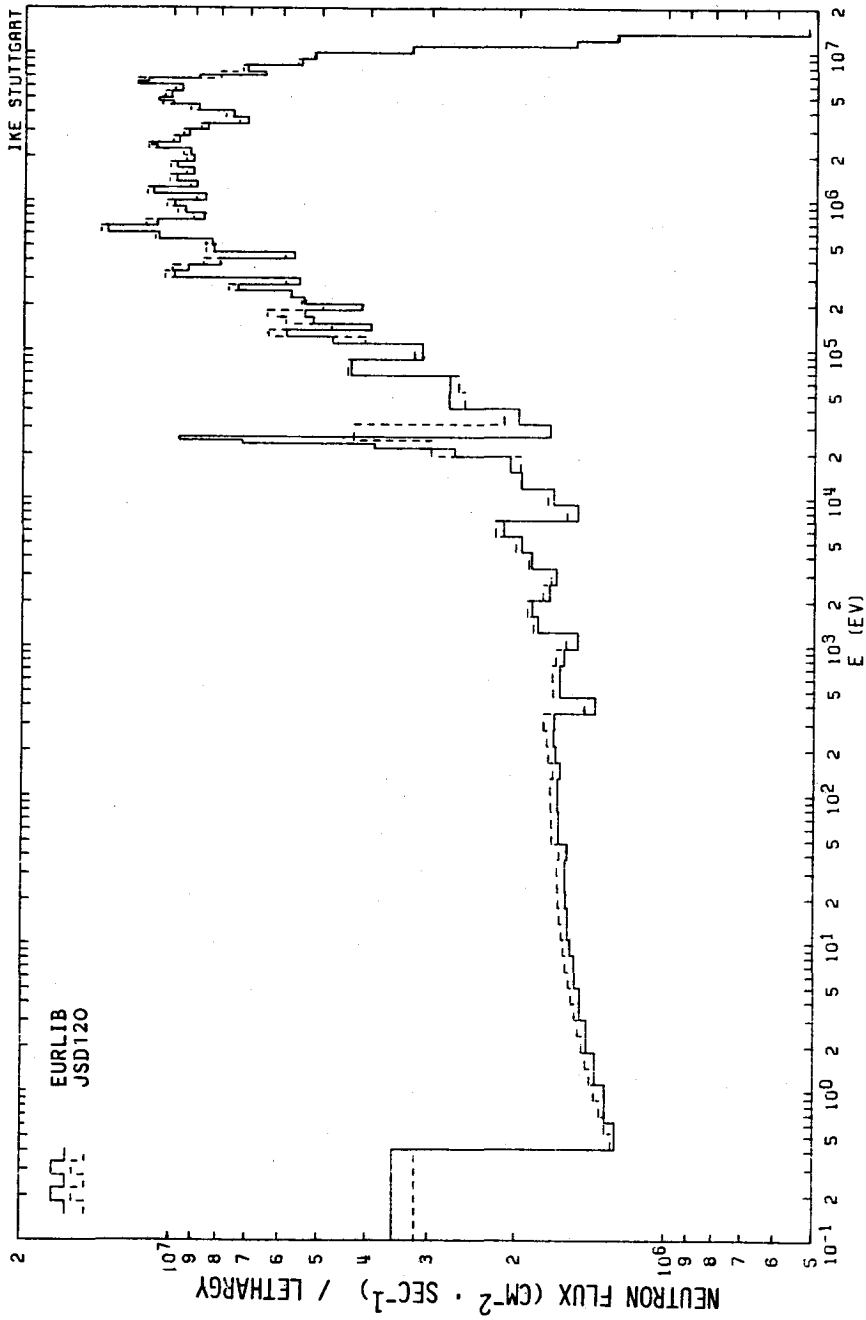

FIG. 2 NEUTRON SPECTRUM IN PRESSURE VESSEL (BWR, KRB-II, 1300 MW_{EL})-
EURLIB-IV AND JSD120

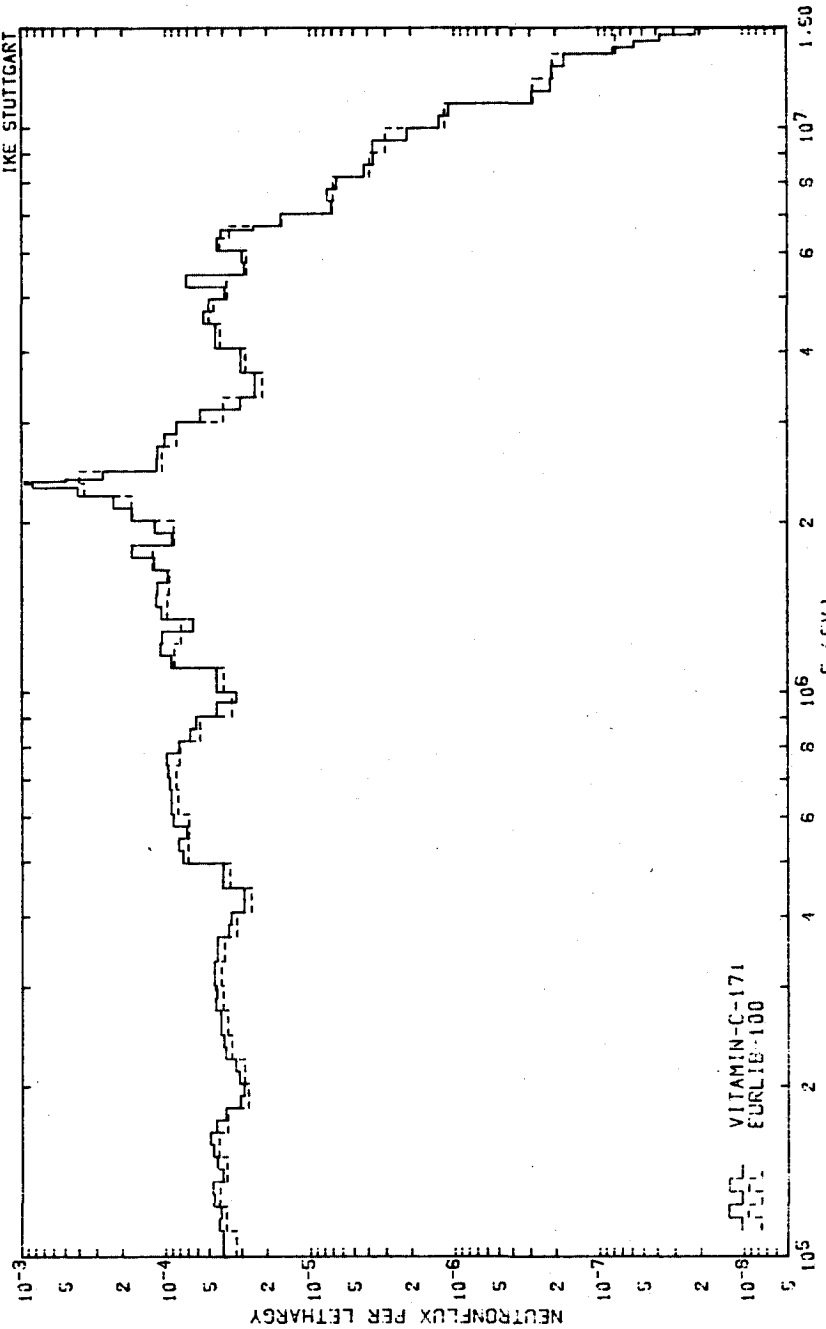

FIG. 3: NEUTRON SPECTRUM AT THE EXIT OF 1 M CONCRETE SLAB
FISSION SOURCE

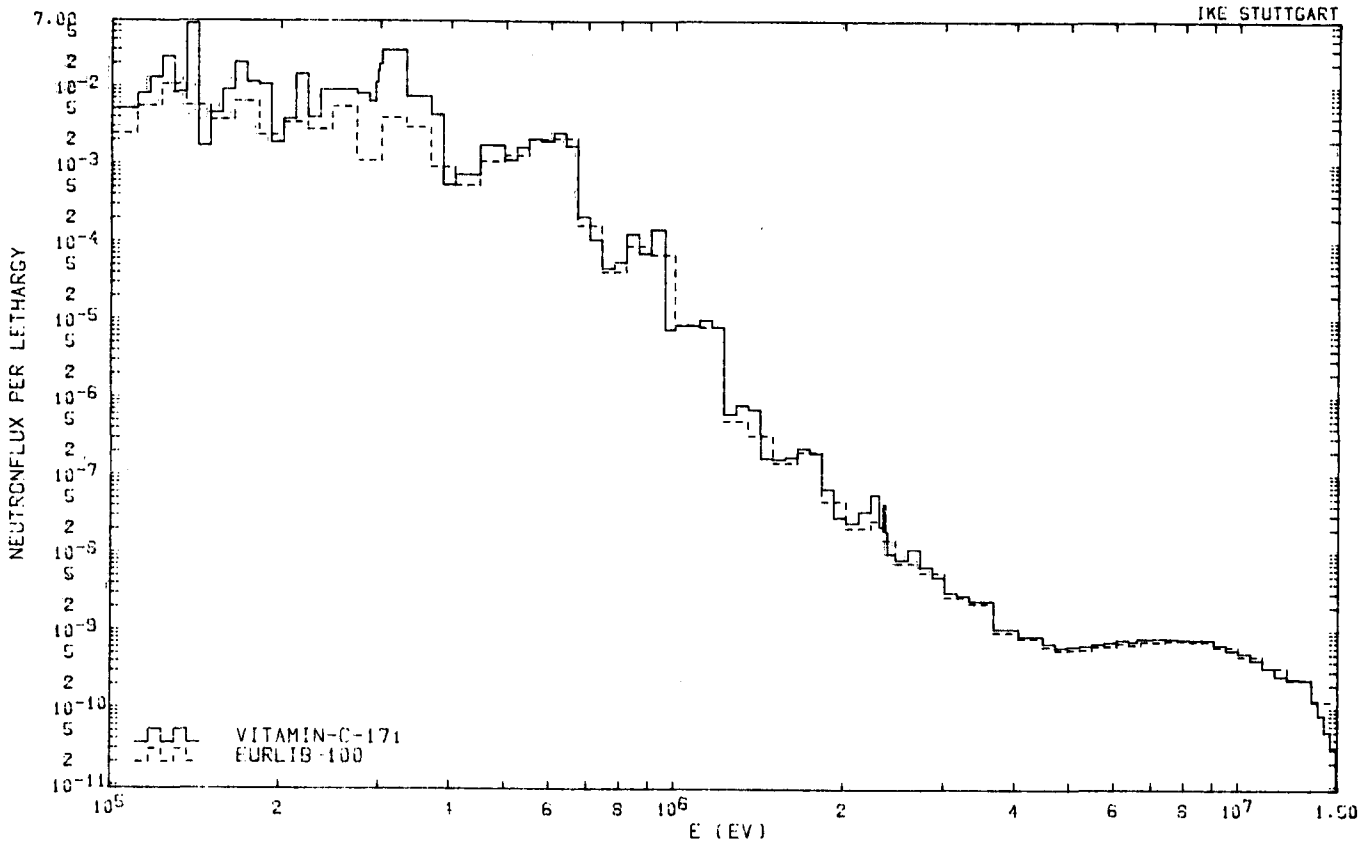

FIG. 4: NEUTRON SPECTRUM AT THE EXIT OF 1 M STEEL SLAB
FISSION SOURCE

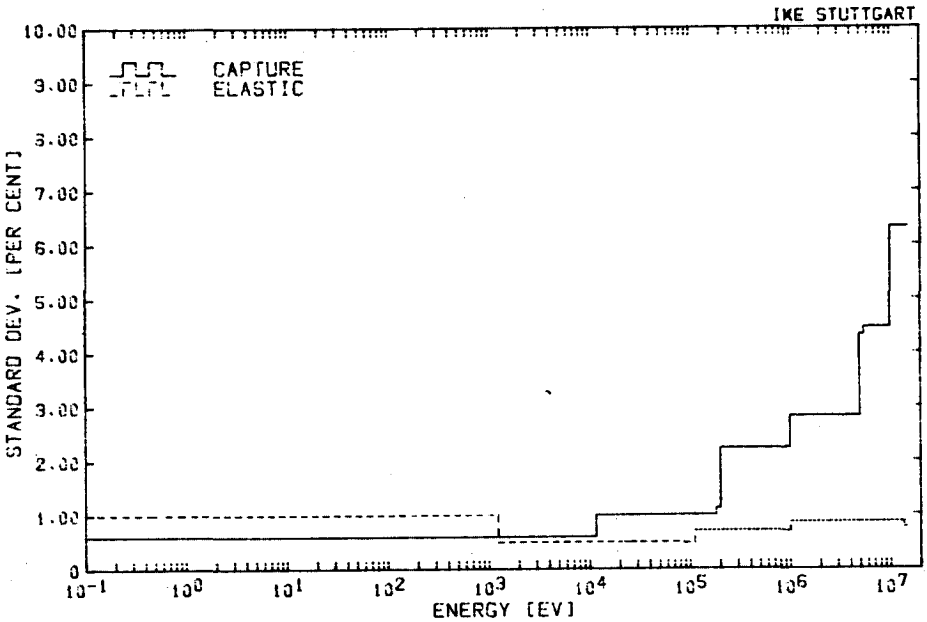

FIG.5 STANDARD DEV. H-1 EURLIB-100 ENDF/B-5

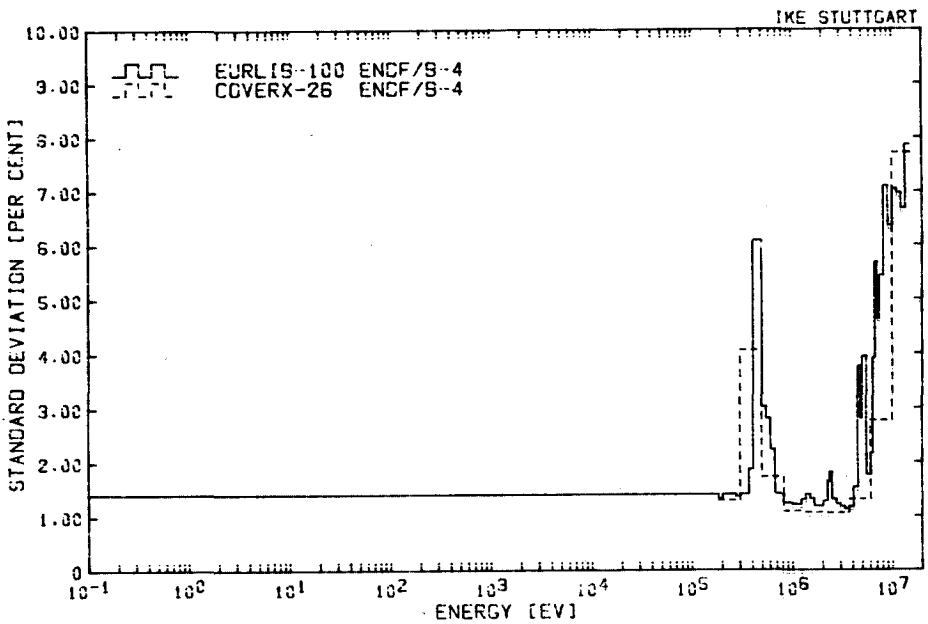

FIG.6 STANDARD DEV. O-16 ELASTIC

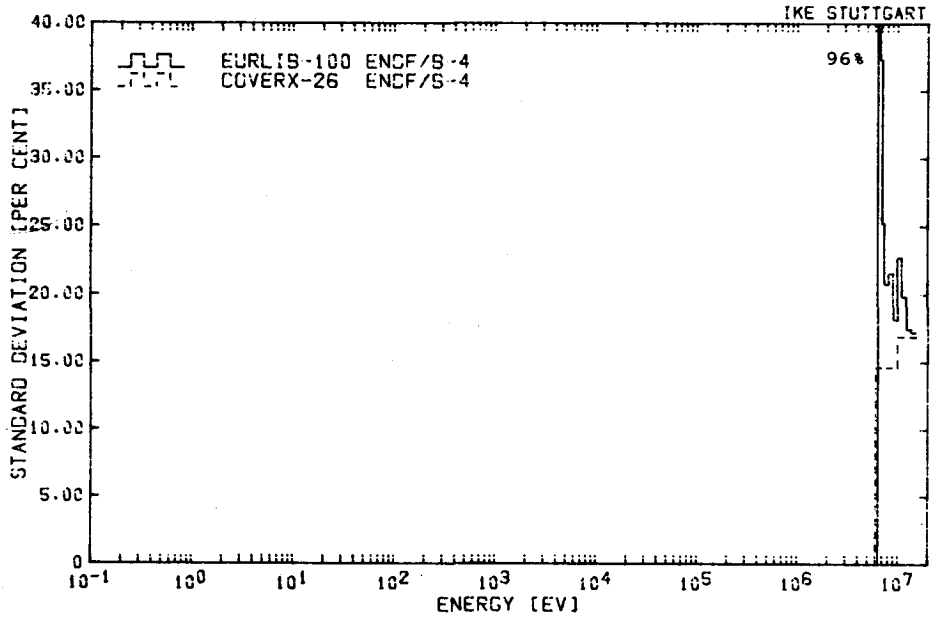

FIG.7 STANDARD DEV. O-16 INELASTIC

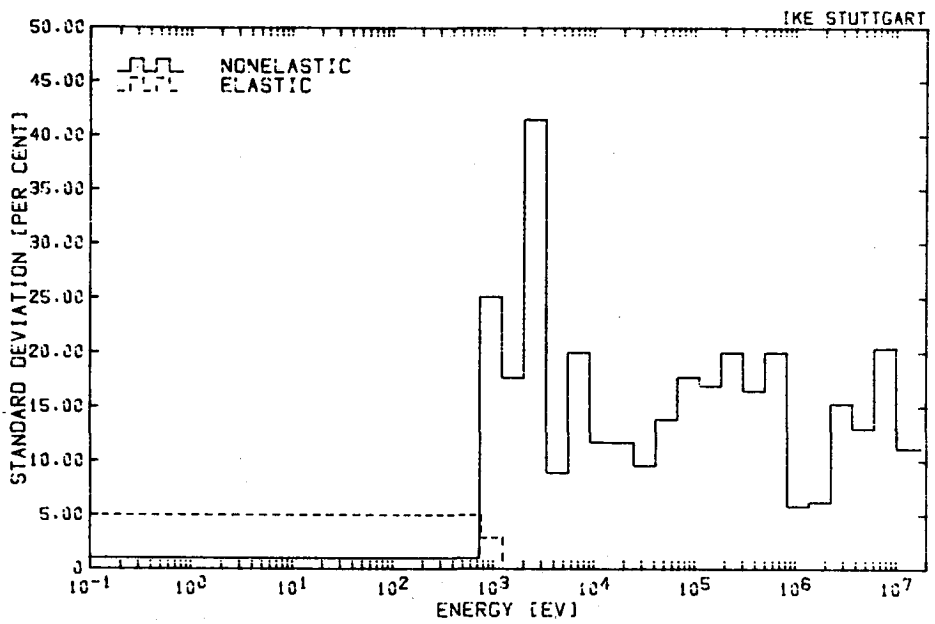

FIG.8 STANDARD DEV. FE-26 COVERX-26 ENDF/B-4

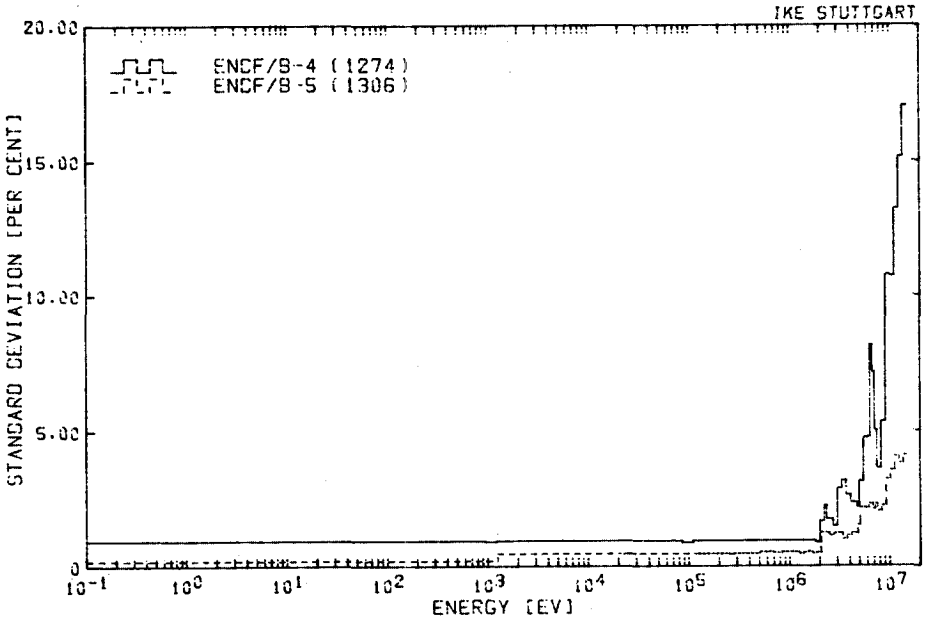

FIG.9 STANDARD DEV. C-12 ELASTIC EURLIB-100

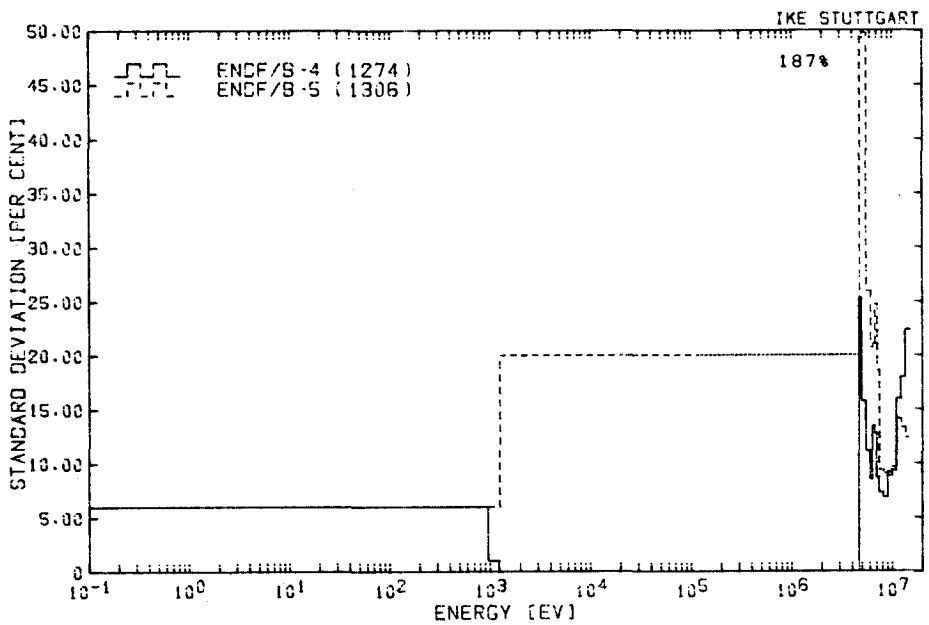

FIG.10 STANDARD DEV. C-12 NONELASTIC EURLIB-100

STATUS OF MULTIGROUP CROSS-SECTION LIBRARIES AVAILABLE FROM THE RADIATION SHIELDING INFORMATION CENTER

R. W. Roussin, D. K. Trubey, and B. F. Maskewitz
Radiation Shielding Information Center
Oak Ridge National Laboratory
Oak Ridge, Tennessee, U.S.A.

ABSTRACT

Multigroup cross-section libraries for shielding applications in formats for direct use in discrete ordinates codes have long been a part of the Radiation Shielding Information Center's (RSIC) Data Library Collection (DLC). In recent years libraries in more flexible and comprehensive formats which allow the user to derive his own problem-dependent sets have been added to the collection. The current status of both types is described as well as well as projections for adding data libraries based on ENDF/B-V.

1. INTRODUCTION

The Radiation Shielding Information Center (RSIC) has long provided multigroup cross sections in discrete ordinates format as part of its Data Library Collection (DLC) [1]. These are generally developed for a particular application and users with similar types of problems have applied them with reasonable success. In recent years, more extensive libraries in flexible formats with an appropriate set of retrieval codes have become available. These allow the user to derive his own problem dependent library taking into account temperature and self shielding effects. The status of both types of libraries now available from RSIC is described in the sections that follow. Useful response function-type libraries are also identified. Libraries which are of both types that are expected to be made part of the DLC are indicated and the availability of new libraries based on ENDF/B-V is discussed.

2. FINE-GROUP LIBRARIES IN DISCRETE ORDINATES FORMAT

The term "discrete ordinates" format generally means that the particular multigroup library can be read into codes developed at Oak Ridge National Laboratory (ORNL) or Los Alamos Scientific Laboratory (LASL) including 1-D, 2-D discrete ordinates Codes as well as multigroup Monte Carlo codes. Care needs to be taken whether the particular code requires a $(2\ell+1)$ term be present in the cross sections.

Some "fine-group" Libraries, i.e., 100 or more neutron groups are available as part of the DLC.

2.1 DLC-27/AMPX01 (104n,22g) Library for Concrete and Air Transport

The 104 neutron (104n), 22 gamma-ray (22g) group, P_5, library was generated with 1/E weighting with AMPX [2] from ENDF/B-III [3] and the Defense Nuclear Agency Working Cross-Section Library (DNAWCSL) [4]. Data are included for the constituents of concrete and air. The group structure is equal lethargy except near the 2.3 MeV oxygen minimum.

2.2 DLC-37/EPR (100n,21g) Library for Fusion Neutronics

The (100n, 21g), P_8, library was generated using 1/E weighting with AMPX from ENDF/B-IV [5] for fusion neutronics studies at ORNL [6]. It has been applied to neutronics design studies for the fusion Experimental Power Reactor (EPR) and many other projects prior to the release of DLC-41/VITAMIN-C (see section 4.1). Data are provided for 46 materials and kerma factors based on ENDF/B-III are also included. Thermal group cross sections are for an 800°K Maxwellian spectrum.

2.3 DLC-35/EURLIB (100n,20y) Coupled Shielding Standard Library

The (100n, 20g), P_3, was generated with AMPX at EURATOM/Ispra from ENDF/B-IV using a 1/E tied to fission spectrum [7], except for iron where $1/E \cdot \sigma_t$ was used. Special treatment for the thermal region was used to obtain proper thermal values. The version currently in RSIC, denoted DLC-35B/EURLIB-III, has data for 13 elements.

2.4 DLC-51/JSD-100/120 Cross Sections for Shield Materials

The Japan Atomic Energy Research Establishment (JAERI) provided two libraries as part of their shielding calculational scheme CCC-300/RADHEAT [8]. The cross sections were generated using the MACS system using ENDF/B data and POPOP-IV [9] for gamma-ray production. One hundred neutron group, P_5, infinitely dilute, data are provided for some 50 materials and dectector responses. Coupled (100n,20g) self shielded data for typical reactor materials is also provided. Use of the library outside the RADHEAT-V3 system would require library translation to appropriate format.

3. BROAD GROUP LIBRARIES IN DISCRETE ORDINATES FORMAT

Broad group (60 or less groups) libraries are typically generated for a particular application and care is required in applying them to problems not closely related to the original application. Some broad group libraries have seen wide usage and may not have always been used with due consideration of the particular application.

3.1 DLC-23/CASK (22n,18g) Shipping Cask Library

The (22n,18g) library was generated with SUPERTOG [10] and POPOP-IV with 1/E weighting into a (104n,18g) structure and was then collapsed to (22n,18g) using a spectrum typical for a U-H_2O mixture [11]. P_3 data are provided for 29 materials. The source of the evaluated neutron data is ENDF/B-II (1970).

3.2 DLC-31/FEWG1 (37n,21g) Defense Nuclear Agency Library

The (37n,21g), P_3, library was developed on behalf of the U.S. Defense Nuclear Agency and was tested against typical air and concrete transport problems [12]. The data were generated with 1/E weighting from ENDF/B-IV and the DNA WCSL using AMPX. Cross sections for 43 materials are provided as well as various useful response functions.

3.3 DLC-36/CLAW-IV (30n,12g) LASL Library

The (30n,12g) library was generated from ENDF/B-IV using NJOY [13] with a fusion-fission-1/E-Maxwellian weight function. The "P_4-corrected" P_3 library [14] includes essentially all materials from ENDF/B-IV. The library includes prompt and steady state transfer arrays, as well as various response functions and fission spectra.

3.4 DLC-75/BUGLE-80 (47n,20g) ANS 6.1.2 Standards Studies Library

The (47n, 20g), P_3, library was generated by collapse from DLC-41/VITAMIN-C (see section 4.1) with a spectrum typical of that in the concrete shield of a PWR [15]. It was developed at ORNL for studies by the American Nuclear Society ANS 6.1.2 Working Group for Shielding Cross Sections in its efforts to develop a Standard for Shielding Cross Sections. BUGLE-80 was found to perform well for typical LWR and concrete shielding problems and will be cited as a library conforming to their Draft Standard [16]. The library contains data for most ENDF/B-IV materials as well as response functions and source spectra.

3.5 DLC-58/HELLO (47n,21g) Cross Sections for E<60 MeV

The (47n,21g) library was developed at ORNL [17] by merging data for E_n > 15 MeV with a (35n,21g) library based on DLC-41/VITAMIN-C (see Section 4.1). The high energy data were developed from optical model and intranuclear cascade evaporation model. The P_3 library contains data for 10 elements to allow shielding calculations for heavy concrete for neutrons generated by Li(D,n) sources.

3.6 DLC-64/UKCTRI (46n) Fusion Reactor Cross Sections

The 46n library was generated at U. Birmingham [18] from UKNDL [19] using GALAXY [20] with a $1/E \cdot \Sigma_t$ weighting function. Data are provided for 25 materials in P_4 expansion for use in fusion (CTR) calculations. Special treatment was used for the thermal region for H and D.

4. FINE-GROUP LIBRARIES FOR DERIVING APPLICATION-DEPENDENT SETS

To avoid using cross-section libraries which may not be appropriate for a given application, a user can generate a new library from the basic evaluated data file. The expense of such an approach usually makes it impractical for most users to exercise this option. An alternative is to derive application-dependent

libraries from a fine-group library. Such libraries for shielding applications have become available in recent years and are now a part of the RSIC DLC. These utilize the AMPX [2] or CCCC [21] formats which allow the user access to all partial cross sections and permit him to account for temperature and self-shielding effects for a particular application. The computing technology for performing such manipulations is available in the RSIC package PSR-117/MARS [22]. Libraries available from RSIC which are in this category are described in section 4.1 through 4.4 below.

4.1 DLC-41/VITAMIN-C (171n,36g) Library for LMFBR and Fusion Neutronics

The (171n,36g) library [23] was generated at ORNL using PSR-105/MINX [24] for neutrons and the LAPANGAS and SMUG modules of AMPX for gamma rays. The output format is AMPX master library format.

Resonance self shielding and temperature effects are accounted for by the Bondarenko [25] approach and the "smooth" weighting function used in the procedure was fusion-fission-1/E-Maxwellian. P_3 data are provided at 300, 900, and 2100 K for 66 materials from ENDF/B-IV. The library was developed for LMFBR core and shield analysis and fusion neutronics and has been applied successfully to applications in those fields [26]. As indicated earlier, several of the libraries listed in section 3 were derived from DLC-41. A CCCC version, DLC-53/VITAMIN-4C is also available in the DLC.

4.2 DLC-42/CLEAR (126n,36g) LMFBR Library

The (126n,36g) library is a subset of DLC-41 but also has data in both AMPX and CCCC formats. This arrangement was necessary to allow CCCC users a technique to include gamma-ray production data in the CCCC framework. DLC-42 has been used for much LMFBR neutronics work at ORNL.

4.3 DLC-43/CSRL (218n) Criticality Safety Library

The 218n library was generated from ENDF/B-IV using AMPX. Designed for out-of-core criticality safety analysis for the U.S. Nuclear Regulatory Commission, DLC-43 has a multithermal group treatment and utilizes the NITAWL resonance calculations in AMPX. Data are provided in P_3 expansion for 84 materials.

4.4 DLC-52/EPRMASTER (100n)

This (100n) library in AMPX format is the neutron file from which DLC-37/EPR (see section 2.2) was prepared. This was packaged to allow users to access to all partial cross sections that are available in the AMPX library format (the same reactions given on ENDF).

5. MISCELLANEOUS LIBRARIES OF RESPONSE FUNCTIONS

It is often very important to have reaction cross sections, response functions, etc., to be used in conjunction with a multigroup library in discrete ordinates format. As indicated above, some DLCs include such as part of the basic cross-section libraries. Listed in sections 5.1 through 5.6 are DLCs which provide useful "response" function data to be used in conjunction with a normal transport calculation.

5.1 DLC-55/RECOIL Recoil Spectra Data Base

A data base of recoil spectra in 104 energy groups has been prepared at ORNL using a modified version of the XLACS module of AMPX on ENDF/B-IV. Data are provided for one hundred incident neutron energy groups for 26 materials of interest to the radiation damage community. An analysis code RECOIL [27] is included to derive primary recoil spectra, damage energy, and displacement cross sections.

5.2 DLC-60/MACKLIB-IV (171n,36g) Kerma Factors

The (171n,36g) library of reaction cross sections and kerma factors [28] was generated from ENDF/B-IV using MACK-IV [29]. Data are provided in the group structure of DLC-41/VITAMIN-C and the two DLCs provide a comprehensive data base for neutronics studies. A retrieval code is provided for group collapse.

5.3 DLC-71/GAMMON Activation Library

The (100n,25g) library was prepared at LASL from a variety of sources and contains activation cross sections for 420 reactions, multigroup decay spectra in 25 gamma-ray groups for 107 unique daughter products, maximum permissible concentrations for 200 reaction products and absorbable decay energy for 85 products. The GAMMON library [30] supersedes the DLC-33/MONTAGE library developed earlier by LASL. A retrieval code is provided to select and rebin the data.

5.4 DLC-72/MONTUK (100n) Transmutation and Activation Library

The (100n) library contains data for 1010 transmutation and activation reactions. The MONTUK [31] library augments the neutron activation reactions in DLC-71/GAMMON with additional transmutation reaction cross sections.

6. LIBRARIES EXPECTED TO BE ADDED TO THE DLC

Additional libraries are expected to be added to the collection in the near future. These include data based on both ENDF/B-IV and ENDF/B-V [32].

6.1 Fine-Group Libraries Based on ENDF/B-IV

The EURLIB-IV (100n,20g) is now being packaged in RSIC.

6.2 Broad-Group Libraries Based on ENDF/B-IV

A (47n,20g) library [33] derived at ORNL from DLC-41/VITAMIN-C for specific LWR models and collapsed with typical spectra calculated for such models will be added to the DLC this fall.

Another library, with (22n,21g) has been derived at ORNL from DLC-41/VITAMIN-C for use in nuclear fuel cycle shielding calculations [34]. It will also be added to the collection this fall.

A 60 neutron group library, covering the energy range from 60 MeV to thermal, has been developed at LASL [35]. The P_5 library was derived from ENDF/B-IV below 20 MeV using MINX and above 20 MeV using an intranuclear cascade and evaporation model. Data are provided in P_5 expansion for 8 materials used in the analysis of a shield-collimator unit for fast neutron radiotherapy.

6.3 Fine-Group Libraries Based on ENDF/B-V

An updated version of VITAMIN-C, denoted VITAMIN-E [36], is now in production at ORNL. The (174n,37g) library will be based on ENDF/B-V using methodology similar, but improved, to that used for VITAMIN-C.

A fine-group coupled cross-section library, LIB-V [37], in generalized format is also under development at LASL. The library will have a detailed thermal treatment and will be generated using NJOY. It is expected that the library will have about 250 total groups.

An ENDF/B-V based version of DLC-43/CSRL, CSRL-V [38], is also planned at ORNL. This version will contain 227 neutron groups and will likewise be applied to criticality safety work.

6.4 Broad-Group Libraries Based on ENDF/B-V

There will likely be many broad-group libraries for shielding based on ENDF/B-V which will be available during the next year and beyond.

There are definite plans at ORNL to provide an updated version of DLC-31/FEWG1 (see section 3.2) based on a collapse from VITAMIN-E.

It is planned that an adjusted library, ORACLE [39], based on collapse from VITAMIN-E and adjustment with FORSS [40], be made available for distribution and testing.

7. LIMITS ON DISTRIBUTION OF ENDF/B-V BASED MULTIGROUP LIBRARIES

Current policy in the U.S. limits the distribution of the ENDF/B-V General Purpose File to the United States. This same restriction also applies to "fine-group libraries" such as VITAMIN-E, LIB-V and CSRL-V. Broad-group libraries are not likely to have the same limited distribution but will have to be available within the United States for a reasonable period of time, nominally one or more years, before general distribution is permitted.

ACKNOWLEDGMENTS

A review paper of this nature surveys the work of many individuals as indicated in the numerous references cited. The reader is directed to the references to indicate proper credit for the developments listed in the text.

The efforts of Eddie Bryant is preparing this manuscript are appreciated.

REFERENCES

1. R. W. Roussin and J. B. Wright, "Abstracts of the Data Library Packages Assembled by the Radiation Information Center," ORNL-RSIC-30 (Rev. 1973).

2. N. M. Greene, J. L. Lucius, L. M. Petrie, W. E. Ford, III, J. E. White, and R. Q. Wright, "AMPX: A Modular Code System for Generating Coupled Neutron-Gamma Libraries from ENDF/B," ORNL/TM-3706 (1976).

3. O. Ozer and D. Garber, Assemblers, "ENDF-201 ENDF/B Summary Documentation," BNL-17541 (ENDF-201) (ENDF/B-III) (1973).

4. R. W. Roussin, "The Defense Nuclear Agency Working Cross-Section Library: Description and Contents," ORNL-RSIC-34 (1973).

5. D. Garber, Compiler, "ENDF-201 ENDF/B Summary Documentation," BNL-17541 (ENDF-201) 2nd Edition (ENDF/B-IV) (1975).

6. W. E. Ford, III, R. T. Santoro, R. W. Roussin, and D. M. Plaster, "Modification Number One to the Coupled 100n-21γ Cross-Section Library for EPR Calculations," ORNL/TM-5249 (1976).

7. E. Cagliotti, R. Nicks, H. Penkuhn (Euratom, Ispra), G. Hehn, M. Mattes (IKE-Stuttgart), and V. Herrnberger (EIR, Würenlingen), "Generation and Testing of the Shielding Data Library EURLIB for Fission and Fusion Technology," Proceedings of the Fifth International Conference on Reactor Shielding," Knoxville, Tennessee (1977), Science Press, Princeton.

8. K. Koyama, Y. Taji, K. Minami, T. Okada, S. Miyasaka, and T. Asaoka, "RADHEAT-V3, A Code System for Analyzing the Radiation Transport in a Nuclear Reactor and Shield," JAERI Report (1976).

9. W. E. Ford, III and D. H. Wallace, "POPOP4 - A Code for Converting Gamma-Ray Spectra to Secondary Gamma-Ray Production Cross Sections," CTC-12 (1969).

10. R. Q. Wright, N. M. Greene, J. L. Lucius, and C. W. Craven, Jr., "SUPERTOG: A Program to Generate Fine-Group Constants and P_n Scattering Matrices From ENDF/B," ORNL-TM-2679 (1969).

11. G. W. Morrison, E. A. Straker, and R. H. Odegaarden, "A Coupled Neutron and Gamma-Ray Library for Use in Shielding Calculations," Trans. Am. Nuc. Soc. 15, 535 (1972).

12. D. E. Bartine, J. R. Knight, J. V. Pace, III, and R. W. Roussin, "Production and Testing of the DNA Few-Group Coupled Neutron-Gamma Cross-Section Library," ORNL/TM-4840 (1977).

13. R. E. MacFarlane, R. J. Barrett, D. W. Muir, and R. M. Boicourt, "The NJOY Nuclear Data Processing System: User's Manual," LA-7584-M (ENDF-272) (1978).

14. R. J. Barrett and R. E. MacFarlane, "Coupled Neutron and Photon Cross Sections for Transport Calculations," LA-7808-MS (1979).

15. RSIC Package DLC-75/BUGLE-80, "Coupled 47 Neutron, 20 Gamma-Ray, P_3, Cross-Section Library for LWR Shielding Calculations," R. W. Roussin, Informal Notes (1980).

16. ANS-6.1.2, "Neutrons and Gamma-Ray Cross Sections for Nuclear Radiation Protection Calculations (N410)," Proposed American National Standard (1979).

17. R. G. Alsmiller, Jr. and J. Barish, "Neutron-Photon Cross Sections for Neutron Energies $\leq$ 60 MeV," ORNL/TM-6486 (1978).

18. T. D. Benyon and N. P. Taylor, "The UKCTRI Data Library: 46-Group Neutron Cross Sections for Fusion Reactor Calculations," U. Birmingham Dept. of Physics Paper No 79-02 (1979).

19. A. L. Pope, "The Current Edition of the Main Tape NDL-1 of the UK Nuclear Data Library," AEEW M 1208 (1973).

20. J. A. Price, "A Guide to Galaxy 6," AWRE 0 13/75 (1975).

21. B. M. Carmichael, "Standard Interface Files and Procedures for Reactor Physics Codes, Version III," LA-5486-MS (1974).

22. RSIC Package PSR-117/MARS, "Collection of Computer Codes for Manipulating Multigroup Cross-Section Libraries in AMPX or CCCC Formats," available from RSIC.

23. R. W. Roussin, C. R. Weisbin, J. E. White, N. M. Greene, R. Q. Wright, and J. B. Wright, "VITAMIN-C: The CTR Processed Multigroup Cross-Section Library for Neutronics Studies," ORNL/RSIC-37 (ENDF-296) (1980).

24. C. R. Weisbin, P. D. Soran, R. E. MacFarlane, D. R. Harris, R. J. LaBauve, J. S. Hendricks, J. E. White, and R. B. Kidman, "MINX: A Multigroup Interpretation of Nuclear Cross Sections from ENDF/B," LA-6486-MS (ENDF-237) (1976).

25. I. I. Bondarenko, Ed., "Group Constants for Nuclear Reactor Calculations," Consultants Bureau, New York (1964).

26. R W. Roussin, C. R. Weisbin, J. E. White, R. Q. Wright, N. M. Greene, W. E. Ford, III, J. B. Wright, and B. R. Diggs, "Experience in Developing and Using the VITAMIN-C 171-Neutron, 36-Gamma-Ray Multigroup Coupled Cross-Section Library," p.107 of "A Review of Multigroup Nuclear Cross-Section Processing," Proceedings of a Seminar-Workshop, Oak Ridge, Tennessee March 1978, ORNL/RSIC-41 (1978).

27. T. A. Gabriel, J. D. Amburgey, and N. M. Greene, "Radiation Damage Calculations: Primary Recoil Spectra, Displacement Rates, and Gas-Production Rates," ORNL/TM-5160 (1976).

28. Y. Gohar and M. A. Abdou, "MACKLIB-IV, A Library of Nuclear Response Functions Generated with the MACK-IV Computer Program from ENDF/B-IV," ANL/FPP/TM-106 (1978).

29. M. A. Abdou, Y. Gohar, and R. Q. Wright, "MACK-IV, A New Version of MACK: A Program to Calculate Nuclear Response Functions from Data in ENDF/B Format," ANL/FPP/TM-77-5 (1978).

30. M. E. Battat, R. J. LaBauve, and D. W. Muir, "The GAMMON Activation Library," LA-8040-MS (1979).

31. O. N. Jarvis, "Description of the Transmutation and Activation Data Library UKCTRIII," AERE-R 9601 (1979).

32. R. E. Kinsey, Compiler, "ENDF-201 ENDF/B Summary Documentation," BNL-NCS-17541 (ENDF-201) 3rd Edition (ENDF/B-V) (1979).

33. G. Simmons and R. Roussin, "A New Cross-Section Library for Light Water Reactor Shielding and Pressure Vessel Dosimetry Applications," Presented at ANS Topical Meeting - 1980 Advances in Reactor Physics and Shielding, Sun Valley, Idaho (1980).

34. W. E. Ford, III, C. C. Webster, B. R. Diggs, R. E. Pevey, and A. G. Croff, "FCXSEC: Multigroup Cross-Section Libraries for Nuclear Fuel Cycle Shielding Calculations," ORNL/TM-7038 (ENDF-287) (1980).

35. W. B. Wilson, "Nuclear Data Development and Shield Design for Neutrons Below 60 MeV," LA-7159-T (1978).

36. C. R. Weisbin, R. W. Roussin, J. J. Wagschal, J. E. White, and R. Q. Wright, "VITAMIN-E: An ENDF/B-V Multigroup Cross-Section Library for LMFBR Core and Shield, LWR Shield, Dosimetry, and Fusion Blanket Technology," ORNL-5505 (ENDF-274) (1979).

37. R. E. MacFarlane, "ENDF/B-IV and V Cross-Section Libraries for Thermal Power Reactor Analysis," International Conference on Nuclear Cross Sections for Technology," Knoxville, Tennessee, October 22-26, 1979 (to be published).

38. W. E. Ford, III, R. M. Westfall, B. R. Diggs, C. C. Webster, and J. R. Knight, "CSRL-V: An ENDF/B-V 227-Group Cross-Section Library for Criticality Safety Studies," Trans. Am. Nuc. Soc. 34, 331 (1980).

39. J. Wagschal, J. Marable, Y. Yeivin, and C. Weisbin, "ORACLE: An Adjusted Cross Section and Covariance Library for Fast Reactor Analysis," Presented at ANS Topical Meeting - 1980 Advances in Reactor Physics and Shielding, Sun Valley, Idaho (1980).

40. J. L. Lucius, C. R. Weisbin, J. H. Marable, J. D. Drischler, R. Q. Wright, and J. E. White, "A User's Manual for the FORSS Sensitivity and Uncertainty Analysis Code System," ORNL-5316 (In Press).

Examples of optimized broad energy group structures generated by the automatic collapsing scheme AGRUKO

V. Herrnberger and S. Padiyath
Swiss Federal Institute for Reactor Research
Würenlingen, Switzerland

Abstract

Basic ideas of the automatic group collapsing scheme AGRUKO are briefly described. The errors introduced by the collapsing process are controled by criteria, which are constructed by the sensitivity profiles and the required target accuracies of the specific shielding type configurations. The group widths are optimized to reduce the calculation time with respect to the fine group calculations.

Optimized group structures were generated for two rather different shielding benchmarks: Neutron and gamma transport in a LWR-shield and in air using a fusion source respectivly. In the case of the LWR-shield the 100/20 groups EURLIB-3 structure was collapsed to 45/16 and 15/5 groups. In the case of the "air" problem the original 22/18 groups were collapsed to 4/8 groups. The accuracies achieved were in general within the required accuracies for the targets activation, radiation damage, radiation heating and dose rates.

Because the broad group structures were optimized in view of basic physical and numerical principles, they are nearly free from arbitrary assumptions as constant lethargy width e.g. Therefore they may be recommended for further use in the field of more complex transport calculations or cross section adjustment procedures.

1. Introduction and problem description

Broad energy group cross section libraries are currently employed in tackling energy dependent transport problems in the fields of shield design, benchmark experiment interpretation and adjusting cross sections to experimental results. Their main goals are to restrict computer storage and costs to reasonable limits, without introducing intolerable errors into the results.

To achieve these goals the proper and optimized selection of group boundaries and weighting spectra in the condensation procedure is the central point. In general the selection of the weighting spectra is not difficult, because they are defined by the problems to be solved.

Fig. 1 GROUP BOUNDARY SELECTION.

PRINCIPLES : 1. COMMON BOUNDARIES
2. FROM HIGHER TO LOWER ENERGIES

EXAMPLE : F = 4

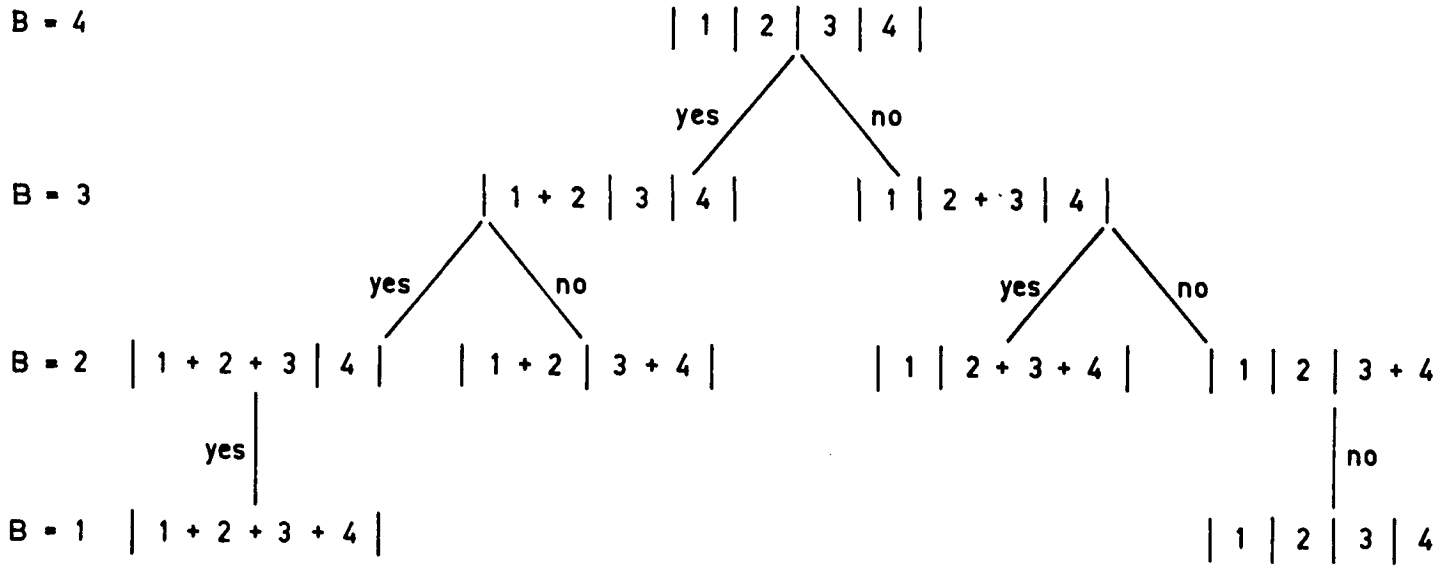

The selection of a proper group boundary structure in less evident. Depending on the user's physical feeling or the possibilities of the data processing codes, more or less important resonance and anti-resonance details of the cross-sections are taken into account. The structure is varified a posteriori, if the errors introduced into the results are tolerable. Then the structure has to be modified eventually.

This approach by trial and error is perhaps sufficient in simple cases with one detector response, but not in real cases with complicated particle transport environments and more than one detector type and position.

More systematic approaches which are able to tackle real cases and to avoid as far as possible arbitrary assumptions were proposed by [1], [2] and one of the authors [3], [4] in which our approach is discussed in any detail. Here after its short descriptions we will give our main results in form of several group structures and the accuracies which were achieved by them in the case of two benchmark problems. The results are quite satisfactory, so that their further application may be recommended.

2. Outline of the collapsing scheme AGRUKO

The scheme reduces the number of groups $f \leq F$ to a number of broad groups $b \leq B$, needed to solve a specific problem with the following constraints [4]:

1st: The change in detector response R (their sensitivity to energy group condensations) should remain within given experiment or design margins $(\frac{\delta R}{R})_a$ (error criterion):

$$\left| \frac{R^{(b)} - R^{(f)}}{R^{(f)}} \right| < \left| \left(\frac{\delta R}{R} \right)_a \right| \qquad (1)$$

2nd: A strong reduction in calculational effort, e.g. measured in number of iterations I_b should result (Iteration criterion):

$$\sum_{b=1}^{B} I_b \ll \sum_{f=1}^{F} I_f \qquad (2)$$

The design margins were evaluated elsewhere [5]. The number of broad groups B collapsed from F groups and their group boundary structure will depend upon the design margins, the iterative efficiency of the transport method and the method of fine group collapsing. The method chosen begins with the highest energy group and works down progressively to the lowest one (figure 1). For the group collapsing groupwise iteration and error criteria have to be fullfilled, which were deduced from the critera (1) and (2). The groupwise error criterion takes into account the importance of the groups by their sensitivity profiles P_f, P_b or groupwise detector responses:A low error is allowed for collapsing groups of high importance and vice versa.

Different functional relationships between groupwise error margin and sensitivity profile can be assumed. Appendix 1 shows possible "Ansätze", which are available in AGRUKO. Some discussions of the crite-

Fig. 2

Flow chart of AGRUKO

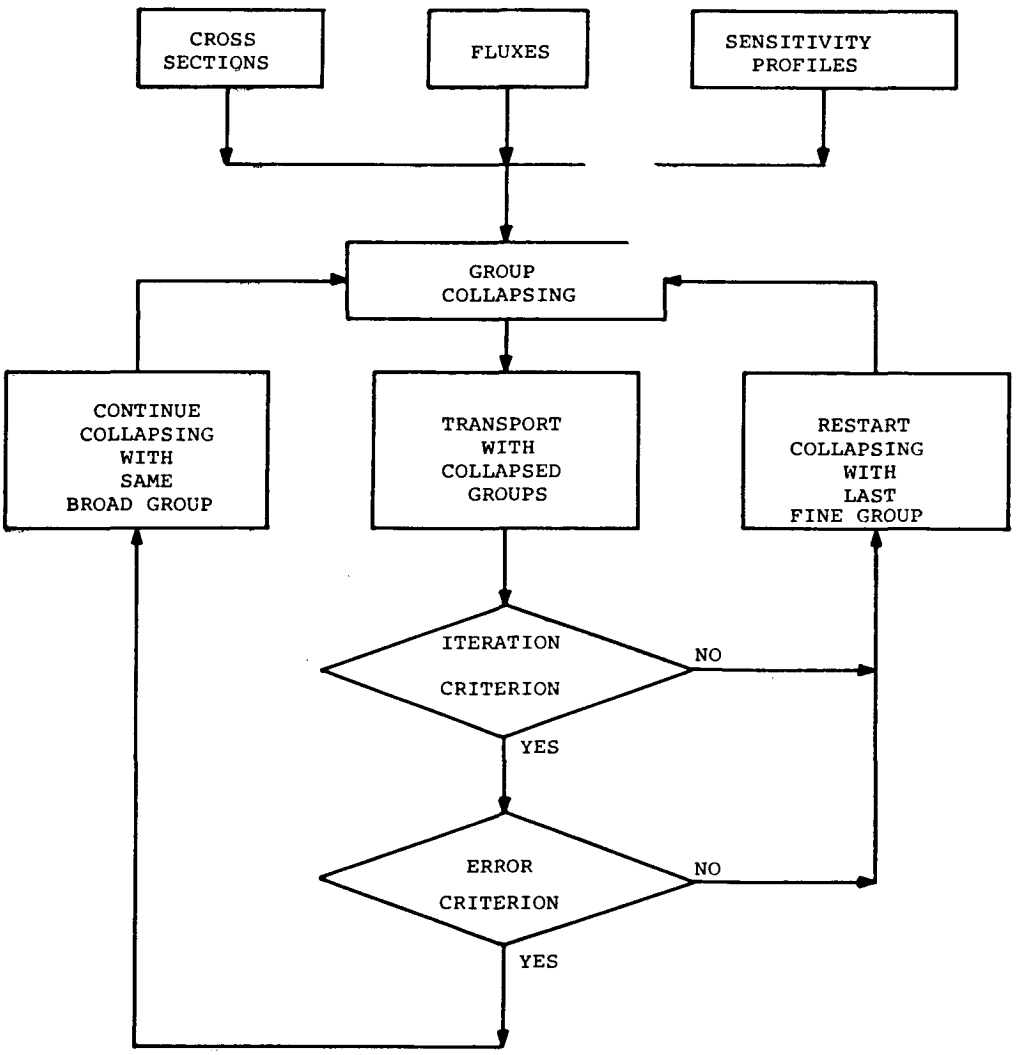

ria can be found elsewhere [4].

The groupwise iteration criterion guarantees a reduction of the calculational effort roughly proportional to the final number of collapsed groups.

Figure 2 gives an overview of the logical flow in AGRUKO and shows the central role of the error and iteration criteria. Neutron and gamma cross sections are condensed separately.

3. Examples of collapsed energy group structures

Two typical shielding benchmark problems were chosen, to check the collapsing procedure particularly with regard to the different error criteria to find the most useful criterion on the one hand and to generate collapsed group cross sections with it, on the other hand, which can be recommended for further use in design and cross section adjustment work.

3.1 Neutron and gamma transport in air

This example is a fusion type source in air [7]. The dose rate is measured at a distance of two thousand meters, which was selected as detector position. The effect of different criteria was examined for a "required design accuracy", RDA, of 50% on the neutron dose rate. The reference case uses the highest number of spatial mesh and a 22/18 (n/γ)-coupled cross section library. Table 1 shows the results of the study. The definitions of the columns are:

TYPE : type of transport calculation, direct (D) or adjoint (A).

APP : transport approximation

IM : number of spatial mesh points

IGM : number of groups

CRIT : criterion used: P, with sensitivity profile or A, with groupwise relative detector response

%-DEV. COND : % deviation of broad group from fine group results for low IM (=9).

%-DEV. REF : as abouve but for the reference case with high IM (=169).

Criteria P/2, A/3 and P/3 are rather strong, because the collapsed group cross sections show an accuracy of 10-80 x below the required one. The application of the weaker criteria P/4, A/4 (A/3 shows the same effect) results in a complete condensation of all 22 groups into a single one. The accuracy was only a factor 2 below the required one. On the other hand, when looking at the reference case, the deviations are much graeter and only A/2 seemed to have a reasonable safety margin of a factor 2 with regard to the required 50% deviation.

In consequence criterion A/2 was used for the coupled n,γ-case.

The detailed results of AGRUKO are given in table 2 and 3. The new group structures for neutron and gamma cross sections, the relati-

TABLE 1

COMPARISON OF FINE/BROAD GROUP RESULTS

NEUTRON TRANSPORT IN AIR, RDA = 50%

TYPE	APP.	IM	IGM	CRIT.	%-DEV. COND.	%-DEV. REF.
D	S40P3	9	22	-	-	(100x)
A	"	"	"	-	-	(60x)
D	"	169	"	-	-	[0.72]
A	"	9/169	"	-	-	∿ 3.
D	"	9/169	1	A/3+4 P/4	28	-96.
"	"	9/169	3	P/3	4.9	-41.
"	"	9/169	4	A/ 2	2.9	-26.
"	"	9/169	10	P/2	0.69	- 6.5

TABLE 2

AIR, S40/P3,9 INT. CONDENSATION FROM 22 GR.WITH RELATIVE ACTIVITY

NEUTRON GROUPS TAKEN

NUMBER OF TARGETS = 1
TARGET = DOSE RATE
RDA % = 50
CRITERION = 2
INTERVAL NO. = 8
FINE GROUP TARGET RESPONSE = 7.1E-15

BROAD GROUPS	FINE GROUPS	RELATIVE DEVIATION	PERMISSIBLE DEVIATION	FAILED CRITERION
1	1 - 10	-40.1E-2	55.4E-2	FEH
2	11 - 12	-47.8E-2	65.9E-2	FEH
3	13 - 15	-33.3E-2	41.9E-2	FEH
4	16 - 22	-16.8E-1	14.6	NO

ITE = ITERATION CRITERION

FEH = ERROR CRITERION

THE TOTAL RELATIVE DEVIATION OF
4 GROUP CROSS SECTIONS = -2.9 %

TABLE 3

AIR, S40/P3,9 INT. CONDENSATION FROM 18 GR.WITH RELATIVE ACTIVITY

GAMMA GROUPS TAKEN

NUMBER OF TARGETS = 1
TARGET = DOSE RATE
RDA % = 50
CRITERION = 2
INTERVAL NO. = 8
FINE GROUP TARGET RESPONSE = 4.1E-16

BROAD GROUPS	FINE GROUPS	RELATIVE DEVIATION	PERMISSIBLE DEVIATION	FAILED CRITERION
1	23 - 23	-24.8E-2	97.5E-2	ITE
2	24 - 24	-36.7E-1	49.4E-2	ITE
3	25 - 25	-90.0E-2	15.9E-2	FEH
4	26 - 26	-22.3E-2	48.5E-2	ITE
5	27 - 27	27.9E-2	49.1E-2	ITE
6	28 - 31	-22.9E-2	30.1E-2	FEH
7	32 - 38	-16.4E-2	50.3E-2	FEH
8	39 - 40	-69.7E-3	98.6E-1	NO

ITE = ITERATION CRITERION

FEH = ERROR CRITERION

THE TOTAL RELATIVE DEVIATION OF
8 GROUP CROSS SECTIONS = -2.5 %

ve deviation, the permissible deviation and the failed criterion per group as the total deviation are given.

It is very interesting to see, that the gamma groups are much less collapsed for the same required accuracy. This fact shows their relative importance in this type of transport problem, which was allready reflected in the unusually high fine number of γ-groups compared to that of the neutron groups (18:22). The %-deviation from the reference case was less than 1% for the γ-dose rate.

3.2 Neutron transport in a PWR shield

In a first step the displacement rate at the inner side of a PWR pressure vessel was selected as target [8] to check the error criteria. The EURLIB-B library with 100/20 n/γ-groups was used as fine group data base [6] . Only the most efficient criterion 3 and 4 were examined (table 1) and the RDA were varied. The results for criterion P/4 are shown in table 4.

The reference case was S8P3 IM=146, IGM=100. Between 10% - 100% RDA the collapsing process gives satisfying results. The number of groups are reduced with reducing accuracy. The %-deviation shows some fluctuation, because error compensation gets more important with lower numbers of groups. For extremly "low" RDA of about 300% a reversed tendency appears in the sense, that the number of groups increase slightly, but the %-DEV. increases remarkably. The overall result of the check of the criteria 3 and 4 was, that as in table 1 the P/4 is the more efficient one with regard to the reduction of the number of groups. A/4 is less efficient, but it does not show the reversed tendency for very low required accuracies.

In a second step the whole PWR-benchmark was treated and the 100/20 group were collapsed in two sets ot 45/16 and 15/5 groups respectively. Three detectors (targets) were used, the displacement rate at the inner side of the pressure vessel as above, the γ-heating (energy deposition) at the inner side of the concrete shield and the dose rate at the outer side of the concrete shield. The required design accuracies were 20%, 40% (30%) and 100% for each n- and γ-dose rate respectively. The criterion A/4 was applied for two reasons: First, for its uniform tendency in the collapsing procedure. Second, for the reduction of calculational effort (no additional adjoint S_n- and sensitivity profile calculations for the other detectors are necessary). The resulting group structures are shown in tables 5-8. Table 5 and 6 give the example of the dose rate at the outer concrete shield for the 45 neutron and 16 gamma groups. Table 7 and 8 show the examples of the two targets displacement rate and γ-heating for the 15 neutron and 5 gamma groups. The effect of the error compensation can be seen: The high relative deviation of the last (thermal) neutron group, which cannot be controlled by this type of a non iterative collapsing scheme, is largely compensated by those of the higher groups. Only one spectrum for the condensation was chosen in order to restrict the corss sections to one set per material zone. The spectrum in the pressure vessel seemed to be one of the most typical of the shield system. The 15/5 structure was obtained by repeated collapsing of the 45/16 groups using mostly the same RDA, which was the most difficult task. It turned out, that a direct condensation of the 100/20 group scheme to very few groups (<20) led to uncontrollable large errors in the γ-reponses and to convergence problems in the KeV-neutron- energy region of the cross sections (1-10^2KeV) within the pressure vessel of the reference case (with high angular and spatial mesh). Therefore the condensation was perfor-

TABLE 4

LWR- BENCHMARK, CRIT. P/4

TYPE	APP.	IM	IGM	RDA[%]	%-DEV. COND.	%-DEV. REF.
D	S4P1	20	100	-	-	52.
A	"	"	"	-	-	196.
D	S8P3	146	"	-	-	[0.264]
"	S4P1/S8P3	20/146	42	10	3.41	-15.3
"	S4P1/S8P3	20/146	36	30	6.9	9.2
"	S4P1/S8P3	20/146	17	100	-0.71	1.5
"	S4P1/S8P3	20/146	21	300	41.9	54.2

TABLE 5

LWR, S4/P1,28 INT. CONDENSATION FROM 100 GR.WITH RELATIVE ACTIVITY

NEUTRON GROUPS TAKEN

NUMBER OF TARGETS = 3
TARGET = DOSE RATE
RDA % = 100
CRITERION = 4
INTERVAL NO. = 28
FINE GROUP TARGET RESPONSE = 7.5E+01

BROAD GROUPS	FINE GROUPS	RELATIVE DEVIATION	PERMISSIBLE DEVIATION	FAILED CRITERION
1	1 - 7	-73.6E-4	22.5	FEH
2	8 - 8	74.6E-5	26.4E-1	FEH
3	9 - 9	10.6E-4	20.0E-1	FEH
4	10 - 10	15.8E-4	15.2E-1	FEH
5	11 - 11	18.2E-4	14.3E-1	FEH
6	12 - 12	29.2E-4	11.8E-1	FEH
7	13 - 13	39.7E-4	10.2E-1	FEH
8	14 - 14	24.4E-4	13.2E-1	FEH
9	15 - 15	23.1E-4	13.5E-1	FEH
10	16 - 17	-41.9E-4	22.1E-1	FEH
11	18 - 18	23.8E-4	12.5E-1	FEH
12	19 - 19	41.4E-4	91.4E-2	FEH
13	20 - 21	33.5E-3	12.9E-1	FEH
14	22 - 22	10.9E-3	51.4E-2	FEH
15	23 - 23	91.9E-4	53.9E-2	FEH
16	24 - 24	96.2E-4	47.6E-2	FEH
17	25 - 25	64.5E-4	58.8E-2	FEH
18	26 - 26	95.9E-4	46.9E-2	FEH
19	27 - 27	81.3E-4	50.3E-2	FEH
20	28 - 28	91.9E-4	47.4E-2	FEH
21	29 - 29	79.54-4	50.8E-2	FEH
22	30 - 31	-93.4E-3	11.3E-1	FEH
23	32 - 32	-12.6E-3	66.8E-2	FEH
24	33 - 33	-82.2E-5	53.1E-2	FEH
25	34 - 34	-28.5E-4	45.0E-2	FEH
26	35 - 35	-85.4E-5	43.7E-2	FEH
27	36 - 37	97.9E-3	86.6E-2	FEH
28	38 - 39	-17.5E-2	10.6E-1	FEH
29	40 - 41	-16.4E-3	15.0E-1	FEH
30	42 - 43	22.6E-4	13.3E-1	FEH
31	44 - 47	-14.8E-3	29.2E-1	ITE
32	48 - 50	32.1E-3	23.6E-1	ITE
33	51 - 52	21.2E-4	16.4E-1	ITE
34	53 - 53	-80.8E-5	85.5E-2	FEH
35	54 - 54	-18.1E-4	59.6E-2	FEH
36	55 - 55	-76.9E-5	61.8E-2	FEH
37	56 - 57	45.9E-3	14.0E-1	ITE
38	58 - 67	96.9E-2	13.2	ITE
39	68 - 69	-95.3E-4	22.5E-1	ITE
40	70 - 73	81.1E-3	41.4E-1	ITE
41	74 - 77	86.4E-3	37.2E-1	ITE
42	78 - 93	18.9E-1	11.4	ITE
43	94 - 98	16.1E-1	18.4E-1	ITE
44	99 - 99	73.2E-3	39.1E-2	FEH
45	100 - 100	20.6E-1	34.0E-3	NO

ITE = ITERATION CRITERION
FEH = ERROR CRITERION
THE TOTAL RELATIVE DEVIATION OF
45 GROUP CROSS SECTIONS = 6.74 %

TABLE 6

LWR, S4/P1,28 INT. CONDENSATION FROM 20 GR.WITH RELATIVE ACTIVITY

GAMMA GROUPS TAKEN

NUMBER OF TARGETS = 3
TARGET = DOSE RATE
RDA % = 100
CRITERION = 4
INTERVAL NO. = 28
FINE GROUP TARGET RESPONSE = 4.4E+1

BROAD GROUPS	FINE GROUPS	RELATIVE DEVIATION	PERMISSIBLE DEVIATION	FAILED CRITERION
1	101 - 104	-14.3	96.8	FEH
2	105 - 105	-47.2E-1	63.5E-3	FEH
3	106 - 106	-28.9E-1	77.0E-3	FEH
4	107 - 107	-26.9E-1	78.8E-3	FEH
5	108 - 108	-13.3E-1	11.7E-2	FEH
6	109 - 109	-14.1E-1	10.2E-2	FEH
7	110 - 110	-10.2E-1	11.5E-2	FEH
8	111 - 111	-95.2E-2	13.2E-2	FEH
9	112 - 112	-10.0E-1	12.9E-2	FEH
10	113 - 113	-65.4E-2	16.1E-2	FEH
11	114 - 114	-71.4E-2	15.4E-2	FEH
12	115 - 115	-81.1E-2	14.3E-2	FEH
13	116 - 116	-48.7E-2	18.4E-2	FEH
14	117 - 117	-54.8E-2	17.1E-2	FEH
15	118 - 118	-63.8E-2	15.8E-2	FEH
16	119 - 120	-68.1E-3	14.0E-1	NO

ITE = ITERATION CRITERION

FEH = ERROR CRITERION

THE TOTAL RELATIVE DEVIATION OF
16 GROUP CROSS SECTIONS = -34.3 %

med stepwise form 45/16 to 21/4 and to 13/3 n/γ-groups.

To reduce divergence problems due too large group widths the iteration criterion was changed to

$$I_{b+f} < a \cdot I_b$$

where (b+f) means the condensation of broad group with the next fine group f and a is an experimental parameter depending upon the numerical iteration scheme of the transport code.

a=0.8 was too strong,because more than 70% of the group limits were defined by the iteration criterion. a=1.2 seemed to be reasonable, but did'nt solve (as a=1.0) completely the convergence problems. In consequence the original 21 group structure of 3 groups had to be maintained for group 10 of the 13 group structure (table 7). The resulting 15 groups were used to collapse the 16 γ-groups (table 6) to the 5 γ-groups (table 8), which showed reasonalbe errors in the reference case. Table 9 shows the accuracies achieved by the two structures. They are very satisfying. The condensation was made in a S_4P_1-approximation with IM=28. The reference case was calculated in a S_8P_3-approximation with IM=202 intervalls.

4. Conclusions

The generated broad group structures for the particle transport in air and in a PWR shield are very satisfying. They guarantie the reguired design accuracies of the different detector responses and they reduce the calcuational effort roughly proportional to the number of groups. Up to now the use of group dependent relative detector responses instead of sensitivity profiles leads to satisfactory results. Condensation to very few groups is still difficult, as to guarantee convergence of the iterative transport methods, and not yet completely straight forward.

TABLE 7

LWR, S4/P1,28 INT. CONDENSATION FROM 45 GR.WITH RELATIVE ACTIVITY

NEUTRON GROUPS TAKEN

NUMBER OF TARGETS = 3
TARGET = DISPLACEMENT RATE
RDA % = 20
CRITERION = 4
INTERVAL NO. = 17
FINE GROUP TARGET RESPONSE = 5.3E+12

BROAD GROUPS	FINE GROUPS	RELATIVE DEVIATION	PERMISSIBLE DEVIATION	FAILED CRITERION
1	1 - 6	22.1E-7	31.1E-2	FEH
2	7 - 10	57.7E-2	11.3E-1	FEH
3	11 - 11	55.1E-3	56.4E-2	FEH
4	12 - 15	14.5E-2	36.1E-2	FEH
¢ 5	16 - 16	46.2E-3	50.4E-2	FEH
6	17 - 20	-53.7E-2	86.9E-2	ITE
7	21 - 26	-18.6E-1	29.1E-1	FEH
8	27 - 29	-24.8E-2	32.9E-2	FEH
9	30 - 36	44.4E-2	12.0E-1	FEH
10	37 - 37			
11	38 - 38	74.3E-2*	33.1E-1*	FEH*
12	39 - 40			
13	41 - 42	17.2E-3*	40.5E-1*	FEH*
14	43 - 44	66.1E-4*	41.7E-1*	FEH*
15	45 - 45	-25.2E-1*	30.4E-2*	NO

ITE = ITERATION CRITERION
FEH = ERROR CRITERION

THE TOTAL RELATIVE DEVIATION OF
13 GROUP CROSS SECTIONS = -3.1%

* VALID FOR THE 13 GROUP STRUCTURE.THE TENTH GROUP WAS SUBDIVIDED INTO 3 GROUPS

TABLE 8

LWR, S4/P1,28 INT. CONDENSATION FROM 16 GR.WITH RELATIVE ACTIVITY

GAMMA GROUPS TAKEN

NUMBER OF TARGETS = 3
TARGET = GAMMA HEATING
RDA % = 30
CRITERION = 4
INTERVAL NO. = 21
FINE GROUP TARGET RESPONSE = 2.9E-4

BROAD GROUPS	FINE GROUPS	RELATIVE DEVIATION	PERMISSIBLE DEVIATION	FAILED CRITERION
1	46 - 47	-82.5E-2	21.2E-1	FEH
2	48 - 48	-15.5E-1	14.0E-1	FEH
3	49 - 56	-87.6E-1	13.4	FEH
4	57 - 58	-10.6E-1	44.8E-1	ITE
5	59 - 61	11.0E-1	86.0E-1	NO

ITE = ITERATION CRITERION

FEH = ERROR CRITERION

THE TOTAL RELATIVE DEVIATION OF
5 GROUP CROSS SECTIONS = -11.1 %

TABLE 9

ACCURACIES OF COLLAPSED GROUP

STRUCTURES FOR THE PWR-BENCHMARK

TARGET TYPE	IGM	RDA [%]	%-DEV. COND.	%-DEV. REF.
DISPLACEMENT RATE	45	20	- 0.4	5
DISPLACEMENT RATE	15	20	-3*) (Table 7)	20
γ-HEATING	45/16	40	-27	-6
γ-HEATING	15/5	30	-11 (Table 8)	-7
n/γ-DOSE RATE	45/16	100/100	7/-34 (Tables 5/6)	11/-1
n/γ-DOSE RATE	15/5	100/100	-3*)/3	-68/-52

*) VALID FOR THE 13 GROUP STRUCTURE.
THE TENTH GROUP WAS SUBDIVIDED
INTO 3 GROUPS, WHICH DEFINE THE 15 GROUPS.

References:

[1] E. Oblow et al.
"Selection of Group Energy Boundaries Using Sensitivity Theory",
Trans. ANS 17 (1) 1973

[2] F. Bouteau et al.
"Formulaire de propagation de neutrons dans les milieux acier-sodium pour les protection de la filière rapide",
OECD, Paris 1975

[3] V. Herrnberger
"Application of Sensitivity Theory to Energy Group Structure definition",
OECD Trans. 1975

[4] V. Herrnberger
"A Computational Scheme for Energy Group Boundary Selection Using Sensitivity Theory",
5th Int. Conf. on Reactor Shielding, Knoxville, Tenn. April 17-23 1977

[5] V. Herrnberger et al.
"Target Accuracies Required in Radiations Shielding",
OECD / IAEA, Vienna 1976

[6] E. Caglioti et al.
Generation and Testing of the Shielding Data Library EURLIB for Fission and Fusion Technology.
5th Int. Conf. on Reactor Shielding, Knoxville, Tenn. April 17-23 1977

[7] D.E. Bartine et al.
Radiation-Transport Cross-Section Sensitivity Analysis. A General Approach Illustrated for a Thermonuclear Source in Air.
NSE 53, 304-318 (1974)

[8] G. Hehn and J. Koban
"Reactor Shield Benchmark No. 2",
ESIS-Newstetter, Special Issue No. 4, Jan. 1976

Appendix 1

GROUPWISE CRITERIA

1. ITERATIONS

$$I_b < I_{b'} + I_p << \sum_{f \in b} I_f$$

2. ERRORS

CRITER. 1 (GENERAL)

$$\frac{\delta R_b}{R} = \left|\frac{\delta R}{R}\right|_a \cdot \underbrace{F(P_b)}$$

DISTRIBUTION FUNCTION WITH $F'(P_b) < o$

$$\frac{\delta R_b}{R} = \frac{R_b - \sum_{f \in b} R_f}{R^{(f)}}$$

$$\left|\sum_{b=1}^{B} \frac{\delta R_b}{R}\right| < \left|\frac{\delta R}{R}\right|_a \Rightarrow \underbrace{\left|\sum_{b=1}^{B} F(P_b)\right|}_{C(f,b)} < 1$$

CRITER. 2

$$F(P_b) = C_2 \cdot P_b^{-1}$$

$$\left|C_2\right| < \left|\sum_{b=1}^{B} P_b^{-1}\right|^{-1}$$

APPROXIMATION NEEDED:

$$P_b \approx \sum_{f \in b} P_f$$

LOWER LIMIT OF C_2:

$$\left|C_2^*\right| = \left|\sum_{b'=1}^{b} P_{b'}^{-1} + \sum_{f>b} P_f\right|^{-1} < \left|C_2\right|$$

CRITER. 3

$$F(P_b) = C_3 \cdot \sum_{f \in b} P_f^{-1}$$

$$\left|C_3\right| \leq \left|\sum_{f=1}^{F} P_f^{-1}\right|^{-1}$$

CRITER. 4

$$F(P_b) = C_4 \cdot \sum_{f \in b} P_f \left|\cdot P_f\right|^{-3/2}$$

$$\left|C_4\right| \leq \left|\sum_{f=1}^{F} P_f \cdot \left|P_f\right|^{-3/2}\right|^{-1}$$

CRITER. 5

$$F(P_b) = C_5 \cdot \sum_{f \in b} P_f \left|P_f\right|^{-5/4}$$

$$\left|C_5\right| \leq \left|\sum_{f=1}^{F} P_f \cdot \left|P_f\right|^{-5/4}\right|^{-1}$$

POSSIBLE SIMPLIFICATION:

$$P_f \approx \frac{R_f}{R^{(f)}}$$

PRELIMINARY VERSION OF THE EURLIB VARIANCE-COVARIANCE MATRICES

by

M C G Hall
Imperial College, London*

Radiation Physics and Shielding Group
Reactor Physics Division
AEE Winfrith

* Work performed during author's attachment to Radiation Physics and Shielding Group, Reactor Physics Division, AEE Winfrith.

1. Introduction and Background

In the uncertainty analysis of any calculation involving nuclear data, correlations between errors of the data must be considered. This can be demonstrated by considering the uncertainty of a multigroup calculation of some response R. The perturbation of R can be written

$$\delta R = \sum_{K} \sum_{i} \frac{\partial R}{\partial x_{Ki}} \delta x_{Ki} \qquad 1.$$

where x_{Ki} is a group cross-section of type K for group i, and

$\sum_{K} x_{Ki} = T_i$, the total cross-section for group i.

More specifically, if it is proposed to analyse the variation of the response with respect to, say, the non-elastic cross-section X and the elastic scattering cross-section N, then

$$\delta R = \sum_{i} \left(\frac{\partial R}{\partial X_i} \delta X_i + \frac{\partial R}{\partial N_i} \delta N_i \right) \qquad 2.$$

The expected value of the square of equation 2 is:-

$$\sigma^2(R) = \sum_{j} \sum_{i} \left[\frac{\partial R}{\partial X_i} \frac{\partial R}{\partial X_j} \operatorname{cov}(X_i, X_j) + \frac{\partial R}{\partial N_i} \frac{\partial R}{\partial N_j} \operatorname{cov}(N_i, N_j) + 2 \frac{\partial R}{\partial X_i} \frac{\partial R}{\partial N_j} \operatorname{cov}(X_i, N_j) \right] \qquad \ldots. 3.$$

Defining a sensitivity coefficient U_{Xi} in the conventional manner by

$$U_{Xi} = \frac{\partial R}{\partial X_i} \frac{X_i}{R} \qquad 4.$$

equation 3 can be expressed in terms of fractional covariance matrices:-

$$\frac{\sigma^2(R)}{R^2} = \sum_{j} \sum_{i} \left[U_{Xi} U_{Xj} \frac{\operatorname{cov}(X_i, X_j)}{X_i X_j} + U_{Ni} U_{Nj} \frac{\operatorname{cov}(N_i, N_j)}{N_i N_j} + 2 U_{Xi} U_{Nj} \frac{\operatorname{cov}(X_i, N_j)}{X_i N_j} \right] \qquad \ldots. 5.$$

The evaluation of this expression clearly requires covariance information.

In the absence of detailed covariance information an upper limit for this expression can be obtained as follows. For most isotopes N is derived from independent measurements of X_i and T_i in which case $COV(X_i N_j)$ can be replaced by $-COV(X_i X_j)$ to give:-

$$\frac{\sigma^2(R)}{R^2} = \sum_i \sum_j \left\{ \left(U_{Xi} U_{Xj} - 2 \frac{X}{N_j} U_{Xi} U_{Nj} \right) \frac{cov(X_i X_j)}{X_i X_j} + U_{Ni} U_{Nj} \frac{cov(N_i N_j)}{N_i N_j} \right\} \quad \ldots . 6$$

$COV(X_i X_j)$ and $COV(N_i N_j)$ are invariably non-negative so their upper limits are given by respectively $\sigma(X_i)\sigma(X_j)$ and $\sigma(N_i)\sigma(N_j)$.
This yields an upper limit for the fractional variance:-

$$\left(\frac{\sigma^2(R)}{R^2}\right)_{MAX} = \sum_i \sum_j \left\{ \left| U_{Xi} U_{Xj} - 2 \frac{X_i}{N_j} U_{Xi} U_{Nj} \right| \sigma(X_i)\sigma(X_j) + \left| U_{Ni} U_{Nj} \right| \sigma(N_i)\sigma(N_j) \right\} \quad \ldots . 7$$

An essentially similar approach (1) has been used before in which only the independent variables X and T were considered. This method of error assessment - making the best of a bad job with what information was easily available - is being rendered obsolete by production of covariance matrices.

Recently published covariance matrices by Drischler (2) and Weisbin of ORNL consist of values of

$$\frac{cov(\gamma_i \gamma_j)}{\gamma_i \gamma_j}$$

where ζ embraces several reaction types. These have been obtained by collapsing evaluated covariance data into a fifteen-group structure using E^{-1} weighting. These covariance matrices are of course strictly appropriate only to the ENDF data for which they are derived - they can however be used with reasonable confidence with data which is not very dissimilar to that in the ENDF library.

The purpose of this note is to expand the fifteen-group ORNL matrices, in a simple way, into the EURLIB 100-group structure for use in detailed uncertainty analysis.

2. Calculation of the EURLIB Matrices

Unfortunately the ORNL fifteen-group structure is not a subset of the EURLIB 100-group structure. The procedure has been to introduce additional energy boundaries where necessary into the EURLIB structure - this resulted in a 109-group scheme. For all groups in this super group scheme it was assumed that

$$\frac{cov(\zeta_i \zeta_j)}{\zeta_i \zeta_j} = \frac{cov(Z_p Z_q)}{Z_p Z_q}$$

where the fine group cross-sections ζ_i, ζ_j correspond respectively to ORNL group cross-sections Z_p, Z_q. This means in practice that all the elements of the fine group matrices which comprise an element of an ORNL matrix will have the same value as the latter, and that the expanded services will collapse to the latter with any weighting function. The 109 group matrices are then collapsed to the EURLIB group scheme by assuming that

$$\frac{cov(\zeta'_K \zeta'_L)}{\zeta'_K \zeta'_L} = \frac{\sum cov(\zeta_i \zeta_j) \delta U_i \delta U_j}{\sum \zeta_i \zeta_j \delta U_i \delta U_j}$$

where the prime indicates the EURLIB cross-sections and the δU are the lethargy

widths of the expanded EURLIB group scheme. This expression should be used for collapsing the EURLIB covariance matrices to any subset of the EURLIB structure.

3. Conclusions

Covariance matrices for iron and sodium have been provided in the EURLIB group scheme from basic information given in (2). More complicated, and perhaps more realistic, expansions of the basic data can be postulated. These simple expansions have been produced in the spirit that they will encourage rigorous methods of calculating errors in readiness for the time when covariance information is supplied as a matter of course with evaluated nuclear data.

4. Results

The covariances are illustrated in figures 1 to 6 as contour plots. The contours are labelled in percentages which express values of

$$\sqrt{\frac{cov(\bar{\gamma}_i, \bar{\gamma}_j)}{\bar{\gamma}_i \bar{\gamma}_j}}$$

If i is equal to j this expression reduces to $\sigma(\bar{\gamma}_i)/\bar{\gamma}_i$ so that along the relevant diagonals the percentages are fractional standard deviations.

The coarse structure of the contour maps reflects the fifteen-group origin of the matrices. For practical use the 100 x 100 matrices $COV(X_i, X_j)$, $COV(N_i, N_j)$, $COV(X_i, N_j)$ for iron and sodium are being written on to tape and will be available on request.

References

1. McCracken, A. K.
The Application of Sensitivity Analysis to the Identification of Data Requirements for Shielding.
NEACRP-A-298, 1977.

2. Drischler, J. D., Weisbin, C. R.
Compilation of Multigroup Cross-Section Covariance Matrices for Several Important Reactor Materials.
ORNL-5318, 1977.

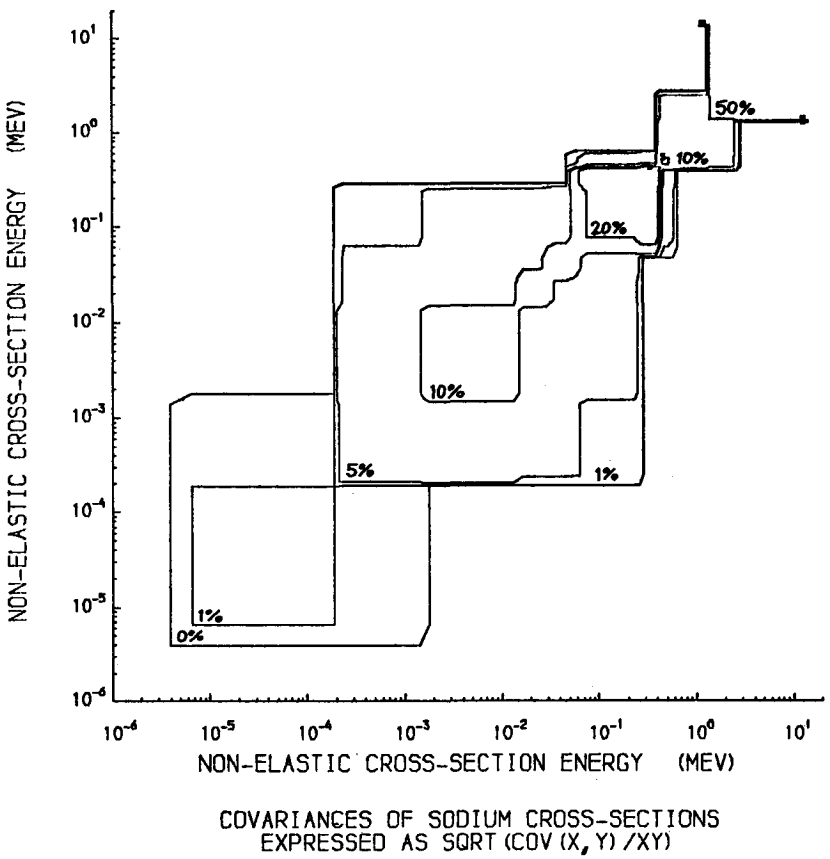

COVARIANCES OF SODIUM CROSS-SECTIONS
EXPRESSED AS SQRT (COV (X, Y) /XY)

FIGURE ONE

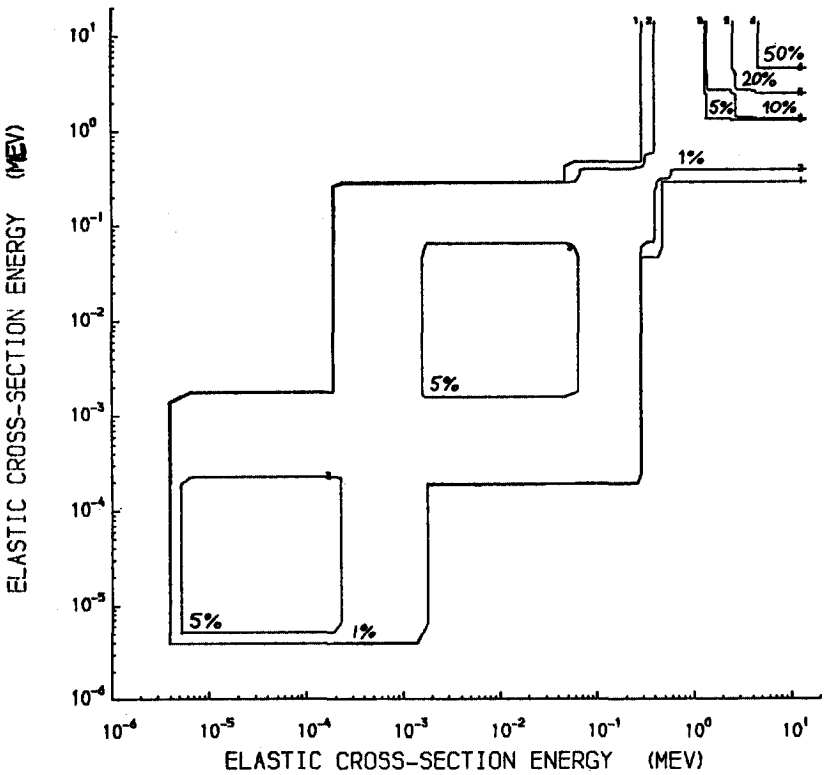

COVARIANCES OF SODIUM CROSS-SECTIONS
EXPRESSED AS SQRT (COV (X, Y) /XY)

FIGURE TWO

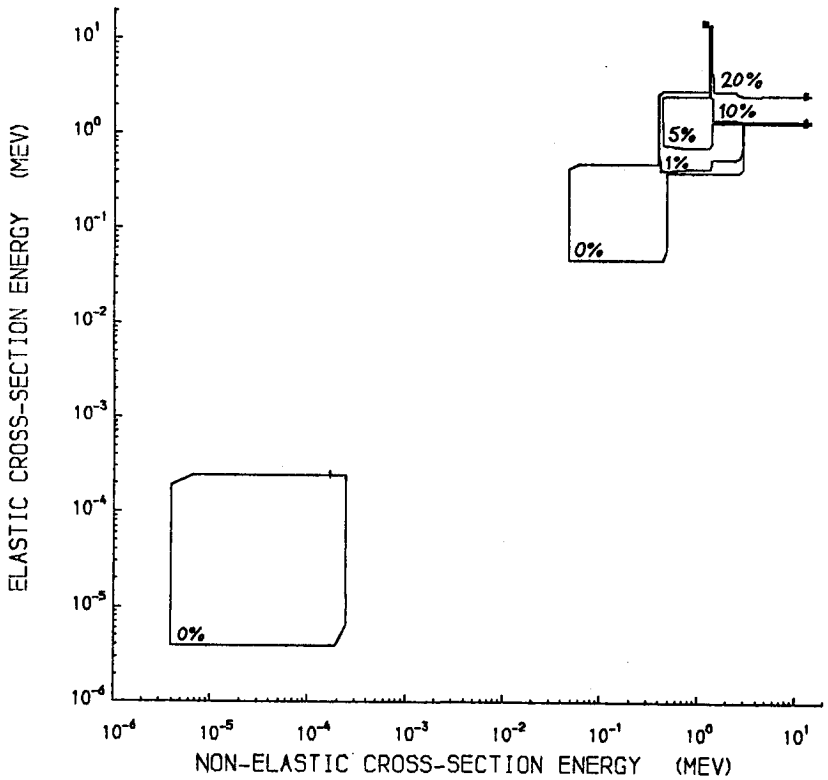

COVARIANCES OF SODIUM CROSS-SECTIONS
EXPRESSED AS SQRT-(COV (X, Y) /XY)

FIGURE THREE

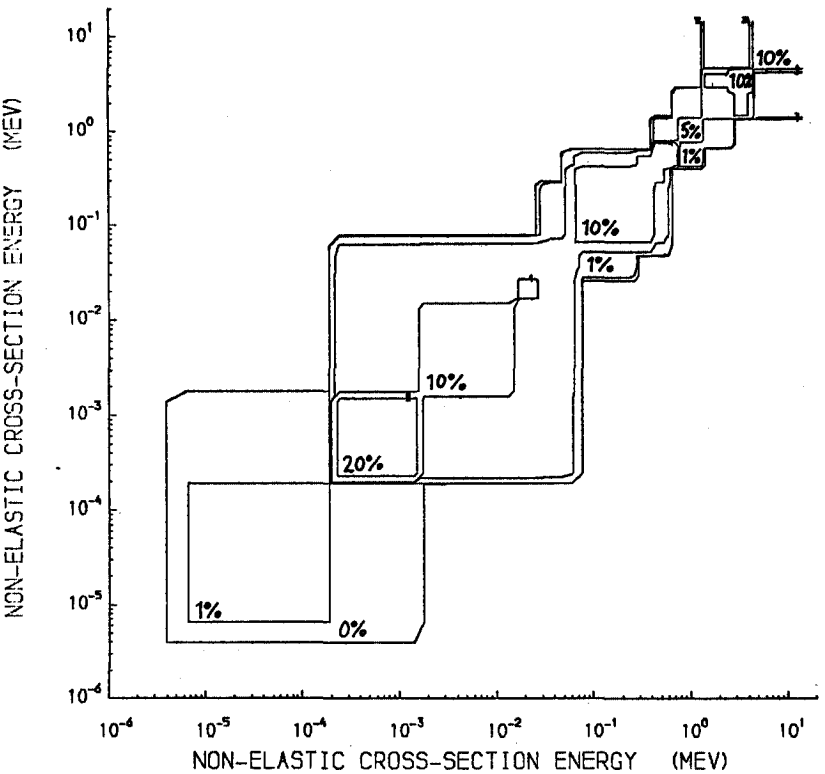

COVARIANCES OF IRON CROSS-SECTIONS
EXPRESSED AS SQRT (COV (X, Y) /XY)

FIGURE FOUR

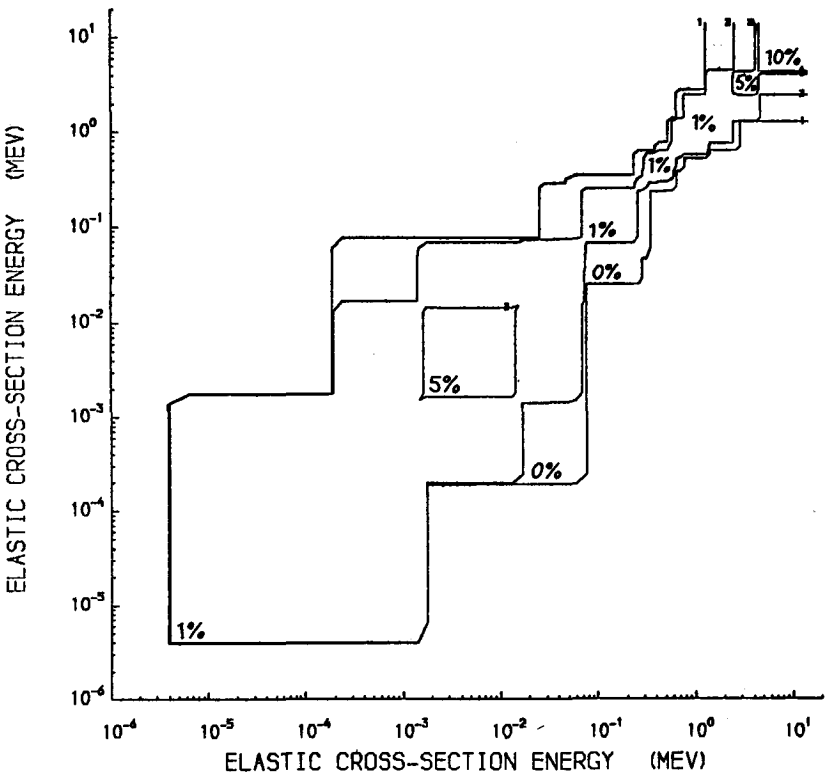

COVARIANCES OF IRON CROSS-SECTIONS
EXPRESSED AS SQRT (COV (X, Y) /XY)

FIGURE FIVE

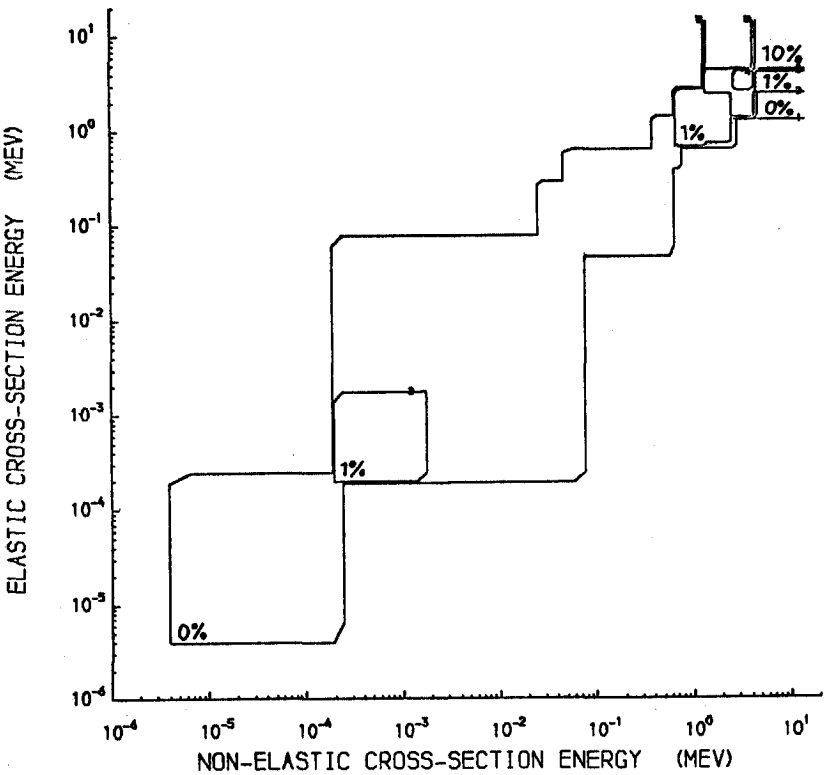

COVARIANCES OF IRON CROSS-SECTIONS
EXPRESSED AS SQRT-(COV (X, Y) /XY)

FIGURE SIX

STATUS OF MULTIGROUP SENSITIVITY PROFILES AND COVARIANCE MATRICES AVAILABLE FROM THE RADIATION SHIELDING INFORMATION CENTER

R. W. Roussin,* J. D. Drischler, ** and J. H. Marable**
*Radiation Shielding Information Center
**Oak Ridge National Laboratory
Oak Ridge, Tennessee, U.S.A.

ABSTRACT

In recent years multigroup sensitivity profiles and covariance matrices have been added to the Radiation Shielding Information Center's Data Library Collection (DLC). Sensitivity profiles are available in a single package, DLC-45/SENPRO, and covariance matrices are found in two packages, DLC-44/COVERX and DLC-77/COVERV. The contents of these packages are described and their availability is discussed.

1. INTRODUCTION

Multigroup sensitivity profiles and covariance matrices are now a part of the Radiation Shielding Information Center's (RSIC) Data Library Collection (DLC). Both are in trial CCCC formats [1], SENPRO for sensitivity profiles, and COVERX for covariance matrices. The RSIC package DLC-45/SENPRO contains several sets of profiles for fast reactor, thermal reactor, and shielding benchmarks. The DLC-44/COVERX package contains multigroup covariance files for fission, LMFBR, and 1/E weighting based on ENDF/B-IV covariance data and informal evaluations. Each package contains a retrieval code for editing and format conversion so that they can be used in the CCC-334/FORSS [2] Sensitivity and Uncertainty Analysis System. As is indicated in another paper at this Conference [3], these can be used directly in the FORSS system.

Archival storage of sensitivity profiles appears prudent since the benchmark experiments have long lasting value and the sensitivities themselves are relatively stable with respect to cross-section changes (i.e., ENDF/B-IV and ENDF/B-V sensitivities for fast reactor benchmarks are virtually identical).

In the following sections the data in DLC-44 and DLC-45 are described and new data which are now being packaged in RSIC are discussed. The availability of these new data is also indicated.

2. FAST REACTOR BENCHMARK SENSITIVITY PROFILES IN DLC-45

Fast reactor benchmark sensitivity profiles in the current version of the package, DLC-45C/SENPRO (1980), are described in sections 2.1 through 2.4 below. Some of these are for benchmark problems approved by the Cross Section Evaluation Working Group (CSEWG) [4].

2.1 126 Neutron Group Profiles for CSEWG Fast Reactor Benchmarks

The initial set of profiles in 126 neutron group structure, which were generated at ORNL [5] with FORSS, have been expanded to include 650 profiles for CSEWG fast reactor assemblies ZPR 6/7, ZPR 6/6A, ZBR 3/56B, ZPR 3/11, GODIVA, and JEZEBEL.

2.2 12 Neutron Group Profiles for CSEWG Fast Reactor Benchmarks

The 12 group profiles were generated at Argonne National Laboratory with VARY-1D [6,7] and placed in SENPRO format at ORNL. CSEWG assemblies ZPR 3/48, ZPR 6/7, ZPR 6/6A, and ZPR 9/31 are included.

2.3 Profiles for the Large Core Code Evaluation Working Group (LCCEWG) Study

A four group set of 10 profiles for ZPR-6/7, collapsed from the 126 group profiles, was used as a part of the LCCEWG study. In addition, 32 group profiles for a 2D model of a large LMFBR, used in the LCCEWG study [8], are included.

2.4 26 Neutron Group Profiles for Fast Reactor Benchmarks

Some 1263 profiles in a 26 group structure were prepared by collapsing or expanding the sets listed earlier. These form the major set that has been used at ORNL for various studies [9]. Models included are ZPR-3/48, ZPR-6/7, -6/6A, ZPR-9/31, ZPR-3/56B, -3/11, GODIVA, JEZEBEL, Advanced Fuels, and the LCCEWG model.

3. THERMAL REACTOR BENCHMARK PROFILES IN DLC-45

CSEWG thermal reactor benchmarks in DLC-45C/SENPRO are described in sections 3.1 and 3.2 below.

3.1 131 Neutron Group Profiles for TRX-2

The 131 group profiles for TRX-2 were generated at ORNL with FORSS [10].

3.2 57 Neutron Group Profiles for a CSEWG Mixed Oxide Benchmark

The 57 group profiles for the U-L212 (Pu + U) mixed oxide benchmark were generated at ORNL with FORSS [11].

4. FAST REACTOR SHIELDING BENCHMARK PROFILES IN DLC-45

A set of 171 neutron group profiles for a fast reactor shielding benchmark (Steel-Sodium-Iron) were prepared at ORNL with FORSS [12]. A range of steel-sodium-iron thicknesses are included.

5. CURRENT STATUS OF THE RSIC PACKAGE DLC-45/SENPRO

The latest version of the package, DLC-45C, contains the profiles discussed in sections 2, 3, and 4 above. Minor updates were made to the data in 2.2, 2.4, and 4, in July 1980 and these changes are reflected in the current package. The SENDIN [13] retrieval code is also provided for editing and format conversion.

6. SENSITIVITY PROFILES NOW BEING PROCESSED

Sensitivity profiles derived in the pre-analysis of the ORNL fusion integral experiment [14] are currently being packaged at RSIC for inclusion in DLC-45.

7. COVARIANCE MATRICES IN DLC-44

The current version of the package, DLC-44C/COVERX, contains multi-group covariance matrices based on ENDF/B-IV [15] and informal evaluations performed at ORNL prior to the preparation and release of ENDF/B-V [16]. The DLC-44 files are documented in References [17] and [18] and were generated with the PUFF code [19] at ORNL. Particular files are described in sections 7.1 through 7.4 below.

7.1 Fission Spectrum Covariance Library in DLC-44

The so-called fission spectrum was processed into 6 neutron groups using a GODIVA spectrum. Data are provided for ^{235}U, ^{238}U, ^{239}Pu, ^{240}Pu, and ^{241}Pu.

7.2 Core Physics Covariance Library in DLC-44

The core physics covariance library was processed using a ZPR-6/7 spectrum into 10 neutron groups. Data for C, N, O, ^{235}U, ^{238}U, ^{239}Pu, ^{240}Pu, and ^{241}Pu are included.

7.3 Shielding Covariance Library in DLC-44

The shielding covariance library was processed into 15 neutron groups using a 1/E spectrum. Data are provided for Na, Fe, N, O, and C.

7.4 ORNL Fast Reactor Benchmark Covariance Library in DLC-44

The ORNL fast reactor benchmark covariance library was generated at ORNL using PUFF into a 26 neutron energy group structure using a fusion-fission-1/E-Maxwellian weighting function. Data are included for N, O, C, Na, Fe, ^{235}U, ^{238}U, ^{239}Pu, ^{240}Pu, ^{241}Pu.

8. CURRENT STATUS OF THE RSIC PACKAGE DLC-44/COVERX

The latest version of the package, DLC-44C, contains the covariance data described in sections 7.1 through 7.4 above. The COVERX Service Module [20] is included for file editing, manipulation, and format conversion.

9. MULTIGROUP COVARIANCE FILES BASED ON ENDF/B-V

ENDF/B-V has a more detailed set of covariance information (compared to ENDF/B-IV) for some materials in the General Purpose File as well as Special Purpose Files such as the Dosimetry File.

At present the General Purpose File is limited to distribution within the United States and the same restriction applies to the covariance files for materials in the General Purpose Files. Since Special Purpose Files are not limited in distribution the associated covariance files are likewise not restricted (This includes the so called Standards materials for ENDF/B-V). Multigroup covariance files derived from the General Purpose File are, in general, not limited in their distribution after first being made available within the United States for a suitable period of time, nominally, one or more years. There are currently projects under way to generate multigroup covariance files based on ENDF/B-V as indicated below.

9.1 ORNL 52 Group Covariance Library

The PUFF-II code [21] has been used at ORNL to generate a 52 group covariance library. The initial version, now being packaged in RSIC, contains data for ^{10}B, C, ^{16}O, ^{23}Na, Cr, Fe, Ni, ^{235}U, ^{238}U, ^{239}Pu, ^{240}Pu, and ^{241}Pu. When packaged, a new DLC number will be used to distinguish these data from the ENDF/B-IV based data in DLC-44. The new package will be called DLC-77/COVERV.

9.2 ORNL 24 Group Covariance Library

Another PUFF-II generated data set is being prepared at ORNL for application to Light Water Reactor Pressure Vessel Dosimetry Problems [22,23]. This set is not yet in RSIC for packaging but is expected soon.

9.3 LASL 30 Group Covariance Library

The NJOY [24] system has been used to generate a 30 neutron group covariance library from ENDF/B-V for uncertainty analysis of a fusion reactor [25]. Data are included for ^{1}H, ^{10}B, C, Cr, Fe, Ni, Cu, and W. These data are expected to be sent to RSIC for packaging as a DLC.

10. COVARIANCES FOR INTEGRAL EXPERIMENTS AND CALCULATIONAL METHODS

Integral experiment covariances as well as calculational methods uncertainties will also be computerized and stored in future work at ORNL so that an entire uncertainty analysis sequence can be audited.

ACKNOWLEDGMENTS

A review paper of this nature surveys the work of many individuals as indicated in the numerous references cited. The reader is directed to the references to indicate proper credit for the developments listed in the text.

The efforts of Eddie Bryant in preparing this manuscript are appreciated.

REFERENCES

1. J. L. Lucius and C. R. Weisbin, "Interface Specifications for Sensitivity Profiles (SENPRO) and Covariance Files (COVERX)," Presentation to the Committee on Computer Code Coordination, Los Alamos Scientific Laboratory (May 1976).

2. C. R. Weisbin, J. H. Marable, J. L. Lucius, E. M. Oblow, F. R. Mynatt, R. W. Peelle, and F. G. Perey, "Application of FORSS Sensitivity and Uncertainty Methodology to Fast Reactor Benchmark Problems," ORNL/TM-5563 (1976).

3. R. W. Roussin, C. R. Weisbin, and J. L. Lucius, "A Review of the Capabilities of the FORSS Sensitivity and Uncertainty Analysis System," Presented at NEA Specialists' Meeting on Nuclear Data and Benchmarks for Reactor Shielding, Paris (1980).

4. ENDF-202 Cross-Section Evaluation Working Group Benchmark Specification, BNL-19302 (ENDF-202) (1974).

5. J. H. Marable, J. L. Lucius, and C. R. Weisbin, "Compilation of Sensitivity Profiles for Several CSEWG Fast Reactor Benchmarks," ORNL-5262 (ENDF-234) (1977).

6. E. M. Bohn, I. K. Olson, and K. E. Freese, "A Compilation of Cross-Section Sensitivity Coefficients for ZPR-6/6A, ZPR-6/7, and ZPR-3/48," ZPR-TM-240 (1976).

7. H. H. Hummel and W. M. Stacy, Jr., "Cross-Section Sensitivity Studies for ZPR-6 Assembly 7 with the VARI-1D Code," ANL/FRA-TM-54 (1973).

8. J. H. Marable and C. R. Weisbin, "Uncertainties in the Breeding Ratio of a Large LMFBR," in E. G. Silver, Ed., Advances in Reactor Physics, CONF-780401, U.S. Dept. of Energy, p.231 (1978).

9. J. H. Marable, C. R. Weisbin, and G. DeSaussure, "Uncertainty in the Breeding Ratio of a Large Liquid-Metal Fast Breeder Reactor: Theory and Results," Nuc. Sci. Engr. 75, 30-55 (1980).

10. E. T. Tomlinson, J. L. Lucius, and J. D. Drischler, "A Compendium of Energy-Dependent Profiles for the TRX-2 Thermal Lattice," ORNL-5336 (ENDF-253) (1978).

11. R. L. Childs, G. deSaussure, J. L. Lucius, J. D. Drischler, V. C. Baker, J. H. Marable, and R. M. Westfall, "Sensitivity and Uncertainty Analysis for Mixed Oxide Thermal Lattice U-L212," EPRI-NP-1248 (1979).

12. E. M. Oblow and C. R. Weisbin, "Fast Reactor Shielding Studies for Steel-Sodium-Iron Systems", Proceedings of the Fifth International Conference on Reactor Shielding, Knoxville, Tennessee, Science Press (1977).

13. J. H. Marable, J. D. Drischler, and C. R. Weisbin, "SENDIN and SENTINEL: Two Computer Codes to Assess the Effects of Nuclear Data Changes," ORNL/TM-5946 (ENDF-250) (1977).

14. Y. Seki, R. T. Santoro, E. M. Oblow, and J. L. Lucius, "Comparison of One- and Two-Dimensional Cross-Section Sensitivity Calculations for a Fusion Reactor Shielding Experiment," ORNL/TM-6667 (1979).

15. D. Garber, Compiler, "ENDF-201 ENDF/B Summary Documentation," BNL-NCS-17541 (ENDF-201) 2nd Edition (ENDF/B-IV) (1975).

16. R. Kinsey, Compiler, "ENDF-201 ENDF/B Summary Documentation," BNL-NCS-17541 (ENDF-201) 3rd Edition (ENDF/B-V) (1979).

17. J. D. Drischler and C. R. Weisbin, "Compilation of Multigroup Cross-Section Covariance Matrices for Several Important Reactor Materials," ORNL-5318 (ENDF-235) (1977).

18. D. K. Olson and G. de Saussure, to C. R. Weisbin, R. W. Peelle, and F. G. Perey, "^{238}U Inelastic Scattering Covariance Matrix," Intra-Lab Correspondence (1978).

19. C. R. Weisbin, E. M. Oblow, J. Ching, J. E. White, R. Q. Wright, and J. D. Drischler, "Cross Section and Method Uncertainties: The Application of Sensitivity Analysis to Study their Relationship in Radiation Transport Benchmark Problems," ORNL-TM-4847 (ENDF-218) (1975).

20. J. D. Drischler, "The COVERX Service Module of the FORSS System," ORNL/TM-7181 (ENDF-291) (1980).

21. J. D. Smith, III, "Processing ENDF/B-V Uncertainty Files into Multigroup Covariance Matrices," ORNL/TM-7221 (1980).

22. J. D. Smith, III and B. L. Broadhead, "Multigroup Covariance Matrices for Fast Reactor Studies," ORNL/TM-7389 (in press).

23. J. Wagschal, R. Maerker, and B. Broadhead, "LWR-PV Damage Estimate Methodology," Presented at ANS Topical Meeting - 1980 Advances in Reactor Physics and Shielding, Sun Valley, Idaho (1980).

24. R. E. MacFarlane, R. J. Barrett, D. W. Muir, and R. M. Boicourt, "The NJOY Nuclear Data Processing System: Users' Manual," LA-7584-M (1978).

25. S. A. W. Gerstl, R. J. LaBauve, and P. G. Young, "A Comprehensive Neutron Cross Section and Secondary Energy Distribution Uncertainty Analysis for a Fusion Reactor," LA-8333-MS (1980).

A SIMPLE COMPARISON OF ADJUSTED DATA SETS FOR IRON BASED ON MEASUREMENTS IN ASPIS AND IN THE CORES OF FAST REACTOR CRITICALS

by

M C G Hall
Imperial College, London*

Radiation Physics and Shielding Group
Reactor Physics Division
AEE Winfrith

* Work performed during author's attachment to Radiation Physics and Shielding Group, Reactor Physics Division, AEE Winfrith.

1. Introduction

The object of this comparison is to determine whether the adjustment sets for iron obtained in one case from integral measurements in ASPIS and in another case from the cores of fast reactor criticals produce the same effect when used in calculations. The reasons that they may produce different effects are:

(a) The adjustments may reflect shortcomings in the way integral quantities are calculated from data, for example approximations in transport theory or group averaging errors, rather than errors in nuclear data.

(b) The quantities measured in ASPIS and the cores of fast reactor criticals have different sensitivities to iron cross-sections so the adjustments may be complementary rather than equivalent, for example they may span different energy ranges.

(c) The standard deviations assumed for the differential data may be unrealistic. Again this will give rise to adjustments which do not reflect real errors in nuclear data.

2. The Adjustment Sets

ASPIS: The integral measurements in ASPIS were made by spectrometers and activation detectors at penetrations up to 100 cm in iron, with a fission plate source. The calculations were performed using discrete-ordinates multigroup transport codes. The total, inelastic and absorption cross-sections of iron DFN 908 were adjusted in 100 groups according to the Principle of Maximum Likelihood.

REACTOR CORES: The integral measurements in ZEBRA, Los Alamos and Argonne critical assemblies comprised of k_{eff}, k_{∞}, central buckling, central reaction-rate-ratios, central spectra and central reactivity worths. The calculations were performed using collision-probability cell-averaging with anisotropic scattering treated using transport approximations. The scattering and absorption cross-sections of iron DFN 906 were adjusted, along with other cross-sections, to give a least squares fit to differential cross-

section data and integral measurements. The ten-group adjustments were interpolated to produce a smooth set of adjustments.

3. The Calculation

The flux was calculated by McBEND in eleven energy groups from 15 MeV to 10 KeV for the following configuration:

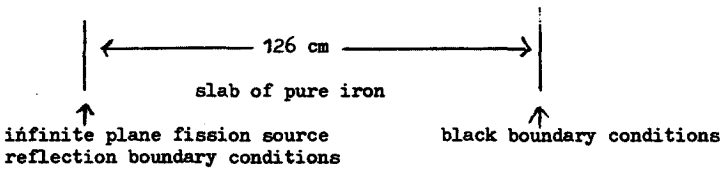

McBEND was used in the DICE mode with 1000 group data. The data was prepared, and if necessary adjusted, by a modified version of MOULD.

This calculation is suitable for the comparison because:

(a) The configuration is physically similar to ASPIS so at least the ASPIS adjustments will be applicable;

(b) McBEND in the DICE mode uses unprocessed scattering laws to track neutrons. The only processing of data which takes place is the conversion of energy-dependent cross-sections of each reaction or PCN into very fine multigroup form. This means the calculation is free of the group averaging and transport theory approximations which might be causing the adjustments to differ.

4. Results

Plotted are fractional deviations of adjusted fluxes at 75 cm and 100 cm penetration, relative to the unadjusted flux of DFN 908. The errors plotted are the standard deviations estimated by McBEND. Features of the results are:

(a) The first three groups of the flux using reactor core adjusted cross-sections are unperturbed, because these groups are outside the range of the ten-group adjustment scheme; this is

an example of the different energy range of sensitivities in the reactor cores and ASPIS.

(b) There is quite good agreement in groups four to eleven. In both cases the flux is reduced at energies above the inelastic threshold and increased at energies below. This is consistent with the increase in the inelastic cross-section found in both adjustment sets.

5. Conclusions

The adjustments sets appear to complement each other; the possibility of producing a rationalised data to embrace both shielding and core calculations cannot be ruled out.

The results also suggest it may not always be necessary to adjust in a many-group scheme. It might be possible to introduce a sensitivity capability into McBEND and calculate, with reasonably small stochastic error, sensitivities in about ten groups, while retaining the versatility and reliability of McBEND in the DICE mode. These sensitivities could then be used in a simplified adjustment scheme.

M C G HALL

Radiation Physics and Shielding Group
Reactor Physics Division
AEE Winfrith

May 1979

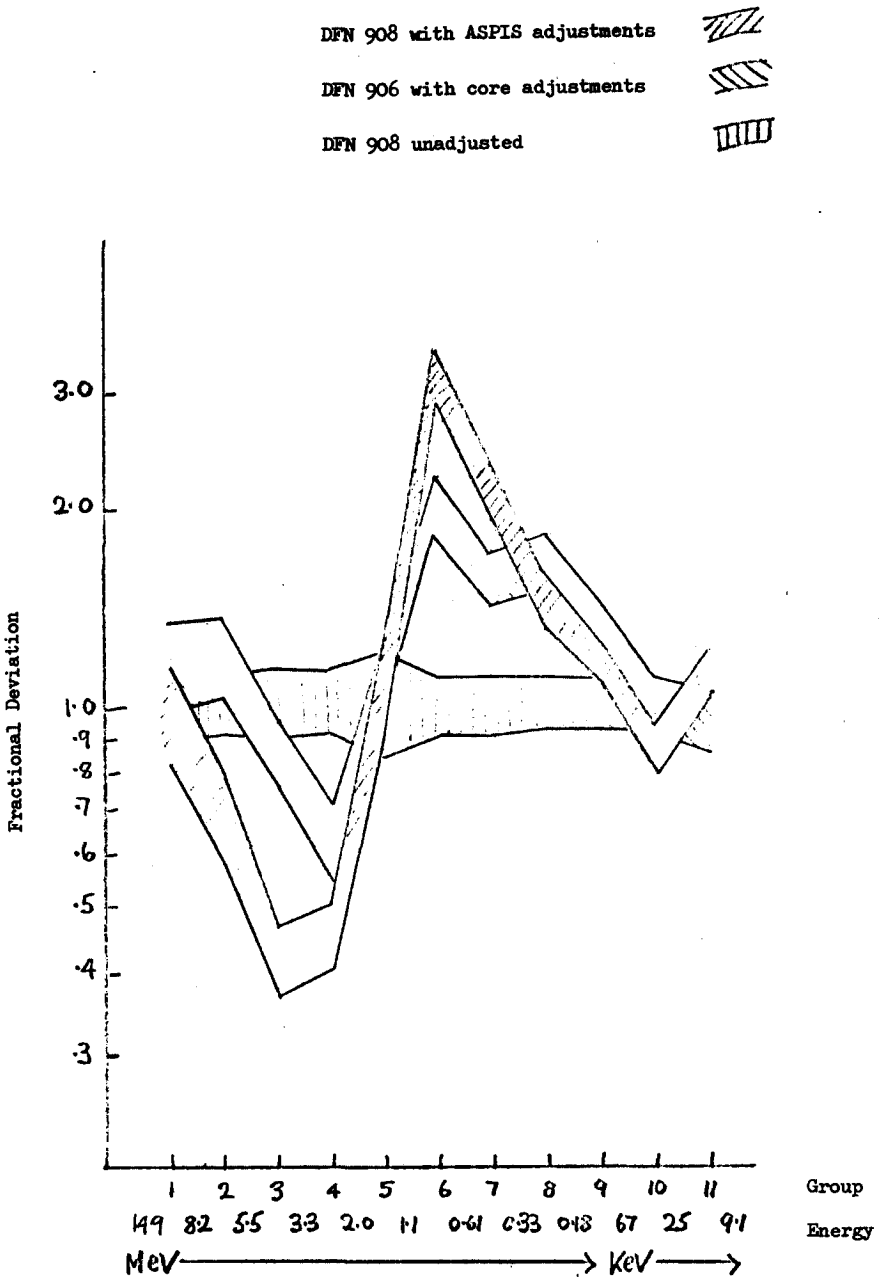

Fractional Deviation of Adjusted Fluxes
at 75 cm Penetration in Iron

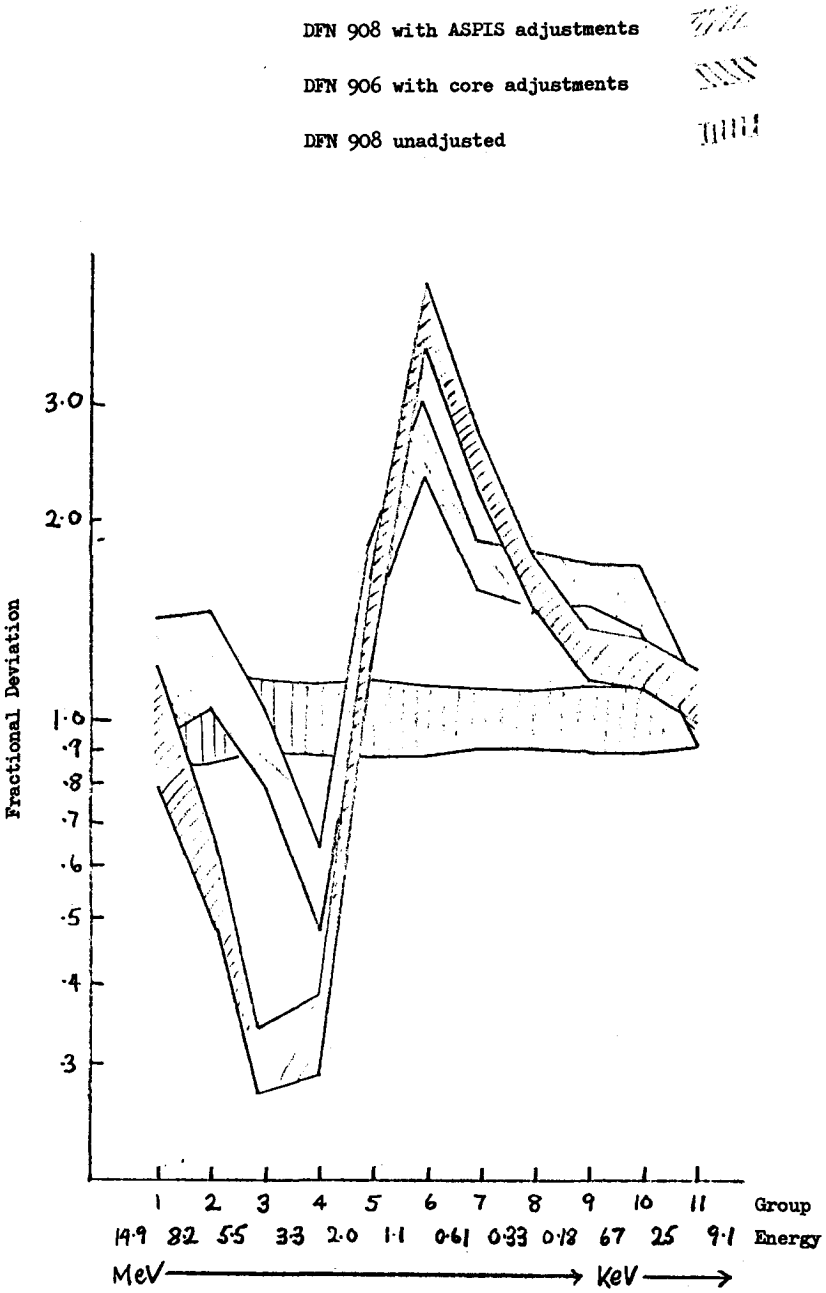

Fractional Deviation of Adjusted Fluxes
at 100 cm Penetration in Iron

SESSION II

COMPILATION OF GENERIC PROBLEMS FOR ANALYSIS TO ASSESS SHIELDING DATA REQUIREMENTS

Chairman - Président

S. AN

(Japan)

SEANCE II

COMPILATION DES PROBLEMES ACTUELS POUR LES ANALYSES DESTINEES A EVALUER LES BESOINS DE DONNEES EN MATIERE DE PROTECTION

SUMMARY OF THE SESSION II RESUME DE LA SEANCE II

Compilation of Generic Problems for Analysis to Assess Shielding Data Requirements

Prof. S. An

Four papers were presented during this session, one of which related to the safety problems of reprocessing facilities and the remainder assessed the shielding data requirements for power reactor design using sensitivity and uncertainty analyses. Two of these latter papers concerned thermal power reactors and the third was for a Fast Breeder Reactor. In general, the data requirements for practical power reactor design were identified and the uncertainties in design parameters due to individual data errors were calculated. The Monte Carlo and S_n transport codes used in the analyses have progressed considerably in recent years.

For a large BWR plant, Dr. Hehn presented sensitivity studies on the radiation damage in the pressure vessel and on the neutron and gamma dose rates in the primary concrete shield. The uncertainties in both the neutron damage and the neutron dose are dominated by the iron inelastic cross-section, so the improvement in this quantity between 4 and 10 MeV, represents the most important nuclear data requirement for LWR. The uncertainty of the fission spectrum in the same energy region is also of high importance. For gas-cooled reactors, the total sensitivity of radiation damage in the liner has high contributions from carbon and iron, and the sensitivity of neutron dose in the concrete shield is dominated by the iron cross section between 2.3 MeV and 7 MeV.

The program DUCKPOND has been applied by Mr. Hall et al to the Oak Ridge Pool Critical Assembly 'blind' test to assess the sensitivity of the flux above 1 MeV and 0.1 MeV and of the $^{58}Ni(n,p)^{58}Co$ reaction rate in the middle of the simulated pressure vessel. The individual contributions from the data errors and from the Monte Carlo statistics, to the total uncertainty of the calculations, were determined. The total uncertainty due to all data errors in the test was about $\pm$ 15 %.

A second paper by Mr. Hall presented a sensitivity analysis of a sodium-cooled fast reactor. The sodium activation-rate in the heat exchanger and the damage rate at the edge of the on-lattice steel shield were studied and best estimates and upper uncertainty limits were derived. Improvement of the sodium-elastic scattering cross-section between approximately 10 keV and 500 keV would lead to a significant reduction in this uncertainty.

The safety study (Mr. Landeyro et al) of the product storage cell of a reprocessing plant involved the Monte Carlo calculation of the criticality risk analysis and the dose rate to personnel, in both operating and emergency conditions. The conclusions were that the amount of fissile material stored could be increased by a factor of 2, compared with the old geometrical conditions.

SHIELDING DATA REQUIREMENT FOR THERMAL POWER REACTORS OF BOILING WATER AND GAS COOLED TYPE

G. Hehn, G. Kicherer
IKE University of Stuttgart
Stuttgart (FRG)

ABSTRACT

The assessment of data requirements for reactor shielding have been extended to a modern BWR-plant (KRB II, 1300 MW_e at Gundremmingen) as well as to high temperature gas cooled reactor (THTR-300,300 MW_e at Uentrop). The sensitivity studies of the light water reactor were performed for the radial shield configuration with the EURLIB group structure. Together with a previous investigation of a shielding benchmark problem for a PWR plant we established a priority list of data improvements needed for LWR shielding. The uncertainties presently given in the high energy part of the neutron fission spectrum as well as for the inelastic cross sections of stainless steel and for some foil activation data don't meet the high safety requirements of pressure vessel loading. Reasonable large dimensions are given for the radial shield of the pebble bed reactor with prestressed concrete pressure vessel. Here upscatter of thermal neutrons have to be treated by several thermal groups to get the gamma production and gamma heating correctly. The uncertainty analysis is performed for water and graphite in EURLIB structure and for iron in the twentysix group information available.

1. INTRODUCTION

Most of the systematic studies on data requirements for shielding of light water reactors had been performed for the PWR type characterized by a compact core and relatively small diameters of the pressure vessel and primary concrete shield [1], [2]. Recently sensitivity studies and error analysis were applied to a small BWR (VAK,15 MW_e at Kahl) for neutron damage and foil detector rates at surveillance capsule position and in the pressure vessel [3]. But this could not be taken as representative for a large power reactor. So a study had been conducted for the radial shield of a large BWR (KRB II, 1300 MW_e at Gundremmingen) and the results should be compared with those of the PWR (Biblis B, 1300 MW_e at Biblis) investigated previously.
Quite different data requirements should be expected for shielding of a gas cooled high temperature reactor with extreme large dimensions of the core , graphite reflector, thermal shield and prestressed concrete pressure vessel. For this the plant THTR-300 at Uentrop was chosen.

2. SENSITIVITY STUDIES AND ERROR ANALYSIS FOR THE BWR

The onedimensional cylindrical calculations were performed at core midplane not along the main symmetry axis but along an angle of 45° through the core edge to get the maximum of the outstreaming radiation as shown in Figure 1.The local distribution of the neutron and gamma dose rate is given in Figure 2. As an example the neutron spectrum at the inner side of the pressure vessel is shown in Fig.3. The energy structure of the spectrum can be correlated with the sensitivity profiles given later. The importance of hydrogen and oxygen with respect to radiation damage in the pressure vessel is quite similar to that of the PWR study , see Figure 4. According to the small thermal shield the importance of iron, nickel and chromium is reduced by a factor of two, whereas the nuclides of the reactor core become little bit more important [4].
The sensitivity analysis for gamma heating in the primary concrete shield give likewise similar results compared with the PWR study for the three most important nuclides iron, oxygen and hydrogen as shown in Figure 5. The total sensitivity of the neutron and gamma dose stresses the importance of the iron data in Figure 6 and Figure 7, which will result in a large effect on the uncer - tainty of the dose.
The sensitivity profiles in Figure 8 and Figure 9 show a little

broader energy range of importance for neutrons between 2 and 10 MeV. Nearly the same energy range is of importance for the gamma radiation as given in Figure 10 for heating.A stronger energy peak between 6 and 8 Mev is observed in Figure 11 for the gamma dose.

In the error analysis covariance matrices have been applied in the EURLIB structure for hydrogen and oxygen from ENDF/B-IV/V. The data for iron were taken from the 26 group COVERX library [5]. The results of the analysis are given in Table I for neutron damage and neutron dose. For damage we get the same uncertainties as in the PWR benchmark from hydrogen and oxygen and a reduced contribution from iron according to the reduced sensitivity [3] . Therefore we can conclude that the most stringent requirement does exist for the PWR originating from the high uncertainty of the nonelastic cross section in a narrow energy range between 5 and 7 MeV.
The uncertainty of the neutron dose is dominated by the same iron inelastic cross section for both reactors, so most of the data requirements of light water reactors can be solved by improving the iron cross sections for neutrons and gamma rays in the upper MeV-region between 4 and 10 MeV. In the same energy region the uncertainty of the fission spectrum of uranium and plutonium is of high importance to nearly all target quantities in reactor shielding and has the next priority after the iron data.

3. SENSITIVITY STUDIES FOR GAS COOLED REACTOR

The radial shield configuration of a gas cooled reactor is given in Figure 12. The local distribution of the neutron and gamma dose rate is shown in Figure 13 indicating a backward current of gamma rays produced by thermal neutrons at the inner side of the thermal shield. Figure 14 shows the soft neutron spectrum in the liner with a strong dominance in the keV region and very few MeV neutrons. The total sensitivity of radiation damage in the liner shows a very high contribution from carbon in Figure 15. The iron sensitivity is by a factor of three higher than that of the PWR, so that the error will be dominated by iron nonelastic cross section at 7 MeV as can be deduced from the sensitivity profile of Figure 18.
The sensitivity of the neutron dose in the concrete shield is extremly dominated by the iron cross section at 2.3 MeV and 7 MeV as indicated by Figure 16 together with the profile in Figure 19. The gamma heating in the graphite reflector at the core edge is determined by the gamma cross section of carbon and thorium as shown

in Figure 17 with a relative soft sensitivity profile of Figure 20. Of course also the neutron cross section of carbon may be of importance. A detailed error analysis is in progress for the gas cooled reactor.

4. REFERENCES

(1) Hehn G., Koban J.

Reactor shield benchmark No. 2
ESIS, Special Issue No.4, 1976

(2) Hehn G.

Conclusions from the sensitivity benchmark results of a PWR shield.
IAEA - 207, Vienna, 1978

(3) Prillinger G., Almalah K., Hehn G., Pfister G.

Accuracy of neutron spectrum calculations for prediction of radiation damage in PV - steel
3. ASTM - EURATOM Symp. on Reactor Dos., Ispra 1.- 5. Oct. 1979

(4) Devilles C.

Sensitivity studies and data requirements for thermal reactor shielding
IAEA - 207 , Vienna , 1978

(5) Drischler, J.D., Weisbin, C.R.

Compilation of multigroup cross-section covariance matrices for several important reactor materials
ORNL - 5318 (ENDF-235) ,1977
Available from RSIC as DLC-44/COVERX

Tab. I : Error analysis for damage in the pressure vessel and neutron dose after 1 m ordinary concrete shield for a BWR (KRB-II, 1300 MW_{el})

		Neutron dose	damage
H - 1	elastic	4.8 %	4.3 %
	total	4.8 %	4.3 %
O - 16	elastic	6.1 %	2.2 %
	inelastic	5.5 %	2.3 %
	(n-p)-Reaction	3.7 %	1.5 %
	(n,)-Reaction	0.12 %	0.04 %
	total	6.02 %	2.24 %
Fe	elastic	0.2 %	0.0 %
	nonelastic	62.3 %	7.5 %
	total	62.3 %	7.5 %
total		62.78 %	8.97 %

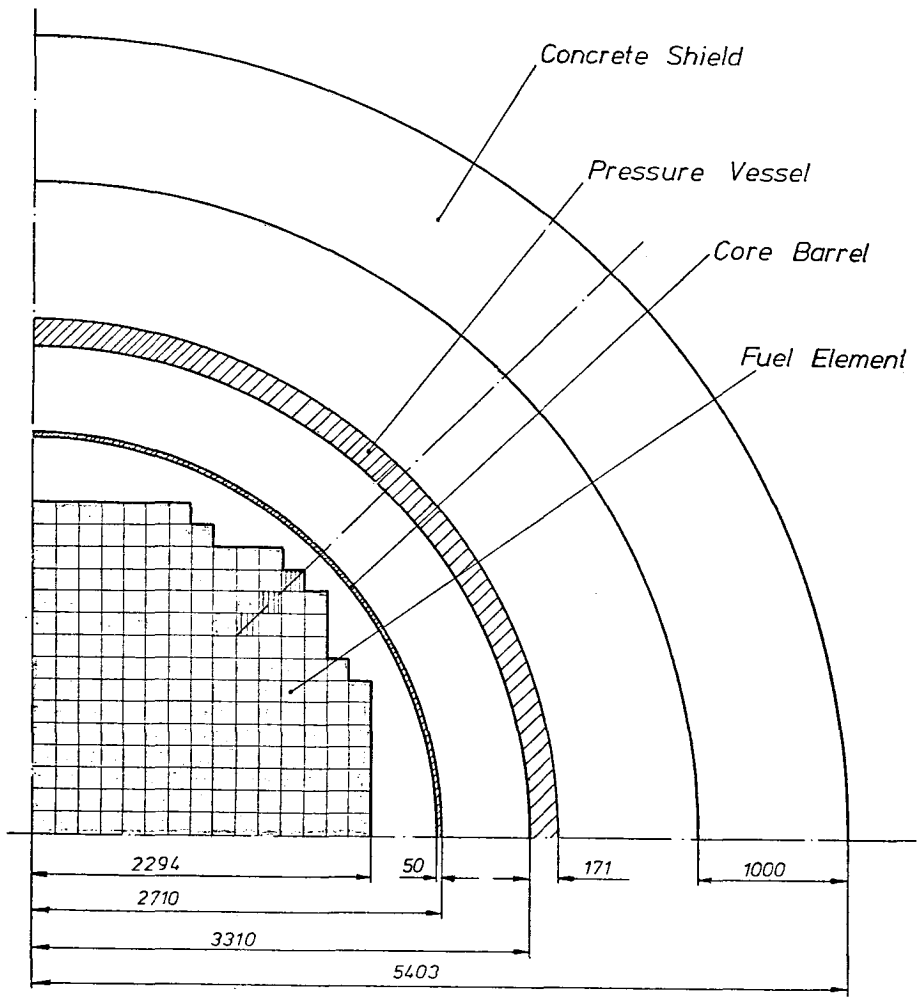

FIG.1 *Cylindrical Geometry Model of a BWR (KRB II, 1300 MW_{el})*

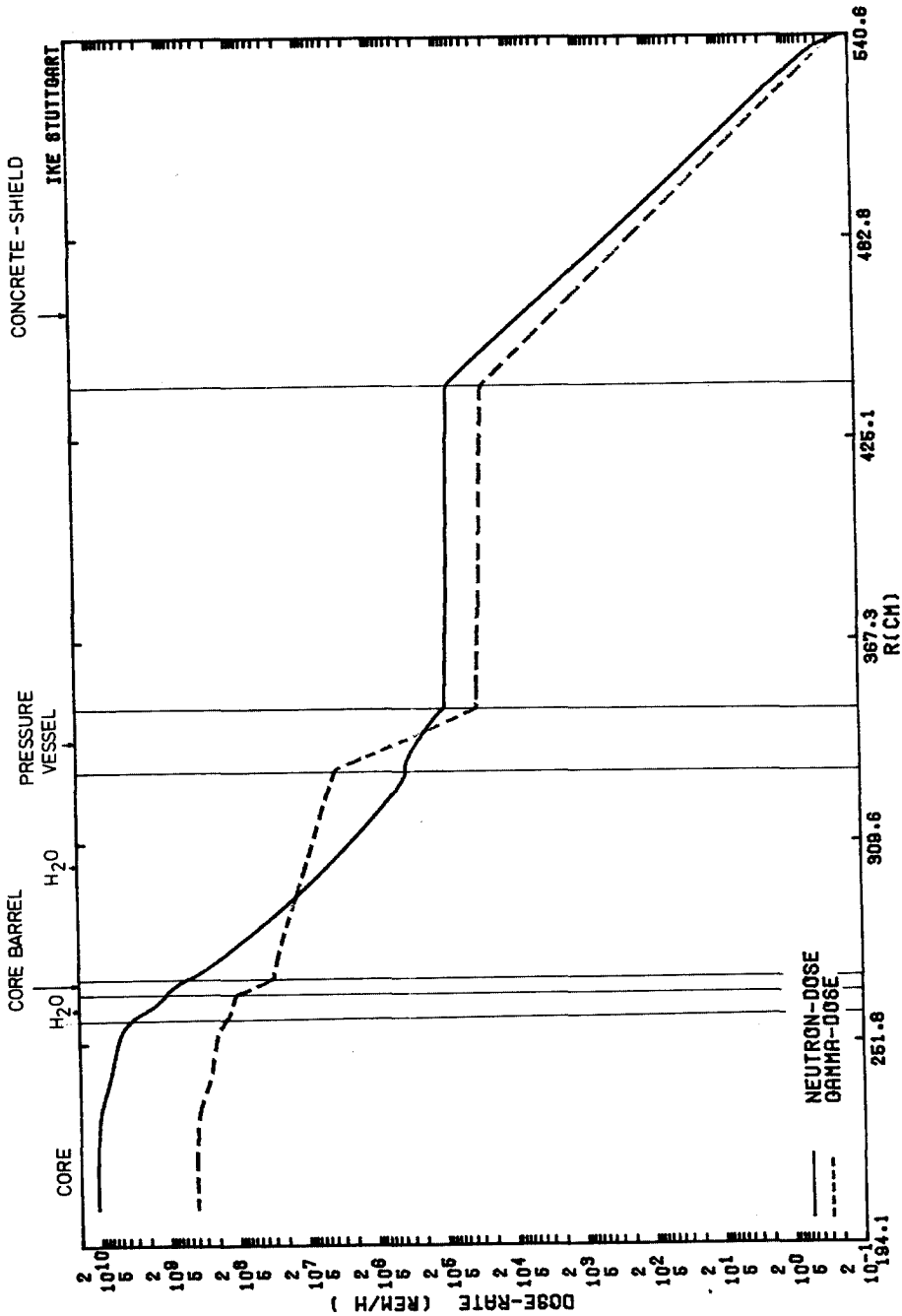

FIG. 2 NEUTRON- AND GAMMA-DOSE ATTENUATION ALONG RADIAL AXIS/BWR KRBII

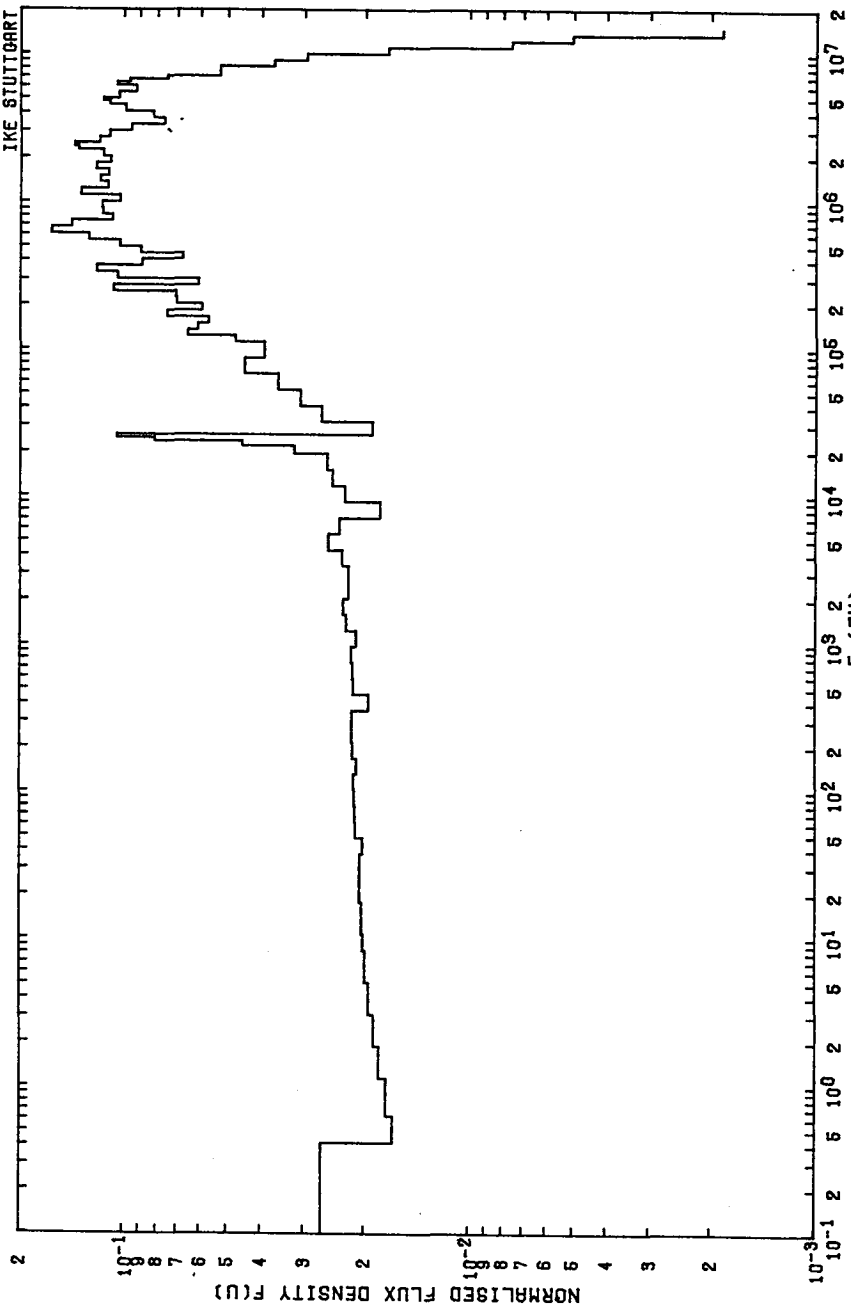

FIG. 3 NEUTRON SPECTRUM IN PRESSURE VESSEL/BWR KRBII

FIG. 5

SENSITIVITY OF RAD.-HEAT AT THE BEGINNIG OF CONCRETE SHIELD FOR VARIOUS ELEMENTS INTEGRATED OVER ALL ZONES

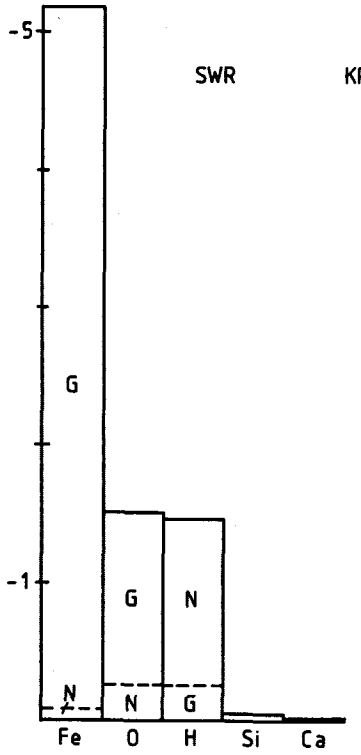

FIG. 4

SENSITIVITY OF RAD. DAMAGE IN PRESSURE VESSEL FOR VARIOUS ELEMENTS INTEGRATED OVER ALL ZONES

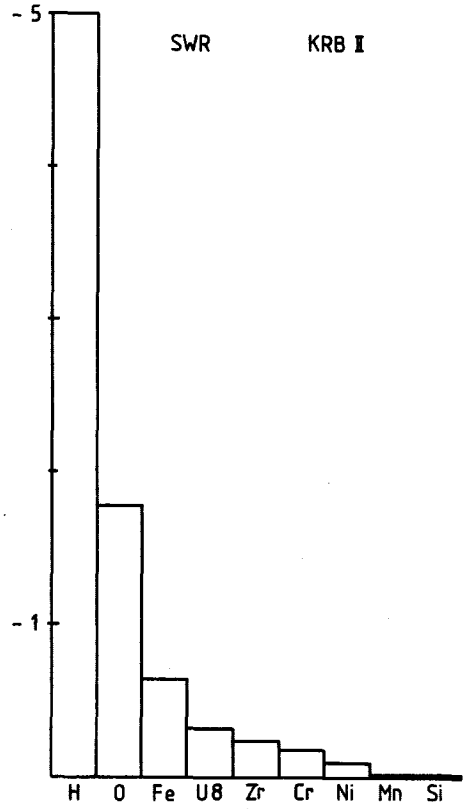

FIG. 6

NEUTRON - DOSE SENSITIVITY IN CONCRETE SHIELD (1M)
FOR VARIOUS ELEMENTS INTEGRATED OVER ALL ZONES

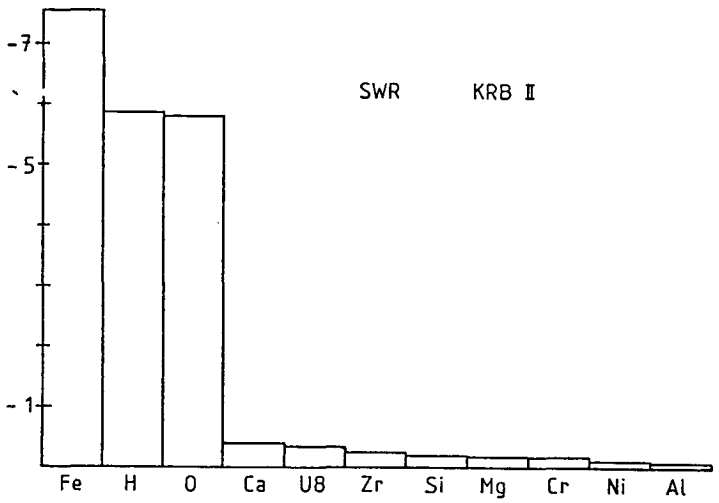

FIG. 7 ·

GAMMA-DOSE SENSITIVITY IN CONCRETE SHIELD (1M)
FOR VARIOUS ELEMENTS INTEGRATED OVER ALL ZONES

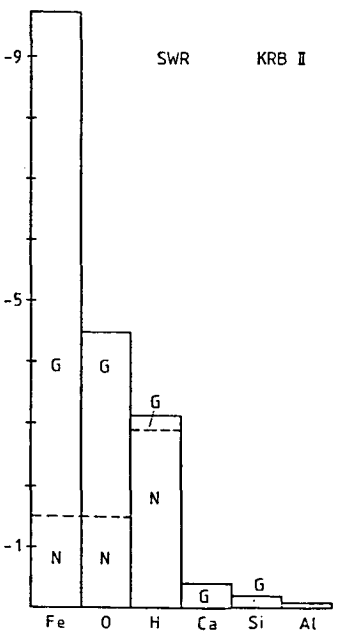

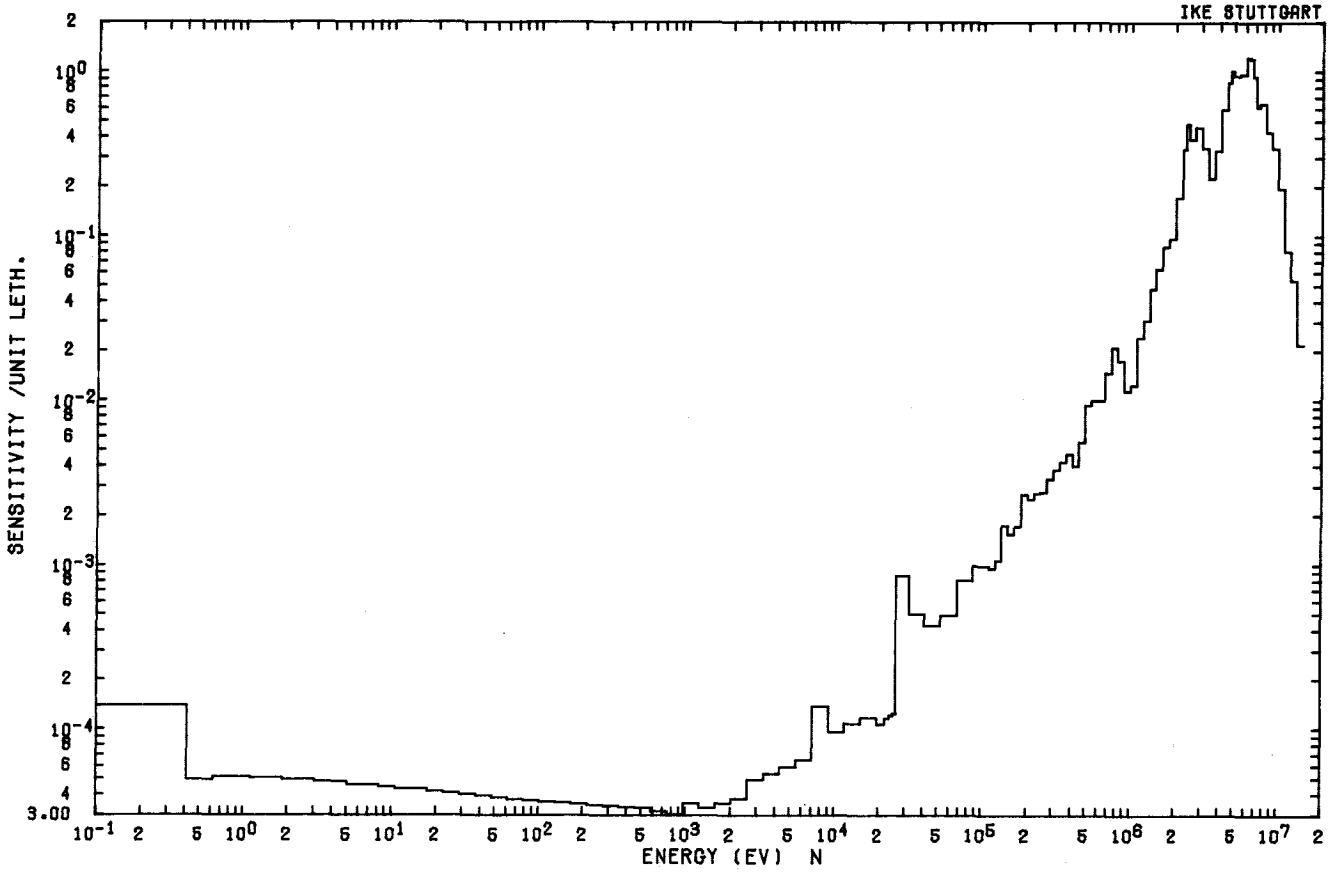

FIG. 8 SENSITIVITY OF DPA (H-1)

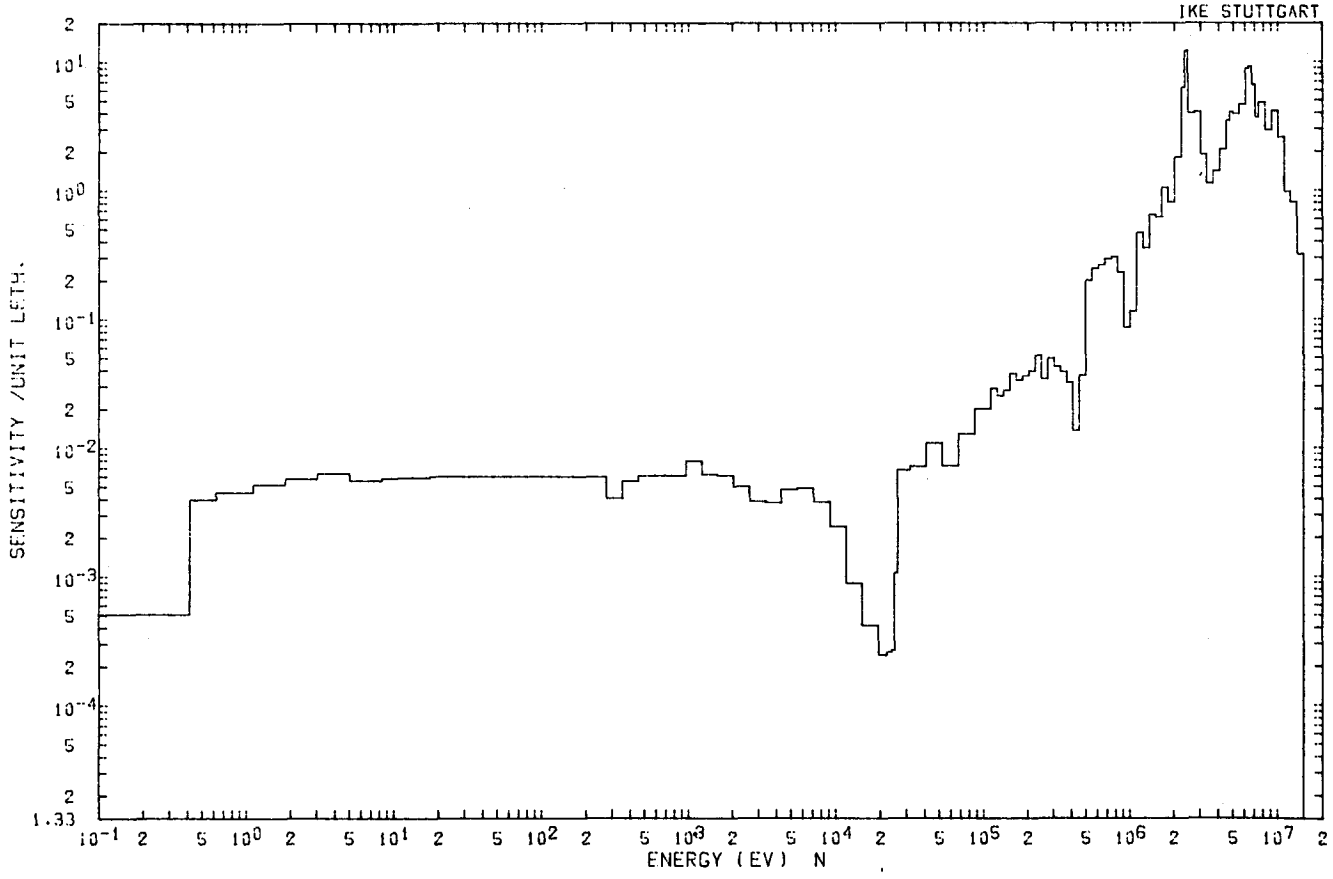

FIG. 9 SENSITIVITY OF N-DOSE (FE) .KRB II. 100N 20G

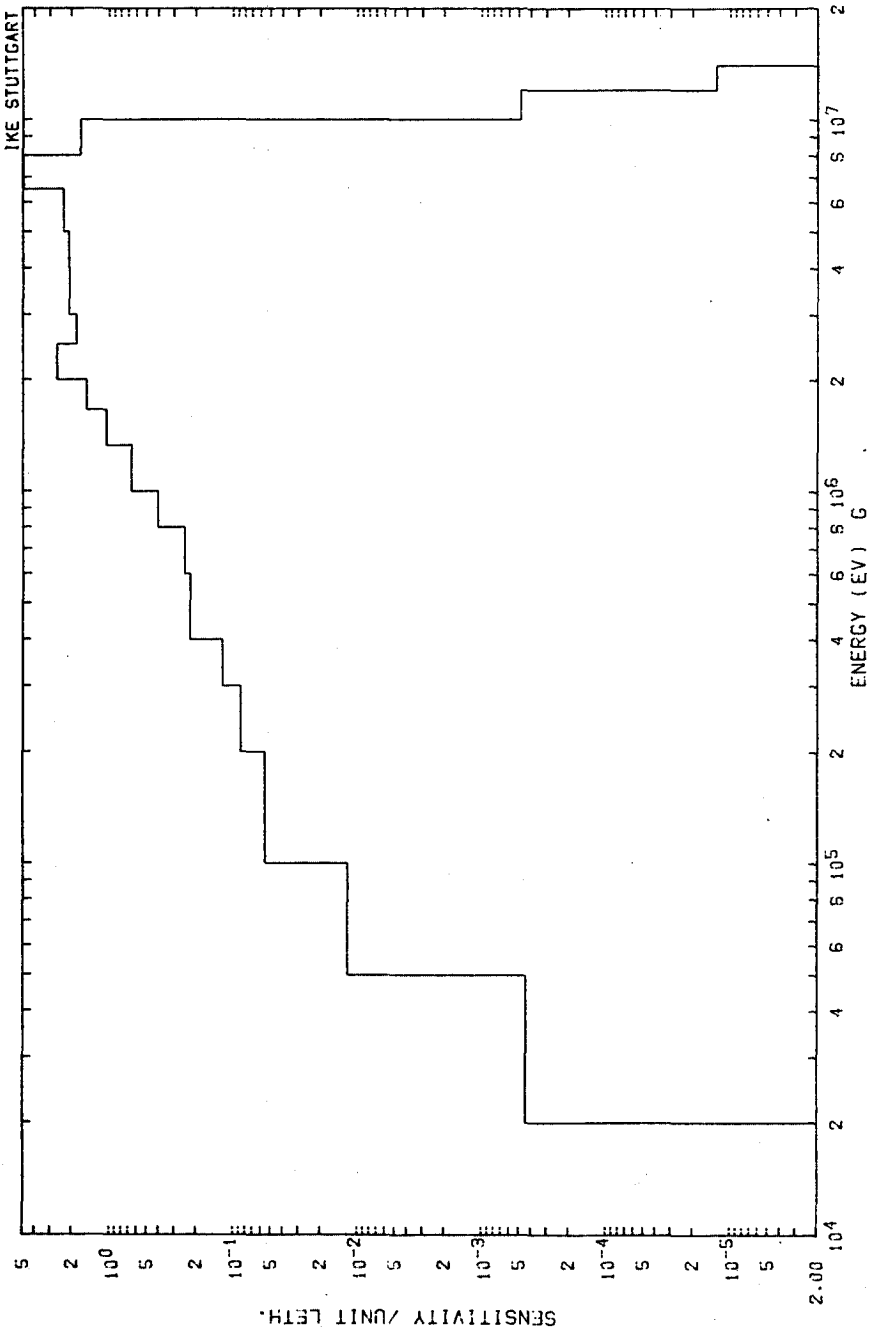

FIG. 10 G-SENSITIVITY OF KERMA (FE).KRB II. 100N 20G

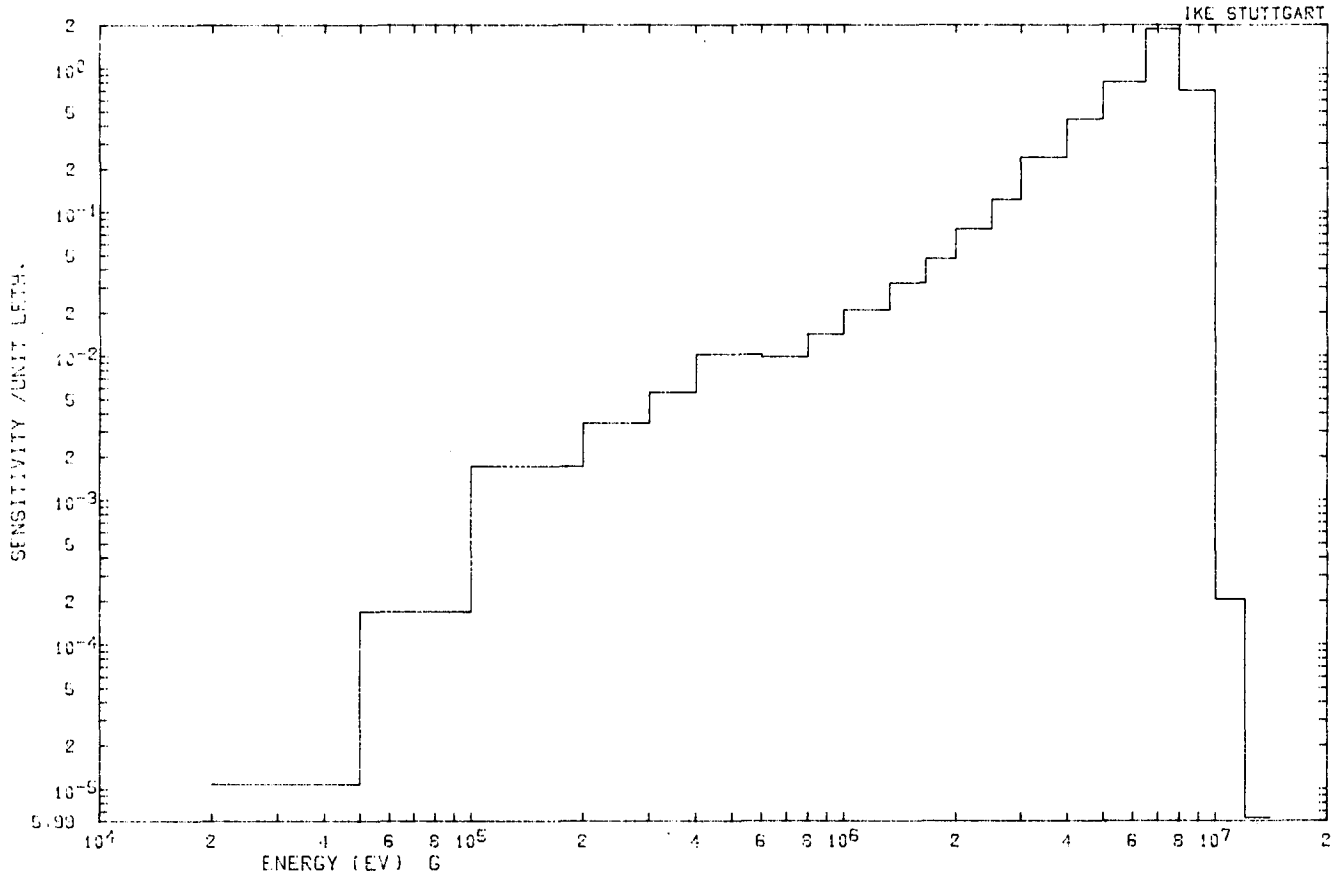

FIG. 11 G-SENSITIVITY OF G-DOSE (FE)

FIG. 12 *Cylindrical Geometry Model of a pebble bed reactor (THTR-300)*

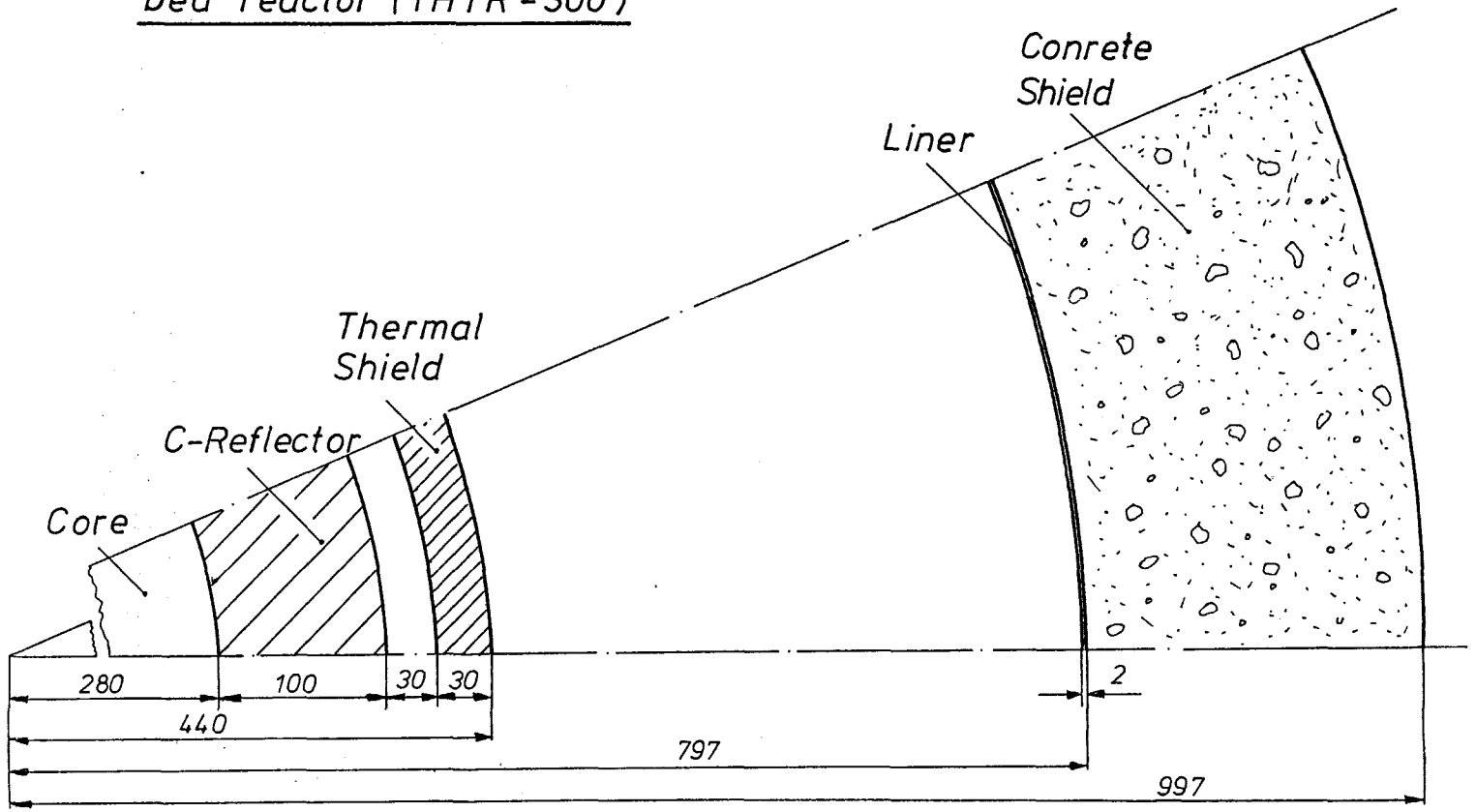

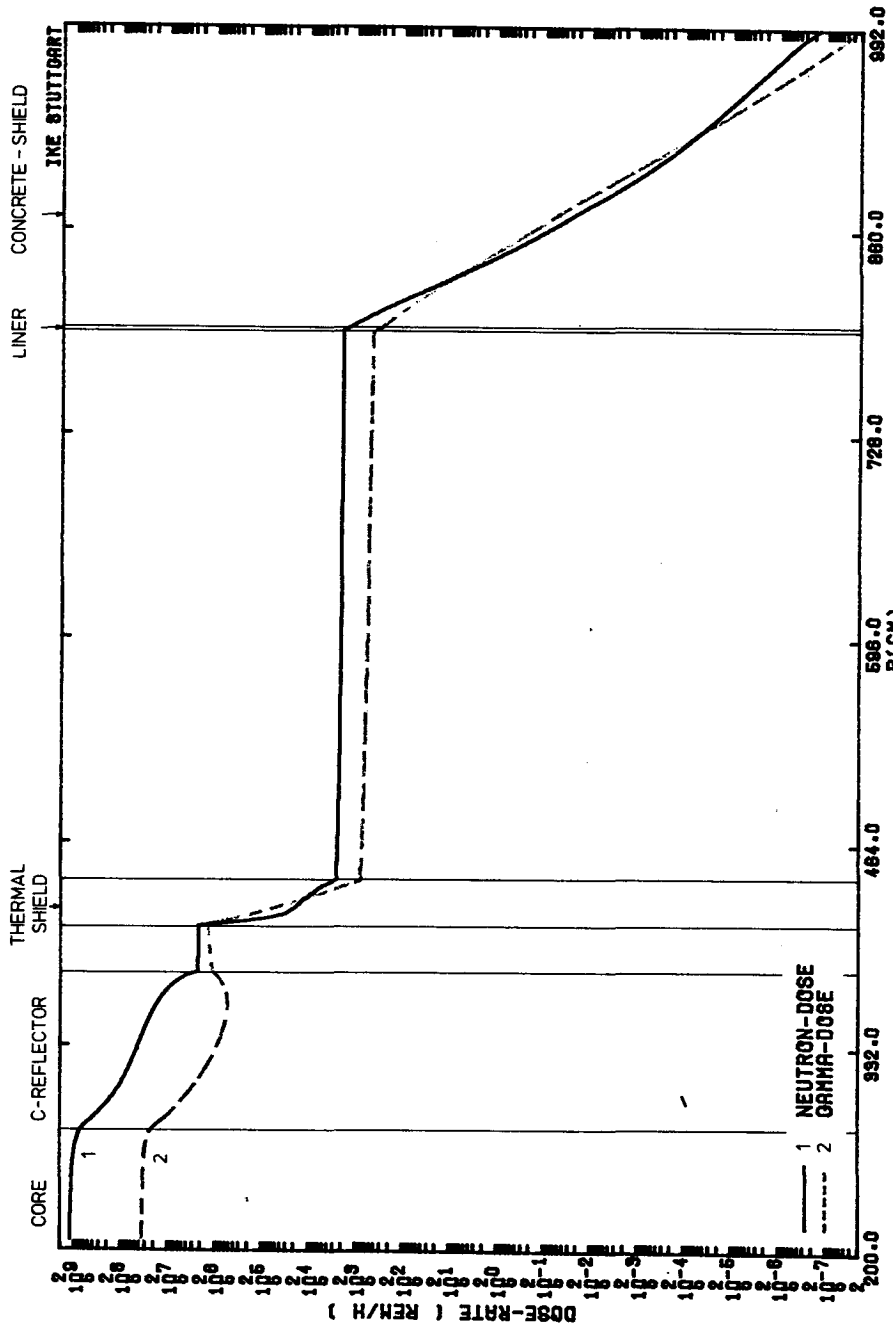

FIG. 13 GAMMA- AND NEUTRON-DOSE ATTENUATION ALONG RADIAL AXIS/ THTR-300

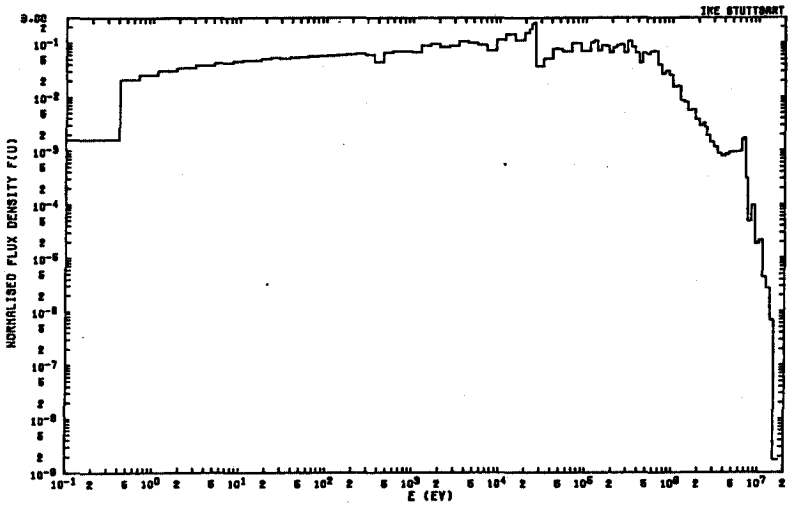

FIG. 14 NEUTRON SPECTRUM IN THE LINER /THTR-300

FIG. 15

SENSITIVITY OF RAD. DAMAGE IN LINER FOR VARIOUS ELEMENTS INTEGRATED OVER ALL ZONES

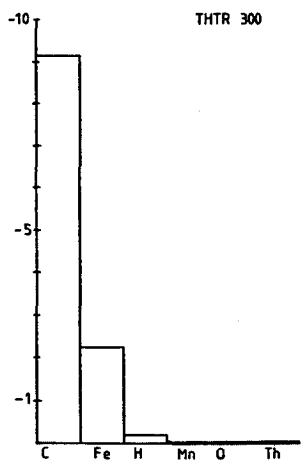

FIG. 16

NEUTRON-DOSE SENSITIVITY IN CONCRETE SHIELD (2M. FOR VARIOUS ELEMENTS INTEGRATED OVER ALL ZONES

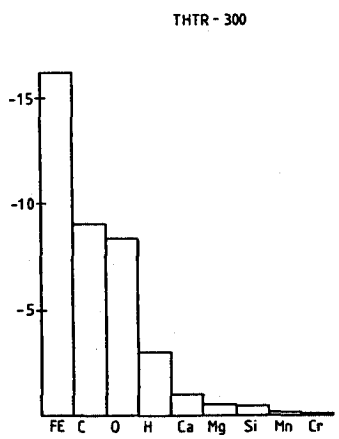

FIG. 17

SENSITIVITY OF RAD. HEAT IN C-REFLECTOR FOR
VARIOUS ELEMENTS INTEGRATED OVER ALL ZONES

THTR 300

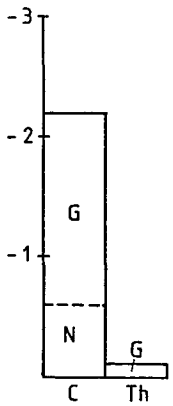

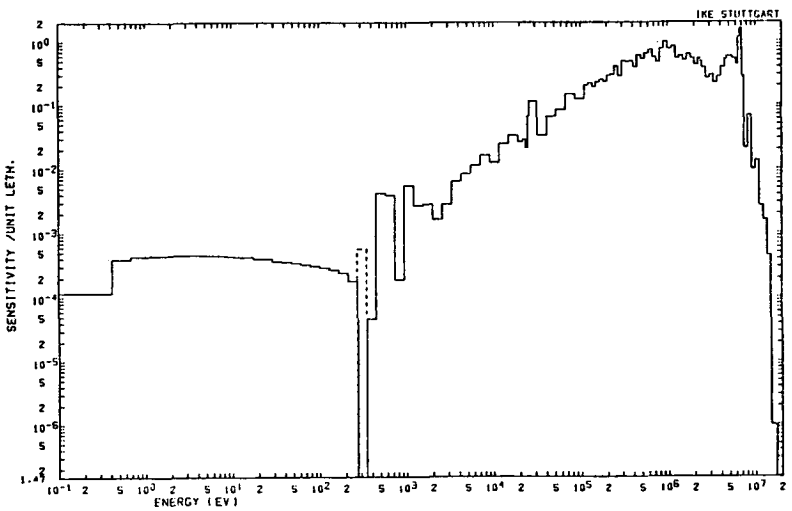

FIG. 18 SENSITIVITY OF DPA (FE) 10IN THTR

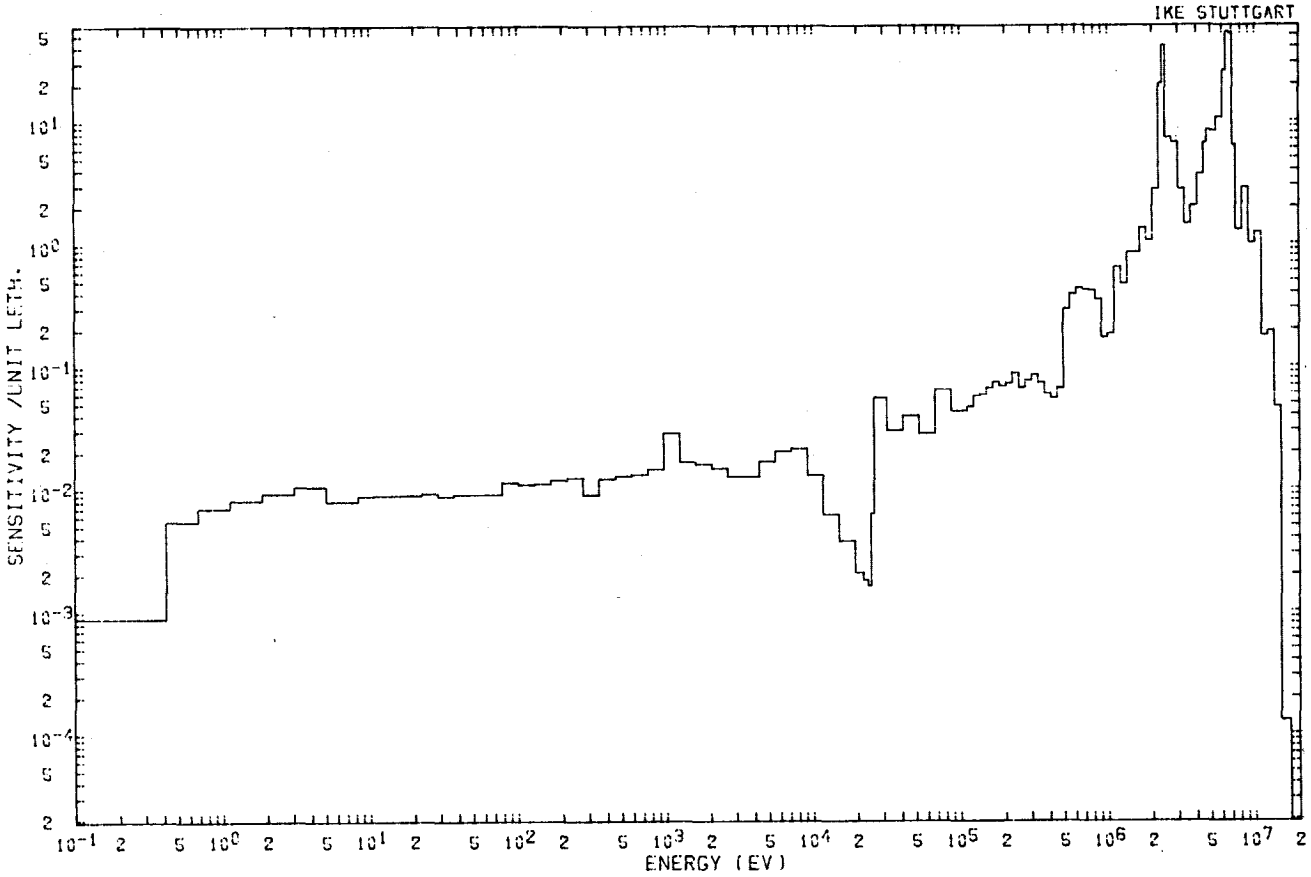

FIG. 19 SENSITIVITY OF N-DOSE (FE) 101N THTR

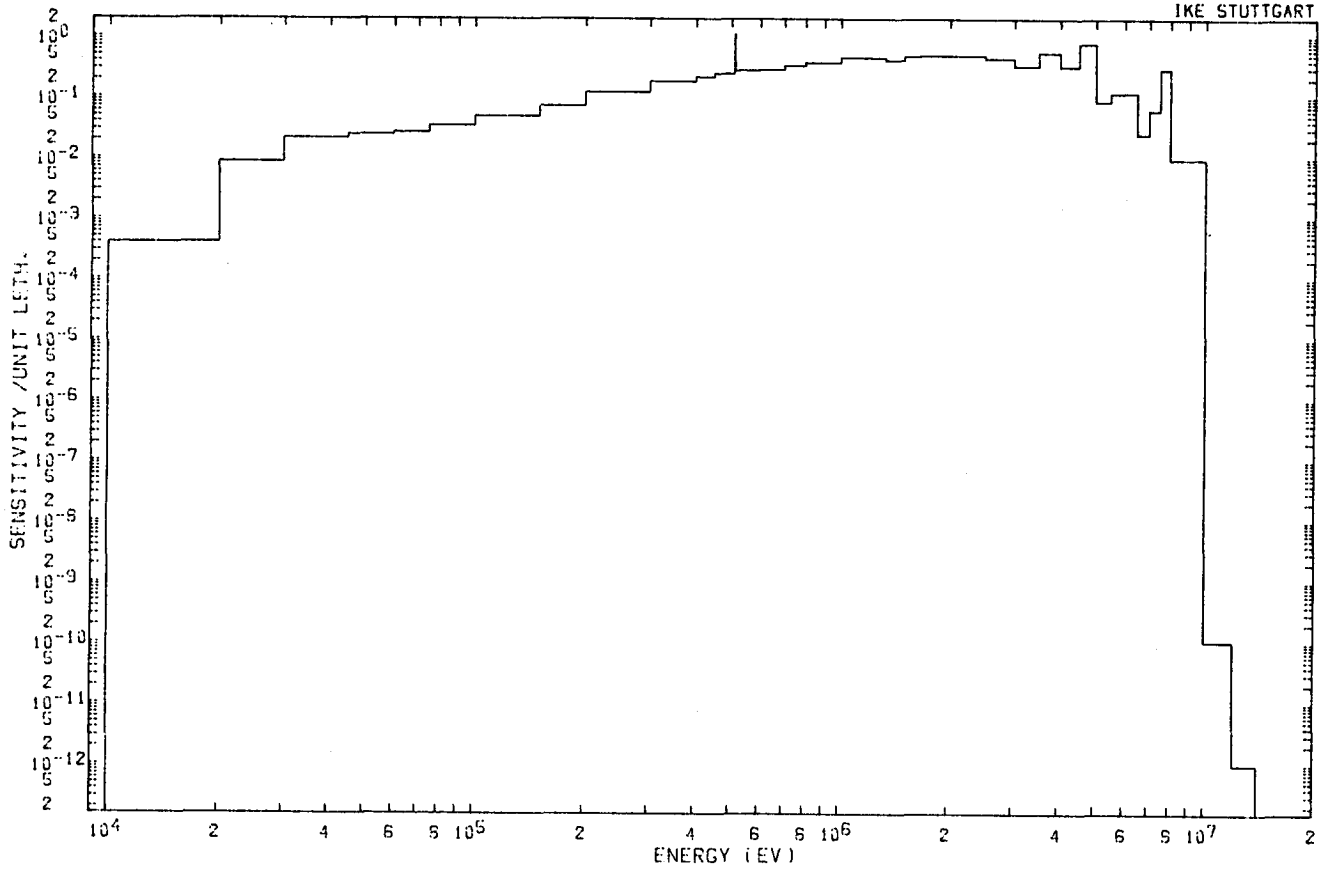

FIG. 20 G-SENSITIVITY OF KERMA (C-12) 101N 36G THTR

SAFETY STUDIES FOR A CELL PRODUCT STORAGE IN REPROCESSING PLANTS

P.A. Landeyro, S.Marcondes
Dipartimento Ciclo del Combustibile
C.N.E.N. (Rome - Italy)

RIASSUNTO

Il presente studio pone l'accento sull'analisi di sicurezza di una cella di stoccaggio di prodotto in un impianto di riprocessamento.

Lo studio di sicurezza comprende il calcolo del fattore K effettivo e della dose per il personale esposto. Sono state considerate condizioni operative e di emergenza.

I calcoli di criticità sono stati eseguiti con KENO IV un codice Montecarlo, mentre i calcoli della dose sono stati fatti applicando il codice Montecarlo MORSE C.G. e usando una libreria neutronica prodotta dal codice SUPERTOG-IV. I calcoli di dose sono stati ripetuti per differenti vettori di Pu.

ABSTRACT

The present study emphasizes the safety analysis of a product storage cell in a reprocessing plant. Moreover safety studies were made for calculations of the K-effective factor and of the dose rate to the exposed personnel.

Operating and emergency conditions were considered.

Criticality calculations were achieved with KENO IV Montecarlo code. The dose calculations were carried out applying the MORSE C.G. Montecarlo code using a neutron library produced by SUPERTOG-IV code.

The dose calculations were repeated for different types of Pu vectors.

Introduction

The safety study of any cell containing fissile material in a fuel cycle, have two steps first criticality risk analysis, secondly dose rate to the exposed personel in operating and emergency conditions.

Presently new Montecarlo programs for transport calculation have been developed, and it is possible to represent with such codes any normal or abnormal situation, with the desired precision. These can be represented for any component or component's configuration for whatsoever fuel cycle plant. With the purpose of analyzing the hazardous criticality accident or dose intensity calculations (neutron, gamma or both).

In the Fuel Cycle Department CNEN such codes have been qualified and routinely used for plant design.

The present work represents code applications e.g., the calculations of a storage cell for fissile material, Plutonium nitrate, just in the step which precedes the transformation of the fissile salt in the oxide state. The work is representative in these conditions, from the criticality risk point of view for several process cells (mixer-settlers cell, centrifugal extractors cell, pulsed columns cell, etc., etc.). The criticality calculations have been performed with KENO IV /1/, and the dose intensity calculations by MORSE C.G. /2/ both Montecarlo codes. These are further analyzed to the design conditions for 6 accidental cases with Plutonium nitrate solution of 200 gr/litre of Pu, containing in all 86 kg of Pu.

In this paper only the results of neutron dose calculations are shown, because those concerning the gamma and gamma neutron dose are still under studies.

Cell Description

The cell dimensions are (7.40 x 1.725 x 4.40) in meters, with 30 cm wall thickness, concrete. The containers for the storage of fissile material consist of two sets of 9 cylinders each, in stainless steel, of 10.2 cm O.d., 180 cm of height and 3 mm of wall thichkness, placed in file at 40 cm to the nearest wall. The distance between the cylinders axis is 31,5 cm and the distance from the last cylinder to the wall is 29,5 cm. In the cell and in a parallel plane to that of the 18 cylinders, at 35 cm. from another long wall there are 4 cylinders, 3 storage vessel and a condenser, all with an external diameter of 12.5 cm. Two of them are 305 cm in length, one is 155 cm, and the little 85 cm in length. In the plane of 18 cylinders is an evaporator, which for the calculation purposes has been considered as 2 vertical cylinders of 10.2 cm of external diameter and 260 cm of length with 50 cm distance between its axis and 80 cm from the last of 18 cylinders.

Analyzed Cases Criticality

CASE A. Normal conditions. All the vessels have been considered filled with Plutonium nitrate solution 200 gr/litre of Pu.

CASE B. In the described solution breaking of a set of 9 storage vessels with the formation of a solution slab over the floor by the first 9 cylinders.

CASE C. Breaking of a set of storage vessels with the formation of a

slab of solution over the floor by emptying of the second set of 9 cylinders.

CASE D. Precipitation of Pu as PuO2-5H2O filling the vessel at a height proportional to the Pu content considering each cylinder as in case A.

CASE E. Solution in the same conditions of case A and the cell flooded.

CASE F. Identical as case D and the cell flooded.

CASE G. All the vessels filled with mixture PuO2-5H2O and cell flooded.

Analyzed Cases Neutron Dose

CASE A. Was considered the design case (the same of criticality calculations) changing the percent composition of Pu, corresponding to fuel discharged by L.W.R. for burnups of 20000, 30000, 40000 MWD/Ton, for CANDU reactor 10000 MWD/Ton, and for F.B.R. for 80000 MWD/Ton respectively.

CASE B. Identical as case B of criticality calculations, with Pu percent composition corresponding to fuel discharged by L.W.R. with 30000 MWD/ton of burnup.

CASE D. Identical as case D of criticality calculations, with Pu percent composition corresponding to fuel discharged by L.W.R. with 30000 MWD/ton of burnup.

Criticality Calculation Method

The KENO IV calculations were approximately for 80 batches of 1200 neutrons each, of which the first three batches in each case were skipped.

For KENO IV in all cases was used as an average statistical weight of 0,5, for russian roulette, for any energetic group.

In all cases for KENO IV calculations was used MIXED BOX type geometry.

The KENO IV calculations were realized considering the influence of the wall as represented by its albedo data.

In all cases were used the Hansen-Roach sixteen group cross section library.

The plutonium composition used was 95% of 239-Pu and 5% 240-Pu.

Dose Intensity Calculation Method

The percent Pu composition was calculated with ORIGEN code /3/, and is shown in table I.

As fixed neutron source was considered the set of alpha-neutron reactions and spontaneous fission reactions.

As spectrum of alpha-neutron reactions was utilized the data of reference /4/, and as spontaneous fission spectrum the fission spectrum of 239-Pu.

In all calculations was used the MORSE C.G. option that permits to consider the neutron fission as secondary particles and to add their contribute to the neutrons of fixed source.

All the dose intensity calculations were performed with a cross section library of 100 energy group, created by SUPERTOG-4 code /5/.

All the calculations were realized with a number of histories between

TABLE I - PERCENT COMPOSITION of PU

R E A C T O R	H W R	L W R			F B R
BURNUP	10000 MWD/ton	20000 MWD/ton	30000 MWD/ton	40000 MWD/ton	80000 MWD/ton
% 236 - Pu	1.79 E-6	2.04 E-6	5.13 E-6	9.27 E-6	2.21 E-6
% 238 - Pu	3.18 E-1	6.97 E-1	1.62000	2.70000	8.89 E-2
% 239 - Pu	5.91 E+1	7.07 E+1	6.06 E+1	5.48 E+1	6.6 E+1
% 240 - Pu	3.18 E+1	2.05 E+1	2.39 E+1	2.45 E+1	2.84 E+1
% 241 - Pu	6.59000	6.7500	1.05 E+1	1.24 E+1	3.93000
%242 - Pu	2.18000	1.2700	3.3800	5.62000	1.57000

24000 and 34000 in order to keep the percentage error lower than 32%.

The points considered in the analysis were in the center of the cell and on the long wall close to the 18 cylinders in the center of external face.

In every MORSE C.G. calculation was employd the COMBINATORIAL GEOMETRY.

The parameters of the russian roulette for MORSE C.G. calculation for each energy group were 0,1, the low weight, and 0,3, the average weight.

Results

It is clear from table II the criticality calculation results, and is obvious from the first 4 cases that the k-eff factor changes negligibly within the design of emergency conditions in air medium.

K-eff is increased by more than 25% for the flooding cases. Highest k-eff values are observed for theoretical incidents (practically impossible), shown by case G. This accident is practically equivalent to the old "geometrical safety" conditions.

The values of k-eff for a cylinder 12,5 cm in diameter, 305 cm in lenght, reflected by 20 cm of water filled with Plutonium nitrate solution 200 gr/litre of Pu or $PuO2-5H2O$, homogeneous mixture, are 0.77384 and 0.96851 respectively. Comparing this value with the results of case E and G, it is clear that, in flooded cell conditions, the K-eff is determined only by the cylinder with the maximum diameter.
Therefore the interaction between vessels is negligeable.

Looking at table III, it is clear that the difference between the dose intensity in normal and emergency conditions is little.

Low level dose corresponding to F.B.R. is explained by the level of 238-Pu concentration.

Comparing the dose results of table III for a L.W.R. fuel with a burnup of 40000 MWD/ton with the calculations using expression of reference /6/ for the internal point, the results of both methods are in good accordance : 5.49 mrem/h against to 8.80 mrem/h for Montecarlo method.

Conclusions

The Montecarlo calculations permit to release the old "geometrical safety" conditions. So it allows to increase the amount of fissile material stored whitout risk by a factor greater than 2, when considering as the most dangerous accident the precipitation and flooding, which is little likelyhood, and by a factor greater than 3, considering only the flooding case.

It is clear that in all flooding accident cases, where the vessels behave as full reflected, it is not necessary to calculate the neutron dose.

The neutron dose obtained by a Montecarlo method is in accord with other methods or it result more conservative.

TABLE II - RESULTS OF CRITICALITY CALCULATIONS

C A S E	K EFFECTIVE	STANDARD DEVIATION
A	0.62772	0.257 E-2
B	0.62874	0.266 E-2
C	0.60766	0.306 E-2
D	0.59905	0.473 E-2
E	0.77361	0.387 E-2
F	0.79435	0.628 E-2
G	0.96286	0.367 E-2

TABLE III - RESULTS of NEUTRON DOSE CALCULATIONS

CASE A	CENTRAL CELL POINT		EXTERNAL POINT	
	Dose mrem/h	error %	Dose mrem/h	error %
HWR 10000 MWD/ton	3.7688	32.40	1.6696	30.110
LWR 20000 MWD/ton	4.0628	34.50	1.5526	31.620
LWR 30000 MWD/ton	6.447	32.40	2.3898	30.216
LWR 40000 MWD/ton	8.8018	32.40	3.5630	31.581
FBR 80000 MWD/ton	1.27988	35.20	0.5817	30.045
CASE B 30000 MWD/ton	4.4570	27.60	2.2624	26.70
CASE D 30000 MWD/ton	5.1576	28.90	1.9120	29.80

Reference

1.- Petrie L.M. Cross N.F. "KENO IV an improved Montecarlo criticality program". ORNL-4938 (1975).

2.- MORSE C.G. "A General Pourpose Montecarlo Moultigroup Neutron and Gamma Ray Transport Code with Combinatorial Geometry", CCC-203.

3.- Bell M.J. "ORIGEN - the ORNL Isotope Generation and Depletion Code" ORNL-4628 (1973).

4.- Hajtaba Taburzadeh, "Neutron Yeld from the Isotope Oxigen-18", Jet Propulsion Laboratory, Nuclear Science on Engeneering 44, 190-193 (1971).

5.- Wright R.Q. Lucius J.L. Greene N.M. and Craven Jr. C.W. "SUPERTOG: A Program To Generate Fine Group Constants And Pn Scattering Matrices From ENDF/B", ORNL-TM-2679 (1969).

6.- Etherington H. NUCLEAR ENGENEERING HANDBOOK, sec 7-3, page 7-106 (1958).

Acknowledgements

The authors are very grateful to Maria Carotenuto and Mohammed Azeem for their valuable contribution in the writing this report.

Thanks are also due to Miss Stefania Messa for her valuable contribution in typing this report.

UNCERTAINTY ANALYSIS IN A FAST BREEDER REACTOR USING ANISN/SWANLAKE

by

M C G Hall
Imperial College, London*

Radiation Physics and Shielding Group
Reactor Physics Division
AEE Winfrith

* Work performed during author's attachment to Radiation Physics and Shielding Group, Reactor Physics Division, AEE Winfrith.

1. Introduction

The use of the one-dimensional program ANISN (1) and the perturbation program SWANLAKE (2) to estimate uncertainties in design parameters arising from uncertainties in multi-group cross-section data has previously been demonstrated in studies of a typical PWR (3) and a sodium-cooled fast reactor (4). The present work represents an advance on these early studies in the following respects:-

(i) A more detailed and up-to-date model of a sodium-cooled fast reactor has been chosen;

(ii) Calculations have been carried out in the EURLIB 100-group structure - so sensitivity features which were to some extent masked by the 37-group structure previously used are now resolved;

(iii) Recently available cross-section correlation data (5) for iron and sodium* has been processed into the EURLIB group scheme (6) and used in the analysis. Realistic design parameter uncertainties can now be compared with upper limit estimates of uncertainty whose use has been enforced through lack of information on correlated uncertainties.

2. The Shielding Calculations

Tables A1 and A2 detail the configuration chosen. The two parameters studied were the sodium activation-rate in the heat-exchanger (radius 835.5 cm), and the damage-rate at the edge of the on-lattice steel shield where a core restraint structure would be positioned (radius 261 cm). Calculations of flux throughout the shield were carried out with ANISN in the P_3S_8 approximation in spherical geometry. Neutron sources for the calculation are given in Table A3. All data, with the exception

---

* Matrices from this source for Na and Fe are shown in Appendix B

of the iron damage cross-section, were processed into the EURLIB group scheme from the UK Nuclear Data File - the Data File Numbers are given in Table A1. The iron damage cross-section was calculated by applying the IAEA recommended displacement cross-section to iron data (7). The principal cross-sections of interest are shown in Figures 1 to 4.

3. Calculation of Uncertainties and Sensitivities

For a single material of interest the perturbation of the calculation of a quantity R which depends on data $\underline{\alpha}$ is given by

$$\delta R = \sum_{K} \sum_{i} \frac{\partial R}{\partial \alpha_{iK}} \delta \alpha_{iK} \qquad 1.$$

where α_{iK} is the cross-section of reaction type K in group i and $\sum_{K} \alpha_{iK} = T_i$ the total cross-section for group i.

A simple and unambiguous expression for the perturbation of R is

$$\delta R = \sum_{i} \left\{ \frac{\partial R}{\partial N'_i} \delta N'_i + \frac{\partial R}{\partial N_i} \delta N_i + \frac{\partial R}{\partial A_i} \delta A_i \right\} \qquad 2.$$

where N', N and A are respectively cross-sections for inelastic and elastic scattering and absorption. In practice below the threshold energy of inelastic scattering $N' = 0$ and above this energy $A \ll N'$ throughout the energy range of interest to the problem. In this case equation 2 is simplified by the use of the non-elastic cross-section $X_i = N'_i + A_i$:-

$$\delta R = \sum_{i} \left\{ \frac{\partial R}{\partial X_i} \delta X_i + \frac{\partial R}{\partial N_i} \delta N_i \right\} \qquad 3.$$

Squaring equation 3 and taking the expectation gives for the fractional variance of R :-

$$\frac{\sigma^2(R)}{R^2} = \frac{1}{R^2} \sum_{i} \sum_{j} \left\{ \frac{\partial R}{\partial X_i} \frac{\partial R}{\partial X_j} \operatorname{cov}(X_i, X_j) + \frac{\partial R}{\partial N_i} \frac{\partial R}{\partial N_j} \operatorname{cov}(N_i, N_j) + 2 \frac{\partial R}{\partial X_i} \frac{\partial R}{\partial N_j} \operatorname{cov}(X_i, N_j) \right\} \qquad 4.$$

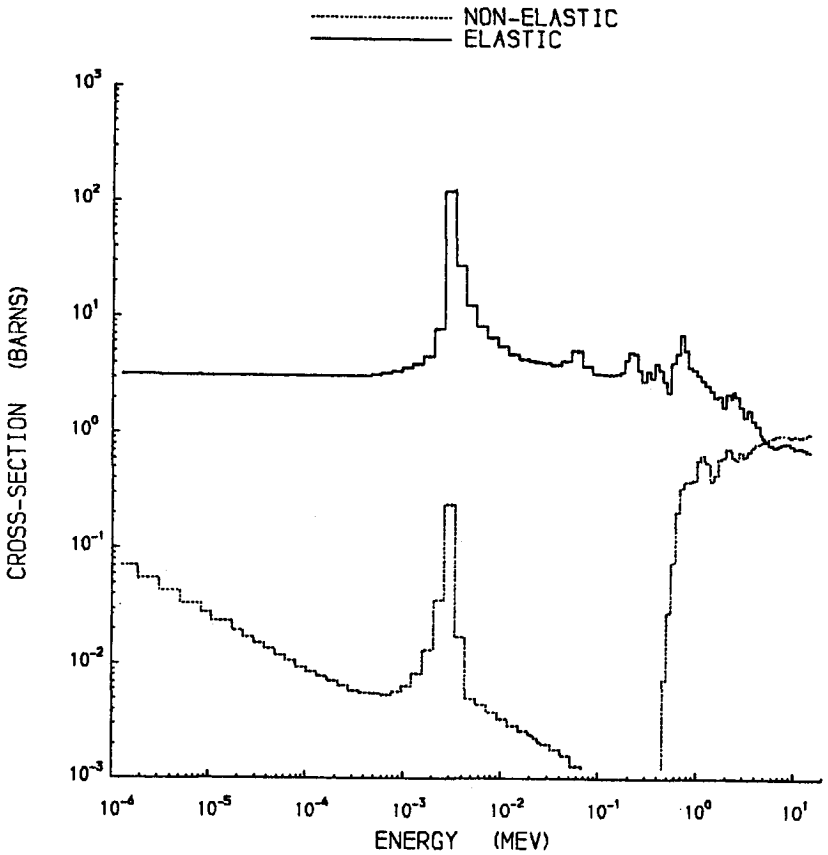

SODIUM CROSS-SECTIONS

FIGURE ONE

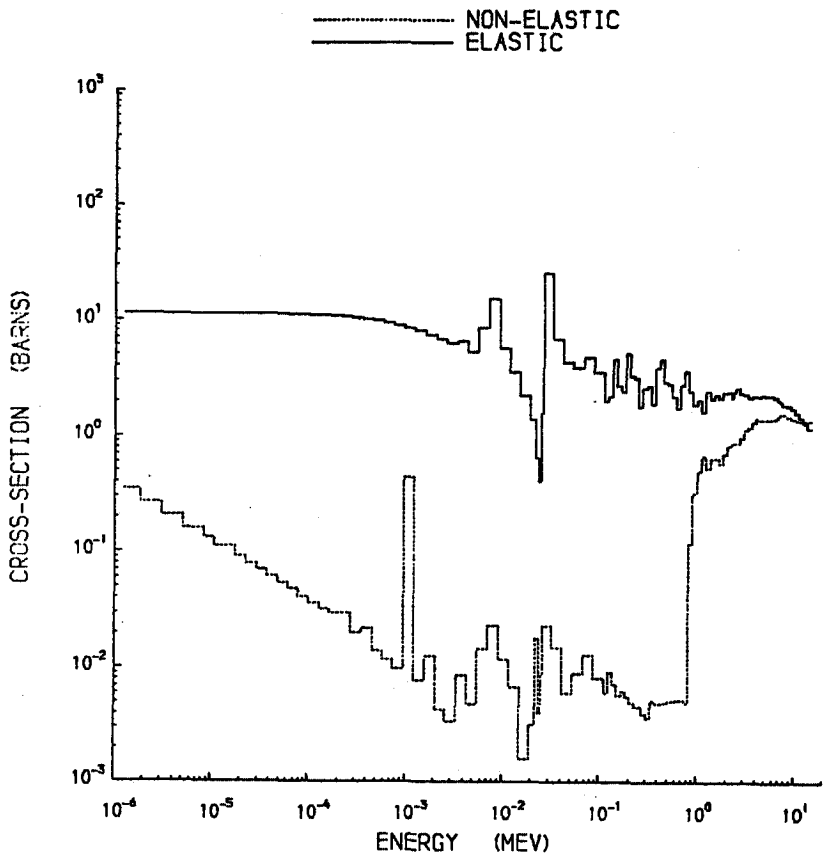

IRON CROSS-SECTIONS

FIGURE TWO

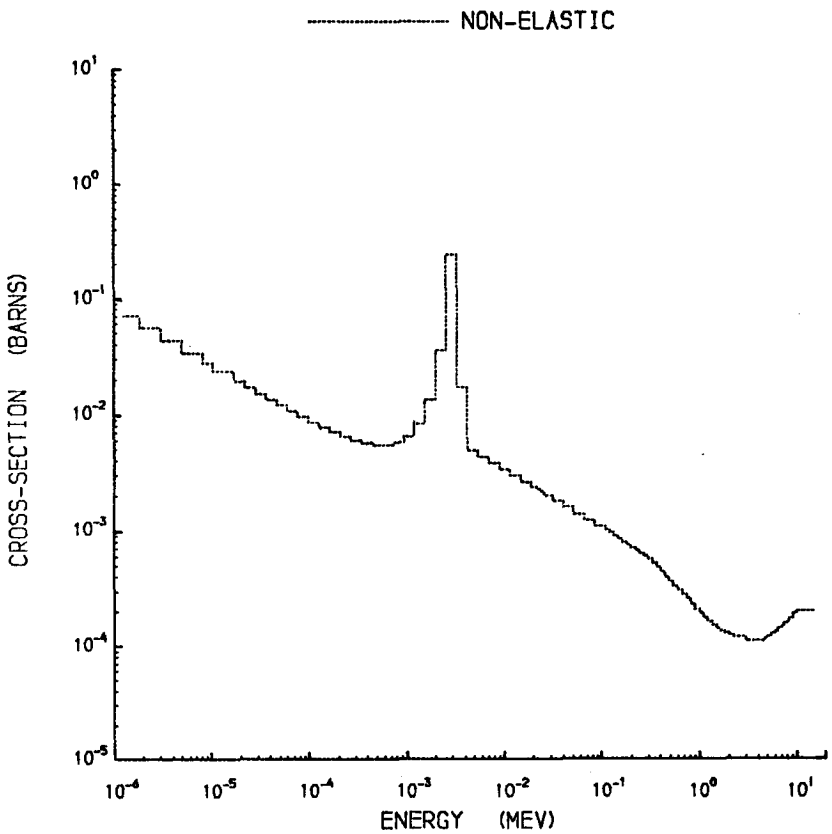

SODIUM ACTIVATION CROSS-SECTIONS

FIGURE THREE

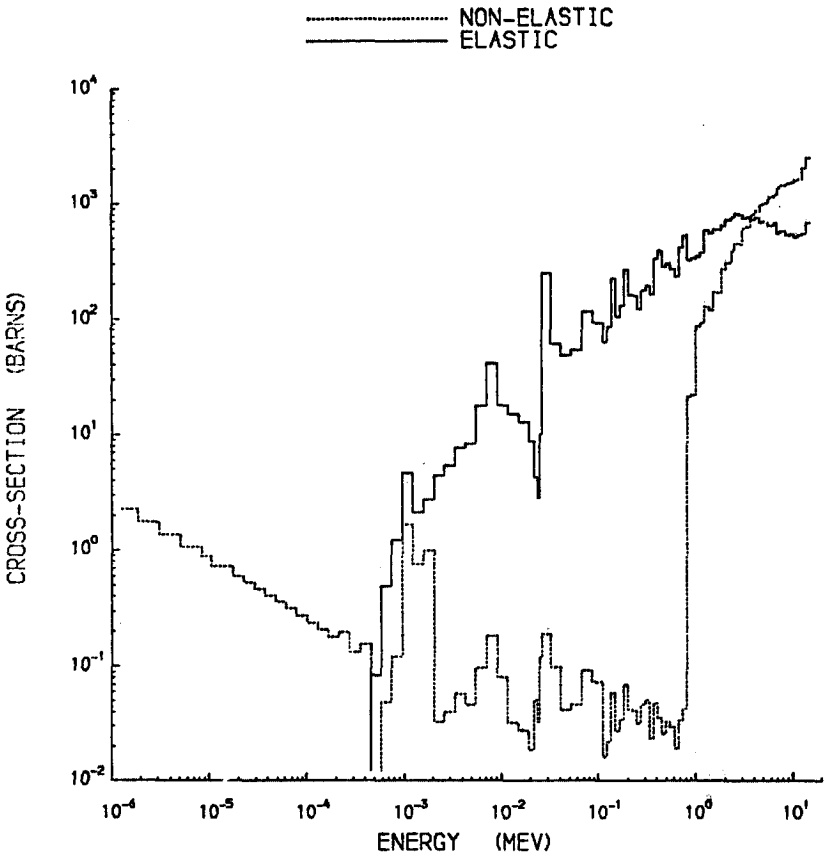

IRON DAMAGE CROSS-SECTIONS

FIGURE FOUR

Sensitivities given by SWANLAKE are defined by $U_{x_i} = \frac{\partial R}{\partial X_i} \frac{X_i}{R}$ and equation 4 therefore becomes

$$\frac{\sigma^2(R)}{R^2} = \sum_i \sum_j \left\{ U_{x_i} U_{x_j} \frac{cov(X_i X_j)}{X_i X_j} + U_{N_i} U_{N_j} \frac{cov(N_i N_j)}{N_i N_j} + 2 U_{x_i} U_{N_j} \frac{cov(X_i N_j)}{X_i N_j} \right\} \quad 5.$$

The fractional ovariances of equation 5 are described for iron and sodium in (5) and in their expanded 100- group form (6) represent the only relevant uncertainty information which has been available for this analysis. Equation 5 takes no account of the possibility that a cross-section used in the SWANLAKE calculation may also be a detector cross-section. In this case (for example the uncertainty in sodium activation-rate due to uncertainty in the sodium cross-sections) a simple correction to the sensitivity is required - this is discussed in (4).

The sensitivities used in equation 5 of the sodium activation rate in the heat-exchanger and of the iron displacement rate at the edge of the on-lattice shield to iron and sodium non-elastic and elastic cross-sections are shown in figures 5 to 8. The covariance information used is shown schematically in Appendix B.

4. Calculation of Measurement Sensitivities

Conventional sensitivity coefficients of the type $U_{x_i} = \frac{\partial R}{\partial X_i} \frac{X_i}{R}$ give a useful insight into which cross-sections and energy ranges are likely to be significant contributors to the fractional uncertainty $\sigma(R)/R$. A more useful quantity, however, is the so-called measurement sensitivity

$$M_{x_i} = \frac{\partial \sigma(R)}{\partial \sigma(x_i)} \frac{\sigma(x_i)}{\sigma(R)} \quad 6.$$

originally defined in (4); this points more precisely to the most profitable areas of data refinement. The measurement sensitivities to X_i and N_i derived from equation 5 by differentiation are:-

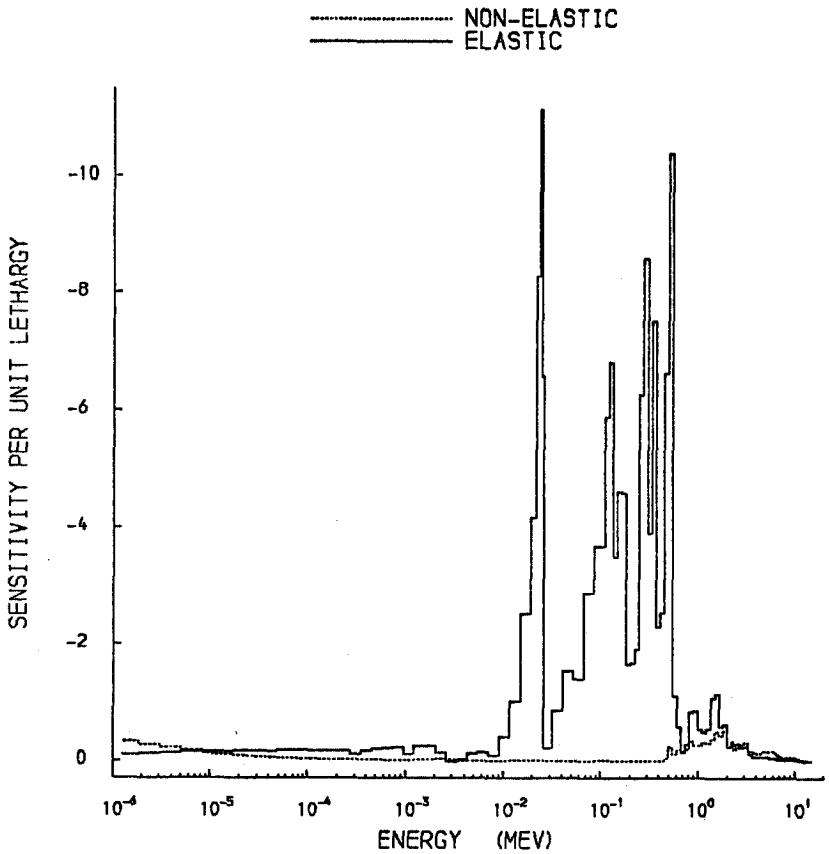

SENSITIVITY PER UNIT LETHARGY
OF SODIUM ACTIVATION RATE IN THE HEAT EXCHANGER
TO SODIUM CROSS-SECTIONS

FIGURE FIVE

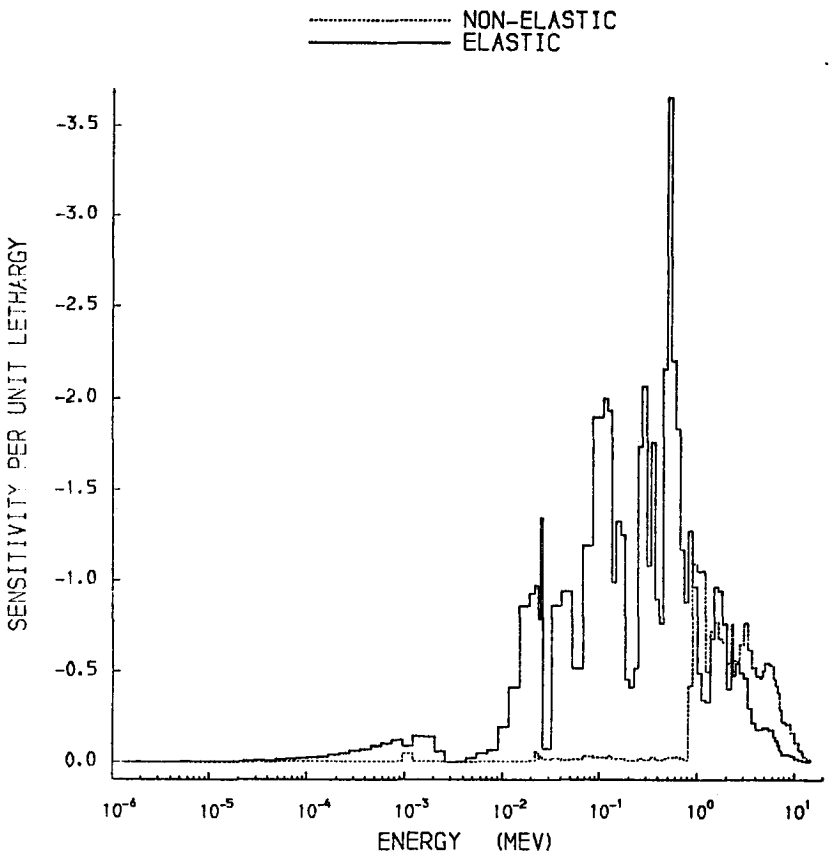

SENSITIVITY PER UNIT LETHARGY
OF SODIUM ACTIVATION RATE IN THE HEAT EXCHANGER
TO IRON CROSS-SECTIONS

FIGURE SIX

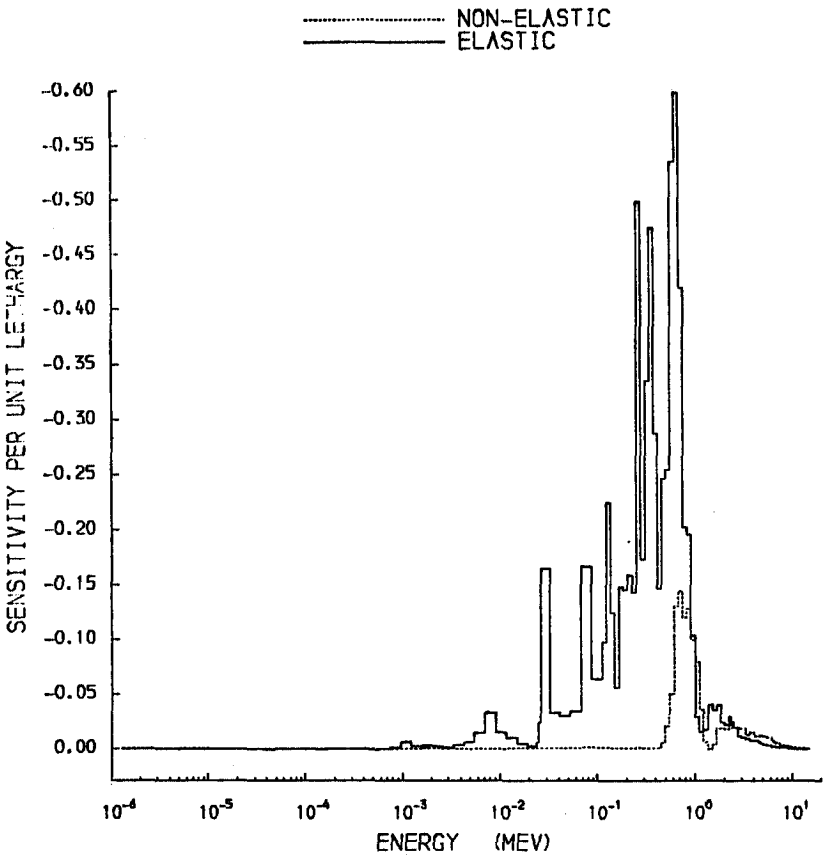

SENSITIVITY PER UNIT LETHARGY
OF IRON DAMAGE RATE IN THE CORE RESTRAINT STRUCTURE
TO SODIUM CROSS-SECTIONS

FIGURE SEVEN

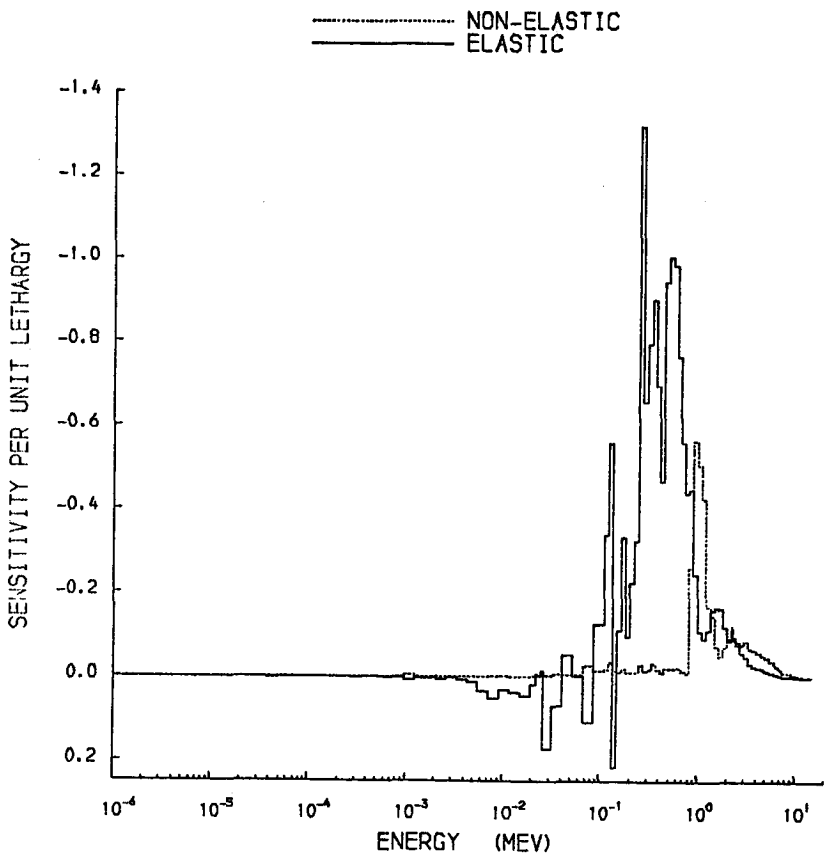

SENSITIVITY PER UNIT LETHARGY
OF IRON DAMAGE RATE IN THE CORE RESTRAINT STRUCTURE
TO IRON CROSS-SECTIONS

FIGURE EIGHT

$$M_{xi} = \frac{1}{\sigma^2(R)} \sum_j \left\{ U_{Ri} U_{Xj} \frac{cov(X_i X_j)}{X_i X_j} + U_{Xi} U_{Nj} \frac{cov(X_i N_j)}{X_i N_j} \right\}$$

$$M_{Ni} = \frac{1}{\sigma^2(R)} \sum_j \left\{ U_{Ri} U_{Nj} \frac{cov(N_i N_j)}{N_i N_j} + U_{Xj} U_{Ri} \frac{cov(X_j N_i)}{X_j N_i} \right\}$$

Measurement sensitivities for the problem studied are shown in figures 9 to 12.

5. Calculation of Upper Limits

Before the general availability of covariance matrices it was suggested in (4) that an upper limit for the fractional uncertainty of a design parameter be found by assuming that full correlation existed between the values of a given cross-section at all energies. This recipe applied to equation 5 leads to

$$\left[\frac{\sigma^2(R)}{R^2}\right]_{MAX} = \sum_j \sum_i \left\{ |U_{xi} U_{xj} - 2\frac{X_j}{N_j} U_{xi} U_{Nj}| \frac{\sigma(X_i)\sigma(X_j)}{X_i X_j} + |U_{Ni} U_{Nj}| \frac{\sigma(N_i)\sigma(N_j)}{N_i N_j} \right\} \quad \ldots 7$$

for the case where $\underline{X}$ and $\underline{T}$ are independent (which applies for the data in this study). In the present analysis regions of significant sensitivity correspond to those where $X_j \ll N_j$ in which case

$$\left[\frac{\sigma^2(R)}{R^2}\right]_{MAX} \simeq \sum_j \sum_i \left\{ |U_{xi} U_{xj}| \frac{\sigma(X_i)\sigma(X_j)}{X_i X_j} + |U_{Ni} U_{Nj}| \frac{\sigma(N_i)\sigma(N_j)}{N_i N_j} \right\} \quad \ldots 8$$

This expression was used to calculate the upper limit of uncertainties quoted in the table of section 6.

6. Results and Discussion

Calculated fractional uncertainties (equation 5) and upper limit uncertainties (equation 8) for the design parameters are shown in the table together with suggested target accuracies (8) for the quantities are shown in the Table.

Table. Results of Uncertainty Analysis

Parameter	Reaction-rate Atom^{-} 5	Uncertainty Per Cent		Target‡ Accuracy%
		Best Estimate	Upper Limit	
Sodium Activation-rate Heat-Exchanger	1.50×10^{-23}	49	83	50
Fe Damage Rate at Edge of Shield	2.16×10^{-10}	3	6	15

‡ This is required to accommodate all sources of uncertainty - conventionally errors in data are required to contribute no more than half of this.

The use of available covariariance data gives uncertainty estimates which are considerably smaller than the upper limit uncertainty estimates. Interestingly, for the case studied, their use does not alter one's view of the adequacy of the data used; both estimates for sodium activation are unsatisfactory and both estimates for the iron damage-rate are satisfactory. Figures 9 and 10 show that only improvement of the sodium elastic scattering cross-sections between roughly 10KeV and 500 KeV will lead to significant reductions in the uncertainty of the sodium activation-rate in the heat-exchanger.

The essential features of the uncertainty analysis are covariance data and a method of calculating sensitivities. Although both of these exist there are serious shortcomings in each. SWANLAKE, for example, is restricted to one-dimensional calculations and it is awkward to use since the sensitivities it calculates often need modifying. In addition SWANLAKE must be provided with multigroup partial cross-sections which are often not considered an essential part of a multigroup cross-section library.

Covariance data is limited in availability and reliability. This results in it being more common to ignore uncertainties due to data than to calculate them.

The shortcomings of covariance data can only be overcome by the release of more evaluated covariance information. The best way to improve the software for calculating uncertainties, though, is not so obvious. One way would be to incorporate a sensitivity capability into a Monte Carlo code which samples point nuclear data. The point data would already exist as partial cross-sections, sensitivities could be estimated at the same time as responses and calculations could be carried out in three dimensions. In addition group-averaging errors, which can be as large as data errors, would be removed.

References

1. Engle, W. W. A One-Dimensional Discrete Ordinates Transport Code with Anisotropic Scattering.
   K-1693 (1967)
2. Dartine D. E. et al. SWANLAKE - A Computer Code Utilising ANLSN Radiation Transport Calculations for Cross-Section Sensitivity Analysis.
   ORNL-TM-3809
3. Lympany, S. D. et al. Contribution to the Exercise on Sensitivity Studies for the NEA Theoretical PWR Benchmark. Proceedings of the NEA Specialists Meeting on Sensitivity Studies and Shielding Benchmarks, Paris 1975.
4. Lympany, S. D. et al. Contribution to the Exercise on Sensitivity Studies for the NEA Theoretical Fast Reactor Benchmark. Ibid.
5. Drischler, J. D., Weisbin, C. R. Compilation of Multigroup Cross-Section Covariance Matrices for Several Important Reactor Materials.
   ORNL-5318
6. Hall, M. C. G. Preliminary Version of the URLIB Variance - Covariance Matrices. To be presented at the NEA Specialists Meeting on Sensitivity Studies, Paris 1979
7. Norget, M. J. et al. Proc. IAEA Specialists Meeting on Radiation Damage for Ferritic and Stainless Steels, Washington 1972
8. Herrenberger V. et al. Required Target Accuracies. Proc. NEA Specialists Meeting on Sensitivity Studies and Shielding Benchmarks, Paris 1975

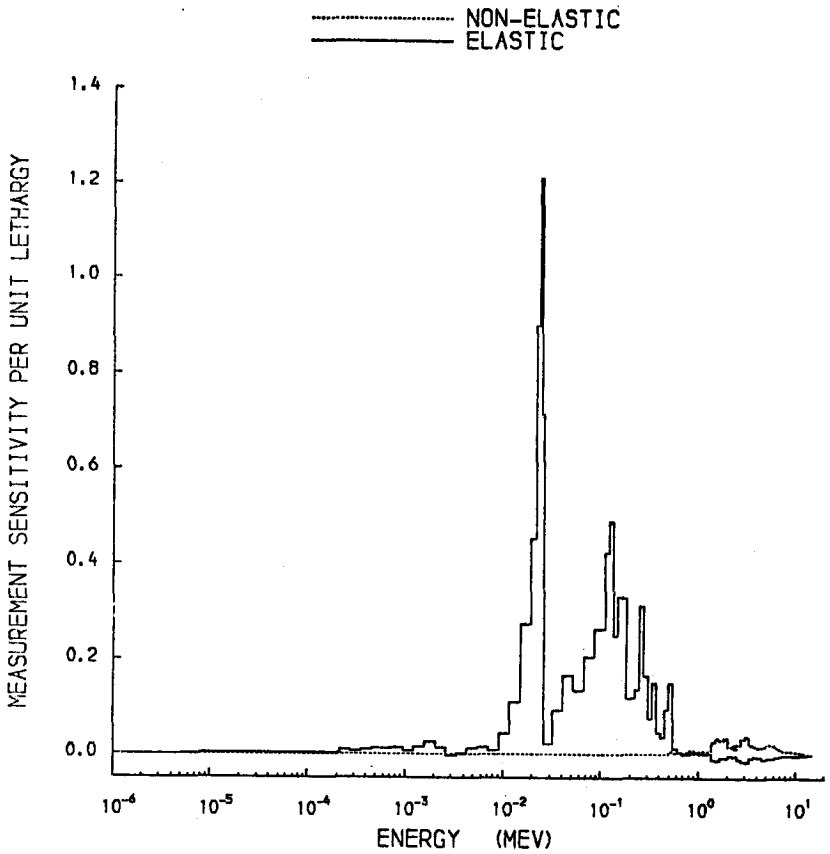

MEASUREMENT SENSITIVITY PER UNIT LETHARGY
OF SODIUM ACTIVATION RATE IN THE HEAT EXCHANGER
TO SODIUM CROSS-SECTIONS

FIGURE NINE

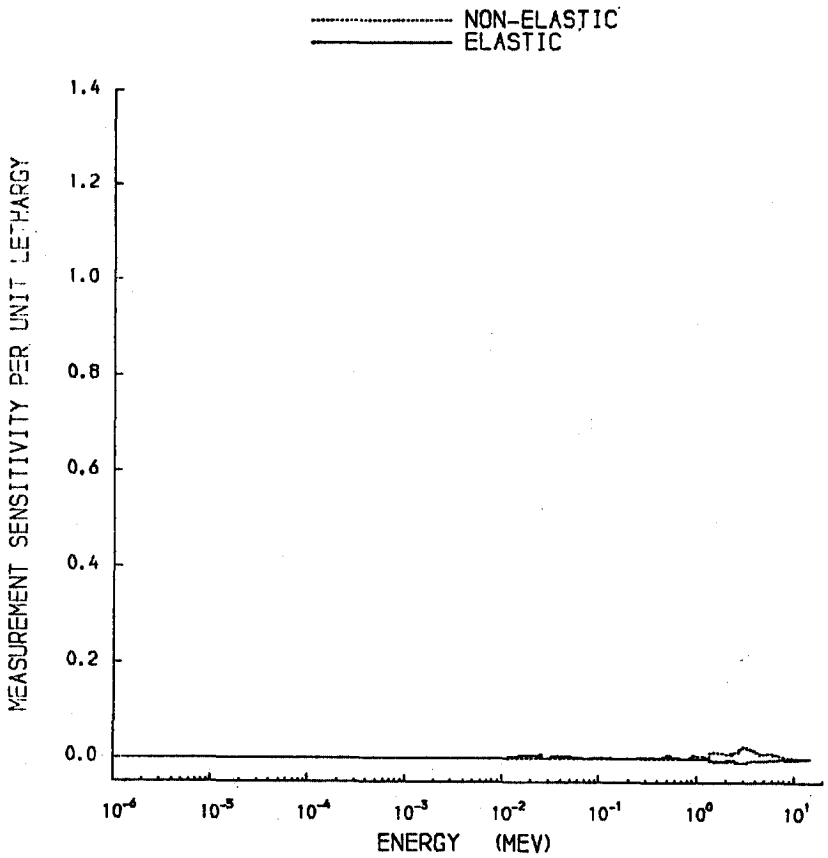

MEASUREMENT SENSITIVITY PER UNIT LETHARGY
OF SODIUM ACTIVATION RATE IN THE HEAT EXCHANGER
TO IRON CROSS-SECTIONS

FIGURE TEN

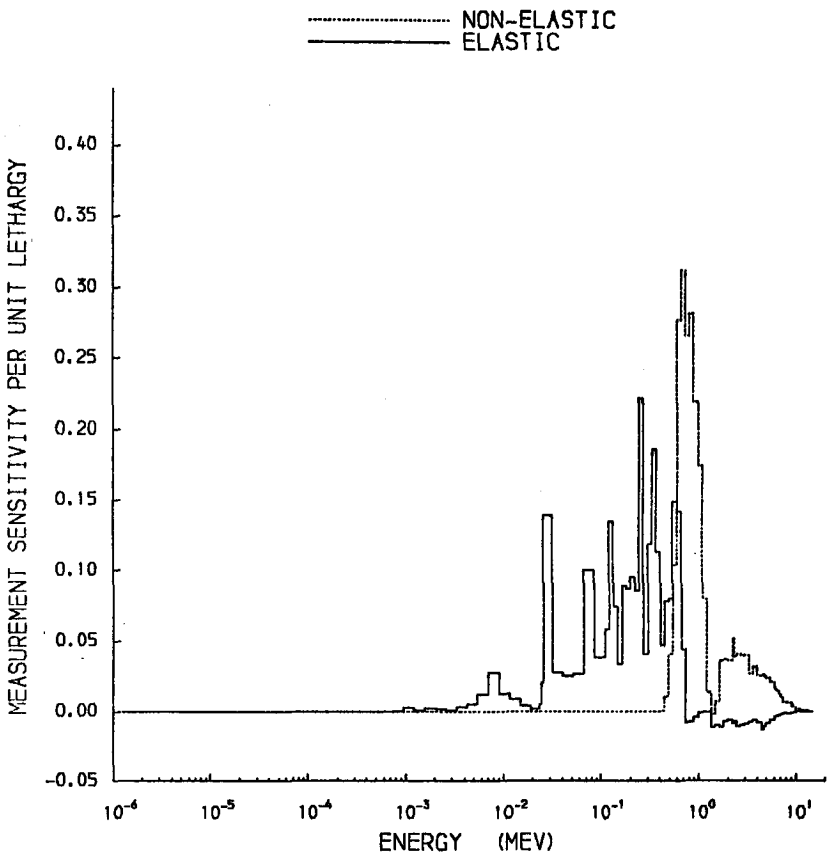

MEASUREMENT SENSITIVITY PER UNIT LETHARGY
OF IRON DAMAGE RATE IN THE CORE RESTRAINT STRUCTURE
TO SODIUM CROSS-SECTIONS

FIGURE ELEVEN

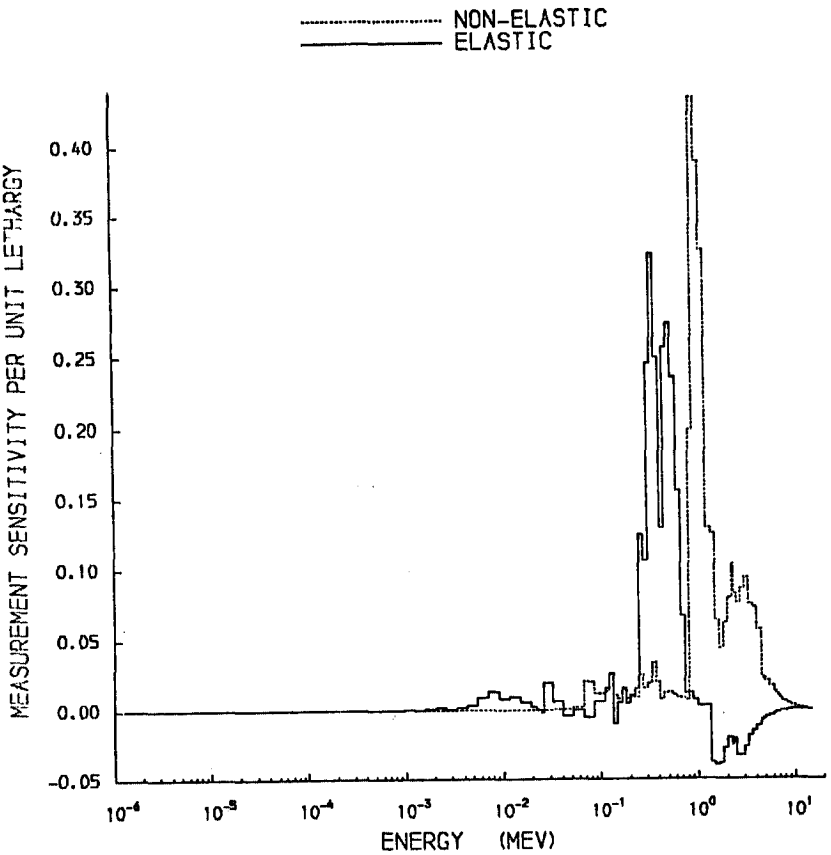

MEASUREMENT SENSITIVITY PER UNIT LETHARGY
OF IRON DAMAGE RATE IN THE CORE RESTRAINT STRUCTURE
TO IRON CROSS-SECTIONS

FIGURE TWELVE

A P P E N D I X A

CALCULATIONAL MODEL

TABLE A1 Model of Core and Radial Shield

Region Description	Thickness cm	Outer Radius cm	Composition Volume Fraction
Inner core	115.54	115.54	CORE1 0.8889/Na 0.1111
Outer core	39.31	154.85	CORE2 0.8889/Na 0.1111
Hollow fuel breeder	15.19	170.04	BREEDER1 1.00
Solid fuel breeder	26.90	196.94	BREEDER2 1.00
On-lattice shield	64.95	261.89	M316 0.75/Na 0.25
Sodium	47.06	420.00	Na 1.00
Low density steel shield	220.00	640.00	CRM-2 0.20/Na 0.80
High density steel shield	30.00	670.00	CRM-2 0.67/Na 0.33
Sodium	20.00	690.00	Na 1.00
IHX sheath	3.00	693.00	EN58B 1.00
IHX tube bundle	80.00	773.00	EN58B 0.0427/Na 0.9573
IHX inner tube	122.00	895.00	Na 1.00
IHX tube bundle	100.00	995.00	EN58B 0.0427/Na 0.9573

TABLE A2

Compositions and Densities of the Materials in Table A1

Mixture	Density gr/cm^3	Element (weight percentages)											
		Fe	Cr	Ni	Mo	Mn	Na	C	O	^{235}U	^{238}U	^{239}Pu	^{240}Pu
Inner core CORE1	4.926	15.98	5.52	8.53	0.90	0.31	8.22		7.17	0.18	44.03	7.57	1.59
Outer core CORE2	4.934	15.97	5.52	8.52	0.90	0.31	8.22		7.23	0.16	40.21	10.70	2.25
Hollow fuel breeder BREEDER1	7.585	9.83	3.54	6.65	5.25	0.16	6.92	3.29		0.26	64.09		
Solid fuel breeder BREEDER2	8.550	8.45	2.91	5.07	4.94	0.15	2.74	3.67		0.29	71.76		
M316 steel	7.97	65.12	17.14	13.61	2.42	1.71							
Na (temp 470°C)	0.8394						1.00						
CRM-2 steel	7.80	96.75	2.25		1.00								
EN58B steel	7.80	73.00	18.00	8.00		1.00							
UK Data File No.		906	45	907	81	88	182	902	933	159	160	159	159

TABLE A3

Neutron Sources in Core and Breeder Regions (3230 MW)

Region	Radius cm	Source n/cm^3-sec at core mid-height
Inner core	0	3.94,13
	11.55	3.87,13
	23.11	3.79,13
	34.66	3.78,13
	46.21	3.77,13
	57.77	3.70,13
	69.32	3.64,13
	80.88	3.62,13
	92.43	3.52,13
	103.99	3.39,13
	115.54	3.26,13
Outer core	115.54	4.09,13
	123.40	3.86,13
	131.26	3.56,13
	139.13	3.14,13
	146.99	2.67,13
	154.85	2.17,13
Hollow fuel radial breeder	154.85	6.92,12
	157.89	6.38,12
	160.93	5.83,12
	163.96	5.28,12
	167.00	4.73,12
	170.04	4.18,12
Solid fuel radial breeder	170.04	6.88,12
	175.42	5.15,12
	180.80	3.56,12
	186.18	2.27,12
	191.56	1.85,12
	196.94	1.33,12

APPENDIX B

FIFTEEN-GROUP FRACTICNAL COVARIANCE MATRICES FOR SODIUM AND IRON

ELEMENTS OF THE CORRELATION MATRIX (10**3) FOR
MATERIAL 1156 REACTION 1 WITH RESPECT TO MATERIAL 1156 REACTION 1

$Na(T,T)$

ENERGY RANGE (EV)	% REL STD-DEV	GROUP	1	2	3	4	5	6	7	8	9	10	11	12	13	14	15
1.492E+07-- 4.400E+06	3.2	1	1000														
4.400E+06-- 2.600E+06	3.3	2	516	1000													
2.600E+06-- 1.350E+06	2.7	3	457	812	1000												
1.350E+06-- 7.080E+05	2.6	4	471	463	581	1000											
7.080E+05-- 5.800E+05	3.5	5	359	353	423	693	1000										
5.800E+05-- 4.100E+05	3.7	6	340	334	400	413	566	1000									
4.100E+05-- 3.095E+05	5.0	7	26	25	30	31	24	88	1000								
3.095E+05-- 2.620E+05	4.6	8	0	0	0	0	0	0	159	1000							
2.620E+05-- 6.200E+04	3.4	9	0	0	0	0	0	0	88	191	1000						
6.200E+04-- 3.000E+04	9.4	10	0	0	0	0	0	0	0	0	184	1000					
3.000E+04-- 1.500E+04	6.7	11	0	0	0	0	0	0	0	0	225	143	1000				
1.500E+04-- 1.585E+03	6.2	12	0	0	0	0	0	0	0	0	245	156	236	1000			
1.585E+03-- 2.145E+02	4.2	13	0	0	0	0	0	0	0	0	225	143	199	304	1000		
2.145E+02-- 1.068E+01	7.0	14	0	0	0	0	0	0	0	0	0	0	0	0	638	1000	
1.068E+01-- 5.043E+00	7.0	15	0	0	0	0	0	0	0	0	0	0	0	0	638	1000	1000

ELEMENTS OF THE CORRELATION MATRIX (10**3) FOR
MATERIAL 1156 REACTION 2 WITH RESPECT TO MATERIAL 1156 REACTION 2

$Na(N,N)$

ENERGY RANGE (EV)	% REL STD-DEV	GROUP	1	2	3	4	5	6	7	8	9	10	11	12	13	14	15
1.492E+07-- 4.400E+06	52.5	1	1000														
4.400E+06-- 2.600E+06	22.6	2	907	1000													
2.600E+06-- 1.350E+06	6.5	3	722	847	1000												
1.350E+06-- 7.080E+05	3.7	4	51	82	409	1000											
7.080E+05-- 5.800E+05	3.7	5	48	76	278	658	1000										
5.800E+05-- 4.100E+05	3.7	6	46	74	218	343	556	1000									
4.100E+05-- 3.095E+05	5.0	7	3	6	16	25	23	88	1000								
3.095E+05-- 2.620E+05	4.6	8	0	0	0	0	0	0	159	1000							
2.620E+05-- 6.200E+04	3.9	9	0	0	0	0	0	0	77	167	1000						
6.200E+04-- 3.000E+04	6.0	10	0	0	0	0	0	0	0	0	882	1000					
3.000E+04-- 1.500E+04	6.0	11	0	0	0	0	0	0	0	0	882	1000	1000				
1.500E+04-- 1.585E+03	6.0	12	0	0	0	0	0	0	0	0	882	1000	1000	1000			
1.585E+03-- 2.145E+02	4.2	13	0	0	0	0	0	0	0	0	674	765	765	765	1000		
2.145E+02-- 1.068E+01	7.0	14	0	0	0	0	0	0	0	0	0	0	0	0	634	1000	
1.068E+01-- 5.043E+00	7.1	15	0	0	0	0	0	0	0	0	0	0	0	0	634	1000	1000

$N_a(x,x)$

ELEMENTS OF THE CORRELATION MATRIX (10**3) FOR
MATERIAL 1156 REACTION 3 WITH RESPECT TO MATERIAL 1156 REACTION 3

ENERGY RANGE (EV)	% REL STD-DEV	GROUP	1	2	3	4	5	6	7	8	9	10	11	12	13	14	15
1.492E+07-- 4.400E+06	42.6	1	1000														
4.400E+06-- 2.600E+06	41.2	2	922	1000													
2.600E+06-- 1.350E+06	21.8	3	819	908	1000												
1.350E+06-- 7.080E+05	16.9	4	0	0	322	1000											
7.080E+05-- 5.800E+05	17.0	5	0	0	320	877	1000										
5.800E+05-- 4.100E+05	20.3	6	0	0	266	653	725	1000									
4.100E+05-- 3.095E+05	50.0	7	0	0	0	0	0	7	1000								
3.095E+05-- 2.620E+05	50.0	8	0	0	0	0	0	7	1000	1000							
2.620E+05-- 6.200E+04	20.2	9	0	0	0	0	0	6	774	774	1000						
6.200E+04-- 3.000E+04	13.8	10	0	0	0	0	0	0	0	0	160	1000					
3.000E+04-- 1.500E+04	14.5	11	0	0	0	0	0	0	0	0	115	442	1000				
1.500E+04-- 1.585E+03	12.1	12	0	0	0	0	0	0	0	0	137	293	297	1000			
1.585E+03-- 2.145E+02	7.4	13	0	0	0	0	0	0	0	0	136	290	276	998	1000		
2.145E+02-- 1.068E+01	1.0	14	0	0	0	0	0	0	0	0	0	0	0	0	54	1000	
1.068E+01-- 5.043E+00	1.0	15	0	0	0	0	0	0	0	0	0	0	0	0	54	1000	1000

$N_a(N,T)$

ELEMENTS OF THE CORRELATION MATRIX (10**3) FOR
MATERIAL 1156 REACTION 1 WITH RESPECT TO MATERIAL 1156 REACTION 2 T

ENERGY RANGE (EV)	GROUP	1	2	3	4	5	6	7	8	9	10	11	12	13	14	15
1.492E+07-- 4.400E+06	1	136	70	62	64	49	46	3	0	0	0	0	0	0	0	0
4.400E+06-- 2.600E+06	2	114	222	180	103	78	74	6	0	0	0	0	0	0	0	0
2.600E+06-- 1.350E+06	3	240	428	527	306	223	211	16	0	0	0	0	0	0	0	0
1.350E+06-- 7.080E+05	4	377	371	465	800	555	330	25	0	0	0	0	0	0	0	0
7.080E+05-- 5.800E+05	5	350	344	412	675	975	551	23	0	0	0	0	0	0	0	0
5.800E+05-- 4.100E+05	6	340	334	400	413	566	1000	88	0	0	0	0	0	0	0	0
4.100E+05-- 3.095E+05 N	7	26	25	30	31	24	88	1000	159	88	0	0	0	0	0	0
3.095E+05-- 2.620E+05	8	0	0	0	0	0	0	159	1000	191	0	0	0	0	0	0
2.620E+05-- 6.200E+04	9	0	0	0	0	0	0	77	167	874	161	197	214	197	0	0
6.200E+04-- 3.000E+04	10	0	0	0	0	0	0	0	0	286	1560	224	243	223	0	0
3.000E+04-- 1.500E+04	11	0	0	0	0	0	0	0	0	252	160	1118	264	223	0	0
1.500E+04-- 1.585E+03	12	0	0	0	0	0	0	0	0	252	161	243	1030	313	0	0
1.585E+03-- 2.145E+02	13	0	0	0	0	0	0	0	0	223	142	198	302	993	634	634
2.145E+02-- 1.068E+01	14	0	0	0	0	0	0	0	0	0	0	0	0	638	1000	1000
1.068E+01-- 5.043E+00	15	0	0	0	0	0	0	0	0	0	0	0	0	638	1000	1000

ELEMENTS OF THE CORRELATION MATRIX (10**3) FOR
MATERIAL 1156 REACTION 2 WITH RESPECT TO MATERIAL 1156 REACTION 3

N

ENERGY RANGE (EV)	GROUP	1	2	3	4	5	6	7	8	9	10	11	12	13	14	15
1.492E+07-- 4.400E+06	1	-991	-899	-696	0	0	0	0	0	0	0	0	0	0	0	0
4.400E+06-- 2.600E+06	2	-914	-975	-771	0	0	0	0	0	0	0	0	0	0	0	0
2.600E+06-- 1.350E+06	3	-811	-885	-850	-193	-72	-8	0	0	0	0	0	0	0	0	0
1.350E+06-- 7.080E+05	4	0	0	-273	-599	-196	-20	0	0	0	0	0	0	0	0	0
7.080E+05-- 5.800E+05	5	0	0	-272	-526	-224	-23	0	0	0	0	0	0	0	0	0
5.800E+05-- 4.100E+05	6	0	0	-227	-392	-162	-31	0	0	0	0	0	0	0	0	0
4.100E+05-- 3.095E+05	7	0	0	0	0	0	0	-1	-2	-1	0	0	0	0	0	0
3.095E+05-- 2.620E+05	8	0	0	0	0	0	0	-1	-2	-1	0	0	0	0	0	0
2.620E+05-- 6.200E+04	9	0	0	0	0	0	0	-1	-2	-1	0	0	0	0	0	0
6.200E+04-- 3.000E+04	10	0	0	0	0	0	0	0	0	0	0	0	0	0	0	0
3.000E+04-- 1.500E+04	11	0	0	0	0	0	0	0	0	0	0	0	0	0	0	0
1.500E+04-- 1.585E+03	12	0	0	0	0	0	0	0	0	0	0	0	0	0	0	0
1.585E+03-- 2.145E+02	13	0	0	0	0	0	0	0	0	0	0	0	0	0	0	0
2.145E+02-- 1.068E+01	14	0	0	0	0	0	0	0	0	0	0	0	0	0	-1	-2
1.068E+01-- 5.043E+00	15	0	0	0	0	0	0	0	0	0	0	0	0	0	-1	-2

Na(N,X) X

ELEMENTS OF THE CORRELATION MATRIX (10**3) FOR
MATERIAL 1192 REACTION 1 WITH RESPECT TO MATERIAL 1192 REACTION 1

ENERGY RANGE (EV)	% REL STD-DEV	GROUP	1	2	3	4	5	6	7	8	9	10	11	12	13	14	15
1.492E+07-- 4.400E+06	1.4	1	1000														
4.400E+06-- 2.600E+06	2.4	2	41	1000													
2.600E+06-- 1.350E+06	1.6	3	0	45	1000												
1.350E+06-- 7.080E+05	1.5	4	0	0	175	1000											
7.080E+05-- 5.800E+05	2.6	5	0	0	0	502	1000										
5.800E+05-- 4.100E+05	2.2	6	0	0	0	0	170	1000									
4.100E+05-- 3.095E+05	3.0	7	0	0	0	0	0	456	1000								
3.095E+05-- 2.620E+05	2.8	8	0	0	0	0	0	36	79	1000							
2.620E+05-- 6.200E+04	1.2	9	0	0	0	0	0	0	0	46	1000						
6.200E+04-- 3.000E+04	3.5	10	0	0	0	0	0	0	0	0	7	1000					
3.000E+04-- 1.500E+04	4.2	11	0	0	0	0	0	0	0	0	0	666	1000				
1.500E+04-- 1.585E+03	6.3	12	0	0	0	0	0	0	0	0	0	180	186	1000			
1.585E+03-- 2.145E+02	2.2	13	0	0	0	0	0	0	0	0	0	110	93	509	1000		
2.145E+02-- 1.068E+01	0.0	14	0	0	0	0	0	0	0	0	0	0	0	0	0	0	
1.068E+01-- 5.043E+00	0.0	15	0	0	0	0	0	0	0	0	0	0	0	0	0	0	0

Fe (T,T)

ELEMENTS OF THE CORRELATION MATRIX (10**3) FOR
MATERIAL 1192 REACTION 2 WITH RESPECT TO MATERIAL 1192 REACTION 2

Fe (N,N)

ENERGY RANGE (EV)	% REL STD-DEV	GROUP	1	2	3	4	5	6	7	8	9	10	11	12	13	14	15
1.492E+07-- 4.400E+06	12.2	1	1000														
4.400E+06-- 2.600E+06	9.3	2	21	1000													
2.600E+06-- 1.350E+06	3.5	3	13	619	1000												
1.350E+06-- 7.080E+05	1.8	4	0	0	187	1000											
7.080E+05-- 5.800E+05	2.6	5	0	0	0	473	1000										
5.800E+05-- 4.100E+05	2.2	6	0	0	0	0	170	1000									
4.100E+05-- 3.095E+05	3.0	7	0	0	0	0	0	456	1000								
3.095E+05-- 2.620E+05	2.8	8	0	0	0	0	0	36	79	1000							
2.620E+05-- 6.200E+04	1.2	9	0	0	0	0	0	0	0	46	1000						
6.200E+04-- 3.000E+04	3.5	10	0	0	0	0	0	0	0	0	7	1000					
3.000E+04-- 1.500E+04	4.2	11	0	0	0	0	0	0	0	0	0	666	1000				
1.500E+04-- 1.585E+03	6.3	12	0	0	0	0	0	0	0	0	0	180	186	1000			
1.585E+03-- 2.145E+02	4.6	13	0	0	0	0	0	0	0	0	0	53	45	247	1000		
2.145E+02-- 1.068E+01	5.0	14	0	0	0	0	0	0	0	0	0	0	0	0	872	1000	
1.068E+01-- 5.043E+00	5.0	15	0	0	0	0	0	0	0	0	0	0	0	0	872	1000	1000

ELEMENTS OF THE CORRELATION MATRIX (10**3) FOR
MATERIAL 1192 REACTION 3 WITH RESPECT TO MATERIAL 1192 REACTION 3

Fe (X,X)

ENERGY RANGE (EV)	% REL STD-DEV	GROUP	1	2	3	4	5	6	7	8	9	10	11	12	13	14	15
1.492E+07-- 4.400E+06	14.1	1	1000														
4.400E+06-- 2.600E+06	15.5	2	20	1000													
2.600E+06-- 1.350E+06	7.9	3	17	845	1000												
1.350E+06-- 7.080E+05	5.8	4	0	0	326	1000											
7.080E+05-- 5.800E+05	20.0	5	0	0	0	19	1000										
5.800E+05-- 4.100E+05	15.6	6	0	0	0	18	941	1000									
4.100E+05-- 3.095E+05	20.0	7	0	0	0	0	0	338	1000								
3.095E+05-- 2.620E+05	20.0	8	0	0	0	0	0	338	1000	1000							
2.620E+05-- 6.200E+04	13.0	9	0	0	0	0	0	234	691	691	1000						
6.200E+04-- 3.000E+04	9.9	10	0	0	0	0	0	0	0	0	38	1000					
3.000E+04-- 1.500E+04	10.3	11	0	0	0	0	0	0	0	0	0	473	1000				
1.500E+04-- 1.585E+03	12.4	12	0	0	0	0	0	0	0	0	0	392	388	1000			
1.585E+03-- 2.145E+02	23.0	13	0	0	0	0	0	0	0	0	0	191	188	157	1000		
2.145E+02-- 1.068E+01	1.0	14	0	0	0	0	0	0	0	0	0	0	0	0	4	1000	
1.068E+01-- 5.043E+00	1.0	15	0	0	0	0	0	0	0	0	0	0	0	0	4	1000	1000

ELEMENTS OF THE CORRELATION MATRIX (10**3) FOR
MATERIAL 1192 REACTION 1 WITH RESPECT TO MATERIAL 1192 REACTION 2

T

ENERGY RANGE (EV)	GROUP	1	2	3	4	5	6	7	8	9	10	11	12	13	14	15
1.492E+07-- 4.400E+06	1	207	8	0	0	0	0	0	0	0	0	0	0	0	0	0
4.400E+06-- 2.600E+06	2	16	393	18	0	0	0	0	0	0	0	0	0	0	0	0
2.600E+06-- 1.350E+06	3	0	28	623	109	0	0	0	0	0	0	0	0	0	0	0
1.350E+06-- 7.080E+05	4	0	0	165	983	473	0	0	0	0	0	0	0	0	0	0
7.080E+05-- 5.800E+05	5	0	0	0	502	1000	170	0	0	0	0	0	0	0	0	0
5.800E+05-- 4.100E+05	6	0	0	0	0	170	1000	456	36	0	0	0	0	0	0	0
4.100E+05-- 3.095E+05	7	0	0	0	0	0	456	1000	79	0	0	0	0	0	0	0
3.095E+05-- 2.620E+05	8	0	0	0	0	0	36	79	1000	46	0	0	0	0	0	0
2.620E+05-- 6.200E+04	9	0	0	0	0	0	0	0	46	1000	7	0	0	0	0	0
6.200E+04-- 3.000E+04	10	0	0	0	0	0	0	0	0	7	1000	666	180	110	0	0
3.000E+04-- 1.500E+04	11	0	0	0	0	0	0	0	0	0	666	1000	186	93	0	0
1.500E+04-- 1.585E+03	12	0	0	0	0	0	0	0	0	0	180	186	1000	509	0	0
1.585E+03-- 2.145E+02	13	0	0	0	0	0	0	0	0	0	53	45	247	485	0	0
2.145E+02-- 1.068E+01	14	0	0	0	0	0	0	0	0	0	0	0	0	0	0	0
1.068E+01-- 5.043E+00	15	0	0	0	0	0	0	0	0	0	0	0	0	0	0	0

$F_e(\bar{T}N)$ N

ELEMENTS OF THE CORRELATION MATRIX (10**3) FOR
MATERIAL 1192 REACTION 2 WITH RESPECT TO MATERIAL 1192 REACTION 3

N

ENERGY RANGE (EV)	GROUP	1	2	3	4	5	6	7	8	9	10	11	12	13	14	15
1.492E+07-- 4.400E+06	1	-978	-18	-13	0	0	0	0	0	0	0	0	0	0	0	0
4.400E+06-- 2.600E+06	2	-20	-920	-661	0	0	0	0	0	0	0	0	0	0	0	0
2.600E+06-- 1.350E+06	3	-16	-777	-782	-108	0	0	0	0	0	0	0	0	0	0	0
1.350E+06-- 7.080E+05	4	0	0	-255	-332	0	0	0	0	0	0	0	0	0	0	0
7.080E+05-- 5.800E+05	5	0	0	0	-6	-18	-9	0	0	0	0	0	0	0	0	0
5.800E+05-- 4.100E+05	6	0	0	0	-6	-17	-10	-3	-5	-4	0	0	0	0	0	0
4.100E+05-- 3.095E+05	7	0	0	0	0	0	-3	-9	-14	-11	0	0	0	0	0	0
3.095E+05-- 2.620E+05	8	0	0	0	0	0	-3	-9	-14	-11	0	0	0	0	0	0
2.620E+05-- 6.200E+04	9	0	0	0	0	0	-2	-6	-10	-17	0	0	0	0	0	0
6.200E+04-- 3.000E+04	10	0	0	0	0	0	0	0	0	-1	-4	-1	-1	-12	0	0
3.000E+04-- 1.500E+04	11	0	0	0	0	0	0	0	0	0	-2	-3	-1	-12	0	0
1.500E+04-- 1.585E+03	12	0	0	0	0	0	0	0	0	0	-2	-1	-3	-10	0	0
1.585E+03-- 2.145E+02	13	0	0	0	0	0	0	0	0	0	-1	-1	-1	-62	0	0
2.145E+02-- 1.068E+01	14	0	0	0	0	0	0	0	0	0	0	0	0	0	-1	-3
1.068E+01-- 5.043E+00	15	0	0	0	0	0	0	0	0	0	0	0	0	0	-1	-3

$F_e(N,X)$ X

THE APPLICATION OF DUCKPOND TO THE OAK RIDGE PCA CALCULATIONAL BLIND TEST

by

M C G Hall*
A K McCracken
A Packwood

Radiation Physics and Shielding Group
Reactor Physics Division
AEE Winfrith

* Work performed during authors attachment to Radiation Physics and Shielding Group, Reactor Physics Division, AEE Winfrith

1 INTRODUCTION

The Pool Critical Assembly (PCA) at Oak Ridge was an experimental simulation of the shield and pressure-vessel regions of a Pressurised Water Reactor.

Extensive measurements were carried out and laboratories were invited to calculate "blind", ie without knowledge of the experimental results, various quantities throughout the shield. The Technical Letter for the PCA Blind Test (1) published by the Nuclear Regulatory Commission stated:

"The Intent of the Blind Test is to assess current neutron transport theory methods as applied to the publication of neutron penetration in LWR water-steel environments .... The Calculations from the various participants will be compared with each other and with the best available measurements on the PCA benchmark". Hall briefly mentions DUCKPOND calculations for the PCA in (2) and gives a fuller discussion in (3). This note draws on (3) and also includes some unpublished work (4). Sensitivities to cross sections used in the calculation are derived for various reaction-rates in the middle of the simulated pressure-vessel and the influence of data uncertainties on the accuracy of calculation of the 58Ni(n,p)58Co reaction rate in the middle of the pressure vessel is calculated.

2 The Experiment and Calculations

Figure 1 shows in plan the configuration of the PCA experiments and in this paper we concentrate on the prediction of quantities in scoring region A5 - the middle of the simulated pressure vessel. The calculations were carried out with DUCKPOND, a perturbation code based on the Monte Carlo code McBEND (5).

The quantities calculated were the total flux above energies of 1 MeV and 0.1 MeV and the 58Ni(n,p)58Co reaction-rate. The first two of these quantities have often been used as theoretical monitors of physical damage processes and the last of these as an experimental monitor. For the purpose of the blind test the prediction of the 58Ni(n,p)58Co reaction-rate is the most important as this was measured - sensitivities calculated by DUCKPOND of the integral fluxes to cross sections are shown for interest. Tables 1, 2 and 3 show respectively the sensitivities to the iron and oxygen elastic and non elastic group cross sections of the calculated fluxes above 0.1 MeV and 1 MeV and the calculated 58Ni(n,p)58Co reaction-rate. Sensitivities to uranium cross sections and the hydrogen elastic cross section are not given - the former are orders of magnitude smaller than the iron and oxygen cross-section sensitivities and the hydrogen elastic cross section is so well- known as to be of small interest. All the sensitivities not marked with + in the tables are negative. The definition of sensitivity appropriate to these tables is that of common usage, ie

$$U_{ij} = \frac{\partial C_i}{\partial x_j} \frac{x_j}{C_i}$$

where U_{ij} is the sensitivity of calculated reaction C_i to group cross-section x_j.

Table 1 - Sensitivity of the flux 0.1 MeV in position A5 to iron and oxygen cross-sections

Energy Mev	Iron		Oxygen	
	Elastic	Nonelastic	Elastic	Nonelastic
15.0 - 10.0	0.0	0.004	0.004	0.005
10.0 - 7.0	+0.032	0.058	0.054	0.033
7.0 - 4.4	0.054	0.166	0.144	0.018
4.4 - 3.5	0.033	0.069	0.093	0.006
3.5 - 2.6	0.076	0.104	0.132	0.0
2.6 - 1.35	0.187	0.166	0.146	0.0
1.35 - 0.86	0.028	0.026	0.098	0.0

Table 2 - Sensitivity of the flux 1.0 MeV in position A5 to iron and oxygen cross-sections

Energy MeV	Iron		Oxygen	
	Elastic	Nonelastic	Elastic	Nonelastic
15.0 - 10.0	0.003	0.004	0.001	0.004
10.0 - 7.0	+0.021	0.103	0.076	0.043
7.0 - 4.4	0.134	0.304	0.229	0.019
4.4 - 3.5	0.034	0.091	0.058	0.007
3.5 - 2.6	0.204	0.270	0.190	0.0
2.6 - 1.35	0.203	0.577	0.155	0.0
1.35 - 0.86	0.022	0.143	0.014	0.0

Table 3 - Sensitivity of the 58Ni(n,p)58Co reaction-rate at position A5 to iron and oxygen cross-sections

Energy MeV	Iron		Oxygen	
	Elastic	Nonelastic	Elastic	Nonelastic
15.0 - 10.0	0.014	0.024	0.002	0.014
10.0 - 7.0	+0.012	0.368	0.149	0.081
7.0 - 4.4	0.365	0.929	0.431	0.031
4.4 - 3.5	0.059	0.152	0.074	0.006
3.5 - 2.6	0.201	0.288	0.140	0.0
2.6 - 1.35	0.088	0.198	0.043	0.0
1.36 - 0.86	0.001	0.007	0.001	0.0

The results of Table 3 are displayed graphically in a broader group scheme, in Figure 2 which is taken from Reference (3). (Note that the sensitivities have not been normalised to gtoup energy or lethargy width).

The iron non-elastic cross-sections are clearly those which most influence the accuracy of calculation of threshold reaction-rates within the pressure vessel. Using the sensitivities of Tables, 1, 2 and 3 in conjunction with covariance matrices for iron and oxygen given by Drischler[6] and Weisbin we can estimate the uncertainties in the three calculated quantities which arise from uncertainties in the calculational data. Table 4 shows these together with the uncertainties associated with finite Monte Carlo sampling statistics.

Table 4 Contributions to the Total Uncertainty of Calculations from Data Errors and Monte Carlo Statistics

Error Source	Calculated Quantity		
	ϕ>0.1 MeV	ϕ>1.0 MeV	$^{58}Ni(n,p)^{58}Co$
Data	5.0%	9.0%	14.0%
M/C Statistics	4.7%	6.9%	9.5%
Total	6.9% (6.0%)	11.3% (10.2%)	16.9% (15.5%)

The data errors and Monte Carlo statistical errors are independent and are added quadratically to give the total - errors in the $^{58}Ni(n,p)$ cross-section contribute a negligible amount to the total in the last column. The above calculations were the result of a DUCKPOND run of forty minutes on an IBM 370 and we can see immediately that the relatively large contribution of the data errors makes further refinement of the total error by increased Monte Carlo running time a bad economic proposition - the last row, in parenthesis, in Table 4 shows the meagre increase in accuracy that would be achieved by running the Monte Carlo code for eighty minutes instead of forty minutes. This in itself justifies the use of DUCKPOND rather than its faster parent McBEND. For this problem McBEND and DUCKPOND sampled particles roughly in the ratio of 7:4 per unit time. Using McBEND therefore for forty minutes we would have achieved statistical uncertainties of 3.6%, 5.2% and 7.2% instead of respectively 4.7%, 6.9% and 9.5% for the three calculations. We should also grossly underestimate the three uncertainties on the calculations through having no knowledge of the largest components of the errors. The quoted measured value of the $^{58}Ni(n,p)^{58}Co$ reaction-rate (without an error assessment) in position A5 is 2.2×10^{-33} activations per atom per second. This is in reasonable agreement with the calculated value of 1.9 ± 16.9%. Without a knowledge of the data contribution to the total calculational error, the agreement would be much less satisfactory. The information of Tables 1, 2 and 3 also clearly gives a rough idea of those cross-sections whose refinement is important for improving the quality of the calculations. Apparently important cross-sections may, however, be rather well-known, and it might be more profitable to direct one's efforts towards rather badly-known cross-sections of less apparent importance. The most important display parameter, which takes cognisance of this, is the 'measurement sensitivity' $\tilde{I}_K$ defined and used by McCracken[7] et al in 1976:

$$\tilde{I}_K = \frac{\partial \sigma(C)}{\partial \sigma_K} \frac{\sigma_K}{C}$$

where the calculation C has standard deviation $\sigma(C)$ and the K^{th} cross-section has standard deviation σ_K. This parameter is shown in Figure 3 for iron and oxygen cross-sections used in the calculation of the $^{58}Ni(n,p)^{58}Co$ reaction-rate in position A5. Referring to Figure 2, one would attribute top priority to the inspection of the high-energy iron inelastic cross-section, followed by the slightly less important high-energy oxygen elastic and iron elastic cross-sections. Figure 3 supports the first of these judgements but completely refutes the latter two - the iron elastic cross-section is of minor importance and the oxygen elastic cross-section despite the apparent evidence in Figure 2, is not worth a moment's attention.

Acknowledgement

We are obliged to Mr M Austin and Mr A Thomas for making available some unpublished results of their work.

References

1 Technical letter for the PCA Blind Test, US Nuclear Regulatory Commission, 1970.

2 Hall, M C G. *DUCKPOND - A Perturbation Monte Carlo and its Applications*, Paper 6, Session III of this meeting.

3 Hall, M C G. Monte Carlo Perturbation Theory in Neutron Transport Calculations. Thesis, Imperial College, London, 1980.

4 Austin, M, Packwood, A and Thomas, A. Private Communication, 1980.

5 Bendall, D E and Brissenden, R J. McBEND Programme Users Guide. To be published as an AEEW report, 1980.

6 Drischler, J D and Weisbin, C R. Compilation of Multigroup Cross-section Covariance Matrices for Several Important Reactor Materials. ORNL-5318 (END5-235), 1977.

7 McCracken, A K, Packwood, A and Lympany, S. Contribution to the Exercise on Sensitivity Studies for the NEA Theoretical Fast Reactor Benchmark. Proc. Specialists' Meeting on Data Requirements for Shielding Calculations, Vienna, October 1976. IAEA-207.

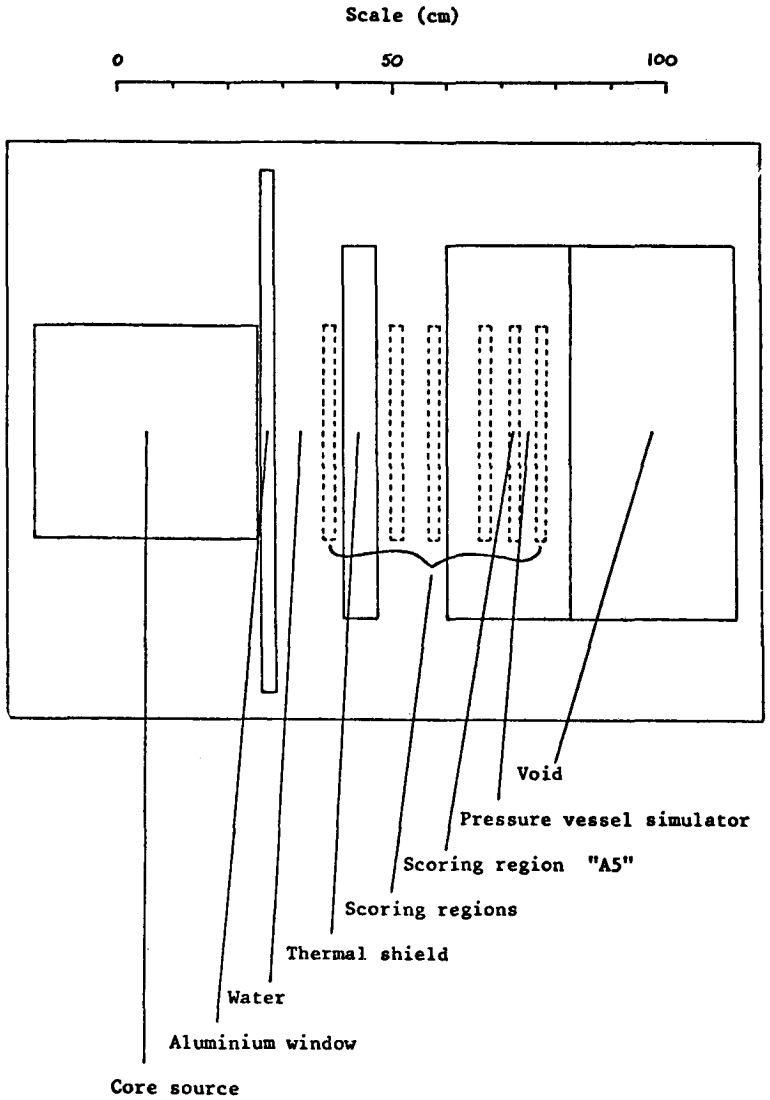

Figure 1 PCA 12/13 Configuration. This is a plan of the geometric model. In an elevation the core is slightly taller.

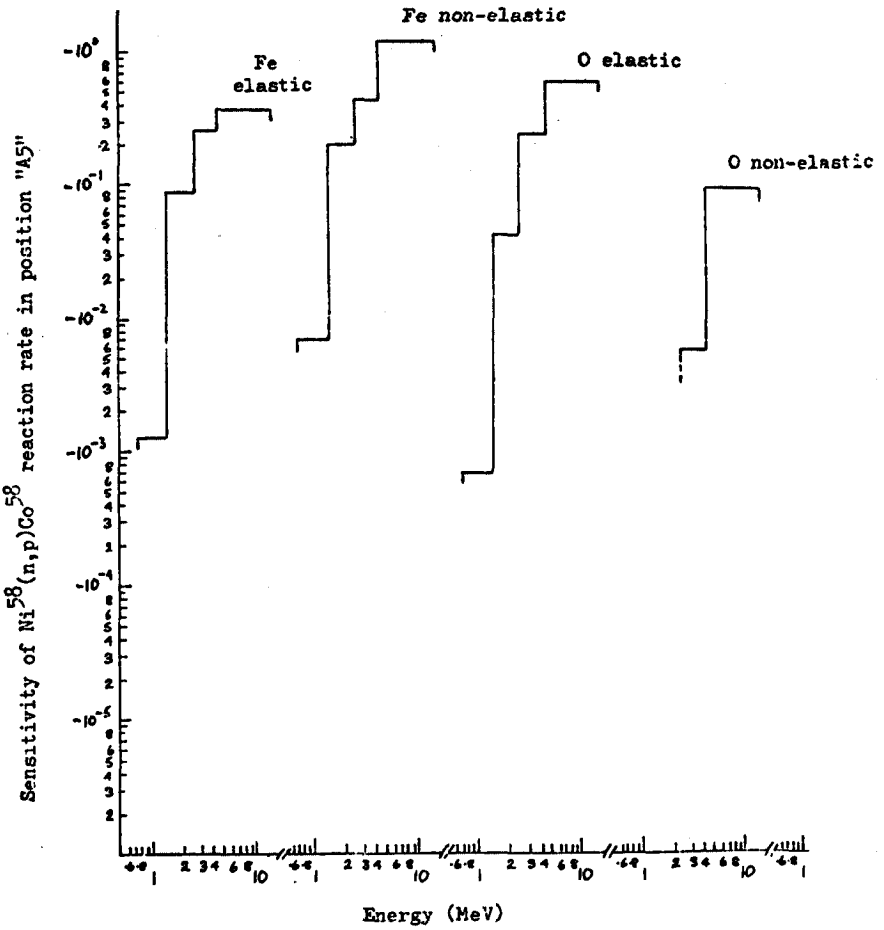

Figure 2. Sensitivities calculated by "Duckpond" for the PCA "Blind Test". The estimated statistical error of the sensitivities was typically about 25%. Sensitivities have been divided by the response, and are dimensionless. All the sensitivities were negative.

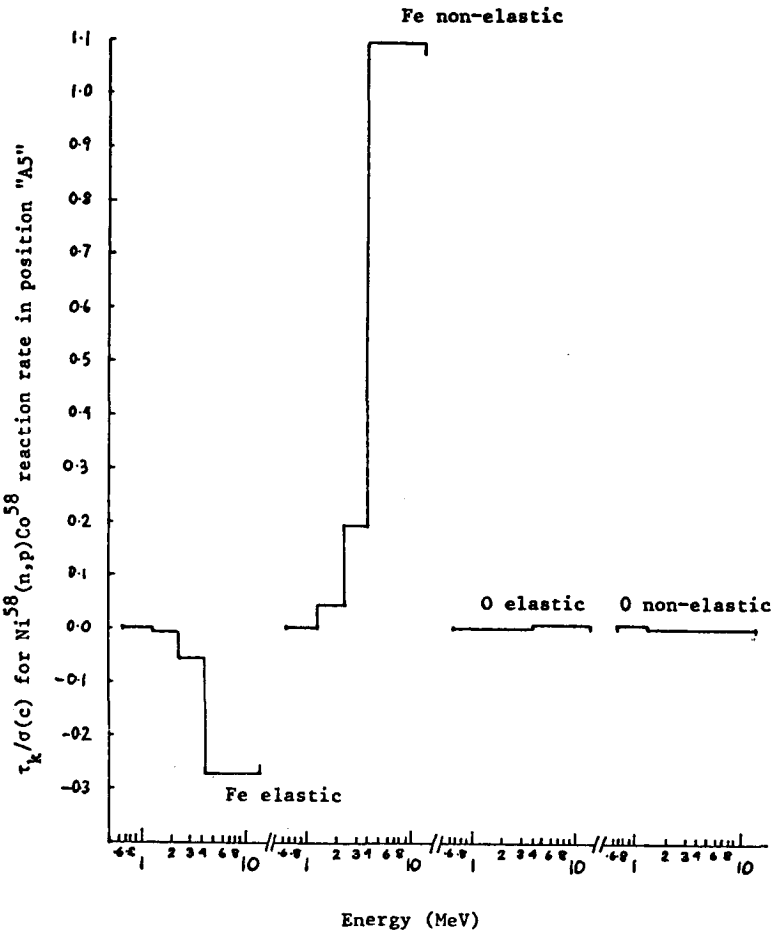

Figure 3 Values of τ_k for the PCA "Blind Test" showing the most useful areas of re-measurement. The values have been divided by $\sigma(c)$, and are dimensionless. Negative values indicate that the corresponding cross-sections are not measured directly.

SESSION III

SENSITIVITY METHODS AND THEIR APPLICATIONS

Chairman - Président

G. HEHN

(Federal Republic of Germany)

SEANCE III

METHODES D'ANALYSE DE SENSIBILITE ET LEURS APPLICATIONS

SUMMARY OF THE SESSION III RESUME DE LA SEANCE III

Sensitivity Methods and their Applications

Dr. G. Hehn

Reports on the development of sensitivity methods for three-dimensional geometries dominated this session. The Monte Carlo codes TIMOC (EURATOM/Ispra), TRIPOLI (CEA/Saclay), and DUCKPOND (AEE/Winfrith) have been used with a correlated tracking option, a method which has already been successfully applied in reactor core perturbation studies (e.g. with MORSE-K at Stuttgart University). However, for application to bulk shielding and for the evaluation of benchmark experiments characterised by deep penetration, the inherent problems of the Monte Carlo method have not been solved. Considerable effort is underway to specialise and improve the correlated tracking method for shielding applications up to medium penetration depths. In this range the sensitivities are normally small, so that a linear perturbation is sufficient. If the group data are improperly weighted in the resonance region, point nuclear data can be used to overcome certain problems. Of course, it is impossible to utilise the fine energy detail of the input cross-sections in the sensitivity output, so that the sensitivity results must be reduced to normal multigroup or few-group structure. Specific attention must be given to the statistical noise of the sensitivity method in data adjustment procedures. In general, the reports presented showed that the Monte Carlo method can be used for sensitivity studies and error analyses, in cases where the representation of the exact three-dimensional geometry is essential.

The code system SAMPO, developed in an Italian-French cooperation, utilises the basic work of refined perturbation theory in a multigroup, one-dimensional transport calculation. The status of the various modules was described. SAMPO can be used for general sensitivity and higher order perturbation studies, variational group condensation, complete error analysis and data adjustment for reproducing integral experiments.

A review paper from Oak Ridge Laboratory presented the status of the FORSS sensitivity and uncertainty analysis system, the first version of which had been demonstrated in an RSIC workshop in 1978 and is now available. The new applications are in two-dimensional sensitivity studies with angular fluxes from DOT and three-dimensional diffusion fluxes from VENTURE. In core physics, time-dependent sensitivities have been investigated for burnup effects. Of special interest are studies showing the importance of resonance self-shielding factors for shielding applications. Uncertainty analyses of integral experiments are in progress with adjustment of the cross sections performed by the modules UNCOVER and ADJUST. Based on ENDF/B-V cross sections and covariance information, the adjusted multigroup library ORACLE is presently under development. The adjustments are confined to measurements in fast reactor and dosimetry integral experiments. An interesting new activity has started with the module NUTCRCKR, in which the inverse problem of reactor sensitivity is solved for more objective data evaluation. Sensitivity studies with the Monte Carlo method were not reported, but the trends in sensitivity studies of more complex geometries and the use of integral experiments for data adjustments are becoming common aims.

The final release of the code SENSIT from Los Alamos Laboratory has coincided with the initiation of new studies on advanced NEA shielding design benchmarks for LWR and fast breeder reactors. The code will be applied in a common test to calculate sensitivity profiles for secondary energy distributions of special interest.

Finally, the application of cross-section sensitivity analysis

to the main shield of the fast reactor JOYO/Japan has been reported. A detailed study has been performed with one- and two-dimensional transport calculations including error analysis and comparison with experimental results.

APPLICATION OF CROSS SECTION SENSITIVITY ANALYSIS TO "JOYO" MAIN SHIELD

N. Ohtani*
M. Yamauchi**, J. Itoh**, and M. Kawai**
* Power Reactor and Nuclear Fuel Development Corporation
** Nippon Atomic Industry Group Co., Ltd.
JAPAN

ABSTRACT

Cross section sensitivities of shielding characteristics, such as dose rate or gamma heating rate, in the main shields of experimental fast reactor "JOYO" are studied with linear perturbation theory by ANISN-SWANLAKE code system.

With regard to materials, reactions, spatial regions and energy ranges, the kinds of cross sections which exert large influences upon shielding calculations are assessed and the errors of the shielding characteristics due to cross section uncertainties are evaluated.

This sensitivity analysis shows that the method is useful for the estimation of the reliability of the shielding design calculation, and for the judgement of the important part of cross sections to reduce the calculational errors.

I. Introduction

"JOYO", the experimental fast reactor in JAPAN, achieved criticality in April 1977, and after the low-power and power-up tests, it is now being operated in 75MW thermal. In these tests, various shielding characteristics were measured in the main shield and it has been proved that the shielding performance of "JOYO" is quite satisfactory.

On the other hand, for the assessments of the shielding design calculations of the fast reactors, shielding characteristics of "JOYO" main shield were analyzed by the detailed two-dimensional discrete ordinate calculations and the calculational results were compared with the measured data. Moreover, in order to evaluate the uncertainties of the two dimensional calculations, effects of selections of the calculational parameters and the uncertainties due to the errors of the cross section data were estimated by one dimensional calculations.

In this paper, the cross section sensitivity analysis for the "JOYO" main shield by ANISN-SWANLAKE code system [1] is reported.

Sensitivities to the cross section data were analyzed for one dimensional models of "JOYO" main shield; in radial direction the region is from the core center to the biological concrete shield, and in axial direction it is from the core center to the pit room upon the shielding plug.

Nuclear group constants used in the analysis were made mainly from ENDF/B-IV file by RADHEAT code system [2], and are composed of 100 neutron energy groups and 20 gamma-ray groups. This set of 120 groups was digenerated and the sensitivities were analyzed in 120, 64 or 28 groups.

Shielding characteristics or detector responses analyzed in this study are,

(1) atomic displacement rate of the reactor vessel,
(2) gamma heating rate in the biological concrete shield,
(3) total dose rate at the outside of the concrete shield, and
(4) total dose rate on the rotating plug.

Sensitivities of responses were obtained both to the macroscopic cross sections of regions and for the microscopic cross sections of elements in each region. Macroscopic cross section analyzed are total, capture, in-group scattering, down-scattering, and secondary gamma-ray production cross sections of sodium, graphite(carbon), SUS304(stainless steel), and concrete. For microscopic cross sections, sensitivities were calculated for total, elastic scattering, inelastic scattering, (n,2n), (n,α), (n,p), (n,γ) and the secondary gamma-ray production cross sections of seven elements such as sodium, iron, chromium, nickel, carbon, silicon and oxigen.

As the results of macroscopic cross section analyses, important cross sections in shielding analyses were shown, that is, sensitivities to the neutron cross sections of sodium and SUS304, and those to the gamma-ray cross sections of concrete are large in radial calculations, and in axial calculations sensitivities to the neutron cross sections of sodium and gamma-ray cross sections of graphite, which is the principal constituent of the rotating plug of "JOYO", are large. Besides, it has become clear that the responses are highly sensitive to the down scattering cross sections of fast neutrons in regions near the core, while sensitivities to the neutron capture and in-group scattering cross sections and those to the gamma-ray cross sections gradually increase as the location comes nearer to the detector region.

Main results of microscopic cross section analyses are as follows: The atomic displacement rate of the reactor vessel and the total dose rate at the outside of the biological concrete shield are both remarkably sensitive to cross sections of sodium and iron. For example, they increase by 2.0% and 3.4% respectively by the 1% decrease of the neutron total cross section of iron. As for the partial cross sections, sensitivities to the elastic scattering cross sections are more than 70% of those to the total cross sections and sensitivities to the inelastic scattering cross sections are at most

20% for both responses. Sensitivities to the other neutron reaction cross sections are comparatively small. As for the spatial distributions of the sensitivities, that of the total dose rate at the outside of the concrete to the capture cross section of iron in the carbon steel between the graphite and the concrete shield is fairly large, and it is 80-90% of that to the total cross section. This sensitivity to the secondary gamma-ray production cross section of iron is also large in this region. This means that the total dose at the outside of the concrete shield is mostly due to the gamma-ray produced in the iron between the graphite and the concrete region.

In this sensitivity study of "JOYO", important materials, reactions, spatial regions and energy ranges for the cross section data were quantitatively estimated, and the errors of shielding characteristics due to uncertainties of cross section data were obtained as an application of this study. Compared with the discrepancies between two dimensional calculations and measurements, the errors due to the cross section data turned out to be not so small.

These sensitivity analyses of "JOYO" show that the sensitivity study and the system of the analysis in this report are very helpful to shielding designs and analyses of fast reactors.

II. Transport Calculation

Nuclear cross section sensitivities of the shielding characteristics in "JOYO" main shield were analyzed by ANISN-SWANLAKE code system. The vertical cross section of "JOYO" is shown in Figure 1, and the analyzed one dimensional models are in Table I. In radial direction, the analyzed region is from the core center to the outside of the biological concrete shield, and in axial direction, it is from the core center to the upside of the shielding plug. In the shielding system of "JOYO", graphite is used in the shielding plug and in the space outside of the reactor vessel.

Nuclear group constants used in this analysis were produced by RADHEAT code system of JAERI and are composed of 100 neutron groups and 20 gamma ray groups. The energy range of neutron is from 14.9MeV to thermal, and that of the gamma ray is from 14MeV to 20keV. Energy group structure of the neutron is identical with that of DLC-2 of ORNL-RSIC, and the structure of the gamma ray is identical with that of EURLIB-2. Angular distribution of the scattering is represented by P-3 approximation. As for the neutron transport cross sections, ENDF/B-IV nuclear data file was processed to the microscopic cross section set JSD100, and the resonance disadvantage factor was multiplied to make effective microscopic and regional macroscopic cross sections. Transport cross sections of gamma ray were calculated by GAMLEG-JR code, and the gamma ray production cross sections were obtained from POPOP-4 library of JAERI.

Sensitivities were analyzed with 120 groups, and also with degenerated sets of 64 and 28 energy groups. Constants of 64 groups were obtained with the weighting flux of (fission+1/E) spectrum, and those of 28 groups were obtained with the spectrum of the one dimensional transport calculation. Group structures of 64 and 28 groups were both chosen not to cancel the effects of resonance peaks and windows.

Neutron and gamma ray transports were calculated by ANISN code with the external distributed sources; the external sources of the forward calculations are the one dimensional profiles of the power distribution multiplied by the fission spectrum. Sources of adjoint calculations are the response functions of shielding characteristics. These are the atomic displacement rate of the reactor vessel, the gamma heating rate in the biological concrete shield, the total dose rate at the outside of the concrete shield, and the total dose rate on the rotating plug.

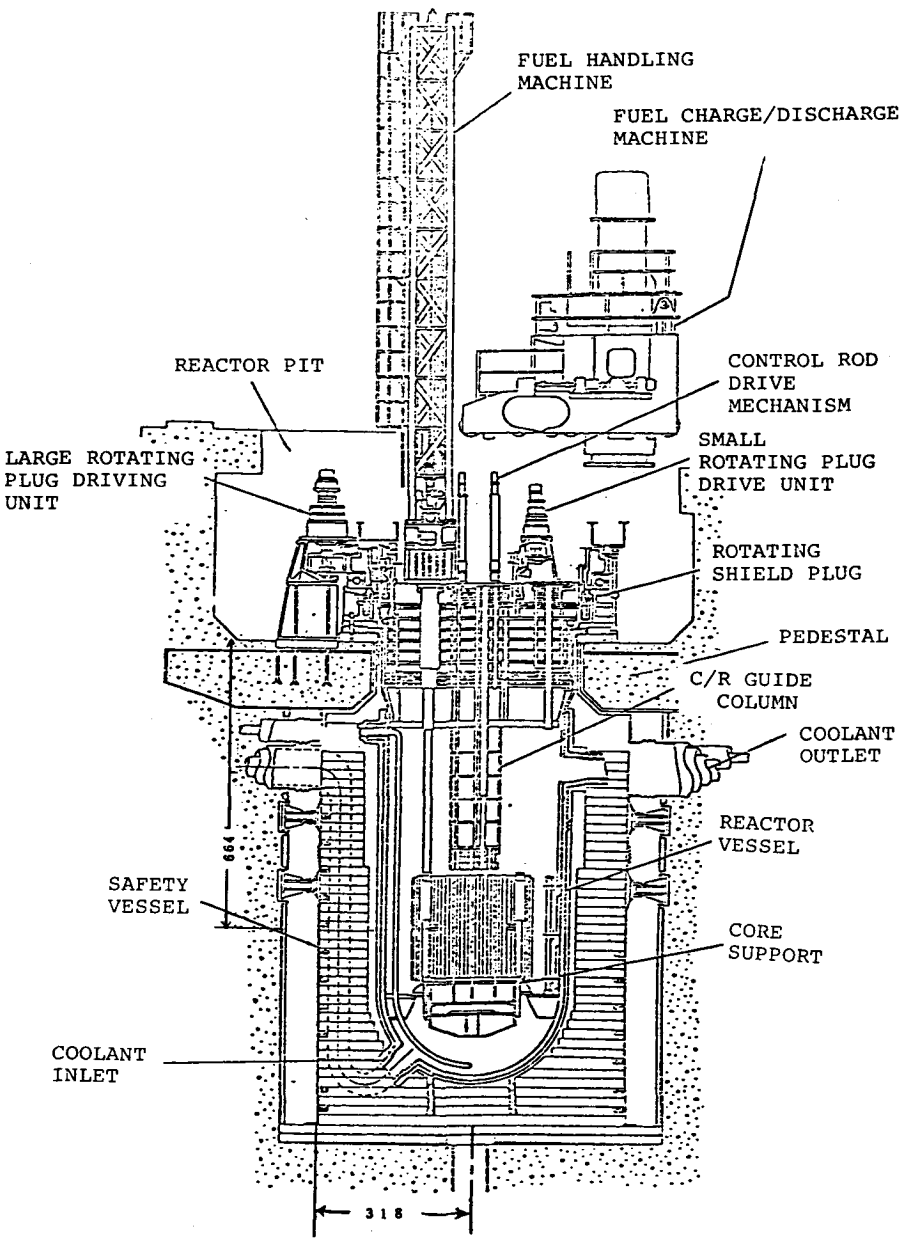

Figure 1 Vertical Cross Section of "JOYO"

Table I

One Dimensional Geometries of "JOYO" Main Shield

Radial

		Radius	Wid.
		0.0	
1	Inner Core		20.4
		20.4	
2	Control Rod		2.56
		23.0	
3	Outer Core		14.5
		37.4	
4	Radial Blanket		32.5
		69.9	
5	Movable Reflector		6.07
		76.0	
6	Sodium		6.01
		82.0	
7	Inner n. Shield		5.0
		87.0	
8	Fuel Strage Rack		22.5
		109.5	
9	Core Barrel		2.5
		112.0	
10	Outer n. Shield		14.0
		126.0	
11	Sodium		24.0
		150.0	
12	Sodium		25.0
		175.0	
13	Thermal Shield		5.0
		180.0	
14	Reactor Vessel		2.5
		182.0	
15	N2 Gas		2.5
		185.0	
16	Leak Jacket		1.2
		186.2	
17	Thermal Insulator		10.0
		196.2	
18	N2 Gas		18.8
		215.0	
19	Graphite		35.0
		250.0	
20	Graphite		35.0
		285.0	
21	Graphite		33.0
		318.0	
22	N2 Gas		2.0
		320.0	
23	Carbon Steel		1.9
		321.9	
24	N2 Gas		64.6
		386.5	
25	Carbon Steel		10.0
		396.5	
26	Carbon Steel Lining		13.5
		400.0	
27	Ordinary Concrete		50.0
		450.0	
28	Ordinary Concrete		50.0
		500.0	
29	Carbon Steel Lining		0.6
		500.6	

Axial

		Hight	Wid.
		773.0	
34	SUS304		10.5
		762.5	
33	Borated Steel		32.0
		730.0	
32	N2 Gas		5.4
		725.1	
31	SUS304		1.8
		723.3	
30	Ar Gas		5.0
		718.3	
29	Graphite		20.0
		698.3	
28	Carbon Steel		3.6
		694.7	
27	Graphite		20.5
		674.2	
26	Carbon Steel		3.6
		670.6	
25	Graphite		20.5
		650.1	
24	Carbon Steel		3.6
		646.5	
23	Graphite		20.5
		626.0	
22	Carbon Steel		3.6
		622.4	
21	Graphite		20.5
		601.9	
20	Carbon Steel		4.2
		597.7	
19	Graphite		20.5
		577.2	
18	Carbon Steel		4.0
		573.2	
17	SUS wool		23.8
		549.4	
16	SUS304		3.0
		546.4	
15	Ar Gas		70.4
		476.0	
14	Sodium		6.0
		470.0	
13	Dip Plate		15.0
		455.0	
12	Sodium		90.0
		365.0	
11	Sodium		90.0
		275.0	
10	Sodium		90.5
		184.5	
9	Above Core Structure		5.0
		179.5	
8	Above Core Structure		8.0
		171.5	
7	Above Core Structure		34.5
		137.0	
6	Handling Head		11.4
		125.6	
5	Wrapper Tube Zone		10.8
		114.3	
4	End Cap (Top)		4.0
		110.8	
3	Gas Plenum Space		40.6
		70.2	
2	Axial Blanket		40.1
		30.1	
1	Inner Core		30.1
		0.0	

In Table II, calculated cases by ANISN are listed. A numerical calculation of a transport equation by ANISN is an established method, but in each case, selections of parameters for the convergence of a solution are not so clear. For example, in Case AR-4 of Table II, the spatial meshes of Case AR-3 were modified mainly in the void regions, and the total mesh number was changed from 422 to 394 for the improvement of convergence. (The results were edited to 422 mesh form and used as an input for SWANLAKE.)

To estimate the convergences of calculations, agreements of the reaction rates by the forward and by the adjoint fluxes were checked; if it is so defined as $R=(\Sigma,\phi)$ and $R^*=(S,\phi^*)$, R should be equal to R* mathematically, and the error of R* from R is one of the parameters for the convergences or accuracies of the numerical solutions. Reaction rates and their discrepancies are shown in Table III. As above mentioned, the adjoint calculation with 422 meshes and the source of the dose conversion factor at the outside of the concrete does not converge near the void regions, and the reaction rate R* does not agree with R. The calculation with modified meshes was carried out. As shown in Table III, the adjoint calculation of 120 groups with the source of the gamma heating rate coefficients at the center of the concrete also does not converge. (Re-calculation was not performed.)

III. Macroscopic Cross Section Sensitivity

General properties of the cross section sensitivities for a fast reactor shielding system were studied by the analyses of the sensitivities to the macroscopic cross sections for the shielding characteristics of "JOYO". These analyses give the important kinds of nuclear reactions, regions and energy ranges for the errors of the shielding calculations.

Sensitivities to the macroscopic cross sections of sodium, SUS304, graphite and ordinary concrete were analyzed for the shielding characteristics of "JOYO", which are the atomic displacement rate of the reactor vessel, the gamma ray heating rate in the biological concrete shield, the total dose rate at the outside of the concrete shield, and the total dose rate on the rotating plug. Table IV shows the sensitivities of the shielding characteristics to the macroscopic total cross sections. In this table, sensitivities are summed up for all regions.

Table V shows the sensitivities of the atomic displacement rate of the reactor vessel to the total neutron cross sections of sodium, SUS304, and carbon of each region. Displacement productions by gamma rays are small and neglected. Among the cross sections analyzed, the sensitivities to the sodium cross section are large and the sum of the sensitivity coefficients for all regions is -3.5, and the sensitivities to the cross section of carbon(graphite) is remarkably small compared with those to sodium and SUS304.

Table IV shows the sensitivities of the total dose rate at the outside of the concrete shield to the total neutron and gamma ray cross sections of sodium, SUS304, carbon and concrete. In this calculational model, 99.9% of the total dose at the outside of the concrete is the dose by gamma ray. Therefore, as for the sodium and SUS304, which are the structural materials mainly near the reactor core, sensitivities to the neutron cross sections are large, while to the cross sections of the concrete, only the sensitivities to the gamma ray cross sections have the significant values. This is because the gamma rays which contribute to the dose are produced inside of the concrete shield and transport in the concrete, and the production of the gamma rays at the outer regions near the concrete depends on the neutron cross sections of the regions near the core.

The sensitivities of the gamma heating rate at the center of the concrete shield were also analyzed, and the behaviours were proved to be similar to those of the total dose rate at the outside of the

Table II Calculations by ANISN

FORWARD

Case	FR-1	FR-2	FR-3	FZ-1
Geometry	Cylinder	Cylinder	Cylinder	Slab
No. of Regions	29	29	29	34
No. of Mesh Intervals	422	422	205	392
No. of Energy Groups	120 (100n+20g)	28 (21n+7g)	64 (57n+7g)	28 (21n+7g)
Source	(Power Distribution)*(Fission Spectrum)			
Source Region	Inner Core, Outer Core, Blanket			Inner Core Axial Blanket
Approx. of Angular Distribution	P3-S8	P3-S8	P3-S8	P3-S8

ADJOINT

Case	AR-1	AR-2	AR-3	AR-4
Geometry	Cylinder	Cylinder	Cylinder	Cylinder
No. of Regions	29	29	29	29
No. of Mesh Intervals	422	422	422	394
No. of Energy Groups	120 (100n+20g)	120 (100n+20g)	28 (21n+7g)	28 (21n+7g)
Source	Atomic Disp. Production C.S. of SUS304	KERMA Factor of Concrete for γ-ray	Dose Conv. Factor	Dose Conv. Factor
Source Position	Reactor Vessel	Center of Concrete	C.Steel Lining outside of Concrete	
Approx. of Angular Distribution	P3-S8	P3-S8	P3-S8	P3-S8

ADJOINT

Case	AR-5	AR-6	AZ-1
Geometry	Cylinder	Cylinder	Slab
No. of Regions	29	29	34
No. of Mesh Intervals	205	205	392
No. of Energy Groups	64 (57n+7g)	64 (57n+7g)	28 (21n-7g)
Source	Dose Conv. Factor	Atomic Disp. Production C.S. of SUS304	Dose Conv. Factor
Source Position	C.Steel Lining outside of Concrete	Reactor Vissel	Top of the Rotating Plug
Approx. of Ang. Dis.	P3-S8	P3-S8	P3-S8

Table III Reaction Rates and Errors

	Reaction	unit	Geom.	ϕ	ϕ^*	$R=<\Sigma\phi>$	$R^*=<S\phi^*>$	R^*/R
1	Displacement Prod. Rate of Reactor Vessel	DPA/year	R	FR-1	AR-1	1.1(-3)	1.1(-3)	1.015
2	Gamma Heating Rate (Center of Concrete)	watt/cm^3	R	FR-1	AR-2	1.8(-7)	2.3(-6)	13.0
3a	Total Dose Rate (Outside of Concrete)	m.rem/hr	R	FR-2	AR-3	1.1(3)	1.4(4)	12.9
3b	Total Dose Rate (Outside of Concrete)	m.rem/hr	R	FR-2	AR-4	1.1(3)	1.2(3)	1.18
4	Displacement Prod. Rate of Reactor Vessel	DPA/year	R	FR-3	AR-6	1.2(-3)	1.3(-3)	1.05
5	Total Dose Rate (Outside of Concrete)	m.rem/hr	R	FR-3	AR-5	1.6(3)	1.8(3)	1.11
6	Total Dose Rate (On the Rotating Plug)	m.rem/hr	Z	FZ-1	AZ-1	7.6(-5)	7.7(-5)	1.00

*) Values are normalized as the total neutron flux at the center of the core is 3.2(15) n/cm /sec.
**) DPA: Displacement Per Atom
1.1(-3) means 1.1×10^{-3}

Table IV Sensitivities to the Macroscopic Cross Sections (sum of all regions)

	Sodium	SUS304	Carbon	Concrete
	Neutron (Gamma)	Neutron (Gamma)	Neutron (Gamma)	Neutron (Gamma)
Displacement Prod. Rate of Reactor Vessel	-3.468 (-)	-2.184 (-)	-0.024 (-)	0.0 (-)
Gamma Heating Rate (Center of Concrete)	-2.343 (-0.003)	-2.808 (-0.019)	-0.645 (-0.082)	-0.001 (-0.223)
Total Dose Rate (Outside of Concrete)	-2.234 (-0.042)	-2.585 (-0.229)	-1.612 (-0.995)	-0.009 (-4.820)
Total Dose Rate (On the Rotating Plug)	-8.756 (-0.704)	-0.229 (-3.216)	-0.312 (-4.080)	- (-)

Table V Sensitivity of Displacement Production Rate of Reactor Vessel to Total Neutron Cross Section

	Region	Na	SUS304	Carbon		Region	Na	SUS304	C
1	Inner Core	-.013			11	Sodium	-.850		
2	C/R	-.007			12	Sodium	-.893		
3	Outer Core	-.080			13	Thermal Shield	-.080	-.350	-.003
4	R. Blanket	-.360							
5	Mov. Reflector	-.047			14	React. Vess.		-.070	-.002
6	Sodium	-.238			16	Leak Jacket		.060	.0
7	Inner N. Shield	-.040	-.390	-.003	17	Therm. Ins.		.018	.0
8	Fuel Stor. Rack	-.715	-.447	-.004	19	Graphite			-.004
9	Core Barrel			-.002	20	Graphite			.001
10	Outer N. Shield	-.145	-1.00	-.009	21	Graphite			.0
						All Regions	-3.47	-2.18	-.024

concrete.

The sensitivities of the dose rate on the rotating plug to the total cross sections of sodium, SUS304, and carbon were analyzed along the axial direction of "JOYO". In the result of the one dimensional transport calculation, which is used in the sensitivity analysis, 97% of the total dose is due to gamma ray, but this is different from the results of the two dimensional calculation and the measurements. In these results, most of the total dose are due to neutron flux. This is because the streaming along the direction of the radial axis cannot be considered in the one dimensional calculation and the neutron flux is underestimated on the rotating plug. This case is one of the examples that a two dimensional analysis is necessary for the estimation of the sensitivities of shielding characteristics. By this one dimensional analysis, the sensitivities to the neutron cross sections of the sodium, whose depth is 476cm from the core center to the sodium surface, and the sensitivities to the gamma ray cross sections of the regions near the top of the plug were proved to be large.

As an example of the sensitivity spectra, which show the energy dependences of the sensitivity coefficients, Figure 2 shows the sensitivity spectrum of the atomic displacement rate of the reactor vessel to the total cross section of SUS304. The profile of the sensitivity spectrum is similar to the neutron spectrum from the inner neutron shield to the thermal shield. However, the sensitivity is large in high energy range, $E \geq 100$keV, because the atomic displacement production cross section of the reactor vessel (SUS304) is large in such high energy range. Moreover, fine structure of the spectrum by the resonance of iron, cobalt, manganese and sodium can be observed. At the resonance energies of 130keV, 330keV, and 2.8keV, the sensitivity becomes small, and at the resonance window regions of iron and sodium, such as 24keV and 300keV, there are peaks in the sensitivity spectrum. Especially at the resonance window energy of iron, 24keV, the higher neutron flux makes the sensitivity very large.

Analyses of sensitivities to the partial cross sections of the principal regions give the following results for the sensitivity coefficients and spectrums.

(1) In the radial direction, the sensitivity to the sodium cross section is very large, and the sensitivity to the neutron slowing down cross section takes the dominant part in the sensitivity to sodium.

(2) Spatially in radial direction for sodium and SUS304, sensitivities to the neutron slowing down cross sections are large near the core, and those to the absorption and in-group scattering cross sections become larger in outer regions.

(3) To the scattering cross sections, which determine the transmission of neutron, sensitivities are large in the energy ranges where the neutron flux is high.

(4) Sensitivities to the absorption and secondary gamma ray production cross sections of sodium, SUS304, carbon, and concrete have been proved to be small: In these spectrums, sensitivities are large both at the energies of the peaks of neutron spectrum and resonance peaks of cross sections.

(5) Spectra of gamma ray fluxes are almost flat in all regions, and sensitivities to the gamma ray cross sections are large at the energies where the cross sections and the response function are large.

(6) In the radial direction, the neutron cross sections of sodium and SUS304 are important and their important energy ranges are; 10keV-5MeV for the displacement production rate of the reactor vessel, and for the shielding characteristics near the concrete shield, 1keV-5MeV for sodium and 1eV-1MeV for SUS304.

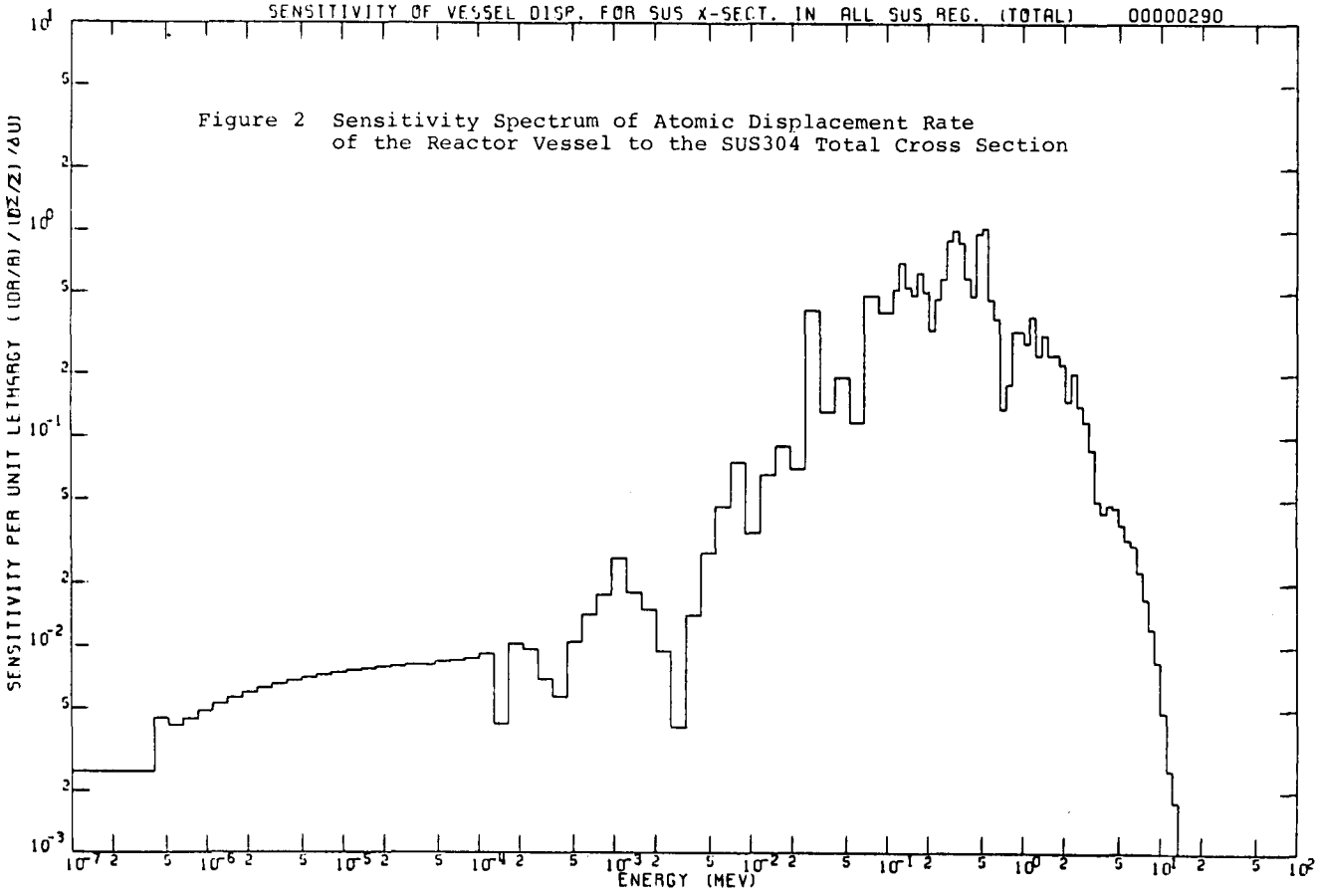

Figure 2 Sensitivity Spectrum of Atomic Displacement Rate of the Reactor Vessel to the SUS304 Total Cross Section

IV. Microscopic Cross Section Sensitivity

Sensitivities to the microscopic cross sections of each element were analyzed to estimate the important elements and the kinds of cross sections for the shielding calculations of fast reactors.

The main shield of "JOYO" was modeled in one dimension along the radial direction and the sensitivities of the atomic displacement rate of the reactor vessel and the total dose rate at the outside of the concrete shield to the microscopic cross sections of sodium, iron, chromium, nickel, carbon, silicon and oxigen were analyzed. The model of the main shield is shown in Table I and the calculations by ANISN are listed in Table II. In Table II, Case FR-3, AR-5, and AR-6 were used in microscopic cross section analyses.

In order to analyze the sensitivities to the cross sections of each reaction, a set of the reaction-wise microscopic cross sections of each element was prepared besides the cross section set used in the transport calculations. In these cross section sets, the resonance disadvantage factor (f-factor) for each region is multiplied to the infinite dilution cross sections. Moreover, in order to calculate the sensitivities to the parastic absorption cross sections, (n,p) reaction for example, "SWANLAKE" code had to be improved slightly.

Table VII shows the sensitivities of the atomic displacement rate of the reactor vessel to the total and the individual reaction cross sections of each element. As for the total cross sections, sensitivities to sodium and iron are remarkably large and it has been proved they are important in the shielding calculations of fast reactors.

Among the sodium cross sections, response is highly sensitive to the elastic scattering cross section and the sensitivity is 91% of that to the total cross section of sodium. Spatially it is 50% near the core and 98% just inside of the reactor vessel. The sensitivity to the inelastic scattering cross section is 50% near the core and it decreases to 1-2% near the reactor vessel. This spatial distribution corresponds to the slowing down of fast neutrons.

As for the iron cross sections, the inelastic scattering cross section, which appears above the threshold energy of about 800keV, is relatively important, and its sensitivity is 22% of that to the total cross section. The sensitivity to the elastic scattering cross section is 75% of that to the total cross section. The spatial distributions of these sensitivities of iron are similar to those to the sodium cross sections. Contribution of the capture cross section is small and negligible.

Table IIX shows the sensitivities of the total dose rate at the outside of the concrete shield to the total and partial cross sections of the elements. Similar to the previous case, sensitivities to the sodium and iron are large. Almost of the total dose at the outside of the concrete is due to the gamma ray, and the sensitivity to the neutron cross section of silicon, which is the main constituent of the concrete, is very small. For the production of the sencondary gamma ray, the contribution of the low energy neutron is larger than in the case of the atomic displacement rate of the vessel, and the ratio of the sensitivities to the capture cross sections is larger than in the case of the atomic displacement. Especially for the iron, 37%(sum of all regions) or 80-90%(at the region of the carbon steel between the graphite and the concrete) of the sensitivity to the total cross section is that to the capture cross section. This shows that the gamma ray at the outside of the concrete is produced from the absorption of thermal neutrons in the region of the carbon steel.

Table VI Sensitivity of Total Dose Rate at the Outside of the Concrete Shield to the Total Cross Section

	Region	Sodium		SUS304*		Carbon		Concrete	
		n	γ	n	γ	n	γ	n	γ
1	Inner Core	-.014	0.0						
2	C/R	-.007	0.0						
3	Outer Core	-.073	0.0						
4	R.Blanket	-.301	0.0						
5	Mov.Refl.	-.039	0.0						
6	Sodium	-.194	0.0						
7	Inner N.Shil.	-.032	0.0	-.366	-.001	-.003	0.0		
8	Fuel Rack	-.548	-.001	-.444	-.002	-.003	0.0		
9	Core Barrel					-.001	0.0		
10	Outer N.Shil.	-.088	-.001	-.968	-.039	-.006	0.0		
11	Sodium	-.453	-.018						
12	Sodium	-.451	-.020						
13	Thermal Shil.	-.034	-.003	-.388	-.045	-.001	0.0		
14	R.Vessel			-.294	-.072	-.001	0.0		
16	Leak Jacket			-.113	-.059	0.0	0.0		
17	T.Insulator			-.012	-.011	0.0	0.0		
19	Graphite					-.565	-.330		
20	Graphite					-.571	-.330		
21	Graphite					-.460	-.319		
23	C.Steel					0.0	0.0		
25	C.Steel					0.0	-.003		
26	C.St.Lining					0.0	-.001		
27	Concrete					0.0	-.006	-.006	-2.415
28	Concrete					0.0	-.006	-.003	-2.405
29	C.St.Lining					0.0	0.0		
All Regions		-2.23	-.042	-2.59	-.229	-1.61	-.995	-.009	-4.820

*) SUS304:Stainless Steel

Table VII Sensitivities of the Displacement Production Rate of the Reactor Vessel (sum of all regions)

	Na	Fe	Cr	Ni	C	Si	O
Total	-3.55	-2.02	-0.76	-0.58	-7(-4)	-0.054	-1.108
Elastic Scat.	-3.23	-1.50	-0.63	-0.49	0.002	-0.053	-1.097
Inela. Scat.	-0.31	-0.45	-0.10	-0.051	-5(-6)	-7(-4)	-0.002
(n,2n)	-2(-6)	-4(-5)	-3(-5)	-3(-6)	0.0	-2(-8)	0.0
Capture	-0.01	-0.067	-0.027	-0.032	-0.002	4(-4)	-0.009
(n,p)	-0.001	-0.005	-4(-4)	-0.012	0.0	0.0	-3(-5)
(n,α)	-5(-4)	-3(-4)	-3(-5)	-7(-4)	0.0	0.0	-0.009
(n,γ)	-0.009	-0.062	-0.026	-0.032	-0.002	0.0	0.0

Table VIII Sensitivities of the Total Dose Rate at the Outside of the Biological Concrete Shield (sum of all regions)

	Na	Fe	Cr	Ni	C	Si	O
Total	-2.521	-3.408	-0.793	-0.737	-1.397	-0.038	-1.213
Elastic Scat.	-2.250	-1.890	-0.581	-0.592	-1.142	-0.034	-1.205
Inela. Scat.	-0.197	-0.254	-0.057	-0.031	2(-4)	-2(-4)	-0.001
(n,2n)	6(-7)	-8(-6)	-4(-6)	-1(-7)	0.0	3(-8)	0.0
Capture	-0.091	-1.265	-0.155	-0.114	-0.255	-0.004	-0.007
(n,p)	-7(-4)	-0.004	-3(-4)	-0.009	0.0	-2(-5)	-2(-5)
(n,α)	-3(-4)	-2(-4)	-2(-5)	-5(-4)	-3(-5)	-1(-5)	-0.007
(n,γ)	-0.090	-1.261	-0.154	-0.104	-0.255	0.004	-1(-5)
Gamma Prod.	0.006	3.060	0.113	0.083	0.014	1(-5)	9(-4)

* -2(-6):-2×10^{-6}

V. Errors of Shielding Characteristics

Errors of shielding characteristics of "JOYO" due to the uncertainties of cross section data have been evaluated by using the results of the SWANLAKE calculations and rough estimations of cross section data errors.

For these evaluations, a limitation of the error calculation by the linear perturbation theory was checked. Changes of the reaction rates by the linear perturbation theory and those by the direct calculations are compared in Table IX. As shown in this table, for the 30% change of the reaction rate, the change by the linear perturbation theory differs about 30% from that by the direct calculation.

Making rough estimations and assumptions of the errors of cross section data, the errors of the shielding characteristics were evaluated. As for the errors of cross section data, the reports by Steiner[3] and by McKnight[4] were reffered. Table X shows the errors of shielding characteristics due to the assumed cross section errors. If the full correlation of the cross section errors is supposed, the errors of the atomic displacement rate is 53% and that of the dose rate is 150%. Of cource, it should be noted that the obtained values of the errors are both in excess of the limitation of the linear perturbation theory.

For the main shield of "JOYO", the detailed two dimensional calculations were carried out, and the results were compared with the measured data of "JOYO". However the atomic displacement rate of the reactor vessel and the dose rate at the outside of the concrete shield were not measured and compared, C/E(calculation/experiment) values of the reaction rates near the reactor vessel are about factor 2 for the neutron reaction and about factor 3 for the gamma ray dose rate. Moreover, the C/E value of the gamma ray dose rate just inside of the concrete shield is about factor 5. In the analysis of "JOYO" main shield, the C/E values for the gamma ray are generally not good and it was concluded that it is because of the inaccuracies of the gamma ray production cross sections.

Another one dimensional analysis for the selections of calculational parameters shows the changes of the neutron dose rate by taking the calculational parameters of higher approximations: it is about 7% near the reactor vessel and about 40% at the outside of the concrete shield. One dimensional calculations with the parameters which are the same order of the approximation to the two dimensional calculation have been compared with those with the higher approximations. Calculational parameters considered here are number of energy groups, number of spatial meshes, order of Pn, and order of Sn.

These results show that for the shielding characteristics of fast reactors the contribution of the errors due to the cross section data errors is not so small in the discrepancies between the calculaional and measured values.. This means that the improvement of the accuracies of the nuclear cross section data and the arrangement of detailed error files are enough effectual in the shielding analyses of fast reactors. However, in the detailed shielding design of the prototype fast breeder reactor of Japan, two dimensional discrete ordinate calculations are being applied, and the design margins for the modeling of the shielding configurations and for the estimations of the streamings through various pathes are greatly required besides the margin for the cross section data uncertainties. For the more rational shielding design, it is important to reduce these margins, and it will be possible by the accumulation of the shielding analyses of many kinds of fast reactors.

Table IX Comparison of Reaction Rate Changes (%)

Reaction	X.Sec. Perturb.	Direct Calc.	Linear Perturb.	Exact Perturb.
Displacement Rate (Reactor Vessel)	5%	9.1(1.0)	10.1(1.11)	9.6(1.05)
	10%	17.4(1.0)	20.2(1.16)	18.3(1.05)
Total Dose Rate (Outside of Concrete)	5%	14.2(1.0)	17.0(1.20)	15.5(1.09)
	10%	26.1(1.0)	34.1(1.31)	28.4(1.09)

Table X Estimated Error based on Sensitivity

Cross Section			Atomic Diplacement Rate (Reactor Vessel)		Total Dose Rate at the Outside of the Concrete	
Element	Reaction	Uncertainty	Sensitivity	Error	Sensitivity	Error
Sodium	N.Total	5%	-3.550	18%	-2.521	13%
	G.Prod.	20%	-	-	0.006	0.12%
Iron	N.Total	10%	-2.015	20%	-3.408	34%
	G.Prod.	25%	-	-	3.060	77%
Chromium	N.Total	10%	-0.757	7.6%	-0.793	7.9%
	G.Prod.	25%	-	-	0.113	2.8%
Nickel	N.Total	10%	-0.578	5.8%	-0.737	7.4%
	G.Prod.	25%	-	-	0.083	2.1%
Carbon	N.Total	1%	-0.001	0.001%	-1.397	1.4%
	G.Prod.	-	-	-	0.014	-
Silicon	N.Total	10%	-0.054	0.54%	-0.038	0.38%
	G.Prod.	-	-	-	-	-
Oxigen	N.Total	1%	-1.108	1.1%	-1.213	1.2%
	G.Prod.	-	-	-	-	-
Estimated Error due to N.Total C.S.	Full Correl.		53%		65%	
	Uncorrel.		29%		38%	
Total Estimated Error	Full Correl.		53%		150%	
	Uncorrel.		29%		86%	

References

[1] D.E.Bartine, F.R.Mynatt & E.M.Oblow: SWANLAKE, A Computer Code Utilizing ANISN Radiation Transport Calculations for Cross Section Sensitivity Analysis, ORNL-TM-3809

[2] K.Koyama, K.Minami, Y.Taji & S.Miyasaka: RADHEAT-V3, A Code System for Generating Coupled Neutron and Gamma-Ray Group Constants and Analyzing Radiation Transport, JAERI-M 7155

[3] D.Steiner: The Status of Neutron Induced Nuclear Data for Controlled Thermonuclear Research Applications, Critical Review of Current Evaluations, USNDC-CTR-1(1974)

[4] R.D.McKnight & L.G.LeSage: Proc. of Int. Conf. on Advanced Reactors - Physics, Design and Economics, Atlanta, p.620(1974)

A REVIEW OF THE CAPABILITIES OF THE ORNL FORSS SENSITIVITY AND UNCERTAINTY ANALYSIS SYSTEM

R. W. Roussin, C. R. Weisbin, and J. L. Lucius
Oak Ridge National Laboratory
Oak Ridge, Tennessee U.S.A.

ABSTRACT

The ORNL FORSS Sensitivity and Uncertainty Analysis System was demonstrated in the 1978 Radiation Shielding Information Center (RSIC) Workshop. The first versions of this code system for both IBM and CDC computers are now packaged and are available from RSIC. Features of the FORSS system are described and guidelines for its use are given. An assessment of the status of the system and plans for future updates are provided. Examples of applications of the system to fast reactor and fusion integral experiments, to reactor dosimetry problems, and to the adjustment of a cross-section library are discussed.

1. INTRODUCTION

The ORNL FORSS [1] Sensitivity and Uncertainty Analysis System was demonstrated in the Workshop portion of a 1978 Radiation Shielding Information Center (RSIC) Seminar/Workshop on the Theory and Application of Sensitivity and Uncertainty Analysis [2]. The system has been packaged and is generally available from RSIC as CCC-334/FORSS. Early development of the system focused on fast reactor physics and shielding problems. The technology continues to be developed and applied to fast reactor physics and other shielding applications at ORNL, including fusion neutronics and light water reactor (LWR) pressure vessel dosimetry.

The following sections describe the current status of the FORSS system and related technology and possible future extensions of the system. Applications of the system to shielding problems at ORNL are described and results from a cross-section library adjustment problem are discussed.

2. ELEMENTS OF THE FORSS SYSTEM

The FORSS Sensitivity and Uncertainty Methodology is not a single code system but rather a collection of code systems and stand-alone codes that contribute to the solution of a FORSS problem. The technology includes multigroup cross section processing, uncertainty file processing, neutronics calculations, source calculations, sensitivity profile generation, uncertainty analysis, data adjustment, and estimation of accuracy requirements for nuclear data to meet pre-determined design constraints and error margins. A modular code system under driver control has been developed and is commonly called FORSS; however, it does not at present place all the FORSS methodology under the control of a single driver. The following sections will discuss the relationship of the codes and code systems that contribute to the solution of a FORSS problem. A discussion of FORSS methodology is found in Reference 1 and detailed user instructions are provided in Reference 3.

3. DATA PROCESSING FOR FORSS

Multigroup cross sections and covariance matrices are required in the FORSS system in particular formats. The user may generate these or perhaps obtain data already processed at some other installation. As indicated in section 7.3 below and in another paper at this Conference [4], such libraries are available from RSIC.

3.1 Cross-Section Processing

Multigroup cross sections must be prepared for the neutronics calculation selected to model the assembly being investigated. The MINX-SPHINX [5,6], AMPX [7], and NJOY [8] cross-section processing systems are examples of cross-section processors that provide this capability. In sensitivity and uncertainty analysis partial cross sections must be available, so FORSS uses the proposed CCCC [9] file MATXS [10] as the data base for partial cross sections. For cross-section processors which do not directly produce a MATXS file, the FORSS system includes three translators for producing MATXS from the more mature ISOTXS [9], AMPX master, or ANISN [11] formats.

3.2 Uncertainty (Covariance) File Processing

Uncertainty analysis with the FORSS system requires that multigroup covariance matrices be available. These can be produced for example, from ENDF/B-IV formatted uncertainty data [12] using the PUFF [13] code. The resulting matrices are placed in the format of a proposed CCCC file COVERX [14]. FORSS requires such COVERX files before uncertainty analysis can be initiated. Uncertainty files in ENDF/B-V [15] format can be processed with PUFF-II [16] or NJOY. As is indicated in another paper at this conference [17], such multigroup uncertainty files are available from RSIC.

4. NEUTRONICS AND SENSITIVITY COEFFICIENT CALCULATIONS

The ANISN, DOT [18], and VENTURE [19] neutronics codes are used in the FORSS methodology. ANISN is a module in the FORSS driver controlled system and its interaction with the other modules in the system is somewhat automated. *Comments about the use of DOT and VENTURE in FORSS are made in section 4.2 below.*

The number of neutronics calculations required for a study is a function of the number and type of responses under consideration. Sensitivity analysis for criticality requires a forward and adjoint neutronics calculation; reaction rate ratio analysis requires, in addition, the computation of a generalized adjoint. For worth sensitivity, four neutronics calculations are required; these being a forward and adjoint, and a generalized forward and adjoint. The JULIET module uses the fluxes produced by these neutronics calculations.

4.1 The JULIET Module

This module calculates sources, responses, normalization parameters, and sensitivity coefficients. The JULIET algorithms for generalized sources, responses, and normalization parameters use FORSS ANISN (FANISN) produced angular fluxes. The sources calculated by JULIET are returned to FANISN as input to generalized neutronics calculations. The sensitivity coefficients calculated by JULIET are placed in a proposed CCCC file SENPRO [14].

JULIET is organized into execution paths, i.e., it has multiple entry points. A source calculation may be performed and execution terminated without generating sensitivity coefficients. When sufficient results are available from preliminary calculations, JULIET may be asked to generate sensitivity coefficients and bypass the source calculations.

4.2 Two-Dimensional Analysis with DOT or VENTURE

With an understanding of how ANISN and JULIET interact to produce generalized fluxes, sources, and normalization parameters, the use of 2-D neutronics in FORSS can be clarified. Before sensitivity coefficients are generated, JULIET prepares a so-called <Ø*Ø> file. This is symbolic since it could be <Γ*Ø> or <Ø*Γ> (brackets imply integration over spatial regions and angles). This file is used in the generation of sensitivity coefficients. When 2-D neutronics is used in FORSS, the selected 2-D code system, DOT or VENTURE, is used to produce the equivalent fluxes as produced by ANISN and the JULIET-SOURCE algorithms. The VIP [20] code is then used to prepare the <Ø*Ø> file. The selected 2-D code system must also produce the normalization parameters required by the JULIET sensitivity profile calculation. With appropriate <Ø*Ø> files and normalization parameters available, the JULIET-SENSE execution path is entered and the problem solution path is the same as when ANISN neutronics is used.

A recent major study of a two-dimensional LMFBR Conceptual Design Study Reactor [21] has been completed and multi-dimensional sensitivities generated for homogeneous and heterogeneous designs. Current work [22] is directed toward the generation of multi-dimensional time-dependent sensitivities (i.e., burnup effects). Further work [23] is directed toward understanding how uncertainties in resonance parameters propagate through to uncertainties in integral results through the vehicle of the multigroup self-shielding factor. Finally, the JULIET module also has a provision for including constraints on the sensitivities (e.g., k-reset, constant power).

5. FEATURES AND APPLICATIONS OF THE FORSS SYSTEM

5.1 Manipulation of SENPRO and COVERX Files

JULIET generates the SENPRO file containing sensitivity profiles. However, before using the file in uncertainty analysis, it may be desirable to examine the file(s) in detail. The SENPRO SERVICE MODULE [24] operates on the file providing a number of services including plotting and listing.

As stated in section 3.2, COVERX files must be available before uncertainty analysis can be initiated with FORSS modules. The COVERX Service Module [25] operates on the file providing a number of services such as binary to card image conversion, listing, and merging.

5.2 Assessing Effects of Proposed Cross-Section Changes

When the calculation of sensitivity coefficients is complete and SENPRO file(s) are available, the effects of proposed cross-section modifications may be investigated. The SENTINEL [26] module computes the percentage (or fractional) change in the performance parameter of a given assembly due to specified percentage (or fractional) changes in designated reaction cross sections over a number of energy regions. An edited list of the most significant individual contributions to the response change is also provided.

5.3 Uncertainty Analysis Considering Only Nuclear Data Uncertainties

When COVERX and SENPRO files are available, uncertainty analysis may be initiated. The CAVALIER [27] module folds sensitivity profiles (SENPRO) and covariance matrices (COVERX) to estimate reactor performance uncertainties which result from uncertainties in nuclear data.

5.4 Uncertainty Analysis with Integral Experiments Taken into Account

The module UNCOVER [28] finds the adjustments of both integral and differential data which are most consistent (in a general least squares sense) with the data and with the calculational model as represented by the sensitivity coefficients. The input to UNCOVER includes data from SENPRO sensitivity and COVERX (a priori) covariance files. The output includes a posteriori covariances for the adjusted data in addition to the adjustments themselves. The adjusted data and associated covariances can be applied to design models for improved predictions of performance parameter and of their uncertainties. Input for UNCOVERS is greatly facilitated through the use of a module called COVERS.

A major effort is now underway (see section 8.5) to create and test a comprehensive adjusted library including explicitly estimates of calculational uncertainties. The library will soon be undergoing major testing in LMFBR design applications.

5.5 Cross-Section Adjustment

The ADJUST module modifies the cross sections on an AMPX master file by the percent changes calculated by the UNCOVER module. ADJUST also calculates the fission spectrum using the Watt formulism with adjusted values of a and b. A Maxwellian fission spectrum is calculated when b is input as zero. This creates an adjusted cross-section library for dissemination via the AMPX system. It should be noted that the operation of AMPX modules AJAX, COMET, RADE, and DIAL are to be used in conjunction with ADJUST to insure a consistent cross-section data set following an adjustment procedure.

5.6 The Inverse Problem

The NUTCRCKR module is a first attempt at solution of the "Inverse Problem" of reactor sensitivity. The objective is to provide quantitative guidance to data acquisition, data evaluation, and associated data processing code development programs by giving estimated accuracy requirements on various multigroup nuclear data to meet predetermined design constraints and error margins. Recent improvements include bounds on required standard deviations (e.g., measurements required can result in uncertainties no larger than those perceived to currently exist), a variety of objective functions for minimization, and estimated bounds on proposed experimental correlations.

6. FORSS SYSTEM STRUCTURE

The system is composed of modules which may be executed under DRIVER control or they may be executed as stand-alone programs. Under DRIVER CONTROL, a run is executed from a procedure which includes most of the IBM JCL needed. The DRIVER and procedure technology are based on those used in AMPX.

Data interchange between modules is accomplished by well defined files which are located on external storage devices such as magnetic tape or disks. Proposed CCCC files are used for partial cross sections (MATXS), sensitivity coefficients (SENPRO), and covariance matrices (COVERX). In the current version of the system, FORSS ANISN uses a traditional ANISN formatted tape. The COVERS module prepares from SENPRO and COVERX files two other files which are suitably formatted for the flexible structure of the UNCOVER module. FORSS ANISN and JULIET interchange data via a repository which is implemented with the FMANG module.

FORSS is designed to permit multiple entry points into the system. A comprehensive calculation may be designed to generate fluxes, normalization parameters, sensitivity coefficients and perform an adjustment in a single computer run. Conversely, many computer runs may be used to obtain the same results. The latter approach requires that the appropriate files (Repository, SENPRO, COVERS files, etc.) must be saved on semipermanent external storage devices. It is also good policy to do this for the comprehensive run unless the calculation is small enough to make little demand on computer resources. A correct calculational hierarchy must be defined and executed for either the comprehensive or the segmented solution.

A correct hierarchy is determined by the prerequisites of the modules needed to solve the problem of interest. An example of a correct hierarchy is:

1. Processing of ENDF/B files into multigroup neutron cross sections. Resulting files may be an AMPX master, ISOTXS, or ANISN cross-section library.
2. Processing of ENDF/B uncertainty files resulting in a COVERX file. NOTE: The FORSS DRIVER controlled program does not include the modules needed to implement steps 1 and 2; these are external preparatory steps for FORSS.
3. Generating forward and adjoint fluxes on the repository with FANISN.
4. Translating AMPX, ISOTXS, or ANISN cross sections to the MATXS file with the appropriate translation module.
5. Generating normalization parameters and generalized sources on the repository with JULIET.
6. Generating generalized forward and adjoint fluxes on the repository with FANISN.
7. Calculating sensitivity coefficients and preparing a SENPRO file(s) with JULIET.
8. Operating on SENPRO files with the SENPRO SERVICE module.
9. Performing perturbation analysis with SENTINEL.
10. Operating on COVERX files with the COVERX SERVICE module.
11. Performing uncertainty analysis with CAVALIER.
12. Preparing input for UNCOVER WITH COVERS.
13. Performing uncertainty analysis (adjustment) with UNCOVER.
14. Implementing the resulting adjustments with ADJUST.

The multiple entry feature of FORSS permits entry at the module level and in some situations at the submodule level. Some modules perform more than one task and some of these tasks may be selected for execution in a particular run and others excluded. This concept is referred to as execution paths.

FORSS has a very powerful and flexible free field data input scheme called Improved FIDO.

7. AVAILABILITY OF THE FORSS TECHNOLOGY

Versions of the FORSS system are available from RSIC under the designations CCC-334A for IBM-360 from ORNL and CCC-334B for CDC-7600 systems from University of California at Berkeley.

7.1 Contents of the RSIC Versions

The RSIC versions are designed to be run with modules as stand-alone codes rather than under DRIVER control. The technology contained in the RSIC FORSS packages does not include cross section or uncertainty processing or two-dimensional neutronics. The user can perform detailed sensitivity and uncertainty analysis through the UNCOVER stage (see section 5.1 through 5.4).

7.2 Expected Future Updates

It is anticipated that the next update of FORSS will be the inclusion of the ADJUST module with appropriate documentation to guide in producing a consistent adjusted AMPX master library. An update coming at a somewhat later time will be the NUTCRACKR module for solving the Inverse Problem.

7.3 Availability of Processed Cross Sections, Covariances, and Sensitivity Profiles

Multigroup cross sections, covariance matrices, and sensitivity profiles have been packaged and are available from RSIC. Details of the available libraries are given in two other papers at this Conference.

8. SHIELDING APPLICATIONS OF FORSS AT ORNL

8.1 Fast Reactor Integral Experiment Analysis

Oblow and Weisbin [29] performed sensitivity and uncertainty studies for steel-sodium-iron systems. They concluded that the use of integral data from the ORNL Tower Shielding Facility Measurements in adjustment procedures will significantly reduce uncertainties in LMFBR shield designs of steel/sodium and iron.

8.2 Analysis of a Benchmark Standard Neutron Field

Broadhead and Marable [30] performed a FORSS analysis of the National Bureau of Standards - Intermediate Energy Standard Neutron Field (NBS-ISNF) to obtain the most likely estimates of the NBS-ISNF flux spectrum and several dosimetry cross sections as well as their covariances based on several integral experiments. Satisfactory results were obtained when analysis was repeated a finer energy mesh for cross sections (171 neutron groups) and fission spectrum.

8.3 Fusion Integral Experiment

The FORSS system has been applied to the pre-analysis of the experimental program sponsored at ORNL by the Department of Energy Office of Fusion Energy (DOE-OFE). Both two dimensional [31] and one dimensional [32] sensitivity analysis were performed by Seki, et al. and the results were used to aid in designing a streaming experiment. A post-analysis study is currently underway.

8.4 LWR Pressure Vessel Damage Methodology

The Electric Power Research Institute is sponsoring at ORNL the development of an advanced methodology for the determination of LWR pressure vessel damage. Recent work [33] considers the inclusion of ORNL Pool Critical Assembly (PCA) benchmark. Bias factors for group fluxes, sensitivities of the flux to the fission spectrum and structural material cross sections, ENDF/B-V based cross sections and covariance matrices, and new fission spectrum covariance matrices are being employed. These represent substantial progress towards implementing the methodology to the PV damage estimate of a working LWR.

8.5 Development of an Adjusted Library (ORACLE)

An Oak Ridge Adjusted Cross section and covariance multigroup library based on ENDF/B-V (ORACLE) differential data evaluation and information from fast reactor and dosimetry integral experiments is presently under development [34]. ORACLE is a major testbed of the generalized least-squares procedure for producing credible results with a minimum of data-related bias. Cross sections and covariance files used for ORACLE are based on ENDF/B-V.

8.6 Analysis of the CFRMF Facility

An extensive analysis of the Coupled Fast Reactivity Measurement Facility (CFRMF) is now being performed using FORSS [35]. A relative flux covariance matrix for the central neutron spectrum due to neutron cross section and fission spectrum uncertainties and correlations has been calculated. The uncertainties in the associated flux spectrum are an integral part of the characterization of this benchmark field.

ACKNOWLEDGMENTS

A review paper of this nature surveys the work of many individuals as indicated in the numerous references cited. The reader is directed to the references to indicate proper credit for the developments listed in the text.

The efforts of Eddie Bryant in preparing this manuscript are appreciated.

REFERENCES

1. C. R. Weisbin, E. M. Oblow, J. H. Marable, R. W. Peelle, and J. L. Lucius, "Application of Sensitivity and Uncertainty Methodology to Fast Reactor Integral Experiment Analysis," Nucl. Sci. Eng. 66, 307-333 (1978).

2. C. R. Weisbin, R. W. Roussin, H. R. Hendrickson, and E. W. Bryant, "A Review of the Theory and Application of Sensitivity and Uncertainty Analysis," Proceedings of a Seminar-Workshop, Oak Ridge, Tennessee, August 1978, ORNL/RSIC-42 (1978).

3. J. L. Lucius, C. R. Weisbin, J. H. Marable, J. D. Drischler, R. Q. Wright, and J. E. White, "A User's Manual for the FORSS Sensitivity and Uncertainty Analysis Code System," ORNL-5316 (ENDF-291) (1980).

4. R. W. Roussin, "Status of Multigroup Cross-Section Libraries Available from the Radiation Shielding Information Center," Presented at NEA Specialists' Meeting on Nuclear Data and Benchmarks for Reactor Shielding, Paris (1980).

5. C. R. Weisbin, P. D. Soran, R. E. MacFarlane, D. R. Harris, R. J. LaBauve, J. S. Hendricks, and J. E. White, "MINX, A Multigroup Interpretation of Nuclear Cross Sections from ENDF/B," Los Alamos Scientific Laboratory (LA-6486-MS); see also, Trans. Am. Nucl. Soc., 16, 127 (1973).

6. W. J. Davis, M. G. Yarbrough, and A. B. Bortz, "SPHINX, A One-Dimensional Diffusion and Transport Nuclear Cross Section Processing Code," WARD-XS-3045-17 (1977).

7. N. M. Greene, J. L. Lucius, L. M. Petrie, W. E. Ford III, J. E. White, R. Q. Wright, "AMPX: A Modular Code System for Generating Coupled Multigroup Neutron-Gamma Libraries from ENDF/B," ORNL/TM-3706 (March 1976).

8. R. G. MacFarlane, R. J. Barrett, D. W. Muir, and R. M. Boicourt, "The NJOY Nuclear Data Processing System: User's Manual," LA-7584-M (1978).

9. B. M. Carmichael, "Standard Interface Files and Procedures for Reactor Physics Codes, Version III," LA-5486-MS (February 1974).

10. R. J. Barrett, R. E. MacFarlane, and R. M. Boicourt, Los Alamos Scientific Laboratory (to be published).

11. W. W. Engle, Jr., "A Users Manual for ANISN, A One-Dimensional Discrete Ordinates Transport Code with Anisotropic Scattering," K-1693, Computing Technology Center, Oak Ridge Gaseous Diffusion Plant (1967).

12. M. K. Drake, "Data Formats and Procedures for the ENDF Neutron Cross Section Library," Brookhaven National Laboratory report BNL-50274 April 1974 Revision).

13. C. R. Weisbin, E. M. Oblow, J. Ching, J. E. White, R. Q. Wright, and J. D. Drischler, "Cross Section and Method Uncertainties: The Application of Sensitivity Analysis to Study Their Relationship in Radiation Transport Benchmark Problems," ORNL-TM-4847 (ENDF-218) (August 1975) see also, RSIC Code Collection PSR-93.

14. J. L. Lucius and C. R. Weisbin, "Interface Specifications for Sensitivity Profiles (SENPRO) and Covariance Files (COVERX)," Presentation to the Committee on Computer Code Coordination, Los Alamos Scientific Laboratory (May 1976).

15. R. Kinsey, "Data Formats and Procedures for the Evaluated Nuclear Data File, ENDF," BNL-NCS-50496 (ENDF 102), 2nd Edition (ENDF/B-V) (1979).

16. J. D. Smith, III, "Processing ENDF/B-V Uncertainty Data into Multigroup Covariance Matrices," ORNL/TM-7221 (June 1980).

17. R. W. Roussin, J. D. Drischler, and J. H. Marable, "Status of Multigroup Sensitivity Profiles and Covariance Matrices Available from the Radiation Shielding Information Center," Presented at the NEA Specialists' Meeting on Nuclear Data and Benchmarks for Reactor Shielding, Paris (1980).

18. W. A. Rhoades and F. R. Myantt, "The DOT III Two-Dimensional Discrete Ordinates Transport Code," ORNL-TM-4280 (September 1973).

19. D. R. Vondy. T. B. Fowler, and G. W. Cunningham, "VENTURE: A Code Block for Solving Multigroup Neutronics Problems Applying the Finite-Difference Diffusion-Theory Approximation to Neutron Transport," ORNL-5062 (October 1975).

20. R. L. Childs, D. E. Bartine, and W. W. Engle, Jr., Trans. Am. Nucl. Soc., 21, 542 (1975).

21. J. Kallfelz (Ga. Tech.), C. Cowan (GE), J. Marable, M. Williams, C. Weisbin, J. Drischler, and T. Fowler (ORNL), "Design and Sensitivity Analysis of CDS-Type Heterogeneous Core," Presented at ANS Topical Meeting 1980 Advances in Reactor Physics and Shielding, Sun Valley Idaho (1980).

22. J. White, T. Burns, and M. Williams, "On the Implementation, Verification, and Application of Multicycle Depletion Perturbation Theory," Presented at ANS Topical Meeting 1980 Advances in Reactor Physics and Shielding, Sun Valley Idaho (1980).

23. E. Greenspan, Y. Carni, and D. Gilai, "High Order Effects in Cross-Section Sensitivity Analysis," p.231 of "A Review of the Theory and Application of Sensitivity and Uncertainty Analysis, Proceedings of a Seminar-Workshop, Oak Ridge, Tennessee, August 1978," ORNL/RSIC-42 (1979).

24. J. L. Lucius, "The SENPRO Service Module of the FORSS System," ORNL (to be published).

25. J. D. Drischler, "The COVERX Service Module of the FORSS System," ORNL/TM-7181 (ENDF-291) (1980).

26. J. H. Marable, J. D. Drischler, and C. R. Weisbin, "SENDIN and SENTINEL: Two Computer Codes to Assess the Effects of Nuclear Data Changes," ORNL/TM-5946, ENDF-250 (July 1977).

27. J. D. Drischler, J. H. Marable, and C. R. Weisbin, "COVERT and CAVALIER: Two Computer Codes for Reactor Performance Uncertainty Estimation Using SENPRO Sensitivity and COVERX Covariance Files," ORNL/TM-6078, ENDF-256 (to be published).

28. UNCOVER is a revision of the AMARA program permitting the solution of problems with a large number of energy groups. See also A. Gandini and M. Petilli, "AMARA: Code Using the Lagrange Multiplier Method for Nuclear Data Adjustment," private communication, M. Salvatores (1975).

29. E. M. Oblow and C. R. Weisbin, "Fast Reactor Shield Studies for Steel-Sodium-Iron Systems," Proceedings of the Fifth International Conference on Reactor Shielding," Knoxville, Tennessee, Science Press (1977).

30. B. L. Broadhead and J. H. Marable, "Sensitivity and Uncertainty Analysis Applied to the NBS-ISNF," see Reference 2, page 161.

31. Y. Seki, R. T. Santoro, E. M. Oblow, and J. L. Lucius, "Cross-Section Sensitivity Analysis of a Proposed Neutron Streaming Experiment with a Two-Dimensional Model," ORNL/TM-6588 (1979).

32. Y. Seki, R. T. Santoro, E. M. Oblow, and J. L. Lucius, "Comparison of One- and Two-Dimensional Cross-Section Sensitivity Calculations for a Fusion Reactor Shielding Experiment," ORNL/TM-6667 (1979).

33. J. Wagschal, R. Maerker, and B. Broadhead, "LWR-PV Damage Estimate Methodology, "Presented at ANS Topical Meeting - 1980 Advances in Reactor Physics and Shielding, Sun Valley, Idaho (1980).

34. J. Wagschal, J. Marable, Y. Yeivin, and C. Weisbin, "ORACLE: An Adjusted Cross Section and Covariance Library for Fast Reactor Analysis," Presented at ANS Topical Meeting - 1980 Advances in Reactor Physics and Shielding, Sun Valley, Idaho (1980).

35. J. M. Ryskamp, R. A. Anderl (EGG-Idaho), B. L. Broadhead, W. E. Ford, III, J. L. Lucius, and J. H. Marable, "Sensitivity and a Priori Uncertainty Analysis of the CFRMF Central Flux Spectrum," to be presented at the Washington, D.C. ANS Meeting, November 1980.

A NOTE ON SOME ASPECTS OF SENSITIVITY ANALYSIS IN MONTE CARLO

A. Dubi[1)], H. Rief

Work performed at the
Joint Research Centre of the European
Communities, Ispra Establishment-Italy
1) Ben Gurion University of the Negev
Beer-Sheva, Israel

ABSTRACT

Correlated tracking has become a means of sampling perturbation effects and sensitivity profiles in several Monte Carlo programs. Whilst the algorithm as it is used in the TIMOC code had already been described in earlier reports, this paper deals with investigations concerning the variance of the perturbation as a function of its magnitude and the so called "cross group" relations occuring in the calculation of sensitivity profiles.

Introduction

Monte Carlo methods are fast becoming a significant tool in sensitivity analysis and perturbation calculations. The use of the method is enhanced due to two exclusive features which are shared by no other method. First, the Monte Carlo method is not limited to first order perturbation theory thus in principle in one run a complete set of sensitivity profiles may be achieved (whereas in deterministic methods based on first order perturbation theory each sensitivity profile centered at a given value of the perturbed parameter requires a separate forward and adjoint calculation). Second, complicated realistic three dimensional structures can be studied.

Thus the Monte Carlo method bares the potential of becoming a unique tool in the design and analysis of realistic systems and in data evaluation of complicated geometries. A perturbation algorithm, based on correlated tracking, including the sampling of sensitivity profiles, was already included into TIMOC several years ago [1,2,3]. In the meantime also other multi-purpose Monte Carlo codes like DUCKPOND, MCNP and TRIPOLI were reported to have been equipped with this feature [4,5,6]. In most cases the perturbation features are still being evaluated and studied as to their correctness, reliability and efficiency, this mainly by testing them against ANISN-SWANLAKE calculations[7].Such studies are naturally limited to simple 1-D geometries (to which ANISN is limited) and there is still much to be learned about the efficient use of the correlated sampling used in the perturbation features especially in deep penetration situations, complicated geometries or when detailed sensitivity information is desired in a larger number of energy intervals. In the following we discuss some special points of interest raised while studying the perturbation scheme in TIMOC [8]. A general, however simplified, description of the method has been given in a recent paper [7].

General Considerations Concerning Correlated Sampling

The basic idea in using correlated sampling in perturbation calculations may be based on the following two Lemmas. Let $f(x, \alpha)$ be a probability density function (p.d.f.) of a random variable x and a parameter α. Let $\alpha' = \alpha + \Delta\alpha$, $\Delta\alpha$ being a perturbation on α. Let $\langle x \rangle$ be the expected value of x averaged over $f(x, \alpha)$ ($\langle x \rangle$ is the unperturbed response) and $\langle x' \rangle$ the average of x' over $f(x', \alpha')$ (the perturbed response). The random variable $\Delta x = x' - x$ then yields an average $\langle \Delta x \rangle = \langle x' \rangle - \langle x \rangle$ which will be referred as the perturbation. Then the following lemmas hold:

Lemma 1 : If we calculate $\langle \Delta x \rangle$ by independently calculating $\langle x' \rangle$ (sampling from $f(x', \alpha')$ and $\langle x \rangle$ (sampling from $f(x, \alpha)$) then the relative standard deviation of Δx defined as

$$e(\Delta x) = \frac{\sigma(\Delta x)}{\Delta x}$$ (where $\sigma_{\Delta x}$ is the standard deviation of Δx)

diverges as Δx approaches zero i.e.:

$$\lim_{\Delta x \to o} e(\Delta x) = \infty$$

Proof: consider first the variance of Δx. Since x and x' are independent we get:

$$V_{\Delta x} = \iint (x'-x)^2 \, f(x, \alpha) \, f(x', \alpha') \, dx dx' =$$
$$= \langle x'^2 \rangle - \langle x' \rangle^2 + \langle x^2 \rangle - \langle x \rangle^2 \qquad (1)$$

As $\Delta \alpha$ approaches zero we get

$$f(x', \alpha') = f(x', \alpha + \Delta \alpha) = f(x', \alpha) + \frac{\partial f}{\partial x'} \Delta \alpha$$

so that in the limit were $\Delta \alpha$ approaches zero we may write

$$\langle x'^2 \rangle = \int x'^2 f(x', \alpha') dx' = \int x'^2 f(x', \alpha) dx' +$$
$$+ \Delta \alpha \int x'^2 \frac{\partial f(x', \alpha)}{\partial \alpha} dx' = \langle x^2 \rangle + A \Delta \alpha \qquad (2)$$

and similarly we get

$$\langle x' \rangle = \langle x \rangle + B \Delta \alpha \quad \text{where} \quad B = \frac{\int x' \, \partial f(x', \alpha)}{\partial \alpha} dx' \qquad (3)$$

A and B are clearly constants independent of $\Delta \alpha$. Substituting equations (2) and (3) into (1) we obtain (as $\Delta \alpha \to 0$)

$$V_{\Delta x} = 2V_x + [A - 2 \langle x \rangle B] \Delta \alpha - B^2 \Delta^2 \alpha \quad , \quad V_x = \langle x^2 \rangle - \langle x \rangle^2$$
$$= 2V_x \left\{ 1 + \frac{A - 2 \langle x \rangle B}{2V_x} \Delta \alpha - \frac{B^2}{2V_x} \Delta^2 \alpha \right\} = \qquad (4)$$
$$= 2V_x \left\{ 1 + a \Delta \alpha - b \Delta^2 \alpha \right\}$$

thus

$$\sigma_{\Delta x} = \sqrt{V_x} = \sqrt{2} \, \sigma_x [1 + a \Delta \alpha - b \Delta^2 \alpha]^{\frac{1}{2}}$$
$$= \sqrt{2} \, \sigma_x \left(1 + \frac{a}{2} \Delta \alpha - \frac{b}{2} \Delta^2 \alpha\right) \qquad (5)$$

where in the last equality we utilized the approximation $(1+y) = 1+\frac{y}{2}$ for small y ($a \Delta \alpha$ and $b \Delta^2 \alpha$ can be made as small as necessary in the process of $\Delta \alpha$ approaching zero). Now using eq.(5)

and (3) we get

$$\lim_{\Delta x \to o} e(\Delta x) = \lim_{\Delta x \to o} \frac{\sigma_{\Delta x}}{\Delta x} = \lim_{\Delta x \to o} \frac{\sqrt{2}\,\sigma_x}{B} \left(\frac{1}{\Delta \alpha} + \frac{a}{2} - \frac{b}{2} \Delta \alpha \right) = \infty \qquad (6)$$

Q.E.D. (due to the $\frac{1}{\Delta \alpha}$)

The above lemma indicates that as the perturbation $\Delta \alpha$ goes to zero the separate Monte Carlo calculation of the perturbation response Δx, by independently calculating $< x >$ and $< x' >$, will not do, since its relative statistical error will diverge. The above Lemma is a mathematical statement of the fact that for small perturbations the statistical uncertainties accompanying both the calculations of $< x' >$ and $< x >$ will "mask" the difference between them. Even in the extreme case of $< x' > = < x >$ (i.e. $\Delta \alpha = 0$) being calculated indepedently there will be a finite variance to x. Indeed then the relative error will be infinite. Correlated sampling is a way to avoide the above described problem. This can be made clear with the following Lemma.

Lemma 2: The random variable y defined as

$$y = x \left[\frac{f(x, \alpha')}{f(x, \alpha)} - 1 \right] \quad \text{where } x \text{ is sampled from } f(x, \alpha),$$

an unbiased estimate of $< \Delta x >$ with a finite relative standard deviation as $\Delta x \to o$.

Proof: since x is sampled from $f(x, \alpha)$ we get

$$< y > = \int y\, f(x, \alpha) dx = \int \frac{x\,[\, f(x, \alpha') - f(x, \alpha)\,]}{f(x, \alpha)}\, f(x, \alpha)\, dx = \qquad (7)$$

$$= \int x\, f(x, \alpha') dx - \int x\, f(x, \alpha) dx = < x' > - < x > = < \Delta x >$$

which completes the proof that y is an unbiased estimator of $<\Delta x>$. Next we consider the variance of y.

$$V_y = \int y^2\, f(x, \alpha) dx = \int x^2 \left\{ \frac{f(x, \alpha') - f(x, \alpha)}{f(x, \alpha)} \right\}^2 f(x, \alpha)\, dx \qquad (8)$$

Using now the expression $f(x, \alpha') + \frac{\partial f}{\partial \alpha} \Delta \alpha$ for $\Delta \alpha$ approaching zero we obtain

$$V_y = \left\{ \int x^2 \left(\frac{\partial f}{\partial \alpha} \right)^2 \frac{dx}{f(x, \alpha)} - \left[\int x\, \frac{\partial f(x, \alpha)}{\partial \alpha}\, dx \right]^2 \right\} \Delta \alpha = (C - B^2)\, \Delta^2 x \qquad (9)$$

Thus

$$\lim_{\Delta x \to o} e(x) = \lim_{\Delta x \to o} \frac{\sqrt{V_y}}{\Delta x} = \frac{\sqrt{C-B^2}}{B}$$ which is finite (unless B=0 or

C is undefined).

The method described in the above Lemma has therefore a finite relative error for vanishing small perturbations and is thus adequate for perturbation calculations by Monte Carlo. Since in the above sampling scheme $x' = x \frac{f(x, \alpha')}{f(x, \alpha)}$, x' and x are correlated. It is indeed this correlation between x and x' that causes the enhancement of the perturbation expressed in the weight $f(x, \alpha')/f(x,\alpha)$. Also note that for $\Delta \alpha = 0$ it follows $y = 0$ which means zero variance.

In principle correlated sampling may be utilized for calculating large perturbations and in fact by defining $\alpha_1, \alpha_2, \ldots\ldots \alpha_n$ one may get in one run a complete scan over values of $< x(\alpha_i) >$ averaged over $f(x, \alpha_1)$; this merely by defining a set of estimators $x'_i = x \frac{f(x, \alpha_i)}{f(x, \alpha)}$ (where $i = 1,..,n$) which is one of the features that makes Monte Carlo attractive for perturbation calculations.There is however a point of causion in the above scheme. Applying the idea one may create a situation of a very high or even infinite variance which will render the calculation unreliable. As the variance $V_{\Delta x}$ in correlated sampling can be expressed by

$$V_{\Delta x} = \int (x'- x)^2 f(x, \alpha)dx - < x'- x >^2 =$$

$$\int x^2 [f(x, \alpha') - f(x, \alpha)]^2 \frac{dx}{f(x,\alpha)} - < x'- x >^2 = \qquad (10)$$

$$= S^2(\alpha, \alpha') - < x' - x >^2$$

It follows that the integral is the second moment of (x'-x), which in some situations may be infinite. Consider the important case [8] $f(x, \alpha) = \alpha \exp(-\alpha x)$ (the p.d.f. for sampling the next collision point in transport calculations). Substituting this p.d.f. into equation (10) yields for the second moment the form

$$S^2(\alpha, \alpha') = \frac{2\alpha'^2}{(2\alpha'- \alpha)^3} - \frac{4}{\alpha'^2} + \frac{2}{\alpha^2}$$

We may note that for $\alpha = \alpha'$ ($\Delta\alpha = 0$) it follows that $S^2(\alpha, \alpha')=0$ as expected; yet for $\alpha'= \alpha/2$ we get an infinite variance. Thus if the perturbation in a Monte Carlo calculation of the total cross section is reduced to 50% a very high variance and consequently an unreliable result may be expected, and indeed in our tests of TIMOC on two groups spherical problems we noted at the vicinity of 50% perturbation a jump from 5% error to 65% which could not be explained at the time[7].

The following example might illustrate this fact. Consider the transmission through a one dimensional slab of thickness d with an absorption cross section Σ_a and a scattering cross section Σ_s ($\Sigma_a + \Sigma_s = \Sigma_t$). We also assume that only forward scattering is possible. In the case of no absorption the probability of a particle to make n collisions along a trajectory d is given by

$$P(n|d) = \frac{(\Sigma_t d)^n}{n!} \exp(-\Sigma_t d) \tag{11}$$

When absorption is present we utilize survival biasing such that a particle can not be absorbed in a collision and is only foreward scattered with its weight reduced by a factor $C = \Sigma_s / \Sigma_t$. Thus the weight of a particle leaking through the slab after n collisions is the random variable $x = C^n$.

The average weight or transmission is given by:

$$\langle x \rangle = T = \sum_{n=0}^{\infty} C^n \frac{(\Sigma_t d)^n}{n!} \exp[-\Sigma_t d = \exp[-\Sigma_t d(1-C)] =$$

$$= \exp(-\Sigma_a d)$$

Suppose that Σ_t is varied into $\Sigma_t' = \Sigma_t + \Delta\Sigma_t$ such that Σ_a and Σ_s are multiplied by the same factor.Using correlated sampling the perturbed transmition will be estimated by the random variable

$$x' = x \cdot \frac{(\Sigma'_t d)^n}{(\Sigma_t d)^n} \frac{\exp(-\Sigma'_t d)}{\exp(-\Sigma_t d)} = C^n(\Sigma'_t/\Sigma_t)\exp[-(\Sigma'_t - \Sigma_t)d]$$

clearly the mean of x' will yield the perturbed transmission. Let us now determine the second moment of x'

$$S^2_{x'} = \sum_{n=0}^{\infty} x'^{2n} \frac{(\Sigma_t d)^n}{n!} \exp(-\Sigma_t d)$$

$$= \sum_{n=0}^{\infty} C^n \left(\frac{\Sigma'_t}{\Sigma_t}\right)^{2n} \exp[-2(\Sigma'_t - \Sigma_t)d] \frac{(\Sigma_t d)^n}{n!} \exp(-\Sigma_t d)$$

$$= \exp[-(2\Sigma'_t - \Sigma_t)d] \exp\left(C\Sigma'^2_t d/\Sigma_t\right) \tag{12}$$

$$= \exp\left\{d\left(\frac{C\Sigma'^2_t}{\Sigma_t} + \Sigma_t - 2\Sigma'_t\right)\right\}$$

Though there is no singularity in that second moment still if $\Sigma'^2_t \gg \Sigma_t$ the exponent may increase very fast, yielding an exponentially increasing variance.

In view of the above one should exercise care when attempting to calculate large perturbations with correlated sampling. Sudden increases in the variance of the perturbed response may occur when one gets into the proximity of singularities.

Correlated Sampling Applied to Sensitivity Analysis

Another point of interest concerns the comparison of calculations of sensitivities and perturbations in different energy groups. Consider a target response R (of any general nature) calculated with g energy groups. A perturbation is introduced into one of the parameters in all g energy groups (usually if Σ_r is perturbed, then $\frac{\Delta \Sigma_{ri}}{\Sigma_{ri}}$ is taken equal for all energy groups i = 1....g). A common tally of the perturbation is $\frac{\Delta R(i)}{R}$, defined as the relative change in the target response R due to a change in the i th' group only. The ratio ($\frac{\Delta R(i)}{R} / \frac{\Delta \Sigma_{ri}}{\Sigma_{ri}}$) for each "i" is the sensitivity profile. The total perturbation i.e. ΔR_t the change in the target response R due to a simultaneous change in all energy groups is calculated as the sum of the individual perturbations per group "i".

$$\Delta R_t = \sum_{i=1}^{g} \Delta R(i) \qquad (13)$$

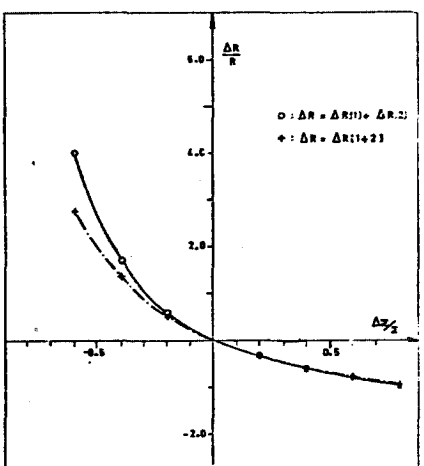

Fig.1- Cross group effect in a 2 group calculation of the leakage sensitivity

It is important to note that the above equation assumes no interference among the various groups i.e. it is assumed that $\Delta R(i)$ is independent of $\Delta \Sigma_r(i-1)$ (higher group). Such an assumption is only approximately correct. Because changing the group structure may also change ΔR_t especially when all g detector groups are collapsed into one group(resulting in an exact estimation of ΔR_t). This"cross group" effect can be demonstrated with the following simple arguments. Consider a case of two groups only (g=2) and let the total response be defined for simplicity over the lower group only. Let W_1 denote the weight acquired by a particle of the unperturbed game in the top group and W_1^* the weight of the perturbed game. W_2 and W_2^* are the corresponding quantities in the lower group

Clearly now $\Delta R(1)$ will be an average over weights of the form $W_1^* W_2$ thus

$$\Delta R(1) = \sum_{j=1}^{N} \frac{W_1^{*j} W_2^j - W_1^j W_2^j}{N}$$

(j referring to the j th particle) while $\Delta R(2)$ is given by

$$\Delta R(2) = \sum_{j=1}^{N} \frac{W_1^j W_2^{*j} - W_1^j W_2^j}{N}$$

No terms of the form $W_1^* W_2^*$ will appear in any of the cases. Now suppose the two groups are collapsed into one group, then

$$\Delta R_t = \sum_{j=1}^{N} \frac{W_1^{*j} W_2^{*j} - W_1^j W_2^j}{N} \qquad (14)$$

calculating ΔR_1 from the sum of $\Delta R(1) + \Delta R(2)$ we get

$$\Delta R_t^{(1,2)} = \sum_{j=1}^{N} \frac{W_1^{*j} W_2 + W_1^j W_2^{*j} - 2W_1^j W_2^j}{N} \qquad (15)$$

Equations (14) and (15) clearly demonstrate the dependence of ΔR_t on the group structure. It is therefore recommended to make comparisons between sensitivity profiles calculated by different codes with identical group structures. Not much can be said at this point on the extent and importance of this effect. While testing the perturbation features implemented in "TIMOC" we have searched for this effect on a limited number of problems. In Fig.1 results are shown for a two group calculation of a spherical geometry and a point source at the center (R_a = 5 cm). The response is leakage. The cross sections used are shown in Table I.

Table I

	Σ_t [cm^{-1}]	Σ_a/Σ_t	Σ_s/Σ_t	Σ_{11}/Σ_t	Σ_{12}/Σ_t
group 1 (top)	0.5	0.1	0.9	0.5	0.5
group 2	2.0	0.1	0.9	1.0	0

We see in the figure that at negative $\Delta \Sigma_t$ large differences (and errors if the summing method is used) may occur for perturbations larger then 20%. However in the range of first order perturbation theory (1% - 5%) no significant differences could be observed.

Next we considered an Iron sphere of radius 20 cm with a Californium point source at the center. The energy range between 52 KeV - 24.9 Mev was devided into 4 to 28 groups (using the EURLIB library). The response was total leakage through the sphere's surface. In table II results are given for this case for a 1% perturbation of the total cross section.

Table II

	sum of 28 groups	sum of 12 groups	sum of 4 groups	1 group
$\Delta R/R$	1.269×10^{-2}	1.242×10^{-2}	1.236×10^{-2}	1.231×10^{-6}

Some systematic differences may be noted yet these differences are small compared to the statistical accuracy so that no definite conclusion may be drawn. However, it seems that for 1% - 5% perturbation the difference will not exceed a few percent.

Finally in Table III we bring some comparative results between TIMOC and ANISN-SWANLAKE for the sensitivity profile of four energy groups for the above mentioned iron-sphere problem.

Table III

(Sensitivity Profiles)

	0.05-0.33 (MeV)	0.33-1.35 (MeV)	1.35-4.72 (MeV)	4.72-14.9 (MeV)	Total
TIMOC	6.8×10^{-2}	5.4×10^{-2}	2.3×10^{-2}	2.1×10^{-3}	0.147
SWANLAKE	5.89×10^{-2}	4.7×10^{-2}	1.999×10^{-2}	2.55×10^{-3}	0.135

These results are well within the statistical uncertainty of the calculations.

Conclusions

Though correlated sampling is becoming fast a common place tool of sensitivity studies in complicated systems. Still a lot must be learned and experience gathered as to its efficient and reliable use. Care should be exercised concerning the points raise in this note. There are still two problems worth investigating, one is the case of perturbations in deep penetration and the other is the calculation of sensitivity profiles for small energy intervals. One may assume that the first problem depends on the progress made in deep penetration in general. The second problem becomes important when detailed sensitivity profiles are required(for example in resonance regions). As energy intervals become smaller the accuracy of the perturbation of each group deteriorates due to the decrease of sample values. Further work should be done in that area. Possible approaches may be energy splitting and even scattering cross section biasing to direct more particles into important energy groups.

References

[1] Rief, H.: "An Attempt of Sensitivity Calculations in 3-D Geometries by Monte Carlo Techniques",Proceedings of the Specialists' Meeting on Sensitivity Studies and Shielding Benchmark,p.68 OECD Paris (Oct.1975)

[2] Rief, H.: "Sensitivity Studies in 3D Shielding Configurations", Differential and Integral Nuclear Data Requirements for Shielding Calculations, IAEA, Vienna (1976)

[3] Rief, H.: "Threedimensional Effects in Sensitivity Studies", Proc.of the 5th Intern.Conf.on Reactor Shielding, Knoxville (1977)

[4] Hall, M.C.G.: "Monte Carlo Perturbation Theory in Neutron Transport Calculations", ORNL-RSIC/44 (1980)

[5] LA-7396-M, (Los Alamos Sci.Lab.) November (1979)

[6] Dejonghe, G., Gonnord, J., Nimal, J.C.: "Study of Perturbations Using Correlated Monte Carlo Method", ORNL-RSIC/44 (1980)

[7] Rief,H., Dubi, A., Sundararaman, S.: "Experience with Correlated Tracking in Deep Penetration Monte Carlo Sensitivity Analysis", 1980 Advances in Reactor Physics and Shielding, ANS-Topical Meeting, Sun Valley (Sept.1980)

[8] Rief,H., Dubi,A.: "Manual of the TIMOC Sensitivity Version" EUR-Report to be published, 1980
Jaarsma,R., Rief, H.: "TIMOC-72 Code Manual", EUR-5016 Ispra(1973)

ETUDE DE PERTURBATIONS UTILISANT LA METHODE DE MONTE CARLO

G. DEJONGHE - J. GONNORD - J.C. NIMAL

COMMISSARIAT A L'ENERGIE ATOMIQUE
SERMA/LEP/
B.P. N° 2 - 91190 - GIF SUR YVETTE - FRANCE -

RESUME

L'influence de petites perturbations de sections efficaces sur un ensemble de réponses (flux, taux de réaction) ne peut être estimée avec une précision acceptable par des calculs de Monte Carlo indépendants.

Le code TRIPOLI différentiel, un programme de Monte Carlo à trois dimensions polycinétique, permet de calculer de telles variations en corrigeant les poids attribués aux particules préalablement simulées par un calcul TRIPOLI standard pour le problème non perturbé. Des exemples sont traités.

ABSTRACT

The influence of light perturbations of cross section on a set of responses (flux, reaction rates) cannot be estimated with an acceptable precision by statistically independent Monte Carlo calculations.

Differential TRIPOLI, a tridimensional, polykinetic code of Monte Carlo, permits to calculate such variations by correcting the weights of particles previously simulated by a standard TRIPOLI calculation for the non perturbed problem. Some examples are treated.

1 - INTRODUCTION

Les propriétés neutroniques d'un milieu sont caractérisées par les constantes nucléaires suivantes :

- pour chaque élément, un ensemble de sections efficaces microscopiques qui décrivent toutes les interactions possibles entre la particule et cet élément. Cet ensemble est complété par des lois de renvois en énergie et direction après interaction.

- pour chaque matériaux, la densité atomique de chaque nucléide.

L'ensemble de ces données nucléaires et de la description géométrique définit l'opérateur linéaire de l'équation de Boltzmann.

La théorie des perturbations consiste à évaluer l'évolution des réponses (flux, courants de particules, taux de réaction) lorsqu'on perturbe l'opérateur de Boltzmann. Cette théorie peut être appliquée à des problèmes variés, tels que les effets de température, de concentrations ou d'origine de bibliothèques ou encore les études de sensibilité. Nous avons exclu de notre étude les perturbations de géométrie.

L'influence des perturbations a été évaluée en utilisant le programme de Monte Carlo polycinétique à trois dimensions TRIPOLI [17].

2 - METHODE DE MONTE CARLO

La méthode de Monte Carlo résout l'équation de Boltzmann en simulant les histoires d'un grand nombre de particules.

Le comportement d'une particule est caractérisé par une chaîne d'évènements $(x_0, \ldots x_N)$ où x_i représente les coordonnées de position d'énergie et de direction $(\vec{r}_i, E_i, \vec{\Omega}_i)$ de la $i^{ème}$ collision de la particule.

A cause des splitting éventuels ayant lieu au cours de la simulation, un arbre d'évènements est associé à chaque particule. Une chaîne est par suite une séquence d'évènements successifs depuis la racine x_0 (naissance de la particule jusqu'à sa disparition x_N (fin de l'arbre).

Quand x_i est fixé, le prochain évènement x_{i+1} est choisi en accord avec les lois de probabilités qui dépendent des sections efficaces après l'état x_i. Un poids π_i est attribué à chaque noeud i de la chaîne, il est mis à jour après chaque collision. A partir de ces poids π_i nous calculons des flux courants et taux de réaction.

3 - METHODE DE MONTE CARLO POUR LE CALCUL DES PERTURBATIONS

Une perturbation de l'opérateur du transport apparaît du point de vue Monte Carlo comme une modification des lois de probabilité $(x_i \longrightarrow x_{i+1})$.

Comme pour les méthodes analytiques, deux calculs indépendants peuvent être faits pour trouver l'effet de perturbation, par différence entre deux résultats. Deux ensembles indépendants d'arbres sont alors créés.

Si ce procédé est valable pour de grandes perturbations, il est important de noter que des perturbations infinitésimales ne peuvent être atteintes de cette façon. L'incertitude statistique relative est inversement proportionnelle à ΔR où ΔR est la différence entre les deux réponses, si bien que l'incertitude relative devient infinie pour des perturbations tendant vers zéro.

Cette impossibilité n'existe plus si les deux calculs sont corrélés. La voie la plus naturelle pour introduire une corrélation est de considérer que le même échantillon d'arbres a été créé par les deux simulations. Avec ce modèle, l'influence de la perturbation n'est plus considérée comme une modification des lois de collision, mais comme une modification des poids des évènements.

Considérons l'ensemble des arbres et des poids non perturbés. Nous appellerons jeu initial cet ensemble. La méthode utilisée, consiste à reconstruire chaque arbre du jeu initial et à multiplier par un facteur correctif le poids à chaque noeud, ce facteur correctif tient compte de la perturbation. Pour un noeud donné c'est le produit cumulé sur tous les noeuds antérieurs des rapports des probabilités après perturbation aux probabilités correspondantes sans perturbation.

Cette méthode appelée méthode des échantillons corrélés est exacte et ne fait aucune hypothèse sur l'importance de la perturbation. Cependant, la dispersion des poids corrigés s'accroît avec l'amplitude de la perturbation, si bien que l'incertitude statistique croît aussi.

Ce procédé présente certains avantages :

- nous avons pu montrer que l'incertitude relative sur le résultat restait fini lorsque la perturbation tendait vers 0 [2]
- le temps de calculs des corrections de poids est faible de sorte que l'étude de plusieurs perturbations est plus brève en temps d'ordinateur que le calcul de Monte Carlo initial.
- plusieurs perturbations peuvent être traitées simultanément.

Les limitations de l'amplitude des perturbations dépendent seulement du comportement de l'incertitude statistique. Ces limitations n'ont pas encore fait l'objet d'études approfondies sur la solution de l'équation de Boltzmann.

Nous allons montrer ces limitations sur quelques exemples.

4 - METHODE DES ECHANTILLONS CORRELES APPLIQUEE AUX LOIS DE PROBABILITE EXPONENTIELLE ET ROULETTE RUSSE

Ces deux lois interviennent dans le processus de Monte Carlo permettant à une particule de passer de l'état x_i à l'état x_{i+1}.

4.1. Sensibilité du parcours moyen d'un neutron à la section efficace totale d'un milieu

4.1.1. Simulations non corrélées

Le parcours cumulé moyen d'un neutron diffusant dans un milieu dont la section efficace totale est σ_0, est $\frac{n}{\sigma_0}$ après n collisions.

Une façon simple pour simuler le parcours total d'un neutron est de choisir un ensemble de n valeurs indépendantes $(x_1, \ldots\ldots x_N)$ avec la probabilité $\sigma_0 e^{-\sigma_0 x_i} dx_i$ pour chaque évènement.

Nous cumulons les quantités x_i pour obtenir le parcours total en n collisions. La variance sur le résultat est n/σ_0^2 et l'incertitude relative e (σ_0) est $\frac{1}{\sqrt{n}}$, indépendant de σ_0.

Soit $\sigma_1 = \sigma_0 + \Delta\sigma$ la section efficace du milieu perturbé. Une simulation indépendante donnerait pour espérance mathématique de la réponse n/σ_1 avec la variance n/σ_1^2.

Avec deux calculs indépendants, la réponse différentielle

(1) $\Delta R = \frac{n}{\sigma_1} - \frac{n}{\sigma_0}$ est obtenue avec la variance $\frac{n}{\sigma_1^2} + \frac{n}{\sigma_0^2}$,

si bien que l'incertitude statistique relative sur ΔR est :

(2) $$e\left(\frac{\Delta\sigma}{\sigma_0}\right) = \frac{1}{\sqrt{n}} \frac{\sqrt{\sigma_0^2+\sigma_1^2}}{\Delta\sigma}$$

Elle tend vers l'infini lorsque $\Delta\sigma$ tend vers 0.

4.1.2. Méthode des échantillons corrélés

Supposons que la chaîne apparaisse avec la même probabilité :

(3) $$\prod_{i=1}^{N} \left\{ \sigma_0 e^{-\sigma_0 x_i} \right\} dx_1 \cdots dx_n$$

Lorsque la section efficace totale devient σ_1, nous attribuons un poids C_i à chaque évènement, c'est-à-dire à chaque x_i, déterminé comme suit :

(4) $$C_0 = 1$$
$$C_i = C_{i-1} \times C(X_i)$$
où $C(X_i) = \frac{\sigma_1 e^{-\sigma_1 x_i}}{\sigma_0 e^{-\sigma_0 x_i}}$

est le rapport de la densité de probabilité dans le jeu perturbé à la même densité dans le jeu non perturbé. On démontre, que si on cumule les produits $C_i x_i$ pour chaque i, le score total est le résultat attendu $\frac{n}{\sigma_1}$. La variance n'est plus n/σ_1^2 mais est donnée par σ^{*2} :

(5) $$\sigma^{*2} = \frac{2\sigma_1\sigma_0}{(\Delta\sigma)^2}\left[(1-\xi)(1-\xi^n)\frac{\sigma_0}{\sigma_1} + \xi^n - n\xi + n - 1\right] - \frac{n^2}{\sigma_1^2}$$

(6) où $$\xi = \frac{\sigma_1^2}{\sigma_0(2\sigma_1-\sigma_0)}$$

On démontre que pour σ^{*2} soit fini, il faut et il suffit que ξ soit positif. Il est donc indispensable que σ_1 soit plus grand que $\sigma_0/2$

(7) $$\sigma_1 > \frac{\sigma_0}{2}$$

La figure 1 donne l'évolution du rapport de l'incertitude relative $e^*(\sigma_1)$ par la méthode des échantillons corrélés à l'incertitude du calcul indépendant avec la section efficace σ_1.

FIGURE 1

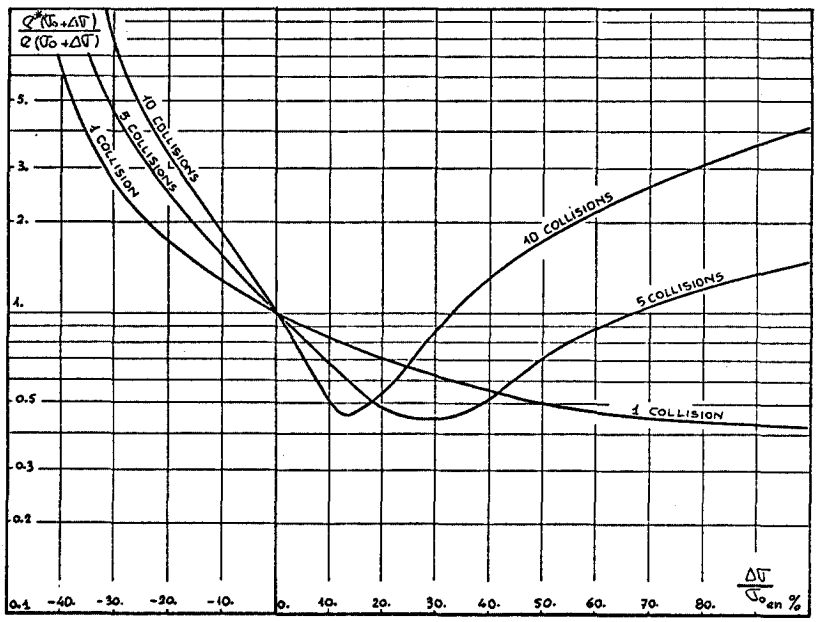

Nous avons évalué la variance sur l'effet différentiel ΔR par la méthode des échantillons corrélés. Cette variance s'écrit sous la forme (8) :

$$(8) \qquad \sigma^{*2}(\Delta R) = \frac{n}{\sigma_0^2} + \sigma^{*2} - 2\,cov$$

où cov est la covariance des deux estimateurs qui s'écrit :

$$cov = \frac{n}{2\sigma_1}\left\{\frac{n+3}{\sigma_1} + \frac{n+1}{\sigma_0}\right\}$$

A partir de l'expression (8), il est possible de calculer l'expression (9) de l'incertitude relative e^* sur l'effet différentiel estimée par la méthode des échantillons corrélés lorsque $\Delta\sigma$ tend vers 0. Cette incertitude relative limite est finie, contrairement à celle obtenue lorsqu'on calcule l'effet de perturbation par différence de deux calculs de Monte Carlo indépendants.

$$(9) \qquad e^*(\Delta\sigma, \sigma_0) \xrightarrow[\Delta\sigma \to 0]{} e(\sigma_0)\sqrt{\frac{n^2+9n+29}{3}}$$

La figure 2 représente les variations en fonction de $\frac{\Delta\sigma}{\sigma_0}$ du rapport $e^*(\Delta\sigma,\sigma_0)/e(\sigma_0)$ dans les deux cas suivants :

- méthode des échantillons corrélés (asymptote $\frac{\Delta\sigma}{\sigma} = -50\ \%$)
- méthode de différence de deux calculs indépendants (asymptote à $\Delta\sigma = 0$).

Cette figure 2 montre la zone d'amélioration apportée par la méthode des échantillons corrélés.

FIGURE 2

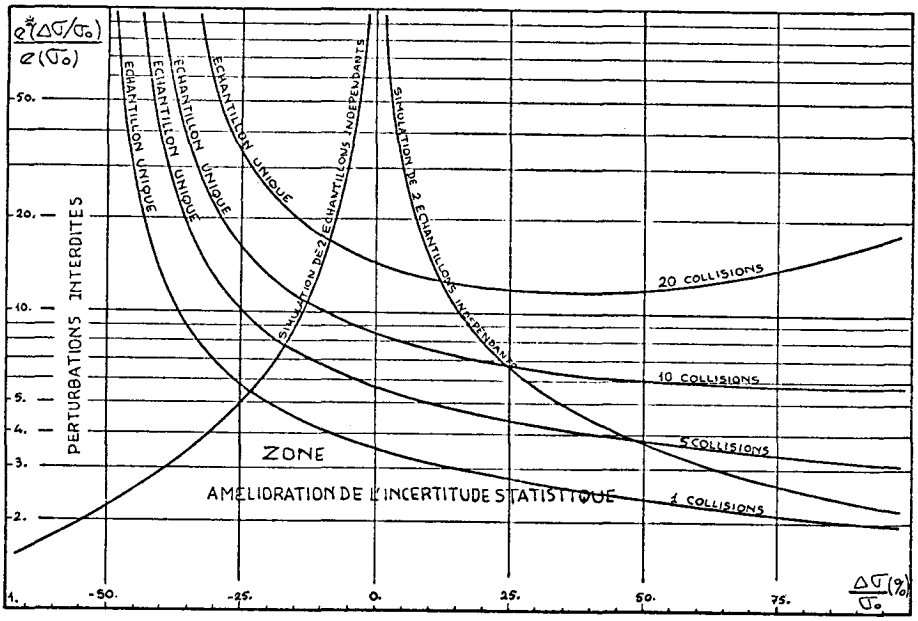

4.2. Sensibilité du nombre de collisions à la probabilité de non absorption Co

4.2.1. Simulation originale

Dans cet exemple nous créons des chaînes de longueur variable (x_1, x_2... x_N). Si Co est la probabilité de non absorption, la particule survit après chaque collision avec la probabilité Co et nous ajoutons $x_i = 1$ au score total S défini par (10).

(10) $$S = \sum_{i=1}^{n} x_i = n$$

La particule est tuée avec la probabilité (1 - Co).

L'espérance mathématique du score est $\frac{1}{1-Co}$. Si la probabilité de non absorption devient $C_1 = Co + \Delta C$, une simulation indépendante donne une incertitude relative (11) sur la réponse différentielle ΔR donnée par (12).

(11) $$e(\Delta C, C_0) = \frac{1}{\Delta C} \sqrt{C_1(1-C_0)^2 + C_0(1-C_1)^2}$$

(12) $$\Delta R = \frac{\Delta C}{(1-C_1)(1-C_0)}$$

Cette incertitude relative $e\ (\Delta C, C_0)$ tend vers l'infini lorsque ΔC tend vers 0.

4.2.2. Méthode des échantillons corrélés

Nous attribuons un poids Pi à chaque évènement défini par (13)

(13) $P_0 = 1$

$$P_i = P_{i-1} \times \frac{C_1}{C_0}$$

Le score perturbé devient $\sum_i P_i x_i$ et son espérance mathématique est $\frac{1}{1 - C_1}$. La variance σ^{*2} n'est définie que pour $C_1 < \sqrt{C_0}$ et à l'expression (14) :

(14) $$\sigma^{*2} = \frac{C_1}{(1-C_1)^2} \frac{1-C_0}{(C_0-C_1^2)}$$

La méthode des échantillons corrélés n'est applicable que pour $C_1 < \sqrt{C_0}$.

Nous avons enfin démontré que l'incertitude relative sur l'effet de différence ΔR évaluée par la méthode des échantillons corrélés restait fine pour ΔC tendant vers 0. L'incertitude limite est donnée par (15).

(15) $$e(C_0)\sqrt{\frac{5C_0 + (1-C_0)^2}{C_0^2}}$$

5 - TRANSPORT DANS UNE PLAQUE

5.1. Référence

Une comparaison a été effectuée entre TRIPOLI DIFFERENTIEL et un calcul analytique dans le cas d'un milieu infini homogène pour des neutrons monocinétiques diffusant isotropiquement. Dans ce cas la théorie du transport montre que le flux intégré sur les angles peut être décomposé en 2 termes : φ_{as} et φ_t. Seul le premier terme prédomine à grande distance de la source et de la face de sortie. Il est alors possible de calculer avec une grande précision les valeurs de $\varphi_{as}\ (\sigma,\ C,\ x)$ pour toutes valeurs des paramètres :

σ section totale du milieu
C probabilité de non absorption du milieu
x distance à la source.

Ces valeurs nous servirons ensuite de référence.

5.2. Calcul non perturbé par TRIPOLI

La composition du milieu est faite de deux éléments fictifs :

TABLEAU I -

Eléments	Masse	σ_a barn	σ_s barns	Densité N/cm^3
1	10^6	0.4	1.6	$2\ 10^{23}$
2	10^6	0.3	2.7	$3\ 10^{23}$

La masse atomique des deux éléments est choisie égale à 10^6 de telle sorte que les collisions soient isotropes dans le système du laboratoire et la perte

d'énergie après chaque collision négligeable. La géométrie est une plaque de 17 cm d'épaisseur divisée en 13 zones.

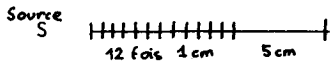

Une fonction spatiale d'importance $\vec{J}(x) = \exp(k_0 x)$ est attribuée au milieu, K_0 étant facteur d'atténuation théorique pour le flux asymptotique, de telle sorte que le nombre de collisions simulées soit pratiquement constant par unité de volume en fonction de x.

Le flux moyen par zone a été calculé à partir d'un échantillon de 300 neutrons.

Les résultats de TRIPOLI sont en parfait accord avec le calcul analytique sauf dans les deux premières régions où le flux non asymptotique prédomine. Les 300 arbres sont stockés pour être utilisés par TRIPOLI DIFFERENTIEL.

5.3. Perturbation de la section totale σ_0

L'influence de 15 perturbations de σ pour une valeur fixe de C=0.86923.

TABLEAU II- VARIATION DU FLUX MOYEN PERTURBE DANS LA ZONE CENTRALE DE LA PLAQUE (5 - 9 cm) en fonction de σ

Perturbation	φ_{AS} Calcul analytique	φ_{MC} Calcul TRIPOLI DIFF.	Variance en %	$\frac{\lvert\varphi_{MC} - \varphi_{AS}\rvert}{\varphi_{AS}}$ en %
σ : - 75 %	5.333 E-1	3.025 E-1	59.68	43.28
σ : - 50 %	1.488 E-1	1.095 E-1	18.11	26.40
σ : - 40 %	9.047 E-2	7.941 E-2	15.26	12.22
σ : - 30 %	5.536 E-2	5.268 E-2	11.51	4.84
σ : - 20 %	3.409 E-2	3.329 E-2	6.92	2.36
σ : - 10 %	2.112 E-2	2.085 E-2	4.11	1.27
σ : - 1 %	1.381 E-2	1.366 E-2	3.83	1.05
problème non perturbé	1.316 E-2	1.315 E-2	3.53	9.44 E-2
σ : + 1 %	1.255 E-2	1.247 E-2	3.85	0.64
σ : + 10 %	8.240 E-3	8.385 E-3	3.63	1.75
σ : + 20 %	5.186 E-3	5.425 E-3	4.17	4.62
σ : + 30 %	3.278 E-3	3.541 E-3	5.44	8.01
σ : + 40 %	2.081 E-3	2.307 E-3	7.68	10.87
σ : + 50 %	1.326 E-3	1.485 E-3	11.02	12.01
σ : + 75 %	4.359 E-4	4.460 E-4	21.74	2.31
σ : + 100 %	1.459 E-4	1.094 E-4	30.57	25.03

Nous remarquons que pour des perturbations variant de -0.3 à + 0.5 les résultats sont corrects. De plus le rapport des incertitudes statistiques des jeux perturbés et non perturbés ne dépasse pas le facteur 3.

Une dégradation très importante de la précision apparaît pour

$-0.75 < \frac{\Delta\sigma}{\sigma_0} < -0.5$. La valeur limite théorique de la perturbation étant de -0.796 compte tenu de la transformation exponentielle.

TABLEAU III - VARIATION DE L'EFFET DIFFERENTIEL DANS LA ZONE CENTRALE (5cm-9cm) en fonction de σ

Perturbation	$\frac{\Delta\varphi_{MC}}{\varphi_{MC}}$	$\Delta\varphi_{AS}$ Calcul analytique	$\Delta\varphi_{MC}$ TRIPOLI	Variance sur $\Delta\varphi_{m.c}$ en %	$\frac{\lvert\Delta\varphi_{MC} - \Delta\varphi_{AS}\rvert}{\Delta\varphi_{AS}}$ en %
σ: - 75 %	22	5.201 E-1	2.893 E-1	62.29	44.38
σ: - 50 %	7.33	1.357 E-1	9.641 E-2	20.36	28.94
σ: - 40 %	5.04	7.731 E-2	6.625 E-2	17.93	14.30
σ: - 30 %	3.01	4.220 E-2	3.953 E-2	14.69	6.32
σ: - 20 %	1.53	2.093 E-2	2.014 E-2	10.03	3.78
σ: - 10 %	5.86 E-1	7.962 E-3	7.708 E-3	6.25	3.19
σ: - 1 %	4.64 E-2	6.341 E-4	6.108 E-4	4.86	3.67
σ: + 1 %	-4.43 E-2	-6.046 E-4	-5.821 E-4	3.94	3.72
σ: + 10 %	-3.62 E-1	-4.918 E-3	-4.759 E-3	3.82	3.23
σ: + 20 %	-5.87 E-1	-7.972 E-3	-7.720 E-3	3.48	3.17
σ: + 30 %	-7.30 E-1	-9.880 E-3	-9.604 E-3	3.22	2.79
σ: + 40 %	-8.24 E-1	-1.108 E-2	-1.084 E-2	3.05	2.16
σ: + 50 %	-8.87 E-1	-1.183 E-2	-1.166 E-2	3.01	1.48
σ: + 75 %	-9.66 E-1	-1.272 E-2	-1.270 E-2	3.18	1.90 E-1
σ: + 100 %	-9.91 E-1	-1.301 E-2	-1.303 E-2	3.39	1.67 E-1

FIGURE 3

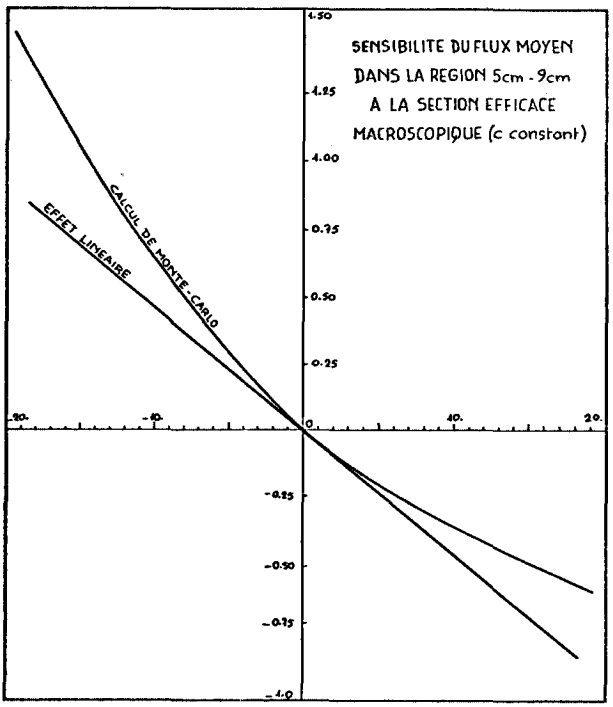

Le tableau III où sont représentées les variations de l'effet différentiel en fonction de σ et la courbe 4 montre que la méthode des échantillons corrélés reste valable dans le domaine de non linéarité de la perturbation.

5.4. Perturbation de la probabilité de non absorption C

Des flux perturbés ont été calculés pour différentes variations de C à σ constant. Le tableau IV montre la forte non linéarité de la réponse en fonction de ΔC.

TABLEAU IV- VARIATION DU FLUX MOYEN PERTURBE DANS LA ZONE CENTRALE (5cm-9cm) EN FONCTION DE C

Perturbation	α (C) (pente)	φ AS Calcul analytique	φ MC Calcul TRIPOLI	Variance sur φ_{MC} en %	$\frac{\lvert\varphi_{MC} - \varphi_{AS}\rvert}{\varphi_{AS}}$ (en %)
C : - 20 %	0.83302	9.550 E-4	9.589 E-4	2.17	4.08 E-1
C : - 10 %	0.73501	2.884 E-3	2.859 E-3	2.83	8.62 E-1
C : - 1 %	0.60985	1.098 E-2	1.096 E-2	3.36	1.82 E-1
C : - 0.1 %	0.59456	1.292 E-2	1.290 E-2	3.52	1.43 E-1
problème non perturbé	0.59283	1.316 E-2	1.315 E-2	3.53	9.44 E-2
C : + 0.1 %	0.59108	1.340 E-2	1.339 E-2	3.55	7.46 E-2
C : + 1 %	0.57498	1.590 E-2	1.590 E-2	3.74	6.29 E-3
C : + 5 %	0.49364	3.802 E-2	3.799 E-2	5.22	8.55 E-2

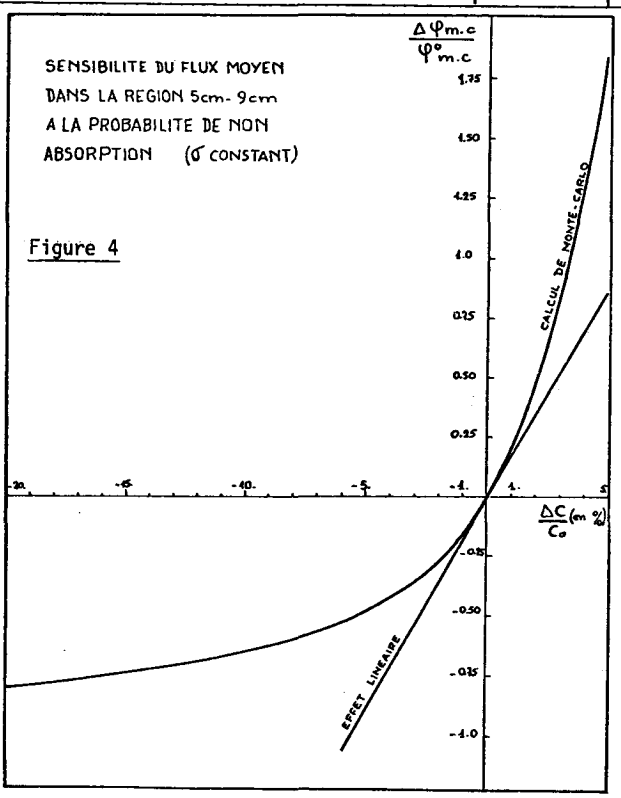

La figure 4 montre la non linéarité des effets observés dans la zone centrale de la plaque et calculée par TRIPOLI DIFFERENTIEL.

6 - SENSIBILITE DE L'ECHAUFFEMENT D'UN THERMOMETRE GAMMA A LA SECTION EFFICACE TOTALE DE $^{238}_{92}U$

Le problème posé est le calcul de l'échauffement d'un crayon d'acier situé en (0, 0) dû uniquement à l'émission de gamma dans le crayon combustible situé en (8, 7). La figure 5 représente un huitième d'assemblage PWR immergé dans l'eau. Des conditions de symétrie sont appliquées aux limites de la géométrie. Les gamma ont été émis uniformément dans le bande 1.75 - 1.25 MeV. L'intensité de la source est de 0.7269 γ/s.

Le calcul TRIPOLI standard a donné les résultats suivants :

- échauffement	4.32 E-19 watt/g
- incertitude relative	4.75 % à 66 % de confiance

Nous avons perturbé la section efficace totale de l'uranium 238.

Les tableaux V et VI donnent les variations relatives de l'échauffement en fonction de l'amplitude de la perturbation de section efficace totale de $^{238}_{92}U$. Cette perturbation de section efficace a été faite dans deux créneaux d'énergie 1.75 MeV - 1.26 MeV et 1.26 MeV - 0.708 MeV.

FIGURE 5

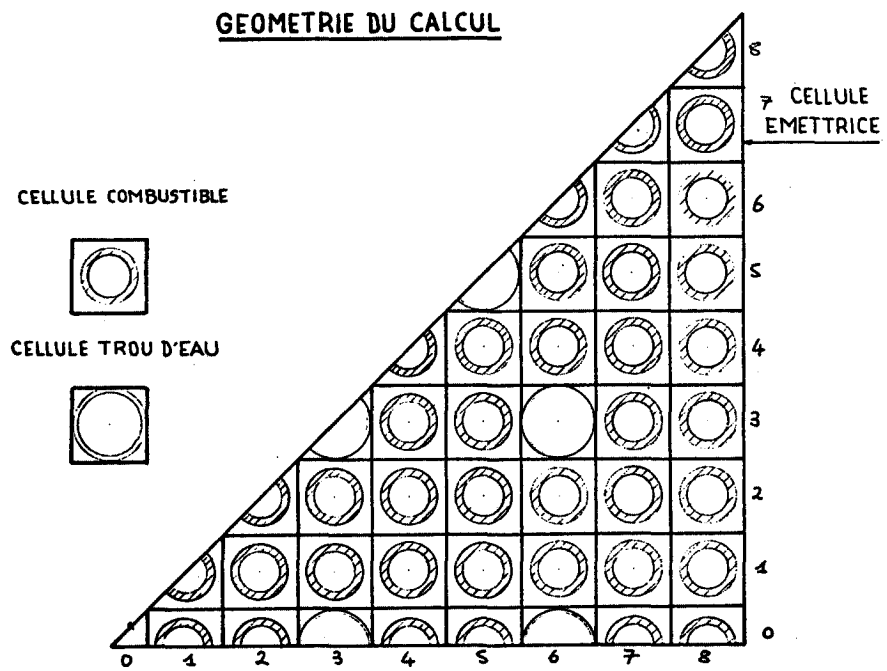

TABLEAU V - SENSIBILITE DE L'ECHAUFFEMENT DU THERMOMETRE GAMMA A LA SECTION EFFICACE TOTALE DE U^{238}_{92} PERTURBE DANS LE CRENEAU 1.75 - 1.26 MeV

Perturbation $\frac{\Delta\sigma}{\sigma}$ en %	- 20	- 10	- 5	- 1	+ 1	+ 5	+ 10	+ 20
Variation relative de la réponse en % $\Delta R/R_o$	31.4	14.4	6.88	1.33	- 1.31	- 6.32	- 12.1	-22.4
Quotient de l'incertitude relative sur ΔR à l'incertitude relative sur R_o	1.41	1.38	1.37	1.36	1.35	1.34	1.33	1.31

TABLEAU VI- SENSIBILITE DE L'ECHAUFFEMENT DU THERMOMETRE GAMMA A LA SECTION EFFICACE TOTALE DE U^{238}_{92} PERTURBEE DANS LE CRENEAU 1.26 - 0.708 MeV

Perturbation $\frac{\Delta\sigma}{\sigma}$ en %	- 20	- 10	- 5	- 1	+ 1	+ 5	+ 10	+ 20
Variation relative de la réponse en % $\Delta R/R_o$	6.79	3.14	1.51	0.293	-0.289	- 1.40	- 2.71	- 5.05
Quotient de l'incertitude relative sur ΔR à l'incertitude relative sur R_o	1.82	1.80	1.80	1.80	1.79	1.79	1.79	1.79

REFERENCES

1 J.C. NIMAL et coll.
Programme de Monte Carlo Polycinétique à trois dimensions TRIPOLI 01
Note CEA.N.1919 (1 à 7) tomes 1 à 7 - Septembre 1976

2 G. DEJONGHE
Thèse d'ingénieur docteur de la Faculté d'Orsay
(à paraître)

DUCKPOND - A PERTURBATION MONTE CARLO AND ITS APPLICATIONS

by

M C G Hall*

ABSTRACT

The need to obtain sensitivities in complicated geometrical configurations has resulted in the development of Monte Carlo sensitivity estimation. A new method has been developed to calculate energy-dependent sensitivities of any number of responses in a single Monte Carlo calculation with a very small time penalty. This estimation typically increases the tracking time per source particle by about 30%. The method of estimation is explained. Sensitivities obtained are compared with those calculated by discrete ordinates methods. Further theoretical developments, such as second order perturbation theory and application to k_{eff} calculations are discussed. The application of the method to uncertainty analysis and to the analysis of benchmark experiments is illustrated.

INTRODUCTION

The result of a neutron transport calculation can be very sensitive to nuclear data, and experimental error in these data may cause the result to be misleading. To determine how important this effect is, it is necessary to calculate sensitivities and combine them with covariance information to obtain the standard deviation of the result. If the uncertainty arising in this way is unacceptably large, then the nuclear data must be improved. One way to do this is to adjust on the basis of a benchmark experiment, which also involves the calculation of sensitivities. The motivation for this work is the need to calculate sensitivities in geometries which, because of their complexity, require a Monte Carlo calculation.

There are additional advantages in using a Monte Carlo method for the analysis of benchmark experiments. All the sensitivity information can be estimated simultaneously, whereas conventional methods require a separate adjoint calculation for each channel of experimental information. Also group-averaging errors can be avoided by the use of point nuclear data, so the adjustments should reflect shortcomings in the basic data, rather than difficulties in a group-averaging process. The number of

* Work performed during author's attachment to Radiation Physics and Shielding Group, Reactor Physics Division, AEE Winfrith.

sensitivity coefficients which need to be estimated though, can be as many as a thousand, so it is essential that each should be scored with very little time penalty.

The method described here has been implemented with all this in mind, although the approach has been kept as general as possible, so that different applications can be catered for.

METHOD

Any response R can be considered as an average value associated with the set P of all neutron paths:

$$R = \sum_{m \in P} r^m p^m . \tag{1}$$

Here p^m is the probability of path m, and r^m is the estimator for path m. If $\hat{D}$ is a linear perturbation operator, then $\hat{D}$ operating on Eq. (1) gives

$$\hat{D}R = \sum_{m \in P} \hat{D}(r^m p^m) . \tag{2}$$

Writing Eq. (2) in the form of Eq. (1)

$$\hat{D}R = \sum_{m \in P} dr^m p^m \tag{3}$$

where

$$dr^m = \{\hat{D}(r^m p^m)\}/p^m , \tag{4}$$

so dr^m is an estimator of $\hat{D}R$. Re-arranging Eq. (4)

$$dr^m = v^m r^m \tag{5}$$

where

$$v^m = \{\hat{D}(r^m p^m)\}/(r^m p^m) , \tag{6}$$

so dr^m is a weighted version of r^m.

This estimator has the disadvantage that it is bad at estimating the component of a change which is zero because of physical restrictions. For example, in a non-multiplying medium a perturbation of a cross-section at low energy usually cannot affect the flux at high energy. But even if $\hat{D}$ only operates on cross-sections at low energy and r^m only scores flux at high energy, the estimator dr^m given by Eq. (4) will still in general be non-zero, although it will have zero expectation. A more discerning estimator would itself be zero under these circumstances. To achieve this r^m and p^m are split into components associated with each trajectory of path m:

$$r^m = \sum_{i \le t^m} s_i^m \qquad (7)$$

and

$$p^m = \prod_{j \le t^m} q_j^m \ . \qquad (8)$$

In this context: a trajectory is a section of a path along which no collisions or boundary crossings occur; t^m is the number of trajectories in path m; s_i^m is the contribution to the estimator for path m arising from the i^{th} trajectory; q_j^m is the probability of the j^{th} trajectory, given that the $(j-1)^{th}$ trajectory has occurred. It is shown in the appendix that another estimator for $\hat{D}R$ is given by

$$dr^m = \sum_{i \le t^m} \left\{ \hat{D}\left(s_i^m \prod_{j \le i} q_j^m\right) \right\} \Big/ \prod_{j \le i} q_j^m \ . \qquad (9)$$

This estimator will always be zero in the circumstances which have just been mentioned. This is because, in Eq. (9), by the time i is large enough for $\hat{D}$ to operate on s_i^m and q_j^m, the value of s_i^m is zero. Re-arranging as before

$$dr^m = \sum_{i \le t^m} \omega_i^m s_i^m \qquad (10)$$

where

$$\omega_i^m = \left\{ \hat{D}\left(s_i^m \prod_{j \le i} q_j^m\right) \right\} \Big/ \left(s_i^m \prod_{j \le i} q_j^m\right) \ . \qquad (11)$$

These are the key expressions used in the method. The two expressions for dr^m in Eqs. (5) and (10) can be compared by writing Eq. (5) as

$$dr^m = \sum_{i \le t^m} v^m s_i^m \qquad (12)$$

IMPLEMENTATION

Implementation consists of specifying $\hat{D}$, s_i^m and q_j^m of Eq. (11), evaluating the weights ω_i^m, and scoring the estimator dr^m in the same way as the estimator r^m.

Specifying $\hat{D}$

The form of $\hat{D}$ is determined by the nature of the perturbations of interest. In the analysis of a benchmark experiment it is usual to regard the result R of a calculation as a function of the nuclear data $\underline{x}$:

$$\hat{z} = R(\underline{x}) \tag{13}$$

$\underline{x}$ is subject to experimental error and may be perturbed by an amount $\delta\underline{x}$. The Taylor expansion of R about $\underline{x}$ is

$$\delta R = \sum_i \delta x_i \frac{\partial}{\partial x_i} R + \frac{1}{2!} \sum_{ij} \delta x_i \delta x_j \frac{\partial^2}{\partial x_i \partial x_j} R + \tag{14}$$

Writing this in dimensionless terms

$$\frac{\delta R}{R} = \sum_i \frac{\delta x_i}{x_i} \frac{x_i}{R} \frac{\partial}{\partial x_i} R + \frac{1}{2!} \sum_{ij} \frac{\delta x_i}{x_i} \frac{\delta x_j}{x_j} \frac{x_i x_j}{R} \frac{\partial^2}{\partial x_i \partial x_j} R + \tag{15}$$

Often some of the values of $\delta x_i / x_i$ are constrained to be equal—for example they may be subject to a systematic error. Suppose for a set of integers K and associated constant c_K there is a constraint

$$\delta x_i / x_i = c_K \quad i \in K \tag{16}$$

—similarly for another set L and constant c_L. In this case Eq. (15) can be factorised:

$$\frac{\delta R}{R} = \sum_K c_K \sum_{i \in K} \frac{x_i}{R} \frac{\partial}{\partial x_i} R + \frac{1}{2!} \sum_K \sum_L c_K c_L \sum_{i \in K} \sum_{j \in L} \frac{x_i x_j}{R} \frac{\partial^2}{\partial x_i \partial x_j} R + \cdots \tag{17}$$

The terms which it is useful to know are

$$\sum_{i \in K} \frac{x_i}{R} \frac{\partial}{\partial x_i} R \tag{18}$$

and

$$\sum_{i \in K} \sum_{j \in L} \frac{x_i x_j}{R} \frac{\partial^2}{\partial x_i \partial x_j} R \,. \tag{19}$$

The first of these terms can be written as

$$(1/R) \hat{D} R \tag{20}$$

where

$$\hat{D} = \sum_{i \in K} x_i \frac{\partial}{\partial x_i} \,. \tag{21}$$

This is the form of $\hat{D}$ considered in this section.

Specifying S and q

The quantities S and q are determined by the type of trajectory and by the method of estimation. Suppose a trajectory starts with a neutron undergoing a reaction type α at energy E. The neutron is scattered through an angle θ to energy E', continues for a length λ and then collides. The cross-section for reaction β at energy E is x_j^β. For convenience x_j^B is defined by

$$x_j^B = \sum_{\beta \in B} , \tag{22}$$

where B is a set of partial cross-sections. The probability of the trajectory alone is given by

$$q = (x_j^\alpha / x_j^T)\, p(\theta)\, d\theta\, p(E,E')\, dE' \exp(-x_j^T \lambda)\, x_j^T\, d\lambda . \tag{23}$$

Here T is the set of all reactions making up the total cross-section and $p(\theta)d\theta\, p(E,E')dE'$ is the probability distribution function in phase-space of the secondary neutron. If a Monte Carlo code uses point nuclear data, then values such as x_j^β are used in the sampling procedure. In this case $\hat{D}$ might be given by

$$\hat{D} = \sum_{\beta \in P} \sum_{h \in G} x_h^\beta \frac{\partial}{\partial x_h^\beta} . \tag{24}$$

Here P is a set of cross-section types, for example non-elastic, and G is a set of values of h comprising an energy interval. In this case $(1/R)\hat{D}R$ would be the sensitivity of R to the non-elastic cross-section in the G^m energy interval.

If track length estimation is used, the contribution to the estimator for the trajectory will be given by

$$s = \lambda \sigma_j , \tag{25}$$

where σ_j is a response cross-section at energy E'. If collision density estimation is used, then

$$s = \sigma_j / x_j^T . \tag{26}$$

Evaluating ω_i^m

The symbol δ_α^P is defined to be unity if α belongs to the set P, and otherwise to be zero. If $\hat{D}$ is given by Eq. (24) and track length estimation is used, the weight ω_i^m is given by

$$\omega_i^m = \sum_{j \le i} \left\{ \delta_\alpha^P - \delta_j^G (x_j^P / x_j^T) - \delta_j^G (x_j^P, \lambda) + \delta_j^G (x_j^P / x_j^T) \right\} \quad . \qquad (27)$$

If collision density estimation is used, then

$$\omega_i^m = \sum_{j \le i} \left\{ \delta_\alpha^P - \delta_j^G (x_j^P / x_j^T) - \delta_j^G (x_j^P, \lambda) \right\} \quad . \qquad (28)$$

Fortunately the weights can be evaluated using a recursion formula—for example with track length estimation

$$\omega_i^m = \omega_{i-1}^m + \left\{ \delta_\alpha^P - \delta_j^G (x_j^P / x_j^T) - \delta_j^G (x_j^P, \lambda) + \delta_j^G (x_j^P / x_j^T) \right\} \quad . \qquad (29)$$

It can be seen from Eq. (29) why the method is so fast. The values of x_j^P, x_j^T, $x_{j'}^P$, $x_{j'}^T$ and λ are all available in an unperturbed calculation, so the weight ω_i^m only has to assemble information which is already there. In addition, the weight ω_i^m can be applied to any estimator s_i^m, which means that sensitivities to any number of responses can be scored simultaneously.

Scoring dr^m

A code called DUCKPOND[1] has been written to score the estimator dr_i^m. Full use has been made of the Winfrith Shielding Group's suite of Monte Carlo modules. This has meant that DUCKPOND has been coded with a minimum of effort yet includes the powerful capabilities familiar to users of McBEND[2]. In addition to a sensitivity capability, DUCKPOND can score a covariance matrix for all the estimated responses. This is useful in analysing benchmark experiments.

COMPARISON

Sensitivities can be obtained in limited circumstances using discrete ordinates (S_N) calculations, so an important test is to compare results of this type with answers estimated using the Monte Carlo method. The only difficulty with the comparison is that the discrete ordinates calculation may involve group averaging errors, whereas this will not be the case with Monte Carlo estimation using point nuclear data. To determine the extent of this problem, fluxes are compared in addition to sensitivities.

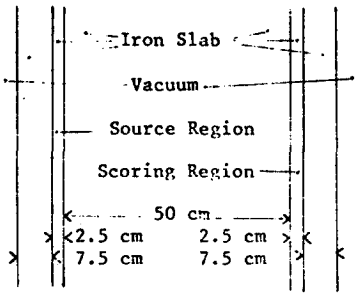

Fig. 1. The Geometry of the Test Problem.

The geometry of the test problem is illustrated in Fig. 1. The response function is for total flux per unit volume betweem 14.9 MeV and 407 KeV; the source has a fission spectrum normalised to $1.0\ cm^{-3}\ s^{-1}$. Sensitivities to the elastic and non-elastic cross-sections of iron are calculated in forty groups of approximately equal lethargy width between 14.9 MeV and 407 KeV, corresponding to the first forty groups of the 100-group EURLIB[3] structure. Flux per unit volume in the scoring region is calculated in the same group scheme.

ANISN[4] and SWANLAKE[5] were used for the S_n calculations and DUCKPOND for the Monte Carlo estimation. Fluxes and sensitivities are compared in Figs. 2 and 3; the errors plotted for the Monte Carlo results are an estimate of one standard deviation.

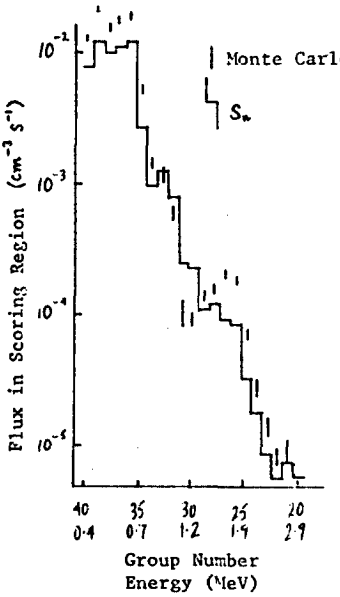

Fig. 2. Comparison of Flux in Scoring Region calculated by Monte Carlo and S_n Methods.

The Monte Carlo sensitivity estimation is working well. The agreement with the S_n method is convincing and, equally important, acceptable variances have been obtained with a workable sample size. DUCKPOND was run in this case for twenty minutes on an IBM 3033 using automatically-generated importance sampling, and the test problem is representative in scale of a realistic calculation. Moreover a comparison of running times between DUCKPOND and its non-perturbative equivalent McBEND show that sensitivity estimation typically slows down tracking by 30%. To give an example—for the same price a response might either be estimated by McBEND with a standard deviation of 10%, or estimated by DUCKPOND with a standard deviation of 11.4% but with a full set of sensitivity profiles. If the sensitivities reveal uncertainty of 20% arising from data errors, then the DUCKPOND calculation would be the more useful. It would be sensible to perform an uncertainty analysis of this kind on all Monte Carlo calculations.

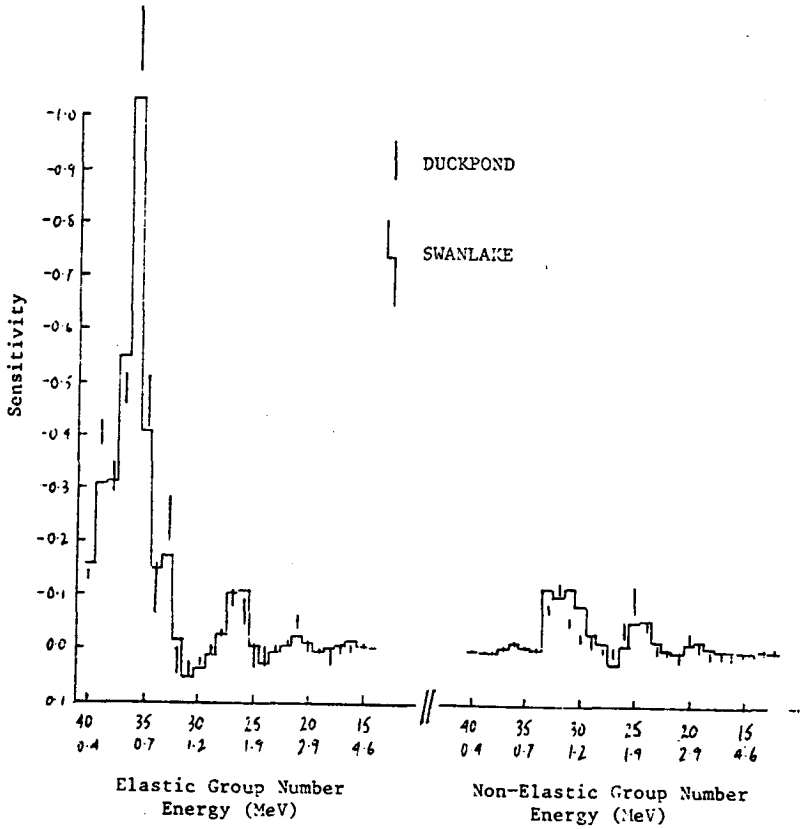

Fig. 3. Comparison of Sensitivities of Flux above 407 KeV to Elastic and Non-Elastic Cross-Sections of Iron, as calculated by DUCKPOND and SWANLAKE.

A disturbing aspect of the results is the discrepancy between the fluxes calculated by the Monte Carlo and S_n methods. The low energy flux, which is the main contributor to the total flux, is undercalculated by about 50% by the S_n method. The sensitivity profiles suggest that an explanation of this is a group averaging overestimate of about 30% in the cross-sections for groups 35 to 39. Such an error could easily arise: the elastic cross-section of iron is rapidly changing by factors of about five in this energy range, which puts great importance on the weighting function used in the averaging process.

DEVELOPMENT

There are three interesting ways in which this method can be developed: higher order perturbation coefficients could be scored, sensitivities to geometric data obtained, and the method could be applied to eigenvalue calculations.

Higher Order Coefficients

A second order operator has already arisen in Eq. (19). Such an operator is now defined by

$$\hat{D}_{KL} = \sum_{i\in K}\sum_{j\in L} x_i x_j \frac{\partial^2}{\partial x_i \partial x_j} \quad . \tag{30}$$

It is also convenient to redefine corresponding first order operators:

$$\hat{D}_K = \sum_{i\in K} x_i \frac{\partial}{\partial x_i} \tag{31}$$

and

$$\hat{D}_L = \sum_{j\in L} x_j \frac{\partial}{\partial x_j} \quad . \tag{32}$$

The first order weights are given by Eq. (11) and turn out to be

$${}^{K}\omega_i^m = \frac{1}{s_i^m}\hat{D}_K s_i^m + \sum_{j\le i}\frac{1}{q_j^m}\hat{D}_K q_j^m \tag{33}$$

and

$${}^{L}\omega_i^m = \frac{1}{s_i^m}\hat{D}_L s_i^m + \sum_{j\le i}\frac{1}{q_j^m}\hat{D}_L q_j^m \quad , \tag{34}$$

and the second order weights are given by

$$\begin{aligned} {}^{KL}\omega_i^m = {}&{}^{K}\omega_i^m\,{}^{L}\omega_i^m + \frac{1}{s_i^m}\hat{D}_{KL} s_i^m - \left(\frac{1}{s_i^m}\hat{D}_K s_i^m\right)\left(\frac{1}{s_i^m}\hat{D}_L s_i^m\right) \\ &+ \sum_{j\le i}\left\{\frac{1}{q_j^m}\hat{D}_{KL} q_j^m - \left(\frac{1}{q_j^m}\hat{D}_K q_j^m\right)\left(\frac{1}{q_j^m}\hat{D}_L q_j^m\right)\right\} \quad . \end{aligned} \tag{35}$$

These equations are illustrated by referring to the specifications of $\hat{D}$, S and q appearing in the section on implementation. $\hat{D}_K$ and $\hat{D}_L$ are given by

$$\hat{D}_K = \sum_{\beta\in P}\sum_{h\in G} x_h^\beta \frac{\partial}{\partial x_h^\beta} \tag{36}$$

and

$$\hat{D}_L = \sum_{\beta\in Q}\sum_{h\in H} x_h^\beta \frac{\partial}{\partial x_h^\beta} \quad , \tag{37}$$

with a corresponding definition of $\hat{D}_{KL}$. The previous definitions of S and q still stand. For track length estimation all the terms involving S in Eqs. (33) to (35) are zero. The other terms are given by

$$(1/q_j^m)\hat{D}_K q_j^m = S_K^P - \delta_K^G (x_j^P / x_j^T) - \delta_{j'}^G (x_{j'}^P, \lambda) + \delta_{j'}^G (x_{j'}^G / x_{j'}^T), \quad (38)$$

$$(1/q_j^m)\hat{D}_L q_j^m = S_L^Q - \delta_j^H (x_j^Q / x_j^T) - \delta_{j'}^H (x_{j'}^Q \lambda) + \delta_{j'}^H (x_{j'}^Q / x_{j'}^T), \quad (39)$$

$$(1/q_j^m)\hat{D}_{KL} q_j^m = -(\delta_K^P + \delta_L^Q)(x_j^P x_j^Q)/(x_j^K x_j^T) - 2\delta_j^G \delta_j^H (x_j^P x_j^Q)/(x_j^T)^2 + \delta_{j'}^G \delta_{j'}^H (x_{j'}^P x_{j'}^Q \lambda^2), \quad (40)$$

so second order weights are not much more difficult to evaluate than first order, although there may be more of them. The most likely use of second order coefficients would be in testing the validity of a first order approximation.

Geometric Sensitivities

Suppose a geometrical configuration is defined in terms of rectangular co-ordinates r_1, r_2 and r_3. A plane with unit normal $\underline{n}$ which separates two different media may be described by the equation

$$\underline{n} \cdot \underline{r} = l . \quad (41)$$

An operator which describes a first order change in the position of the plane is

$$\hat{D} = \partial/\partial l \quad (42)$$

Again using the previous specifications for S and q, the only variable which can depend on l is λ. If u_1, u_2 and u_3 are the direction cosines of a trajectory then

$$\partial\lambda/\partial l = k/\underline{n} \cdot \underline{u} . \quad (43)$$

Here $k = -1$ for boundary crossing at the beginning of the trajectory, $k = 1$ for boundary crossing at the end of the trajectory, and $k = 0$ otherwise. If collision density estimation is used, the weight given by Eq. (11) is

$$\omega_j^m = -k x_j^T / \underline{n} \cdot \underline{u} . \quad (44)$$

This could be used to score the geometric sensitivity $\partial R/\partial l$.

Eigenvalue Calculations

Monte Carlo eigenvalue calculations differ from shielding calculations in that superimposed on the normal processes of tracking and scoring is an iterative procedure. An eigenvalue calculation in a code such as MONK[6] will usually start with a fission source guess represented by N_0 particles. These particles are tracked to leakage, absorption or fission. N_0 of the resulting N_1 secondary particles are sampled at random and the process continues for successive generations. The ratio K_j is defined by

$$K_j = N_j / N_0 \tag{45}$$

where N_j is the number of secondary particles at the end of the j^{th} generation.

Each trajectory involved is labelled according to the particle from which it originated (m) and the generation in which it occurs (j). The probability of the i^{th} trajectory of this type is defined in the same way as before to be q_{ij}^m. The probability of all the trajectories up to and including the k^{th} generation which originate from the m^{th} particle is given by

$$P_k^m = \frac{1}{N_0} \prod_{j=1}^{k} \frac{1}{K_{j-1}} \prod_i q_{ij}^m . \tag{46}$$

If τ_k^m is the number of secondaries at the end of the k^{th} generation originating from the m^{th} particle, then another expression of the ratio K_k is

$$K_k = \lim_{N_0 \to \infty} \sum_{m=1}^{N_0} \tau_k^m P_k^m . \tag{47}$$

Furthermore the eigenvalue k_{eff} is given by

$$k_{eff} = \lim_{k \to \infty} K_k , \tag{48}$$

so for k sufficiently large, τ_k^m is an estimator of k_{eff}. If α is some perturbation parameter then

$$\frac{\partial K_k}{\partial \alpha} = \lim_{N_0 \to \infty} \sum_{m=1}^{N_0} \tau_k^m \frac{\partial P_k^m}{\partial \alpha} , \tag{49}$$

or

$$\frac{\partial K_k}{\partial \alpha} = \lim_{N_0 \to \infty} \sum_{m=1}^{N_0} d\tau_k^m P_k^m \tag{50}$$

where

$$d\tau_k^m = \frac{1}{P_k^m} \frac{\partial P_k^m}{\partial \alpha} \tau_k^m . \tag{51}$$

This means that $d\tau_k^m$ is an estimator of $\partial K_k/\partial x$ and, for k sufficiently large, $\partial k_{eff}/\partial x$. Re-arranging Eq. (51)

$$d\tau_k^m = y_k^m r_k^m \tag{52}$$

where

$$y_k^m = \frac{1}{P_k^m}\frac{\partial p_k^m}{\partial x}. \tag{53}$$

The evaluation of the weight y_k^m may be troublesome. Substituting for p_k^m from Eq. (46)

$$y_k^m = \sum_{j=1}^{k}\left(\sum_i \frac{1}{q_{ij}^m}\frac{\partial}{\partial x}q_{ij}^m - \frac{1}{K_{j-1}}\frac{\partial K_{j-1}}{\partial x}\right) \tag{54}$$

so

$$y_k^m = y_{k-1}^m + \sum_i \frac{1}{q_{ik}^m}\frac{\partial}{\partial x}q_{ik}^m - \frac{1}{K_{k-1}}\frac{\partial K_{k-1}}{\partial x}. \tag{55}$$

The difficulty is in evaluating the term $\partial K_{k-1}/\partial x$. An exact value is not available, so an estimate using $d\tau_{k-1}^m$ has to be used. If N_0 is not sufficiently large, the estimates of $\partial K_k/\partial x$ may get progressively worse, and the method may not converge.

APPLICATION

DUCKPOND has been applied to a variety of practical problems. Preliminary results of the uncertainty analysis for the NRC Blind Test[7] have already been produced and sensitivity calculations have been carried out for the analysis of the Winfrith Iron Benchmark[8] . Some of these results are presented here.

NRC Blind Test

This test is to see how well a series of experimental reaction rates in a simulated pressure vessel can be predicted by various methods. It is useful to be able to isolate each source of error in the predictions, and DUCKPOND has been used to evaluate uncertainties arising from errors in nuclear data. The significant sensitivities of one of the reaction rates. as calculated by DUCKPOND, are illustrated in Fig. 4. These sensitivities were combined with covariance information about nuclear data[9] to obtain an uncertainty of 14%. The geometrical configuration involved in the calculation precluded an S_n method.

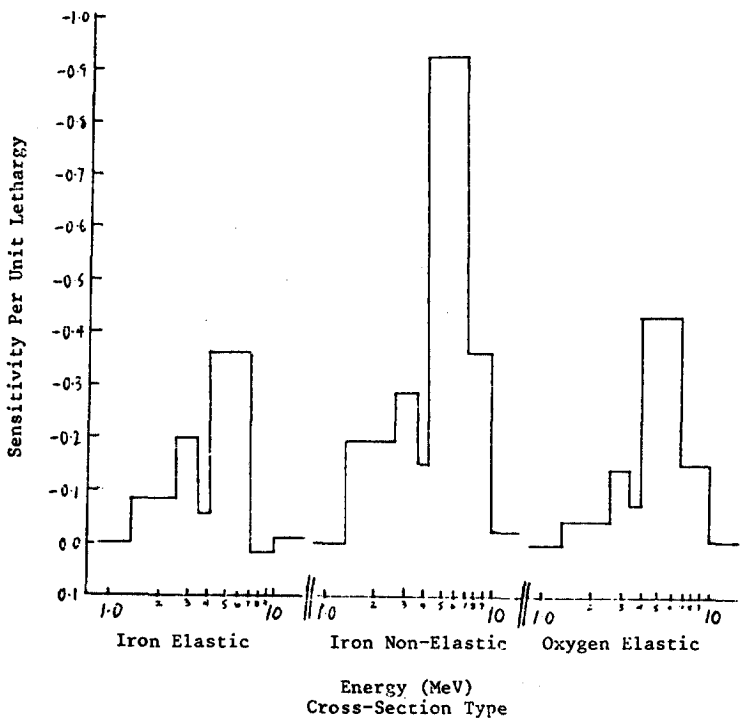

Fig. 4. Sensitivity per Unit Lethargy of $^{58}Ni(n,p)^{58}Co$ Reaction Rate in a Simulated Pressure Vessel, to Various Cross-Sections.

Winfrith Iron Benchmark

The objective of this benchmark is to adjust the evaluated cross-section of iron on the basis of count rates measured in an iron block with a fission source at one end. Each count rate is calculated along with a sensitivity profile: the sensitivities determine which adjustments would improve the agreement between calculation and experiment, and cross-section covariance information indicates which the likely adjustments are.

DUCKPOND was used for the calculations. The experimental configuration was modelled very accurately using combinatorial geometry. Sixty count rates and sensitivity profiles were scored, which involved tracking neutrons in iron to a depth of 75 cm and down to 5 KeV. After twenty minutes running on an IBM 3033 the statistical error on the estimated count rates

had reached the same level as the experimental error (about 15%). One of the sensitivity profiles is illustrated in Fig. 5. The pronounced positive sensitivity is probably a three-dimensional effect: an increase in the cross-section will reduce the leakage and hence increase the count rate. The results of an adjustment procedure based on this DUCKPOND calculation are shortly to be produced.

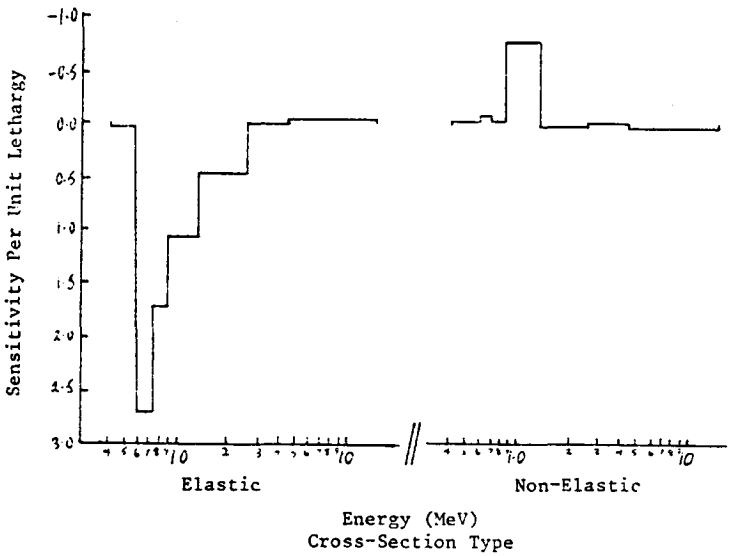

Fig. 5. Sensitivity Per Unit Lethargy of an Hydrogen/Argon Proportional Count Rate at 50 cm Penetration, to Iron Cross-Sections. (The threshold of the detector is about 4.7 MeV.)

CONCLUSION

It is now a simple and inexpensive matter to carry out the uncertainty analysis of a transport calculation, however complicated the geometrical configuration. It is also clearly feasible to analyse a shielding benchmark experiment on the basis of a Monte Carlo calculation. Application of this method to core calculations is as yet untested, and this would be a sensible option to try out. Geometric and second order developments would be easy to implement, although they might be of limited use. There is no reason why the method should not be applied to calculations using multigroup data if necessary.

REFERENCES

1. M. C. G. Hall, DUCKPOND - A Monte Carlo Code for Determining the Unknown Consequences of Known Perturbations of Nuclear Data, to be published.

2. D. E. Bendall and R. J. Brissenden, McBEND Programme Users Guide, To be published.

3. "EURLIB Library", ESIS Newsletter No. 12, January 1975.

4. W. W. Engle, A Users Manual for Anisn, a One-Dimensional Discrete Ordinates Transport Code with Anisotropic Scattering K-1673, Computing Technology Centre, Oak Ridge, Gaseous Diffusion Plant, 1967.

5. D. E. Bartine, F. R. Mynatt and E. M. Oblow, Swanlake, A Computer Code Utilising Anisn Radiation Transport Calculations for Cross-Section Sensitivity Analysis, ORNL-TM-3809, Mathematics Division, Oak Ridge National Laboratory, May 1973.

6. V. S. W. Sherriffs, Monk - A General Purpose Monte Carlo Neutronics Program, SRD Culcheth No. 86, January 1978.

7. Technical Letter for PCA Blind Test, NRC April 1979.

8. M. D. Carter and A. Packwood, The Winfrith Benchmark Experiment in Iron - Experimental Results, Proc. of Specialists Meeting on Sensitivity Studies and Shielding Benchmarks NEA/OECD, Paris, 1975.

9. J. D. Drischler and C. R. Weisbin, Compilation of Multigroup Cross-Section Covariance Matrices for Several Important Reactor Materials, ORNL-5318 Neutron Physics Division, Oak Ridge National Laboratory, October 1977.

APPENDIX

A path segment is defined to be a set of contiguous trajectories which make up the initial part of the path. R_k is the set of paths which start with segment k. ${}^{k}S_i$ and ${}^{k}q_i$ are defined by

$$ {}^{k}S_i = S_i^m \qquad m \in R_k \tag{56} $$

and

$$ {}^{k}q_i = q_i^m \qquad m \in R_k \; . \tag{57} $$

The number of trajectories in segment k is u^k. The response R can now be regarded as the average value associated with the set S of all segments:

$$R = \sum_{k \in S} {}^{k}S_{u^k} \prod_{j \le u^k} {}^{k}q_j \quad . \tag{58}$$

$\hat{D}$ operating on Eq. (58) gives

$$\hat{D}R = \sum_{k \in S} d^k S_{u^k} \prod_{j \le u^k} {}^{k}q_j \tag{59}$$

where

$$d^k S_{u^k} = \left\{ \hat{D}\left({}^{k}S_{u^k} \prod_{j \le u^k} {}^{k}q_j \right) \right\} / \prod_{j \le u^k} {}^{k}q_j \quad . \tag{60}$$

T_i is the set of segments with exactly i trajectories ($u^k = i$). The sum over segments ($\sum_{k \in S}$) is now regarded as a sum over i, and a sum over segments with exactly i trajectories ($\sum_i \sum_{k \in T_i}$). From the definition of a probability

$$\sum_{m \in R_k} \prod_{u^k < l < t^m} q_l^m = 1 \quad . \tag{61}$$

Also $u^k = i$ for $k \in T_i$. Using all this in Eq. (59)

$$\hat{D}R = \sum_i \sum_{k \in T_i} d^k S_i \prod_{j \le i} {}^{k}q_j \left(\sum_{m \in R_k} \prod_{i < l < t^m} q_l^m \right) . \tag{62}$$

Re-arranging and using Eqs. (56) and (57)

$$\hat{D}R = \sum_i \sum_{k \in T_i} \sum_{m \in R_k} ds_i^m \prod_{j \le t^m} q_j^m \tag{63}$$

where

$$ds_i^m = \left\{ \hat{D}\left(s_i^m \prod_{j \le i} q_j^m \right) \right\} / \prod_{j \le i} q_j^m \quad . \tag{64}$$

Q_i is the set of paths with at least i trajectories. The sum over all such paths ($\sum_{m \in Q_i}$) can be regarded as the sum over paths which contain a segment with exactly i trajectories ($\sum_{k \in T_i} \sum_{m \in R_k}$). This double sum is replaced in Eq. (63) to give

$$\hat{D}R = \sum_i \sum_{m \in Q_i} ds_i^m \prod_{j \le t^m} q_j^m \quad . \tag{65}$$

Re-arranging Eq. (65)

$$\hat{D}R = \sum_{m \in P} \sum_{i \le t^m} ds_i^m \prod_{j \le t^m} q_j^m \quad , \tag{66}$$

so an estimator of $\hat{D}R$ for paths is given by

$$dr^m = \sum_{i \le t^m} \left\{ \hat{D}\left(s_i^m \prod_{j \le i} q_j^m \right) \right\} / \prod_{j \le i} q_j^m \quad . \tag{67}$$

SAMPO : UN SYSTEME DE CODE POUR LES ANALYSES DE SENSIBILITE ET DE PERTURBATION A DIFFERENTS ORDRES D'APPROXIMATION

J.C. Estiot*, G. Palmiotti**, M. Salvatores*
*CEA/CEN/CADARACHE (France) **NIRA/GENES (Italie)

RESUME

On présente les caractéristiques du système de codes SAMPO (Système d'Analyse Mulitigroupe par Perturbations Optimisées), en théorie du transport à une dimension spatiale, qui est utilisé pour les calculs suivants :

. analyses de sensibilité pour des fonctionnelles linéaires ou bi-linéaires du flux direct ou adjoint et leurs rapports;
. analyse de perturbation classique.

Les méthodes employées peuvent être au premier ordre ou à un ordre supérieur.

ABSTRACT

We present the characteristics of SAMPO, a one dimension transport theory code system, which is used for the following types of calculation :

. sensitivity analysis for functionals linear or bi-linear on the direct or adjoint flux and their ratios ;
. classic perturbation analysis.

First order calculations, as well higher order, can be presented.

-oOo-

TABLEAU 1

ISOTOPE	REGION	Effets sur : σ_{tot}	$\nu\sigma_f$	σ_s
U.238	CŒUR	-0.90	0.03	0.82
	COUVERTURE	2.09	-0.15	-1.28
	TOTAL	1.19	-0.12	-0.46
Fe	CŒUR	-0.45		0.43
	COUVERTURE	0.86		-0.62
	TOTAL	0.41		-0.19
Oxy.	CŒUR	-0.78		0.76
	COUVERTURE	1.24		-0.96
	TOTAL	0.46		-0.20
Na	CŒUR	-0.61		0.59
	COUVERTURE	0.83		-0.64
	TOTAL	0.22		-0.05

Coefficients de sensibilité $(\delta R/R)/(\delta\Sigma/\Sigma)$ pour :

$$R = \frac{F8\ (\text{interface cœur/couverture})}{F8(\text{interface couverture/écran})}$$

pour la configuration typique de réacteur rapide

1. INTRODUCTION

Un système de codes a été développé pour effectuer des analyses de sensibilité et de perturbation en théorie du transport à une dimension. Ce système de codes, appelé SAMPO [1], est utilisé soit pour des études de protection, soit dans l'analyse de problèmes spécifiques liés aux expériences intégrales. Le système SAMPO est schématisé dans le Figure 1. Les options suivantes peuvent être utilisées :

1.1. Calcul de sensibilité pour les paramètres suivants :

a) dose à un point donné ou sur une région donnée ;
b) taux de réaction et leurs rapports ;
c) coefficients de réactivité (par exemple : coefficient de vide Sodium).

Ces calculs de sensibilité peuvent être effectués dans des milieux multipliants ou non (cas des protections) en utilisant la théorie des perturbations généralisées (T.P.G.) au premier ordre. Si le système n'est pas multipliant, les coefficients de sensibilité peuvent être calculés à un ordre supérieur en utilisant la méthode des fonctions auxiliaires [2].

1.2. Calculs des perturbations :

a) perturbations au premier ordre ou perturbations exactes de la valeur propre ;
b) calcul du flux perturbé par la méthode des harmoniques.

1.3. Condensation des constantes multigroupes :

a) méthode variationnelle basée sur la conservation de la réactivité ;
b) méthode variationnelle basée sur la conservation d'une fonctionnelle quelconque.

1.4. Analyses d'incertitudes et ajustements des données de base.

2. DESCRIPTION DES MODULES

On résume ici les caractéristiques principales de chaque module du système SAMPO.

2.1. Giant-NL

Le code GIANT-NL (New-Look) est une version modifiée et complétée du code GIANT [3].

Les caractéristiques principales de ce code sont les suivantes :

. le code utilise la méthode aux ordonnées discrètes ;
. le code peut traiter des solutions négatives.

De telles solutions peuvent apparaître dans des calculs de fonctions d'importance généralisées, liées à des rapports de fonctionnelles.

Les codes aux ordonnées discrètes doivent être modifiés pour traiter d'une façon correcte de tels problèmes.

a) S'il y a des solutions négatives, l'accélération par rééquilibrage variationnel ("coarse mesh rebalancing) n'est pas utilisée pour les itérations internes afin d'éviter des oscillations dans la convergence.

b) Des tests sélectifs de convergence ponctuelle ont été introduits, en particulier pour éviter de donner un poids excessif aux points situés près d'un éventuel changement de signe de la fonction importance.

c) Le code GIANT-NL calcule les sources pour les calculs d'importance généralisées ainsi que les effets directs dus aux variations sur les valeurs des fonctions réponses.

d) Le code GIANT-NL calcule les fonctions auxiliaires utilisées dans les calculs de sensibilité d'ordre supérieur.

Ces fonctions ψ_i^+ et ψ_i sont définies de la façon suivante [2] :

$$A^+\psi_i^+ + G_i\psi^+ = 0 \qquad\qquad A\psi_i + G_i\psi = 0 \tag{1}$$

où ψ^+ est la solution de :

$$A^+\psi^+ + S^+ = 0 \tag{2}$$

et :

$$S = \int S^+ \varphi \, d\Omega \tag{3}$$

est la fonctionnelle à laquelle on s'intéresse. ψ^+ est donc la fonction d'importance généralisée qui permet d'obtenir les effets au premier ordre.

Si l'on considère une variation δpi de l'opérateur A de BOLTZMANN, on a :

$$G_i = \frac{\delta A^+}{\delta_{pi}} \tag{4}$$

La variation de S -jusqu'au second ordre- due à δpi est exprimée alors de la façon suivante :

$$\delta S = \int \psi^+ \delta A \varphi \, d\Omega + \frac{1}{2!} \sum_{J=1}^{J} \left(\int \psi_J^+ \delta A^+ \varphi \, d\Omega + \int \psi^+ \delta A \psi_J \, d\Omega \right) \tag{5}$$

Pour les calculs de fonctions d'importance généralisées liées aux fonctionnelles bi-linéaires et pour les calculs de fonctions auxiliaires, toutes les valeurs des sources angulaires sont calculées au centre de la maille (au lieu de la définition habituelle à la frontière de la maille).

La correction de contamination du mode fondamental est appliquée [4] à toutes les itérations externes i :

$$^i\psi^+_{corr.} = {}^i\psi^+ - \frac{\langle {}^i\psi^+ F\varphi \rangle}{\langle \varphi^+ F\varphi \rangle} \psi^+ \tag{6}$$

pour assurer la convergence de la fonction importance recherchée.

2.2. Code ANHARC :

Ce code calcule les harmoniques supérieures du flux réel ou adjoint avec une méthode LOMS (Lower Order Mode Sweeping) [5], qui permet l'élimination, dans le calcul de chaque harmonique de la contamination des autres harmoniques. Cette procédure est une généralisation de la procédure décrite précédemment (6) :

$$\varphi_n^{corr.} = \varphi_n - \sum_{J=1}^{n-1} \frac{\langle \varphi_n^+ \; F \; \varphi_J \rangle}{\langle \varphi_J^+ \; F \; \varphi_J \rangle} \varphi_J \qquad (7)$$

Les caractéristiques de la procédure itérative sont identiques à celles du code GIANT-NL (voir 2.1.).

Avec les harmoniques φ_n, il est possible de calculer le flux perturbé φ' résultant d'une perturbation δA, avec des approximations successives [6], par exemple au premier ordre (P.O.), on a :

$$\varphi'_{PO} = \varphi_1 - \sum_{n=2}^{\infty} \frac{\langle \varphi_n^+ \; \delta A \; \varphi_1 \rangle}{\lambda_1 - \lambda_n} \varphi_n \qquad (8)$$

où φ_1 est le mode fondamental, et λ_i les valeurs propres relatives à chaque harmonique. Des expressions plus complexes peuvent être utilisées pour le calcul du flux perturbé à des ordres supérieurs.

2.3. Code RO-SCOFF :

Ce code, dérivé du code SCOFF [3], calcule, à partir des fonctions calculées par GIANT-NL et ANHARC, les quantités suivantes :

- composantes de la réactivité ($\delta K/K$) ;
- composantes des variations $\delta R/R$ selon la théorie des perturbations généralisées ;
- les coefficients de sensibilité $(\delta R/R)/(\delta a/a)$.

Ces coefficients de sensibilité peuvent inclure des relations de conservation selon la définition de MacCracken [7], (RO-SCOFF calcule les deux types de coefficients de sensibilité) :

- à partir de l'équation (5), les effets au deuxième ordre pour les calculs de protection peuvent être obtenus ;
- à partir de l'équation (8), ou d'expressions similaires pour les ordres supérieurs, le code RO-SCOFF calcule les coefficients nécessaires à l'évaluation d'un flux perturbé.

Le code RO-SCOFF prépare donc les matrices de coefficients de sensibilité qui doivent être exploitées dans les analyses d'incertitudes ou dans les procédures d'ajustement des données de base.

Les perturbations sont introduites dans le code RO-SCOFF d'une façon très générale et ne dépendent pas de la structure géométrique qui a été utilisée pour le calcul des fonctions φ, φ^+, ψ, ψ^+, ψ_i, φ_n, etc...

2.4. Le code CORDAJ

Ce code est une version améliorée du code AMARA [8]. Ce code inclut :

. le calcul de la déviation standard d'un paramètre intégral R, due à une matrice de dispersion B. Les matrices de dispersion contiennent en général, soit des corrélations entre différentes sections efficaces, soit des corrélations en énergie pour une section efficace donnée [9] ;

. le calcul d'ajustement des données selon la méthode statistique ; c'est-à-dire, en prenant en compte toutes les erreurs d'origine statistique et distribuées avec une loi gaussienne [10]. Cette méthode permet de tenir compte d'éventuelles corrélations entre données intégrales et microscopiques, ou bien de corrélations entre différentes données intégrales ;

. le calcul de la nouvelle matrice de dispersion $\hat{B}$, après ajustement des sections efficaces ;

. un test de χ^2 sur les ajustements effectués.

Le code CORDAJ a une interface avec un code d'exploitation (SECOR) qui, à partir des ajustements, recalcule des sections multigroupes modifiées et les fournit dans le format lu par GIANT-NL, ANHARC ou ANISN/DOT.

2.5. Le code BASIC :

Ce code calcule les "sources" nécessaires aux calculs des fonctions importance liées aux fonctionnelles bi-linéaires.

Si, par exemple, on a une fonctionnelle bi-linéaire R (e.g; réactivité d'une barre) :

$$R = \frac{1}{F}\int \varphi \varphi^+ \delta\Sigma d\Omega = \frac{a}{F} \qquad (9)$$

où F est l'intégrale de normalisation de la réactivité, on a pour une modification δA des caractéristiques du système :

$$\frac{\delta R}{R} = \int \varphi\, \delta\, A\psi_R^+ d\Omega + \int \varphi^+\, \delta A^+ \psi_R d\Omega \qquad (10)$$

où ψ_R^+ et ψ_R sont données par les équations suivantes :

$$A^+\psi_R^+ = \frac{1}{a}\,\varphi^+\,\delta\Sigma - \frac{1}{F}\,\nu\Sigma_f\,\chi\varphi^+ \qquad (11)$$

$$A\,\psi_R = \frac{1}{a}\,\varphi\,\delta\Sigma - \frac{1}{F}\,\nu\Sigma_f\,\chi\varphi \qquad (12)$$

Le code BASIC calcule les termes de source des équations (11) et (12). Ces équations sont ensuite résolues par le code GIANT-NL (voir 2.1.), et les perturbations sont calculées selon l'équation (10) par le code RO-SCOFF (voir 2.4.).

2.6. Le code VACANT :

Une méthode variationnelle a été proposée pour la condensation des constantes multigroupes à un nombre réduit de groupes. Cette méthode, développée pour les calculs en diffusion, s'applique également aux calculs en théorie du transport.

Le code VACANT en est la réalisation pratique. Pour les calculs de protection, une méthode variationnelle encore plus générale, a été envisagée, qui prévoit la condensation des constantes à partir d'une loi de conservation d'une fonctionnelle quelconque du flux [11].

Le code VACANT peut condenser les constantes selon cette procédure généralisée. Habituellement, VACANT utilise des formules de condensation du type :

$$\sigma_I = \frac{\sum_{i \in I} \varphi_i \ \sigma_i \ \varphi_i^+}{\sum_{i,J \in I} \varphi_i \ \varphi_J^+} \qquad (13)$$

où φ_i^+ peut être ou le flux adjoint (conservation de la réactivité), ou la fonction importance relative à une fonctionnelle linéaire quelconque du flux, auquel on applique la loi de conservation.

3. QUELQUES EXEMPLES D'UTILISATION

Dans ce paragraphe, on donne, à titre d'information, quelques exemples d'utilisation du système SAMPO.

3.1. Sensibilité aux sources neutroniques :

Le système SAMPO peut être appliqué aux calculs de sensibilité relatifs aux spectres des sources utilisés dans les calculs de protection. Dans le Figure 2, on présente un cas typique : il s'agit des coefficients de sensibilité du flux total au spectre de la source. On donne le profil de sensibilité pour les deux cas suivants :

. bloc de Fer (≃ 100 cm de profondeur) ;
. bloc d'Acier (≃ 100 cm de profondeur).

Dans les deux cas, le flux total, dont on veut connaître la sensibilité, est calculé à la sortie du bloc (face opposée à la source).

3.2. Analyse de sensibilité dans une couverture :

Dans le Tableau I, on montre le résultat d'une analyse de sensibilité effectuée pour un problème de couverture. Il s'agit donc d'un système multipliant, où l'utilisation du transport est souvent nécessaire.

L'exemple du Tableau I montre les effets des incertitudes des sections efficaces sur l'atténuation du taux de fission de l'Uranium 238 (cest-à-dire sur le rapport des valeurs de ce même taux à l'interface coeur/couverture et couverture/protection).

Les résultats obtenus à partir d'un calcul de fonction importance avec GIANT-NL et de calculs RO-SCOFF, sont présentés sous la forme de coefficients de sensibilité intégrés sur l'énergie, et donnés par région, par isotope, et par type de réaction.

3.3. Un calcul de sensibilité au deuxième ordre :

Dans la Figure 3, on présente la distribution spatiale du coefficient de sensibilité du flux total aux variations des sections d'absorption dans le système mono-dimensionnel suivant :

Fig. 2

SENSIBILITE A LA SOURCE POUR DES EXPERIENCES DE PROPAGATION EN FER OU ACIER

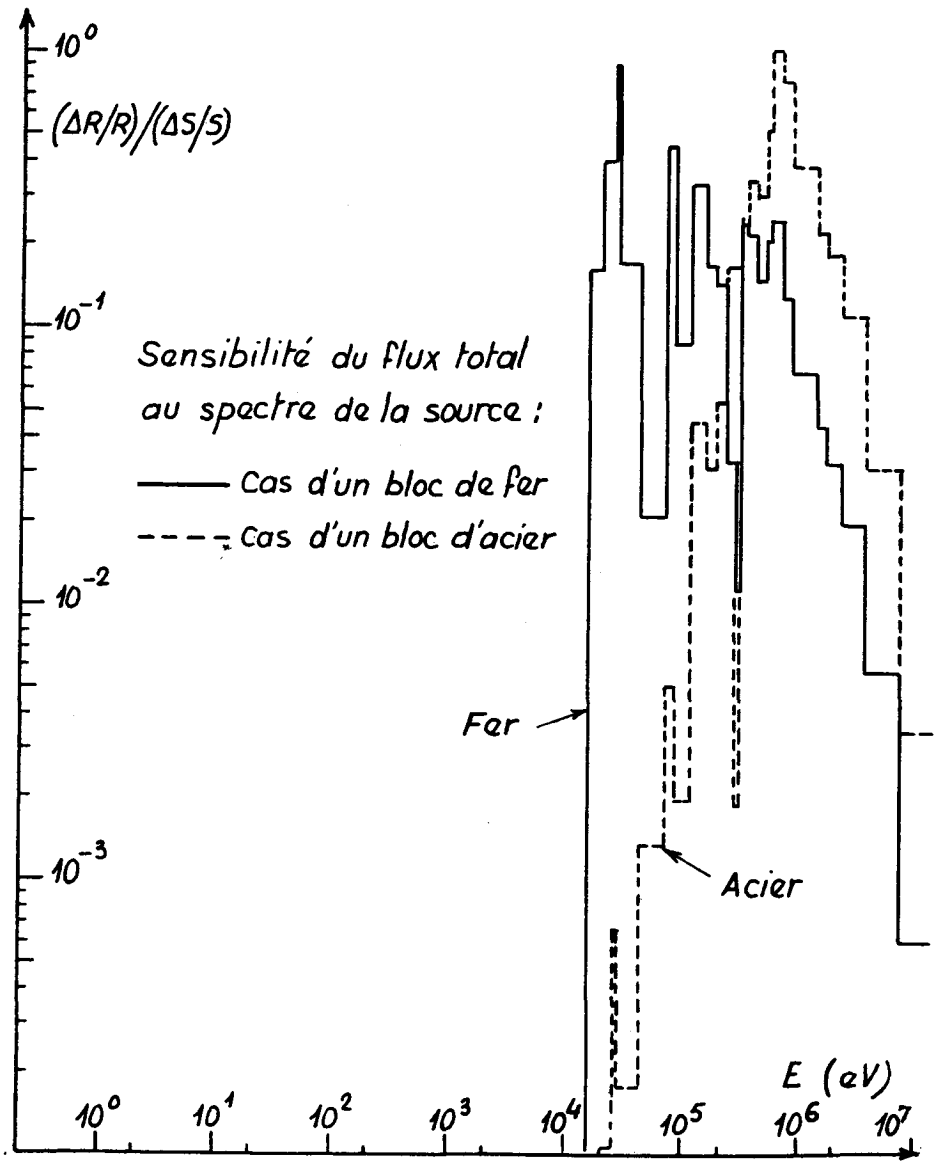

SAMPO : Système d'Analyse Multigroupe pour Perturbations Optimisées

Fig. 1

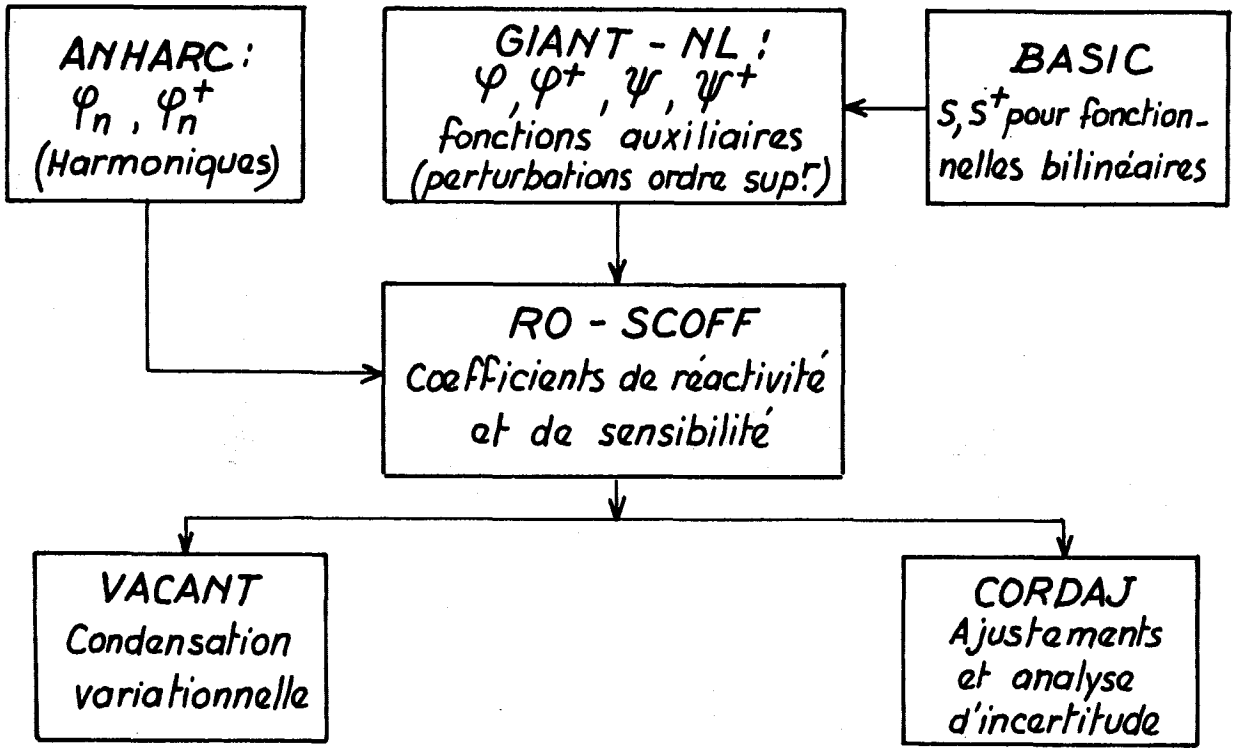

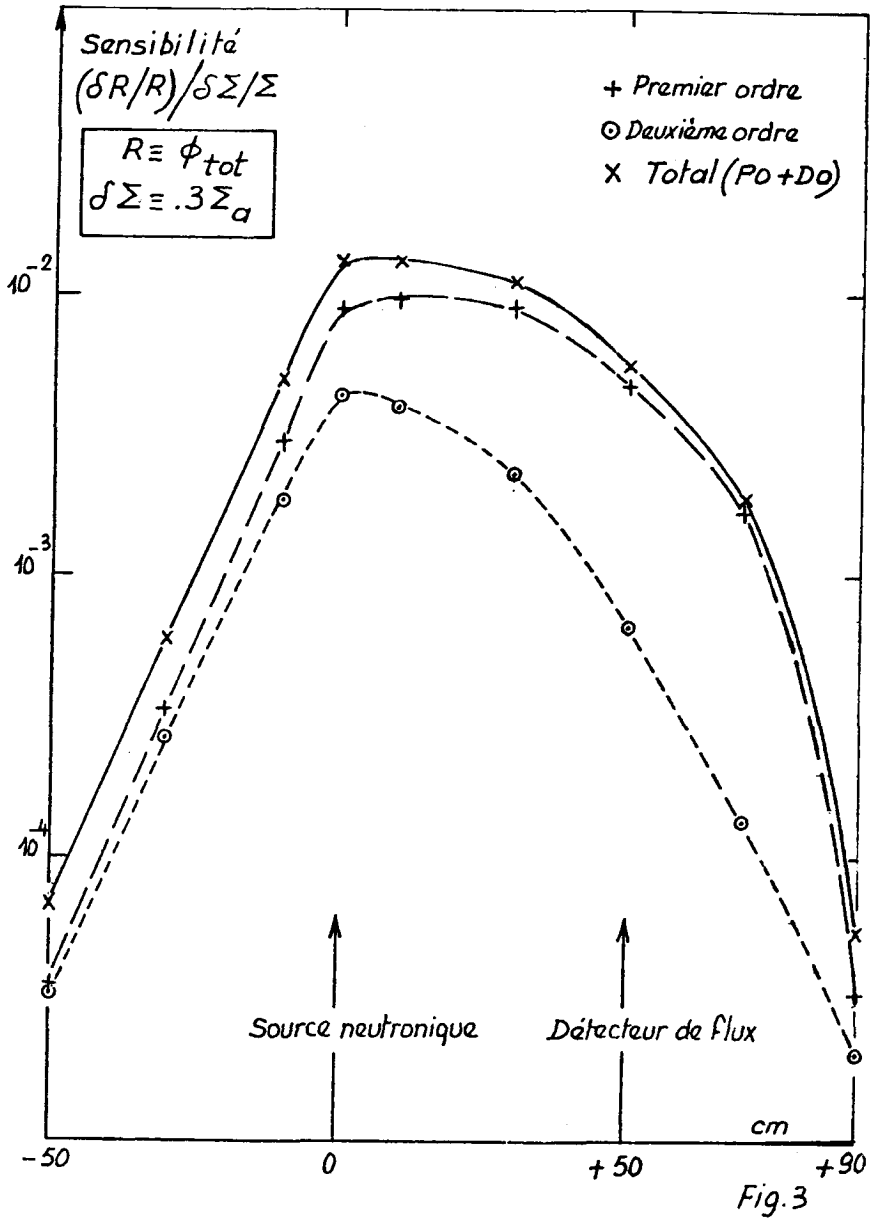
Sensibilité
$(\delta R/R)/\delta\Sigma/\Sigma$
$R \equiv \phi_{tot}$
$\delta\Sigma \equiv .3\Sigma_a$
+ Premier ordre
⊙ Deuxième ordre
× Total (Po + Do)
10^{-2}
10^{-3}
10^{-4}
Source neutronique
Détecteur de flux
cm
-50
0
+50
+90

Fig. 3

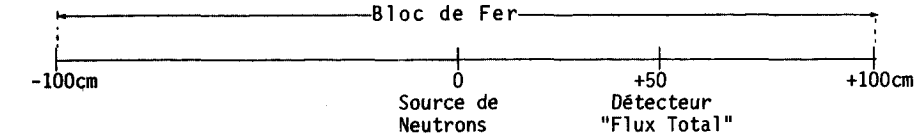

Une variation de 30% sur les sections d'absorption du Fer, conduit à des effets non linéaires dans l'évaluation des variations du flux total à 50 cm de la source neutronique.

En particulier, on vérifie qu'il existe des effets non linéaires très importants loin du détecteur, et près de la source. Ces effets peuvent être de l'ordre de 50% de l'effet au premier ordre. L'intégration de la perturbation sur l'espace, conduit aux valeurs suivantes :

. $\delta\varphi_{tot}/\varphi_{tot}$ (calcul exact) = .82
. $\delta\varphi_{tot}/\varphi_{tot}$ (premier ordre) = .53
. $\delta\varphi_{tot}/\varphi_{tot}$ (deuxième ordre) = .73

3.4. Calcul de flux perturbé :

On a calculé les harmoniques (jusqu'à l'ordre 7) pour un système rapide à deux zones (coeur/couverture) -voir Figure 4-. On a considéré comme "perturbations" l'insertion de zones fertiles correspondantes à la transformation de ce système en système hétérogène. Pour ce faire, on a introduit des perturbations $\Sigma_{fis} \rightarrow \Sigma_{fert.}$ dans deux zones (une zone centrale et un anneau).

Dans la Figure 5, on présente le flux "perturbé" obtenu successivement avec un calcul direct du système perturbé, et avec l'utilisation des harmoniques. En particulier, on considère un flux perturbé "au permier ordre" (voir 2.2., équation (8)), et un flux perturbé "au deuxième ordre". Ce flux perturbé permet de calculer, avec une bonne précision, les paramètres intégraux du système perturbé [5].

3.5. Condensation variationnelle pour un cas de protection :

On a considéré le système suivant :

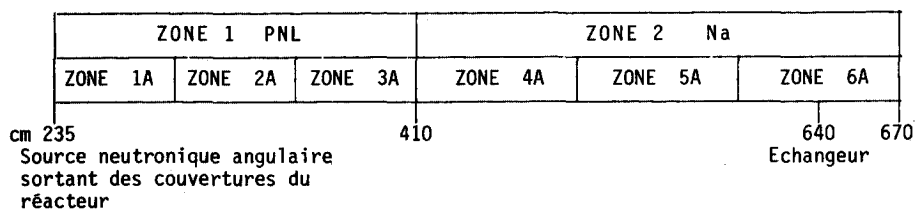

constitué par une PNL de 140 cm en Acier/Sodium 50/50 suivi par du Sodium pur jusqu'à la paroi de l'échangeur à 640 cm du centre coeur. On a effectué le calcul de propagation neutronique à 45 groupes d'énergie (structure PROPANE Do) et aussi avec un découpage énergétique beaucoup plus réduit, à 10 groupes. On a effectué la condensation d'abord de façon tout à fait classique, c'est-à-dire en utilisant le flux neutronique (une condensation pour le découpage à deux zones, et ensuite, pour celui à six zones -voir schéma ci-dessus-), et puis de façon variationnelle en utilisant les deux fonctions importance qui conservaient dans les deux zones du système (PNL et Na) le flux total respectif. Dans le tableau suivant, on montre les résultats obtenus pour le flux total évalué en deux positions différentes :

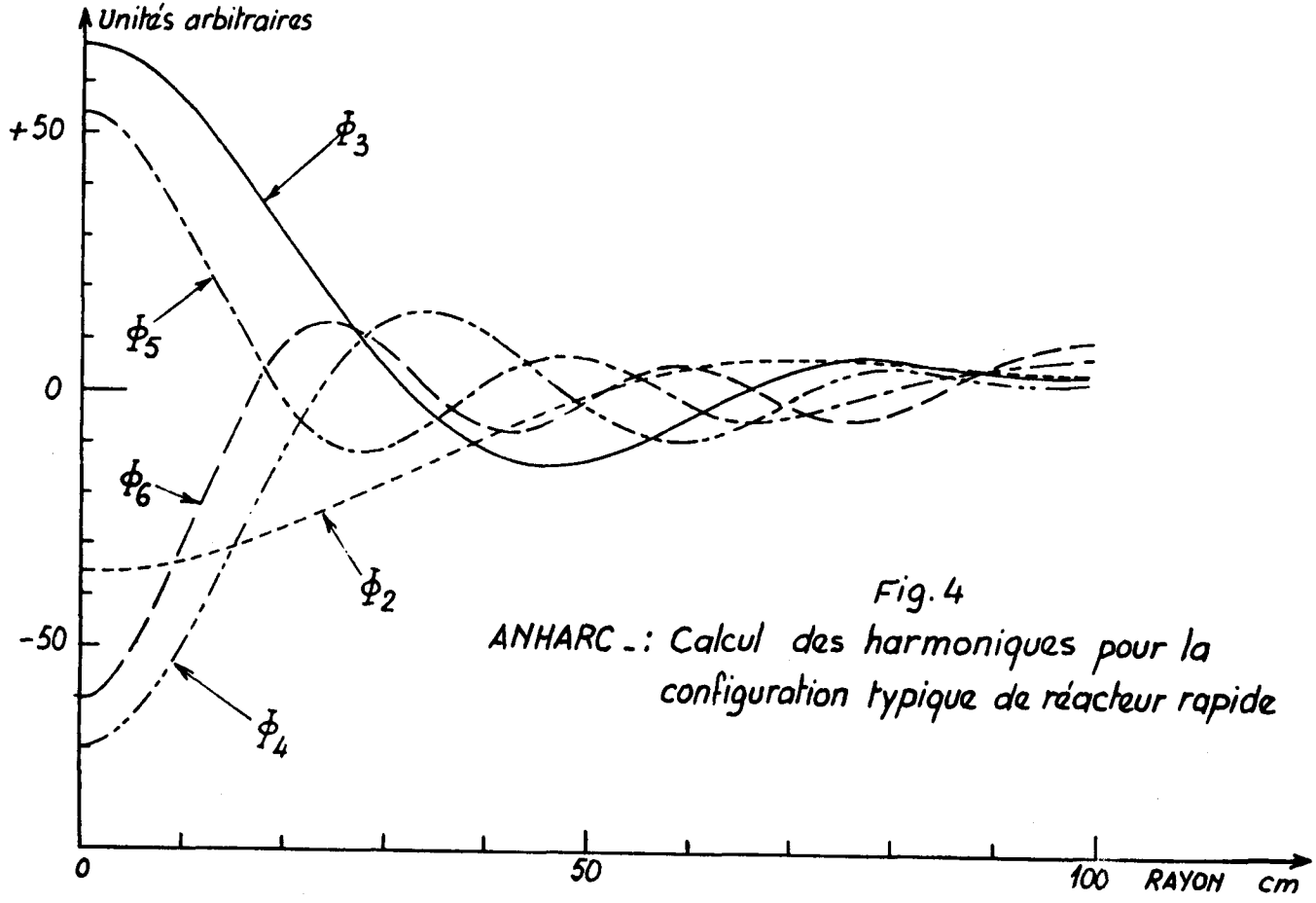

Fig. 4

ANHARC _ : Calcul des harmoniques pour la configuration typique de réacteur rapide

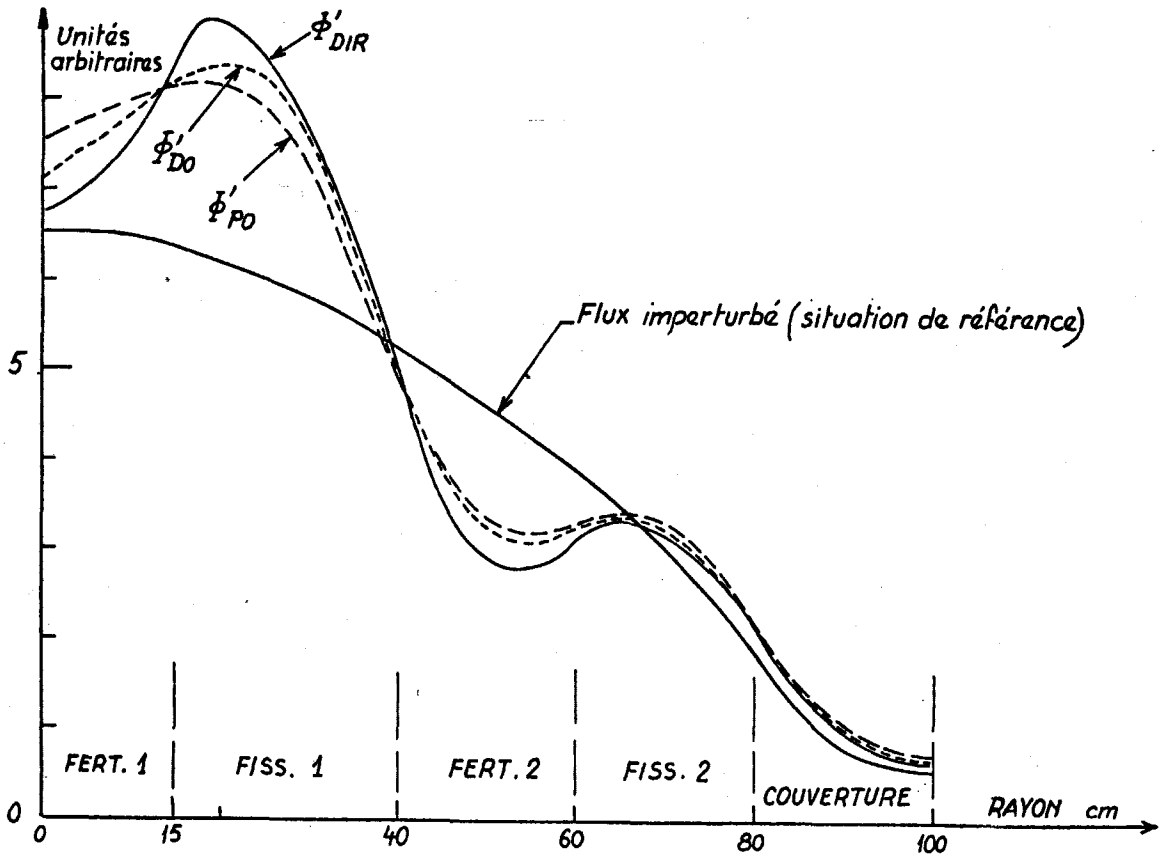
Unités arbitraires
Φ'_{DIR}
Φ'_{DO}
Φ'_{PO}
Flux imperturbé (situation de référence)
5
0
FERT. 1
FISS. 1
FERT. 2
FISS. 2
COUVERTURE
RAYON cm
0
15
40
60
80
100

Fig. 5

Méthode \ Position	Sortie PNL	Paroi Echangeur
Référence 45 groupes	2.429×10^{10}	5.037×10^{7}
Condensation flux deux zones	2.538×10^{10}	7.547×10^{7}
Condensation flux six zones	2.113×10^{10}	5.240×10^{7}
Condensation variationnelle	2.385×10^{10}	5.186×10^{7}

On peut observer, que la condensation variationelle donne toujours les résultats les meilleurs, et que, même si l'on prend jusqu'à six zones en condensation classique -ce qui alourdit le calcul en multiplicant le nombre de corps et de régions à traiter- on améliore le résultat sur la paroi de l'échangeur, mais on détériore celui de la sortie de la PNL. Ce type de résultats obtenus fait espérer pour le futur, la possibilité de réduire drastiquement le coût du calcul de propagation neutronique en utilisant la condensation variationnelle, qui permettra d'effectuer des calculs à deux dimensions, mais à peu de groupes.

5. CONCLUSIONS

Le système SAMPO, pour les calculs de perturbation à une dimension en théorie du transport (approximation aux ordonnées discrètes), peut être utilisé pour les analyses de sensibilité nécessaires aux calculs d'optimisation ou aux analyses paramétriques des protections. Ce système permet de prendre en compte les effets non linéaires qui résultent de modifications importantes du système de référence.

Le système SAMPO, peut aussi être utilisé pour l'évaluation des effets de transport dans l'analyse des expériences intégrales, en particulier celles liées aux problèmes de couvertures ou de propagation neutronique.

Enfin, le système SAMPO permet l'étude paramétrique d'un système perturbé avec l'utilisation des harmoniques. En effet, à partir d'une bibliothèque d'harmoniques calculées une fois pour toutes, on peut évaluer les paramètres intégraux.

-oOo-

REFERENCES

[1] Kalevala de E. Lonnroth, Trad. J.L. Perret.

[2] Gandini A. : "Higher order perturbation methods", Rapport CNEN RIT/LTCR (78)3 (1978)

[3] Palmiotti G., Salvatores M. : "Transport calculations of the generalized importance functions for sensitivity analysis", Proc. Specialist's Meeting on Sensitivity studies, OECD, Paris (1975)

[4] Cecchini G.P., Salvatores M. : Nucl. Sci. Eng., 45, 304, (1971)

REFERENCES (suite)

[5] Palmiotti G. : "Explicite higher order perturbative formulation : Transport application", soumis à Nucl. Sci. Eng.

[6] Gandini A. : Nucl. Sci. Eng., 67, 347 (1978)

[7] MacCracken A. : "The application of sensitivity analysis to the identification of data requirements", Proc. Spec. Meeting, OECD Vienne, (1977)

[8] Gandini A., Petilli M. : "AMARA : a code using the Lagrange multipliers method for nuclear data adjustments", Rapport CNEN TR/FI(73) 39, (1973)

[9] Drischler J.D., Weisbin C.R. : "Compilation of multigroupe cross-section covariance matrices for several important reactor materials", ORNL, 5318 (1979)

[10] Gandini A. : "Nuclear data and integral measurements correlations for fast reactors", Rapport CNEN RT/FI(73)5, (1973)

[11] Salvatores M. : Nucl. Sci. Eng., 57, 340 (1975)

-oOo-

SENSIT: A CROSS-SECTION AND DESIGN SENSITIVITY AND UNCERTAINTY ANALYSIS CODE

S. A. W. Gerstl
Theoretical Division
Los Alamos Scientific Laboratory
Los Alamos, New Mexico 87545, U.S.A.

ABSTRACT

SENSIT computes the sensitivity and uncertainty of a calculated integral response (such as a dose rate) due to input cross-sections and their uncertainties. Sensitivity profiles are computed for neutron and gamma-ray reaction cross-sections of standard multigroup cross-section sets and for secondary energy distributions (SED's) of multigroup scattering matrices. In the design sensitivity mode, SENSIT computes changes in an integral response due to design changes and gives the appropriate sensitivity coefficients. Cross-section uncertainty analyses are performed for three types of input data uncertainties: (a) cross-section covariance matrices for pairs of multigroup reaction cross-sections, (b) spectral shape uncertainty parameters for secondary energy distributions (integral SED uncertainties), and (c) covariance matrices for energy-dependent response functions. For all three types of data uncertainties SENSIT computes the resulting variance and estimated standard deviation in an integral response of interest, based on generalized perturbation theory. SENSIT attempts to be more comprehensive than earlier sensitivity analysis codes, such as SWANLAKE.

Introduction

Sensitivity analysis in radiation transport theory attempts to determine quantitatively how sensitive a calculated integral response is to the input data for the transport calculation. Such input data may concern either cross-section data, geometry specifications (design data), methods approximations, or any other input required to perform a transport calculation. In an uncertainty analysis, the sensitivity information is used, together with additional data about the uncertainty of the input data, to calculate or estimate the uncertainty of a calculated integral response which results from these input data uncertainties. In a cross-section uncertainty analysis the data uncertainties may be quantified in cross-section covariance matrices and in spectral shape uncertainty parameters for secondary energy distributions (SED's), while the resulting response uncertainty is best quantified by a variance or relative standard deviation. In a design sensitivity analysis, usually a specific design change, e.g. a material replacement or a geometry modification, and its effect on a calculated integral response is of concern. Therefore, in such cases a resulting response change is calculated based on generalized perturbation theory.

The SENSIT code is in some respects more comprehensive than earlier sensitivity codes presently in use [1]. Specifically, SENSIT includes the calculation of sensitivity profiles for secondary energy distributions (SED's) and performs also an SED uncertainty analysis. In addition, SENSIT also allows design sensitivity analyses and detector response uncertainty analyses to be performed in addition to the standard cross-section sensitivity and uncertainty analysis.

Detailed documentation on SENSIT is published separately in a comprehensive Los Alamos Scientific Laboratory Report, Ref. [2]. This 128-pages report contains detailed descriptions of the SENSIT input specifications, the underlying theory, the computational outline, details of program options, eight sample problems, retrieving and running SENSIT on two different CDC-7600 computers, references, and listings of all sample problems' input and output files. A separate Los Alamos Scientific Laboratory report, Ref. [3], documents in detail the application of SENSIT to a comprehensive neutron cross-section and secondary-energy-distribution uncertainty analysis for a fusion reactor. Due to the availability of this detailed documentation in the open literature, we restrict ourselves in the following to a summary of the significant features of SENSIT.

Computer Code Abstract

1. Program Identification: SENSIT
2. Computer for which program is designed: CDC-7600, IBM 360
3. Description of Function and Method of Solution:

The basic theory upon which the present sensitivity and uncertainty analysis methods are based has developed over the past several years. We refer to only a few selected references here which can provide the user an overview of the field, Refs. [4] through [7]. More mathematical detail is given in Ref. [8] with special emphasis on discrete-ordinates formulations. SENSIT is based on the one-dimensional discrete-ordinates formulation of radiation transport theory and operates in four different modes which can be selected by setting an input parameter ITYP to an integer value between zero and three as indicated below:

A. Standard Cross-Section Sensitivity Analysis (ITYP = 0)

Conventional sensitivity profiles P_{Σ} may be derived from the expression for the forward difference approximation, Eq. (36) in Ref. [8], or Eq. (17) in Ref. [4], or Eq. (26) in Ref. [5]. The analytical definition of a cross-section sensitivity function $F_{\Sigma}(E)$ expresses the sensitivity of a calculated integral response I to a particular cross section Σ_x at energy E and may be expressed as

$$F_{\Sigma_x}(E) = (1/I)\int d\underline{r} \int d\underline{\Omega} \left\{ - \phi(\underline{r},\underline{\Omega},E)\, \Sigma_{x,T}(\underline{r},E)\, \phi^*(\underline{r},\underline{\Omega},E) \right. \tag{1}$$

$$\left. + \int d\underline{\Omega}' \int dE'\, \phi(\underline{r},\underline{\Omega},E)\, \Sigma_{x,S}(\underline{r},\underline{\Omega}\to\underline{\Omega}',E\to E')\, \phi^*(\underline{r},\underline{\Omega}',E') \right\} .$$

In a multigroup formulation one usually prefers to identify and work with a sensitivity profile P^g_{Σ}, which is related to the above sensitivity function through the scaling factor Δu^g by $P^g_{\Sigma} = \bar{F}_{\Sigma}(E_g)/\Delta u^g$ and refers to a group-averaged sensitivity. Δu^g is the lethargy width of energy group g. The exact numerical definition of a multigroup cross-section sensitivity profile for the macroscopic cross section Σ^g_x is:

$$P^g_{\Sigma_x} = \left\{ - \Sigma^g_{x,T} \cdot \chi^g + \sum_{\ell=0}^{LMAX} \sum_{g'=g}^{GMAX} \Sigma^{g \to g'}_{s,\ell} \cdot \psi^{gg'}_{\ell} \right\} \Big/ I_{\phi} \cdot \Delta u^g \quad , \tag{2}$$

where $\Sigma^g_{x,T}$ = total macroscopic cross section for reaction type x,

$\Sigma^{g \to g'}_{s,\ell}$ = ℓ'th Legendre coefficient of the scattering matrix element for energy transfer from group g to group g', as derived from the differential scattering cross section for reaction type x,

$$\chi^g = \sum_{i=1}^{IPERT} V_i \sum_{m=1}^{MM} \phi^g_m(i) \cdot \phi^{*g}_m(i) \cdot w_m \quad ,$$

= numerical integral of the product of forward and adjoint angular fluxes over all angles and all spatial intervals described by i = 1,...,IPERT.

$$\psi^{gg'}_{\ell} = \sum_{i=1}^{IPERT} V_i X^g_{\ell}(i) \cdot Y^{g'}_{\ell}(i) \quad ,$$

= spatial integral of the product of Legendre coefficients of forward and adjoint angular fluxes.

$$X^g_{\ell}(i) = \sum_{m=1}^{MM} \phi^g_m(i) \cdot P_{\ell}(\mu_m) \cdot w_m$$

$$Y^{g'}_{\ell}(i) = \sum_{m=1}^{MM} \phi^{*g'}_m(i) \cdot P_{\ell}(\mu_m) \cdot w_m$$

$\phi^g_m(i), \phi^{*g}_m(i)$ = discrete-ordinates representations of forward and ajoint angular fluxes for group g, spatial mesh point i and discrete direction m.

$P_{\ell}(\mu_m)$ = Legendre polynomial of order ℓ at direction cosine μ_m.

$\{\mu_m, w_m\}$ = discrete-ordinates quadrature direction cosines μ_m and associated quadrature weights w_m.

V_i = volume of spatial mesh interval i.

Δu^g = lethargy width of energy group g,
= $\ell n(E^g/E^{g+1})$, where E^g and E^{g+1} are upper and lower energy group boundaries.

I_ϕ = integral response as calculated from forward fluxes only,

$$= \sum_{i=1}^{IDET} \sum_{g=1}^{IGM} \sum_{m=1}^{MM} V_i R_i^g \cdot \phi_m^g(i) \cdot w_m$$

R_i^g = spatially and group-dependent detector response function.

The basic Eq. (2), as well as its corresponding Eq. (1), consist of two terms on the right-hand side. The first term, which is always negative, is called the "loss term" [4,8] and involves always the total (collision) cross section for a certain reaction type. The second term involves only the differential scattering cross section and is always positive; it is called the "gain term" [4,8]. In order to facilitate the interpretation of sensitivity results, SENSIT prints loss and gain terms in addition to the net sensitivity profiles.

B. Design Sensitivity Analysis (ITYP = 1)

The objective in a design-sensitivity analysis is to estimate the change of an integral response I due to a given design change without repeating the transport calculation for the altered design. Methods, based on generalized perturbation theory, have been developed which allow such estimates to be made with second-order accuracy in respect to the associated flux changes [5,8]. These perturbation methods require only the forward and adjoint flux solutions to a reference case and the specification of a perturbation to this reference design, which is equivalent to a postulated design change. All such design changes can be described then by a perturbation, ΔL, in the linear Boltzmann operator L.

Due to the dualism of forward and adjoint formulations for radiation transport calculations, two different but equivalent expressions can be derived for the estimated integral response in the perturbed system [5,8]. These expressions are both second-order with respect to flux changes but first-order with respect to the perturbation and are denoted as the adjoint difference (AD) and the forward difference (FD) formulation. Using the convenient operator notation of Refs. [5] and [8], we obtain for the integral response in the perturbed system the two expressions

$$I_{AD}^{(2)} = \langle R,\phi \rangle - \langle \phi^*, \Delta L \phi \rangle \equiv I_\phi^{(1)} - \Delta I_{AD}^{(2)} , \tag{3}$$

$$I_{FD}^{(2)} = \langle Q,\phi^* \rangle - \langle \phi, \Delta L^* \phi^* \rangle \equiv I_{\phi^*}^{(1)} - \Delta I_{FD}^{(2)} , \tag{4}$$

where $\langle , \rangle$ indicates integrations over all independent variables, and ϕ, ϕ^* are the forward and adjoint angular fluxes for the reference design. If the operators ΔL and ΔL^* are written down explicitly [8], it is noted that the second-order term in Eq. (4) is equivalent to the negative of the numerator of Eq. (2) when the cross sections Σ_x are replaced by cross-section changes $\Delta\Sigma$, and when an additional integration over all energies E, namely, a summation over all groups g, is performed:

$$\Delta I_{FD}^{(2)} = \sum_{g=1}^{IGM} \Delta\Sigma_T^g \cdot \chi^g - \sum_{\ell=0}^{LMAX} \sum_{g'=g}^{IGM} \Delta\Sigma_{x,\ell}^{g \to g'} \cdot \psi_\ell^{gg'} \tag{5}$$

The analogous expression for the second-order term in Eq. (3) becomes

$$\Delta I_{AD}^{(2)} = \sum_{g=1}^{IGM} \left\{ \Delta\Sigma_T^g \cdot \chi^g - \sum_{\ell=0}^{LMAX} \sum_{g'=1}^{g} \Delta\Sigma_{s,\ell}^{g' \to g} \cdot \psi_\ell^{g'g} \right\} . \tag{6}$$

The perturbation, as expressed by macroscopic cross-section changes in Eqs. (5) and (6) is calculated in SENSIT from two sets of input cross-section tables, the unperturbed or reference cross-section set $\{\bar{\Sigma}\}$ and the perturbed cross-section set $\{\Sigma\}$:

$$\Delta\Sigma_T^g = \Sigma_T^g - \bar{\Sigma}_T^g \ , \tag{7}$$

$$\Delta\Sigma_{s,\ell}^{g\to g'} = \Sigma_{s,\ell}^{g\to g'} - \bar{\Sigma}_{s,\ell}^{g\to g'} \tag{8}$$

$$\Delta\Sigma_{s,\ell}^{g'\to g} = \Sigma_{s,\ell}^{g'\to g} - \bar{\Sigma}_{s,\ell}^{g'\to g} \tag{9}$$

A design sensitivity coefficient X is then defined for both (AD and FD) formulations according to

$$X_{AD} = I_{AD}^{(2)}/I_\phi^{(1)} = 1 - \Delta I_{AD}^{(2)}/I_\phi^{(1)} \ , \tag{10}$$

$$X_{FD} = I_{FD}^{(2)}/I_{\phi^*}^{(1)} = 1 - \Delta I_{FD}^{(2)}/I_{\phi^*}^{(1)} \ , \tag{11}$$

from which the estimated fractional change of the integral response I due to the introduction of the perturbation can be easily determined. SENSIT prints all design sensitivity information, as defined in Eqs. (3) through (11), separately for neutrons and gamma rays, and for each perturbed zone, as well as integrated over all perturbed zones.

C. Vector Cross-Section Sensitivity and Uncertainty Analysis (ITYP = 2)

The term "vector cross-section" has been chosen to identify a multigroup cross-section set which consists of a linear string of numbers with one group-averaged reaction cross-section per group, but no scattering matrix. Existing correlations between two individual vector cross-sections are easily described by a simple two-dimensional correlation matrix. As a consequence, therefore, it is also straightforward to describe correlated cross-section uncertainties of pairs of vector cross-sections by a two-dimensional covariance matrix [6]. For ITYP = 2, SENSIT performs a complete sensitivity and response uncertainty analysis for given sets of vector cross-section pairs $\{\Sigma_1^g\}$ and $\{\Sigma_2^g\}$ with an associated covariance matrix $\mathrm{Cov}(\Sigma_1^g,\Sigma_2^g)$ attached to each pair. As a first step SENSIT calculates the sensitivity profiles P_1^g and P_2^g for each individual vector cross section. Then the covariance matrix $\mathrm{Cov}(\Sigma_1^g,\Sigma_2^g)$ is used to compute the resulting integral response uncertainty due to the correlated cross-section uncertainties of this pair of vector cross sections according to [6]

$$\mathrm{Var}(I_\phi) = \sum_{g=1}^{IGM1}\sum_{g'=1}^{IGM1} P_1^g \cdot P_2^{g'} \cdot \mathrm{Cov}\left(\Sigma_1^g,\Sigma_2^{g'}\right). \tag{12}$$

Both, the variance $\mathrm{Var}(I_\phi)$ as well as the relative standard deviation

$$\frac{\delta I}{I} = \sqrt{\mathrm{Var}(I_\phi)}, \tag{13}$$

are printed by SENSIT for each vector cross-section pair.

D. SED Sensitivity and Uncertainty Analysis (ITYP = 3)

It has only recently been recognized [9] that sensitivity profiles for secondary energy and angular distributions are obtained as adjoints of the standard sensitivity profiles, i.e., from the differential form of the adjoint difference (AD) formulation. For ITYP = 3, SENSIT computes and prints the double-differential and single-differential sensitivity profiles for secondary energy distributions (SED's) and performs also an SED uncertainty analysis based on the hot/cold concept of integral SED uncertainties [10].

As shown in Ref. [9], a double-differential SED sensitivity profile is described by the differential form of the gain term in the AD-formulation:

$$p_{SED}^{g',g} = \left\{ \sum_{\ell=0}^{LMAX} \Sigma_{s,\ell}^{g' \to g} \cdot \psi_{\ell}^{g'} \right\} \Big/ I_{\phi} \cdot \Delta u^{g'} \cdot \Delta u^{g} \quad . \tag{14}$$

This double-differential SED sensitivity profile quantifies the sensitivity of the integral response I_{ϕ} to the scattering matrix element $\Sigma_s^{g' \to g}$. Therefore, $p_{SED}^{g',g}$ is a pure gain term for the sensitivity gain due to the transfer of neutrons from the incident energy group g' to the final energy group g.

In order to perform an SED uncertainty analysis based on the hot/cold concept introducted in Ref. [10], it is required to specify the median energy group of the SED for each incident neutron energy group, GMED(g'), as well as the associated integral SED uncertainty (spectral shape uncertainty parameter), $F_{SED}(g')$, for each SED with incident energy group g'. GMED(g') and $F_{SED}(g')$ are expected input arrays in SENSIT if ITYP = 3. Hot and cold integral SED sensitivity coefficients, $S_{HOT}(g')$ and $S_{COLD}(g')$, are then computed by SENSIT according to [10]:

$$S_{HOT}(g') = \Delta u^{g'} \cdot \sum_{g=g'}^{GMED(g')} p_{SED}^{g',g} \cdot \Delta u^{g} \quad , \tag{15}$$

$$S_{COLD}(g') = \Delta u^{g'} \cdot \sum_{g=GMED+1}^{IGM1} p_{SED}^{g',g} \cdot \Delta u^{g} \quad . \tag{16}$$

From these two components of an integral SED sensitivity, SENSIT obtains the net integral SED sensitivity coefficient

$$S(g') = S_{HOT}(g') - S_{COLD}(g') \quad , \tag{17}$$

which quantifies how much more sensitive the integral response I_{ϕ} is to the hot component of the SED at incident energy group g' than to its cold component. The simplest possible response uncertainty estimate due to estimated SED uncertainties is then obtained from [10]

$$\left(\frac{\delta I}{I}\right)_{SED} = \sum_{g'=1}^{IGM1} |S(g')| \cdot F_{SED}(g') \quad . \tag{18}$$

Values for the SED sensitivity profile, as defined in Eq. (14), all integral SED sensitivity coefficients, Eqs. (15) through (17), and the estimated response uncertainty due to all integral SED uncertainties according to Eq. (18), are printed by SENSIT for each set of material cross sections and associated integral SED uncertainties.

4. Input Formats:

SENSIT uses the angular flux output from one-dimensional discrete-ordinates codes as input files. Slab, spherical and one-dimensional cylindrical geometries are allowed. An input parameter ITAPE allows to read angular forward- and adjoint-flux tapes in two different formats. ITAPE = 1 is the preferred option to read the standardized CCCC-flux format which is defined precisely [11] and is recommended by the Committee on Computer Code Coordination as a code and computer independent standard interface format. The LASL code ONETRAN [12], e.g., generates a CCCC-formated angular flux tape on TAPE31 if both control integers IFO and IANG are set to 1. If ITAPE = 0, SENSIT reads the angular flux tapes as generated by the ORNL code ANISN [13] or the older LASL code DTF [14].

Three options are built into SENSIT to read standard neutron (or coupled neutron/gamma-ray multi-group cross-section sets: first, LASL format cross sections from cards; second, LASL format cross sections from tape; and third, limited FIDO (ORNL) format cross sections from cards. The general structure of all transport cross-section tables is as described in the transport code literature; e.g., the ONETRAN [12] or ANISN manual [13]. The LASL format is simply a string of 6E12.5 formatted numbers, while the FIDO format allows certain abbreviations for strings of zeroes, etc. For covariance data input a convenient ENDF-like input format is adopted which is identical to the output format from the cross-section processing code system NJOY [15].

5. Data Management and Storage Requirements:

SENSIT uses one-, two-, and three-dimensional arrays to manage the large amount of numerical data involved in its execution. Core storage is reserved for a particular dimensioned array only during the time the corresponding data are required to be in-core; at other times, the space is made available for the storage of other data. In order to alleviate bookkeeping chores associated with such dynamic storage allocation techniques, Argonne National Laboratory developed a collection of subroutines, called the BPOINTR package [16,17], which is incorporated in SENSIT. The user needs to know nothing about the BPOINTR routines themselves, only that they require two large blocks of workspace called "containers" for data storage during execution of a job. The container sizes are set in the main program by four FORTRAN statements as explained in Ref. [2], and the choice of sizes is problem dependent. The first container, the FCM (fast-core memory) or SCM (small-core memory) container, is in the CDC-7600's fast memory. The second, the ECM (extended-core-memory) or LCM (large-core memory) container, is in the slower memory banks of the CDC-7600. On IBM machines, both containers are in fast memory [16,17].

6. Machine Requirements and Restrictions

Due to the variable dimensioning as described above, large flexibility exists to adjust the storage requirements for a specific problem to the available machine core. On a CDC-7600 all of the 8 sample problems and the realistic applications described in Ref. [3] could be executed within a maximum of 24000 words of fast (SCM) core and 80000 words of extended-core (ECM) memory.

7. Running Time

A typical execution time on the CDC-7600 for a standard cross-section sensitivity analysis, together with an SED uncertainty analysis is about 4 seconds CPU (central processor units) time. Here a coupled neutron/gamma group structure of 30 × 12 groups, P_3 cross-sections, and 137 spatial intervals was used. A typical vector cross-section sensitivity and uncertainty analysis with 30 × 30 covariance matrices requires about 2 seconds of CPU time per case.

8. Material Available:

The SENSIT code package is available in a CDC as well as an IBM version and is distributed through the RSIC/EPIC code center for the U.S. and the ESIS code center for Europe. The package contains the FORTRAN source code together with complete input and output files for 8 sample problems.

REFERENCES

1. D. E. Bartine, F. R. Mynatt, and E. M. Oblow, "SWANLAKE, a Computer Code *Utilizing ANISN Radiation Transport Calculations for Cross-Section* Sensitivity Analysis," Oak Ridge National Laboratory report ORNL-TM-3809 (May 1973).

2. S. A. W. Gerstl, "SENSIT: A Cross-Section and Design Sensitivity and Uncertainty Analysis Code," Los Alamos Scientific Laboratory report LA-8498-MS (Aug. 1980).

3. S. A. W. Gerstl, R. J. LaBauve, and P. G. Young, "A Comprehensive Neutron Cross-Section and Secondary Energy Distribution Uncertainty Analysis for a Fusion Reactor," Los Alamos Scientific Laboratory report LA-8333-MS (May 1980).

4. D. E. Bartine, E. M. Oblow, and F. R. Mynatt, "Radiation-Transport Cross-Section Analysis - A General Approach Illustrated for a Thermonuclear Source in Air," Nucl. Sci. Eng., 55, 147 (1974).

5. S. A. W. Gerstl and W. M. Stacey, Jr., "A Class of Second-Order Approximate Formulations of Deep Penetration Radiation Transport Problems," Nucl. Sci. Eng., 51, 339 (1973).

6. S. A. W. Gerstl, D. J. Dudziak, and D. W. Muir, "Cross-Section and Uncertainty Analysis with Application to a Fusion Reactor," Nucl. Sci. Eng. 62, 137-156 (1977).

7. C. R. Weisbin et. al., Eds., "A Review of the Theory and Application of Sensitivity and Uncertainty Analysis," Proc. Seminar-Workshop, Oak Ridge, Tenn., Aug. 22-24, 1978, Oak Ridge National Laboratory report ORNL/RSIC-42 (February 1979).

8. S. A. W. Gerstl, "The Application of Perturbation Methods to Shield and Blanket Design Sensitivity Analyses," Argonne National Laboratory report AP/CTR/TM-25 or FRA-TM-67 (October 1974).

9. S. A. W. Gerstl, "Sensitivity Profiles for Secondary Energy and Angular Distributions," R. W. Roussin et. al., Eds., Proc. Fifth Int. Conf. Reactor Shielding, Knoxville, Tenn., April 18-22, 1977 (Science Press, Princeton) pp. 101-111.

10. S. A. W. Gerstl, "Uncertainty Analysis for Secondary Energy Distributions," Proc. Seminar-Workshop on Theory and Appl. of Sens. and Uncert. Analysis," Oak Ridge, Tenn., Aug. 23-25, 1978; ORNL/RSIC-42, pp. 219-229 (February 1979).

11. R. D. O'Dell, "Standard Interface Files and Procedures for Reactor Physics Codes, Version IV," Los Alamos Scientific Laboratory report LA-6941-MS (September 1977).

12. T. R. Hill, "ONETRAN: A Discrete Ordinates Finite Element Code for the Solution of the One-Dimensional Multigroup Transport Equation," Los Alamos Scientific Laboratory report LA-5990-MS (June 1975).

13. W. W. Engle, Jr., "A User's Manual for ANISN, a One-Dimensional Discrete Ordinates Transport Code with Anisotropic Scattering," Union Carbide Corporation report K-1693 (March 1967).

14. K. D. Lathrop, "DTF-IV - A FORTRAN-IV Program for Solving the Multigroup Transport Equation with Anisotropic Scattering," Los Alamos Scientific Laboratory report LA-3373 (November 1965).

15. R. E. MacFarlane, R. J. Berrett, D. W. Muir, and R. M. Boicourt, "The NJOY Nuclear Data Processing System: User's Manual," Los Alamos Scientific Laboratory report LA-7584-M/ENDF-272 (December 1978).

16. L. C. Just, H. Henryson II, A. S. Kennedy, S. D. Sparck, B. J. Toppel and P. M. Walker, "The System Aspects and Interface Data Sets of the Argonne Reactor Computation (ARC) System," Argonne National Laboratory report ANL-7711 (1971).

17. C. H. Adams, Argonne National Laboratory, personal communication, March 1980.

SESSION IV

REVIEW OF EXPERIMENTAL PROGRAMS

Chairman - Président

M. SALVATORES

(France)

SEANCE IV

RESUME DES PROGRAMMES EXPERIMENTAUX

SUMMARY OF THE SESSION IV RESUME DE LA SEANCE IV

Review of Experimental Programs

Dr. M. Salvatores

This session offered a review of current experimental programs in different laboratories.

Standard iron benchmark experiment results were reported, and a variety of penetration experiments in different media were also presented, both planned or recently completed.

In particular, the ASPIS iron benchmark experiment was fully documented in the McCracken paper, making this experiment the most suitable for intercomparison among different laboratories.

The present EURACOS experiment results were presented together with a discussion of experimental techniques for neutron spectra measurements and the problems related to their analysis.

With regard to other propagation media, experiments in sodium performed in Japan were reported by Prof. An. The results concerned both neutron and gamma-ray propagation in 180 cm of sodium. The analysis of the neutron detector ^{115}In (n,n') and ^{197}An (n,γ) responses did show disagreement above the measurement error range (in general C/E > 1.). Much better agreement was found in the gamma-ray dose measurements with TLD. The concurrent neutron data disagreement indicates however the ambiguity of these results.

Experiments performed in several sodium/steel mixtures (about 150 cm propagation length) at the TAPIRO reactor, were analysed in the framework of the joint French/Italian program on Fast Reactor Physics. These results show a significant increasing discrepancy between experiment and calculation with increasing steel content in the mixture, but they are, in general, consistent with previous propagation experimental results in pure sodium.

The French participants also presented a new experimental program (JASON), which will be devoted to the performance assessment of natural boron carbide and of some special steel (e.g. high Ni content) as shielding material for fast reactors. Some new concepts (e.g. localised shield) will also be studied in the same program.

From the Japanese side, a number of experimental results were shown concerning fast neutron streaming. Analysis of the data is still in progress.

Finally, a paper presented by M.C. Scott of the University of Birmingham gave a carefull review of the problems encountered in the use of proton-recoil proportional and scintillation counters. Even if the paper was mainly addressed to 14 MeV neutron measurements, the principal suggestions were also of strong interest for similar measurements of fission neutron spectra.

LE PROGRAMME EXPERIMENTAL JASON ASSOCIE A L'OPTIMISATION DES PROTECTIONS NEUTRONIQUES DE LA FILIERE RAPIDE FRANCAISE

J.P. Trapp, R. Valenza , R. Vienot
CEA/CEN/CADARACHE (France)

RESUME

Après une étude des performances de nouveaux concepts ou de nouveaux matériaux utilisables en protection neutronique, on présente le programme expérimental JASON qui doit débuter en Septembre 1980 sur le réacteur HARMONIE à CADARACHE. Ce programme est destiné à vérifier l'intérêt de ces matériaux et concepts, et à valider le formulaire PROPANE destiné au calcul de protections neutroniques.

On présente aussi les résultats expérimentaux préliminaires au programme JASON, concernant l'emploi de B4C en association avec l'Acier.

ABSTRACT

Following a study of the performances of the new concepts and the new materials to be utilised in neutron shielding, we present the epxerimental program JASON which will start on September 1980 on the HARMONIE reactor in CADARACHE. The purpose of this program is to verify the interest in new materials and concepts and the validation of the PROPANE "formulaire" used in the calculation of the neutron shielding.

The preliminary experimental results of the JASON program concerning the use of B4C associated with SS are also presented.

-oOo-

INTRODUCTION

Le formulaire de propagation neutronique PROPANE dans sa version actuelle Do, est adapté au traitement des protections neutroniques (en Acier-Sodium) des réacteurs rapides de la filière rapides française.

Dans une version ultérieure, ce formulaire devra être validé pour le traitement de matériaux et de concepts nouveaux, envisageables pour l'optimisation de ces protections.

Ce papier présente à la fois les études qui ont présidé à la définition d'un programme expérimental répondant à cet objectif ainsi que le programme expérimental lui-même.

On présente en outre, les résultats d'un programme expérimental préliminaire destiné à vérifier la validité des hypothèses faites en ce qui concerne l'utilisation du B4C.

1. PROTECTIONS NEUTRONIQUES : MATERIAUX ET CONCEPTS NOUVEAUX

1.1 Aciers

1.1.a) Sensibilité aux divers constituants :

Une étude de sensibilité aux composants de l'Acier permet de définir l'intérêt de chacun des constituants.

Le Tableau I indique l'importance de différents constituants de l'Acier vis-à-vis du flux thermique équivalent après un parcours de 130 cm dans un mélange Acier-Sodium à 50-50% :

TABLEAU I

	Fe	Ni	Cr	Mn	Mo	Ti
Concentrations dans le milieu	63.45%	14%	17%	1.5%	2.75%	0.4%
Sensibilité totale (densité unitaire)	-174.7	-324.6	-199.3	-537.1	-925.7	-372.7
Sensibilité totale (densité du matériau)	- 4.57	- 1.784	- 1.501	- 0.338	- 0.611	- 0.072
Par zone d'énergie (en % de la sensibilité totale)						
En > 820 KeV	15.26	7.5	13.15	5.02	16.5	22.29
21 < En < 44 KeV	3.66	11.21	4.56	5.62	2.76	36.34
E < 454 eV	14.06	12.37	8.52	34.05	50.64	7.28

On peut remarquer l'importance du Nickel dont la sensibilité représente 20% de la sensibilité totale alors que sa concentration dans le milieu n'est que de 14%.

De même, pour le Manganèse, le Molybdène et le Titane, dont les sensibilités représentent 3.8%, 6.88% et 0.81% pour des concentrations respectives de 1.5%, 2.75% et 0.4%.

Par zone d'énergie, on peut aussi remarquer la complémentarité de matériaux tels que Nickel, Titane et Molybdène avec le Fer et le Chrome.

On observe en effet, que la zone du trou du Fer au voisinage de 24 KeV, correspond à une zone de forte sensibilité pour le Nickel et le Titane ; que ce dernier apparaît très efficace au-dessus de 800 KeV, et enfin, que le Manganèse et le Molybdène sont très efficaces en-dessous de 400 eV.

Ainsi, on peut choisir des Aciers qui, du point de vue neutronique, semblent présenter un maximum d'intérêt.

1.1.b) Efficacité de divers Aciers :

Dans le cadre d'une protection neutronique classique, à savoir 180 cm d'Acier-Sodium, on compare l'efficacité de différents Aciers avec l'Acier 304.

Le Tableau II donne la composition des Aciers étudiés, et le Tableau III l'atténuation obtenue sur le flux thermique équivalent à la sortie de la PNL, ainsi qu'après un parcours de 160 cm de Sodium.

TABLEAU II

COMPOSITION DES ACIERS (% en poids)

	Ni	Cr	Fe	Mn	Mo	Ti	B10 + B11	Si	C
Acier 304	8.9	10.2	69.1	1.8					
Z12	35	15	46.4	1.4		1.6		0.6	
Z10	25	20	48.4	1.1	4.5			1	
Z75	4	0	80.25	15.					0.75
Acier Boré	8.55	17.1	71.75	1.6			1		

TABLEAU III

ATTENUATIONS DU FLUX THERMIQUE EQUIVALENT

	Acier 304	Acier Z12	Acier Z10	Acier Z75	Acier Boré
Sortie PNL	$3.45\ 10^{3}$	$3.06\ 10^{4}$	$3.01\ 10^{4}$	$2.0\ 10^{4}$	$7.5\ 10^{3}$
Après 160cm Na	$2.60\ 10^{4}$	$2.27\ 10^{5}$	$1.4\ 10^{5}$	$1.01\ 10^{5}$	$1.03\ 10^{5}$

On peut constater l'intérêt de l'Acier Z12 qui est presque dix fois plus efficace que l'Acier 304. On peut aussi remarquer l'intérêt présenté soit par le passage d'une concentration en Nickel de 25 à 35% (Z10 → Z12), soit par l'association avec le Titane.

Les Aciers absorbants (Z75 et Boré) semblent présenter moins d'intérêt dans le cas d'une conception classique de protection, mais il faut attendre une confirmation expérimentale avant de porter une conclusion définitive.

1.2 Matériaux et concepts nouveaux

1.2.a) Protections composites :

Différentes études ont montré l'intérêt de l'utilisation du B4C et de l'H_2Zr, en particulier en association avec de l'Acier-Sodium. De plus, on a montré que l'efficacité neutronique de tels matériaux était d'autant plus grande que le milieu Acier-Sodium associé possédait une plus forte concentration en Acier.

Le Tableau IV présente les atténuations sur le flux thermique équivalent au niveau de l'échangeur dans la géométrie SUPER-PHENIX pour différentes configurations de protection :

TABLEAU IV

ATTENUATIONS SUR LE FLUX THERMIQUE EQUIVALENT AU NIVEAU DE L'ECHANGEUR

	Référence	1	2	3	4
Côte 600cm	$2.6\ 10^4$	$1.30\ 10^4$	$2.4\ 10^4$	$1.70\ 10^4$	$2.2\ 10^4$

Référence : 180cm [Acier(304)-Sodium(50v/o)]
1 : 32cm [Acier(304)-Sodium (50v/o)]+32cm[B4C-Acier-Na(65-35)]
2 : 32cm [Acier(304)-Sodium (70-30)]+32cm[B4C-Acier-Na(65-35)]
3 : 32cm [Acier(Z12)-Sodium (50v/o)]+32cm[B4C-Acier-Na(65-35)]
4 : 32cm [Acier(Z12)-Sodium (50v/o)]+32cm[H_2Zr-Acier-Na(65-35)]

On peut ainsi vérifier l'intérêt de tels matériaux qui permettent une réduction de la protection de 180 à 70cm environ.

1.2.b) Protections localisées :

Une solution envisageable consisterait à supprimier la protection neutronique au voisinage du coeur ou du moins à le réduire drastiquement, et à transporter la protection au voisinage de la zone à protéger (échangeur par exemple). Dans une telle configuration, le B4C ou l'Acier Boré présentent une grande efficacité car le spectre neutronique incident est déjà suffisamment dégradé par la traversée du Sodium.

Dans une telle configuration -à épaisseur de protection égale- le B4C est vingt fois plus efficace que l'Acier Boré à 1%, qui est lui-même treize fois plus efficace que l'Acier Z12, et seize fois plus que l'Acier 304.

1.3 Choix des matériaux et des configurations à étudier

Le programme expérimental JASON est destiné à étudier les matériaux et concepts nouveaux pouvant être envisagés dans les protections neutroniques.

. Dans le cas d'une protection intégrée classique, l'étude d'Aciers spéciaux tels que ceux à forte teneur de Nickel, Aciers en Manganèse et Aciers Borés, présentent de l'intérêt ainsi que l'association de tels Aciers avec du B4C et de l'H_2Zr.

. Dans le cas d'une protection localisée, l'étude du B4C, et d'Aciers au Bore, présentent aussi de l'intérêt.

2. PROGRAMME EXPERIMENTAL JASON

La Figure 1 représente le dispositf réalisé. Il comprend :

. une cuve inférieure carrée de 200 cm de côté et 25 cm de hauteur. Au centre, un trou carré de 128 cm de côté et de même hauteur est ménagé ;

. une cuve intermédiaire cylindrique de diamètre 200 cm et de hauteur 175 cm. Cinq chaussettes de mesures perpendiculaires à l'axe de propagation sont disposées régulièrement, décalées de 15° les unes par rapport aux autres ;

. une cuve supérieure cylindrique de diamètre 200 cm et de 100 cm de hauteur, comportant aussi trois chaussettes de mesures décalées de 15° les unes par rapports aux autres.

Les parois des cuves sont en Acier, et les fonds ont une épaisseur de 6 mm.

Les trois cuves sont remplies de Sodium. Le dispositif de remplissage est tel que lors du refroidissement du Sodium, le retrait inévitable se produit au niveau des trous d'homme, donc à l'extérieur de la cuve.

Une chaussette verticale de diamètre 30 cm, dont l'axe est décalé de 30 cm par rapport à l'axe des cuves est aménagée dans la cuve intermédiaire. Elle servira ultérieurement à des expériences de streaming (il n'en sera pas question dans cette note).

L'ensemble est disposé sur le socle du réacteur source HARMONIE situé à CADARACHE. Ce réacteur, d'une puissance maximum de 2 KW, fournit une source neutronique à la sortie d'un réflecteur d'Acier.

Dans la configuration expérimentale qui sera utilisée, la position du coeur du réacteur permet l'utilisation d'un espace identique à celui du trou de la cuve inférieure. Des plaques d'Acier peuvent y être disposées ou un assemblage de réglettes UO_2-Na, de manière à simuler une couverture d'un réacteur rapide. Cet assemblage sert de convertisseur de spectre. De telles expériences ont été réalisées lors des expériences de propagation profonde dans le Sodium, [1,2,3].

Les expériences suivantes seront effectuées :

. Configurations A - PNL (voir Figure 2)

1 - Expérience de référence A1 : le trou de la cuve inférieure est rempli de Sodium. La source est la même que celle correspondant aux expériences HARMONIE (25 cm Acier) [1].

Figure 1
Dispositif Expérimental

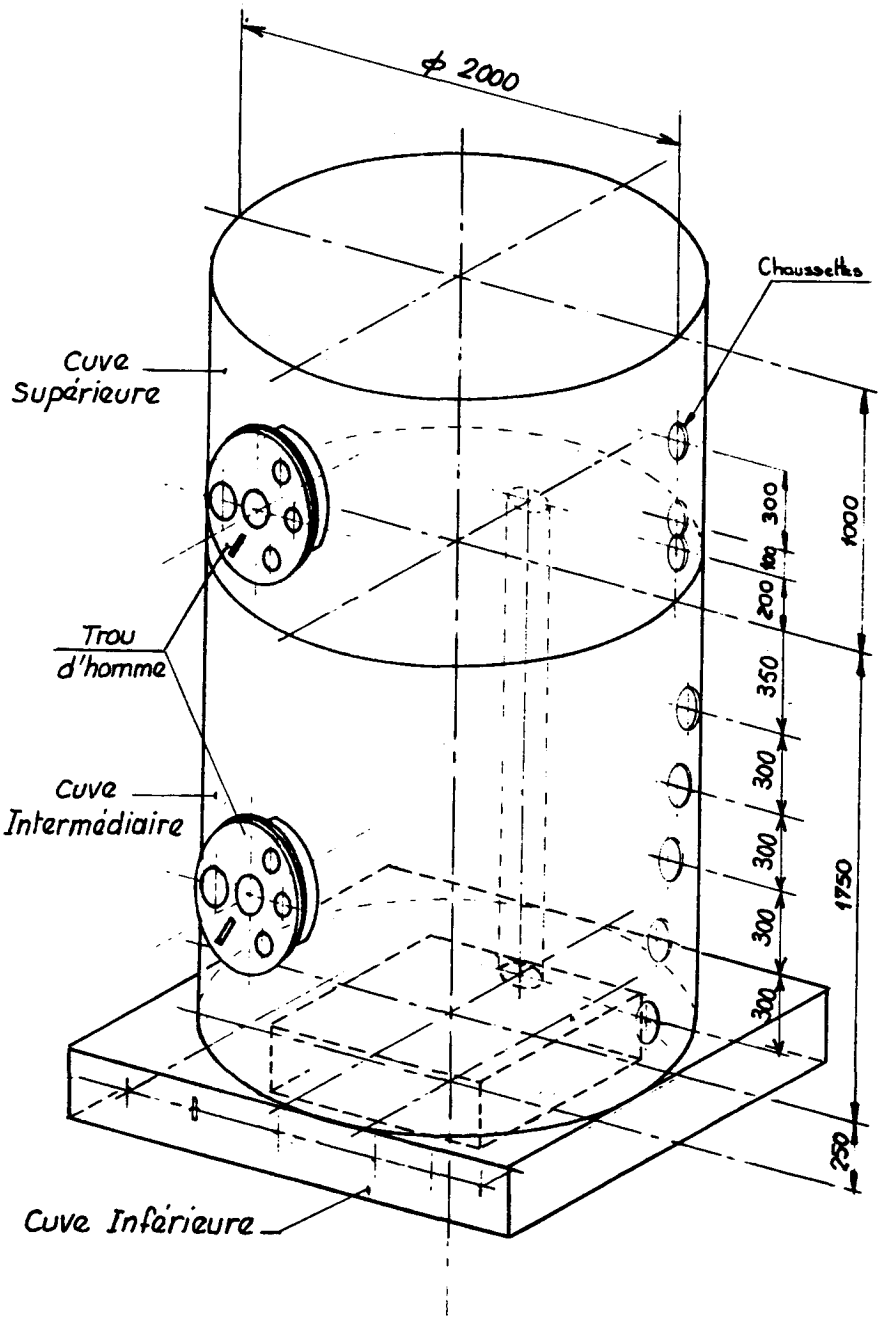

Fig.2

Configurations A

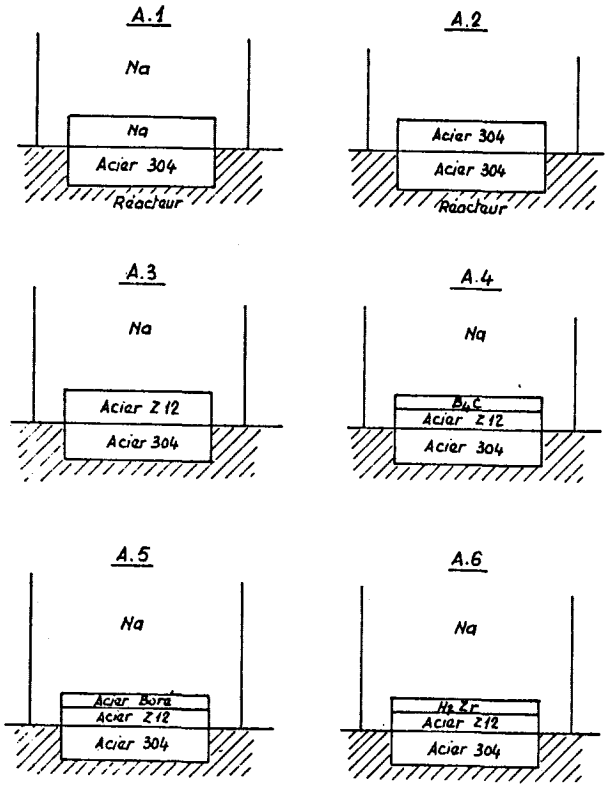

Fig.3

Configurations B

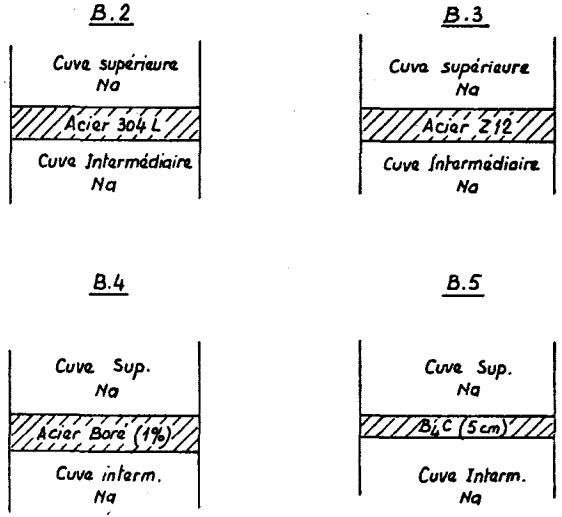

Cette expérience permettra une recalage par rapport aux expériences précédentes ; en particulier, elle permettra de mesurer l'effet des dimensions latérales réduites.

2 - Configuration A2 : on remplace le Sodium dans le trou inférieur par le l'Acier 304.

3 - Configuration A3 : on remplace l'Acier 304 par de l'Acier Z12.

4 - Configuration A4 : on remplace 10 cm d'Acier 304 par du B4C : 15 cm Acier Z12 + 10 cm B4C.

5 - Configuration A4Bis : 15 cm Acier Z12 + 10 cm B4C.

6 - Configuration A5 : 15 cm Acier Z12 + 10 cm H_2Zr.

7 - Configuration A6 : 25 cm Acier Z75.

8 - Configuration A6Bis : 25 cm Acier Boré.

. Configurations B - Protections localisées (voir Figure 3)

1 - Configuration B1 : Entre les cuves intermédiaire et supérieure, on place une plaque d'Acier 304 de 10 cm d'épaisseur.

2 - Configuration B2 : on remplace l'Acier 304 par l'Acier Boré.

3 - Configuration B3 : on remplace l'Acier 304 par l'Acier Z75.

4 - Configuration B4 : on remplace l'Acier 304 par l'Acier Z12

5 - Configuration B5 : on remplace l'Acier par du B4C (5 à 10 cm suivant les possibilités de mesure).

6 - Configuration B6 : on inverse les deux cuves supérieure et intermédiaire ; entre ces cuves on place 10 cm d'Acier Boré. Cette expérience permettra de vérifier l'effet du spectre neutronique à l'entrée de la protection sur l'efficacité de celle-ci.

. Mesures à effectuer :

Pour toutes les expériences, on effectuera :

- des mesures de spectres par protons de recul au niveau du canal 1 ;
- des mesures intégrales à l'aide des détecteurs suivants dans les divers canaux :

  Na nu et sous Cd
  Mn nu et sous Cd
  Au/Cd
  Co 59
  Rhodium, Soufre (n,p), Ni58 (n,p) et In 115 (n,n').

3. PROGRAMME EXPERIMENTAL PRELIMINAIRE

3.1 Dispositif expérimental

Un programme expérimental préalable au programme JASON a été effectué pendant le premier semestre 1980 sur le réacteur HARMONIE en utilisant les cuves Sodium ayant déjà fait l'objet d'expériences de propagation dans le Sodium [1,2,3], (cuve de 3 mètres de haut). Il avait pour but de vérifier qualitativement les propriétés neutroniques du B4C, en particulier dans le cas de son association avec l'Acier.

Sous la cuve de Sodium, on remplace 5 cm d'Acier constituant une partie du réflecteur d'HARMONIE par des boîtiers d'Acier contenant du B4C en poudre, en provenance de SNEAK. La comparaison de ces boîtiers correspond à une proportion de 50% Acier - 50% B4C (en poids).

Les expériences dont les schémas sont donnés ci-dessous, ont été effectuées et les résultats sont comparés à la référence tout Acier (Configuration 0) :

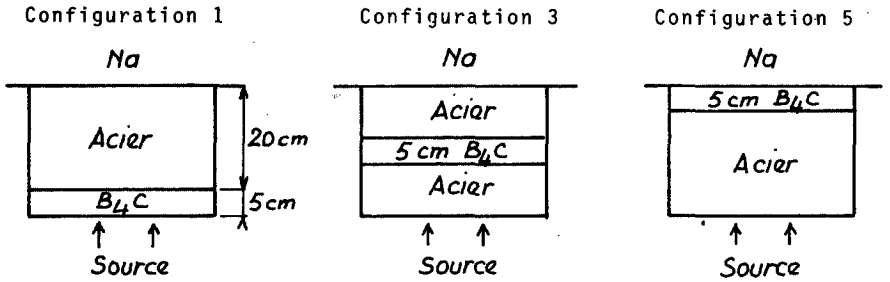

Configuration 0 : 25 cm Acier
Configuration 1 : 5 cm B4C + 20 cm Acier
Configuration 3 : 10 cm Acier + 5 cm B4C + 10 cm Acier
Configuration 5 : 20 cm Acier + 5 cm B4C

3.2 Résultats expérimentaux

Le Tableau V ci-dessous présente les résultats expérimentaux. Toutes les valeurs sont normées à l'activité relevée en canal 0.

TABLEAU V

Détecteur	Mn/Cd				Na/Cd			
Configuration	0	1	3	5	0	1	3	5
Canal 0	1	0.58	0.41	0.15	1	0.58	0.49	0.21
Canal 1	0.82	0.49	0.44	0.30	0.51	0.31	0.28	0.19
Canal 2	0.32	0.19	0.18	0.16	0.25	0.136	0.13	0.097
Canal 6	0.0019	0.00117	0.00110	0.00106	0.0032	0.0018	0.0020	0.0016

TABLEAU V (suite)

Détecteur	Soufre				Rhodium			
Configu-ration	0	1	3	5	0	1	3	5
Canal 0	1.	1.527	1.70	1.104	1.	0.83	0.83	0.58
Canal 1	0.13	0.228	0.221	0.185	0.18	0.14	0.12	0.12
Canal 2	0.0093	0.012	0.0120	0.0116	U.0084	0.0058	0.006	0.0055
Canal 3	0.00092	0.0016	0.0013	0.0010				

Détecteur	Au/Cd			
Configu-ration	0	1	3	5
Canal 0	1.	0.60	0.33	0.0043
Canal 1	0.72	0.50	0.36	0.081
Canal 2	0.39	0.24	0.21	0.065
Canal 6	0.0055	0.0033	0.0031	0.0029

Les Figures 4 à 6 présentent les résutats expérimentaux pour les détecteurs Mn/Cd, Au/Cd et Soufre.

On peut constater :

- pour le détecteur Soufre (seuil à 800 KeV) :

. que le remplacement de 15 cm d'Acier par la même épaisseur de B4C, a pour effet d'augmenter l'activation du détecteur. Cela signifie donc que l'efficacité du B4C est moindre que celle de l'Acier, en ce qui concerne le ralentissement des neutrons rapides (E > 1 MeV).

- pour le détecteur Rhodium (seuil à ≃ 100 KeV) :

. que l'effet signalé ci-dessus ne se produit pas ; en effet, pour le domaine d'énergie couvert par ce détecteur, l'efficacité du B4C devient au moins camparable à celle de l'Acier et même supérieure lorsque le spectre neutronique pénétrant dans le B4C est suffisamment dégradé (cf. C5/C1 ou C3).

- pour les détecteurs basse énergies : MN/Cd, Na/CD, Au/Cd :

. au niveau du canal 0 (entrée dans le Sodium) ; l'efficacité du B4C est d'autant plus grande que ce dernier est précédé d'une épaisseur plus importante d'Acier -pour le détecteur Au/Cd, on constate une atténuation 14 fois plus grande dans la configuration C5 que dans la configuration C1, et 23 fois plus forte que dans la configuration CO- ;

. entre les canaux 0 et 1 ; on observe une remontée des activités mesurées qui est significative du ralentissement -dans le Sodium- des neutrons rapides ayant traversés le B4C sans être absorbés ; cette remontée augmente avec le déplacement du B4C vers la fin du massif (elle n'apparaît qu'à partir de C3). (Dans la configuration C1, l'épaisseur d'Acier est suffisante pour annuler cet effet) ;

. au niveau du canal 6 (après la traversée de 250 cm de Sodium) ; l'effet du B4C apparaît atténuée. Par rapport à la configuration CO, le gain est au plus d'un facteur 2, le déplacement du B4C de C1 en C5 laisse apparaître un gain de l'ordre de 10%. Cela provient du fait que l'efficacité du B4C étant faible pour les neutrons rapides (En > 800 KeV), ce sont ces derniers qui, après ralentissement dans le Sodium, sont comptés par les détecteurs basse énergie au niveau du canal 6.

Fig. 4
Résultats Expérimentaux . Programme Préliminaire
Dat : Mn/Cd

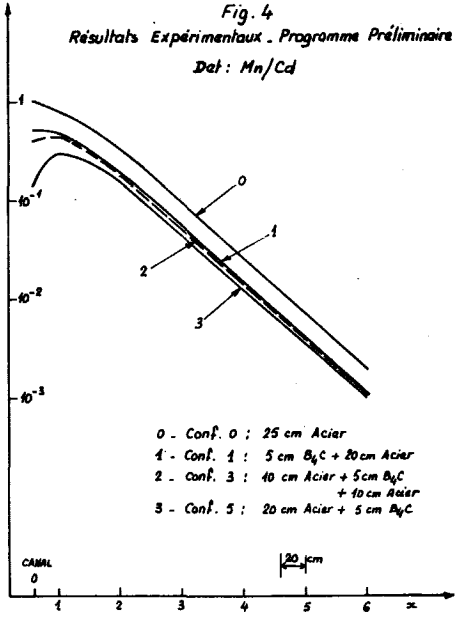

Fig. 5
Résultats Expérimentaux . Programme Préliminaire
Dat : Au/Cd

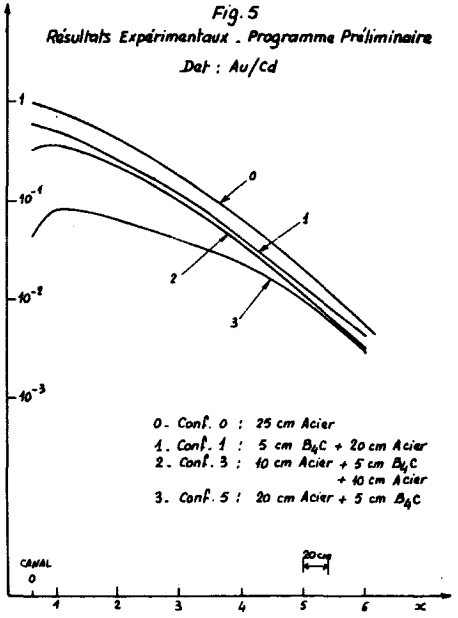

Fig. 6
Résultats Expérimentaux . Programme Préliminaire
Dat. : Soufre

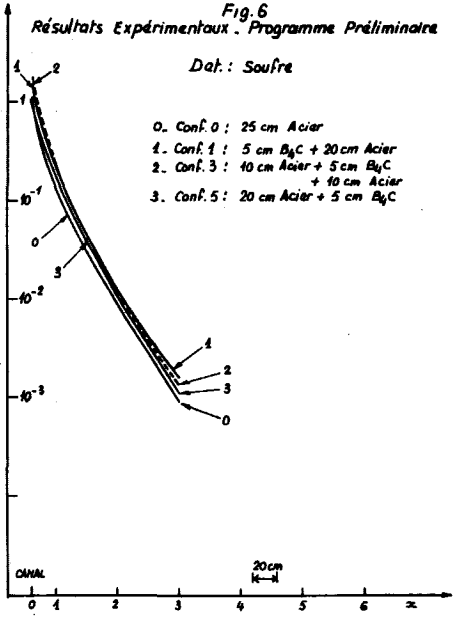

Ces résultats indiquent que si le B4C est intéressant globalement, il présente toutefois un inconvénient, à savoir de laisser passer les neutrons rapides (En > 100 KeV).

Cependant, des calculs paramétriques effectués lors des prévisions de l'expérience, semblent montrer que l'épaisseur respective des matériaux Acier et B4C, a un rôle non négligeable.

4. INFLUENCE DE L'EPAISSEUR DES MATERIAUX

Les résultats des calculs mettant en jeu des épaisseurs supérieures de matériaux -Acier et B4C- dans les positions des configuration C0, C1, C3, C5, sont résumés dans les Tableaux VI et VII :

TABLEAU VI

GAIN PAR RAPPORT A LA SOLUTION TOUT ACIER : Co

(Détecteur Au/Cd)

		C1 (B4C au début)	C3 (B4C au centre)	C5 (B4C à la fin)
Canal 0	25cm dont 5cm B4C	43.9 %	63.4 %	88.8 %
	40cm dont 5cm B4C	27 %		95 %
	40cm dont 10cm B4C	51 %	75 %	97.5 %
	40cm dont 15cm B4C	68 %		98.3 %
Canal 6	25cm dont 5cm B4C	37 %	42.8 %	54.3 %
	40cm dont 5cm B4C	25 %		46 %
	40cm dont 10cm B4C	46 %	59 %	67 %
	40cm dont 15cm B4C	62 %		77 %

TABLEAU VII

GAIN DU A LA POSITION DU B4C

(La norme est la configuration C1)

(Détecteur Au/Cd)

		C3	C5
Canal 0	25cm dont 5cm B4C	34.8 %	80 %
	40cm dont 5cm B4C		93.8 %
	40cm dont 10cm B4C	49.1 %	94.5 %
	40cm dont 15cm B4C		94.5 %
Canal 6	25cm dont 5cm B4C	9.1 %	27.3 %
	40cm dont 5cm B4C		28.6 %
	40cm dont 10cm B4C	28.75 %	37.5 %
	40cm dont 15cm B4C		40.8 %

On peut constater que :

. par rapport à la configuration Co -tout Acier- (Tableau VI) le remplacement d'une zone d'Acier par du B4C est toujours bénéfique. L'augmentation de l'épaisseur de B4C (à épaisseur totale constante), montre un effet de saturation ;

. par rapport à la configuration C1 -B4C au début- (Tableau VII), le déplacement du B4C vers la fin du massif paraît être bénéfique, en particulier lorsque l'épaisseur du B4C augmente. Dans ce cas, il apparaît d'ailleurs une sorte de seuil pour lequel les configurations C3 et surtout C5 présentent un avantage par rapport à la configuration C1.

Les expériences JASON dans lesquelles de telles configurations seront mises en oeuvre devront confirmer ou infirmer ces résultats.

5. CONCLUSION

Les études préliminaires à l'expérience JASON et celles liées à l'optimisation des protections neutroniques de la filière rapide française ont montré que :

. l'utilisation d'Aciers autres que l'Acier 304 utilisé habituellement, présente de l'intérêt ;

. de nouveaux concepts de protection, tels que l'association de matériaux modérateurs et absorbants (H_2Zr et B4C) avec l'Acier ou bien des protections localisées au voisinage de la zone à protéger, pourraient permettre des réductions notables de protections neutroniques.

Les expériences préliminaires au programme JASON concernant l'association du B4C avec l'Acier montrent l'intérêt de l'utilisation du B4C (réduction du flux d'un facteur 1.62 à 2.0 au bout de 250 cm de Sodium lorsqu'on remplace 5 cm d'Acier par la même épaisseur de B4C). Elles mettent cependant en évidence une efficacité moindre que celle de l'Acier en ce qui concerne les neutrons rapides.

Le programme JASON devra permettre de vérifier si l'effet d'épaisseur, indiqué par les calculs prévisionnels, existe en ce qui concerne les positions respectives de l'Acier et du B4C.

Il devra permettre en outre de valider le formulaire PROPANE pour les matériaux et concepts nouveaux qui pourraient être utilisés dans les protections de la filière rapide française.

-oOo-

REFERENCES

[1] Bouteau F. et al. : "Résultats expérimentaux dans HARMONIE et TAPIRO sur la propagation des neutrons", Vienne, Octobre 1976

[2] Calamand D. et al. : "Results of neutron propagation in steel-Sodium mixtures with various source spectra on HARMONIE and TAPIRO", Knoxville, Avril 1977

[3] Estiot J.C. et al. : "Nuclear data for shielding calculations : Na cross-section adjustment using propagation experiments", Knoxville, Octobre 1979

.·.·.·.·.·.

EXPERIENCES DE PROPAGATION DANS DES MILIEUX ACIER-SODIUM A TAPIRO

M. Carta*, A. De Carli*, V. Rado* , M. Salvatores**, J.P. Trapp**
*CNEN/CASACCIA (Italie) **CEA/CEN/CADARACHE (France)

RESUME

On présente les résultats expérimentaux et l'analyse des expériences de propagation dans des milieux Acier-Sodium effectués à TAPIRO, dans le cadre de la collaboration CEA/CNEN sur la Physique des Réacteurs Rapides.

Les écarts Calcul-Expérience observés varient selon le détecteurs et le milieu de propagation, mais la tendance générale est que la calcul sous-estime la valeur expérimentale, et ceci de façon cohérente avec la série d'expériences dans des milieux Sodium pur.

ABSTRACT

The experimental results and the analysis of the neutron propagation experiments in different SS/Na mixtures performed at TAPIRO reactor in the framework of the CEA/CNEN collaboration on the Fast Reactor Physics, are presented.

The observed discrepancies between calculation and experiment depend on the different detectors and mixture of propagation, but the general trend is that the calculation underestimates the experimental value, as observed in the previous series of experiments in pure Na.

-oOo-

1. INTRODUCTION

Le formulaire PROPANE [1], mis au point pour les calculs de protection des réacteurs de la filière rapide, prévoit l'ajustement des données de base multigroupe ; en particulier du Sodium et des isotopes de l'Acier, à l'aide d'expériences de propagation. Une première série d'expériences dans des milieux Sodium pur, effectuée soit à HARMONIE soit à TAPIRO, a permis un premier ajustement des données du Sodium [2]. Dans la présente note, on donne les résultats et l'analyse fine d'expériences effectuées à TAPIRO et portant sur des milieux Acier-Sodium.

2. CONFIGURATION EXPERIMENTALE

Des expériences de propagation de neutrons dans des milieux Acier-Sodium à pourcentage variable, ont été effectuées dans le réacteur TAPIRO (Figure 1). Le réacteur a été modifié en introduisant à la place d'une partie du réflecteur de cuivre, une zone "couverture", telle que le spectre neutronique d'attaque des milieux de propagation soit proche du spectre existant à l'interface couverture/protection dans les réacteurs rapides de puissance (Figure 2). La composition de la couverture est la suivante :

Isotope	At/cm^{3}x10^{24}	Isotope	At/cm^{3}x10^{24}
Na	$1. \times 10^{-2}$	Fe	$6. \times 10^{-3}$
U 235	$4. \times 10^{-5}$	Cr	1.5×10^{-3}
U 238	$1. \times 10^{-2}$	Ni	$8. \times 10^{-4}$
O	$2. \times 10^{-2}$		

Les milieux de propagation sont situés dans deux cuves en Acier, de dimensions globales 149 x 95 x 110 cm^3, remplies de Sodium. Des barreaux d'Acier sont immergés dans ces cuves. Le diamètre des barreaux est : d = 3cm , et ils sont disposés selon trois réseaux différents.

Dans les Figures 3, 4, 5, on indique les réseaux correspondants aux trois pourcentages de Sodium, 25 - 50 - 75% en volume. Dans toutes les configurations, on a utilisé cinq détecteurs d'activation : Mn, Ma, Au, S, Rh. Toutes les mesures ont été effectuées sous Cd pour éliminer d'une part la composante thermique pour les réponses de type (n,γ), et d'autre part les effets d'impuretés dans le cas des détecteurs à seuil. Les incertitudes expérimentales sont les suivantes (en valeur relative) :

$Na(n,\gamma)$, $Mn(n,\gamma)$, $Au(n,\gamma)$: 5 % (2σ)
$S(n,p)$, $Rh(n,n')$: 10 % (2σ)

Les résultats expérimentaux sont montrés dans les Tableaux I, II, III, colonne 4, et sont documentés en référence [5].

3. ANALYSE DES EXPERIENCES

Les calculs en transport à deux dimensions (géométrie R,Z) ont été effectués à l'aide du code aux ordonnées discrètes DOT 3.5. Les options de calcul S_4/P_3 ont été adoptées avec les sections efficaces à 45 groupes d'énergie du formulaire PROPANE Do [1]. Les sections efficaces de ce formulaire ont comme origine la bibliothèque BABEL à 113 groupes [3], et ont été condensées à l'aide de spectres différents, selon les différentes zones (et donc selon les différents pourcentages d'Acier/Sodium).

3.1. Pondérations des sections efficaces

La condensation des sections efficaces à partir de la bibliothèque de référence (BABEL, 113G) a fait l'objet d'une étude particulière :

1) pondération spéciales à partir des flux calculés à 113 groupes sur les trois mélanges Acier-Sodium ;
2) utilisation de PROPANE Do : la bibliothèque PROPANE contient déjà pour un même corps différentes sections efficaces représentatives des effets de spectres dans les trois compositions de mélange envisagées.

Le tableau ci-dessous donne les écarts par rapport à la méthode de référence (113 groupes/S16/P3) pour les deux cas ci-dessus:

ECARTS A LA REFERENCE (%)

[ϕRéf.-45/S4/P3]/ϕRéf.

Détecteur	Distance de propagation (cm)	25%Acier-75%Na		50%Acier-50%Na		75%Acier-25%Na	
		1	2	1	2	1	2
Soufre	55	20%	27.8	46.4%	41.6	45%	30
Au/Cd	55	- 1.8	3.9	-1.4	12.	5.8	12.2
	130	2.1	0.9	-2.9	14.	15.8	11.9

L'utilisation de l'option S16 permet de réduire considérablement les écarts par rapport à la référence (environ 15%).

On observe de faible différences entre les deux ensembles de sections efficaces, ce qui justifie d'une part le choix de PROPANE pour le calcul de propagation dans ces mélanges, et d'autre part le mode de pondération utilisé dans PROPANE.

Pour chaque mélange, on a utilisé deux spectres de condensation, représentatifs de chacune des deux cuves (dans le cas de PROPANE, ces deux spectres correspondent à deux zones successives de la PNL du calcul Benchmark [4]).

3.2. Pondération des sections efficaces de détecteur

Les détecteurs Rhodium, Soufre , Mn/Cd, Au/Cd, Na/Cd, ont été condensés (à partir de 113 groupes) par le mode de condensation 1. Les effets de spectre sont suffisamment peu importants pour justifier l'utilisation d'un seul spectre de pondération (sauf pour le soufre au bout de 130 cm de propagation où ils peuvent atteindre 5%).

L'effet de coupure du Cadmium a été pris en compte ; il intervient à partir du 42ème groupe du découpage PROPANE (8.3 à 3.015 eV). Cependant, dans le cas des mélanges la non prise en compte de cet effet n'a que de faibles conséquences.

3.3. Effet du découpage angulaire et du découpage spatial

Cette étude a été effectuée sur le mélange 75% d'Acier qui est le plus sensible, de ce point de vue.

. Effet du maillage spatial :
A partir d'un calcul de référence 45G/S4/P3 à Δx = 1.5 cm on fait varier le pas en espace jusqu'à 3 puis 5 cm.

A basse énergie (Na/Cd - Mn/Cd - Au/Cd), l'écart par rapport à la référence reste négligeable (< 1%) pour Δx = 3 cm ; il croit fortement pour 5 cm.

A haute énergie (Soufre), le passage de 1.5 cm à 3 cm conduit à un écart inférieur à 14% pour la zone de mesure ; cet écart atteint 60% pour 5 cm.

Le maillage adopté a donc été 1.5 cm.

. Effet du découpage angulaire :
Le calcul de référence est 45G/S32/P3 Δx = 3 cm. On fait varier Sn jusqu'à S16 et S4.

A basse énergie, l'écart est négligeable en S16 et faible en S4 : 7% en plus.

A haute énergie, il reste négligeable en S16 mais devient important en S4 : il atteint 40% pour le Soufre et 15% pour le Rhodium dans la zone mesurée.

L'option S16 apparaît donc nécessaire pour la zone d'énergie couverte par les détecteurs Soufre et Rhodium.

3.4. Calculs spatiaux

La géométrie de l'ensemble TAPIRO+Cuves a conduit à diviser le calcul en deux parties :

1) calcul de préparation de la source ;
2) calcul de propagation dans les différents milieux.

En ce qui concerne le point 1), on a effectué un calcul de criticité avec les sources de fission de la configuration TAPIRO avec couverture. La géométrie a donc été représentée en détail selon un modèle (R,Z) jusqu'au réflecteur de Cu, mais on a présenté seulement une partie réduite d'un milieu de propagation (en particulier le cas avec le mélange 50/50 Sodium/Acier), pour assurer des conditions de réflection réalistes.

De ce calcul, on déduit, pour chaque maille les sources en n/cm^3.sec utilisées dans les calculs de propagation.

2) Le milieu de propagation a été schématisé en géométrie (R,Z) comme un milieu homogène, sauf en ce qui concerne les épaisseurs d'Acier correspondant aux parois des cuves, qui ont été représentées exactement. L'ensemble a été entouré par du béton sur trois côtés. Les effets d'hétérogénéité dus aux barreaux d'Acier ont été calculés séparément comme des corrections à appliquer aux valeurs expérimentales, pour les ramener à des valeurs "homogènes", donc directement comparables au calcul. Les résultats du calcul homogène sont indiqués dans les tableaux I, II, III, colonnes 3.

4. FACTEURS D'HETEROGENEITE

La représentation homogène du milieu de propagation a pour conséquence de négliger les parcours préférentiels des neutrons, en particulier des neutrons rapides dans le Sodium. Pour une analyse correcte de l'expérience, il faut donc corriger les résultats expérimentaux. Le facteur de correction (facteur d'hétérogénéité) est le rapport, pour chaque maille et chaque détecteur, entre la valeur calculée avec le modèle homogène et celle calculée avec le modèle hétérogène.

Pour ces deux descriptions du réseau, on a utilisé la géométrie X-Y, la dimension transverse (hauteur des barreaux d'Acier) étant infinie.

Le calcul DOT a été effectué en S4/P1, avec description détaillée de l'hétérogénéité uniquement pour la zone centrale, le long de la direction de propagation.

Le barreau d'Acier cylindrique a été représenté comme un rectangle avec les deux contraintes suivantes :

. conservation de la section du barreau et conservation de l'épaisseur maximale dans la direction de propagation (épaisseur égale au diamètre).

Cette modélisation a été effectué à l'aide de 2x2 mailles.

Un calcul pour chaque mélange a été effectué, toujours suivant le même principe de conservation des surface et de la dimension du barreau (diamètre de 3 cm) dans la direction de propagation.

Les valeurs obtenues pour les facteurs d'hétérogénéité sont indiquées dans les tableaux I, II, III. Les corrections les plus importantes sont obtenues pour la configuration à 75% de Sodium ($f_{Réf.} \simeq .6$ pour le détecteur Au en bout de propagation).

Pour cette configuration, on a donc effectué une étude détaillée. Les résultats relatifs au détecteur Na(n,γ) sont rassemblés dans le tableau IV. Le tableau ci-dessous résume l'étude effectuée :

ETUDE SPECIFIQUE DU MELANGE

Cas	A	B	C	D	E
Géométrie	XY	XY	XY	XY	XY
Options	S4/P1	S4/P1	S4/P1	S4/P1	S4/P1
Hétérogénéités	Zone centr.	Zone centr.	Zone centr.	zone centr.	Zone centr.
Dimension Transverse	Infinie	Finie*	Finie*	Finie*	Finie*
Description des Barreaux	Surface équivalente + Epaisseur 3 mm dans Pu. Diver-tion de propagation	Surface équivalente + Epaisseur 3 mm dans Pu. Diver-tion de propagation	Pas de con-servation de l'épais-seur	Pas de con-servation de l'épais-seur	Pas de con-servation de l'épais-seur
Nombre de mailles	2 x 2	2 x 2	2 x 2	3 x 3	1 x 1

* Dimension transverse calculée de façon à être cohérente avec les calculs correspondants R,Z.

Les résultats obtenus conduisent aux observations suivantes:

. l'effet des fuites observé entre les cas A et B varie entre environ 1% et 10%, selon la position dans le mélange ;

. l'effet de schématisation du barreau (et la conservation ou non de la dimension dans la direction de propagation) conduit à augmenter les facteurs d'hétérogénéité de 1 à 10% dans le cas C (barreau carré de 2.7 cm de côté) ;

. l'effet de maillage varie d'environ 2% à environ 8%, mais le maillage 2x2 semble être bien adapté.

L'examen de ces résultats a conduit à adapter les facteurs de géométrie du cas A en associant aux valeurs mesurées une incertude supplémentaire croissante avec la distance de propagation (valeurs comprises entre 1% et 10% par une distance de propagation d'environ 120 cm dans le mélange).

5. CONCLUSIONS

Les écarts Calcul/Expérience observés pour les trois mélanges sont indiqués dans les tableaux I, II, III.

On peut observer :

. les écarts (E-C/C) augmentent avec le pourcentage d'Acier ;

. le calcul sous-estime toujours la valeur expérimentale. Cela confirme les résultats déjà obtenus dans le cas du milieu Sodium pur ;

. les incertitudes sur les facteurs d'hétérogénéité ne modifient pas les tendances générales observées plus haut.

L'analyse des résultats présentés ici indique clairement que l'utilisation de telles expériences pour l'ajustement du formulaire PROPANE, nécessite un examen des incertitudes (et de leurs correlations) en ce qui concerne les sections efficaces des isotopes de l'Acier.

Les ajustements déjà effectués sur les milieux Sodium pur [2] ont souligné l'importance de telles données.

-oOo-

REFERENCES

[1] Estiot J.C., Salvatorès M., Trapp J.P. : Basic Nuclear Data and the Fast Reactor Shielding Design. Formulaire PROPANE Do", Proc. Int. Conf. Nucl. Cross-Sections and Tech.; Knoxville 1979

[2] Estiot J.C, et al. : "Nuclear Data for Shielding calculations Na Cross-Section adjustment using propagation experiments", Proc. Int. Conf. Nucl. Cross-Sections and Tech., Knoxville 1979

[3] Estiot J.C., et al. : "Conséquences des incertitudes sur les données de base dans les calculs de protection", Proc. Int. Conf. on Neutron Physics and Nuclear Data, Harwell 1978

[4] "Proc. Specialist Meeting on Differential and Integral Nuclear data requirements for shielding", Vienna 1976.

[5] Antonini D. et al. ; Rapport Technique CNEN - RIT/FIS-LNS(78)1

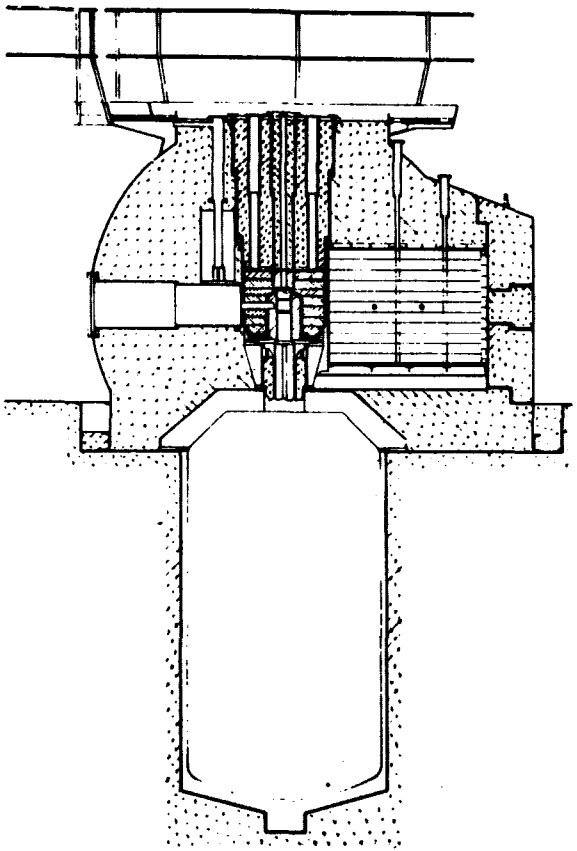

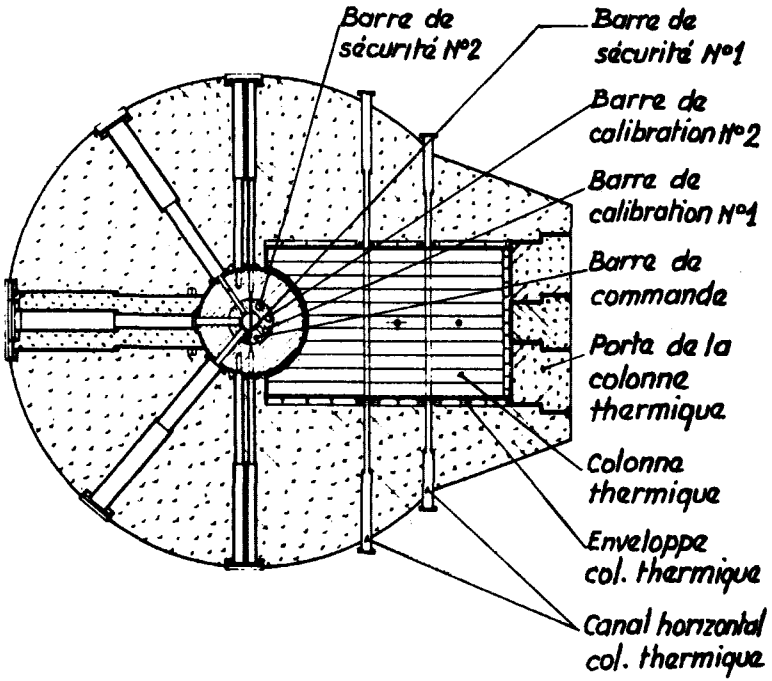

Fig. 1

Réacteur TAPIRO

Vue verticale et horizontale

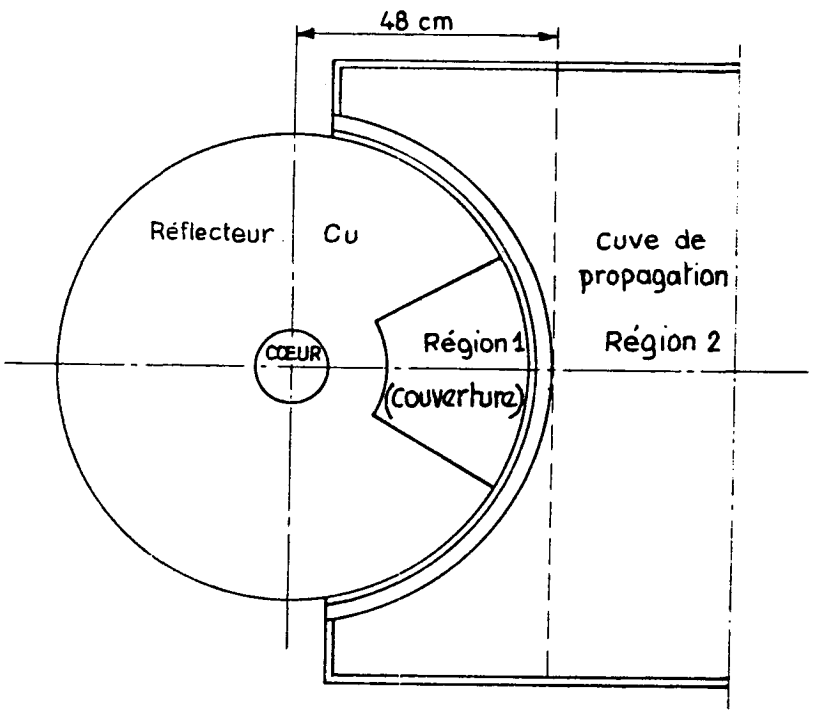

Fig. 2

Configuration TAPIRO avec couverture

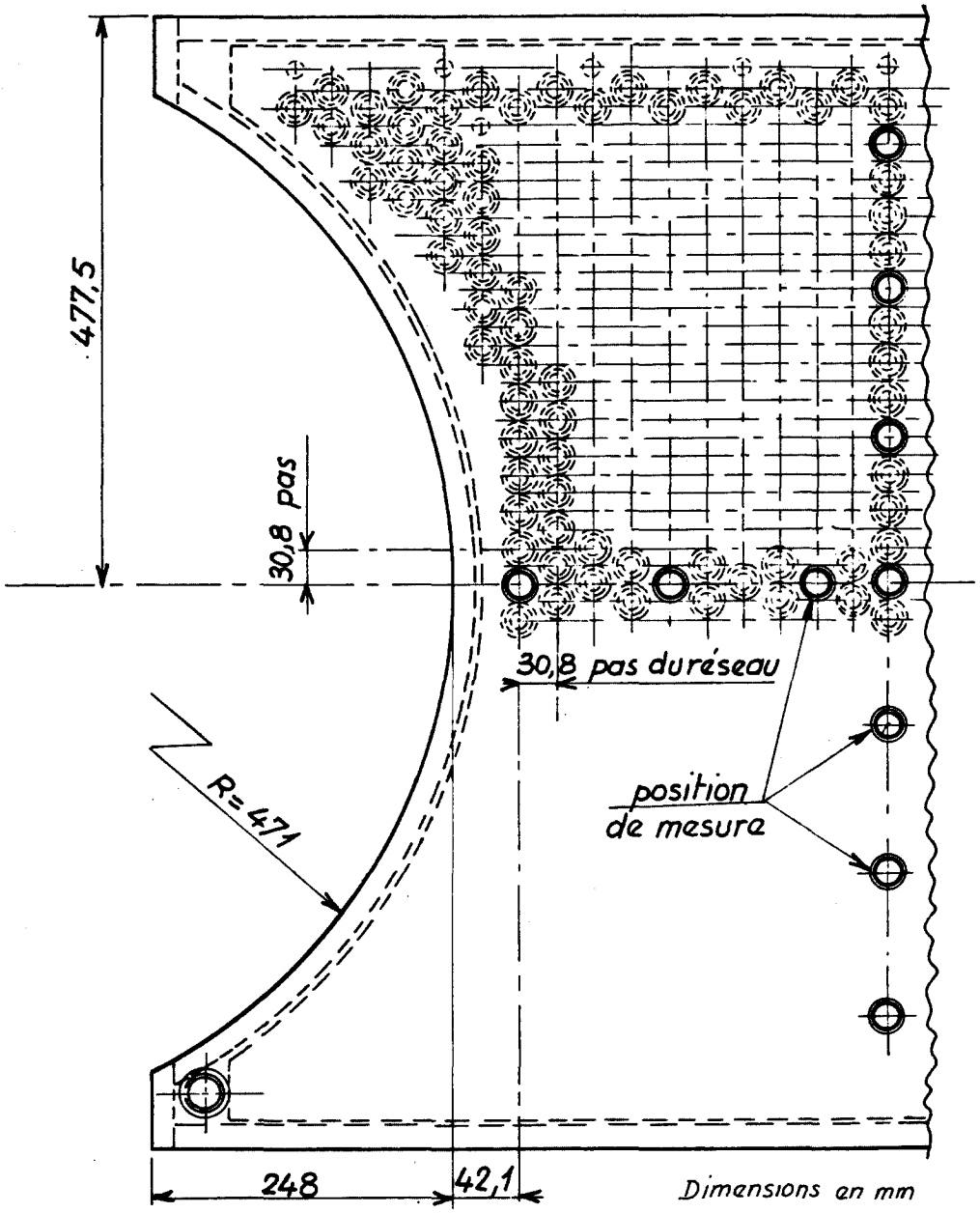

Fig. 3 - Configuration 25 % Na

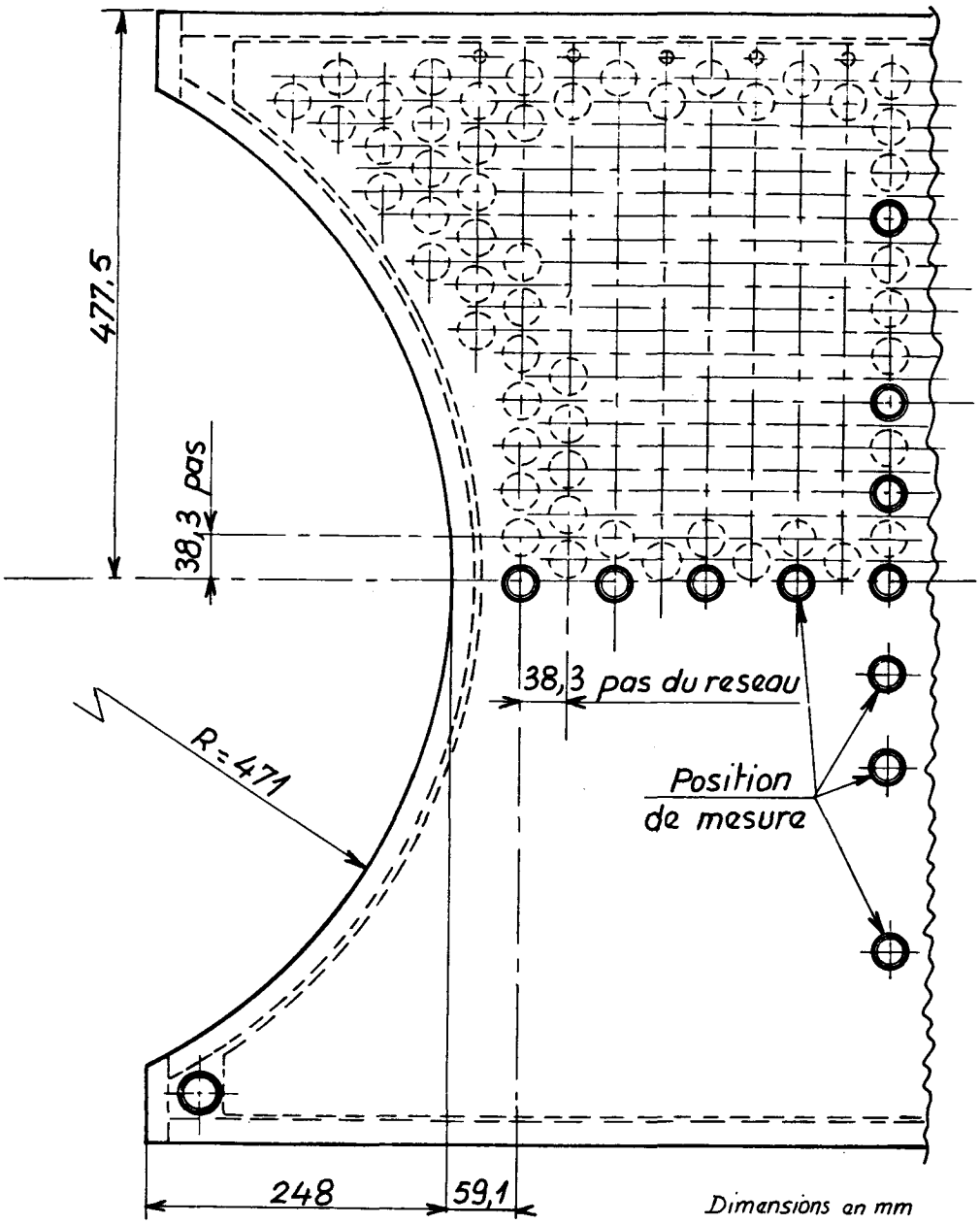

Fig. 4 - Configuration 50 % Na

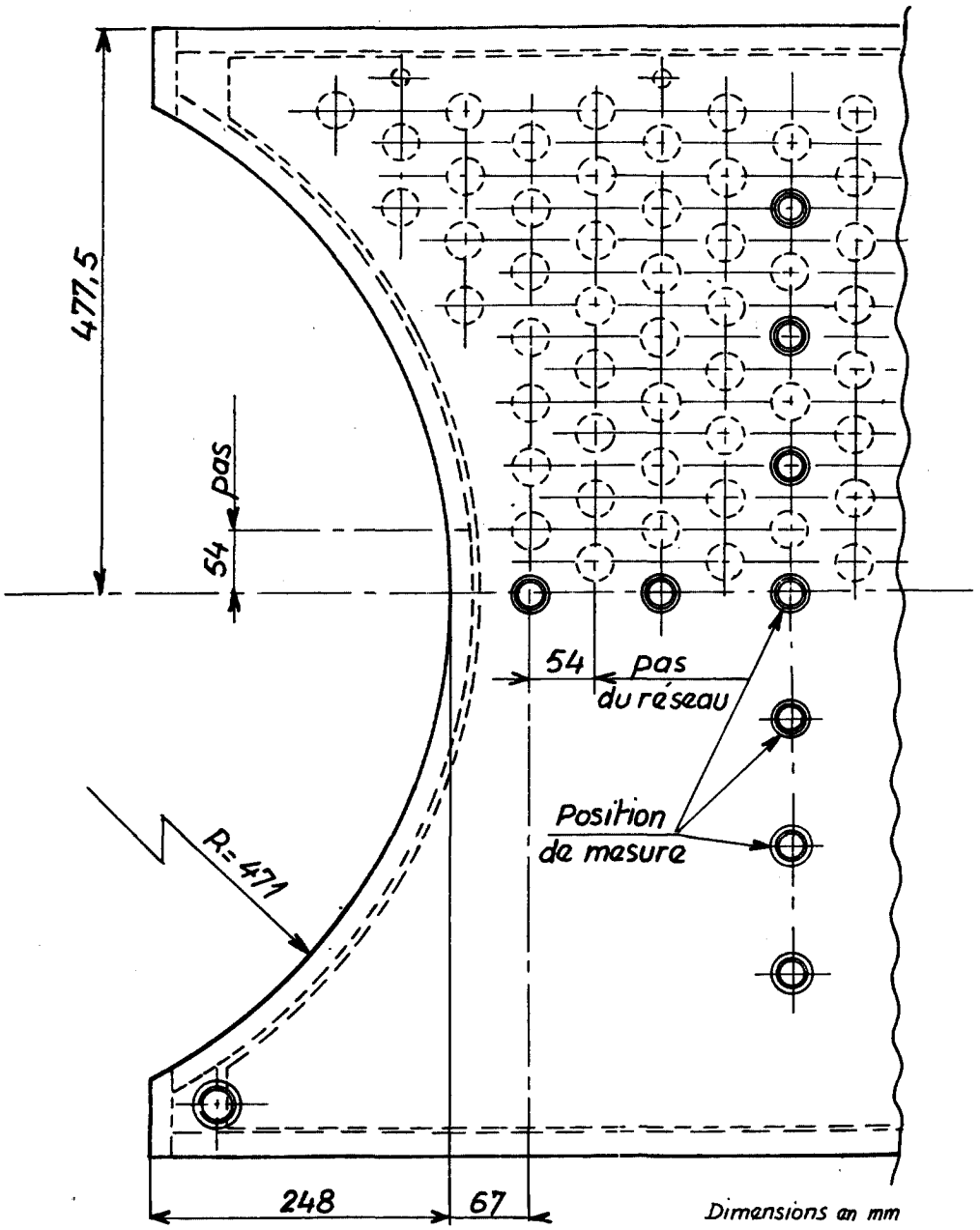

Fig. 5 - Configuration 75 % Na

TABLEAU I

RESULTATS CONCERNANT LE MELANGE 75%Na-25%Acier

Détecteur	Centimètres dans le mélange	Calcul 2D	Mesures	Facteur d'Hétérogénéité	Mesures Corrigées Ec	$\frac{Ec - C}{C}$ %
Na	4.7	1.0	1.0	.992	.992	-0.8
	26.3	.462	.542	.974	.528	14.3
	47.9	.188	.269	.906	.244	29.6
	58.7	.115	.182	.859	.156	35.9
	77.8	.353-1	.590-1	.776	.458-1	29.8
	88.6	.204-1	.366-1	.755	.276-1	35.5
	110.2	.641-2	.138-1	.694	.958-2	49.5
Mn	4.7	1.0	1.0	1.028	1.028	2.8
	15.5	.706	.760	1.014	.771	9.2
	37.1	.278	.345	.938	.323	16.3
	47.9	.165	.244	.895	.218	32.4
	58.7	.950-1	.139	.847	.118	23.9
	77.8	.259-1	.384-1	.783	.301-1	16.1
	88.6	.149-1	.236-1	.774	.183-1	22.6
	110.2	.449-2	.838-2	.721	.604-2	34.5
	131.8	.119-2	.252-2	.666	.168-2	41.0
Au	4.7	1.0	1.0	1.028	1.028	2.8
	15.5	.838	.837	1.029	.861	2.8
	37.1	.453	.494	.969	.479	5.7
	47.9	.305	.362	.924	.334	9.6
	58.7	.198	.256	.870	.223	12.5
	77.8	.646-1	.877-1	.777	.682-1	5.5
	88.6	.382-1	.552-1	.751	.415-1	8.6
	99.4	.221-1	.338-1	.717	.242-1	9.6
	110.2	.125-1	.210-1	.685	.144-1	15.0
	131.8	.357-2	.731-2	.626	.458-2	28.2
S	4.7	1.0	1.0	1.010	1.010	1.0
	15.5	.318	.361	1.000	.361	13.5
	26.3	.106	.133	.941	.125	18.1
	37.1	.355-1	.535-1	.932	.498-1	40.4
	47.9	.127-1	.236-1	.895	.211-1	66.4
	58.7	.473-2	.103-1	.854	.880-2	86.0
Rh	4.7	1.0	1.0	.987	.987	-1.3
	15.5	.392	.446	.980	.437	11.5
	26.3	.160	.181	.960	.174	8.6
	37.1	.666-1	.852-1	.947	.807-1	21.2
	47.9	.284-1	.397-1	.931	.370-1	30.2
	58.7	.123-1	.199-1	.917	.182-1	48.3
	77.8	.255-2	.434-2	.837	.363-2	42.4

TABLEAU II

RESULTATS CONCERNANT LE MELANGE 50%Na-50%Acier

Détecteur	Centimètres dans le mélange	Calcul 2D	Mesures	Facteur d'Hétérogénéité	Mesures Corrigées Ec	$\frac{Ec - C}{C}$ %
Na	3.91	1.0	1.0	.995	.995	-0.5
	19.23	.481	.566	.967	.547	13.7
	34.55	.201	.266	.932	.248	23.4
	57.53	.461-1	.730-1	.882	.644-1	39.7
	84.67	.682-2	.116-1	.761	.883-2	29.5
	107.65	.130-2	.270-2	.761	.206-2	58.5
Mn	3.91	1.0	1.0	.994	.994	-0.6
	19.23	.480	.532	.966	.514	7.1
	34.55	.188	.227	.930	.211	12.2
	57.53	.404-1	.574-1	.891	.511-1	26.5
	84.67	.575-2	.890-2	.781	.695-2	20.9
	107.65	.108-2	.203-2	.786	.160-2	48.2
	130.63	.177-3	.492-3	.788	.388-3	119
Au	3.91	1.0	1.0	1.041	1.041	4.1
	19.23	.647	.691	.995	.687	6.2
	34.55	.309	.365	.945	.345	11.7
	57.53	.779-1	.106	.881	.934-1	19.9
	84.67	.121-1	.175-1	.749	.131-1	8.3
	107.65	.238-2	.408-2	.749	.306-2	28.6
	130.63	.413-3	.101-2	.751	.758-3	83.5
S	3.91	1.0	1.0	.934	.934	-6.6
	19.23	.121	.149	.888	.132	9.1
	34.55	.151-1	.237-1	.863	.205-1	35.8
	42.21	.556-2	.929-2	.849	.789-2	41.9
	49.87	.209-2	.355-2	.834	.296-2	41.6
Rh	3.91	1.0	1.0	.959	.959	-4.1
	11.57	.470	.504	.950	.479	1.9
	19.23	.222	.270	.944	.255	14.9
	26.89	.106	.143	.939	.134	26.4
	34.55	.513-1	.747-1	.935	.699-1	36.3
	42.21	.250-1	.392-1	.931	.365-1	46.0
	49.87	.122-1	.277-1	.926	.257-1	111
	57.53	.600-2	.146-1	.924	.135-1	125
	65.19	.295-2	.606-2	.935	.567-2	92.1
	77.01	.979-3	.202-2	.827	.167-2	70.7

TABLEAU III

RESULTATS CONCERNANT LE MELANGE 25%Na-75%Acier

Détecteur	Centimètres dans le mélange	Calcul 2D	Mesures	Facteur d'Hétérogénéité	Mesures Corrigées Ec	$\frac{Ec - C}{C}$ %
Na	2.21	1.0	1.0	.981	.981	-1.9
	14.53	.465	.525	.955	.502	7.9
	33.01	.119	.153	.960	.147	23.4
	51.49	.272-1	.407-1	.963	.392-1	44.1
	75.27	.377-2	.883-2	.925	.817-2	117
	87.59	.131-2	.355-2	.925	.328-2	150
Mn	2.21	1.0	1.0	.988	.988	-1.2
	14.53	.458	.517	1.00	.517	12.9
	33.01	.112	.143	.996	.142	27.2
	51.49	.255-1	.374-1	.999	.374-1	46.5
	63.81	.988-2	.150-1	.996	.149-1	51.3
	75.27	.349-2	.623-2	.918	.572-2	63.9
	87.59	.122-2	.243-2	.963	.234-2	91.8
Au	2.21	1.0	1.0	1.017	1.017	1.7
	14.53	.645	.662	1.00	.662	2.6
	33.01	.189	.217	.991	.215	13.7
	63.81	.166-1	.241-1	.986	.238-1	43.2
	75.27	.637-2	.103-1	.913	.940-2	47.6
	87.59	.228.2	.419-2	.941	.394-2	72.9
S	2.21	1.0	1.0	.961	.961	-3.9
	14.53	.111	.132	1.00	.132	18.9
	26.85	.130-1	.195-1	1.013	.197-1	51.9
	33.01	.451-2	.848-2	1.014	.860-2	90.6
	39.17	.159-2	.355-2	1.016	.361-2	127
Rh	2.21	1.0	1.0	.978	.978	-2.2
	14.53	.255	.309	.991	.306	20.0
	26.85	.669-1	.922-1	.996	.919-1	37.3
	33.01	.346-1	.509-1	.998	.508-1	46.9
	39.17	.180-1	.295-1	1.00	.295-1	63.9
	51.49	.486-2	.960-2	1.005	.964-2	98.5

TABLEAU IV

FACTEURS D'HETEROGENEITE

cm dans le mélange	A	B	C	D	E
4.7	.992	1.012	1.014	1.019	1.009
26.3	.974	1.003	1.011	1.013	.983
47.9	.906	.927	.950	.957	.927
58.7	.859	.871	.901	.883	.903
77.8	.776	.843	.893	.875	.905
88.6	.755	.822	.872	.859	.879
110.2	.694	.729	.791	.786	.836

THE EURACOS DEEP PENETRATION IRON BENCHMARK EXPERIMENT

G. Perlini, G. Gonano
Joint Research Center
Ispra(Va),Italy

ABSTRACT

The EURACOS II irradiation facility installed at the LENA reactor at Pavia has been used to study the attenuation and spectral deformation of neutron fluxes in an iron block(145x145x140 cm^3)originating from a 235U converter.
The epithermal and fast fluxes were measured along the axis of the block with Cd-canned gold foils and with the S32(n,p) threshold reaction.
Neutron spectra between 20 KeV and 10 MeV were measured with a set of 5 proportional gas counters and a small NE213 liquid scintillator.

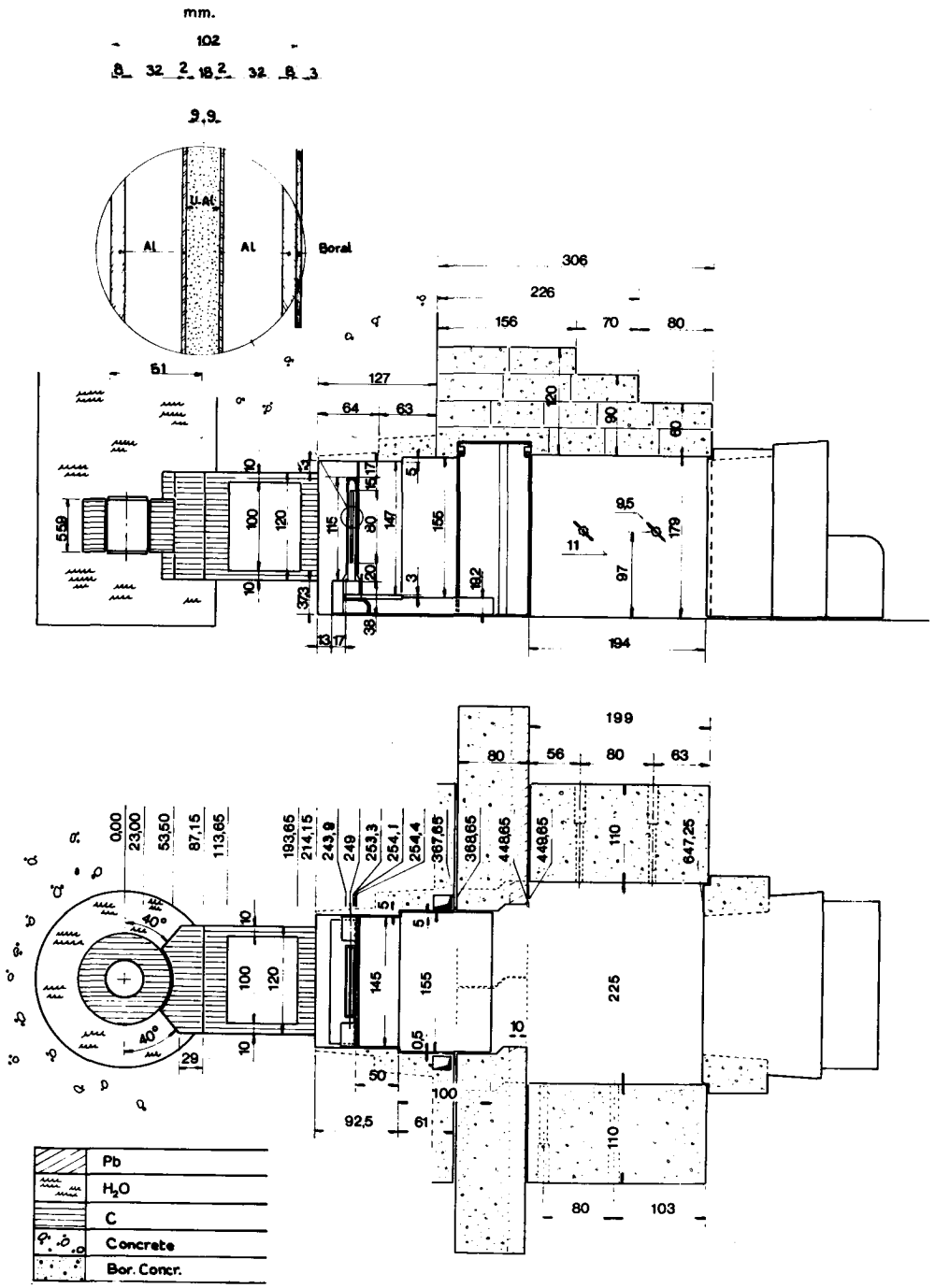

FIG. 1 : The Euracos facility

The Installation

At the LENA-TRIGA reactor of the University of Pavia a spectrum converter is placed at the end of thermal column to study neutron penetration in a large iron block. In order to increase the neutron flux some of the graphite in the central part of the thermal column was removed.(Fig.1)

The converter plate is made up of six plates of an U-Al alloy containing a total of 4.77 Kg of U235 enriched 90%.

The trapezoidal shape of the plates with a variable size has allowed us, by fitting them together, to make an almost circular disc with a diameter of 80 cm.

The converter is contained in an Al chamber in which the two faces of the plates can be air cooled.
The converter has a conversion ratio ϕ_{fiss}/ϕ_{th} of about one. The spectrum leaving the Uranium-Al is very similar to the fission spectrum which at the centre of the external surface of the cooling chamber has a flux strength of $1.167.10^8$ n/(cm^2.sec). This value was obtained by means of the $S^{32}(n,p)P^{32}$ activation measurement using $\overline{\sigma}f(U235) = 65$ mb.

The radial profile of the fast neutron flux (2 MeV) at 6.0 cm from the central plane of the plate, which corresponds to the external surface of the cooling chamber, is represented in Fig.2, while Fig.3 shows the profile along the central axis of the empty irradiating chamber.

The Experiment

The iron block being studied is made up of a group of about thirty iron slabs each with the dimensions 145 x 145 x 4 cm^3. The surfaces were worked to obtain good flatness so that when assembled the block would be as compact as possible.

Half of the plates have a channel penetrating to the central axis of the block. During the measurement this channel is filled by a tightly fitting iron arm, carrying the activation foil. A thicker (8cm) plate of the same structure is used for the positioning of the spectrometers (Fig.4).
There are also available some smaller (100 x 100 x 2 cm^3)iron plates which have been added at the back as appendix.

A chemical analysis of iron assembly showed the following impurities:

Mn : .50%	Cn : .18%
Ni : .15%	Cr : .05%
Sn : traces	

Table I indicates the distances of the detectors and the spectrometers from the initial surface of the iron block and the thickness effectively interposed (sum of the thicknesses of the individual plates). This means that a material density reduction of about 15% should be assumed in the calculation.
Between converter and the iron block there is mounted a 3 mm thick boral slab which is intended to reduce the entering low energy neutron flux from the thermal column.

Table I

Positions of the Detectors in the Iron

Activation Detectors			Neutron Spectrometers		
Pos.	Penetration depth [cm]	Eff.iron depth [cm]	Pos.	Penetration depth [cm]	Eff.iron depth [cm]
1	1.5	1.5	1	9.5	7.4
2	8.1	8.4	2	25.7	23.5
3	16.4	16	3	42	39.8
4	24.4	24	4	58	55.5
5	32.6	32	5	74.2	71.5
6	40.5	40	6	90.5	87.5
7	48.5	48	7	106.5	103.5
8	52.6	52			
9	60.6	60			
10	69.1	68			
11	77.2	76			
12	85.2	84			
13	93.4	92			
14	101.5	100			
15	105.5	104			
16	109.7	108			

The set of slabs making up the iron block is mounted on an Al and concrete bogie which runs along rails. After the detectors and spectrometers have been put in place, the whole assembly is inserted into the irradiating tunnel until it makes contact with the Al chamber containing the converter.

Measurements with activation probes

Activation probes consisting of pure and diluted gold were used to monitor the epithermal flux. The 1%o gold in aluminium was applied (up to a maximum of 60-70 cm) of the iron block penetration depth in order to avoid self-shielding effects in the detectors.

For deeper penetrations pure gold probes were used. The region where the two curves (pure gold, dilute gold) overlapped was at least 30-40 cm, and thus a good fitting was possible.

The gold activation was measured by a 3"x 3" NAI(TL) crystal spectrometer. The gamma-pulse spectrum was processed by using a code which simulate the photo-electric peak with a gaussian distribution and the background with a straight line or a parabola.

A series of different geometric assembly arrangements were studied taking advantage of the relative ease of irradiating and counting of the gold detectors.

Results are shown in Fig.5 and Table II.

Fast neutron fluxes were measured by means of $S^{32}(n,p)P^{32}$ reaction with Sulphur tablets and low-background β counting (Fig.6 and Table III).

Measurements of neutron spectra

Two different types of spectrometers were used both taking advantage of the phenomenon of proton recoil:

1) in gas proportional counters and

2) in a liquid scintillator.

The range of energy explored with the proportional counters was between 20 keV and 2 MeV using different hydrogen pressures and, for higher energies, a mixture of hydrogen and argon. There are various methods for calibration in energy: a) the addition of a small quantity of He_3 to give a thermal peak at 764 keV; b) the deposition of an alpha ^{3}microsource on the central wire; c) the calibration on a spectrum with known resonance peaks (in Fe, Fl, etc.).
Each one has advantages and disadvantages. We have used all three methods to a certain extent.
The measuring set was formed of five spherical proportional counters with a diameter of 4 cm.
The counters together with the preamplifiers were mounted in a bar which was fitted into a specially constructed iron plate.
The pulse spectrum collected by a multichannel analyzer was treated with the unfolding code SPEC4.
For energies higher than 1 MeV a cylindrical NE213 liquid scintillator Ø 1.5 cm x height 1.5 cm was used in connection with a fast rise time photomultiplier. A sophisticated electronic circuit for pulse shape discrimination and pulse shaping /1/ prepared the pulses for the analyzer.

/1/ White, G. : "A Versatile Pulse Shape Discriminator for Charged Particle Separation", 2nd Ispra Nuclear Electronics Symposium (1975) - EUR 5370 e.

Table II

Activation Rate of Gold Detectors

	Dist. (cm)	Act.Rate (dis./gr.sec)
1) Without boral sheet	1.5	435.9165
	8.1	519.6426
	16.4	483.473
	24.4	396.649
2) With boral sheet	1.5	713.01
	8.1	594.1716
	16.4	496.979
	24.4	399.5258
	32.6	342.3891
	40.5	278.8953
	48.5	220.7518
	52.6	191.989
	60.6	150.7165
	68.9	115.5918
	77.2	85.32
	85.3	63.623
3) Iron block lenght cm 112	93.4	41.4168
	101.5	23.5276
	105.5	15.518
	109.5	7.0503
4) Iron block length cm 140	93.4	46.9479
	101.5	33.7461
	105.5	28.5801
	109.7	23.4782
	118.8	14.5402
	128.6	7.1256
	135.4	2.4924

Table III

Absolute Saturation Activity of Sulphur Detectors

Dist. (cm)	Ass. (dis./gr.sec)
1.5	1.3442 E + 5
8.1	2.3875 E + 4
16.4	4.7864 E + 3
24.4	1.0742 E + 3
32.6	2.3596 E + 2
40.5	5.1257 E + 1
52.6	5.5320 E + 0

The calibration in energy was carried out at the Van de Graaf of the JRC-Geel with monoenergetic neutrons of 0.5 to 11 MeV with the reactions T(p,n), D(d,n). The response to the various neutron energies in Cs137 light units is given in Fig.7

A fitting on the experimental data led to the function

$$L = \exp(-1.0000 + 1.7800 * LOG(E) - 0.1550 * LOG(E)^2)$$

which is used in the unfolding code.

Relative neutron spectra measured in different positions of the iron block are represented in the Fig.8 and Tab.IV, V and VI.

Problems encountered in the use of the spectrometers:

1) The NE213-photomultiplier systems showed a 1-2% temperature dependence in energy per C° for the Cs137 reference spectrum.

This can be seen when the apparatus is switched on or displaced. (e.g. when calibrating with a γ source outside the Fe block, and then going inside the block for the measurement.

A temperature probe placed on the outside of the scintillator has allowed us to monitor the temperature variations.

2)Although the pulse shape discrimination circuit may be accurate, it is never perfect: there are always a few impulses due to the presence of γ which enter the neutron coincidence channel; as the energy is lowred this effect becomes more and more pronounced. This effect can be explained as follows:

Let G be the impulses due to the γ present and Gl those which manage to pass into the neutron channel. Let N be the number of impulse due to the neutrons in the neutron channel. A Gl/G ratio of 10^{-3} or 10^{-4} may be considered good. For p.s.d. in some practical cases,however,the Gl/N ratio is more important. In fact,with deep penetrations into the iron,the γ flux present depends on the thermal and epithermal neutron flux with small gradient with respect to the distance); the fast neutron flux ($>$ 1 MeV) falls off rapidly. We thus can find ourselves in situations where even small losses of impulses in p.s.d. may be of the same order as the neutron signals, and completely falsify the spectrum measurement.

Tab.IV - Neutron spectrum at cm. 25.7 of the Iron block

U	F(U)	U	F(U)	U	F(U)
0.0128	4.2636	0.0978	8.8867	0.5240	7.5011
0.0134	5.5125	0.1027	12.4000	0.5373	6.7614
0.0138	6.2687	0.1068	14.2659	0.5512	7.2959
0.0146	8.0502	0.1117	15.4767	0.5650	8.6427
0.0152	8.7634	0.1165	17.4161	0.5665	9.4154
0.0160	9.2493	0.1214	20.1700	0.5914	10.0428
0.0166	9.3126	0.1263	23.3512	0.6225	9.9306
0.0174	9.1972	0.1320	26.7159	0.6474	8.8659
0.0180	9.8847	0.1369	29.1822	0.6848	6.3901
0.0188	11.1089	0.1434	28.7835	0.7159	4.6829
0.0196	12.2357	0.1491	22.9882	0.7532	3.2611
0.0203	14.1607	0.1557	16.1283	0.7906	2.4308
0.0211	17.4824	0.1622	15.8999	0.8279	2.0741
0.0221	22.2835	0.1687	19.9493	0.8653	2.0044
0.0229	24.9222	0.1760	23.6841	0.9089	1.9763
0.0241	24.6154	0.1834	24.8481	0.9462	1.9547
0.0249	20.8454	0.1915	23.2418	0.9960	1.8201
0.0263	10.6491	0.1997	15.9805	1.0396	1.5399
0.0271	6.2011	0.1997	10.5457	1.0956	1.1483
0.0286	3.3602	0.2050	11.4283	1.1454	0.9312
0.0294	3.0232	0.2104	12.9688	1.2077	0.8346
0.0310	1.7711	0.2157	13.9319	1.2575	0.7619
0.0320	1.8918	0.2211	14.4248	1.3259	0.5742
0.0338	3.2514	0.2265	14.1551	1.3820	0.4165
0.0350	3.7494	0.2332	13.7843	1.4567	0.2255
0.0367	4.1942	0.2385	14.2212	1.5189	0.1667
0.0381	4.9522	0.2452	15.1510	1.5998	0.1594
0.0399	6.0992	0.2519	15.8140	1.6530	0.1365
0.0413	6.6878	0.2573	16.2045	1.6683	0.1439
0.0435	6.8903	0.2653	17.6673	1.7355	0.1113
0.0448	6.6682	0.2720	20.4037	1.8225	0.0920
0.0472	6.9590	0.2787	21.9212	1.9135	0.0741
0.0488	8.0559	0.2868	18.6844	2.0090	0.0511
0.0514	8.5846	0.2935	16.7519	2.1095	0.0346
0.0529	7.5610	0.3015	19.4183	2.2150	0.0277
0.0557	6.3692	0.3095	24.5176	2.3255	0.0253
0.0569	8.5050	0.3176	25.8913	2.4420	0.0212
0.0575	7.5368	0.3256	21.4056	2.5645	0.0162
0.0589	9.0299	0.3337	16.0134	2.6925	0.0118
0.0618	9.9986	0.3430	15.7629	2.8135	0.0116
0.0640	11.0519	0.3511	17.4479	2.9550	0.0094
0.0670	11.6980	0.3605	16.1472	3.1170	0.0081
0.0697	12.4928	0.3698	14.6115	3.2725	0.0055
0.0729	15.4998	0.3792	14.0199	3.4360	0.0056
0.0757	16.8549	0.3899	11.6900	3.6080	0.0042
0.0792	14.8197	0.3993	8.5173	3.7885	0.0046
0.0822	14.1771	0.4100	5.9611	3.9780	0.0038
0.0861	15.5276	0.4159	5.9014	4.1770	0.0031
0.0893	13.4422	0.4264	6.3912	4.3860	0.0025
0.0936	9.4813	0.4375	7.5136	4.6050	0.0021
0.0970	9.7469	0.4491	7.8085	4.8350	0.0018
0.1017	12.2599	0.4602	7.8595	5.0770	0.0015
0.1028	12.7589	0.4730	8.9481	5.3310	0.0013
0.1055	13.3450	0.4846	9.2547	5.5975	0.0011
0.0905	10.5856	0.4979	9.3257	5.8775	0.0009
0.0945	8.3898	0.5107	8.8813		

Tab.V - Neutron spectrum at cm. 42 of the Iron block

U	F(U)	U	F(U)
0.0876	19.8755	0.4515	23.2322
0.0907	16.8811	0.4618	23.9319
0.0938	16.9091	0.4747	19.4268
0.0977	17.5941	0.4863	16.6062
0.1008	18.1943	0.4992	20.5033
0.1054	21.7686	0.5121	23.6510
0.1085	25.5763	0.5263	21.5828
0.1132	29.6768	0.5400	22.5104
0.1170	31.7011	0.5760	25.0107
0.1217	35.3424	0.6000	25.4200
0.1263	41.8068	0.6360	22.6068
0.1310	49.0722	0.6660	18.3576
0.1356	50.7218	0.7080	12.9028
0.1411	40.3276	0.7440	9.4573
0.1457	27.1451	0.7860	7.0358
0.1519	20.2134	0.8280	6.8260
0.1566	25.0678	0.8700	7.1002
0.1628	34.3813	0.9180	7.0939
0.1682	40.1048	0.9720	6.5623
0.1744	43.5307	1.0200	5.5571
0.1814	41.4201	1.0800	4.2699
0.1876	35.5088	1.1340	3.7752
0.1953	25.5823	1.2000	3.4987
0.2023	18.8011	1.2600	2.9891
0.2093	21.3160	1.3320	2.2918
0.2178	32.0282	1.4040	1.7898
0.2248	32.9772	1.4760	1.4157
0.2341	30.6146	1.5600	1.1681
0.2418	32.1776	1.6440	1.0629
0.2511	33.2675	1.7280	0.9383
0.2604	35.5204	1.8300	0.8315
0.2697	40.7115	1.9200	0.6751
0.2774	38.6420	2.0340	0.4690
0.2806	41.8533	2.1095	0.4570
0.2851	37.2809	2.1360	0.3582
0.2915	41.5564	2.2150	0.3600
0.3006	51.8493	2.3255	0.3326
0.3070	52.1885	2.4420	0.2529
0.3161	44.7382	2.5645	0.2032
0.3238	37.7414	2.6925	0.2095
0.3315	31.6824	2.8135	0.1149
0.3406	35.0775	2.9550	0.0890
0.3483	40.7723	3.1170	0.1066
0.3586	40.3813	3.2725	0.0772
0.3677	36.2379	3.4360	0.0342
0.3767	30.0760	3.6080	0.0707
0,3870	22.8884	3.7885	0.0530
0.3960	18.2117	3.9780	0.0210
0.4064	16.0384	4.1770	0.0449
0.4180	16.2904	4.3860	0.0204
0.4283	18.0636	4.6050	0.0095
0.4399	20.8862	4.8350	0.0164

Tab.VI - Neutron spectrum at cm. 58 of the Iron block

U	F(U)	U	F(U)
0.5562	74.2916	3.9780	0.6493
0.5871	81.4281	4.1250	0.5143
0.6103	83.5453	4.3930	0.4654
0.6412	80.2597	4.6785	0.3806
0.6721	70.7947	4.9825	0.3305
0.7030	58.9234	5.3060	0.2789
0.7416	46.8806	5.6510	0.2511
0.7725	39.8118	6.0185	0.1816
0.8189	34.8619	6.4100	0.1764
0.8498	34.5231	6.8265	0.1385
0.8961	34.5953	7.2700	0.1253
0.9347	33.5139	7.7425	0.0908
0.9811	30.6584	8.2460	0.0674
1.0274	26.9614	8.7820	0.0689
1.0815	24.3701	9.3525	0.0394
1.1279	23.4731	9.9605	0.0514
1.1897	21.0187	0.0157	18.9053
1.2437	19.1129	0.0161	19.9731
1.3055	17.0105	0.0170	19.4204
1.3673	14.5495	0.0176	18.9846
1.4369	12.7581	0.0183	19.3667
1.4987	11.4491	0.0194	22.0114
1.5836	10.0238	0.0198	22.9747
1.6454	9.4844	0.0211	29.0900
1.7381	8.7663	0.0215	32.3063
1.8077	7.8165	0.0228	42.6799
1.8190	7.0206	0.0234	47.1662
1.9081	6.7685	0.0247	49.5527
1.9140	5.5966	0.0256	43.1449
1.9370	5.7104	0.0269	25.4482
2.0090	4.3643	0.0277	15.1390
2.0630	4.2924	0.0292	7.7098
2.1095	3.6196	0.0301	7.1318
2.1975	3.5608	0.0318	7.3418
2.2150	3.3274	0.0329	7.3107
2.3255	3.2230	0.0344	8.9556
2.3405	3.0700	0.0359	11.7120
2.4420	2.7836	0.0374	13.0079
2.4925	2.5074	0.0389	14.7274
2.5645	2.1880	0.0409	17.0605
2.6545	1.9742	0.0421	17.5752
2.6925	1.9477	0.0443	18.4113
2.8135	1.7614	0.0458	18.6573
2.8270	1.6981	0.0479	18.0248
2.9550	1.5979	0.0499	20.1817
3.0105	1.4708	0.0522	22.7320
3.1170	1.3549	0.0542	21.4733
3.2060	1.2042	0.0570	22.0738
3.2725	1.1764	0.0589	23.5538
3.4145	1.0070	0.0617	27.2051
3.4360	1.0994	0.0641	31.0333
3.6080	0.9196	0.0669	34.7784
3.6365	0.8369	0.0697	37.9064
3.7885	0.7323	0.0729	38.0490
3.8730	0.6316	0.0757	39.0210

U	F(U)	U	F(U)
0.0793	40.7830	0.3472	105.5410
0.0821	38.2937	0.3564	103.1100
0.0862	35.5070	0.3643	90.0584
0.0894	35.1083	0.3749	79.7865
0.0937	34.0873	0.3841	72.7529
0.0972	34.1643	0.3947	65.5691
0.1019	38.1311	0.4052	59.6209
0.1023	38.4836	0.4158	53.4301
0.1047	42.8527	0.4264	47.8843
0.1056	43.0861	0.4369	47.1985
0.1072	46.1238	0.4488	55.4202
0.1104	50.8346	0.4594	66.9356
0.1129	55.5526	0.4726	66.7072
0.1162	62.4422	0.4844	66.2838
0.1194	67.6970	0.4976	78.4459
0.1227	72.9073	0.5372	73.8271
0.1252	77.4068	0.5562	74.2915
0.1292	83.5863	0.1901	58.1550
0.1317	83.4125	0.1940	51.0474
0.1358	76.0168	0.1993	45.8784
0.1391	65.4278	0.2046	49.4446
0.1423	56.3779	0.2099	58.7420
0.1456	52.1554	0.2152	65.4566
0.1497	53.6702	0.2218	65.5607
0.1530	58.8201	0.2270	62.2322
0.1579	67.5532	0.2336	59.2323
0.1612	71.4228	0.2389	58.4824
0.1661	78.2066	0.2455	62.7361
0.1701	86.4594	0.2508	70.3242
0.1751	86.9137	0.2587	83.7056
0.1791	74.9819	0.2640	95.5540
0.1874	64.5808	0.2719	102.8680
0.1927	52.2127	0.2785	89.6840
0.1967	46.8346	0.2864	80.8595
0.2020	46.9184	0.2944	96.8847
0.2072	54.1536	0.3023	118.9310
0.2125	62.3839	0.3102	124.2000
0.2191	66.5456	0.3181	118.1320
0.2244	64.4017	0.3260	98.0027
0.2310	59.8781	0.3340	81.0535
0.2363	59.0375	0.3432	96.6785
0.2429	60.4089	0.3511	107.2780
0.2482	65.6391	0.3617	94.3610
0.2561	77.5762	0.3696	84.6103
0.2614	89.2651	0.3802	75.5263
0.2693	103.5420	0.3894	69.3536
0.2759	95.6274	0.4000	62.4344
0.2825	80.8153	0.4105	56.5711
0.2904	85.6715	0.4211	50.7938
0.2970	105.6700	0.4316	47.2300
0.3049	122.5910	0.4422	49.8354
0.3128	123.2090	0.4541	61.9753
0.3208	112.8110	0.4646	69.0048
0.3300	88.0858	0.4778	64.9239
0.3379	85.2563	0.4897	71.1302
0.3472	105.5410	0.5029	81.0212
0.5029	81.0212		

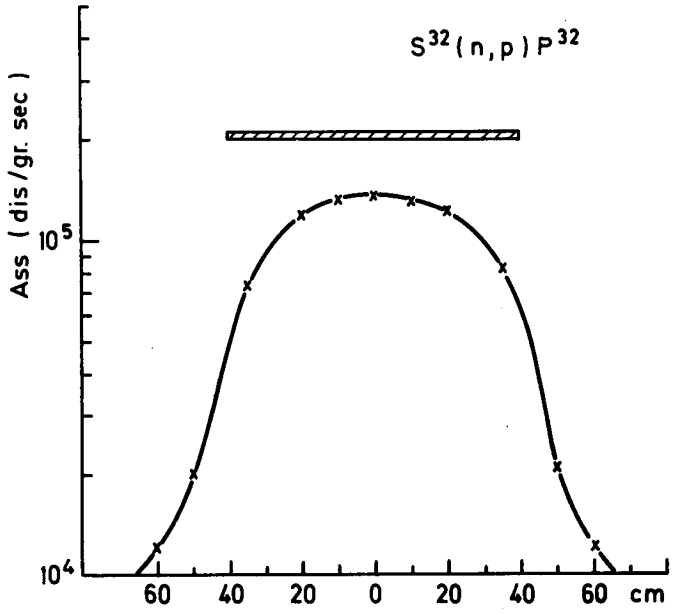

FIG. 2 : Transverse profile of fast neutron flux at 6 cm. from central plane of the source

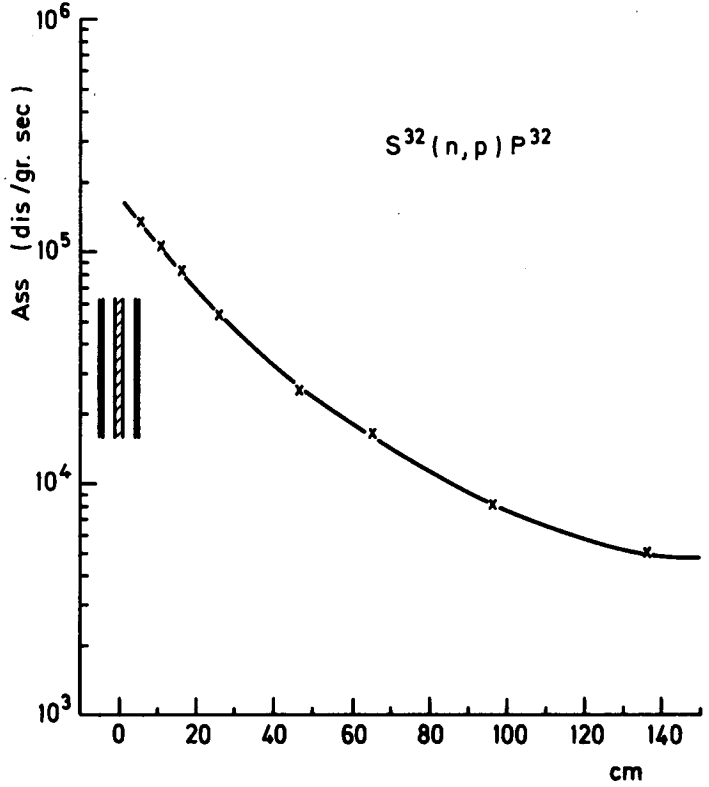

FIG. 3 : Fast neutron flux profile along the central axis in the empty irradiation diameter

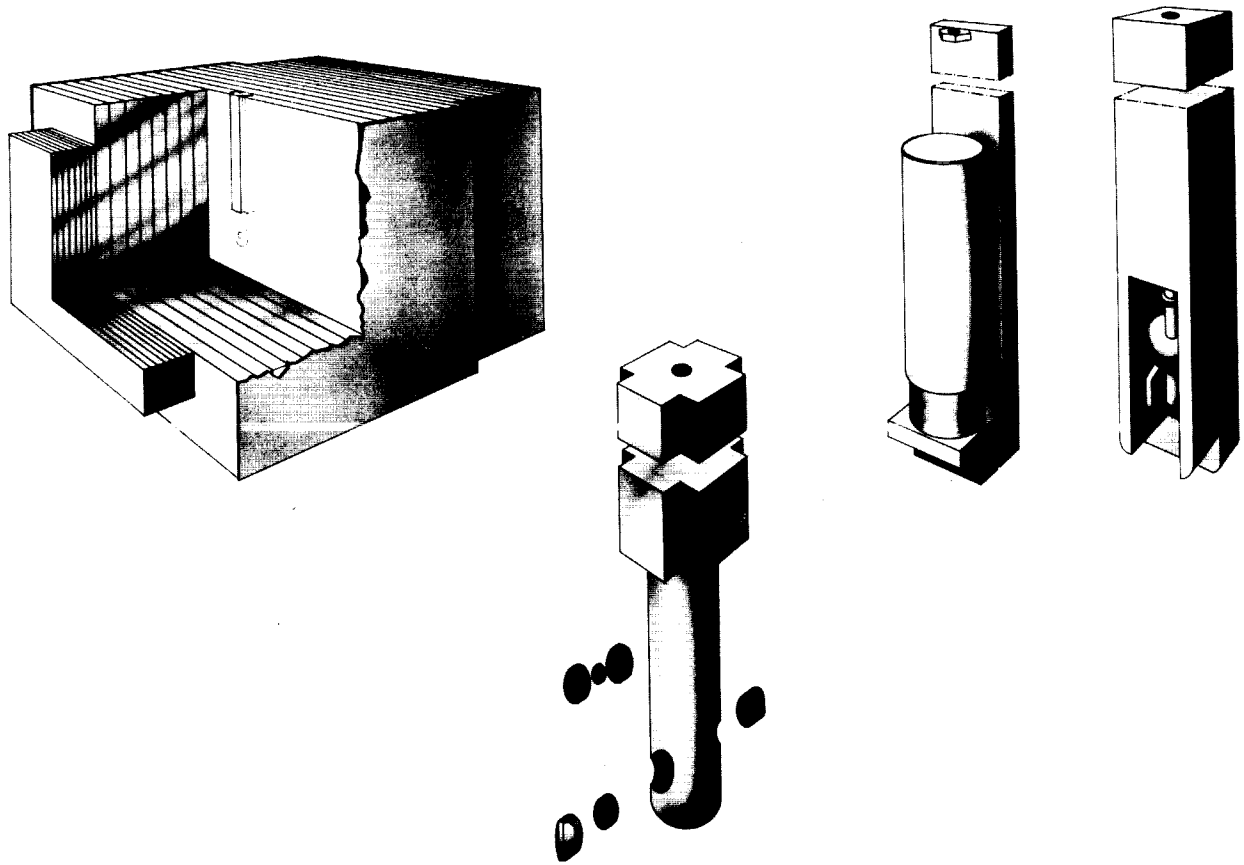

Fig.4-**The Iron block and detector supports**

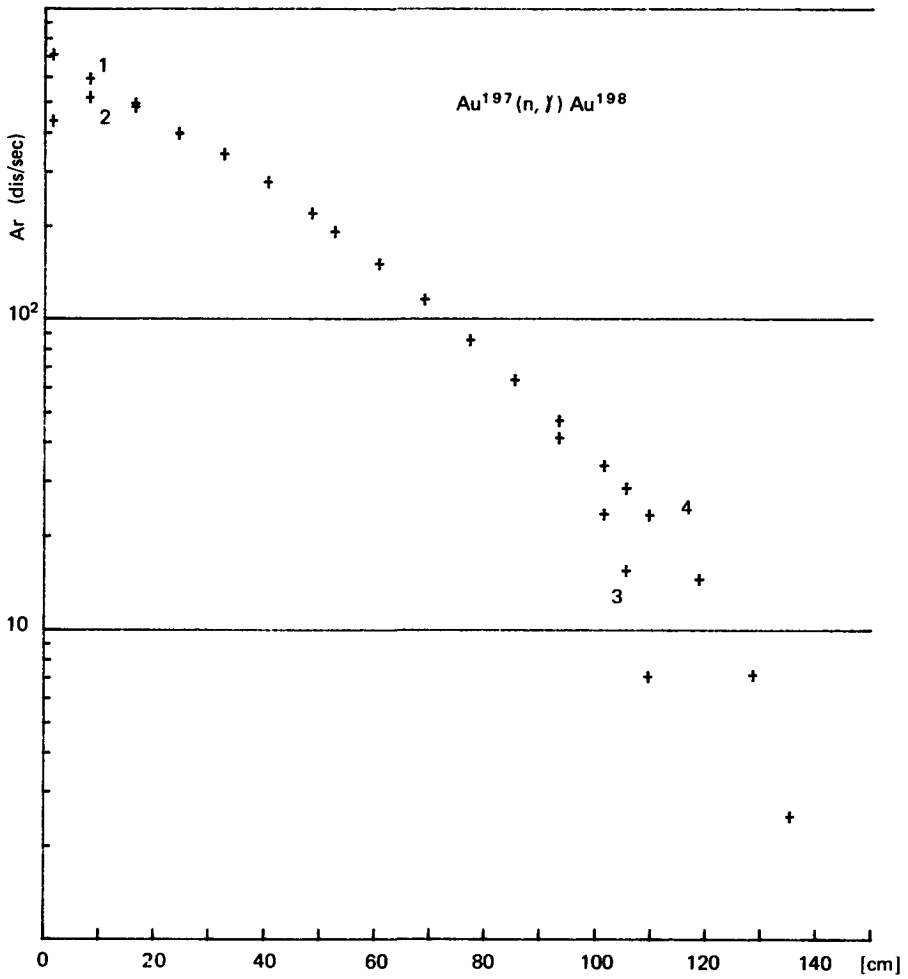

FIG. 5 : Activation rate of gold detectors for different geometrical conditions

1 - Without boral sheet in front of iron block
2 - with boral sheet
3 - iron block of 112 cm total thickness
4 - iron block up 140 cm total thickness

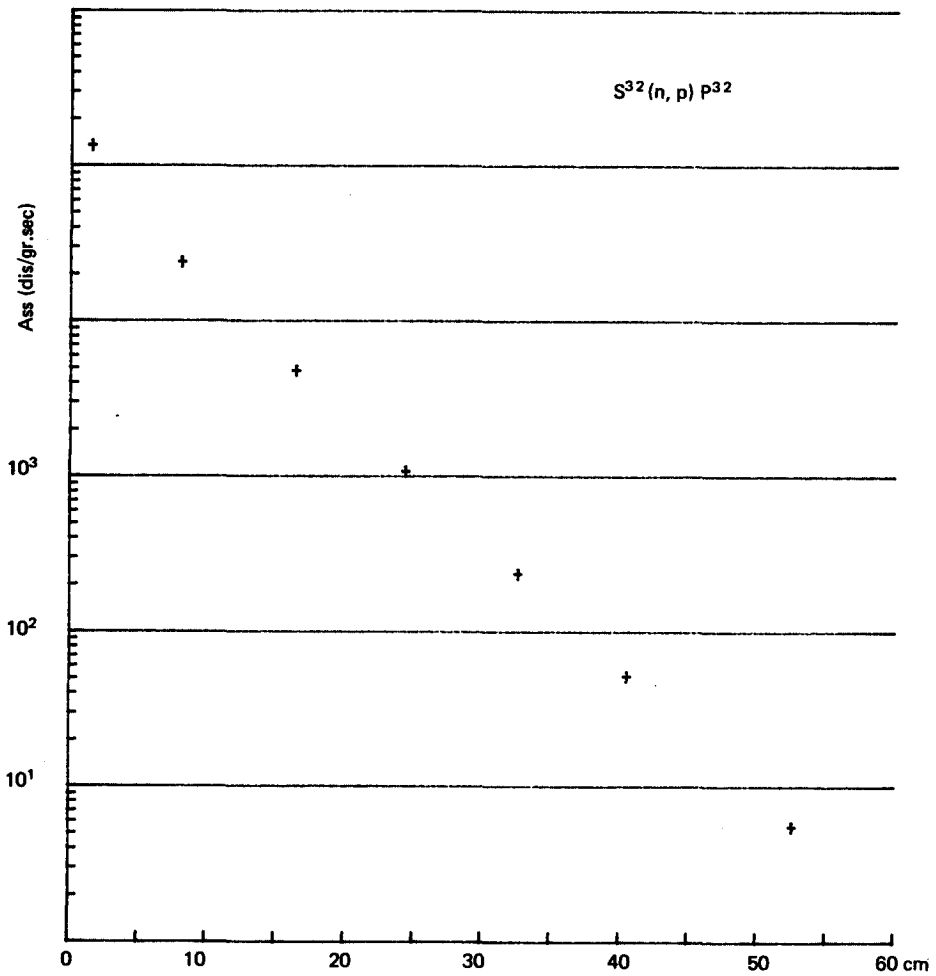

FIG. 6 : Absolute saturation activity of sulphur detectors

FIG. 7 : Neutron light response of NE213 scintillator

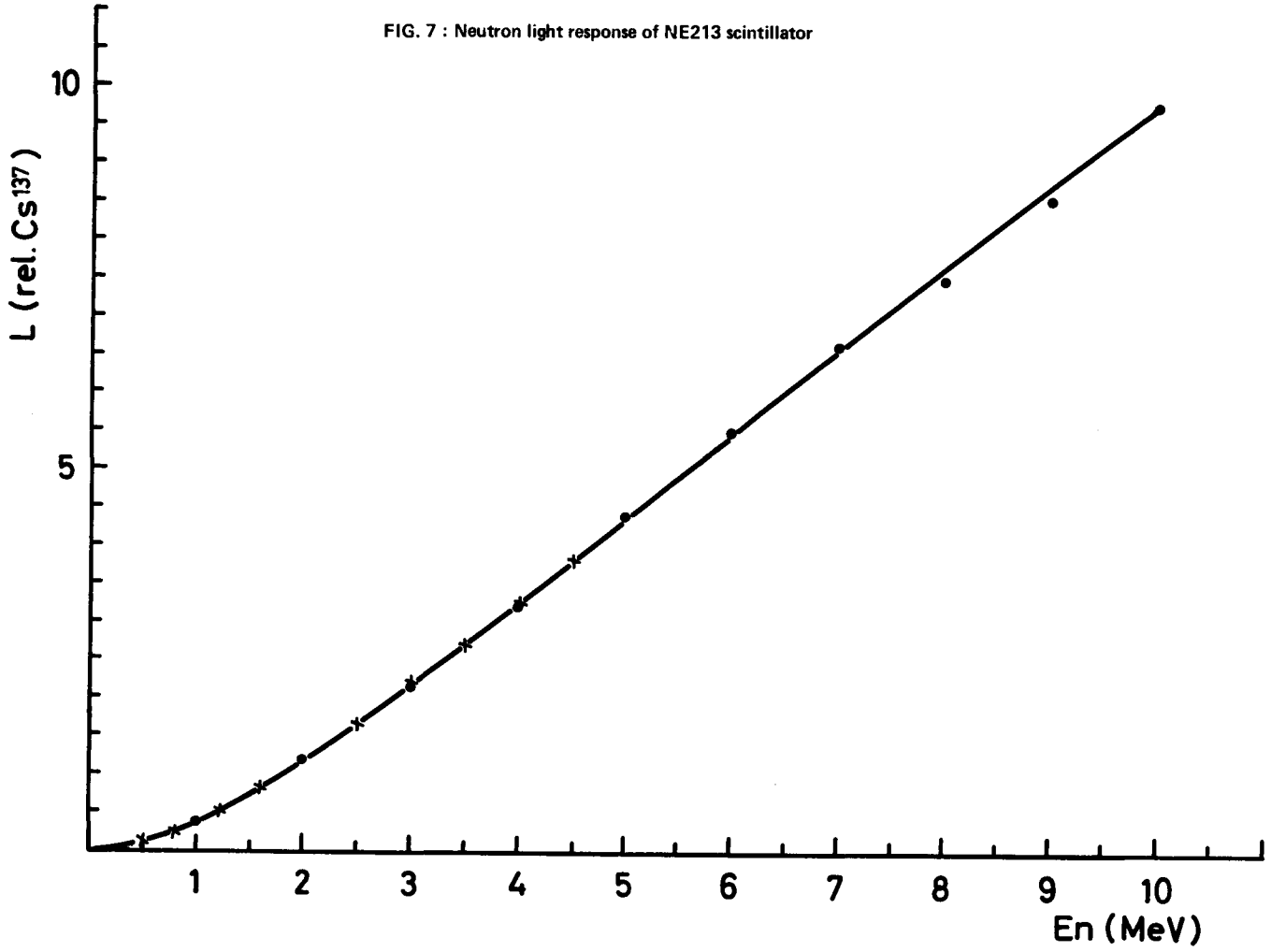

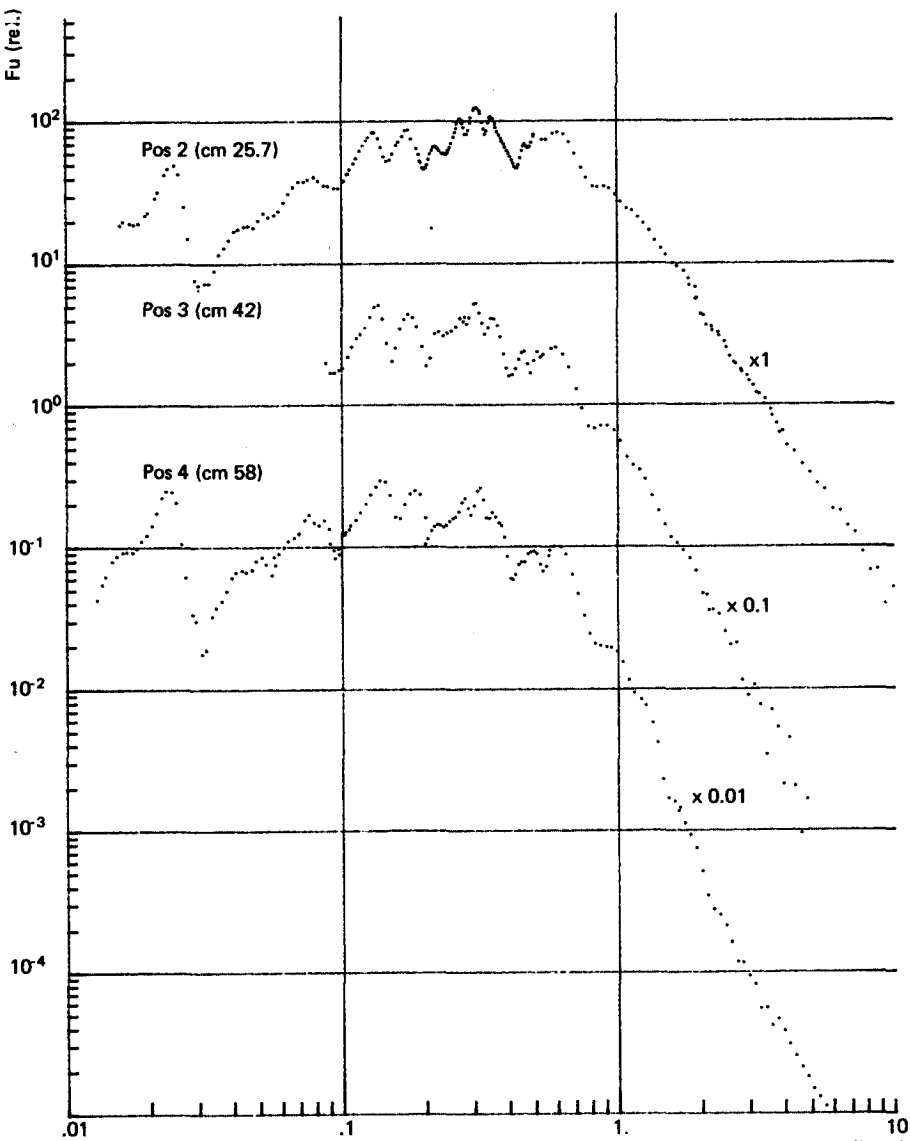

FIG. 8 : Relative neutron spectra at different positions in the iron block

THE ASPIS IRON BENCHMARK EXPERIMENT - RESULTS AND CALCULATIONAL MODEL

by

M D Carter
M M Chestnutt*
A K McCracken

ABSTRACT

The ASPIS experiment on neutron propagation in iron comprises the U.K. contribution to the OECD(NEA) Collaborative Benchmark Exercise on assessing the nuclear data requirements for radiation shielding. Sufficient details are presented in the paper, of the source representation, the geometry of the experiment and of the observations and their associated response functions, to enable other laboratories to quantify the accuracy of their preferred calculational routes and data, whether they be the rigorous many-group transport solutions required for data adjustment or the few-group approximate methods used in reactor design. An analysis of the errors in the response data for the observations has also been included.

Radiation Physics and Shielding Group
Reactor Physics Division
AEE Winfrith

*Work performed during author's attachment to Radiation Physics and Shielding Group, Reactor Physics Division, AEE Winfrith

1. Introduction

The Winfrith iron benchmark experiment comprises a series of measurements at distances up to 1 m in iron of the detector response-rates in the slowing-down flux from a natural uranium fission source. In this report the observed reaction-rate information at the five major measurement positions is given and the measured flux spectra unfolded using the RADAK code are displayed. Sufficient details of the calculational model are given for either 1-D or 2-D transport calculations to be performed.

2. Geometrical Model.

2.1 Description of the Experimental Facility

A schematic diagram of the experimental arrangement is shown in Figure 1, in which the various component regions are named with their relevant equivalent area dimensions. A discussion pertaining to the ASPIS shielding facility and the iron benchmark shield has been given elsewhere[1]. The actual model used for the DOT-III transport calculation, in r-z cylindrical geometry, is illustrated in Figure 2. The effect of neutron backscatter from the lead γ-ray shield in the NESTOR reactor was considered to be negligible. Many of the radial boundaries were adjusted to allow coincidence with the outer radius of the converter plate (r = 66.5cm) thus achieving a considerable reduction in the geometric mesh specification. In contrast with a previous geometric model[2] no axial stretching has been performed - the retention of all axial dimensions as true has allowed conservation of both the material and geometric attenuation. The materials densities appropriate to Figure 2 are given as Table 1.

2.2 Converter Plate Modelling

The converter plate comprised ten aluminium clad fuel elements carried in an aluminuim support plate. Each fuel element could contain a maximum of 46 natural uranium fuel coupons. The spatial distribution of the fuel

in the plate was chosen to represent a disc source, as shown in Figure 3, with mild steel dummy coupons inserted in positions not containing fuel. The inner region of the plate was modelled as a disc source of solid natural uranium and the outer region as an annulus of mild steel. The details of the smearing calculations, which include a modelling factor 0.851, are given elsewhere[3]; the final representation of the smeared converter plate is given as Figure 4 with material densities detailed in Table 2.

2.3 The Source Distribution

At the outset of the experiment the spatial distribution of the fission-rate on the reactor side of the converter plate was measured using 0.05 mm. thick natural uranium foils. The relative flux profile across the converter plate in orthogonal directions was simultaneously monitored with manganese activation foils and the azimuthally averaged values used to establish a value of $1.23 \pm 0.01 \times 10^{-13}$ fissions s^{-1}/atom of U^{235} at 3 kW NESTOR power for the fission-rate on the centre line of the converter plate on the reactor side. The normalised manganese activities were also used to determine a half-width of 71.45 cm for the cosine distribution fitted by the least squares technique to the radial distribution. A comparison of fission-rate with variations in NESTOR reactor power revealed a loss of 2.15% of neutron flux at 3 kW compared with all other powers; since the majority of the experimental measurements were obtained under conditions at 10 kW or 1 kW, a factor 1.022 was included in the fission-rate normalisation to obtain agreement with all other powers. Finally, by use of special fuel plates, the self-attenuation of the fission-rate by the fuel was measured and found to be only $0.865 \pm 1\%$ of that on the reactor side, in the centre of the fuel.

Correspondingly the radial source profile for 2-D reference calculations can be expressed as:

$$\phi(r) = 3.085 \times 10^{-17}\ \bar{\nu}_{235} \cos\left(\frac{\pi r}{142.9}\right) \quad \text{per NESTOR Watt per } U^{235} \text{ atom.} \tag{1}$$

when the modelling factor of 0.851 is incorporated. The total converter plate power predicted using this representation is in very good agreement (+6%) with the power inferred by a Simpson's integration of the measured manganese reaction-rate distribution.

3. Dimensional Transformation from 2-D to 1-D.

For detailed sensitivity analysis it is convenient to define a 1-D working model in which lateral leakage is represented by an increase of $\Delta(z,E)$ in the total cross-section (an increase in the absorption cross-section is implied); by comparison of the 2-D cylindrical and 1-D slab geometry differential neutron transport equations[4], $\Delta(z,E)$ can be identified as:

$$\Delta(z,E) = \lim_{r \to 0} \frac{1}{r\,\phi(r,z,E)} \frac{d}{dr}\left(r\,J_r(r,z,E)\right) \tag{2}$$

For the DOT-III code, utilising the diamond difference algorithm, the discrete form of (2) can be shown to be:

$$\Delta_z^k = \frac{4\,J_{rz}^k}{\Delta r\,\phi_z^k} \tag{3}$$

where J_{rz}^k is the radial current in group k for axial mesh interval z, ϕ_z^k is the corresponding flux and Δr is the width of the first radial mesh interval. For the reference calculation of the ASPIS iron benchmark zone averaging was shown to be acceptable and this scheme produced a 2.8% discrepancy in the comparison of the measurement chi-squared tests for the 2-D and 1-D calculations; the largest fractional group flux difference was 5.5%. The ratios of zone

averaged Δ_z^k with the total and absorption cross-sections for a $1/E\Sigma^T(E)$ condensation of the UKNDL DFN 908A iron data file into the EURLIB-100 group structure[5] are given as Table 3. It seems reasonable that these factors can be used for any data set which closely resembles the UKNDL data set. Table 4 shows a comparison of a selection of the activation foil reaction-rates derived from the 2-D and transformed 1-D calculations at various penetrations.

In contradistinction, the reaction-rates derived from an ANISN calculation using the buckling option with a transverse dimension of 100 cm are given in Table 5. The wide selection of possible bucklings, B, and associated transverse dimensions, r_o, derived by fitting a zeroth order Bessel function to the DOT radial flux profiles, are given as a function of penetration, in Table 6. Despite its common application[6,7] it is clear that the use of the fundamental mode plane wave approximation is insufficiently accurate for shielding benchmark calculations. Recommendations on the choice of input parameters (orders of quadrature and scattering expansion, solution algorithms and convergence tests) for the DOT-III DS_n code have been discussed elsewhere[3].

4. Detectors and Response Data

4.1 The Detectors

The detectors used in the ASPIS iron DATAM experiment[1] can be classified in order of decreasing energy sensitivity into three types - threshold detectors, proton recoil counters and resonance sandwich foils. The threshold detectors monitor the high-energy penetration flux with most of the reaction-rate occurring near the threshold. The proton recoil counters used were of two types: the high-energy region above 0.8 MeV was covered by an NE 213 organic scintillation counter and the energy range below 1.35 MeV down to about 7 keV was spanned by an argon-hydrogen counter and a variety of hydrogen gas proportional counters at different pressures and electronic gains. The low-energy neutron behaviour was estimated over narrow ranges with resonance sandwich foils.

Although the proton recoil counters are conventionally used to provide

differential information with which to determine the energy-dependent flux (by unfolding), each signal channel, M_i, of the pulse height data output from the chamber can be considered as an integral measurement from a threshold detector whose cross-section, a_{ij}, is represented by the row of the integral response matrix corresponding to the i^{th} counting channel. It is this data which is used in the two tier hybrid support method[8,9,10] for the optimisation of iron cross-section data, the corresponding integral response matrix being determined with the PRCM[11] program. Table 7 lists the detectors used in the experiment with their corresponding energy ranges. The lower energy boundary of the hydrogen gas proportional counters represents the energy at which Compton electrons, produced by γ-ray interaction in the chamber wall, start to make a significant contribution to the pulse-height distribution in the counter whilst the upper energy boundary represents the energy limit above which the information produced by the counter is so dominated by wall effect that stable unfolding is not possible.

4.2 Proton Recoil Counter Response Data.

The integral count-rate response matrices for the proton recoil counters are calculated by the PRCM program using the proton range-energy data for hydrogen, argon[12] and xylene napthalene[13] in the leakage formalism derived by Snidow and Warren[14]. Kemshall[15] has found however that the gradient of the theoretical recoil proton distribution is in considerable disagreement with mono-energetic line-shape measurements, especially at low energies where the maximum recoil proton range, $R(E_n)$ is very much less than the counter radius a (Table 8). Accordingly, Kemshall has propsed a set of empirical 'slope correction factors' for the theoretical line-shapes. An assessment of the accuracy with which these slope correction factors can be derived for the trapezoidal line-shapes ($R(E_n)/a < 0.7$) has been performed and the resultant fractional uncertainties on the counter response matrix elements for the EURLIB-100 group structure derived. It can be seen that the error is greatest

for the high energy chamber, but is still satisfactory (Table 9).

For the NE 213 liquid scintillation counter the range of the knock-on protons is considerably shorter and it is sufficient to use the theoretical equi-probable (infinite medium) recoil proton distribution for energies below 7 MeV. However at higher energies, recoil proton leakage from the detection volume becomes significant and at 10 MeV corresponds to an 11% under-estimation of the unfolded flux. The program PRCM calculates the effective recoil proton leakage by approximating the right circular cylindrical NE 213 counter as a sphere of the same volume and uses the Snidow and Warren technique. However the departures from the theoretical infinite medium line-shape are so small as to produce negligible uncertainties in the response cross-sections for the signal channels.

A more important uncertainty arises from the fact that the molecular excitation process in the NE 213 counter detection medium is non-linear and for this reason the pulse height output from the detection system is not proportional to the energy deposition in the sensitive volume of the counter. The response kernel for the system therefore contains a 'light function', L(E), defined as the fraction of quanta emitted relative to the number emitted at the Cs^{137} edge (1.667 MeV neutron equivalent energy) as a function of the proton energy incident upon the detector. The light function has been derived by a least squares log-log fit to measurements made on the IBIS accelerator at AERE Harwell. The function has been expressed in the form:

$$\ln L(E)\,dE \quad . \quad [\alpha + \beta(\ln E) + \gamma(\ln E)^2]\,dE \qquad (4)$$

where α, β and γ, estimated from the fit, had fractional standard deviations of 1.03%, 1.16% and 7.52% respectively. Utilising the variances and covariances on α, β and γ the fractional error in estimating the light output in Cs^{137} units at proton energies of 1.0 and 10.0 MeV has been computed to be 1.03% and 2.1% respectively.

The adequacy of the representation of the NE 213 counter light function

and the recoil proton leakage calculation has been assessed[10] by unfolding spectrum measurements obtained from a standard Cf^{252} fission source; agreement with the Maxwellian distribution of Grundl and Eisenhauer[16] (present NBS recommended fit) above 1 MeV was within 5% (1σ) for the flux grouped into 0.1 lethargy width bins.

4.3 Activation Detector Response Data.

The activation detector response data have been taken from the sources recommended by Farinelli and McCracken[17] for the NEA/OECD Collaborative Benchmark Programme. The uncertainty estimates assumed to apply to these cross-sections have been taken from the SAND-II error file[18], given by McElroy et al[19], for all the cross-sections except rhodium, for which the authors have evaluated an error file from curves given by Vlasov et al[20]. The error estimates derived from the Vlasov et al curve for indium inelastic scattering to the metastable state were some 50% lower than the corresponding SAND-II values; the rhodium error estimates were therefore scaled by a factor 2 to give greater consistency with the SAND-II estimates for the other detectors. Moreover, since the Vlasov et al curves furnished no error information for rhodium near the threshold, a standard error of 30% was assumed, being symptomatic of the general uncertainty for cross-section measurement near the threshold of an inelastic level (Table 10).

For thin detectors of materials different from the bulk transport medium the variance on a calculated response-rate, C_i, arising from uncertainties in the response cross-section data $\underline{a}_i$ can be shown to be:

$$\mathrm{Var}(C_i) = \sum_j \sum_{j'} \phi_j \phi_{j'} \mathrm{cov}(a_{ij}, a_{ij'}) \qquad (5)$$

where $\{\phi_j\}$ represent the group-averaged flux. The upper and lower bound energy-dependent correlation estimates of the expected fractional error on the integral

detector response-rates as a function of position are shown in Table 11. The behaviour displayed can be elucidated by reference to the detector sensitivity profiles[10]. A further assessment of the response data can be made by comparison of the reaction-rates predicted by the recommended detector data with those derived using data taken from other libraries (Table 12). The very good agreement between the SAND-II predictions for indium and the EURLIB calculations may indicate, since they are not primary libraries, that they have a common source; moreover the number of independent measurements of these cross-sections is small so that the primary libraries, notably ENDF/B and UKNDL, represent two samples from a sparse population of measured data and the differences between libraries may reflect more about the credibility of the evaluator than of the data per se.

The disagreement between the ENDF/B-IV dosimetry file predictions of the In(n,n') reaction-rate and that of other libraries arises from the completely different cross-section evaluations which exist between the files (Figure 5). The reaction-rate profile indicates that the important region of the indium cross-section, for the ASPIS iron experiment, lies between threshold and 1 MeV.

The gold reaction-rates for the ASPIS iron benchmark analysis were calculated using a table of 1/E weighted suppressed cross-sections supplied by EURATOM. The comparison of the predictions of these data with an old UKNDL DFN 222 evaluated gold file and with the more recently evaluated UKNDL DFN 1208B gold dosimetry file[21] is given in Table 12. The multi-group suppressed cross-section data were derived from the raw nuclear data using the SUPPRES code[22], which incorporates the use of a single scatter removal kernel for the fine group calculation prior to a 1/E spectrum condensation to the required multi-group form. The resonance integrals, above the cadmium cut-off (0.55eV), of the old and new evaluated files for a 5.08×10^{-2} mm thick foil were determined, using the SUPPRES code, to be 416.3 and 413.7 barns respectively which compare very closely with the measured value of 414 barns obtained by Packwood and McCracken[23] on the GLEEP reactor at AERE Harwell.

5. Comparison of Calculation and Measurement.

A comparison of the integral detector penetration profiles derived from the DOT-III reference calculation[3] (using the UKNDL DFN 908A iron file) with the values inferred from measurement is given as Table 13 and Figure 6. A comparison of the flux spectrum, derived by simultaneous unfolding of all the measured data at all positions, using the RADAK[24] code, with the calculated flux distribution at four penetration depths are given as Figure 7 - 10. The discrepancy manifested in the 24-27 keV region (the energy shift of resonance features) arises from the inability of the spectrum unfolding code, working on the differential data, to adequately represent rapid flux gradients. It is for this reason that the measured and calculated response-rates should be used as the comparators in any data optimisation scheme (Tables 14-18). The measurements at the 22.8 cm position represent a special set of high energy measurements made by Carter et al[25] in 1978 in an attempt to extend the information range of the experiment to the higher energy data on which PWR pressure vessel damage-rate predictions appear to be dependent[26]. The measurements made included the NE 213 pulse height distribution and the S(n,p), In(n,n'), Rh(n,n') and Al(n,α) reaction-rates; a higher fission source power, corresponding to an enriched uranium converter plate, was used to increase the high energy neutron flux and a source normalisation factor has been established to within 2.5% by Arcipiani and Chestnutt[27] for use in scaling these new measurements to a level compatible with the original experiment. The reaction-rates from the Al(n,α) foils were inconsistent with the NE 213 pulse height distribution and with the calculation-to-measurement ratio expected from other detectors and have therefore been omitted. The NE 213 observations extended the flux spectrum characterisation up to 7 MeV.

The measurement standard deviations for the activation foils have been given elsewhere[1] and the standard errors appropriate to the elements of the grouped proton recoil data have been assessed as a combination of the statistical counting error and a reproducibility factor varying between 2-5%, assessed from repeated measurements. The chi-squared value for the reference calculation was 1.9686 + 4 which for 502 degrees of freedom gives χ^2 per degree of freedom to be 39.2.

Acknowledgements.

The work presented in this review has benefited from discussions with Mr. M.D. Carter and Mr. A. Packwood, whose measurements are quoted; Dr. J. Butler, Mr. A.F. Avery and Mr. M.J. Grimstone are thanked for their help and encouragement during the performance of this work.

References.

1. Carter, M.D. and Packwood, A. The Winfrith Benchmark Experiment in Iron - Experimental Results. Paper B5. Proc. of the Specialists' Meeting on Sensitivity Studies and Shielding Benchmarks. Paris NEA/OECD. (1975).

2. "A Calculational Model of the ASPIS Iron Benchmark Experiment". Circulated to Participants at the Specialists' Meeting on Sensitivity Studies and Shielding Benchmarks. Paris. (1975).

3. Chestnutt, M.M. and McCracken, A.K. An Error Estimation for the DOT-III Reference Calculation Performed for the Winfrith Iron Benchmark. Proc. of a Specialists' Meeting on Integral Benchmarks and Data Adjustment. Paris. NEA/OECD. (1977).

4. Grimstone, M.J. and McCracken, A.K. Preliminary Analysis of the Winfrith Iron Benchmark Experiment. Paper C4. ibid(1).

5. ESIS Newsletter No 12 (1975).

6. D'Angelo, A., Oliva, A., Palmiotti, G., Salvatores, M. and Zero, S. Consistent Utilisation of Shielding Benchmark Experiments. Nucl. Sci. Eng. 65 77 (1978).

7. Oka, Y et al. Two-Dimensional Shielding Benchmarks of Sodium and Iron at YAYOI. ibid(2)

8. Chestnutt, M.M. and McCracken, A.K. The Two Tier Hybrid Support Method - A Maximum Likelihood Approach to the Analysis of Experimental Data from Shielding Benchmarks. A.E.E.W.-R (1980)

9. Chestnutt, M.M. and McCracken, A.K. Results of the Analysis of the Winfrith Iron Benchmark Experiment. A.E.E.W.-R (1980)

10. Chestnutt, M.M. Ph.D. Thesis. Univ. of London. (1980)

11. Chestnutt, M.M. The PRCM Users' Manual. Unpublished.

12. Benjamin, P.W., Kemshall, C.D. and Brickstock, A. The Analysis of Proton Recoil Spectra. AWRE O 9/68 (1968)

13. Nuclear Enterprises Scintillator Catalogue 7 (1973).

14. Snidow, N.L. and Warren, H.D. Wall Effect Corrections in Proportional Counter pectrometers. Nucl. Instr. and Methods 51 109 (1967).

15. Kemshall, C.D. The Use of Spherical Proportional Counters for Neutron Spectrum Measurements. AWRE O 31/73 (1973)

16. Grundl, J.A. and Eisenhauer, C. Fission-Rate Measurements for Materials Neutron Dosimetry in Reactor Experiments. 1st ASTM-EURATOM Symposium on Reactor Dosimetry. Petten. (1975).

17. Farinelli, U. and McCracken, A.K. List of Activation Reactions and Cross-Sections suggested for use in Benchmark Shielding Experiments NEACRP-L-1 (1975)

18. Oster, C.A., McElroy, W.N., Lippincott, E.P. and Simmons, R.L. Solution Weighting for the SAND-II Monte Carlo Code BNWL-SA-5736 (1976).

19. Kellogg, L.S. and McElroy, W.N. Fuels and Materials Fast Reactor Dosimetry Data Development and Testing. Nucl. Technol. 25 180 (1975).

20. Vlasov, M.F. Dunford, C.L., Schmidt, J.J. and Lemmel, H.D. Status of Neutron Cross-Section Data for Reactor Radiation Measurements. INDC(NDS) 47/L (1972).

21. Dean, C.J. Private Communication. A.E.E.W. (1978).

22. Chestnutt, M.M. The SUPPRES Code for Calculating Energy-Group Dependent Foil Suppression Factors. Unpublished.

23. McCracken, A.K. and Packwood, A. Private Communication. A.E.E.W. (1978).

24. Grimstone, M.J. The RADAK Users' Manual. AEEW-M1455 (1976).

25. Carter, M.D. and Samways, J. Private Communication. A.E.E.W. (1978).

26. Lympany, S.D., McCracken, A.K. and Packwood, A. Contribution to the Exercise on Sensitivity Studies for the NEA Theoretical Fast Reactor Benchmark. Paper C4. Proc. of a Specialists' Meeting on Differential and Integral Nuclear Data Requirements for Shielding Calculations. IAEA/OECD(NEA). IAEA-207. Vienna. (1976).

27. Arcipiani, B. and Chestnutt, M.M. The Interpretation of the Special High Energy Measurement Data from the ASPIS Iron Benchmark Experiment. Unpublished.

Table 1

Zone Materials Densities for the ASPIS Iron Benchmark Model

Zone No.	Material		Atomic Density atoms $b^{-1}cm^{-1}$.
1	Aluminium		6.024 -2
2	Carbon		8.534 -2
3	Aluminium		6.024 -2
4	Air	N	5.550 -5
5	Converter Plate		-
6	Air	N	5.550 -5
7	Aluminium		6.024 -2
8	Mild Steel	H	2.071 -5
		C	7.996 -4
		Fe	7.404 -2
		Mn	5.660 -4
9,11	Mild Steel	H	2.330 -5
		C	8.996 -4
		Fe	8.330 -2
		Mn	6.370 -4
10,12	Concrete	H	1.128 -2
		C	8.270 -3
		Al	6.610 -4
		Mn	2.130 -4
		Fe	4.990 -2
		O	1.482 -2
		Si	4.760 -3
		Ca	3.690 -3

Table 2

Composition of Modelled Converter Plate

Material		Thickness cm	Atomic Density atoms b^{-1} cm^{-1}
Aluminium (Reactor Side)		8.554 -1	4.808 -2
Mild Steel	H	3.640 -1	1.858 -5
	C		7.174 -4
	Mn		5.080 -4
	Fe		6.643 -2
Natural Uranium	U^{235}	3.988 -1	2.719 -4
	U^{238}		3.746 -2
Mild Steel		3.640 -1	Same as above
Aluminium (Shield Side)		8.930 -1	Same as above

Table 3

Ratios of Dimensional Transformation Coefficients with Absorption and Total Cross-Sections for the ASPIS Iron DATAM Experimental Shield.

Group	Δ/Σ^A	Δ/Σ^T	Group	Δ/Σ^A	Δ/Σ^T	Group	Δ/Σ^A	Δ/Σ^T
1	3.38-1	2.70-2	35	9.26 0	2.16-2	68	4.64-1	7.23-4
2	3.34-1	2.46-2	36	1.29+1	4.77-2	69	1.75+0	1.50-3
3	3.69-1	2.26-2	37	7.77 0	1.98-2	70	8.47-1	9.87-4
4	4.27-1	2.08-2	38	5.56-2	1.05-2	71	1.56 0	9.01-4
5	4.92-1	1.90-2	39	6.47 0	1.27-2	72	5.23-1	4.37-4
6	5.82-1	1.75-2	40	3.27 0	3.80-2	73	4.31-1	7.05-4
7	7.04-1	1.-3-2	41	5.88 0	1.04-2	74	7.45-1	6.80-4
8	8.10-1	1.55-2	42	1.47+1	6.03-2	75	2.24-2	4.90-4
9	8.93-1	1.56-2	43	1.02+1	1.87-2	76	4.76-1	5.45-4
10	9.74-1	1.50-2	44	7.52 0	1.08-2	77	3.84-1	5.00-4
11	1.13 0	1.51-2	45	9.64 0	2.13-2	78	2.82-1	4.57-4
12	1.39 0	1.47-2	46	4.40 0	6.81-3	79	7.81-2	3.38-4
13	1.82 0	1.43-2	47	5.88 0	1.19-2	80	1.86-2	1.80-4
14	2.03 0	1.38-2	48	2.95 0	4.43-3	81	9.19-2	3.94-4
15	2.12 0	1.34-2	49	5.62 0	1.58-2	82	1.34-1	3.95-4
16	2.47 0	1.37-2	50	3.88 0	7.99-3	83	1.24-1	3.91-4
17	3.22 0	1.39-2	51	6.45 0	2.79-2	84	1.10-1	3.84-4
18	4.70 0	1.54-2	52	5.00 0	2.10-2	85	9.63-2	3.78-4
19	6.42 0	1.43-2	53	4.42 0	1.10-2	86	8.43-2	3.74-4
20	9.88 0	1.52-2	54	1.96 0	3.79-3	87	7.41-2	3.70-4
21	1.20+1	1.26-2	55	2.17 0	8.58-3	88	6.45-2	3.66-4
22	1.67+1	1.49-2	56	1.79 0	3.62-3	89	5.64-2	3.62-4
23	1.92+1	1.73-2	57	2.56 0	2.42-3	90	4.95-2	3.59-4
24	1.93+1	1.40-2	58	7.27-1	.04-3	91	4.33-2	3.56-4
25	2.18+1	1.64-2	59	1.66-1	1.56-4	92	3.58-2	3.54-4
26	2.27+1	1.99-2	60	9.94 0	7.23-2	93	2.94-2	3.51-4
27	1.93+1	1.62-2	61	2.44+1	1.95-1	94	2.42-2	3.45-4
28	2.08+1	1.86-2	62	6.88 0	6.66-2	95	1.86-2	3.41-4
29	1.72+1	1.48-2	63	1.01+1	1.56-2	96	1.43-2	3.35-4
30	2.44+1	2.86-2	64	9.47 0	6.97-3	97	1.10-2	3.28-4
31	1.85+1	2.23-2	65	2.34 0	3.11-3	98	8.24-3	3.21-4
32	1.71+1	3.26-2	66	7,91-1	1.36-3	99	8.12-3	4.01-4
33	1.12+1	2.18-2	67	1.28-1	1.93-4	100	2.07-3	3.52-4
34	5.65 0	7.98-3						

Table 4

Comparison of DOT and ANISN Reference Calculation Reaction-Rate Predictions at Various Penetrations

Position (cm)	Calculation	S(n,p)	Rh(n,n')	In(n,n')	Au(n,γ)
-5	DOT	1.152 +2	4.295 +3	6.584 +2	1.803 +5
	ANISN	1.112 +2	4.188 +3	6.374 +2	1.843 +5
	Δ%	-3.47	-2.49	-3.19	2.22
-50	DOT	3.498 -2	7.590 +1	2.133 +0	2.288 +4
	ANISN	3.337 -2	7.632 +1	2.088 +0	2.405 +4
	Δ%	-4.60	0.55	-2.11	5.11
-76	DOT	4.813 -4	1.223 +1	1.825 -1	1.017 +4
	ANISN	4.689 -4	1.213 +1	1.779 -1	1.019 +4
	Δ%	-2.58	-0.82	-2.52	0.20
-101	DOT	5.473 -6	1.867 +0	1.693 -2	3.809 +3
	ANISN	5.458 -6	1.786 +0	1.608 -2	3.587 +3
	Δ%	-0.27	-4.34	-5.02	-5.83

Reaction-rates are given as saturated disintegrations s^{-1} $barn^{-1}$ $atom^{-1}$ NESTOR $Watt^{-1}$

Table 5

Comparison of Buckled ANISN Prediction of Integral Parameters with DOT-III Calculation

Reaction Type	Calculational Method	Position (cm)			
		25.4	50.8	76.2	101.6
S(n,p)	DOT-III	2.80 +0	3.50 -2	4.57 -4	5.97 -6
	ANISN-B	2.60 +0	3.66 -2	5.29 -4	6.33 -6
Rh(n,n')	DOT-III	5.79 +2	7.59 +1	1.19 +1	1.94 +0
	ANISN-B	5.36 +2	6.80 +1	9.92 +0	1.35 +0
In(n,n')	DOT-III	3.97 +1	2.12 +0	1.78 -1	1.77 -2
	ANISN-B	3.72 +1	2.07 +0	1.68 -1	1.44 -2
Au(n,γ)	DOT-III	5.43 +4	2.29 +4	1.01 +4	3.93 +3
	ANISN-B	3.60 +4	1.21 +4	4.53 +3	1.46 +3

Table 6

Bucklings derived from Bessel Function Approximation of DOT-III Radial Profiles

Group	Position (cm)							
	25.4		50.8		76.2		101.6	
	B	r_o	B	r_o	B	r_o	B	r_o
1	3.378-2	71.2	3.408-2	70.6	3.220-2	74.7	2.958-2	81.3
20	3.325-2	72.3	3.304-2	72.8	3.197-2	75.2	3.000-2	80.2
40	3.153-2	76.3	2.958-2	81.3	2.803-2	85.8	2.620-2	91.8
60	2.854-2	84.3	2.624-2	91.7	2.427-2	99.1	2.339-2	102.8
80	2.661-2	90.4	2.436-2	98.7	2.269-2	106.0	2.186-2	110.0
99	2.647-2	90.9	2.385-2	100.8	2.258-2	106.5	2.169-2	110.9

Precision ~ ± 5%

Table 7

Detectors Used in the ASPIS Iron Benchmark Experiment

Detector	Type	Working Energy Range
$Al^{27}(n,\alpha)Na^{24}$	threshold	E > 5.2 MeV
$S^{32}(n,p)P^{32}$	threshold	E > 1.6 MeV
$In^{115}(n,n')In^{115m}$	threshold	E > 0.4 MeV
$Rh^{103}(n,n')Rh^{103m}$	threshold	E > 40 keV
NE 213	proton recoil (organic scintillator)	E > 0.8 MeV
Argon/Hydrogen	proton recoil (gas proportional)	300 keV - 1.75 MeV
10 at. Hydrogen	proton recoil (gas proportional)	160 keV - 930 keV
3 at. Hydrogen	proton recoil (gas proportional)	100 keV - 500 keV
1 at. Hydrogen	proton recoil (gas proportional)	40 keV - 235 keV
½ at. Hydrogen	proton recoil (gas proportional)	24.8 keV - 110 keV
1 at. Hydrogen with High Gain	proton recoil (gas proportional)	10 keV - 85 keV
½ at. Hydrogen with High Gain	proton recoil (gas proportional)	7 keV - 60 keV
$Cd\{Au(n,\gamma)\}$	activation foil	0.55 eV - 100 keV
$Cu^{63}(n,\gamma)$	resonance sandwich foil	580 eV
$W^{186}(n,\gamma)$	resonance sandwich foil	18.8 eV
$Au^{197}(n,\gamma)$	resonance sandwich foil	4.9 eV

Table 8

Percentage Difference in Gradient for Calculated and Measured Line-Shapes[15]

$R(E_n)/a$	Difference w.r.t. Measurement %
0.15	55.8
0.30	34.3
0.45	22.2
0.60	14.5
0.75	11.0
0.90	10.2
1.10	8.24
1.25	6.30
1.40	5.50
1.60	3.40

Table 9

Fractional Error on Gas Proportional Counter Line-Shapes

Counter Type	$R(E_n)/a = 0.20$		$R(E_n)/a = 0.54$	
	Energy (MeV)	$\sigma(a_{ij})/a_{ij}$%	Energy (MeV)	$\sigma(a_{ij})/a_{ij}$%
Argon-Hydrogen	0.990	2.52	1.831	3.33
10 at. Counter	0.579	2.09	1.033	2.27
3 at. Counter	0.271	1.03	0.516	1.58
1 at. Counter	0.102	0.64	0.242	0.94
½ at. Counter	0.046	0.47	0.143	0.79

Table 10

Uncertainty Estimates on Activation Detector Cross-Section Data[19,20]

Lower Boundary (MeV)	S(n,p') %	In(n,n') %	Rh(n,n') %	Au(n,γ) %
1.0,-10	-	-	-	0.5
4.0,-7	-	-	-	4
1.0,-5	-	-	-	5
1.0,-2	-	-	30	6
1.0,-1	-	30	6	6
6.0,-1	-	20	6	7
1.4, 0	100	10	6	7
2.2, 0	20	10	9	7
3.0, 0	8	10	9	7
4.0, 0	8	8	5	7
5.0, 0	8	8	5	7
6.0, 0	8	8	5	7
8.0, 0	8	8	6	7
1.1,+1	8	10	6	7
1.3,+1	8	10	10	7
1.6,+1				

Table 11

Upper and Lower Bound Energy-Dependent Correlation Estimates of the Expected Fractional (%) Error on the Integral Response-Rates as a Function of Position

Position cm.	$S^{32}(n,p)$		$In^{115}(n,n')$		$Rh^{103}(n,n')$		$Au^{197}(n,\gamma)$	
	lower	upper	lower	upper	lower	upper	lower	upper
20.3	15.5	24.3	8.6	15.1	3.6	6.5	3.4	4.7
50.8	22.2	31.0	13.9	21.2	4.7	7.0	3.3	4.5
76.2	28.7	40.5	17.3	24.0	5.3	7.6	3.1	4.3
101.6	35.1	43.6	19.3	24.9	5.6	8.0	2.9	4.0

Table 12

Ratio of the Response-Rates Calculated Using Different Data Libraries Compared with the Response-Rates Determined Using the Recommended Nuclear Data as a Function of Penetration Depth

Position cm.	$S^{32}(n,p)$		$In^{115}(n,n')$			$Au^{197}(n,\gamma)$	
	SAND / UKNDL	ENDF/B / UKNDL	SAND / EURLIB	ENDF/B / EURLIB	UKNDL / EURLIB	UKNDL-222 / EURLIB	UKNDL-1208 / EURLIB
20.3	0.80	0.96	1.00	0.88	0.98	1.04	0.96
50.8	0.73	0.95	1.00	0.73	0.97	1.05	0.96
76.2	0.68	0.93	1.00	0.60	0.94	1.04	0.96
101.6	0.63	0.92	1.00	0.52	0.92	1.04	0.96

Table 13

Comparison of Calculated and Measured Activation Detector Response-Rates

Position (cm)	$Rh^{103}(n,n')$		$S^{32}(n,p)$		$In^{115}(n,n')$		$Au^{197}(n,\gamma)$	
	DOT-III	Measured	DOT-III	Measured	DOT-III	Measured	DOT-III	Measured
5.08	4.11 +3	3.86 +3	1.06 +2	1.10 +2	6.19 +2	5.80 +2	1.75 +5	1.13 +5
10.16	2.38 +3	2.21 +3	3.39 +1	3.75 +1	2.92 +2	2.65 +2	1.23 +5	1.05 +5
15.24	1.44 +3	1.32 +3	1.61 +1	1.35 +1	1.46 +2	1.32 +2	9.03 +4	8.47 +4
20.32	9.05 +2	8.46 +2	6.70 0	5.26 0	7.54 +1	6.44 +1	6.89 +4	6.68 +4
22.86	7.36 +2	7.15 +2	4.36 0	3.33 0	5.51 +1	5.41 +1	-	-
25.40	5.79 +2	5.27 +2	2.80 0	2.02 0	3.97 +1	3.27 +1	5.43 +4	5.48 +4
30.48	3.77 +2	3.41 +2	1.17 0	7.75 -1	2.12 +1	1.69 +1	4.44 +4	4.57 +4
35.56	2.49 +2	-	4.88 -1	2.88 -1	1.17 +1	-	3.71 +4	3.73 +4
40.64	1.67 +2	1.56 +2	2.04 -1	1.17 -1	6.51 +0	5.77 0	3.15 +4	3.15 +4
45.72	1.13 +2	1.12 +2	8.53 -2	4.51 -2	3.71 0	3.50 0	2.68 +4	-
50.80	7.59 +1	7.90 +1	3.50 -2	1.94 -2	2.12 0	2.02 0	2.29 +4	2.24 +4
55.88	5.23 +1	5.84 +1	1.48 -2	7.00 -3	1.27 0	1.27 0	1.96 +4	-
60.96	3.62 +1	4.02 +1	6.29 -3	3.19 -3	7.70 -1	-	1.67 +4	1.56 +4
66.04	2.49 +1	2.97 +1	2.61 -3	-	4.65 -1	-	1.42 +4	-
76.20	1.19 +1	1.66 +1	4.57 -4	2.5 -4	1.78 -1	-	1.01 +4	9.26 +3
81.28	8.30 0	1.21 +1	1.92 -4	-	1.11 -1	-	8.41 +3	7.55 +3
91.44	3.65 0	7.62 0	3.38 -5	-	4.40 -2	-	5.79 +3	5.18 +3
101.60	1.94 0	4.25 0	5.97 -6	-	1.77 -2	-	3.93 +3	3.44 +3

All Reaction-Rates Given as Saturated Disintegrations s^{-1} $atom^{-1}$ $barn^{-1}$ per NESTOR Watt.

TABLE 14

COMPARISON OF CALCULATION WITH MEASUREMENT AT 20.3 CM POSITION.

ENERGY BOUNDARIES (MEV)		M	σ(n,n')/M	C	C/M
		ARGON-HYDROGEN.			
4.0762 -1	4.5049 -1	5.4650 +0	1.0282 -2	4.9394 +0	0.904
4.5049 -1	4.9787 -1	4.6968 +0	1.0330 -2	4.3274 +0	0.921
4.9787 -1	5.5023 -1	3.9903 +0	1.0424 -2	3.5962 +0	0.901
5.5023 -1	6.0810 -1	2.9998 +0	1.0589 -2	2.8907 +0	0.964
6.0810 -1	6.7206 -1	2.1039 +0	1.0764 -2	2.0427 +0	0.971
6.7206 -1	7.4274 -1	1.6034 +0	1.1049 -2	1.3354 +0	0.833
7.4274 -1	8.2085 -1	1.2954 +0	1.1315 -2	1.0051 +0	0.776
8.2085 -1	9.0718 -1	1.0173 +0	1.1591 -2	7.9564 -1	0.782
9.0718 -1	1.0026 +0	7.4114 -1	1.2232 -2	5.8650 -1	0.791
1.0026 +0	1.1080 +0	5.5517 -1	1.3015 -2	4.4316 -1	0.798
1.1080 +0	1.2246 +0	3.9523 -1	1.3967 -2	3.4717 -1	0.878
1.2246 +0	1.3534 +0	2.8380 -1	1.5243 -2	2.6760 -1	0.942
1.3534 +0	1.4957 +0	1.9941 -1	1.7044 -2	2.0390 -1	1.022
1.4957 +0	1.6530 +0	1.4656 -1	1.9048 -2	1.4639 -1	0.999
1.6530 +0	1.8268 +0	9.7193 -2	2.2327 -2	9.7008 -2	0.998
1.8268 +0	2.0190 +0	5.9143 -2	2.7510 -2	6.0041 -2	1.015
		10. AT. COUNTER.			
1.6573 -1	1.8316 -1	2.5474 +1	1.0050 -2	3.0954 +1	1.215
1.8316 -1	2.0242 -1	2.3263 +1	1.0057 -2	2.8903 +1	1.242
2.0242 -1	2.2371 -1	2.2211 +1	1.0056 -2	2.7263 +1	1.227
2.2371 -1	2.4724 -1	2.0990 +1	1.0064 -2	2.5328 +1	1.207
2.4724 -1	2.7324 -1	1.9193 +1	1.0070 -2	2.3044 +1	1.201
2.7324 -1	3.0197 -1	1.7111 +1	1.0080 -2	2.0536 +1	1.200
3.0197 -1	3.3373 -1	1.4433 +1	1.0098 -2	1.8300 +1	1.268
3.3373 -1	3.6885 -1	1.2076 +1	1.0115 -2	1.4612 +1	1.210
3.6885 -1	4.0762 -1	1.0136 +1	1.0139 -2	1.1233 +1	1.108
4.0762 -1	4.5049 -1	9.0122 +0	1.0163 -2	9.8740 +0	1.090
4.5049 -1	4.9787 -1	7.8626 +0	1.0196 -2	8.5507 +0	1.085
4.9787 -1	5.5023 -1	6.6285 +0	1.0229 -2	7.0037 +0	1.057
5.5023 -1	6.0810 -1	5.3463 +0	1.0277 -2	5.5533 +0	1.039
6.0810 -1	6.7206 -1	3.7546 +0	1.0399 -2	3.8697 +0	1.031
6.7206 -1	7.4274 -1	2.6092 +0	1.0570 -2	2.4940 +0	0.956
7.4274 -1	8.2085 -1	1.9456 +0	1.0782 -2	1.8304 +0	0.941
8.2085 -1	9.0718 -1	1.4402 +0	1.1070 -2	1.3957 +0	0.969
9.0718 -1	1.0026 +0	9.8487 -1	1.1506 -2	9.8017 -1	0.995
1.0026 +0	1.1080 +0	6.6367 -1	1.2207 -2	6.8842 -1	1.037
		3 AT. HYGROGEN.			
1.1109 -1	1.2277 -1	1.0538 +1	1.0066 -2	1.3271 +1	1.259
1.2277 -1	1.3569 -1	9.9040 +0	1.0070 -2	1.2476 +1	1.260
1.3569 -1	1.4996 -1	9.0674 +0	1.0076 -2	1.1280 +1	1.244
1.4996 -1	1.6573 -1	8.6034 +0	1.0091 -2	1.0313 +1	1.199
1.6573 -1	1.8316 -1	8.0257 +0	1.0096 -2	9.5617 +0	1.182
1.8316 -1	2.0242 -1	7.3712 +0	1.0096 -2	8.8998 +0	1.206
2.0242 -1	2.2371 -1	6.9975 +0	1.0105 -2	8.3252 +0	1.189
2.2371 -1	2.4724 -1	6.5378 +0	1.0118 -2	7.6578 +0	1.171
2.4724 -1	2.7324 -1	5.9267 +0	1.0128 -2	6.8848 +0	1.162
2.7324 -1	3.0197 -1	5.1775 +0	1.0144 -2	6.0461 +0	1.168
3.0197 -1	3.3373 -1	4.2846 +0	1.0177 -2	5.2815 +0	1.233
3.3373 -1	3.6885 -1	3.4972 +0	1.0219 -2	4.1391 +0	1.184
3.6885 -1	4.0762 -1	2.8885 +0	1.0272 -2	3.1141 +0	1.097
4.0762 -1	4.5049 -1	2.4276 +0	1.0321 -2	2.6127 +0	1.076
4.5049 -1	4.9787 -1	2.0128 +0	1.0282 -2	2.1428 +0	1.065
4.9787 -1	5.5023 -1	1.5678 +0	1.0495 -2	1.6557 +0	1.043
		1 AT. HYDROGEN.			
4.0868 -2	5.2475 -2	8.5295 +0	1.0096 -2	1.1570 +1	1.356
5.2475 -2	6.7379 -2	8.7644 +0	1.0092 -2	1.1650 +1	1.329
6.7379 -2	8.6517 -2	8.7367 +0	1.0095 -2	1.1956 +1	1.330
8.6517 -2	1.1109 -1	8.0219 +0	1.0099 -2	1.0487 +1	1.307
1.1109 -1	1.2277 -1	5.0659 +0	1.0236 -2	3.9905 +0	1.304
1.2277 -1	1.3569 -1	2.0534 +0	1.0270 -2	3.7268 +0	1.306
1.3569 -1	1.4996 -1	2.5711 +0	1.0316 -2	3.3467 +0	1.302
1.4996 -1	1.6573 -1	2.4258 +0	1.0322 -2	3.0239 +0	1.246
1.6573 -1	1.8316 -1	2.1649 +0	1.0348 -2	2.7480 +0	1.269
1.8316 -1	2.0242 -1	1.9219 +0	1.0378 -2	2.4837 +0	1.292
2.0242 -1	2.2371 -1	1.7445 +0	1.0442 -2	2.2056 +0	1.273
2.2371 -1	2.4724 -1	1.5026 +0	1.0514 -2	1.9459 +0	1.313

ENERGY BOUNDARIES (MEV)		M	σ(n,n')/M	C	C/M
		1/2 AT. HYDROGEN.			
2.1870 -2	2.3570 -2	1.6959 +0	1.0309 -2	2.1813 +0	1.286
2.3570 -2	2.4788 -2	1.0440 +0	1.0398 -2	1.5240 +0	1.268
2.4788 -2	2.6050 -2	9.3918 -1	1.0411 -2	1.1406 +0	1.214
2.6050 -2	3.1828 -2	3.5264 +0	1.0209 -2	4.5729 +0	1.297
3.1828 -2	4.0868 -2	4.8449 +0	1.0160 -2	6.2668 +0	1.293
4.0868 -2	5.2475 -2	5.1635 +0	1.0153 -2	6.5467 +0	1.298
5.2475 -2	6.7379 -2	5.2782 +0	1.0153 -2	6.5545 +0	1.242
6.7379 -2	8.6517 -2	4.9806 +0	1.0161 -2	6.2183 +0	1.248
8.6517 -2	1.1109 -1	4.6439 +0	1.0174 -2	5.7126 +0	1.230
1.1109 -1	1.2277 -1	1.6961 +0	1.0458 -2	2.1072 +0	1.242
		1 AT. HIGH GAIN.			
1.1709 -2	1.5034 -2	8.4820 +0	1.0028 -2	1.2859 +1	1.516
1.5034 -2	1.9305 -2	8.4874 +0	1.0029 -2	1.3597 +1	1.602
1.9305 -2	2.1870 -2	4.1165 +0	1.0057 -2	6.8263 +0	1.658
2.1870 -2	2.3570 -2	2.3614 +0	1.0097 -2	3.9298 +0	1.664
2.3570 -2	2.4788 -2	1.4990 +0	1.0149 -2	2.3660 +0	1.578
2.4788 -2	2.6050 -2	1.3683 +0	1.0168 -2	2.0122 +0	1.470
2.6050 -2	3.1828 -2	4.8006 +0	1.0051 -2	8.0242 +0	1.671
3.1828 -2	4.0868 -2	6.3028 +0	1.0039 -2	1.1040 +1	1.752
4.0868 -2	5.2475 -2	6.7317 +0	1.0037 -2	1.1570 +1	1.719
5.2475 -2	6.7379 -2	6.9195 +0	1.0036 -2	1.1650 +1	1.684
6.7379 -2	8.6517 -2	6.6305 +0	1.0037 -2	1.1156 +1	1.683
		1/2 AT. HIGH GAIN.			
7.1017 -3	9.1188 -3	4.2804 +0	1.0030 -2	5.5998 +0	1.308
9.1188 -3	1.1709 -2	4.5174 +0	1.0028 -2	6.4501 +0	1.428
1.1709 -2	1.5034 -2	4.5898 +0	1.0028 -2	7.0948 +0	1.546
1.5034 -2	1.9305 -2	4.5719 +0	1.0028 -2	7.5097 +0	1.643
1.9305 -2	2.1870 -2	2.2383 +0	1.0058 -2	3.7772 +0	1.688
2.1870 -2	2.3570 -2	1.2810 +0	1.0100 -2	2.1813 +0	1.703
2.3570 -2	2.4788 -2	8.0454 -1	1.0151 -2	1.3240 +0	1.646
2.4788 -2	2.6050 -2	7.3351 -1	1.0166 -2	1.1406 +0	1.555
2.6050 -2	3.1828 -2	2.7111 +0	1.0048 -2	4.5729 +0	1.687
3.1828 -2	4.0868 -2	3.6719 +0	1.0036 -2	6.2668 +0	1.707
4.0868 -2	5.2475 -2	3.9111 +0	1.0033 -2	6.5467 +0	1.674
5.2475 -2	6.7379 -2	3.9928 +0	1.0033 -2	6.5545 +0	1.642
		NE 213 COUNTER.			
8.2085 -1	9.0718 -1	1.7212 +1	1.0202 -2	1.8316 +1	1.064
9.0718 -1	1.0026 +0	1.3047 +1	1.0261 -2	1.3651 +1	1.046
1.0026 +0	1.1080 +0	9.4499 +0	1.0367 -2	1.0495 +1	1.111
1.1080 +0	1.2246 +0	7.0074 +0	1.0504 -2	8.4717 +0	1.209
1.2246 +0	1.3534 +0	4.9487 +0	1.0720 -2	6.7740 +0	1.369
1.3534 +0	1.4957 +0	3.6600 +0	1.0961 -2	5.4281 +0	1.483
1.4957 +0	1.6530 +0	2.6902 +0	1.1315 -2	4.1301 +0	1.535
1.6530 +0	1.8268 +0	1.8703 +0	1.1836 -2	2.9287 +0	1.566
1.8268 +0	2.0190 +0	1.2584 +0	1.2554 -2	1.9736 +0	1.520
2.0190 +0	2.2313 +0	9.2179 -1	1.3470 -2	1.3963 +0	1.515
2.2313 +0	2.3460 +0	3.5833 -1	1.7434 -2	5.2915 -1	1.477
2.3460 +0	2.4660 +0	2.9171 -1	1.8674 -2	4.2639 -1	1.462
2.4660 +0	2.7253 +0	4.4393 -1	1.6481 -2	6.5310 -1	1.471
2.7253 +0	3.0112 +0	3.1625 -1	1.8532 -2	4.4572 -1	1.409
3.0112 +0	3.3287 +0	2.2678 -1	2.0940 -2	3.0584 -1	1.347
3.3287 +0	3.6788 +0	1.5759 -1	2.4338 -2	2.1106 -1	1.339
3.6788 +0	4.0657 +0	1.1250 -1	2.8047 -2	1.4547 -1	1.293
4.0657 +0	4.4933 +0	8.3165 -2	3.2193 -2	1.0219 -1	1.229
4.4933 +0	4.7240 +0	3.2772 -2	4.9409 -2	3.8330 -2	1.170
4.7240 +0	4.9659 +0	2.6271 -2	5.4689 -2	3.1621 -2	1.204
4.9659 +0	5.4931 +0	3.5810 -2	4.7416 -2	4.7416 -2	1.313
5.4931 +0	6.0553 +0	2.7356 -2	5.4057 -2	2.8733 -2	1.050
6.0553 +0	6.5763 +0	1.0406 -2	8.6580 -2	9.0563 -3	0.870
6.3765 +0	6.7032 +0	7.0233 -3	1.0470 -1	6.7800 -3	0.965
6.7052 +0	7.0469 +0	5.9466 -3	1.1425 -1	5.0914 -3	0.856
		S IN, P)			
		5.2600 +0	5.0000 -2	6.4538 +0	1.227
		RH IN, N')			
		8.4400 +2	5.0000 -2	8.9755 +2	1.061
		IN IN, N')			
		6.4400 +1	5.0000 -2	7.3566 +1	1.142
		AU IN, G)			
		6.6500 +4	5.0000 -2	7.4765 +4	1.119

TABLE 15

COMPARISON OF CALCULATION WITH MEASUREMENT AT 22.8 CM POSITION.

ENERGY BOUNDARIES (MEV)		N	σ(M) /M	C	C/M
		NE 213 COUNTER.			
8.2085 -1	9.0718 -1	1.1170 +1	1.0024 -2	1.3942 +1	1.248
9.0718 -1	1.0026 +0	9.1830 +0	1.0028 -2	1.0194 +1	1.110
1.0026 +0	1.1080 +0	6.6962 +0	1.0039 -2	7.7182 +0	1.153
1.1080 +0	1.2246 +0	4.8480 +0	1.0055 -2	6.1741 +0	1.273
1.2246 +0	1.3534 +0	3.3876 +0	1.0080 -2	4.8946 +0	1.445
1.3534 +0	1.4957 +0	2.4675 +0	1.0109 -2	3.8981 +0	1.580
1.4957 +0	1.6530 +0	1.8038 +0	1.0154 -2	2.9384 +0	1.629
1.6530 +0	1.8268 +0	1.2505 +0	1.0226 -2	2.0554 +0	1.644
1.8268 +0	2.0190 +0	8.4189 -1	1.0335 -2	1.3621 +0	1.618
2.0190 +0	2.2313 +0	5.9209 -1	1.0487 -2	9.5391 -1	1.611
2.2313 +0	2.3460 +0	2.2252 -1	1.1192 -2	3.5891 -1	1.613
2.3460 +0	2.4660 +0	1.8824 -1	1.1402 -2	2.8780 -1	1.571
2.4660 +0	2.7253 +0	2.7942 -1	1.1006 -2	4.3907 -1	1.571
2.7253 +0	3.0112 +0	1.8939 -1	1.1485 -2	2.9774 -1	1.572
3.0112 +0	3.3287 +0	1.3100 -1	1.2095 -2	2.0304 -1	1.550
3.3287 +0	3.6788 +0	8.7049 -2	1.3093 -2	1.3962 -1	1.604
3.6788 +0	4.0657 +0	6.0702 -2	1.4287 -2	9.6030 -2	1.582
4.0657 +0	4.4933 +0	4.1452 -2	1.6081 -2	6.7663 -2	1.632
4.4933 +0	4.7240 +0	1.6071 -2	2.2538 -2	2.5480 -2	1.585
4.7240 +0	4.9659 +0	1.2907 -2	2.4934 -2	2.1070 -2	1.632
4.9659 +0	5.4881 +0	1.9155 -2	2.1286 -2	3.1404 -2	1.639
5.4881 +0	6.0653 +0	1.2162 -2	2.5907 -2	1.9229 -2	1.581
6.0653 +0	6.3763 +0	4.2024 -3	4.2038 -2	6.0693 -3	1.444
6.3763 +0	6.7032 +0	3.3902 -3	4.6560 -2	4.5515 -3	1.343
6.7032 +0	7.0469 +0	2.5007 -3	5.3373 -2	3.4279 -3	1.371
7.0469 +0	7.4082 +0	1.7022 -3	6.2483 -2	2.6040 -3	1.530
7.4082 +0	8.1873 +0	2.7267 -3	4.9030 -2	3.6155 -3	1.326
8.1873 +0	9.0484 +0	1.2845 -3	7.0812 -2	1.9950 -3	1.553
9.0484 +0	1.0000 +1	6.6393 -4	9.7836 -2	9.6750 -4	1.457
		S(N,P)			
		3.3300 +0	5.0000 -2	4.3628 +0	1.309
		RH(N,N')			
		7.1500 +2	5.0000 -2	7.3557 +2	1.029
		IN(N,N')			
		5.4100 +1	5.0000 -2	5.5131 +1	1.018

TABLE 16

COMPARISON OF CALCULATION WITH MEASUREMENT AT 50.8 CM POSITION.

ENERGY BOUNDARIES (MEV)		N	σ90/M	C	C/N
		AR/H COUNTER.			
3.0197 -1	3.3373 -1	1.1505 +0	1.0161 -2	1.0802 +0	9.389
3.3373 -1	5.4883 -1	8.5603 -1	1.0254 -2	7.4407 -1	0.869
3.6883 -1	4.0762 -1	6.7998 -1	1.0288 -2	4.7879 -1	0.704
4.0762 -1	4.5049 -1	5.5189 -1	1.0338 -2	4.0200 -1	0.728
4.5049 -1	4.9787 -1	4.3186 -1	1.0460 -2	3.3259 -1	0.770
4.9787 -1	5.5023 -1	3.2726 -1	1.0641 -2	2.5272 -1	0.772
5.5023 -1	6.0810 -1	2.1131 -1	1.1005 -2	1.7935 -1	0.849
6.0810 -1	6.7206 -1	1.1598 -1	1.1850 -2	9.7605 -2	0.842
6.7206 -1	7.4274 -1	7.4907 -2	1.2725 -2	4.2568 -2	0.568
7.4274 -1	8.2085 -1	5.3758 -2	1.3612 -2	2.7046 -2	0.503
8.2085 -1	9.0718 -1	3.5067 -2	1.5138 -2	1.8402 -2	0.525
9.0718 -1	1.0026 +0	2.0662 -2	1.7943 -2	1.0350 -2	0.501
1.0026 +0	1.1080 +0	1.2759 -2	2.1712 -2	6.1710 -3	0.484
1.1080 +0	1.2246 +0	7.1098 -3	2.7713 -2	4.2832 -3	0.602
1.2246 +0	1.3534 +0	3.7318 -3	3.6359 -2	2.9443 -3	0.789
1.3534 +0	1.4957 +0	2.3118 -3	4.6317 -2	2.0847 -3	0.902
1.4957 +0	1.6530 +0	1.5646 -3	5.6628 -2	1.3356 -3	0.854
1.6530 +0	1.8268 +0	8.8049 -4	7.4049 -2	7.4751 -4	0.849
1.8268 +0	2.0190 +0	4.8396 -4	1.0055 -1	3.7266 -4	0.770
		10 AT. COUNTER.			
2.0242 -1	2.2371 -1	3.9416 +0	1.0039 -2	4.1341 +0	1.049
2.2371 -1	2.4724 -1	3.5406 +0	1.0046 -2	3.6740 +0	1.038
2.4724 -1	2.7324 -1	3.0757 +0	1.0054 -2	3.1597 +0	1.027
2.7324 -1	3.0197 -1	2.5355 +0	1.0068 -2	2.6179 +0	1.032
3.0197 -1	3.3373 -1	1.9492 +0	1.0091 -2	2.1555 +0	1.106
3.3373 -1	3.6883 -1	1.4753 +0	1.0117 -2	1.4801 +0	1.003
3.6883 -1	4.0762 -1	1.1344 +0	1.0155 -2	9.4922 -1	0.837
4.0762 -1	4.5049 -1	9.2934 -1	1.0198 -2	7.9089 -1	0.851
4.5049 -1	4.9787 -1	7.5262 -1	1.0261 -2	6.4748 -1	0.860
4.9787 -1	5.5023 -1	5.8294 -1	1.0330 -2	4.8531 -1	0.833
5.5023 -1	6.0810 -1	4.1124 -1	1.0452 -2	3.3868 -1	0.824
6.0810 -1	6.7206 -1	2.3504 -1	1.0789 -2	1.8110 -1	0.770
6.7206 -1	7.4274 -1	1.3082 -1	1.1361 -2	7.7618 -2	0.593
7.4274 -1	8.2085 -1	8.3570 -2	1.2118 -2	4.7983 -2	0.574
8.2085 -1	9.0718 -1	5.3445 -2	1.3266 -2	3.1472 -2	0.589
9.0718 -1	1.0026 +0	2.7858 -2	1.5763 -2	1.6967 -2	0.609
1.0026 +0	1.1080 +0	1.5302 -2	1.9084 -2	9.4858 -3	0.620
		3 AT. COUNTER.			
8.6517 -2	1.1109 -1	6.1878 +0	1.0024 -2	7.1990 +0	1.163
1.1109 -1	1.2277 -1	2.3571 +0	1.0056 -2	2.6516 +0	1.125
1.2277 -1	1.3569 -1	2.1744 +0	1.0062 -2	2.3800 +0	1.095
1.3569 -1	1.4996 -1	1.9031 +0	1.0071 -2	2.0168 +0	1.060
1.4996 -1	1.6573 -1	1.6965 +0	1.0082 -2	1.7352 +0	1.023
1.6573 -1	1.8316 -1	1.5336 +0	1.0095 -2	1.5384 +0	1.003
1.8316 -1	2.0242 -1	1.3241 +0	1.0112 -2	1.3700 +0	1.035
2.0242 -1	2.2371 -1	1.2050 +0	1.0125 -2	1.2349 +0	1.025
2.2371 -1	2.4724 -1	1.0794 +0	1.0139 -2	1.0851 +0	1.005
2.4724 -1	2.7324 -1	9.3801 -1	1.0165 -2	9.2060 -1	0.981
2.7324 -1	3.0197 -1	7.4833 -1	1.0209 -2	7.5021 -1	1.002
3.0197 -1	3.3373 -1	5.5572 -1	1.0276 -2	6.0448 -1	1.088
3.3373 -1	3.6883 -1	4.0565 -1	1.0382 -2	4.0681 -1	1.003
3.6883 -1	4.0762 -1	2.9328 -1	1.0527 -2	2.5565 -1	0.872
4.0762 -1	4.5049 -1	2.3864 -1	1.0667 -2	2.0416 -1	0.856
4.5049 -1	4.9787 -1	1.8344 -1	1.0851 -2	1.5804 -1	0.862
4.9787 -1	5.5023 -1	1.3480 -1	1.1124 -2	1.1019 -1	0.817
		1 AT. COUNTER.			
4.0828 -2	5.2475 -2	2.1778 +0	1.0073 -2	2.7258 +0	1.252
5.2475 -2	6.7379 -2	2.1910 +0	1.0071 -2	2.6512 +0	1.210
6.7379 -2	8.6517 -2	1.9972 +0	1.0080 -2	2.4087 +0	1.206
8.6517 -2	1.1109 -1	1.7932 +0	1.0090 -2	2.1172 +0	1.181
1.1109 -1	1.2277 -1	6.6049 -1	1.0220 -2	7.6631 -1	1.160
1.2277 -1	1.3569 -1	5.8200 -1	1.0259 -2	6.8093 -1	1.170
1.3569 -1	1.4996 -1	4.9080 -1	1.0319 -2	5.7277 -1	1.167
1.4996 -1	1.6573 -1	4.4397 -1	1.0347 -2	4.8754 -1	1.098
1.6573 -1	1.8316 -1	3.7037 -1	1.0399 -2	4.2408 -1	1.121
1.8316 -1	2.0242 -1	3.2967 -1	1.0478 -2	3.6771 -1	1.140
2.0242 -1	2.2371 -1	2.8677 -1	1.0543 -2	3.1816 -1	1.127
2.23. -1	2.4724 -1	2.3441 -1	1.0672 -2	2.6587 -1	1.134
2.4724 -1	2.7324 -1	1.8119 -1	1.0870 -2	2.1064 -1	1.162
		1/2 AT. COUNTER.			
2.1870 -2	2.3570 -2	4.7787 -1	1.0136 -2	6.1500 -1	1.283
2.3570 -2	2.4788 -2	2.8412 -1	1.0295 -2	3.4566 -1	1.217
2.4788 -2	2.6050 -2	2.4538 -1	1.0208 -2	2.7651 -1	1.155

ENERGY BOUNDARIES (MEV)		N	σ90/M	C	C/N
2.6050 -2	3.1828 -2	8.7967 -1	1.0089 -2	1.0887 +0	1.238
3.1828 -2	4.0868 -2	1.1820 +0	1.0068 -2	1.4711 +0	1.245
4.0868 -2	5.2475 -2	1.2410 +0	1.0065 -2	1.4965 +0	1.206
5.2475 -2	6.7379 -2	1.2377 +0	1.0067 -2	1.4431 +0	1.166
6.7379 -2	8.6517 -2	1.1080 +0	1.0076 -2	1.2967 +0	1.170
8.6517 -2	1.1109 -1	9.7786 -1	1.0085 -2	1.1163 +0	1.141
1.1109 -1	1.2277 -1	3.4520 -1	1.0233 -2	3.9226 -1	1.136
1.2277 -1	1.3569 -1	2.9496 -1	1.0276 -2	3.4165 -1	1.158
		1 AT. HIGH GAIN.			
9.1188 -3	1.1709 -2	3.1718 +0	1.0038 -2	4.0107 +0	1.264
1.1709 -2	1.5034 -2	3.1733 +0	1.0038 -2	4.2889 +0	1.352
1.5034 -2	1.9305 -2	3.0552 +0	1.0040 -2	4.3405 +0	1.421
1.9305 -2	2.1870 -2	1.4196 +0	1.0086 -2	2.0691 +0	1.457
2.1870 -2	2.3570 -2	7.8128 -1	1.0155 -2	1.1298 +0	1.446
2.3570 -2	2.4788 -2	4.7771 -1	1.0244 -2	6.3229 -1	1.324
2.4788 -2	2.6050 -2	4.2487 -1	1.0265 -2	5.0317 -1	1.184
2.6050 -2	3.1828 -2	1.4117 +0	1.0009 -2	1.9591 +0	1.388
3.1828 -2	4.0868 -2	1.7948 +0	1.0069 -2	2.6630 +0	1.484
4.0868 -2	5.2475 -2	1.8829 +0	1.0066 -2	2.7258 +0	1.448
5.2475 -2	6.7379 -2	1.8802 +0	1.0067 -2	2.6512 +0	1.410
6.7379 -2	8.6517 -2	1.7202 +0	1.0075 -2	2.4087 +0	1.400
8.6517 -2	1.1109 -1	1.5393 +0	1.0081 -2	2.1172 +0	1.375
		1/2 AT. HIGH GAIN.			
7.1017 -3	9.1188 -3	1.5427 +0	1.0024 -2	1.9240 +0	1.247
9.1188 -3	1.1709 -2	1.5950 +0	1.0025 -2	2.1780 +0	1.365
1.1709 -2	1.5034 -2	1.5802 +0	1.0024 -2	2.3261 +0	1.472
1.5034 -2	1.9305 -2	1.5117 +0	1.0025 -2	2.3510 +0	1.555
1.9305 -2	2.1870 -2	7.1103 -1	1.0052 -2	1.1205 +0	1.576
2.1870 -2	2.3570 -2	3.9499 -1	1.0091 -2	6.1300 -1	1.552
2.3570 -2	2.4788 -2	2.4057 -1	1.0148 -2	3.4566 -1	1.438
2.4788 -2	2.6050 -2	2.1084 -1	1.0169 -2	2.7851 -1	1.321
2.6050 -2	3.1828 -2	7.3767 -1	1.0051 -2	1.0887 +0	1.476
3.1828 -2	4.0868 -2	9.7648 -1	1.0038 -2	1.4711 +0	1.506
4.0868 -2	5.2475 -2	1.0269 +0	1.0036 -2	1.4965 +0	1.457
5.2475 -2	6.7379 -2	1.0239 +0	1.0037 -2	1.4431 +0	1.409
		NE 213 COUNTER.			
8.2085 -1	9.0718 -1	3.4728 -1	1.0592 -2	4.4418 -1	1.279
9.0718 -1	1.0026 +0	2.7916 -1	1.0566 -2	2.5202 -1	0.903
1.0026 +0	1.1080 +0	1.8658 -1	1.0761 -2	1.5170 -1	0.813
1.1080 +0	1.2246 +0	1.1125 -1	1.1250 -2	1.0839 -1	0.974
1.2246 +0	1.3534 +0	5.9443 -2	1.2160 -2	7.7262 -2	1.300
1.3534 +0	1.4957 +0	3.6984 -2	1.3343 -2	5.7720 -2	1.561
1.4957 +0	1.6530 +0	2.3600 -2	1.4964 -2	3.9293 -2	1.665
1.6530 +0	1.8268 +0	1.3801 -2	1.7657 -2	2.3503 -2	1.703
1.8268 +0	2.0190 +0	7.5891 -3	2.1645 -2	1.2627 -2	1.664
2.0190 +0	2.2313 +0	4.7042 -3	2.6764 -2	7.8796 -3	1.675
2.2313 +0	2.3460 +0	1.5961 -3	4.2445 -2	2.7422 -3	1.718
2.3460 +0	2.4660 +0	1.2655 -3	4.7641 -2	2.0865 -3	1.649
2.4660 +0	2.7253 +0	1.7914 -3	4.1225 -2	3.0594 -3	1.708
2.7253 +0	3.0112 +0	1.1713 -3	4.9930 -2	1.9464 -3	1.662
3.0112 +0	3.3287 +0	7.3358 -4	6.2027 -2	1.2466 -3	1.699
3.3287 +0	3.6788 +0	4.9169 -4	7.4352 -2	8.3146 -4	1.691
3.6788 +0	4.0657 +0	3.1819 -4	9.4301 -2	5.6558 -4	1.777
4.0657 +0	4.4933 +0	2.4094 -4	1.0770 -1	4.1588 -4	1.726
4.4933 +0	4.7240 +0	1.2351 -4	1.6391 -1	1.6438 -4	1.331
4.7240 +0	4.9659 +0	8.7328 -5	1.7956 -1	1.3974 -4	1.600
4.9659 +0	5.4881 +0	1.2651 -4	1.3727 -1	2.1443 -4	1.669
5.4881 +0	6.0653 +0	8.8782 -5	1.6950 -1	1.3668 -4	1.539
6.0653 +0	6.3763 +0	3.7927 -5	2.3763 -1	4.4772 -5	1.180
6.3763 +0	6.7032 +0	2.6580 -5	2.9454 -1	3.4797 -5	1.217
6.7032 +0	7.0469 +0	2.0630 -5	3.1711 -1	2.7567 -5	1.336
		S ON, P)			
		1.9400 -2	5.0000 -2	3.3365 -2	1.720
		RH ON, N')			
		7.9000 +1	5.0000 -2	7.6318 +1	0.966
		IN ON, N')			
		2.0200 +0	5.0000 -2	2.0809 +0	1.034
		AU ON, G)			
		2.2400 +4	5.0000 -2	2.4051 +4	1.074
		CU ON, G)			
		1.0700 +2	5.0000 -2	1.4592 +2	1.364
		U ON, G)			
		6.5100 +1	5.0000 -2	8.0120 +1	1.231
		AU ON, G) RES SANDWICH			
		4.1900 +1	7.5000 -2	4.3057 +1	1.027

TABLE 17

COMPARISON OF CALCULATION WITH MEASUREMENT AT 76.2 CM POSITION.

ENERGY BOUNDARIES (KEV)		M	σ00 /M	C	C/M
		AR/H COUNTER.			
3.0197 -1	3.3373 -1	1.9938 -1	1.0101 -2	1.6364 -1	0.821
3.3373 -1	3.6883 -1	1.5068 -1	1.0134 -2	1.0093 -1	0.670
3.6883 -1	4.0762 -1	1.1148 -1	1.0202 -2	5.5283 -2	0.496
4.0762 -1	4.5049 -1	8.7664 -2	1.0240 -2	4.5185 -2	0.515
4.5049 -1	4.9787 -1	6.5278 -2	1.0341 -2	3.6273 -2	0.556
4.9787 -1	5.5023 -1	4.6842 -2	1.0472 -2	2.6292 -2	0.561
5.5023 -1	6.0810 -1	2.8525 -2	1.0711 -2	1.7434 -2	0.611
6.0810 -1	6.7206 -1	1.4451 -2	1.1477 -2	8.0309 -3	0.556
6.7206 -1	7.4274 -1	7.9675 -3	1.2512 -2	2.3903 -3	0.300
7.4274 -1	8.2085 -1	5.3823 -3	1.3581 -2	1.3668 -3	0.254
8.2085 -1	9.0718 -1	3.2414 -3	1.5828 -2	8.4332 -4	0.260
9.0718 -1	1.0026 +0	1.7090 -3	1.9375 -2	3.7710 -4	0.221
1.0026 +0	1.1080 +0	9.2742 -4	2.4099 -2	1.7234 -4	0.186
1.1080 +0	1.2246 +0	4.7030 -4	3.2817 -2	1.0786 -4	0.229
		10 AT. COUNTER.			
1.4996 -1	1.6573 -1	1.3521 +0	1.0022 -2	1.1134 +0	0.823
1.6573 -1	1.8316 -1	1.1709 +0	1.0028 -2	9.6341 -1	0.823
1.8316 -1	2.0242 -1	1.0336 +0	1.0033 -2	8.3841 -1	0.811
2.0242 -1	2.2371 -1	9.0045 -1	1.0039 -2	7.4342 -1	0.826
2.2371 -1	2.4724 -1	7.9338 -1	1.0040 -2	6.4043 -1	0.807
2.4724 -1	2.7324 -1	6.6961 -1	1.0050 -2	5.2976 -1	0.791
2.7324 -1	3.0197 -1	5.2693 -1	1.0069 -2	4.1726 -1	0.795
3.0197 -1	3.3373 -1	3.8215 -1	1.0096 -2	3.2591 -1	0.853
3.3373 -1	3.6883 -1	2.7254 -1	1.0130 -2	2.0035 -1	0.735
3.6883 -1	4.0762 -1	1.9648 -1	1.0185 -2	1.0939 -1	0.557
4.0762 -1	4.5049 -1	1.4993 -1	1.0248 -2	8.8709 -2	0.592
4.5049 -1	4.9787 -1	1.1585 -1	1.0313 -2	7.0450 -2	0.608
4.9787 -1	5.5023 -1	8.5752 -2	1.0426 -2	5.0327 -2	0.587
5.5023 -1	6.0810 -1	5.8334 -2	1.0624 -2	3.2801 -2	0.562
6.0810 -1	6.7206 -1	3.0672 -2	1.1165 -2	1.4823 -2	0.483
6.7206 -1	7.4274 -1	1.4869 -2	1.2298 -2	4.3250 -3	0.291
7.4274 -1	8.2085 -1	8.1324 -3	3.2630 -2	2.4008 -3	0.295
8.2085 -1	9.0718 -1	4.7792 -3	4.2637 -2	1.4257 -3	0.298
		3 AT. COUNTER.			
1.1109 -1	1.2277 -1	6.4051 -1	1.0068 -2	5.8020 -1	0.906
1.2277 -1	1.3569 -1	5.8513 -1	1.0075 -2	5.0344 -1	0.860
1.3569 -1	1.4996 -1	4.8942 -1	1.0088 -2	4.0775 -1	0.833
1.4996 -1	1.6573 -1	4.2120 -1	1.0097 -2	3.3694 -1	0.800
1.6573 -1	1.8316 -1	3.6854 -1	1.0115 -2	2.9031 -1	0.788
1.8316 -1	2.0242 -1	3.0653 -1	1.0138 -2	2.5117 -1	0.819
2.0242 -1	2.2371 -1	2.7138 -1	1.0157 -2	2.2067 -1	0.813
2.2371 -1	2.4724 -1	2.3609 -1	1.0176 -2	1.8787 -1	0.796
2.4724 -1	2.7324 -1	1.9595 -1	1.0215 -2	1.5320 -1	0.782
2.7324 -1	3.0197 -1	1.4873 -1	1.0284 -2	1.1859 -1	0.797
3.0197 -1	3.3373 -1	1.0145 -1	1.0423 -2	9.0552 -2	0.893
3.3373 -1	3.6883 -1	6.7936 -2	1.0629 -2	5.4501 -2	0.802
3.6883 -1	4.0762 -1	4.5860 -2	1.0931 -2	2.9209 -2	0.637
4.0762 -1	4.5049 -1	3.5623 -2	1.1159 -2	2.2693 -2	0.637
4.5049 -1	4.9787 -1	2.6435 -2	1.1558 -2	1.7033 -2	0.644
		1 AT. COUNTER.			
4.0868 -2	5.2475 -2	6.4261 -1	1.0062 -2	6.9036 -1	1.074
5.2475 -2	6.7379 -2	6.3475 -1	1.0062 -2	6.5241 -1	1.028
6.7379 -2	8.6517 -2	5.6032 -1	1.0071 -2	5.6827 -1	1.014
8.6517 -2	1.1109 -1	4.8239 -1	1.0084 -2	4.7395 -1	0.983
1.1109 -1	1.2277 -1	1.7199 -1	1.0211 -2	1.6505 -1	0.960
1.2277 -1	1.3569 -1	1.4707 -1	1.0257 -2	1.4164 -1	0.963
1.3569 -1	1.4996 -1	1.1789 -1	1.0333 -2	1.1379 -1	0.965
1.4996 -1	1.6573 -1	1.0432 -1	1.0370 -2	9.2993 -2	0.891

ENERGY BOUNDARIES (KEV)		M	σ (M) /M	C	C/M
1.6573 -1	1.8316 -1	8.5148 -2	1.0442 -2	7.8557 -2	0.923
1.8316 -1	2.0242 -1	7.0078 -2	1.0539 -2	6.6155 -2	0.944
2.0242 -1	2.2371 -1	6.0200 -2	1.0634 -2	5.5836 -2	0.928
2.2371 -1	2.4724 -1	4.8073 -2	1.0813 -2	4.5133 -2	0.939
		1/2 AT. COUNTER.			
2.4788 -2	2.6050 -2	7.3548 -2	1.0259 -2	7.3497 -2	0.999
2.6050 -2	3.1828 -2	2.6842 -1	1.0693 -2	2.8132 -1	1.048
3.1828 -2	4.0868 -2	3.5853 -1	1.0074 -2	3.7583 -1	1.048
4.0868 -2	5.2475 -2	3.7138 -1	1.0071 -2	3.7415 -1	1.007
5.2475 -2	6.7379 -2	3.6247 -1	1.0075 -2	3.4997 -1	0.966
6.7379 -2	8.6517 -2	3.1214 -1	1.0086 -2	3.0096 -1	0.964
8.6517 -2	1.1109 -1	2.6505 -1	1.0102 -2	2.4569 -1	0.927
		1 AT. HIGH GAIN.			
9.1188 -3	1.1709 -2	1.0580 +0	1.0032 -2	1.6193 +0	1.361
1.1709 -2	1.5034 -2	1.0863 +0	1.0031 -2	1.4800 +0	1.362
1.5034 -2	1.9305 -2	1.0638 +0	1.0031 -2	1.4408 +0	1.354
1.9305 -2	2.1870 -2	4.9751 +1	1.0065 -2	6.5620 -1	1.319
2.1870 -2	2.3570 -2	2.7380 -1	1.0115 -2	3.4240 -1	1.250
2.3570 -2	2.4788 -2	1.6532 -1	1.0188 -2	1.7943 -1	1.085
2.4788 -2	2.6050 -2	1.4139 -1	1.0223 -2	1.3411 -1	0.949
2.6050 -2	3.1828 -2	4.5030 -1	1.0074 -2	5.1155 -1	1.136
3.1828 -2	4.0868 -2	5.8969 -1	1.0057 -2	6.8314 -1	1.167
4.0868 -2	5.2475 -2	6.1377 -1	1.0055 -2	6.9036 -1	1.125
5.2475 -2	6.7379 -2	6.0589 -1	1.0056 -2	6.5241 -1	1.077
6.7379 -2	8.6517 -2	5.3665 -1	1.0063 -2	5.6827 -1	1.059
		1/2 AT. HIGH GAIN.			
7.1017 -3	9.1188 -3	4.9597 -1	1.0027 -2	6.8674 -1	1.385
9.1188 -3	1.1709 -2	5.1699 -1	1.0026 -2	7.6577 -1	1.481
1.1709 -2	1.5034 -2	5.2479 -1	1.0025 -2	7.9690 -1	1.518
1.5034 -2	1.9305 -2	5.0956 -1	1.0026 -2	7.7391 -1	1.519
1.9305 -2	2.1870 -2	2.3784 -1	1.0056 -2	3.5201 -1	1.480
2.1870 -2	2.3570 -2	1.3010 -1	1.0100 -2	1.8388 -1	1.413
2.3570 -2	2.4788 -2	7.8394 -2	1.0168 -2	9.7067 -2	1.239
2.4788 -2	2.6050 -2	6.8172 -2	1.0193 -2	7.3487 -2	1.078
2.6050 -2	3.1828 -2	2.2599 -1	1.0059 -2	2.8132 -1	1.245
3.1828 -2	4.0868 -2	2.9051 -1	1.0046 -2	3.7583 -1	1.294
4.0868 -2	5.2475 -2	3.0222 -1	1.0044 -2	3.7415 -1	1.238
5.2475 -2	6.7379 -2	2.9689 -1	1.0045 -2	3.4997 -1	1.179
		NE 213 COUNTER.			
8.2085 -1	9.0718 -1	6.1911 -2	1.0529 -2	2.0798 -2	0.336
9.0718 -1	1.0026 +0	3.4980 -2	1.0858 -2	9.4135 -3	0.269
1.0026 +0	1.1080 +0	1.6760 -2	1.1756 -2	4.3171 -3	0.258
1.1080 +0	1.2246 +0	9.2138 -3	1.3096 -2	2.7794 -3	0.302
1.2246 +0	1.3534 +0	4.3644 -3	1.5991 -2	1.7843 -3	0.409
1.3534 +0	1.4957 +0	2.5693 -3	1.9339 -2	1.2738 -3	0.496
1.4957 +0	1.6530 +0	1.5212 -3	2.3675 -2	8.0346 -4	0.528
1.6530 +0	1.8268 +0	9.5750 -4	2.8707 -2	4.2431 -4	0.443
1.8268 +0	2.0190 +0	5.8003 -4	3.6005 -2	1.8671 -4	0.322
2.0190 +0	2.2313 +0	3.6741 -4	4.4742 -2	1.0618 -4	0.289
		RH (N, N')			
		1.6600 +1	5.0000 -2	1.1852 +1	0.714
		AU (N, G)			
		9.2600 +3	5.0000 -2	1.0069 +4	1.087
		CU (N, G)			
		5.1100 +1	5.0000 -2	6.0702 +1	1.188
		V (N, G)			
		2.6800 +1	5.0000 -2	3.3663 +1	1.256
		AU (N, G)			
		1.7200 +1	7.5000 -2	1.8115 +1	1.053

TABLE 18

COMPARISON OF CALCULATION WITH MEASUREMENT AT 101.6 CM POSITION.

ENERGY BOUNDARIES (MEV)		M	σ(0) /H	C	C/H
		AR/H COUNTER.			
3.0197 -1	3.3373 -1	3.7008 -2	1.0007 -2	2.3047 -2	0.623
3.3373 -1	3.6883 -1	2.3976 -2	1.0012 -2	1.2863 -2	0.536
3.6883 -1	4.0762 -1	1.7340 -2	1.0015 -2	5.8794 -3	0.339
4.0762 -1	4.5049 -1	1.2462 -2	1.0022 -2	4.7204 -3	0.379
4.5049 -1	4.9787 -1	8.8564 -3	1.0031 -2	3.7174 -3	0.420
4.9787 -1	5.5023 -1	6.2894 -3	1.0042 -2	2.6325 -3	0.419
5.5023 -1	6.0810 -1	3.5350 -3	1.0057 -2	1.4592 -3	0.469
6.0810 -1	6.7206 -1	1.6378 -3	1.0171 -2	6.7579 -4	0.413
6.7206 -1	7.4274 -1	8.2894 -4	1.0350 -2	1.2930 -4	0.156
7.4274 -1	8.2085 -1	5.1064 -4	1.0594 -2	6.8195 -5	0.134
8.2085 -1	9.0718 -1	3.1890 -4	1.0921 -2	3.9152 -5	0.123
9.0718 -1	1.0026 +0	1.5346 -4	1.1850 -2	1.4241 -5	0.092
1.0026 +0	1.1080 +0	8.0884 -5	1.3334 -2	4.6459 -6	0.057
1.1080 +0	1.2246 +0	4.1421 -5	1.5964 -2	2.6127 -6	0.631
1.2246 +0	1.3534 +0	2.0490 -5	2.0823 -2	1.4394 -6	0.070
1.3534 +0	1.4957 +0	1.2896 -5	2.4781 -2	9.3264 -7	0.072
1.4957 +0	1.6530 +0	5.9613 -6	3.4324 -2	5.1545 -7	0.086
1.6530 +0	1.8268 +0	3.0885 -6	4.7108 -2	2.2675 -7	0.073
1.8268 +0	2.0190 +0	2.9276 -6	4.7815 -2	7.5200 -8	0.026
		10 AT. COUNTER.			
1.6573 -1	1.8316 -1	2.7456 -1	1.0059 -2	1.6266 -1	0.592
1.8316 -1	2.0242 -1	2.3346 -1	1.0069 -2	1.3831 -1	0.592
2.0242 -1	2.2371 -1	1.9761 -1	1.0091 -2	1.2024 -1	0.608
2.2371 -1	2.4724 -1	1.6912 -1	1.0102 -2	1.0105 -1	0.598
2.4724 -1	2.7324 -1	1.3769 -1	1.0131 -2	8.1056 -2	0.589
2.7324 -1	3.0197 -1	1.0083 -1	1.0176 -2	6.1274 -2	0.608
3.0197 -1	3.3373 -1	6.8004 -2	1.0244 -2	4.5857 -2	0.674
3.3373 -1	3.6883 -1	4.3642 -2	1.0407 -2	2.5504 -2	0.584
3.6883 -1	4.0762 -1	2.8659 -2	1.0604 -2	1.1625 -2	0.406
4.0762 -1	4.5049 -1	2.1448 -2	1.0810 -2	9.2601 -3	0.432
4.5049 -1	4.9787 -1	1.5950 -2	1.1141 -2	7.2141 -3	0.452
4.9787 -1	5.5023 -1	1.1654 -2	1.1490 -2	4.9975 -3	0.429
5.5023 -1	6.0810 -1	7.5245 -3	1.2154 -2	3.1176 -3	0.414
6.0810 -1	6.7206 -1	3.4416 -3	1.4352 -2	1.2448 -3	0.362
6.7206 -1	7.4274 -1	1.3619 -3	1.9466 -2	2.3313 -4	0.171
7.4274 -1	8.2085 -1	7.1692 -4	2.5074 -2	1.1919 -4	0.166
8.2085 -1	9.0718 -1	3.7223 -4	3.3321 -2	6.5770 -5	0.177
9.0718 -1	1.0026 +0	1.5986 -4	5.0041 -2	2.2899 -5	0.143
1.0026 +0	1.1080 +0	5.7697 -5	8.2577 -2	7.0556 -6	0.122
		3 AT. COUNTER.			
1.1109 -1	1.2277 -1	1.7236 -1	1.0069 -2	1.1100 -1	0.644
1.2277 -1	1.3569 -1	1.5144 -1	1.0073 -2	9.3494 -2	0.617
1.3569 -1	1.4996 -1	1.2104 -1	1.0091 -2	7.2761 -2	0.601
1.4996 -1	1.6573 -1	9.9944 -2	1.0114 -2	5.8041 -2	0.581
1.6573 -1	1.8316 -1	8.4458 -2	1.0130 -2	4.8868 -2	0.579
1.8316 -1	2.0242 -1	6.7730 -2	1.0173 -2	4.1305 -2	0.610
2.0242 -1	2.2371 -1	5.9036 -2	1.0206 -2	3.5571 -2	0.603
2.2371 -1	2.4724 -1	4.9458 -2	1.0241 -2	2.9537 -2	0.597
2.4724 -1	2.7324 -1	3.9569 -2	1.0301 -2	2.3345 -2	0.590
2.7324 -1	3.0197 -1	2.7852 -2	1.0411 -2	1.7334 -2	0.622
3.0197 -1	3.3373 -1	1.7429 -2	1.0676 -2	1.2672 -2	0.727
3.3373 -1	3.6883 -1	1.0750 -2	1.1125 -2	6.8931 -3	0.641
3.6883 -1	4.0762 -1	6.6775 -3	1.1736 -2	3.0916 -3	0.463
4.0762 -1	4.5049 -1	5.1525 -3	1.2191 -2	2.3588 -3	0.458
4.5049 -1	4.9787 -1	3.6355 -3	1.2938 -2	1.7363 -3	0.478
		1 AT. COUNTER.			
4.0868 -2	5.2475 -2	1.9257 -1	1.0022 -2	1.5065 -1	0.782
5.2475 -2	6.7379 -2	1.8769 -1	1.0023 -2	1.3888 -1	0.740
6.7379 -2	8.6517 -2	1.6342 -1	1.0027 -2	1.1662 -1	0.714
8.6517 -2	1.1109 -1	1.3536 -1	1.0033 -2	9.2874 -2	0.686
1.1109 -1	1.2277 -1	4.7459 -2	1.0086 -2	3.1281 -2	0.659
1.2277 -1	1.3569 -1	4.0217 -2	1.0103 -2	2.6040 -2	0.647
1.3569 -1	1.4996 -1	3.0924 -2	1.0131 -2	2.0093 -2	0.650
1.4996 -1	1.6573 -1	2.6407 -2	1.0161 -2	1.5849 -2	0.600
1.6573 -1	1.8316 -1	2.0998 -2	1.0207 -2	1.3076 -2	0.623
1.8316 -1	2.0242 -1	1.6651 -2	1.0261 -2	1.0755 -2	0.646
2.0242 -1	2.2371 -1	1.4082 -2	1.0307 -2	8.8918 -3	0.631
2.2371 -1	2.4724 -1	1.0975 -2	1.0385 -2	7.0056 -3	0.638
2.4724 -1	2.7324 -1	7.9745 -3	1.0540 -2	5.1615 -3	0.647
		1/2 AT. COUNTER.			
2.1870 -2	2.3570 -2	5.3225 -2	1.0074 -2	4.8983 -2	0.920
2.3570 -2	2.4788 -2	3.1494 -2	1.0089 -2	2.3895 -2	0.758
2.4788 -2	2.6050 -2	2.6664 -2	1.0128 -2	1.6704 -2	0.626
2.6050 -2	3.1828 -2	8.3442 -2	1.0062 -2	6.2603 -2	0.750
3.1828 -2	4.0868 -2	1.0783 -1	1.0051 -2	8.2852 -2	0.768
4.0868 -2	5.2475 -2	1.0995 -1	1.0051 -2	8.1002 -2	0.737
5.2475 -2	6.7379 -2	1.0570 -1	1.0052 -2	7.3823 -2	0.698
6.7379 -2	8.6517 -2	8.8736 -2	1.0064 -2	6.1120 -2	0.689
8.6517 -2	1.1109 -1	7.1781 -2	1.0079 -2	4.7615 -2	0.663
1.1109 -1	1.2277 -1	2.4103 -2	1.0227 -2	1.5556 -2	0.645
		1 AT. HIGH GAIN.			
9.1188 -3	1.1709 -2	3.6119 -1	1.0031 -2	4.4467 -1	1.231
1.1709 -2	1.5034 -2	3.6762 -1	1.0031 -2	4.5331 -1	1.233
1.5034 -2	1.9305 -2	3.5544 -1	1.0032 -2	4.2538 -1	1.197
1.9305 -2	2.1870 -2	1.6443 -1	1.0069 -2	1.8501 -1	1.125
2.1870 -2	2.3570 -2	9.0029 -2	1.0124 -2	9.1882 -2	1.021
2.3570 -2	2.4788 -2	5.4318 -2	1.0205 -2	4.4484 -2	0.819
2.4788 -2	2.6050 -2	4.6486 -2	1.0230 -2	3.0678 -2	0.660
2.6050 -2	3.1828 -2	1.3913 -1	1.0083 -2	1.1456 -1	0.823
3.1828 -2	4.0868 -2	1.7270 -1	1.0068 -2	1.5276 -1	0.885
4.0868 -2	5.2475 -2	1.7772 -1	1.0066 -2	1.5065 -1	0.848
5.2475 -2	6.7379 -2	1.7272 -1	1.0068 -2	1.3888 -1	0.804
6.7379 -2	8.6517 -2	1.5023 -1	1.0078 -2	1.1662 -1	0.776
8.6517 -2	1.1109 -1	1.2305 -1	1.0096 -2	9.2874 -2	0.755
		1/2 AT. HIGH GAIN.			
7.1017 -3	9.1188 -3	1.8191 -1	1.0021 -2	2.1711 -1	1.193
9.1188 -3	1.1709 -2	1.9344 -1	1.0020 -2	2.3895 -1	1.235
1.1709 -2	1.5034 -2	1.9267 -1	1.0020 -2	2.4293 -1	1.261
1.5034 -2	1.9305 -2	1.8330 -1	1.0022 -2	2.2721 -1	1.240
1.9305 -2	2.1870 -2	8.3801 -2	1.0047 -2	9.8595 -2	1.176
2.1870 -2	2.3570 -2	4.4842 -2	1.0088 -2	4.8983 -2	1.092
2.3570 -2	2.4788 -2	2.5787 -2	1.0150 -2	2.3885 -2	0.926
2.4788 -2	2.6050 -2	2.1491 -2	1.0173 -2	1.6704 -2	0.777
2.6050 -2	3.1828 -2	7.1508 -2	1.0055 -2	6.2603 -2	0.875
3.1828 -2	4.0868 -2	9.3288 -2	1.0043 -2	8.2852 -2	0.888
4.0868 -2	5.2475 -2	9.5123 -2	1.0042 -2	8.1002 -2	0.852
5.2475 -2	6.7379 -2	9.0790 -2	1.0044 -2	7.3823 -2	0.813
		RH (N, N')			
		4.2500 +0	1.0000 -1	1.8515 +0	0.436
		AU (N, G)			
		3.4400 +3	5.0000 -2	3.6623 +3	1.065
		CU (N, G)			
		1.7200 +1	5.0000 -2	2.1746 +1	1.264
		W (N, G)			
		9.8000 +0	5.0000 -2	1.2255 +1	1.250
		AU (N, G)			
		6.5000 +0	7.5000 -2	6.6449 +0	1.022

Table 19

Partition Coefficients and Standard Errors Used in the Analysis of the ASPIS Iron Benchmark Experiment[1]

Detector	Partition Coefft.	% Standard Error	Comments
S(n,p)	1.00	8.00	Error represents burning-off · efficiency + $4\pi\beta$ counter efficiency for P^{32} β^-
In(n,n')	1.00	5.00	Calibration efficiency of NaI(Tl) counter for 330 keV γ-ray uncertain to 5%
Rh(n,n')	1.00	10.00	Uncertainty in internal conversion ratio
Au(n,γ) W(n,γ) Cu(n,γ)	1.00	5.00	Uncertainty in NaI(Tl) photopeak calibration
Ar/H	0.83	5.00	Number density of hydrogen atoms in the counter considered to be lower than specified
All other gas counters	1.00	5.00	5% uncertainty in efficiency of chamber
NE213	1.00	10.00	This counter has never been absolutely calibrated. Only consistency checks with multiple RADAK unfolding have been performed

Table 20

Input Parameters for the PRCM Code

Counter	P_H (at)	P_{CH_4} (at)	P_A (at)	Radius (cm)	Pressure-Range Factor
Ar/H	4.580	0.49	4.580	2.027	1.0965
10 at.	9.630	-	-	2.022	1.0963
3 at.	2.940	-	-	2.024	1.0294
1 at.	0.940	-	-	1.969	1.0094
½ at.	0.488	-	-	1.989	1.00488

TABLE 21

RADAK FLUX/LETHARGY DISTRIBUTION AT FOUR MEASUREMENT POSITIONS.

ENERGY BOUNDARIES (EV)		20.3	50.8	76.2	101.6
7.1017 -3	9.1188 -3	8.1628 +2	3.5808 +2	1.1817 +2	2.7282 +1
9.1188 -3	1.1709 -2	1.0690 +3	4.1817 +2	1.0760 +2	4.2123 +1
1.1709 -2	1.5034 -2	1.2090 +3	4.9548 +2	1.3927 +2	5.5290 +1
1.5034 -2	1.9305 -2	1.3893 +3	5.6837 +2	1.7374 +2	6.6543 +1
1.9305 -2	2.1870 -2	1.6674 +3	6.8074 +2	2.3313 +2	8.8634 +1
2.1870 -2	2.3570 -2	2.5016 +3	1.0538 +3	3.1687 +2	1.4054 +2
2.3570 -2	2.4788 -2	3.6731 +3	1.4057 +3	4.5404 +2	1.7494 +2
2.4788 -2	2.6050 -2	3.6112 +3	1.4368 +3	4.9705 +2	1.8532 +2
2.6050 -2	3.1828 -2	1.3965 +3	4.4563 +2	1.3709 +2	6.1795 +1
3.1828 -2	4.0868 -2	5.6543 +2	1.5931 +2	5.1517 +1	1.7142 +1
4.0868 -2	5.2475 -2	9.3857 +2	2.9762 +2	9.6768 +1	2.9912 +1
5.2475 -2	6.7379 -2	1.2487 +3	3.8434 +2	1.2835 +2	3.8723 +1
6.7379 -2	8.6517 -2	1.8908 +3	5.9762 +2	1.9815 +2	6.1304 +1
8.6517 -2	1.1109 -1	1.4038 +3	4.4461 +2	1.3681 +2	4.0572 +1
1.1109 -1	1.2277 -1	1.7255 +3	5.3938 +2	1.7705 +2	5.6101 +1
1.2277 -1	1.3569 -1	2.0645 +3	8.3156 +2	2.3762 +2	7.9212 +1
1.3569 -1	1.4996 -1	2.7495 +3	8.4417 +2	2.9536 +2	8.2084 +1
1.4996 -1	1.6573 -1	2.0945 +3	5.3236 +2	1.6308 +2	4.5715 +1
1.6573 -1	1.8316 -1	2.6129 +3	7.3592 +2	1.8057 +2	5.5732 +1
1.8316 -1	2.0242 -1	2.3078 +3	5.9582 +2	1.5026 +2	4.0258 +1
2.0242 -1	2.2371 -1	2.0727 +3	4.8327 +2	1.3147 +2	3.4138 +1
2.2371 -1	2.4724 -1	2.3477 +3	5.3947 +2	1.3906 +2	3.5035 +1
2.4724 -1	2.7324 -1	3.7283 +3	6.0335 +2	1.5302 +2	3.8055 +1
2.7324 -1	3.0197 -1	3.2413 +3	6.8981 +2	1.6025 +2	4.0648 +1
3.0197 -1	3.3373 -1	3.4542 +3	6.6386 +2	1.4626 +2	3.1275 +1
3.3373 -1	3.6883 -1	2.8573 +3	5.0178 +2	1.0336 +2	2.3406 +1
3.6883 -1	4.0762 -1	2.1816 +3	3.4273 +2	7.2409 +1	1.3131 +1
4.0762 -1	4.5049 -1	1.8587 +3	2.7856 +2	5.7634 +1	1.1217 +1
4.5049 -1	4.9787 -1	1.9306 +3	2.6783 +2	5.0309 +1	8.5382 +0
4.9787 -1	5.5023 -1	2.0332 +3	2.5489 +2	4.6088 +1	7.3155 +0
5.5023 -1	6.0810 -1	2.5931 +3	2.8948 +2	4.7748 +1	7.2155 +0
6.0810 -1	6.7206 -1	2.1293 +3	1.9630 +2	3.0065 +1	3.9447 +0
6.7206 -1	7.4274 -1	1.3379 +3	9.8612 +1	1.3799 +1	1.5191 +0
7.4274 -1	8.2085 -1	9.1701 +2	5.8925 +1	7.9991 +0	8.4945 -1
8.2085 -1	9.0718 -1	8.2700 +2	5.4870 +1	5.6285 +0	6.6886 -1
9.0718 -1	1.0026 +0	9.2050 +2	4.4663 +1	4.6707 +0	4.5937 -1
1.0026 +0	1.1080 +0	6.1926 +2	1.6539 +1	1.6558 +0	1.8066 -1
1.1080 +0	1.2246 +0	5.6420 +2	1.3399 +1	1.1718 +0	1.7823 -1
1.2246 +0	1.3534 +0	3.8237 +2	7.0887 +0	6.1703 -1	8.9975 -2
1.3534 +0	1.4957 +0	3.0337 +2	5.7962 +0	2.2681 -1	4.1854 -2
1.4957 +0	1.6530 +0	2.4500 +2	2.2138 +0	1.6759 -1	-
1.6530 +0	1.8268 +0	2.0126 +2	2.0361 +0	9.9276 -2	-
1.8268 +0	2.0190 +0	1.4123 +2	9.1799 -1	5.8743 -2	-
2.0190 +0	2.2313 +0	9.3674 +1	5.0868 -1	3.6452 -2	-
2.2313 +0	2.3460 +0	1.0219 +2	4.9563 -1	-	-
2.3460 +0	2.4660 +0	5.4207 +1	3.4466 -1	-	-
2.4660 +0	2.7253 +0	6.1540 +1	2.3243 -1	-	-
2.7253 +0	3.0112 +0	4.7388 +1	1.7563 -1	-	-
3.0112 +0	3.3287 +0	3.2021 +1	-	-	-
3.3287 +0	3.6788 +0	2.5009 +1	-	-	-
3.6788 +0	4.0657 +0	1.7220 +1	-	-	-
4.0657 +0	4.4933 +0	1.3092 +1	-	-	-
4.4933 +0	4.7240 +0	1.0745 +1	-	-	-
4.7240 +0	4.9659 +0	9.7522 +0	-	-	-

ALL DIMENSIONS IN cm.

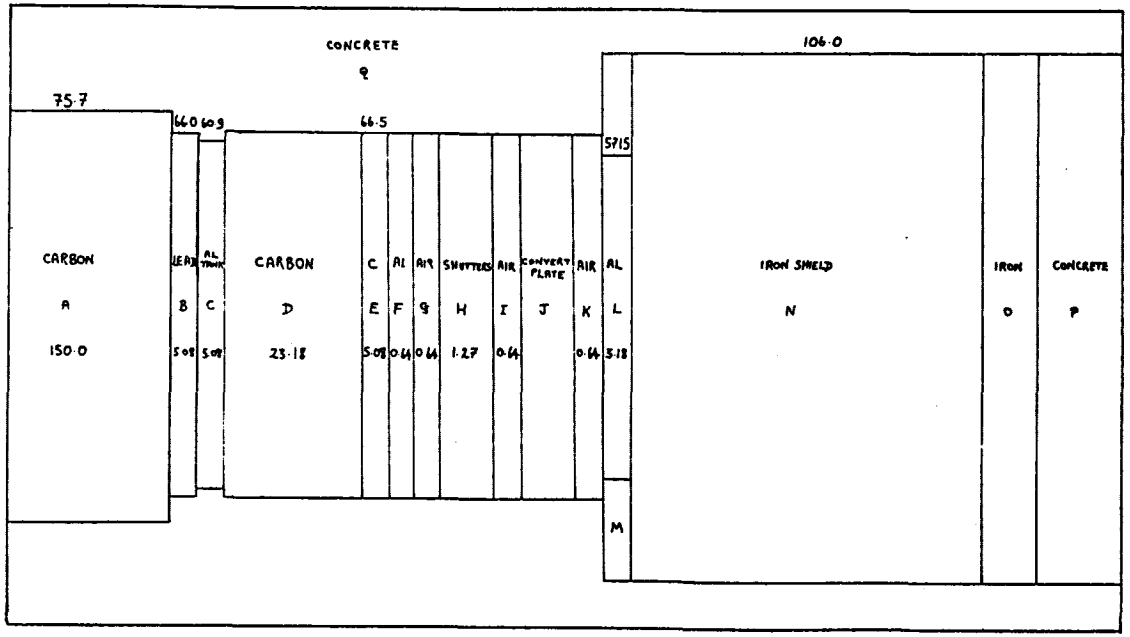

FIG. 1 EQUIVALENT AREA VIEW OF THE ASPIS IRON BENCHMARK EXPERIMENT.

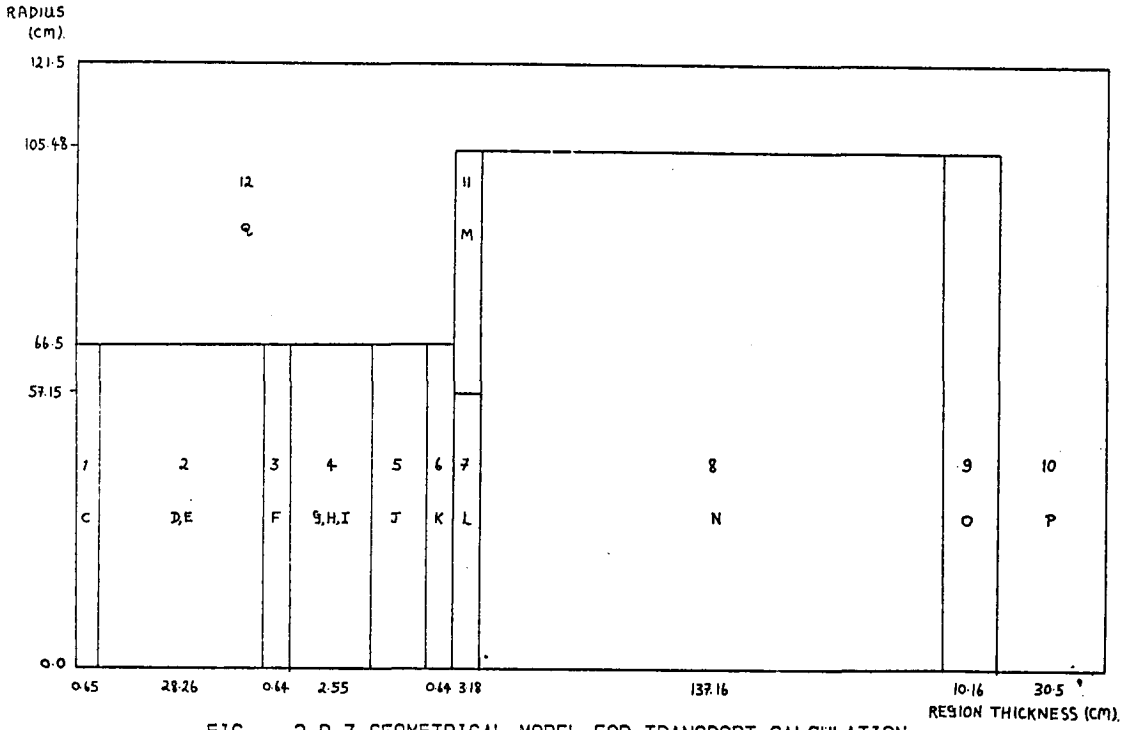

FIG. 2 R-Z GEOMETRICAL MODEL FOR TRANSPORT CALCULATION

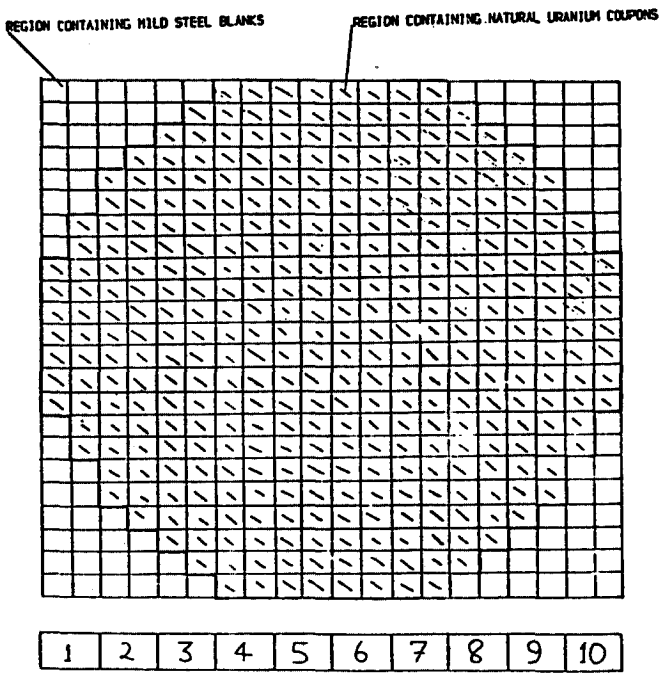

FIG. 3 SPATIAL DISTRIBUTION OF FUEL IN CONVERTER PLATE.

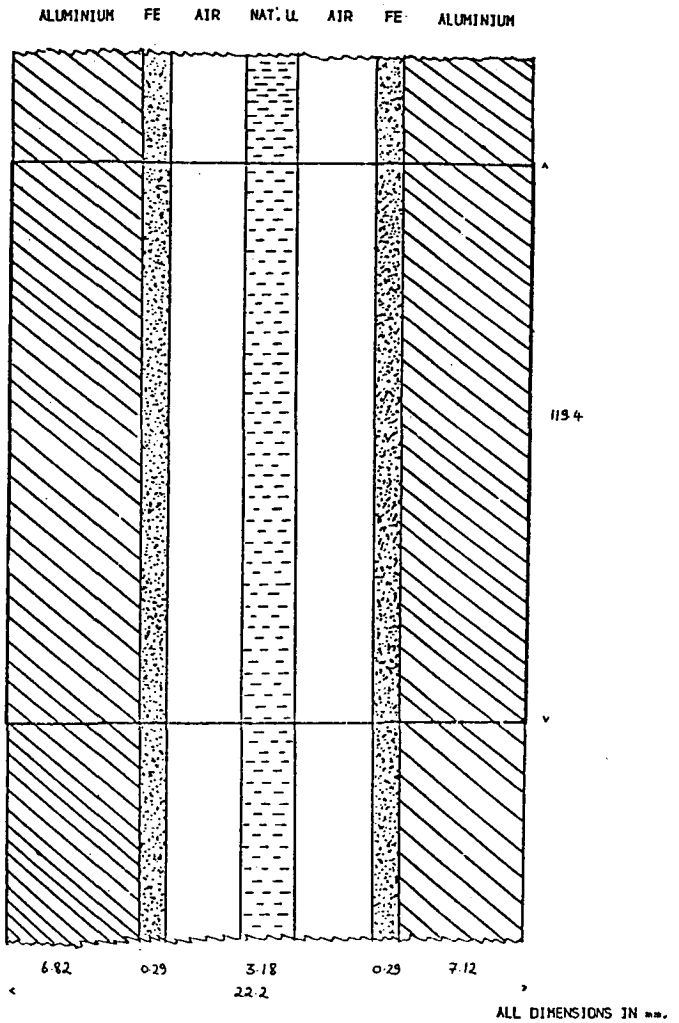

FIG. 4 INTERMEDIATE MODEL OF LATTICE CELL (PLANAR).

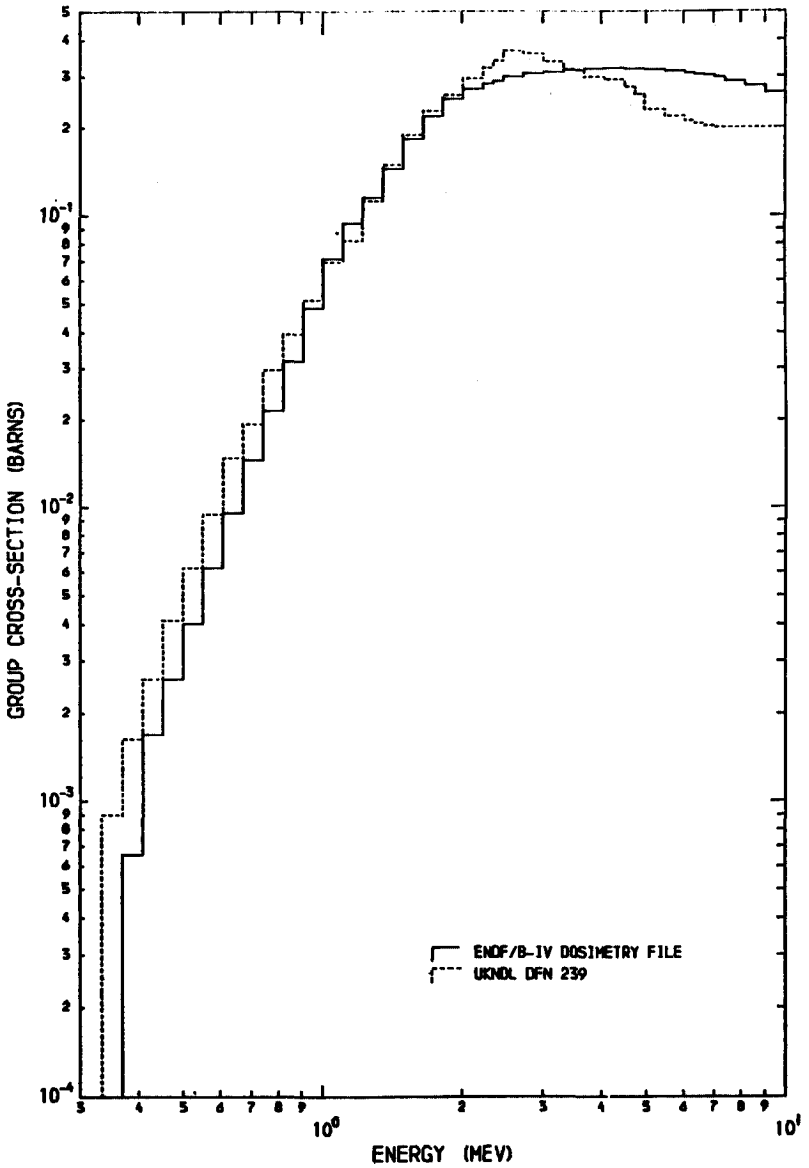

FIG. 5 COMPARISON OF IN-115(N,N') MULTI-GROUP CROSS-SECTION DATA FROM DIFFERENT SOURCES.

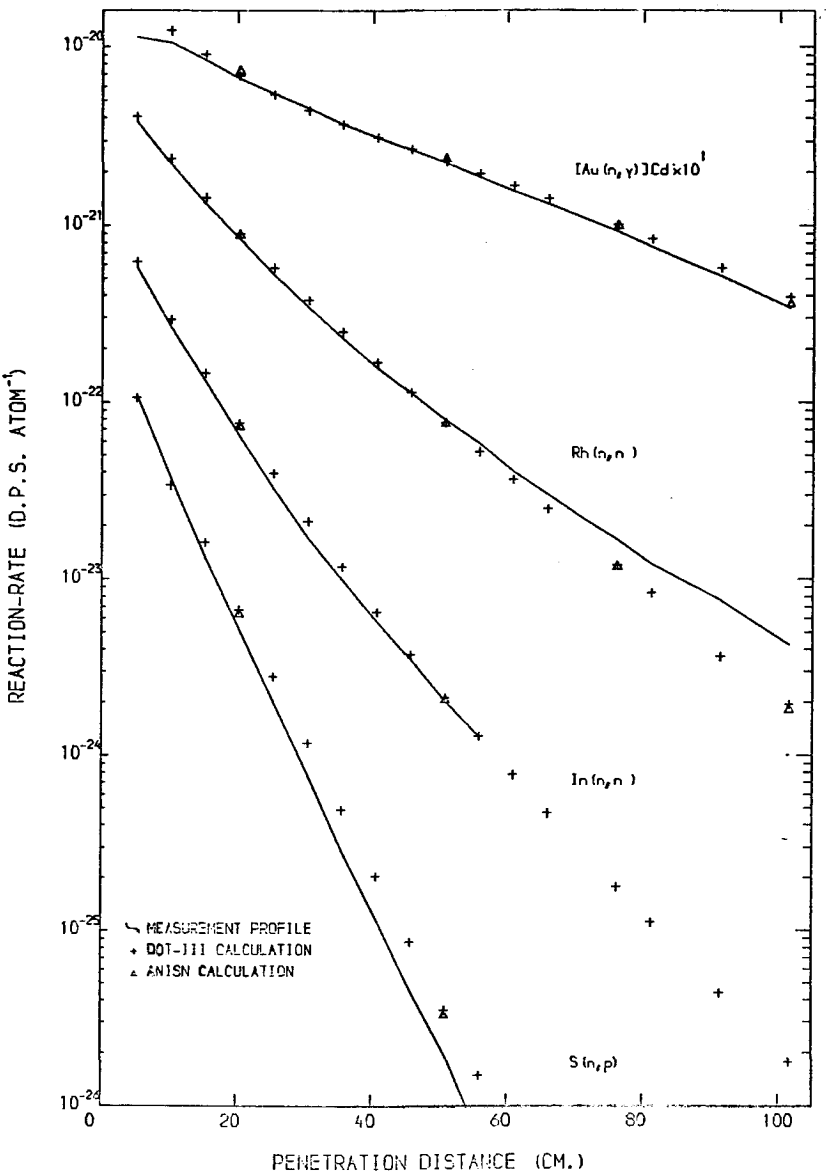

FIG. 6 COMPARISON OF MEASURED AND CALCULATED INTEGRAL DETECTOR REACTION-RATE PENETRATION PROFILES.

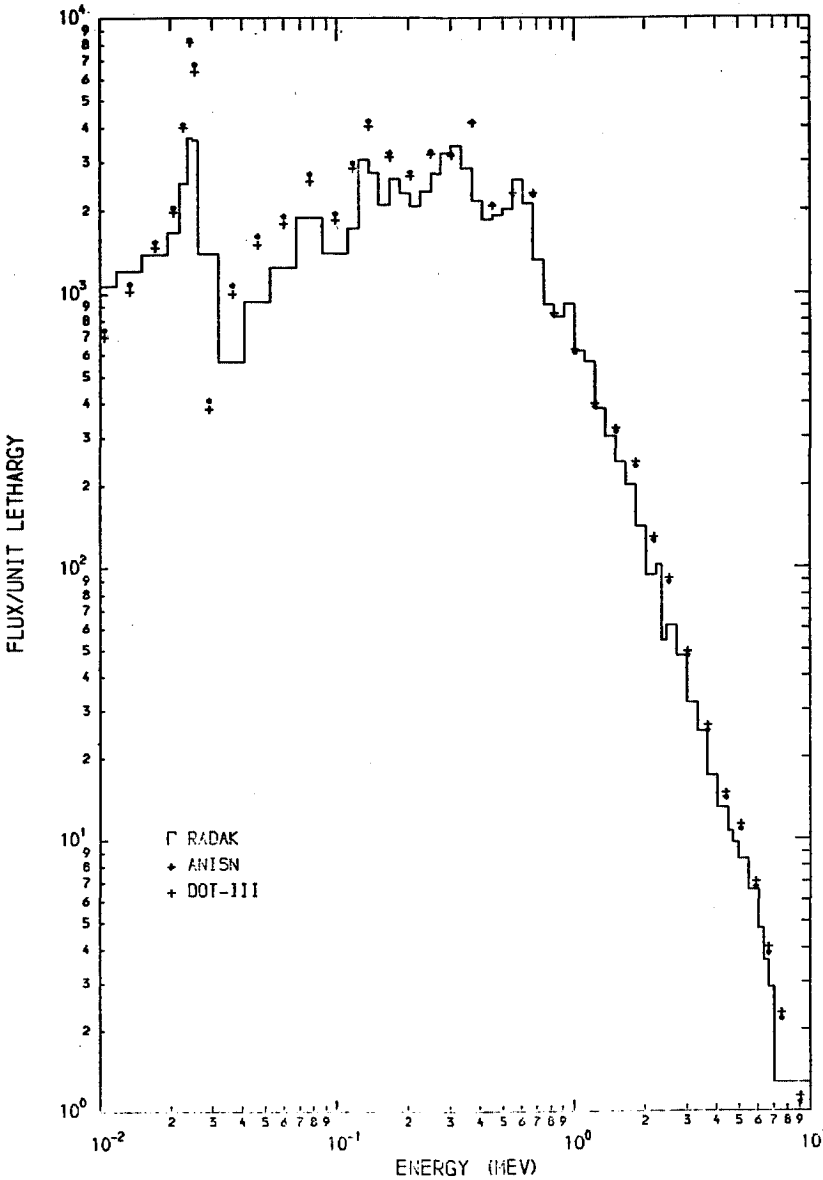

FIG. 7 COMPARISON OF CALCULATED FLUX PROFILES WITH RADAK UNFOLDED SPECTRUM MEASUREMENT AT 20.3CM POSITION.

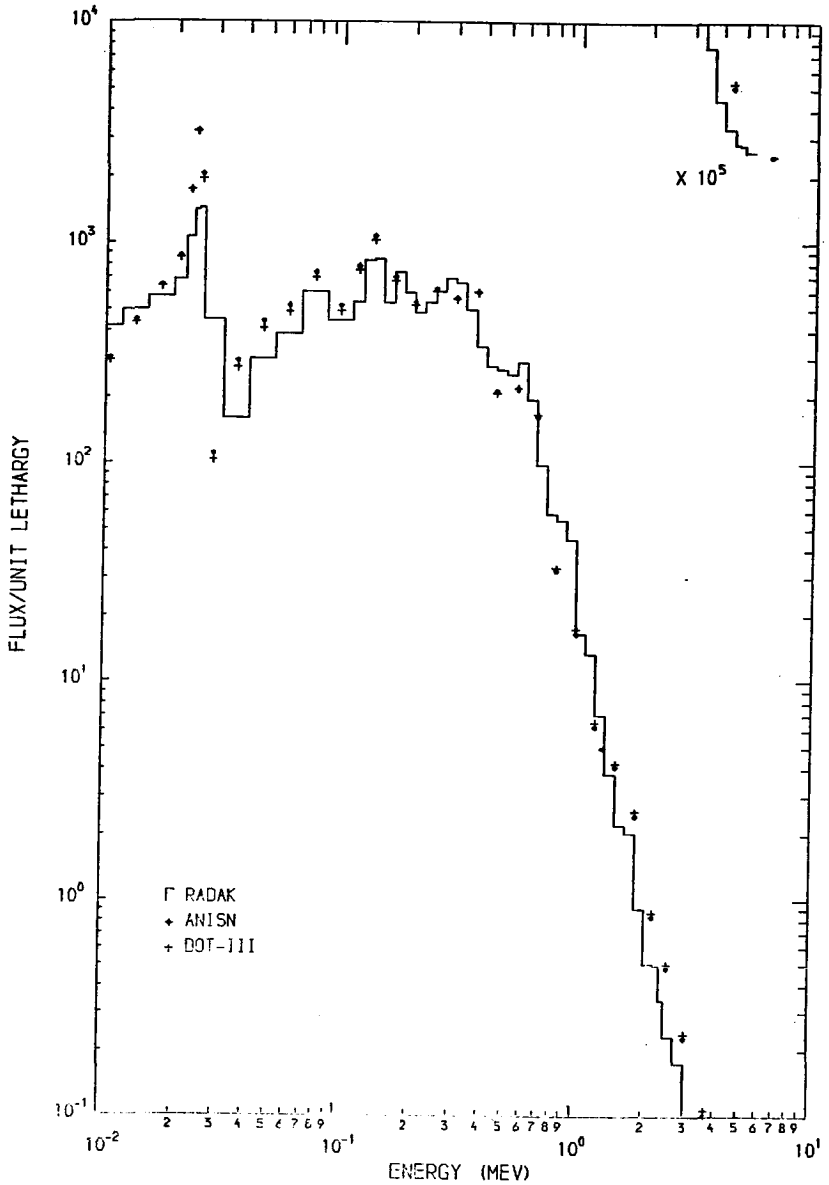

FIG. 8 COMPARISON OF CALCULATED FLUX PROFILES WITH RADAK UNFOLDED SPECTRUM MEASUREMENT AT 50.8CM POSITION.

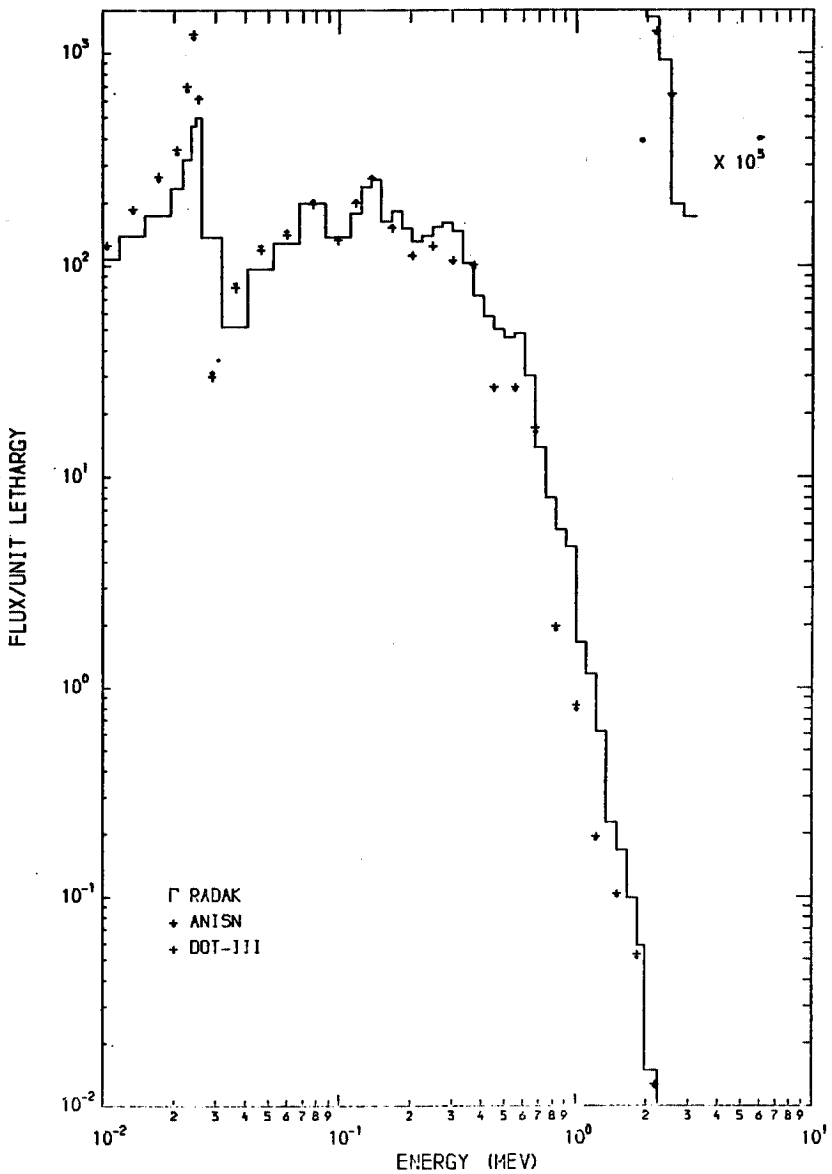

FIG. 9 COMPARISON OF CALCULATED FLUX PROFILES WITH RADAK UNFOLDED SPECTRUM MEASUREMENT AT 76.2CM POSITION.

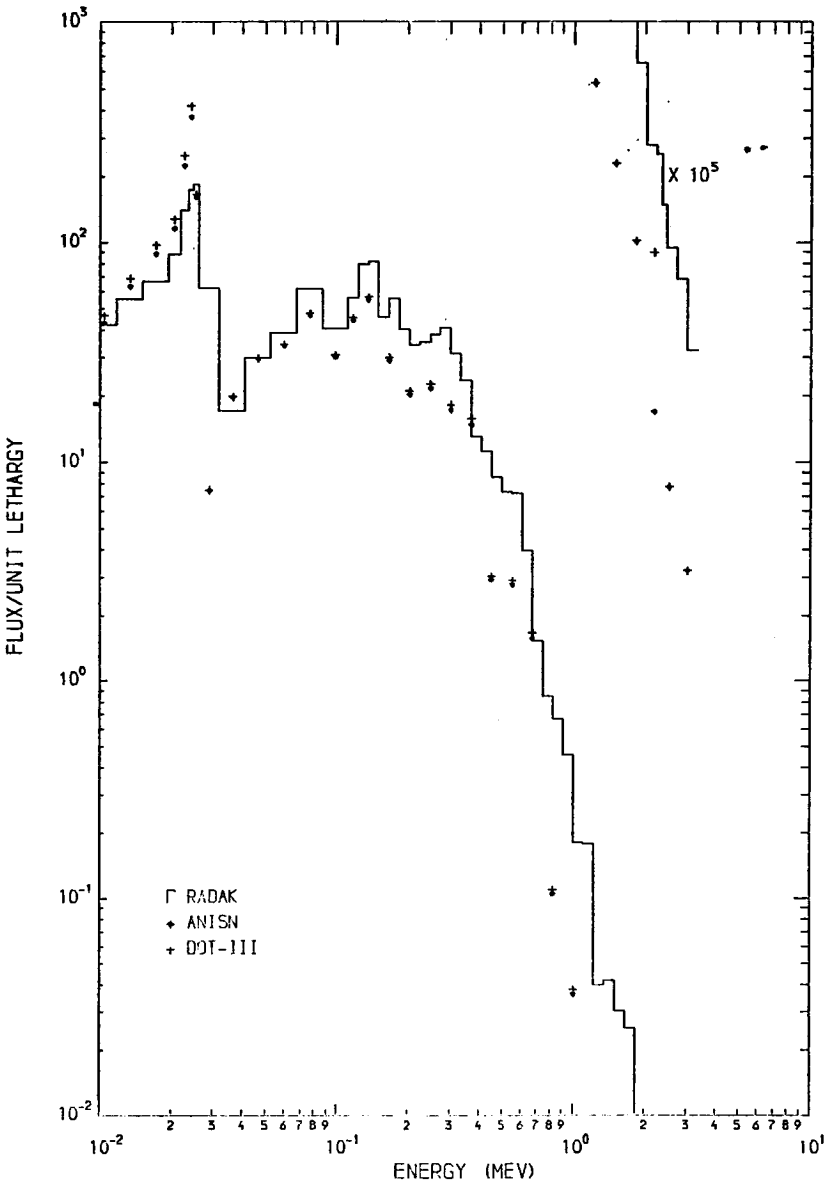

FIG. 10 COMPARISON OF CALCULATED FLUX PROFILES WITH RADAK UNFOLDED SPECTRUM MEASUREMENT AT 101.6CM POSITION.

PROGRESS REPORT ON SHIELDING EXPERIMENTS AT YAYOI

Y. Oka, S. An, H. Hashikura
H. Fukumoto, M. Akiyama
The University of Tokyo, Nuclear Engineering
Research Laboratory, The Faculty of Engineering
Tokai-mura, Ibaraki, 319-11, Japan

S. Miyasaka*
Japan Atomic Energy Research Institute
Tokai-mura, Ibaraki, 319-11, Japan
*present address : Nuclear Material Control Center
Akasaka, 2-3-4, Minatoku,
Tokyo, 107, Japan

ABSTRACT

Rates of neutron reactions have been measured by activation detectors in 177.5cm thick and about 100cm square sodium shields with the fast neutron reactor YAYOI as a source. Spatial distributions of gamma-ray dose rates have been also measured in the shield. The analysis of the experiment by DOT3.5 shows disagreement above the measurement error range. The spatial distributions show rather good agreement with the experiments.

Experiments on the fast neutron streaming through a slit-duct system have been performed. Neutron spectra of the source and in the duct have been obtained by using a NE213 spectrometer and proton recoil spherical gas proportional counters.

Table I Atomic number densities of sodium and stainless steel cans

($\times 10^{24}$ n/cm^3)

material element	stainless steel can	sodium
H	0.0	2.7848-7
C	2.7471-4*	3.7390-7
O	0.0	3.5088-7
Na	0.0	2.3527-2
Al	0.0	0.0
Si	1.0564-3	0.0
K	0.0	7.1804-7
Ca	0.0	2.1893-4
Cr	1.6665-2	0.0
Mn	1.0288-3	0.0
Fe	5.9871-2	0.0
Ni	7.0199-3	0.0

* read as 2.7471×10^{-4}

Table II Measured results at the center of the boundary between the sodium shield and the reflector (at 2kw)

type of reaction	measured reaction rate (s^{-1})
^{24}Mg(n,p)	$4.37(\pm 0.23) \times 10^{-20}$
^{27}Al(n,α)	$2.09(\pm 0.13) \times 10^{-20}$
^{27}Al(n,p)	$1.08(\pm 0.11) \times 10^{-19}$
^{54}Fe(n,p)	$2.79(\pm 0.18) \times 10^{-18}$
^{64}Zn(n,p)	$1.32(\pm 0.04) \times 10^{-18}$
^{58}Ni(n,p)	$4.38(\pm 0.24) \times 10^{-18}$
^{115}In(n,n')	$3.65(\pm 0.59) \times 10^{-17}$
^{197}Au(n,γ)bare	$8.59(\pm 0.59) \times 10^{-14}$
gamma ray	3.2×10^{4} rad/h

1. INTRODUCTION

This report reviews the progress of the works carried out at the YAYOI fast neutron source reactor concerning a benchmark type experiment in thick sodium and an experiment on neutron streaming through a slit-duct configuration. The aim of the first experiment is to verify the calculation of neutron and gamma-ray propagation through thick sodium. The aim of the second experiment is to provide the experimental results to assess the method of analysis for fast neutron streaming.

2. STUDY ON NEUTRON AND GAMMA-RAY PROPAGATION IN THICK SODIUM

2.1 Experiments

A schematic view of the experimental arrangement of the sodium shield is shown in Fig. 1. Three sodium shields were fabricated by casting sodium in thin stainless steel cans. These were made to be closely surrounded by the heavy concrete shield of the reactor when mounted on the reflector of YAYOI. The total thickness of the shields were 180.5cm including three aluminum spacer plates which were placed in order to insert detectors. The shields were fed by the neutrons produced in the core of YAYOI. Neutrons and gamma rays in the shields were measured using activation detectors and thermoluminescent detectors (TLDs) respectively.

The atomic number densities of the sodium and the stainless steel cans are presented in Table I. The compositions of other regions of the reactor are described in detail in [1]. The results of the neutron reaction rates and gamma-ray dose rates at the center of the boundary between the sodium shields and the reflector are presented in Table II. The spatial distributions at the boundary are shown in Fig. 2.

2.2 Analysis

Analysis of the experiment were performed using DOT3.5. Region-wise coupled neutron (13G) and gamma-ray (3G) multigroup cross sections were generated by using the code system RADHEAT-V3 [2]. The neutron data were taken from the ENDF/B-IV library and the secondary gamma-ray production data were taken from the POPOP-4 library. The resonance self-shielding effects were considered by using Bondarenko type self-shielding factors.

In order to obtain source condition for the sodium shield analysis a criticality calculation of the core was performed. The calculated energy spectrum and the spatial distributions of the group fluxes at the boundary between the shield and the reflector were modified until the calculated to experimental (C/E) values become nearly unity. By using the boundary source, two-dimensional analysis of the experiment were performed with a (R,Z) model of the sodium shield. The C/E values on the centerline of the sodium shields are presented in Table III. The results of $^{115}In(n,n')$ and $^{197}Au(n,\gamma)$ reaction show disagreement above the measurement error range. Although C/E values of the gamma-ray dose rate is good, the agreement is not satisfactory in considering the overestimates of the neutron calculations. Further analysis are necessary for clarifying the source of errors.

3. EXPERIMENTS ON NEUTRON STREAMING THROUGH A SLIT-DUCT SYSTEM

Several experiments on neutron streaming have been performed at YAYOI [3], [4], [5]. A fast neutron streaming experiment through a slit-duct system is under way. The experimental arrangement is presented in Fig. 3. The atomic compositions are shown in Table IV. The fast neutrons leak from the YAYOI core through a duct into a slit between the shields. Then the neutron streaming occurs through the duct leading to it. The duct is located off centerline of the neutron beam from the core. The diameter of the duct is 20.5cm. The width of the slit, L, is changed from 0cm to 40cm. The fast neutrons at the inlet of the slit, the source point, and in the duct have been measured by using a NE213 scintillator and proton

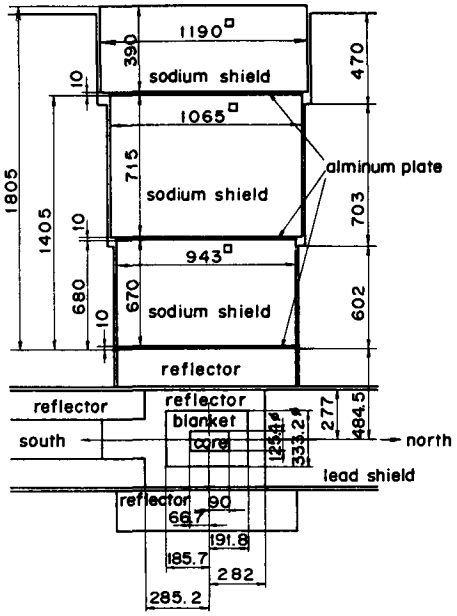

Fig. 1 Schematic view of the experimental arrangement for the study on neutron and gamma-ray propagation in thick sodium (dimensions in millimeters)

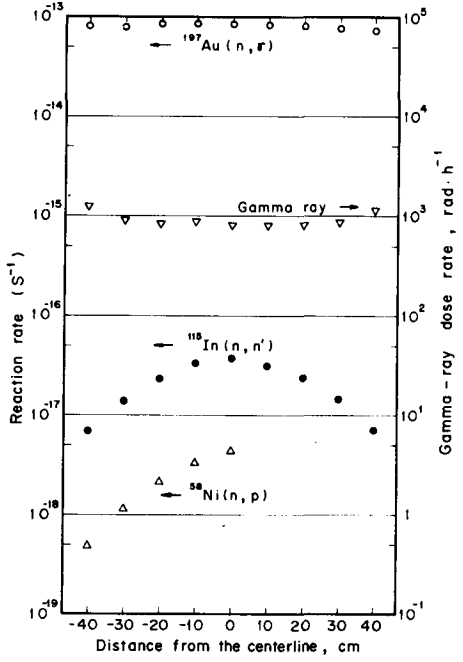

Fig. 2 Experimental distributions of the ^{115}In(n,n'), ^{58}Ni(n,p), ^{197}Au(n,γ) reactions and gamma-ray dose rates at the boundary between the sodium shield and the reflector

recoil spherical gas proportional counters. The measurements have been performed at point (A) to (D) which are shown in Fig. 3. When the measurement is undertaken at point (A), the source point, the 149.9cm square and 140cm thick concrete shield has been removed. The neutron spectra have been obtained by unfolding the measured pulse height distributions. The result for the slit width, L = 40cm is shown in Fig. 4. The experimental results are going to be compared with calculations in order to check the method of analysis for fast neutron streaming.

REFERENCES

[1] Oka, Y. et al. : "Neutron and Gamma-Ray Penetrations in Thick Iron", Nuclear Science and Engineering, 73 (3), 259-273 (1980).

[2] Koyama, K. et al. : "RADHEAT-V3, A Code System for Generating Coupled Neutron and Gamma-Ray Group Constants and Analysing Radiation Transport", JAERI-M-7155, Japan Atomic Energy Research Institute (1977).

[3] Kosako, T. et al. : "Spectral Characterization of Fast Reactor Neutron Fields", Journal of the Faculty of Engineering, The University of Tokyo, series B, 24 (2) 410-480 (1977).

[4] Nakazawa, M. et al. : "Studies on Fast Neutron Behavior in the Reactor Shielding Structure", Reports of Nuclear Safety Research Association of Japan, Oct. 1976 and Oct. 1977. (in Japanese).

[5] Oka, Y. et al. : "Experiments and Analysis of Neutron and Gamma-Ray Streaming in the Cavity-Duct System of a Fast Neutron Source Reactor", Nuclear Science and Engineering, to be published.

Table III Comparison of calculation with experiment on the centerline of the sodium shield

Depth in the Sodium Shield	Type of reaction							
	$^{115}In(n,n')^{115m}In$ S^{-1}		$^{58}Ni(n,p)^{58}Co$		$^{115}Au(n,\gamma)^{198}Au$(bare) S^{-1}		gamma-ray dose rate rad/h	
	Experiment	C/E	Experiment	C/E	Experiment	C/E	Experiment	C/E
0cm	$3.65(\pm0.59)\times10^{-17}$	1.0	$4.38(\pm0.24)\times10^{-18}$	1.0	$8.59(\pm0.97)\times10^{-14}$	1.0	8.00×10^{2} [a]	1.0
68cm	$2.78(\pm0.45)\times10^{-19}$	1.39	$5.42(\pm0.65)\times10^{-20}$	1.10	$2.60(\pm0.16)\times10^{-14}$	1.37	3.34×10^{2}	1.02
140.5cm	----------		----------		$4.41(\pm0.22)\times10^{-15}$	1.27	5.28×10^{2}	1.03
180.5cm	----------		----------		$4.92(\pm0.39)\times10^{-16}$	1.31	9.12	1.18

a. Errors of the TLD measurement may be below 15%

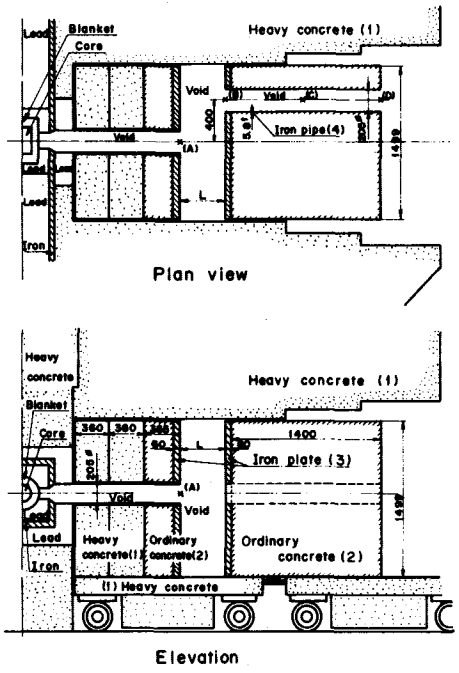

Fig. 3 Experimental arrangement for the study of neutron streaming through a slit -duct system (dimensions in millimeters) (A) to (D) are the points where the neutron spectra are measured. L is changed from 0cm to 40cm. The numbers in parentheses are identification numbers of the regions in Table IV.

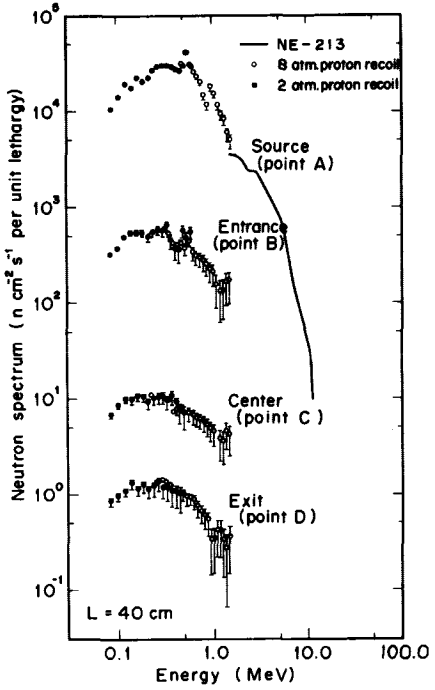

Fig. 4 Measured fast neutron spectra of the source and in the duct for slit width, L=40cm

Table IV Atomic number densities of the regions for slit-duct system ($\times 10^{24}$ atoms/cm^3)

element	(1) heavy concrete	(2) ordinary concrete	(3) iron plate	(4) iron pipe
H	4.997-2*	1.568-2	-	-
B	-	-	8.759-7	1.314-6
C	-	-	7.095-4	2.759-4
O	4.379-2	4.265-2	-	-
Na	-	5.001-4	-	-
Mg	-	3.134-4	-	-
Al	1.890-4	2.146-3	-	-
Si	1.043-3	1.276-2	4.383-4	-
P	-	2.158-5	3.515-5	1.834-5
S	-	5.838-5	2.658-5	2.658-5
K	-	3.009-4	-	-
Ca	2.200-3	3.816-3	-	-
Ti	-	8.375-5	-	-
Cr	-	-	9.105-6	1.821-5
Mn	-	9.734-4	8.962-4	3.016-4
Fe	2.552-2	5.746-4	8.347-2	8.436-2
Ni	-	-	8.065-6	-
Cu	-	-	-	1.490-5
Pb	-	5.807-7	-	-

* read as 4.997×10^{-2}

EXPERIMENTAL TECHNIQUES FOR 14 MEV NEUTRON BENCHMARK STUDIES

Malcolm C. Scott, R. Koohi-Fayegh[§], N. Evans[+], L.J. Perkins[§] and N.P. Taylor
University of Birmingham, Department of Physics, Birmingham B15 2TT, England

[+]Energy Research Group, Cavendish Laboratory, Madingley Road, Cambridge CB3 OHE, England

[§]I.R.T. Corporation, 7650 Convoy Court, P.O. Box 80817, San Diego, California 92138, U.S.A.

ABSTRACT

The use of proton-recoil proportional and scintillation counters for measurements with 14 MeV neutrons is discussed. Details are given of investigations into their performance and that of the unfolding codes used, and examples of their application in LiF and LiF-Be integral assemblies are presented.

1. INTRODUCTION

Because of the relative ease with which known yields of mono-energetic neutrons can be obtained, cross section data points at 14 MeV have long had a special significance in fission reactor data measurements. More recently, increasing activity on the fusion front, particularly investigations of alternative, inertial, methods of plasma confinement and thermonuclear burn initiation, have led to increasing interest in 14 MeV neutron studies.

In this paper we shall discuss the scope and limitations of the techniques used to make 14 MeV benchmark experiments in different experimental assemblies at Birmingham. These measurements involved making absolute spectrum measurements (fluence per source neutron) from 30 keV to ∿16 MeV, and the work breaks down naturally into two parts, namely (i) provision of a monitored neutron source, and (ii) development and use of gas proportional counters and a miniature scintillation counter as neutron spectrometers.

2. NEUTRON SOURCE PROVISION

Because of target deterioration it is not possible to use beam current as a secondary standard in determining neutron yield from tritiated targets under deuteron bombardment. We therefore used associated alpha particle monitoring with a number of different target assemblies. The first two, which are described more fully elsewhere *[1]*, monitored the associated alpha particle in the backward direction, making the target assembly very compact, whilst the third used a 90° monitoring position which, in principle, offers the opportunity of higher precision *[2]*: in both cases, however, the choice of configuration was dictated by the geometry of the bench-mark, integral, assembly.

In the smaller of the two backward monitored targets (4 cm diameter) the beam was incident on the target through the centre of an annular semiconductor detector, the alpha particle count rate being reduced to a reasonable level both by geometry and by the use of an annular collimator. Care was taken to shield the detector from direct beam, and a pair of tantalum discs followed by a ceramic annulus served both to collimate the beam and to prevent radiant heat generated by stopped beam from reaching the detector. In practice, this target geometry limited the beam current which could be used, and a second target was developed, with a very small (7 mm diameter) semi-conductor detector mounted off-axis and screened from stray beam. We note that similar target assemblies have subsequently been reported by the University of Illinois group *[3]*.

As a check that the data and methods used to relate alpha to neutron yield for our assembly were correct, a continuous flow vanadium bath was used to measure the absolute neutron yield per alpha particle: again, full details are given in reference 1. Measurements were made of neutron yield for deuterons from 250 to 500 keV and showed that,within the random and systematic errors of the vanadium bath measurement (11 and 10% respectively), the associated particle monitoring (with an estimated overall error of ±3%) gave good agreement. We therefore concluded that there was no undetermined source of systematic error larger than our quoted experimental errors, and that deuterium build-up on the target together with other possible sources of monitoring error were not significant.

At the same time, since the yield of neutrons from both D-D and D-C reactions increases with target age and incident particle energy, care was taken to ensure that the incident deuteron energy was kept below the threshold for the $^{12}C(d,n)$ reaction of 280 keV, and the targets were changed as soon as there was any evidence of distortion of measured 14 MeV response functions. We note here

that the recent work of Gaiser et al *[4]* confirms our assumption that inclusion in the alpha peak of charged particle from reactions involving no neutron production (e.g. $^{3}He(d,p)^{4}He$ and $D(d,p)T$) does not produce significant errors in fresh targets. For the 90^{o} case they showed that the contribution to the measured alpha peak from these reactions was less than 1% for a fresh target, although it rose to 10% or more for an 'old' target (purchased in 1972 with 4000 μAh service *[5]*).

3. NEUTRON SPECTROMETRY

(a) Gas proportional counters

The counters used were of the design developed by Benjamin et al *[6]*, namely spherical counters of 4 cm diameter with insulators designed to minimise field effect distortion. Because there is a 10 atmosphere pressure limit on these shells, we used a gas mixture to increase the upper neutron energy from 1.2 MeV (using H_2) to 2.5 MeV (using 8.07 atmospheres of argon with 2.27 atmospheres of hydrogen) *[7,8]*. A 2.5 atmosphere hydrogen counter was used to cover the energy range from 30 keV since, even with pulse shape discrimination against gamma rays, the lower energy limit of the mixed gas counter was ∿500 keV.

The use of pulse shape discrimination made it possible to overcome one of the problems of the mixed gas counter in a 14 MeV neutron field, namely the existence of recoil argon ions with energies up to 1.3 MeV. Using the discrimination method of Bennett *[9]* the recoil argon ions could be clearly distinguished on a two-parameter surface, and we could thus use peak search and Gaussian fitting routines to remove both argon recoils and gamma induced electrons from the measured detector response.

The question of energy calibration received considerable attention, and we calibrated each detector using monoenergetic neutrons from different thin targets, resonance filtered spectra and the pulses from the $^{3}He(n,p)T$ reaction generated in traces of ^{3}He using thermal neutrons *[8]*. Examination of the resulting energy versus ionisation curve showed two features. The first was that the 'effective Q' for the ^{3}He reaction differed significantly from the true one of 764 keV, being 779 ± 3 keV for the 2.5 atmos. hydrogen counter and 751 ± 5 for the hydrogen-agron one. A 10 atmosphere hydrogen counter examined in the same study had an effective Q of 784 ± 4 keV. We were able to examine the triton and proton edges for the 2.5 atmos. hydrogen counter and found that the triton edge was 6% too high compared to the proton edge, consistant with difference in W (energy per ion pair) between the two particles: unfortunately, gamma ray interference made it impossible to perform a similar analysis for the mixed gas counter. Our values for hydrogen agree with that of Carter *[10]* (780 keV), but disagree with that of Verbinski and Giovannini *[11]* (756 keV).

The second feature of the energy-ionisation curve was that the energy intercepts were -7.7 ± 0.5 keV for the 2.5 atmos. hydrogen counter, 15.7 ± 2 keV for 10 atmos. hydrogen and 77 ± 4 keV for the mixed gas counter. The sign and value of the intercept is, of course, related both to the variation of the specific energy loss per ion pair with energy, $\bar{w}$, for pure hydrogen, as well as to the presence of gas additives, electronegative and other gaseous impurities. Our intercept values are generally higher than those of other workers. However, we do not think it profitable to attempt to reconcile these differences, given the lack of knowledge of the electronegative impurities present in the counters concerned. In this respect we feel that a systematic investigation of the origins and effects of impurities in gaseous proportional counters would shed considerable light on the differences in counter performance which are a feature of proton-recoil proportional counter work.

Meanwhile, we consider it essential that each individual counter be calibrated over its working energy range. In addition, we would limit the product of gas gain and energy deposited to 48 MeV, as opposed to the value of 93 MeV proposed by Benjamin *[6]*.

Finally, a note on unfolding. We used a slightly modified version of the SPEC-4 code *[12]*. In this, allowance has to be made for proton recoils from neutrons above the detector's operating range. We first note that there is a simple mistake in the published SPEC-4 programme, so that energy deposition from protons having an initial energy greater than 3 MeV is in error. However, the most serious problem arises from the fact that with 14 MeV neutrons charged particle production in the walls and in any noble gases used will distort the detector response prediction used in SPEC-4. We are just completing a programme of work modelling the detector response to all possible reactions in the counter walls and filling gas, the preliminary results of which indicate that these reactions should account for the observed differences between measured and calculated response functions for high energy neutrons. If this is the case, however, we would then probably use a matrix unfolding code, e.g. FERDOR, since allowance for these distortions within SPEC-4 would be difficult.

(b) NE213 proton recoil scintillator

The miniature (∿1.5 c.c.) NE213 scintillator developed for this work was of all glass construction with an integral expansion chamber, coupled to a 1.9 cm diameter fast photomultiplier tube (RCA C31005C). A tapered dynode chain was used to minimise the effect of space charge saturation in such a small tube. The only significant change made since our original paper on this detector *[13]* was to simplify the filling procedure, a specially made long, fine, hyperdermic needle being used to get the NE213 through the constriction in the expansion chamber.

The unfolding procedure used in the first stage of our programme was a differential code based on NEUTSP *[14]*. In order to apply this it was necessary to strip off the alpha particles from $^{12}C(n,\alpha)$ and $^{12}C(n,n'3\alpha)$ reactions. Zero-crossing pulse shape characterisation was therefore used to produce a two-parameter response surface, fitting procedures then being applied to separate the alpha particles from the protons. We note, in this respect that the pulse shape signatures are identical for the two particles at around 1.8 MeV proton energy *[13]* (∿6 MeV alpha particles), so that use of this method is only possible if the alpha particle ridge is well defined, for example, when the neutron spectrum concerned is dominated by a high energy peak.

The other feature which has to be allowed for before using a differential code is that of wall effect and multiple neutron scattering. Here we applied the correction derived by Broek and Anderson *[15]*. However, it must be noted immediately that this correction only applies at an energy point, and allows for particles lost by wall effects and undergoing multiple scattering; it does not, therefore, correct the proton recoil spectra at lower energies.

At a later stage in our programme we were able to implement the matrix unfolding code FERDOR *[16]* which, of course, required us to produce response functions at suitable energy intervals over the entire working range (from ∿0.5 to 16 MeV). Below the threshold for the ^{12}C reactions calculation using, for example, the O5S code *[17]* could be relied upon, since the H(n,p) and total carbon cross sections are very well known. Once one has to include ^{12}C reactions, however, two problems arise, namely (i) the $^{12}C(n,n'3\alpha)$ reaction mechanisms are not well known and there are cross section uncertainties for ^{12}C reactions generally, and (ii) there is not agreement on the alpha to proton light output ratios for NE213.

Of course, one can obviate these difficulties by using measured response functions, but it is necessary to use associated particle gating and high energy accelerators to cover the entire energy range and ensure background free results, whereas with our facilities we could only make such measurements at energies around 15 MeV.

Considering the alpha-proton light output first, comparison of calculated and measured response functions for our cell at 14.3 meV showed the $^{12}C(n,\alpha)$ peak to be displaced using the light output values of Verbinski et al *[18]*, whereas agreement was reached when the alpha-proton ratios were multiplied by 1.2. We make two points here. The first is that Verbinski's light alpha-proton light values were themselves produced by adjustment to fit the response for their cell (5 × 5 cm). The second is that as yet unreported detailed photon calculations from our own laboratory show that geometric factors play an extremely important part in determining the shape of the measured response function, and suggest that, because of their different track length distributions, the alpha-proton light output ratios are likely to be geometry dependent (geometry here including factors such as cell shape, reflecting paint characteristics and photomultiplier photocathode uniformity).

Ideally, of course, one should measure the alpha-proton light output ratio. However, in view of our comment on geometric considerations, use of a point alpha source is likely to lead to errors in magnitude, though not so much in energy dependent shape. What one wants is an alpha emitter in a chemical form such that it will dissolve in the scintillator without changing its characteristics. We believe that we have found such a compound (^{211}At–C$_6$H$_4$–COOH) emitting alpha particles at 5.8 and 7.2 MeV, and work is in hand to investigate its use.

The second problem of the $^{12}C(n,n'3\alpha)$ data, is less tractible: there is clearly a need for much more work, both experimental and theoretical, before the data can be said to be satisfactory, particularly since the reaction is an important one outside the spectrometry field, e.g. in determining radiation effects in fast neutron cancer therapy. Meanwhile we have looked in some detail at the various decay paths for the nuclei produced and then adjusted the branching ratios so as to produce the best fit to our measured spectrum. The result is shown in Figure 1, where it can be seen that, at 14.3 MeV, there is excellent agreement down to 0.3 light units (i.e., a proton energy of ∿1.5 MeV). Full details of all these adjustments are given in reference 19, but the main changes made to the O5S data were (a) to include the reaction branch via ^{9}Be, viz $^{12}C(n,\alpha)^{9}Be^{*}$, and (b) to include five excitation levels for the branch proceeding as $^{12}C(n,n')^{12}C^{*}$. The best agreement between our measured result at 14.3 MeV and prediction was obtained with 45% of the reactions going via $^{9}Be^{*}$, the proportion going through the excited levels of ^{12}C being: via the level at 9.63 MeV, 4%; 10.1 MeV, 4%; 10.84 MeV, 16%; 11.82 MeV, 14% and 12.73 MeV, 17%.

4. EXAMPLES OF APPLICATION

(a) Gas proportional counters

Measurements have been made at a number of positions in a large (1.25 m diameter) sphere of LiF with a central D-T source using the two counters discussed earlier. One example is shown in Figure 2, others being given and discussed in reference 20. In Figure 2 the measurement is compared with an S_n calculation (P_3S_8) using the ENDF/BIV data set. We see firstly that the positions of the resonances in Li and F at 110 and 250 keV are accurately reproduced, but that there are some amplitude and shape differences. We believe that the experimental spectrum could be in error because the allowance for high energy neutron response did not include the charged particle reactions mentioned earlier. However, it is also

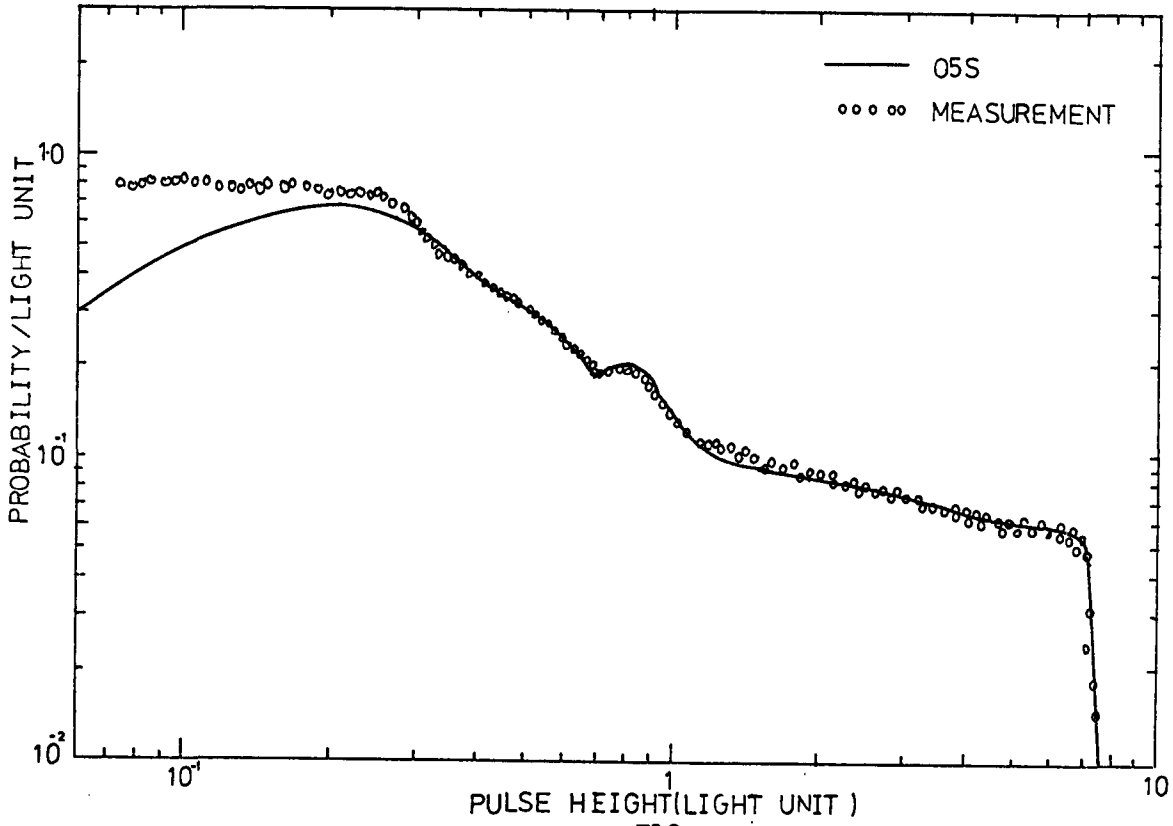

FIG. 1

COMPARISON OF PREDICTION (via O5S with the final madifications) AND MEASUREMENT OF A 14.3MeV RESPONSE FUNCTION

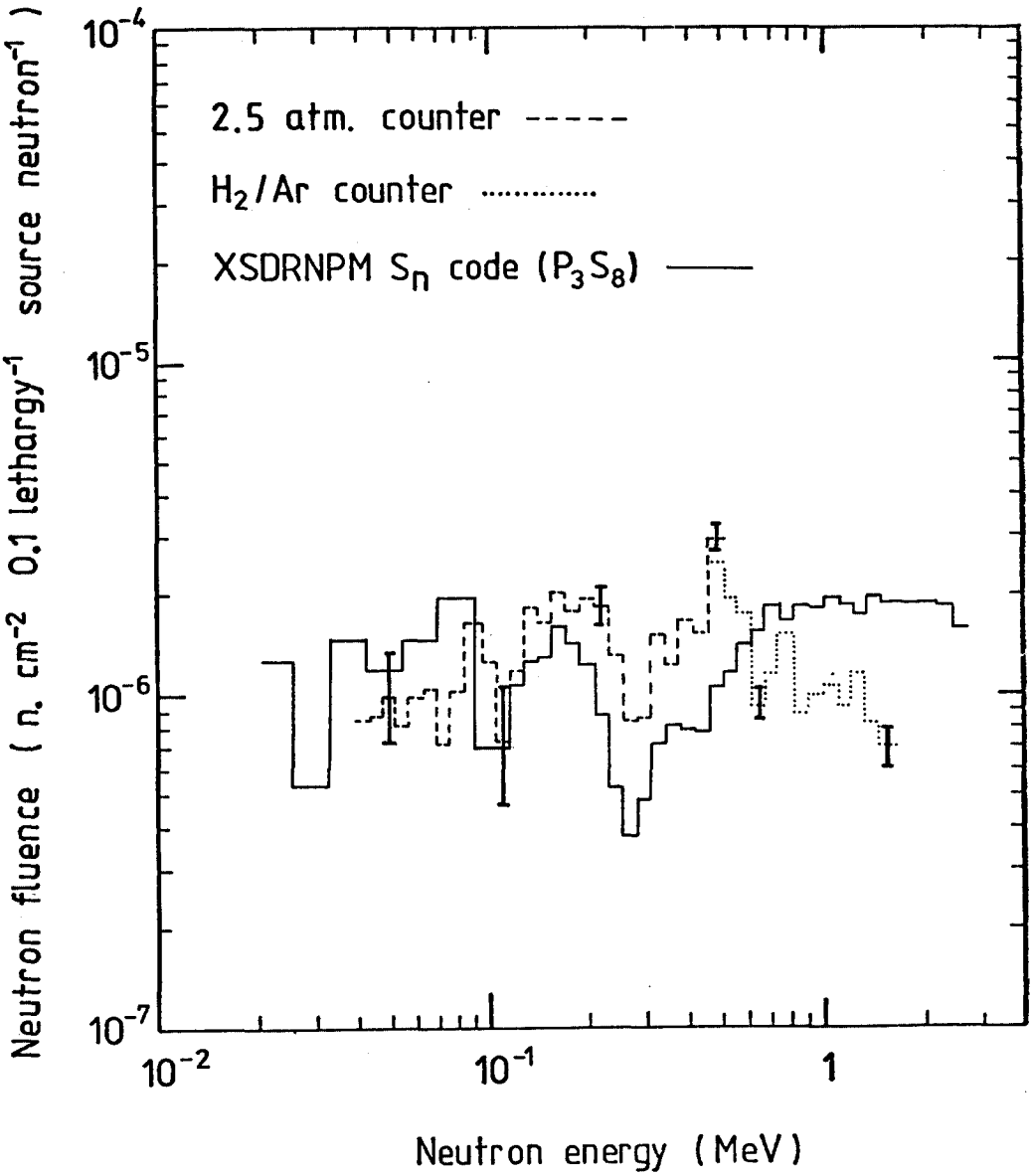

FIG. 2

PROPORTIONAL COUNTER MEASUREMENT OF NEUTRON SPECTRUM IN THE LiF ASSEMBLY AT (Θ=75, r=45.3cm).

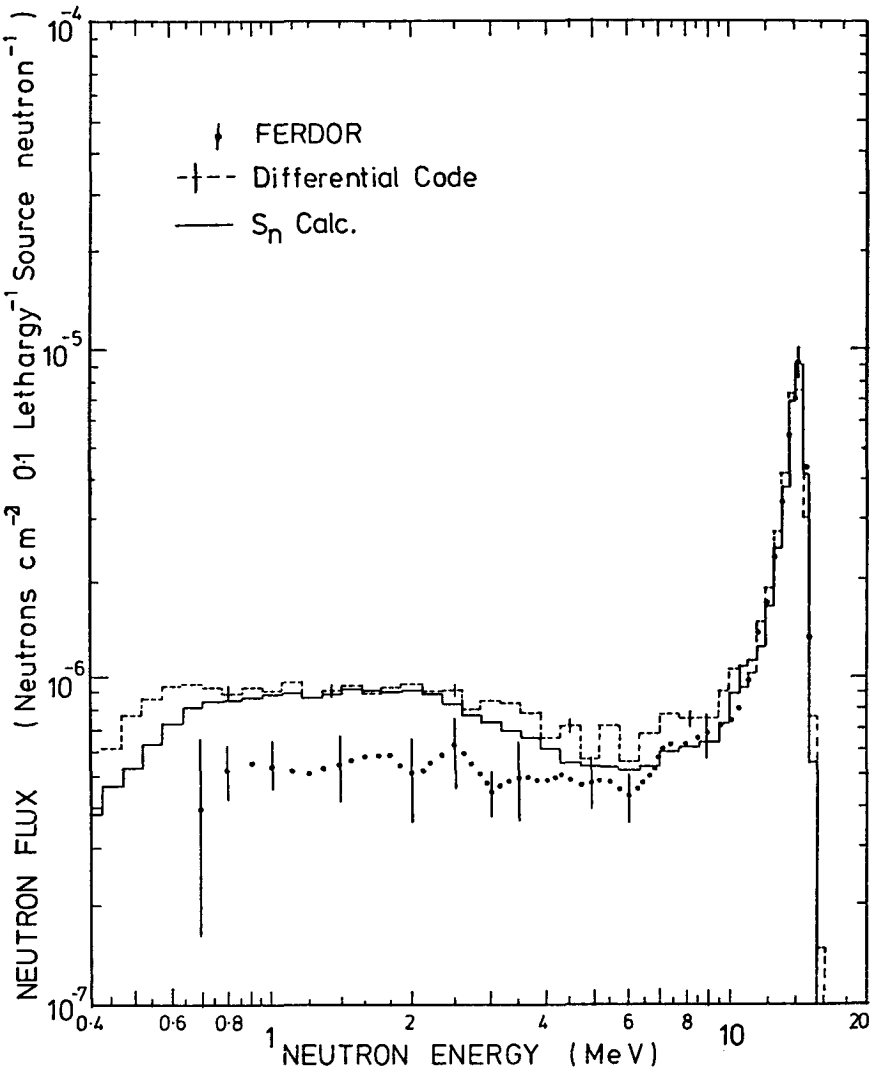

FIG. 3

SCINTILLATION COUNTER MEASUREMENT OF NEUTRON SPECTRUM IN THE LiF ASSEMBLY AT (θ = 75°, r = 55.3 cm)

likely that some of the difference is genuine, in that the lower experimental fluxes at higher energies tie in with scintillation counter measurements unfolded using FERDOR.

(b) NE213 proton recoil scintillator

For scintillator measurements on the LiF sphere mentioned above, the differential unfolding code discussed earlier was used, comparisons being made with an S_n calculation (P_7S_{16}). The ENDF/BIV data used was averaged over 0.1 lethargy steps up to 10 MeV, and over 0.5 MeV steps up to 16 MeV, so as to model the source region with an accuracy slightly better than that of the detector resolution. Again, full details of the measurements, calculations and treatment of the source anisotropy are given in reference 20.

One example is shown in Figure 3, where we see that there is excellent agreement between calculation and the differential unfolding over the source region and down to 10 MeV, but that the measurement is flatter than the calculation from there down to 0.5 MeV.

Without an alternative unfolding method against which to compare, this seemed a satisfactory result: clearly since the object of these experiments is to provide a basis for possible data adjustment - and since the fluorine cross sections, in particular, are not well known - we did not know a priori what to expect. However, we have recently implemented the FERDOR code, so reanalysed the data: the result is also shown on Figure 3. We see that whilst the excellent agreement down to 10 MeV is maintained, below this energy the FERDOR results are very different indeed. In fact, at the corresponding position in the sphere the FERDOR results are in agreement with those from the proportional counter in the region from 1 - 2.5 MeV. In as much as use of the two unfolding codes on standard spectra (^{252}Cf and Am-Be) did not reveal any significant differences (and were the basis of our confidence in the differential unfolding code) we had difficulty in reconciling these two situations.

In an attempt to determine the reasons for the differences we then re-unfolded some earlier 14 MeV response function measurements *[19]*. Using FERDOR, the spectrum peaked around 14 MeV, falling to zero at lower energies and oscillated around zero down to the lower limit of the detector: such behaviour has been observed by other workers (see, for example, reference 12). With the differential unfolding code, however, the unfolded spectrum fell away rapidly below 14 MeV but did not fall to zero. Although the non-zero fluxes were small (being about 1% of that in the main peak) they were significant, showing small peaks at ∿8 MeV and a broad one round 2 MeV. Clearly, for neutron spectra where there are no dominant high energy peak this would not matter, but in our integral assemblies the fluxes below the main peak are between one and two orders of magnitude lower than is the peak, and the effect is therefore important.

We believe that the reasons for this effect with our differential code are two fold. The first is the possibility that the alpha-stripping may have produced a distortion. However, we think this less likely than the fact that both wall effect protons and multiply scattered neutrons are not corrected for at lower energies. Thus, examination of our two parameter surface shows a significant number of particles lying between the main proton and electron ridges. We believe these to be protons terminating in the walls whose pulse shape characteristics would therefore move to that of an electron, since the high dE/dx part of the track would be in the glass. If this is the case, then subtracting these from the measured response would provide the necessary correction to the data. However, whilst we shall examine this to increase our understanding

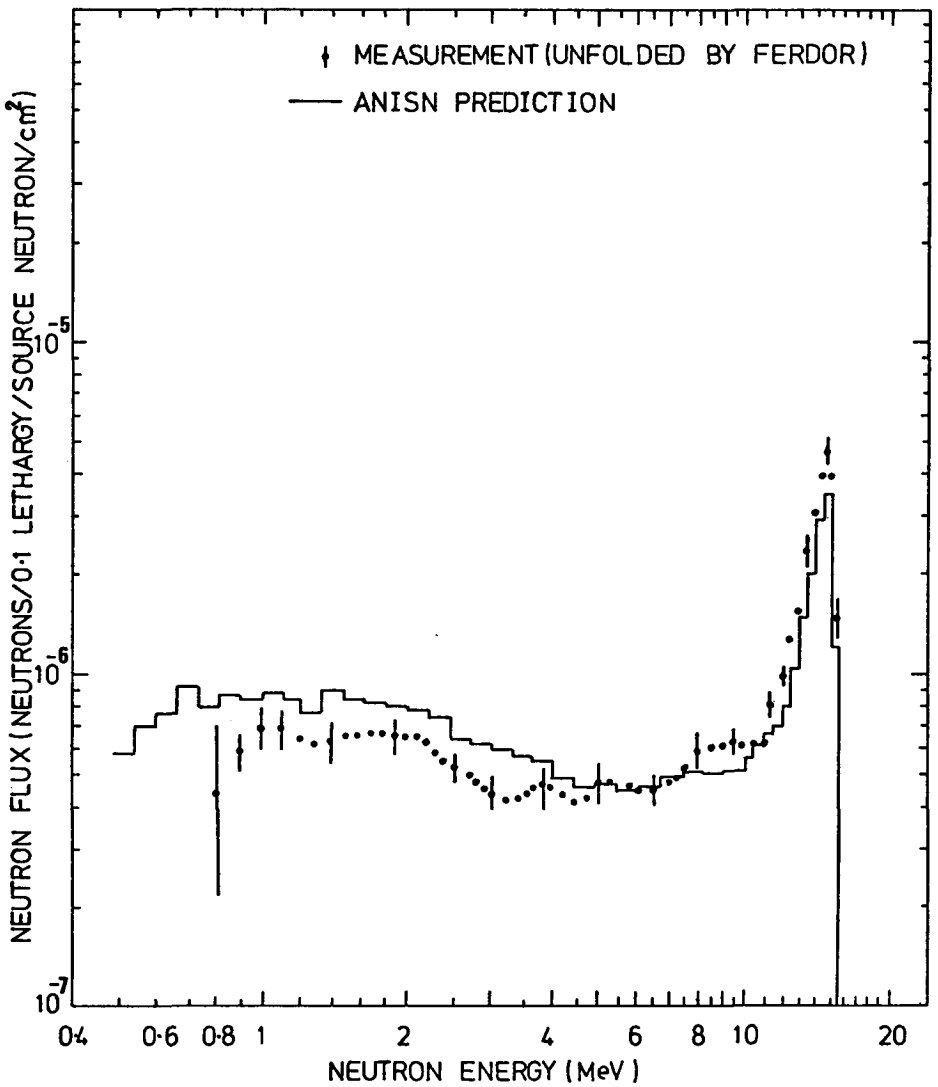

FIG. 4

NEUTRON FLUX IN THE ASSEMBLY AT (r=55.3cm, $\Theta=0^{\circ}$) FOR t=9.65cm

of the physics, in particular to provide a possible cross check on calculations of wall effect, the data processing then required to use differential codes in situations like this would probably further limit their usefulness.

We also note that, because we have had to derive response function data for FERDOR for energies other than 14.3 MeV from adjustments made at that point, we cannot exclude the possibility that errors in these response functions may be producing some of the differences between measurement and calculation noted.

Finally, Figure 4 shows comparison of measurement (using FERDOR) and calculation for the same LiF assembly at a similar position but with a 9.65 cm thick shell of beryllium metal round the target. Here the agreement over the source peak is not so good, but elsewhere the general features of the comparison are similar. We note, however, that the discrepancy in the source region with Be present also shows itself in transmission measurements through bare Be shells, most probably demonstrating the inadequacy of the Be data. More generally, the effect of the beryllium in softening and broadening the spectrum around the source peak can be seen by comparing Figures 3 and 4.

ACKNOWLEDGEMENTS

This work forms part of a fusion reactor neutronics programme funded by the S.R.C., London. This support is acknowledged with gratitude, as is the personal support for two of us (N.E. and L.J.P.). The support of the Iranian Ministry of Science and the University of Ferdosy for R.K-F. is similarly acknowledged. Finally we would like to thank members of the Neutron Physics Group and the staff of the Birmingham Radiation Centre for their invaluable assistance.

REFERENCES

1. Evans, N., Brearley, I.R. and Scott, Malcolm C. : Nucl. Instr. Meth. 160 465 (1979).

2. Fewell, T.R. : Nucl. Instr. Meth. 61 61 (1968).

3. Hertel, N.E. and Wehring, B.W. : Nucl. Instr. Meth. 172 501 (1980).

4. Gaiser, J.E., Harper, R.C., Warren, W.H. and Alford, W.L. : Nucl. Instr. Meth. (1980) in press.

5. Gaiser, J.E. : Private Communication, 1980.

6. Benjamin, P.W., Kemshall, C.D. and Redfearn, J. : Nucl. Instr. Meth. 59 77 (1968).

7. Bore, A. : Ph.D. Thesis, University of Birmingham (1973) "The Development of Proton Recoil Spectrometers for the Measurement of Neutron Slowing Down Spectra in a Lithium Fluoride Assembly".

8. Brearley, I.R. : Ph.D. Thesis, University of Birmingham (1977) "The Calibration of Recoil Proton Proportional Spectrometers and the Measurement of Neutron Slowing Down Spectra in a LiF Assembly".

9. Bennett, E.F. : Rev. Sc. Instr. 33 1153 (1962).

10. Carter, M.D. : Private Communication, 1974.

11. Verbinski, V.V. and Giovannini, R. : Nucl. Instr. Meth. 114 205 (1974).

12. Benjamin, P.W., Kemshall, C.D. and Brickstock, A. : AWRE 09/68 (1968) "The Analysis of Recoil Proton Data".

13. Perkins, L.J. and Scott, Malcolm C. : Nucl. Instr. Meth. 166 451 (1979).

14. Toms, M.E. : Nucl. Instr. Meth. 92 61 (1971).

15. Broek, H.W. and Anderson, C.E. : Rev. Sc. Instr. 31 1063 (1960).

16. Burrus, W.R. : ORNL-3742, Oak Ridge National Laboratory (1964).

17. Textor, R.R. and Verbinski, V.V. : ORNL-4160, Oak Ridge National Laboratory (1968).

18. Verbinski, V.V., Burrus, W.R., Love, T.A., Zobel, W., Hill, N.N. and Textor, R. : Nucl. Instr. Meth. 65 8 (1968).

19. Koohi-Fayegh, R. : Ph.D. Thesis, University of Birmingham (1980) "Neutron Spectrum Measurements in a Be-LiF Assembly using an NE213 Scintillator".

20. Perkins, L.J., Evans, N., Koohi-Fayegh, R., Scott, Malcolm C. and Underwood, B.Y., Nucl. Sc. Eng. (in press).

21. Johnson, R.H., Ingersoll, D.T., Wehring, B.W. and Dorning, J.J.: Nucl. Instr. Meth. 145 337 (1977).

A P P E N D I X

SOME COMMENTS ON THE UTILITY OF MEASURING NEUTRON SPECTRA IN THE CONTEXT OF DATA ADJUSTMENT

Neutron spectra are measured for a variety of reasons. One is because the spectrum is needed for a related calculation, e.g. a reaction rate in a material in which it would be difficult to make a direct measurement. A second is because one can than make direct comparisons with other measurements - for example in an area of energy overlap between two different spectrometers - whilst a third is simply that one can easily relate features in the spectrum to physical parameters of interest, e.g. resonances.

However, when considered in the context of data adjustment, one becomes concerned that the careful analysis which goes into determining the regions of the neutron spectrum sensitive to a cross section parameter of interest may be nullified by a spectrum measurement of the kind described in this paper. This is simply because the unfolding process itself introduces correlated errors which may be large and which are, in many cases, difficult, or impossible, to quantify. Thus the measurement sensitivity profile may be totally different from what is required, and may be (and generally is) unknown.

If, on the other hand, any date adjustments are made with respect to the measured spectrometer response, then the experimental correlations (giving rise to experimental covariance terms) are minimised. Of course, some correlated errors will certainly be introduced through the calculated detector response used in any adjustment, but these effects are much more accessible to analysis and quantification. It does not matter, in this respect, whether the energy dependence of the spectrometer's response functions is calculated or measured.

Thus, whilst the measurement of neutron spectra per se is likely to remain a real challenge to experimentalists, and whilst it undoubtedly has a place and a value, one would suggest that any data adjustment procedures based on integral measurements should be related to the basic, non-unfolded, spectrometer responses.

SESSION V

ANALYTICAL TECHNIQUES

Chairman - Président

A. GANDINI

(Italy)

SEANCE V

TECHNIQUES ANALYTIQUES

SUMMARY OF THE SESSION V

RESUME DE LA SEANCE V

Analytical Techniques

Prof. A. Gandini

The effort on adjustment techniques, as presented at this session may be classified within three areas :

1. Adjustment method development. In this area of special interest appear the global detector technique (Matthes) and the Monte Carlo-based methods (McCracken and Hall). Both these approaches are useful for coping with the difficulties so far encountered for effectively exploiting the large amount of integral information available from the ASPIS, or similar, deep penetration experiments. Both methods use an iterative scheme to reach convergence. Some difficulties have been experienced with respect to the simplifying assumption concerning the adjusted dispersion matrix in the global detector technique, and with regard to the noise introduced by the Monte Carlo method in the sensitivities evaluation. This latter method, however, seems to have the potential advantage of allowing the calculation of the sensitivities, so that an adjustment procedure can be made with respect to the very basic nuclear parameters (consistent method) rather than with respect to the average group cross-sections.

2. Adjustment exercises. Different contributions were presented by the British (McCracken, Hall) and French (Estiot) representatives, relevant to the ASPIS (Fe) and HARMONY/TAPIRO (Na) benchmark experiments, respectively. The former contribution shows a fairly good agreement (i.e. within the statistics) between the results obtained by adopting two different algorithms, based on Monte Carlo and discrete ordinates methods. The second contribution shows an extensive analysis of the influence of the choice of the various parameters (data, errors, etc.) into the adjustment procedure. Many issues such as a priori variances and covariances associated with the cross sections, the acceptable limits of the chi-square values (to be adopted to discriminate against "incompatible" integral data), the calculational method and other systematic errors, still seem to require further investigation.

3. Project-oriented studies. An Italian-French contribution (Palmiotti, Salvatores) showed an effective example of how to apply sensitivity techniques :

a) to optimize integral experiments in view of specified, project-oriented responses;

b) to gain confidence in transposing, via calculated coefficients, or via data adjustment techniques, experimental data (as in propagation experiments in Na/Fe blocks in TAPIRO and HARMONY reactors) to project design.

AN ITERATIVE MULTIGROUP CROSS-SECTION ADJUSTMENT PROCEDURE

W. Matthes
Joint Research Center
Ispra(Va),Italy

ABSTRACT

The method of "Least Squares" was programmed to adjust cross sections in the analysis of Benchmark experiments. To test the efficiency and reliability of this method computer-simulated(Benchmark -)experiments are investigated.

A) Theory

We use the straightforward least-square method for the adjustment. The notation employed is this:

x is the vector of experimentally measured values with error-covariance matrix D.

g = g(p) is the vector of calculated values using the parameter-set p.

p is the vector of parameters to be adjusted (cross-sections, absolute source-strength, source-spectrum, instrument normalization factors etc.) with error-covariance matrix p. y is an initially given approximate parameter set with error matrix C.

We try to adjust p such that

$$Q = (x-g)^T D^{-1}(x-g) + (y-p)^T C^{-1}(y-p) \qquad (1)$$

becomes a minimum.

The standard procedure for solving (1) consists in developing g(p) around an approximate solution b(which can be taken to be y).

The solution for the minimum problem is then:

$$b^* = b + P \left\{ S^T(b)\, D^{-1}(x-g(b)) + C^{-1}(y-b) \right\} \qquad (2)$$

$$P = (C^{-1} + S^T D^{-1} S)^{-1} = C - CS^T(D + SCS^T)^{-1} SC = C - KSC \qquad (3)$$

where P is simultaneously the error covariance matrix of the adjusted data and $S(=\frac{\partial g}{\partial p})$ is the sensitivity matrix.

Equation (2) can now be used as an iterative procedure (put b* for b back into the right side and calculate a new b*) until /b*-b/ fulfills a certain convergence criteria.
We form two iteration schemes from (2). For the first iteration scheme we use (3) in (2) and obtain the usual

1) Newton Iteration

$$b^* = y + K(b) \left\{ e(b) - S(b)\,(y-b) \right\} \qquad (4)$$

$$P = C - KSC$$

$$e = x - g$$

In case the total set of measurements $x = \{ x_i \}$ is made up of a set of uncorrelated measurements, these measurements can successively be added to update the parameter set.

This iteration procedure has the advantage that a proof of convergence exists (for a good enough starting point b) and the disadvantage that it is restricted to a very small number of measurements as (at least for our purpose) the calculation of S is the most time consuming part.

To arrive at the second iteration scheme we transform the first term in the bracket of (2) into a sensitivity vector for only one measurement with a "global detector".

We put:

$$S^T D^{-1} e = \frac{\partial R}{\partial p}, \qquad R = g^T D^{-1} e \tag{5}$$

and consider p in e as constant.

Now we make the assumption, that the error-covariance matrix P for the adjusted data does not differ much from the error-covariance matrix C for the original data, i.e. we put:

$$P \approx C \tag{6}$$

and obtain from (2) the

2) Global Detector Iteration

$$b^* = y + C \frac{\partial R}{\partial p} \tag{7}$$

with C as the (approximate) error-covariance matrix for the adjusted data.

This iteration procedure has the advantage that a Sensitivity vector has to be calculated for one measurement only performed with the "global detector distribution" but the disadvantage, that nothing is known about the effect of the approximation (6) on the convergence properties of (7).

If several independent benchmark-experiments have to be analyzed simultaneously, then R splits into:

$$R = \sum_L R^{(L)} \tag{8}$$

where for each benchmark experiment $R^{(L)}$ has the form (5).
The explicit expression for the calculated values (counting rates) is:

$$g_i = \sum_{jm} \Phi(j,m)\, T^{(n)}(k/jm) \tag{9}$$

the index i splits in two: $i = (k,n)$, where

n : identifies the measurement

k : channel number

$\phi(j,m)$: flux in group j in spatial intervall m

$T^{(n)}(k/jm)$: response matrix for the (multi-channel) instrument used in measurement n.

Using (5) we have for one benchmark experiment:

$$R = \sum_{j,m} \phi(j,m) * R(j,m) \tag{10}$$

with the "Global Detector Distribution";

$$R(j,m) = \sum_{\substack{kk' \\ nn'}} T^{(n)}(k/jm)\, D^{-1}_{kk'}\, (n,n')\, e_{k'}(n') \tag{11}$$

B) Application to cross-section adjustment

The foregoing theory is applied to cross-section adjustment as follows.

The total set of possible parameters p to be adjusted is made up of:

a) the cross sections $\left\{\sigma_T, \sigma_A, \sigma_I, \sigma_E, \sigma_S, \sigma_N\right\}$

- T : Total
- A : Absorption
- I : Inelastic Scattering
- E : Elastic Scattering
- S : Total Scattering
- N : Non-elastic

b) the normalization factors $f = \left\{f_1 f_2 \ldots f_{NI}\right\}$ for the instruments used in the measurement

c) the absolute source-strength's $Q = \left\{Q_1 Q_2 \ldots Q_{NB}\right\}$ of the sources used in the individual benchmark experiments.

Therefore

$$p = \left\{\sigma_T, \sigma_A, \sigma_I, \sigma_E, \sigma_S, \sigma_N, f, Q\right\} = \left\{\sigma, f, Q\right\}$$

and the length of the vector p is

$$NP = 6^{*} NG + NI + NB \qquad (12)$$

where:

NG = Number of (energy -) groups
NI = Number of instruments used
NB = Number of Benchmark experiments

Before our actual application we decide which of the cross-section types are to be adjusted in which groups (in the remaining groups the cross section remain unchanged).

After adjusting (a part of) the cross-sections the other cross sections are recalculated accordingly as to satisfy the relations:

$$\begin{aligned} \sigma_T &= \sigma_A + \sigma_S = \sigma_E + \sigma_N \\ \sigma_S &= \sigma_I + \sigma_E \\ \sigma_N &= \sigma_A + \sigma_I \end{aligned} \qquad (13)$$

For completeness we mention briefly how to evaluate the sensitivity coefficients:

$$S = \frac{\partial X}{\partial p}$$

where X is a measured value and represents:

a) an actually measured counting rate in the "Newton Iteration" and
b) the counting rate of the global detector in the "Global Detector Iteration"

As $p = \{\sigma, f, Q\}$ we have similarly

$$S = \frac{\partial X}{\partial p} = \left\{\frac{\partial X}{\partial \sigma}, \frac{\partial X}{\partial f}, \frac{\partial X}{\partial Q}\right\} = \{S_\sigma, S_f, S_Q\} \qquad (14)$$

Calculation of S

The measured value X is (in our situation) given by an expression of the general form (9).

The standard procedure consists in

1) Calculating the(forward) flux Ø with the code ANISN (Q is the neutron source producing Ø). Knowing Ø we can calculate X.

2) Using the "Detector distribution $T^{(n)}(k/jm)$ as an "Adjoint Source Q^+" in the "ANISN-ADJOINT option" gives the adjoint flux $Ø^+$.

3) Ø and $Ø^+$ together fed as input to the code SWANLAKE gives finally

$$S_\sigma = \frac{\partial X}{\partial \sigma}; \tag{15}$$

Calculation of S_f and S_Q

We write X more explicitly in the form:

$$X = \sum_{njm} Q^{(n)} * f^{(n)} * \varphi^{(n)}(jm) * t^{(n)}(jm) \tag{16}$$

$$= \sum_{n} Q^{(n)} * f^{(n)} * x^{(n)}$$

where:

$Q^{(n)}$: absolute source strength Q used in experiment n

$f^{(n)}$: normalization factor for the instrument I used in experiment n (T = f . t)

$\varphi^{(n)}(jm)$: flux in group j and spatial interval m in experiment n for a unit source (Ø = Q * φ).

Then we have:

$$\frac{\partial X}{\partial f_J} = \sum_{n} Q^{(n)} \delta_{JI(n)} x^{(n)} = \sum_{\substack{\text{over all } l \\ \text{where } J \text{ is used}}} Q^{(l)} x^{(l)} \tag{17}$$

$$\frac{\partial \underset{\sim}{X}}{\partial Q_K} = \sum_{\sim} \int_{KL(n)} f^{(n)}\, x^{(n)} = \sum_{\text{over all } l \text{ in Bench.Exp.K}} f^{(l)}\, x^{(l)} \qquad (18)$$

Note that the index n specifying each measurement splits into two indices (L,l) where

L runs over all Benchmark experiments

l runs over all measurements in one Benchmark experiment.

c) Test of the method

To test the efficiency of the method we simulate an experiment. "Measured"- values (provided with errors) are created using changed cross-sections (and artificial detectors). The programme has to find out which cross-sections are changed in which groups and by how much.

The experimental set-up which is simulated and the response function of the (18 channel) instrument used are sketched in Fig. 1. We use a 60 group cross-section library for the ANISN - and SWANLAKE - calculations in group-independent form.
An example is given to illustrate the type of calculations we made for getting experience about the reliability of the method.

Example (Newton-method):

a) To generate measured values 'x', σ_T was increased by 30% in groups 20→30 (increasing all partial cross-sections correspondingly)

b) The error-covariance matrix of σ_T was chosen to be diagonal with 5% for groups 1→19, 100% for groups 20→30 and 5% for groups 31→60.

c) σ^2_{xx} was taken to be 1% in each channel.

d) σ_T only was chosen for adjustment in groups 1→40.

Fig. 2 shows the result of the adjustment process.

The programme actually adjusted σ_T in groups 20→30 only. No adjustments were indicated for groups not in this range.
After two iterations the adjustments settled to a stable configuration in the sense that in further iterations the adjustment showed very small fluctuations around this configuration. The measured value x is reproduced almost exactly by the final adjusted cross-sections.

Another calculation where the error of σ_T in groups 20→30 was changed from 100% to 10% made the programme to give small adjustments to groups out of the range 20→30 (the bulk of the adjustments however was still in this range).
The procedure therefore adjusts preferably those parameters about which little is known (which have large errors) and only those parameters (with large errors) should be included in the parameter set to be adjusted.

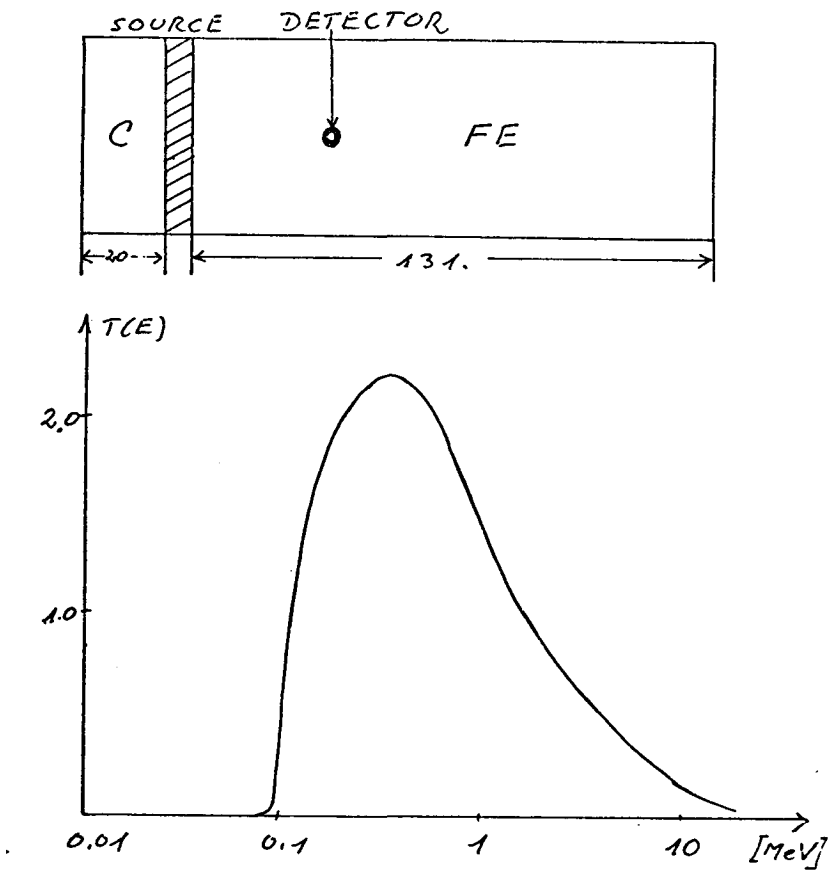

Fig. 1 - Experimental set-up simulated and Response function of the (18 channel-) instrument used.

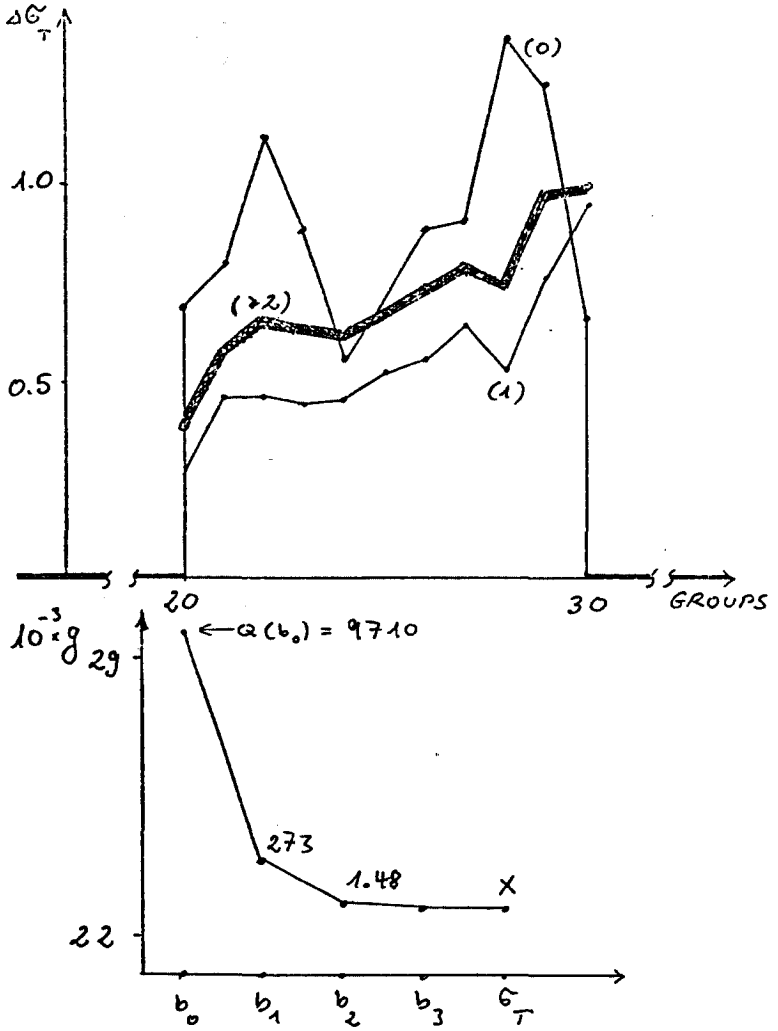

Fig. 2 - Result of an adjustment calculation (see text for conditions) $\Delta \sigma_T = \sigma_T$ (adjusted) - σ_T (initial)

(0) : correct cross-section change

(1) : adjustment after 1-iteration

(2) : adjustment after 2-iteration

All further iterations lead to small fluctuations around (2)

The measured value x was reproduced by the calculated value g almost exactly after the third iteration.

ANALYSIS OF THE WINFRITH IRON BENCHMARK EXPERIMENT WITH DUCKPOND AND COMPARISON WITH THE ANISN/SWANLAKE ANALYSIS

by

A K McCracken
M C G Hall*

Radiation Physics and Shielding Group
Reactor Physics Division
AEE Winfrith

* Work performed during author's attachment to Radiation Physics and Shielding Group, Reactor Physics Division, AEE Winfrith.

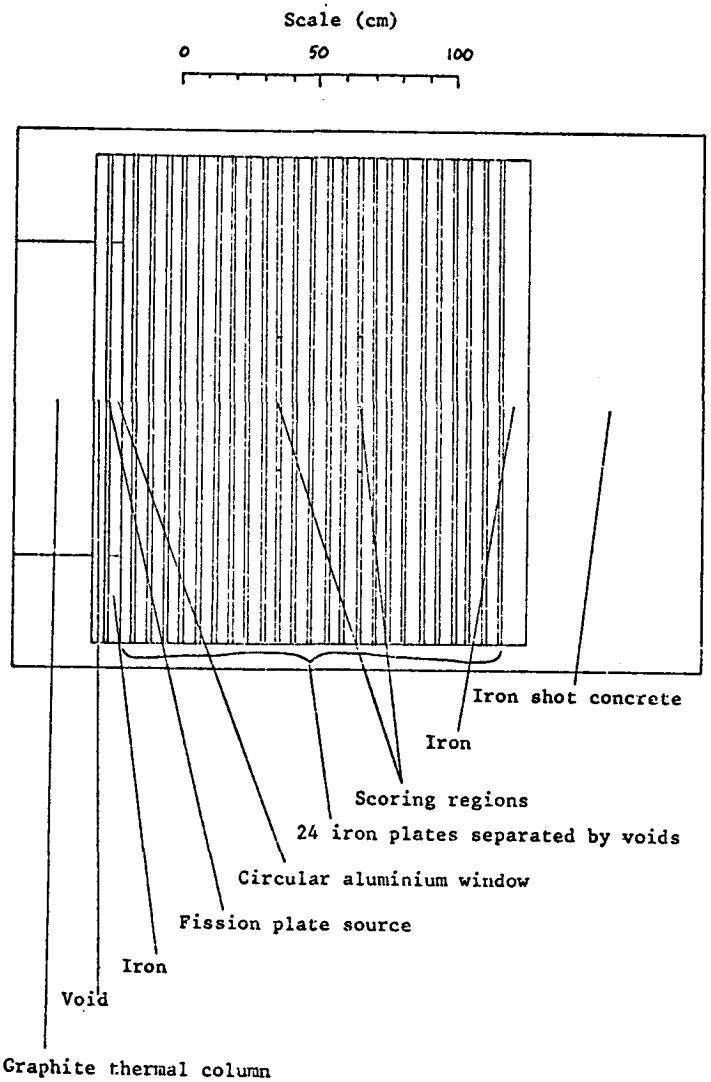

Figure 1 The configuration of the Winfrith Iron Benchmark. This is both a plan and an elevation of the geometric model.

1 Introduction

The program DUCKPOND for finding sensitivity coefficients by Monte Carlo calculation is described in outline in another paper[1] given at this meeting. Strategies for the use of such sensitivity coefficients in conjunction with benchmark experiments to derive adjusted nuclear cross-sections by linear perturbation methods are considered in a further paper[2] at this meeting. A detailed discussion of DUCKPOND, its application to uncertainty analysis and data adjustment and potential developments is given by Hall[3] in a paper which describes in detail the results of the adjustment of iron cross-sections on the basis of the Winfrith iron benchmark experiment[4][5].

Methods of calculation and the iron benchmark experiment description are fully detailed in the above references from which this paper draws freely. A mere outline of the experiment and a verbal commentary on the methods is given here; a critical comparison of the adjustments to the iron cross-sections achieved by two very different methods is the purpose of this paper.

2 The Experiment

The configuration of the Winfrith iron benchmark experiment is shown schematically in Figure 1 which is both a plan and an elevation. Neutron source strengths available from the natural uranium fission-plate ranged up to a maximum of approximately 5 x 10" per second at the (then) maximum NESTOR operating power of 10 KW. Extensive measurements with hydrogen-filled proportional counters and a small ($\sim$3 cm^3) NE213 organic liquid scintillator were made at iron penetration depths of 20.3 cm, 50.8 cm, 76.2 cm and 101.6 cm; in addition, at these and a few other positions, foil activation measurements, which included the reactions $^{103}Rh(n,n')^{103m}Rh$, $^{115}In(n,n')^{115m}In$, and $^{197}Au(n,\gamma)^{198}Au$ were made. The amount of experimental information received from the spectrometers was very much greater than that of the foil detectors which therefore had little influence on the ensuing analysis. The lower energy limit of useful measurement of the hydrogen-filled proportional counters was approximately 10 KeV and the upper energy limit achieved by the NE213 cell varied from (approximately) 2 MeV at 101.6 cm to 10 MeV at 50.8 cm. In the analyses which follow the standard deviation of the fission-plate output was taken as 5% and of the absolute calibration factors of the spectrometers as 10%. Statistical uncertainties on the counting-rates of spectrometers and foils were assumed to follow a Poisson distribution - in general the counting statistics were much smaller than uncertainties ascribed to other parameters in the adjusted process.

3 The Adjustments

3.1 ANISN/SWANLAKE Route

All calculations and perturbations were carried out in the 100-group energy structure of the EURLIB[6] library and each spectrometer signal in every measuring position - several hundred channels - was included in the analysis. Estimates of uncertainties on the iron cross-sections were taken from an early compilation of data by Schmidt[7]. No correlations between values of the same cross-section at different energies were available but correlations between different components of the total cross-section at a given energy could be deduced and were used in the analysis. The iron cross-sections used were those of

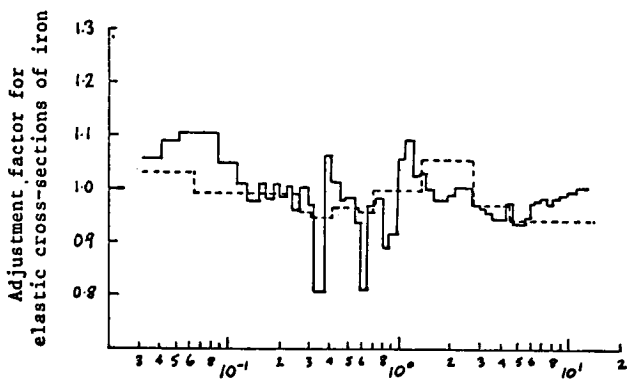

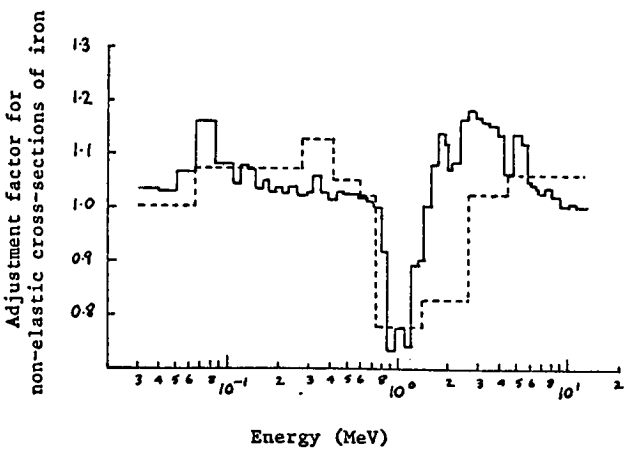

Figure 2. Comparison of adjustments obtained using Monte Carlo and discrete ordinates calculations. The continuous line represents the discrete ordinates analysis.

3 Cont'd

the UK Nuclear Data Library (File number 908A) processed with a $(\Sigma(E), E)^{-1}$ weighting by GALAXY[8]. SWANLAKE[9] is a one-dimensional sensitivity code which can only be used with the one-dimensional discrete ordinates code ANISN[10]; the results of forward and adjoint calculations by ANISN are the required input to SWANLAKE. Used in a conventional manner these codes could only find the sensitivities of cross-sections to a few detector responses, for a separate adjoint ANISN calculation is required for each detector response. In the PLATO analysis this problem was circumvented by introducing the concept of a single fictitious detector which could be used as a source in a single adjoint calculation. Some approximation is involved in the use of this concept and iteration is necessary. Also included in the analysis was an allowance for uncertainties in pulse-height spectra caused by possible changes in the energy-scale calibration of the spectrometers during measurement. The analysis is further complicated by the need to introduce a second fictitious detector for the generation of dispersion matrices of adjusted data. The results shown were achieved after four refinement iterations.

3.2 DUCKPOND Route

DUCKPOND, based on McBEND, is a point-energy Monte Carlo perturbation code. Calculations were carried out using UK Nuclear Data File 908 A for iron in 1000 DICE groups. Sensitivities were scored and iron cross-sections were adjusted in the 15-group scheme used by Drischler[11] and Weisbin for their covariance matrixes for iron cross-sections which were used in the analysis. No activation detector measurements were used in the analysis which used as experimental input 30 spectrometer count-rates at 50.8 cm and 76.2 cm; the sixty counting channels were included simultaneously in a single adjustment. The method lends itself to iterative refinement of adjustments but iteration has not been carried out on the results shown which were achieved after a run of 80 minutes on the Harwell IBM 3033. A run of 20 minutes was then carried out using the adjusted cross-sections to provide a comparison between the predictions of the original and the revised data.

3.3 The Results and Discussion

The adjustment factors derived for the elastic and non-elastic cross-sections of iron by the two methods are shown in Figure 2. For the elastic cross-sections the DUCKPOND cross-section correction factors vary only between 0.95 and 1.06 over the whole energy range 30 KeV to 15 MeV. Between approximately 120 KeV and 1.5 MeV the PLATO results are consistent with a more highly resolved version of the DUCKPOND results. There is some disagreement between 30 KeV to 120 KeV and 1.5 MeV to 2.5 MeV. Above 4.5 MeV an apparent slight disagreement between the two methods is not real. The flux is falling very rapidly with increasing energy and counting statistics are not good. The sensitivity of the PLATO fictitious detector tends to zero and regardless of the quality of the basic data correction factors will tend to unity in these circumstances. In the DUCKPOND analysis most of the sensitivity

3 Cont'd

coefficient is being scored at energies near 4.5 MeV and the whole of the broad group adjustment factor is governed by the requirements of the cross-section at this energy. Bearing in mind that each of the correction factors shown has an associated uncertainty of up to 5%, we can see that there is no fundamental disparity between the findings of the two methods - both agree that the elastic cross-sections are not in serious need of revision.

Consider now the absorption cross-section (ie, the non-elastic cross section below 860 KeV). Up to 70 KeV the methods agree within statistics and between 70 KeV and 300 KeV the PLATO results are an entirely credible high-resolution version of the DUCKPOND results. Between about 300 KeV and 600 KeV the DUCKPOND factors are higher than those given by PLATO but not significantly so for the standard deviations on the former are never less than 15%. The most significant feature of both analyses is the common agreement that near the threshold for inelastic scattering at 860 KeV the cross-section needs reduction by some 20% to 25%. Above 4.5 MeV the findings of both programs are consistent in the same way that the adjustment factors for elastic scattering are consistent in this energy range. Between 1.4 MeV and 4.5 MeV, however, there is marked disagreement between the non-elastic (essentially inelastic in this energy range) adjustment factors found by the two methods.

The theoretical minimum value of χ^2 per measurement (χ^2/N) for the DUCKPOND calculation based on an 80-minute Monte Carlo calculation and the covariance data used if 4.7. This contains a contribution from Monte Carlo statistics - (approximately) 10% per counting channel) and so, even with zero statistical uncertainty (χ^2/N) will be higher than the expected value of unity, but not distressingly so; it appears that some relaxation of the input covariance data is indicated. The DUCKPOND starting value of χ^2/N was 450 and this was reduced after one iteration to 73. At this stage the program output indicated that there was scope for further useful iteration before the process became masked by Monte Carlo noise. The starting value of χ^2/N for the PLATO calculations was 39.2 and this was reduced after four iterations to 8.7. In comparing values of χ^2/N for the two methods, it is important to remember that they are using considerably different input variance data and that the PLATO calculations contain no stochastic uncertainty. DUCKPOND appears to be converging much more rapidly than PLATO. The PLATO calculations may be over-resolved for the quality of the input variance data used. The low-amplitude oscillations seen in the elastic cross-section adjustment factors, near 200 KeV for example, would certainly be inhibited by deresolving or - what is a similar thing - by the inclusion of positive energy-dependent correlations for this cross-section. The large amplitude variations at 330 KeV and 600 KeV given by PLATO for the elastic adjustment factors, however, are very likely to be significant - they correspond closely with cross-section minima at these energies; this effect is missed by the coarse resolution used with DUCKPOND. The discrepancy in the inelastic adjustment factors between 1.4 MeV to 4.4 MeV is at present unexplained but further iteration used with DUCKPOND may (or may not) reduce the difference between the two methods.

3 cont'd

There is no doubt that DUCKPOND has important advantages over PLATO. These are:-

(i) With combinatorial geometry Monte Carlo accurate modelling of an experiment is relatively simple - with ANISN/SWANLAKE it is not.

(ii) Even with extended Monte Carlo computer runs DUCKPOND will be more economical in computer usage than PLATO.

(iii) A converged solution with DUCKPOND will contain no errors caused by approximations in the optimisation. PLATO makes some approximations, (reasonable ones, but nevertheless approximations), in its iterative procedure.

Successful use of DUCKPOND requires the achievement of relatively low Monte Carlo statistical uncertainties on the calculation of each signal which is to be included in the adjustment process and any advances in variance reduction techniques in the code will greatly increase its usefulness. We have not yet shown that we can economically deal with the massive amount of experimental information that was incorporated in a single PLATO unfolding.

Acknowledgement

The measurements used by PLATO and DUCKPOND were made by Mr M D Carter and Mr A Packwood.

References

1 Hall, M C G. DUCKPOND - A perturbation Monte Carlo and its applications. Paper 6, Session III of this meeting.

2 Hall, M C G, McCracken, A K. Adjustment of cross-sections with sensitivities given by Monte Carlo. Paper 3, Session V of this meeting.

3 Hall, M C G. Monte Carlo perturbation theory in neutron transport calculations. Thesis, Imperial College, London (1980).

4 Carter, M D, Packwood, A. The Winfrith benchmark experiment in iron - experimental results. Proc. IAEA/NEA Specialists' meeting on Sensitivity Studies and Shielding Benchmarks, Paris (1975).

5 Chestnutt, M M, McCracken, A K. A review of the Winfrith iron benchmark experiment. Paper 4, Session IV of this meeting.

6 The Eurlib Library, ESIS Newsletter 12 (1975).

7 Schmidt, J J. Neutron cross-sections for fast reactor materials. Part I. KFK-120 (1966).

8 Greenhouse, K G (editor). A users guide to GALAXY. AEEW - R697 (1969).

9 Bartine, D E et al. SWANLAKE, a computer code utilising ANISN radiation transport equations for cross-section sensitivity analysis. ORNL-TM-309 (1973).

10 Engle, W W. A users manual for ANISN, a one-dimensional discrete ordinates transport code with anisotropic scattering. K-1673 ORNL (1967).

11 Drischler, J D, Weisbin, C R. Compilation of multi-group cross-section covariance matrices for several important reactor materials. ORNL-5318 (1977).

ADJUSTMENT OF CROSS-SECTIONS WITH SENSITIVITIES GIVEN BY MONTE CARLO

by

M C G Hall*
A K McCracken

Radiation Physics and Shielding Group
Reactor Physics Division
AEE Winfrith

* Work performed during author's attachment from Imperial College, London

1 Introduction

The calculation $\underline{c}$ and the measurement $\underline{m}$ of a set of reaction-rates will be discrepant and in general neither will agree with the true value $\underline{\hat{c}}$ of these quantities. The error in the calculation can be written

$$\underline{\epsilon}_c = (\underline{\hat{c}} - \underline{c}) = \gamma_p\left(\frac{\underline{\epsilon}_p}{p}\right) + \gamma_q\left(\frac{\underline{\epsilon}_q}{q}\right) + \gamma_f\left(\frac{\underline{\epsilon}_f}{C}\right) + O\left(\left(\frac{\epsilon_p}{p}\right)^2, \left(\frac{\epsilon_q}{q}\right)^2\right) \qquad 1.$$

where $\underline{\epsilon}_p$ and $\underline{\epsilon}_q$ are respectively errors in the basic nuclear data $\underline{p}$ of the calculation and in other parameters $\underline{q}$ used in the calculation (source strength, detector responses etc). The method of calculation itself introduces an error $\underline{\epsilon}_f$. The sensitivity matrix γ_p with elements $Y_{ij} = \partial c_i/\partial p_j$ can be found by the use of sensitivity codes such as SWANLAKE used in conjunction with the discrete ordinates code ANISN[1] or by the perturbation Monte Carlo code DUCKPOND[2], and γ_q is easily constructed. Covariance matrices P, Q can be ascribed to the parameters $\underline{p}$ and $\underline{q}$ (although information required for the construction of P may not be easily available). In a multigroup discrete ordinates calculation $\underline{\epsilon}_f$ includes contributions from errors in modelling, in group-averaging of cross-sections and the implementation of the algorithm itself. Few people would be willing to ascribe a distribution to these errors; it is hoped, in practice, that $\underline{\epsilon}_f$ is small and it is ignored. In a point-energy Monte Carlo with a combinatorial geometry capability, the above sources of error do not arise - in this case $\underline{\epsilon}_f$ is simply the error caused by finite sampling in the Monte Carlo process, and its covariance matrix F is readily calculated by the code itself. The information available in $\underline{c}$, $\underline{m}$, the sensitivity matrices and the covariance matrices allows us to estimate the errors $\underline{\epsilon}_p$, $\underline{\epsilon}_q$ and $\underline{\epsilon}_f$ together with updated covariance matrices $\hat{P}$ and $\hat{Q}$ for $\underline{\hat{p}} = \underline{p} + \underline{\epsilon}_p$ and $\underline{\hat{q}} = \underline{q} + \underline{\epsilon}_q$. The quantities $\underline{\epsilon}_q$ and $\underline{\epsilon}_f$ are of purely local interest and clearly we require $(\underline{\epsilon}_q + \underline{\epsilon}_f) \ll \underline{\epsilon}_p$ in the analysis of a benchmark experiment if high quality information about the state of $\underline{p}$ is to be extracted. The derivation of $\underline{\hat{p}}$, $\underline{\hat{q}}$ and $\hat{P}$ and $\hat{Q}$ in the absence of Monte Carlo statistics is a straightforward unfolding problem using linear perturbation methods. The introduction of Monte Carlo statistics into the problem causes little extra difficulty in obtaining a solution but will influence the amount of refinement by iteration that can be achieved.

2 The Adjustment Method

For the simple case of two calculations, each of which is a function of two cross-sections p_1 and P_2, two other parameters q_1 and q_2, the expanded version of equation 1 to first order terms appears as:-

$$\begin{vmatrix} \epsilon_{c_1} \\ \epsilon_{c_2} \end{vmatrix} = \begin{bmatrix} p_1\frac{\partial c_1}{\partial p_1} & p_2\frac{\partial c_1}{\partial p_2} & q_1\frac{\partial c_1}{\partial q_1} & q_2\frac{\partial c_1}{\partial q_2} & C_1 & 0 \\ p_1\frac{\partial c_2}{\partial p_1} & p_2\frac{\partial c_2}{\partial p_2} & q_1\frac{\partial c_2}{\partial q_1} & q_2\frac{\partial c_2}{\partial q_2} & 0 & C_2 \end{bmatrix} \begin{vmatrix} \epsilon_{p_1}/p_1 \\ \epsilon_{p_2}/p_2 \\ \epsilon_{q_1}/q_1 \\ \epsilon_{q_2}/q_2 \\ \epsilon_{f_1}/C_1 \\ \epsilon_{f_2}/C_2 \end{vmatrix} \qquad 2.$$

The collection of Y_p, Y_q and Y_f into a single matrix Y and the collection of the fractional error vectors into a single vector $\left(\frac{\underline{\epsilon}_r}{\underline{r}}\right)$ illustrated above gives us

$$\underline{\epsilon}_c = Y\left(\frac{\underline{\epsilon}_r}{\underline{r}}\right) \qquad 3.$$

It is convenient to consider fractional errors for in the process of cross-section adjustment a correction factor can be applied to basic cross-sections within a given energy range without having to evaluate an average (ie, spectrally-dependent) cross-section within the range. Writing $\underline{z} = \log_e \underline{r}$ we arrive at a convenient working form of equation 1,

$$\underline{\epsilon}_c = Y\,\underline{\epsilon}_z \qquad 4.$$

The first partition of Y, ie Y_p is provided by a sensitivity code such as DUCKPOND. The second partition Y_q is supplied by the user; if, for example, q_1 represented a source strength used in the calculation of $\underline{c}$ the element $q_1 \partial c_i / \partial q_1$ is simply C_1 and ϵ_{q_1}/q_1 is ϵ_s/s . If method errors are ignored the sensitivity matrix is terminated after Y_q and components (ϵ_f/c) are excluded from the fractional error matrix $\left(\frac{\underline{\epsilon}_r}{\underline{r}}\right)$. For a Monte Carlo calculation, with quantifiable and non-negligible method errors caused by finite sampling, the elements of the diagonal Y_f matrix are simply the Monte Carlo calculations of the quantities which are to be compared with measurements. The covariance matrix Z of $\underline{z}$ is given by

$$Z = \langle \underline{\epsilon}_z \underline{\epsilon}_z^T \rangle \quad \text{where} \langle\ \rangle \text{ denotes expectation.}$$

Referring to equation 2 we see:

$$Z = \begin{bmatrix} \frac{\sigma^2(P_1)}{P_1^2} & \frac{\sigma^2(P_1P_2)}{P_1P_2} & \vdots & 0 & \vdots & 0 \\ \frac{\sigma^2(P_2P_1)}{P_2P_1} & \frac{\sigma^2(P_2)}{P_2^2} & \vdots & & \vdots & \\ \cdots & \cdots & \cdots & \cdots & \cdots & \cdots \\ & & \frac{\sigma^2(q_1)}{q_1^2} & \frac{\sigma^2(q_1q_2)}{q_1q_2} & & \\ 0 & & \frac{\sigma^2(q_2q_1)}{q_2q_1} & \frac{\sigma^2(q_2)}{q_2^2} & 0 & \\ \cdots & \cdots & \cdots & \cdots & \cdots & \cdots \\ & & & & \frac{\sigma^2(f_1)}{c_1^2} & \frac{\sigma^2(f_1f_2)}{c_1c_2} \\ 0 & & 0 & & \frac{\sigma^2(f_2f_1)}{c_2c_1} & \frac{\sigma^2(f_2)}{f_2^2} \end{bmatrix} \qquad 5.$$

The matrix Z is the fractional covariance matrix of the parameters $\underline{r}$ - (information is usually given in this form). The first partition of Z, the covariance of nuclear data, can be taken from the compilation of Drischler[3] and Weisbin. The second partition is supplied without difficulty by the user and the third partition (which is only present in a Monte Carlo analysis) must be scored by the Monte Carlo. In the final partition $\sigma^2(t_i)/C_i^2$ is to be understood to mean the fractional variance on the Monte Carlo calculation of C_p caused by Monte Carlo statistics only. The covariance matrix M of the measurements $\underline{m}$, is supplied by the experimenter. It will usually be given as a diagonal matrix - this may often be a reasonable approximation to make.

Having assembled all the above information, one can express the joint probability density of the measured variables $\underline{z}$ and $\underline{\underline{M}}$ by means of a multivariate normal:-

$$\frac{1}{2\pi\sqrt{|Z||M|}}\ \mathrm{Exp}\ -\frac{1}{2}\Big[\big(\underline{c}(\hat{\underline{z}})-\underline{m}\big)^{T}M^{-1}\big(\underline{c}(\hat{\underline{z}})-\underline{m}\big)+\big(\hat{\underline{z}}-\underline{z}\big)^{T}Z^{-1}\big(\hat{\underline{z}}-\underline{z}\big)\qquad 6.$$

where $\hat{\underline{z}} = \underline{z} + \underline{\epsilon}_z$ represents the true value of the parameters which we wish to estimate. According to the Maximum Likelihood Principle, this is achieved by choosing $\hat{z}$ to maximise equation 6, which is done by minimising

$$\chi^2 = \big(\underline{c}(\hat{\underline{z}})-\underline{m}\big)^{T}M^{-1}\big(\underline{c}(\hat{\underline{z}})-\underline{m}\big)+\big(\hat{\underline{z}}-\underline{z}\big)^{T}Z^{-1}\big(\hat{\underline{z}}-\underline{z}\big)\qquad 7.$$

Since $\underline{c}(\hat{\underline{z}}) = \underline{c}(\underline{z})+\underline{\epsilon}_c \simeq \underline{c}(\underline{z}) + Y\underline{\epsilon}_z$ from equation 4 we have

$$\chi^2 = \big(\underline{c}(\underline{z})-\underline{m}+Y\underline{\epsilon}_z\big)^{T}M^{-1}\big(\underline{c}(\underline{z})-\underline{m}+Y\underline{\epsilon}_z\big)+\underline{\epsilon}_z^{T}Z^{-1}\underline{\epsilon}_z\qquad 8.$$

This is most readily solved by noting that $\underline{\epsilon}_z^{T}Z^{-1}\underline{\epsilon}_z = \underline{\epsilon}_c^{T}C^{-1}\underline{\epsilon}_c$

where $C = \langle \underline{\epsilon}_c\underline{\epsilon}_c^{T}\rangle = YZY^{T}$

and writing

$$\chi^2 = \big(\underline{c}(\underline{z})-\underline{m}+\underline{\epsilon}_c\big)^{T}M^{-1}\big(\underline{c}(\underline{z})-\underline{m}+\underline{\epsilon}_c\big)+\underline{\epsilon}_c^{T}C^{-1}\underline{\epsilon}_c\qquad 9.$$

Differentiation with respect to $\underline{\epsilon}_c$ gives

$$M^{-1}\big(\underline{c}(\underline{z})-\underline{m}+\underline{\epsilon}_c\big)+C^{-1}\underline{\epsilon}_c = 0\qquad 10.$$

From which we find directly

$$\underline{\epsilon}_c = -\big(M^{-1}+C^{-1}\big)^{-1}M^{-1}\big(\underline{c}(\underline{z})-\underline{m}\big)$$

$$= -C\big(M+C\big)^{-1}\big(\underline{c}(\underline{z})-\underline{m}\big)\qquad 11$$

$\underline{\epsilon}_z$ is found directly by using $\underline{\epsilon}_c = Y\underline{\epsilon}_z$

and $C = YZY^{T}$ to get

$$\underline{\epsilon}_z = -ZY^{T}\big(C+M\big)^{-1}\big(\underline{c}(\underline{z})-\underline{m}\big)\qquad 12$$

We now have $\hat{\underline{z}} = \underline{z} - Z\gamma^T(C+M)^{-1}(\underline{c}(\underline{z}) - \underline{m})$ and can find its covariance matrix $\hat{Z} = \langle \delta\hat{\underline{z}}(\delta\hat{\underline{z}})^T \rangle$ to be after a little manipulation 13

$$\hat{Z} = Z - Z\gamma^T(C+M)^{-1}\gamma Z^T \qquad 14$$

Equations 13 and 14 represent the simplest solution to the problem of unfolding revised parameters (including nuclear data) in the presence of Monte Carlo noise - the treatment is an elementary extension of standard methods of linear estimation. This method, code-named PERTAK, used in conjunction with sensitivities given by DUCKPOND, was used to obtain cross-section adjustments from measurements made in the Winfrith Iron Benchmark Experiment.

A second adjustment algorithm called DUCK was then implemented. The adjustments given by DUCK and PERTAK agreed to the fourth significant figure; no iterative refinement was carried out in either case and the agreement simply suggests that both algorithms are doing the same thing and that both have been coded correctly. Both methods can seek refined adjustments by iteration, if this is necessary, and both should give the same answers at any stage. DUCK, however, can be used rather more efficiently in iteration than PERTAK. Before considering iteration and the DUCK algorithm, it is worth remarking that usually only in cases where cross-sections are very badly known will iteration be required. A good benchmark experiment will try to generate very large discrepancies between calculation and experiment. What matters for first order perturbation methods to be adequate is that the sensitivity of the calculation to the cross-section being adjusted shall be high; thus at 1 metre penetration in iron at about 2 MeV a discrepancy of a factor two between calculation and measurement of flux can be accounted for by a mere 10% change in inelastic cross-section at that energy.

If equation 7 is differentiated with respect to $\underline{z}$ we have

$$\gamma^T M^{-1}(\underline{c}(\hat{\underline{z}}) - \underline{m}) + Z^{-1}(\hat{\underline{z}} - \underline{z}) = \underline{h}(\hat{\underline{z}}), \text{ say} \qquad 15$$

and the ideal choice of $\hat{\underline{z}}$ is that for which $\underline{h}(\hat{\underline{z}}) = 0$. Perform a linear perturbation on equation 15 to get

$$\delta\underline{h}(\hat{\underline{z}}) = \gamma^T M^{-1}\gamma\,\delta\hat{\underline{z}} + Z^{-1}\delta\hat{\underline{z}} \qquad 16$$

Setting this equal to $-\underline{h}(\hat{\underline{z}})$ we have the iterative scheme

$$\hat{\underline{z}}_{n+1} = \hat{\underline{z}}_n - \left(\gamma_n^T M^{-1}\gamma_n + Z^{-1}\right)^{-1}\underline{h}(\hat{\underline{z}}_n) \qquad 17$$

where a sensible choice of $\hat{\underline{z}}_1$ would be given by equation 13. In the absence of Monte Carlo statistics this process can proceed indefinitely. Fairly quickly, however, we shall reach the situation where systematic reduction of $\underline{h}(\hat{\underline{z}})$ is inhibited by Monte Carlo statistics which will not reduce with every successive iteration. A procedure would be to inspect $\chi^2(\hat{\underline{z}}_n)$ for each value n and to stop iterating at the onset of noisy behaviour in these quantities. A more economical approach would enable one to see at each stage of the iteration the increasing dominance of Monte Carlo noise on the refinement process, thus saving at least one expensive and unnecessary Monte Carlo calculation. The DUCK algorithm achieves this simply and neatly by separation of the statistical uncertainty in a Monte Carlo calculation from the uncertainties of all the parameters used in the calculation. Referring to equation 1 where PERTAK collected three fractional error

terms into a single vector ($\underline{\epsilon_r/r}$) and transformed this into $\underline{\epsilon_z}$, DUCK collects only ($\underline{\epsilon_p/p}$) and ($\underline{\epsilon_q/q}$) and transforms these into, say, $\underline{\epsilon_v}$. Similarly only the first two sensitivity matrices Y_p and Y_q are compounded into a single sensitivity matrix U. A Monte Carlo calculation $\underline{c}(\underline{\bar{v}})$ using data $\underline{v}$ is regarded as a perfect (ie, zero statistic) calculation $\underline{f}(\underline{v})$ with an error due to Monte Carlo statistics $\underline{\epsilon_f}$

$$\underline{c}(\underline{v}) = \underline{f}(\underline{v}) + \underline{\epsilon_f} \qquad 18$$

From which we have

$$\underline{\epsilon_c} = U\,\underline{\epsilon_v} + \underline{\epsilon_f} \qquad 19$$

and $$\langle \underline{\epsilon_c}\,\underline{\epsilon_c}^T \rangle = C = UVU^T + F \qquad 20$$

where $U_{ij} = \partial f_i(\underline{v})/\partial v_j$ and where V, F and C are respectively the covariance matrices of data $\underline{v}$, the Monte Carlo statistics, and the calculations $\underline{c}$. By precisely the same process given in equations 8 to 11 we can find

$$\underline{\epsilon_c} = -C(M+C)^{-1}(\underline{c}(\underline{v}) - \underline{m}) \qquad 21$$

and $$\hat{\underline{c}} = \underline{c}(\underline{v}) + \underline{\epsilon_c} = \underline{c}(\underline{v}) - C(C+M)^{-1}(\underline{c}(\underline{v}) - \underline{m}) \qquad 22$$

$$= C(M+C)^{-1}\underline{m} + M(M+C)^{-1}\underline{c} \qquad 23$$

The minimum value of χ^2 with this value of $\hat{\underline{c}}$ is

$$\chi^2_{min} = (\underline{c}(\underline{v}) - \underline{m})^T (M+C)^{-1}(\underline{c}(\underline{v}) - \underline{m}) \qquad 24$$

The covariance matrix $\hat{C}$ of the adjusted calculation $\hat{\underline{c}}$ is

$$\hat{C} = C(M+C)^{-1}M \qquad 25$$

It is now desired to choose $\hat{\underline{v}} = \underline{v} + \underline{\epsilon_v}$ and $\underline{\epsilon_f} = \hat{\underline{c}} - \underline{f}(\hat{\underline{v}})$ to minimise

$$\chi^2(\hat{\underline{v}}) = (\hat{\underline{c}} - \underline{f}(\hat{\underline{v}}))^T F^{-1}(\hat{\underline{c}} - \underline{f}(\hat{\underline{v}})) + (\hat{\underline{v}} - \underline{v})^T V^{-1}(\hat{\underline{v}} - \underline{v}) \qquad 26.$$

Differentiation with respect to $\hat{\underline{v}}$ gives the requirement that

$$\underline{h}(\hat{\underline{v}}) = -U^T(\hat{\underline{v}})\,F^{-1}(\hat{\underline{v}})\,(\hat{\underline{c}} - \underline{f}(\hat{\underline{v}})) + V^{-1}(\hat{\underline{v}} - \underline{v}) \qquad 27$$

shall be zero. Setting $\delta\underline{h} = -\underline{h}$ as before we have

$$\delta\underline{h}(\hat{\underline{v}}) = U^T F^{-1} U\,\delta\hat{\underline{v}} + V^{-1}\delta\hat{\underline{v}} = -\underline{h}(\hat{\underline{v}}) \qquad 28$$

giving the iterative scheme

$$\hat{\underline{v}}_{n+1} = \hat{\underline{v}}_n - (U_n^T F_n^{-1} U_n + V^{-1})^{-1}\,\underline{h}_n \quad \text{or} \qquad 29$$

$$\hat{\underline{v}}_{n+1} = \hat{\underline{v}}_n - D_n^{-1}\,\underline{h}_n \quad \text{for brevity.} \qquad 30$$

It has already been mentioned that useful iteration will eventually be inhibited by the purely stochastic uncertainty in the calculation of $\underline{h}(\hat{\underline{v}})$ arising from errors ϵ_u and ϵ_f . The statistical error $\underline{\epsilon}_h$ is given by

$$\underline{\epsilon}_h = (\epsilon U^T) F^{-1} \left\{ \underline{\epsilon}_f + \underline{f}(\hat{\underline{v}}) - \hat{\underline{c}} \right\} + U^T F^{-1} \underline{\epsilon}_f \qquad 31$$

and if $\underline{f}(\hat{\underline{v}}) - \hat{\underline{c}} \sim \underline{\epsilon}_f$ and $(\epsilon U) \ll U$ this reduces to $\underline{\epsilon}_h \simeq U^T F^{-1} \underline{\epsilon}_f$ 32

The covariance matrix H of Monte Carlo statistics in $\underline{h}$ is therefore

$$H \simeq U^T F^{-1} U \qquad 33$$

This quantity is evaluated by DUCK and since $|h_i(\hat{\underline{v}}_n)|$ will not converge to a value less than $\sqrt{H_{ii}}$ a sensible criterion for ending iteration is that $|h_i(\hat{\underline{v}}_n)| \sim \sqrt{H_{ii}}$ for all i. Inspection of the ratios $|h_i(\hat{\underline{v}}_n)|/\sqrt{H_{ii}}$ after each iteration will give a good guide to the usefulness of further iterations. The covariance matrix $\hat{V}_n$ of $\hat{\underline{v}}_n$ after the n'th iteration can be found by perturbing $\underline{h}(\hat{\underline{v}}_n)$ thus

$$\underline{\epsilon}_h = (\epsilon U^T) F^{-1} \left\{ \underline{f}(\hat{\underline{v}}_n) - \hat{\underline{c}} + \underline{\epsilon}_f - \underline{\epsilon}\epsilon \right\} + U^T F^{-1} \left(\underline{\epsilon}_f - \underline{\epsilon}\hat{c} \right) + V^{-1} \underline{\epsilon}_v \qquad 34$$

If $\left(\underline{f}(\hat{\underline{v}}_n) - \hat{\underline{c}}\right) \simeq \underline{\epsilon}_f$ and $\epsilon U \ll U$ and $\underline{\epsilon}_c \ll \underline{\epsilon}_f$ then

$$D\, \underline{\epsilon}_{\hat{v}_n} \simeq U_N^T F_n^{-1} \underline{\epsilon}_f + V^{-1} \underline{\epsilon}_v \qquad 35$$

From which $\hat{V}_n = D_n^{-1}$

3 Conclusions

The inclusion of Monte Carlo statistics into a linear adjustment procedure poses little difficulty and two algorithms, PERTAK and DUCK, which do this have been discussed. Both have been applied to measurements in the Winfrith iron benchmark experiment in conjunction with the perturbation Monte Carlo code; results from both algorithms agreed very closely. Both methods can make use of iterative refinement, but DUCK gives an earlier indication of the point at which iteration should cease and this is the algorithm which has been included in DUCKPOND. Deep penetration measurements are those which focus attention sharply on defects in nuclear data but a rather large stochastic uncertainty is likely in the Monte Carlo prediction of such measurements. As the refinement of nuclear data is inhibited by Monte Carlo statistical uncertainties, we can see that a highly efficient variance reduction stategy is most desirable in Monte Carlo perturbation methods.

There seems little need to embrace the complications of higher order perturbation methods if the size of data adjustments gives rise to misgivings about the use of first order theory - refinement by iteration is simple.

References

1 Engle, W W
A users manual for ANISN, a one-dimensional discrete ordinates transport code with anisotropic scattering.
K-1673 Oak Ridge (1967)

2 Hall, M C G
Monte Carlo perturbation theory in neutron transport calculations. Thesis submitted for the degree of PhD, London University (1980)

3 Drischler, J D and Weisbin, C R
Compilation of multigroup cross-section covariance matrices for several important reactor materials.
ORNL - 5318, Oak Ridge, (1977)

UTILISATION D'EXPERIENCES INTEGRALES POUR LA REDUCTION DES INCERTITUDES AFFECTANT LES PARAMETRES PROJET DANS LES CALCULS DE PROTECTION

G. Palmiotti*, M. Salvatores**
*NIRA (Italie) **CEA/CEN/CADARACHE(France)

RESUME

Les résultats des expériences de propagation de neutrons, en particulier les écarts Calcul-Expérience et les ajustements des données de base effectués à partir de ces écarts, doivent être transposables aux paramètres et aux calculs de projet de protection. Ceci est vérifié dans le cas des protections "autour des sources" type SUPER-PHENIX 1, à l'aide d'une comparaison avec les réponses expérimentales mesurées sur HARMONIE et TAPIRO dans le cadre du programme CNEN/CEA. La même vérification est possible pour des solutions nouvelles de protection, à l'aide des résultats que fournira le programme JASON.

ABSTRACT

The results of the neutron propagation experiments, in particular the discrepancies between Calculation and Experiments and their related basic data adjustments, must be transposed to the shield design parameters and calculations. That is verified in the case of shields, type "around the source" as in the SUPER-PHENIX 1 reactor, by the means of a comparison with the experiments performed at HARMONIE and TAPIRO reactors in the framework of the CEA/CNEN program. The same verification is possible in the case of new concepts for neutron shields by the means of the exploitation of the results provided by the JASON program.

-oOo-

1. INTRODUCTION

Le formulaire PROPANE [1] est utilisé au CEA pour les calculs de protection de la filière rapide, soit pour les calculs de projet, soit pour l'analyse des expériences de propagation [2].

En ce qui concerne les données, PROPANE est basé sur les données ENDF/B.IV mises en groupe avec des méthodes qui prennent en compte l'auto-protection des résonances et les variations de spectre suivant les régions.

En ce qui concerne les méthodes, tous les calculs de protection utilisent la méthode S_N à une ou deux dimensions.

Un important programme expérimental a été réalisé en collaboration entre le CEA et le CNEN/CASACCIA, pour étudier la propagation des neutrons dans des milieux Sodium pur, et dans des mélanges Acier-Sodium à pourcentage variable d'Acier, et avec différents spectres de propagation [2,3]. Un ajustement "global" des données du Sodium et des isotopes de l'Acier est en cours.

En vue de l'utilisation de PROPANE dans les calculs de projet de la filière rapide, on a suivi la démarche suivante :

- définition des paramètres importants pour le projet ;
- définition des configurations et des matériaux de protection intéressants dans le cadre de la filière rapide ;
- vérification de la représentativité des résultats expérimentaux vis-à-vis des paramètres projet. Même vérification pour les configurations expérimentales ;
- vérifier que les incertitudes introduites par les approximations de méthode ne préjugent pas la transposabilité des résultats des expériences aux paramètres projet.

Dans la présente note, on montrera l'état de l'art actuel sur ces problèmes.

Dans une série de communications présentées à cette conférence [2,4,5,6], on fera aussi le point sur :

- la validité de la méthode d'ajustement [4] ;
- les programmes expérimentaux [3,5] ;
- la méthodologie des études de sensibilité [6].

2. PARAMETRES PROJET D'INTERET

Le principal paramètre de projet d'intérêt, est certainement l'activation du Sodium secondaire et donc le flux thermique équivalent sur la paroi de l'échangeur. (On adopte dans cette note, comme géométrie de référence, la géométrie définie en référence 7, et que l'on appelle "SUPER-PHENIX 1").

En ce qui concerne les autres paramètres d'intérêt, on a considéré le cas très général du flux total, et en particulier à la sortie des structures en Acier proches du coeur.

On n'a pas considéré le dommage dans les Aciers, parce qu'il nous semble que ce paramètre prend tout son poids si l'on considère les structures proches du coeur, où le problème de propagation des neutrons est moins important.

3. CONFIGURATIONS D'INTERET

Les configurations d'intérêt sont les configurations classiques de protection en Acier (plus précisément mélanges Acier/Sodium), autour des sources [7]. Mais on a considéré aussi de nouveaux concepts de protection [5] :

a) également autour des sources, mais en utilisant du B4C ;
b) "loin" des sources (protections localisées).

4. PARAMETRES PROJET ET REPONSES EXPERIMENTALES

Le problème de la représentativité des réponses expérimentales par rapport aux paramètres projet, a déjà été abordé dans une précédente note [8].

Dans ce travail, on avait considéré le problème en termes d'atténuation comparable pour les paramètres projet et pour les réponses expérimentales. Ici, on reprend le même critère, mais on le généralise à un ensemble plus cohérent de configurations, y compris des nouvelles configurations qui représentent de nouvelles solutions de protection. Tous les calculs de la présente note sont en géométrie sphérique, et pour tous ces calculs on a utilisé la même source de surface.

Dans les Figures 1 et 2, on compare l'atténuation du flux thermique équivalent et de la réponse Au(n,γ) :

a) dans la configuration projet [7], avec protection neutronique latérale (PNL) en Acier-Sodium (environ 50/50, en environ 250 cm de propagation en Sodium) ;
b) dans la configuration expérimentale HARMONIE : Sodium pur [3].

L'accord entre les atténuations du flux thermique équivalent (ϕtheq) et du Au(n,γ) est remarquable.

En ce qui concerne le flux total ϕtot, on a comparé, suivant l'étude de la référence [8], l'atténuation du ϕtot et de la réponse expérimentale Mn(n,γ), dans la PNL de la configuration projet et dans la configuration expérimentale TAPIRO avec mélange Acier-Sodium 50/50, [2]. Dans la comparaison, on ajoute aussi (voir Figures 3 et 4) d'autres réponses expérimentales envisageables, Cr^{50}(n,γ), Cu^{63}(n,γ), Fe^{58}(n,γ). Comme prévu, toutes les réponses sont "utilisables", les réactions (n,γ) considérées étant de bonnes "intégratrices" de neutrons.

En ce qui concerne les configurations envisageables pour la filière, on a comparé une configuration projet (dites "SUPER-PHENIX 2"), où l'on utilise une PNL en B4C (épaisseur environ 50 cm), et une configuration expérimentale à réaliser dans le programme JASON [5], où 25 cm de B4C sont suivis par une propagation dans environ 200 cm de Sodium.

Sur les Figures 5 et 6, on montre la comparaison entre Au(n,γ) et ϕtheq, calculé au bout de la propagation dans les deux configurations. Malgré les différentes épaisseurs de matériaux, l'accord entre les deux réponses dans les deux configurations est excellent.

En ce qui concerne le flux total, les Figures 7 et 8 montrent la comparaison entre ϕtot et les réponses (n,γ) considérées plus haut. L'atténuation du flux total dans le Sodium après le B4C n'est guère influencée par la faible efficacité du B4C vis-à-vis des neutrons à hautes énergies. Au contraire, toutes les réponses (n,γ) considérées, montrent une remontée due à la contribution des neutrons à hautes énergies, qui n'ont pas été ralentis par le B4C.

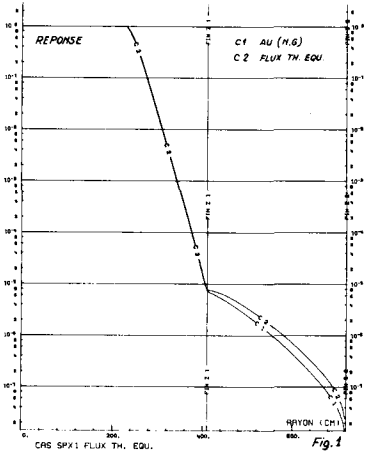

CAS SPX1 FLUX TH. EQU. Fig.1

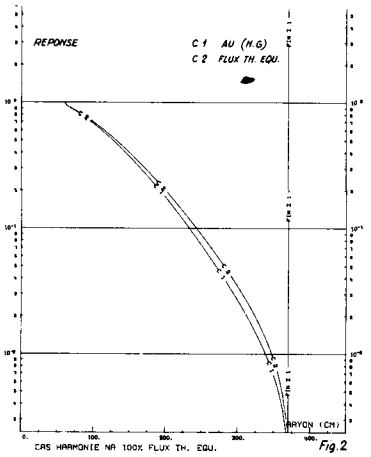

CAS HARMONIE NR 100X FLUX TH. EQU. Fig.2

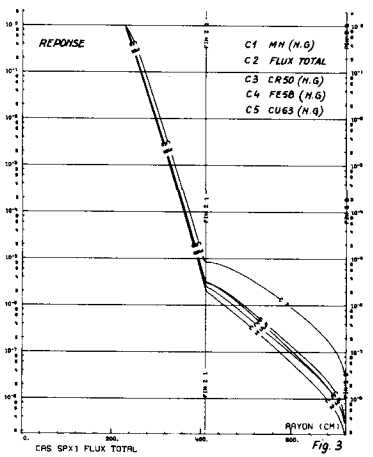

CAS SPX1 FLUX TOTAL Fig. 3

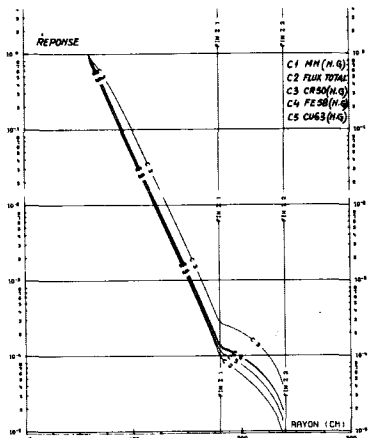

CAS TAPIRO 50/50 FLUX TOTAL

Fig.4

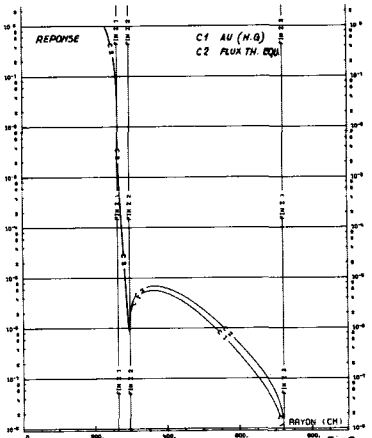

CAS SPX 2 FLUX TH. EQU.

Fig.5

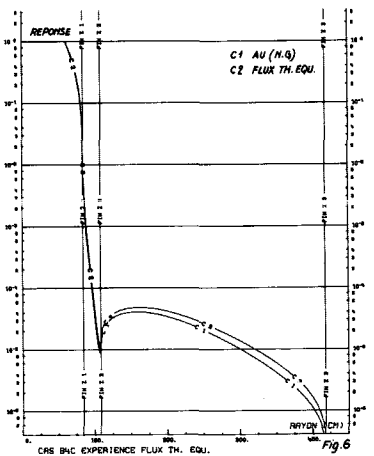

CAS BHC EXPERIENCE FLUX TH. EQU.

Fig.6

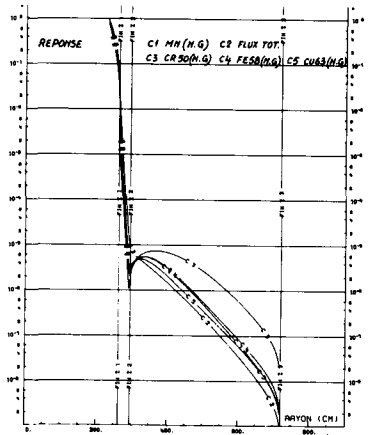

CAS SPX2 FLUX TOTAL Fig.7

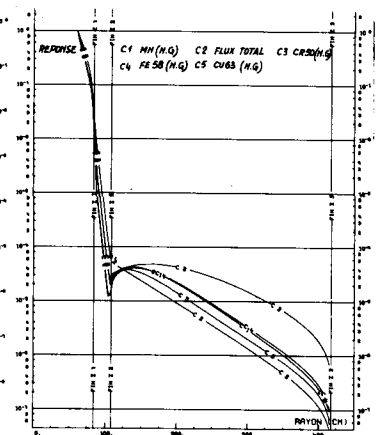

CAS B4C EXPERIENCE FLUX TOTAL Fig.8

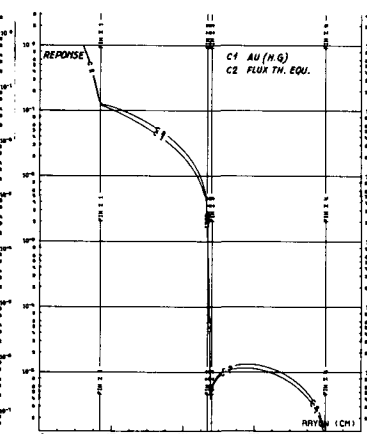

CAS B4C LOCALISE FLUX TH. EQU. Fig.9

Enfin, on a considéré une configuration expérimentale (programme JASON [5]), avec des protections localisées en B4C (5 cm d'épaisseur). Dans la Figure 9, on a comparé comme auparavant, les réponses ϕ_{theq} et Au(n,γ) calculées au bout de la propagation, c'est-à-dire à environ 100 cm derrière la protection localisée.

Dans ce cas également, on observe les mêmes tendances, et on peut tirer les mêmes conclusions que dans le cas où le B4C est placé autour des sources, c'est-à-dire un excellent accord entre l'atténuation du ϕ_{theq} et du Au(n,γ).

5. ANALYSE DES PROFILS DE SENSIBILITE

Dans le paragraphe précédent, on a vérifié que parmi les réponses expérimentales, on peut en choisir qui représentent d'une façon convenable les paramètres projet, et cela en termes d'atténuation. Cette vérification a été faite soit pour les configurations projet, soit pour les configurations expérimentales correspondantes, et pour différentes solutions conceptuelles de protection.

On vérifie maintenant que la représentativité des expériences est valable aussi en termes de profils de sensibilité. Cela doit nous assurer que toutes les conclusions extraites des expériences, soit des valeurs de (E-C)/C ou des ajustements que l'on peut obtenir à partir de ces (E-C)/C, sont transposables aux calculs de projet, sans introduire des erreurs systématiques.

Pour cela, on a effectué, à l'aide du système de codes SAMPO [6], une étude de sensibilité, où l'on a comparé les profils de sensibilité en énergie des différents paramètres dans les différentes configurations, aux données de base. Tous les résultats sont indiqués dans les Figures 10-18.

En ce qui concerne les configurations classiques (Acier/Sodium autour des sources), on vérifie (Figures 10-12) que :

- les sensibilités du ϕ_{tot} et du Mn(n,γ) aux variations des σ du Fe dans la PNL sont très proches ;

- même commentaire pour la sensibilité aux variations des σ du Sodium, du ϕ_{theq} et du Au(n,γ), sauf à très basse énergie ;

- les sensibilités dans la configuration "projet" et dans la configuration expérimentale sont très similaires, sauf à haute énergie (environ 1 MeV). Cela est du au fait que, dans la configuration projet, la sensibilité aux σ du Sodium est influencée par la traversée de la PNL. Dans la configuration expérimentale considérée, on n'a pas de telle traversée, donc on a une sensibilité plus élevée aux neutrons à haute énergie. Il faut remarquer à cet égard, que la partie la plus importante de la sensibilité se trouve au dessous de $\sim$ 1 KeV, où les profils de sensibilité sont très proches.

En ce qui concerne les configurations avec du B4C autour des sources (Figures 13-15), on peut faire les mêmes remarques que précédemment. On remarque également que la configuration projet et la configuration expérimentale donnent des profils très proches sur toute la gamme des énergies, et cela à cause de l'importance prépondérante de la traversée en B4C.

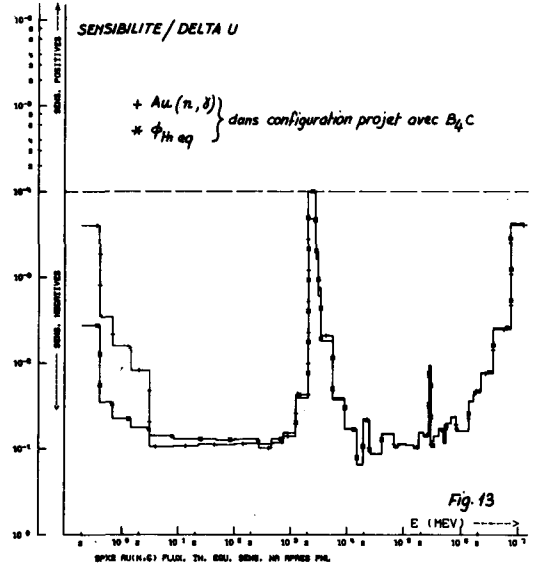

Fig. 13

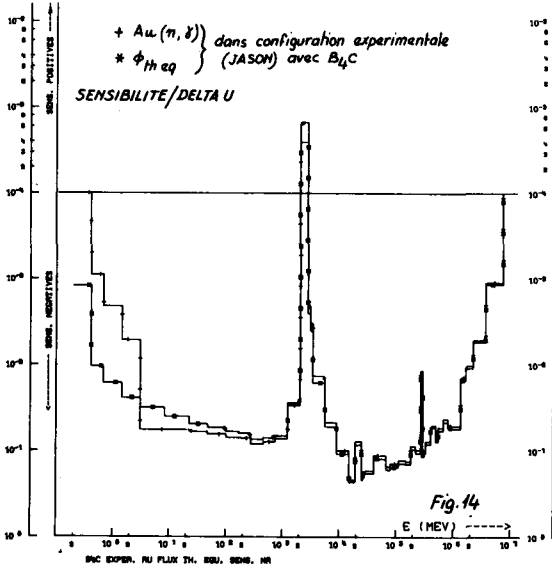

Fig. 14

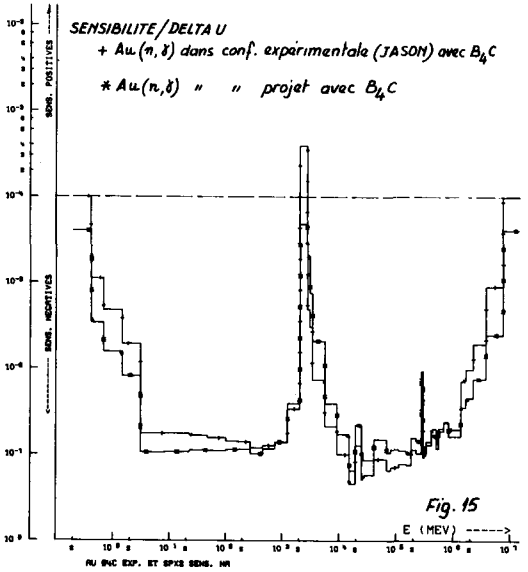

Fig. 15

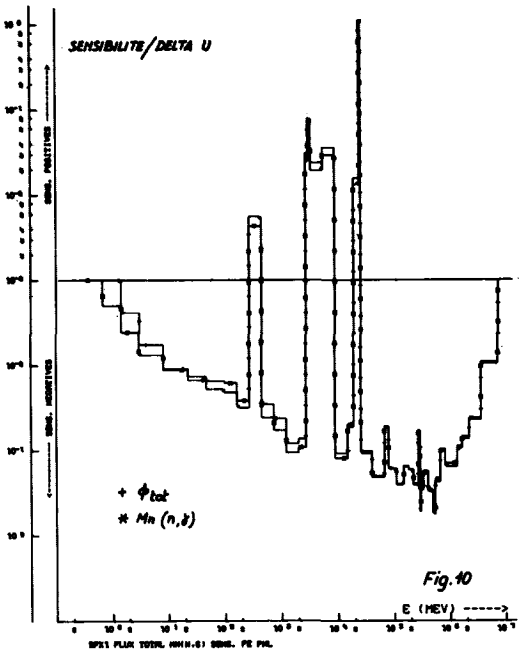
SENSIBILITE/DELTA U
+ ϕ_{tot}
* Mn (n,γ)
E (MEV) ----->
Fig. 10

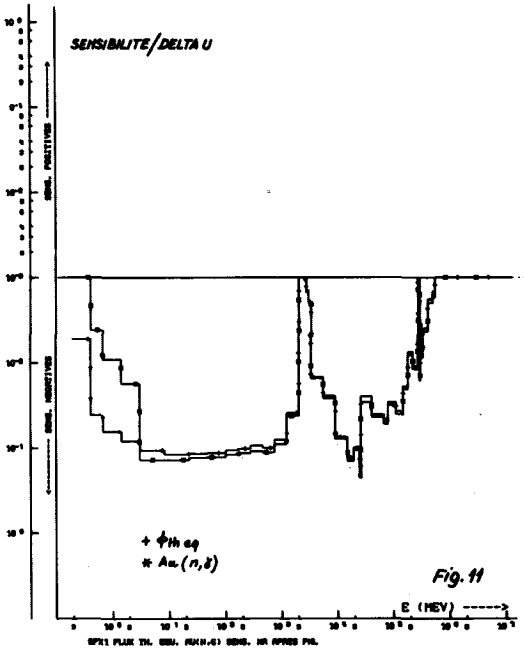
SENSIBILITE/DELTA U
+ $\phi_{th\ eq}$
* Au. (n,γ)
E (MEV) ----->
Fig. 11

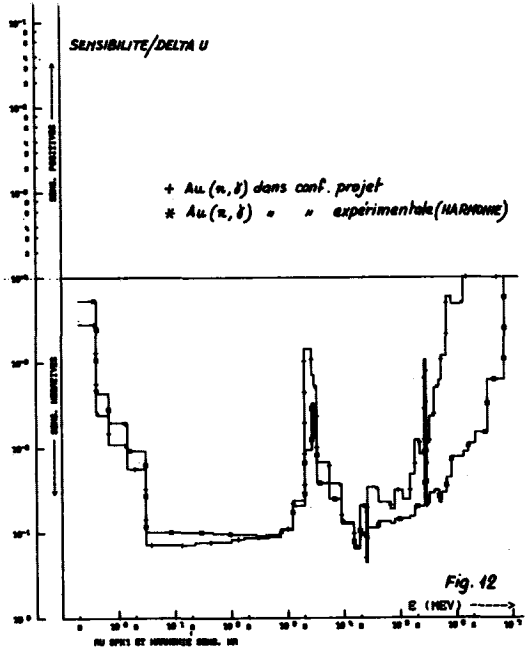
SENSIBILITE/DELTA U
+ Au. (n,γ) dans conf. projet
* Au. (n,γ) " " expérimentale (HARMONIE)
E (MEV) ----->
Fig. 12

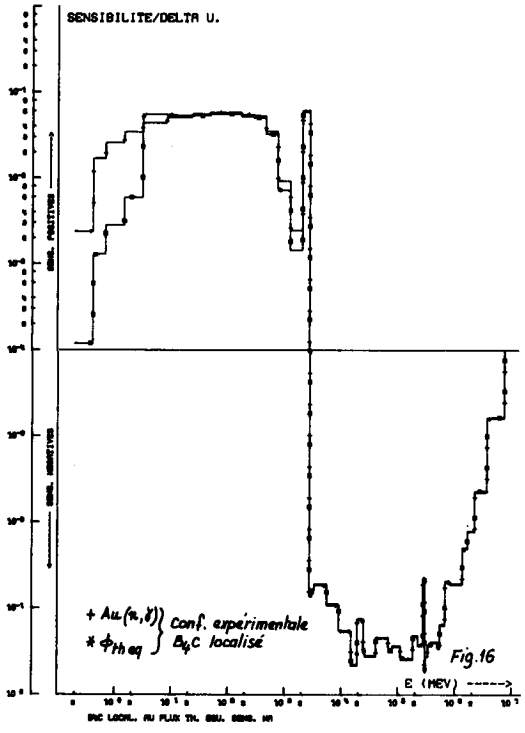

Fig.16

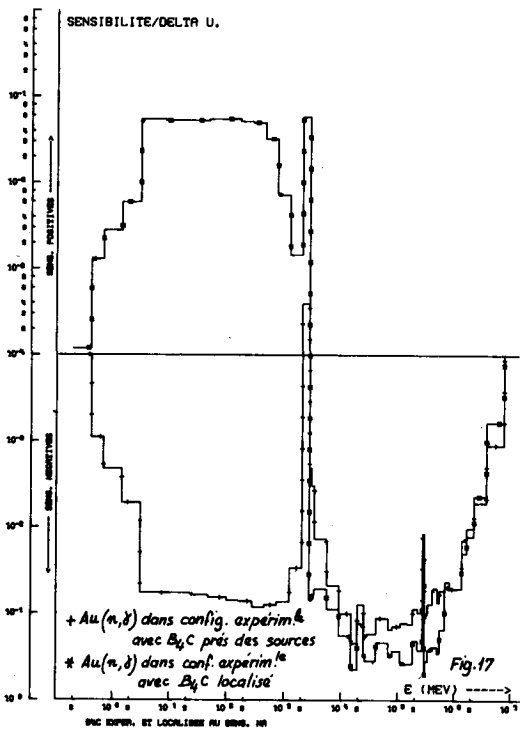

Fig.17

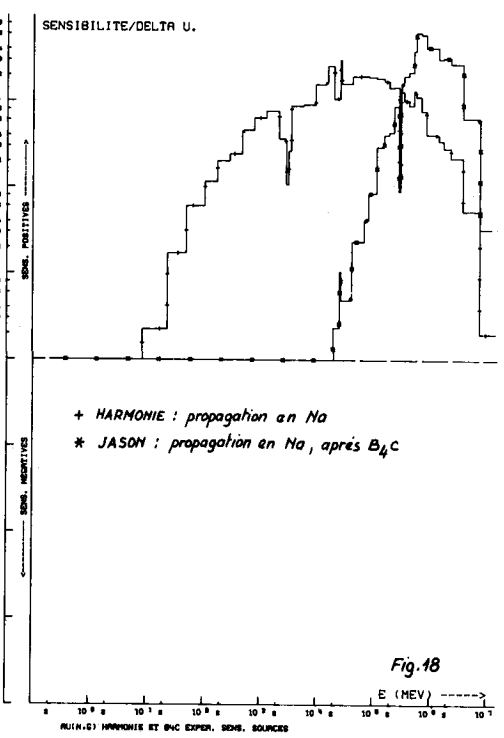

Fig.18

Enfin, dans le cas des protections localisées, la Figure 6 confirme le bon accord entre les profils de sensibilité de l'Au(n,γ) et du ϕ_{theq}.

En ce qui concerne les différences qui peuvent être observées entre les différentes configurations, il est intéressant de comparer (Figure 17) les profils de sensibilité de l'Au(n,γ) aux sections du Sodium quand le B4C est autour ou éloigné des sources. Le profil de sensibilité reste le même aux énergies supérieures à 1 KeV, mais on observe un changement de signe au-dessous de $\sim$1 KeV dans un profil par rapport à l'autre : dans le cas d'une protection localisée en B4C, une augmentation des sections efficaces du Sodium au-dessous de 1 KeV augmente la thermalisation des neutrons (après la protection), et donc le ϕ_{theq} (ou la réponse Au(n,γ)).

Enfin, sur la Figure 18, on compare la sensibilité de la réponse Au(n,γ) au spectre de la source dans deux configurations expérimentales : celle d'HARMONIE (propagation en Sodium pur), et celle de JASON (B4C suivi du Sodium). On remarque encore une fois la sensibilité plus importante aux neutrons à hautes énergies dans le cas de la configuration avec B4C.

6. INFLUENCE DES APPROXIMATIONS DE METHODE

On peut se poser enfin le problème de la transposition d'informations entre une configuration expérimentale et une configuration projet, si on n'introduit pas d'incertitudes dues au modèle de calcul ou aux effets des approximations de méthode. Pour donner une réponse à une telle question, on a comparé dans une situation projet type SUPER-PHENIX 1, quelle était l'influence d'un passage assez drastique d'un modèle à deux dimension (R,Z), à un modèle 1D (sphérique).

Dans la Figure 20, on montre ce facteur de géométrie dans le cas du flux thermique équivalent :

$$f_1 = \frac{\phi_{theq\ 2D}}{\phi_{theq\ 1D}}$$

Les valeurs de "f" sont très proches de 1, même après une grande propagation en Sodium.

En ce qui concerne les approximations de calcul, on a testé l'influence du maillage spatio-angulaire adopté. On a comparé deux calculs 1D de la même configuration projet : le premier utilisait les options PROPANE, c'est-à-dire 45 groupes, découpage angulaire S4 et des mailles spatiales d'environ 3 cm dans l'Acier/Sodium, et d'environ 5 cm en Sodium. Le deuxième calcul utilisait la bibliothèque de référence BABEL [9] à 113 groupes, le découpage angulaire S16 et des mailles réduites d'un facteur 2.

On présente sur la Figure 21, le facteur f_2 :

$$f_2 = \frac{\phi_{theq}\ (S16,\ 113g,\ maillage\ double)}{\phi_{theq}\ (S4\ ,\ \ 45g,\ maillage\ simple)}$$

Le facteur f_2 est lui aussi toujours assez proche de 1. Enfin, le produit $f_1 f_2$ est présenté sur la Figure 22. Les effets de compensation sont favorables, et l'on observe finalement des écarts faibles du calcul approché (1D, 45 groupes, S4, maillage simple), par rapport à un calcul de référence.

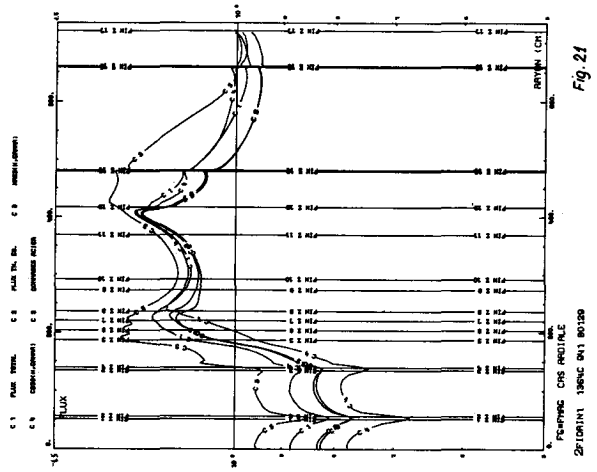

Fig. 21

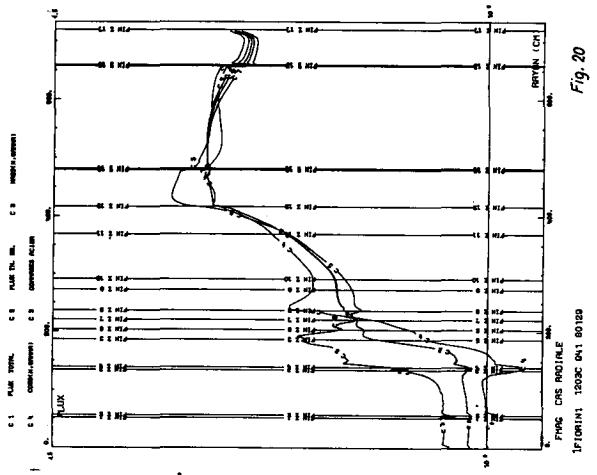

Fig. 20

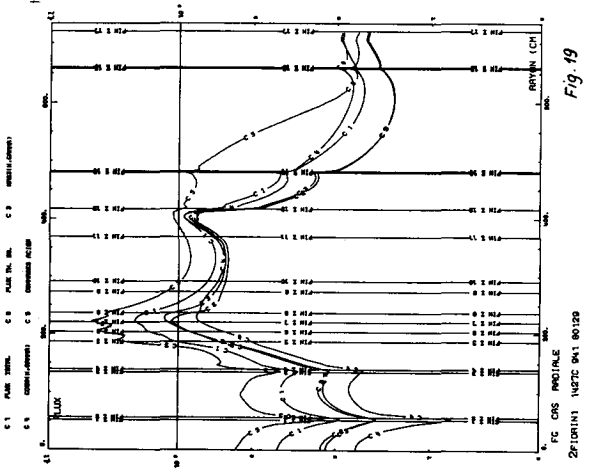

Fig. 19

Cet exemple nous donne confiance pour la transposition des écarts Calcul-Expérience et des ajustements, des situations expérimentales aux situations projet : *on peut en effet penser que si les* effets d'approximations de méthode et de modèle ne sont pas trop importants, cela sera vrai "à fortiori" pour les différences des valeurs de ces effets entre configurations expérimentales et de projet, à condition d'avoir réalisé dans les configurations expérimentales, des propagations significatives.

7. CONCLUSIONS

Les expériences de propagation du programme CNEN/CEA sur HARMONIE et TAPIRO ont permis d'obtenir des informations transposables aux configurations de projet et permettent des ajustements des données de base utilisables dans les calculs de projet de protection "autour des sources" en Acier/Sodium.

Le programme JASON, démarré récemment sur HARMONIE permettra de compléter ces informations avec des ajustements sur des configurations où l'on utilise des matériaux de protection différents (type B4C), ou bien où l'on envisage un emplacement différent des protections (localisées et loin des sources).

-oOo-

REFERENCES

[1] Estiot J.C., Salvatores M., Trapp J.P. : Basic Nuclear Data and the Fast Reactor Shielding Design. Formulaire PROPANE Do", Proc. Int. Conf. Nucl. Cross-Sections and Tech., Knoxville 1979

[2] Estiot J.C. et al. : "Nuclear Data for Shielding Calculations Na Cross-Sections Adjustment using Propagation Experiments", Proc. Int. Conf. Nucl. Cross-Sections and Tech., Knoxville 1979

[3] Carta M., De Carli A., Rado V., Salvatores M., Trapp J.P. : "Expériences de propagation dans des milieux Acier/Sodium à TAPIRO", Réunion de Spécialistes sur les Données Nucléaires et les Expériences Repères en Matière de Protection des Réacteurs, Paris, 27-29 Octobre 1980

[4] Estiot J.C. :"Qualification de la méthode d'ajustement des données nucléaires utilisées pour l'optimisation du formulaire PROPANE", Réunion de Spécialistes sur les Données Nucléaires et les Expériences Repères en Matière de Protection des Réacteurs, Paris, 27-29 Octobre 1980

[5] Trapp J.P. et al. : "Le programme expérimental JASON associé à l'optimisation des protections neutroniques pour la filière rapide", Réunion de Spécialistes sur les Données Nucléaires et les Expériences Repères en Matière de Protection des Réacteurs, Paris, 27-29 Octobre 1980

[6] Estiot J.P., Palmiotti G., Salvatores M. : "Le système SAMPO pour les analyses de sensibilité et de perturbation à différents ordres d'approximation", Réunion de Spécialistes sur les Données Nucléaires et les Expériences Repères en Matière de Protection des Réacteurs, Paris 27-29 Octobre 1980

[7] Proc. Specialists' Meeting on Differential and Integral Nuclear Data Requirements for Shielding, Vienna 1978

[8] Salvatores M. : "Neutron Transport in Structural Materials and Shielding Design", Proc. Int. Conf. Nuclear Cross-Sections and Technology, Knoxville 1979

[9] Estiot J.C. et al. : "Conséquences des incertitudes sur les données de base dans les calculs de protection", Proc. Int. Conf. on Neutron Physics and Nuclear Data, Harwell 1978

-oOo-

QUALIFICATION DE LA METHODE D'AJUSTEMENT DES DONNEES NUCLEAIRES UTILISEES POUR L'OPTIMISATION DU FORMULAIRE PROPANE

J.C. Estiot
CEA/CEN/CADARACHE (FRANCE)

RESUME

Dans la méthode d'ajustement statistique utilisée pour l'amélioration des données de base, plusieurs paramètres jouent un rôle important : le nombre d'expériences intégrales utilisées, les ordres de grandeurs des incertitudes sur les données de base et sur les expériences intégrales, etc. On étudie ici l'influence du choix de ces paramètres dans la procédure d'ajustement.

ABSTRACT

In the statistical adjustment method used to improve basic data, several parameters play an important role : the number of integral experiments used, the magnitudes of incertainties on the basic data and integral experiments, etc. We study here the influence of the choice of these parameters on the adjustment procedure.

1. INTRODUCTION

La méthode d'ajustement statistique [1] est utilisée fréquemment pour l'amélioration des données du formulaire PROPANE [3] de protection de la filière rapide.

Nous avons cherché à tester cette méthode d'ajustement qui est basée sur les calculs de sensibilité des mesures intégrales aux données de base.

Nous avons donc fait varier les paramètres intervenant dans ces ajustements tel le nombre de mesures intégrales dont nous disposons, la précision accordée à ces mesures et leurs compatibilités, les incertitudes sur les données de base et leur corrélation.

On a aussi testé quel intérêt pouvait présenter les passages successifs d'un même cas utilisant comme données les résultats de l'ajustement précédent.

Nous observons à cet effet les différents résultats que nous obtenons telles les valeurs des écarts relatifs expérience/calcul (E-C)/C résultantes, les variations imposées aux données de base pour les obtenir et un test χ^2_i sur la validité de l'ajustement.

L'hypothèse de linéarité des coefficients de sensibilité, implicite dans la méthode d'ajustement, est finalement contrôlée par le passage de cas directs qui utilisent les données de base après correction.

2. PRINCIPE DE LA METHODE UTILISEE

Elle met en oeuvre, en plusieurs étapes, les codes du système SAMPO

Le code de transport GIANT [4] à une dimension dérivé d'ANISN [4] effectue le calcul direct de la réponse d'un détecteur ou d'un rapport de détecteurs ainsi que la fonction adjointe donnant l'importance de la contribution neutronique par énergie à cette réponse ou à ce rapport.

Un calcul de sensibilité de ces mesures intégrales aux données de base est effectué par le code ROSCOFF [4] qui résoud l'équation générale suivante :

$$\frac{dR}{R}(\delta\Sigma_x) = \int_r \int_\Omega \int_E \delta\Sigma_x(r,\Omega,E) \quad \phi(r,\Omega,E) \quad \Psi^*(r,\Omega,E) dr, d\Omega, dE$$

Dans ce code nous avons utilisé la formulation de Mc Cracken [6] qui associe les sensibilités aux sections élastiques, inélastiques et d'absorption dans un rapport tel qu'il permet d'effectuer les calculs d'ajustement en tenant compte implicitement des lois de conservation sur les sections.

L'ajustement proprement dit est réalisé par le code CORDAJ qui effectue la recherche du maximum d'une fonction de probabilité de la forme :

$$\exp \left[(y_i^{ex} - y_i)\ (y_j^{ex} - y_j)\right]$$

qui amène, en utilisant la méthode des multiplicateurs de Lagrange, à la détermination de la valeur estimée $\hat{y}$ de y.

y représente le vecteur que nous voulons évaluer des corrections exactes à apporter aux valeurs intégrales et aux données de base.

Ce code détermine aussi la matrice $\tilde{By}$ à partir de la matrice de dispersion By d'origine et de la matrice des coefficients de sensibilité.

$$By = \begin{vmatrix} P_{CR} & 0 \\ 0 & W_{\sigma} \end{vmatrix}$$

où P_{CR} et W_{σ} sont respectivement les matrices de dispersion liées aux valeurs intégrales et sections efficaces que l'on suppose sans corrélation entre elles.

3. ORIGINE DES DONNEES INTEGRALES

Les expériences intégrales dont nous nous sommes servis pour établir une qualification de la méthode d'ajustement ont été réalisées sur des massifs de sodium pour des installations HARMONIE et TAPIRO (la première étant située à Cadarache, France, et la seconde à Casaccia, Italie).

Ce sont des rapports de détecteurs placés à des distances de pénétration différentes (voir notes du tableau IV) allant de 20 cm à 270 cm.

Les spectres neutroniques de propagation sont représentatifs du spectre après la couverture de SPx1 (A.Cv) et après les protections latérales (S.Cv) (Figure N°1).

Les détecteurs utilisés sont des feuilles ou des pastilles de manganèse, d'or, de sodium, de soufre et de rhodium qui sont sensibles à différentes parties du spectre neutronique utilisés pour les mesures de propagation [5]. La liste des mesures intégrales est donnée dans le table I ci-dessous :

TABLEAU I - LISTE DES MESURES INTEGRALES

Conf.	N° de mesure	Type de mesure (*)	Conf.	N° de mesure	Type de mesure	Conf.		N° de mesure	Type de mesure
HARMONIE Sans couverture (S.Cv)	1	Na 1/3	HARMONIE avec couverture (A.Cv)	11	Au 1/3	TAPIRO	sans couverture	20	Na A/F
	2	Mn 1/3		12	Na 1/3			21	Mn A/F
	3	Mn 1/4		13	Mn 1/3			22	S A/D
	4	Au 1/3		14	Mn 3/6			23	Rh A/D
	5	S 1/2		15	Na 3/6		avec couverture	24	Na A/F
	6	S 2/4		16	Au 3/6			25	Mn A/F
	7	Rh 1/3		17	S 1/2			26	Au A/F
	8	Na 3/5		18	S 2/4			27	S A/B
	9	Na 3/6		19	Rh 1/2			28	Rh A/D
	10	Mn 3/6							

*Nota de la colonne type de mesure :

x 1/3 = Rapport des taux de réaction des détecteurs des positions 20/120 cm
x 1/4 = Rapport des taux de réaction des détecteurs des positions 20/170 cm
x 1/2 = Rapport des taux de réaction des détecteurs des positions 20/70 cm
x 2/4 = Rapport des taux de réaction des détecteurs des positions 70/170 cm
x 3/6 = Rapport des taux de réaction des détecteurs des positions 120/270 cm

} Configuration HARMONIE

x 3/5 = Rapport des taux de réaction des détecteurs des positions 120/220 cm

x A/B = Rapport des taux de réaction des détecteurs des positions 20/35 cm
x A/D = Rapport des taux de réaction des détecteurs des positions 20/70 cm
x A/F = Rapport des taux de réaction des détecteurs des positions 20/120 cm

} Configuration TAPIRO

4. ORIGINE DES DONNEES DE BASE

Nous avons utilisé comme sections efficaces celles de la bibliothèque ENDF/BIV condensées à 45 groupes dans le formulaire PROPANE [3] et les incertitudes sur les données de base ainsi que leurs corrélations ont été fournies à 15 groupes d'énergie par ORNL [2] et étendues à 45 groupes par un code utilisant une méthode d'interpollation logarithmique.

Pour rendre plus compréhensible et plus visuel certains de nos résultats nous avons défini uniquement pour les représentations graphiques et les discussions un découpage en 5 groupes défini dans le tableau II et pour lequel nous donnons les déviations standards définies par ORNL dans le cas du sodium.

TABLEAU II - CARACTERISTIQUES DU DECOUPAGE A 5 GROUPES D'ENERGIE DES DONNEES DE BASE (Na)

N° de groupe	Energie limite des groupes	Deviation standard des sections $\Delta\sigma/\sigma$		
		$\frac{\Delta\sigma_a}{\sigma_a}$ (%)	$\frac{\Delta\sigma_i}{\sigma_i}$ (%)	$\frac{\Delta\sigma_T}{\sigma_T}$ (%)
1	14.7 MeV à 497 KeV	42.3	25.8	3.19
2	497 KeV à 79 KeV	35.7	45.2	4.48
3	79 KeV à 3 KeV	13.1	0.	6.71
4	3 KeV à 8.31 eV	5.02	0.	5.41
5	< 8.31	< 0.1	0.	7.

5. EFFET DES INCERTITUDES SUR LES DONNEES DE BASE

Nous avons étudié cet effet sur une série de 11 expériences intégrales comprenant un échantillonnage représentatif des 28 mesures du tableau I.

Nous avons multiplié par 2 les éléments des matrices de dispersion des données de base pour chacune des réactions d'absorption, inélastique et totale ou pour les 3 ensembles, et ce pour une partie de la bande d'énergie ou pour toutes les énergies.

Les corrélations initiales entre énergies sont conservées. Les résultats sont consignés dans le tableau III.

Les colonnes 1, 2, 3 comparées entre elles montrent que les déviations standards des mesures intégrales sont beaucoup plus sensibles aux basses énergies qu'aux hautes excepté pour le soufre.

Les colonnes 4, 5, 6 montrent que seules les incertitudes sur les sections totales ont des incidences sur les incertitudes des mesures intégrales, le soufre fait encore exception compte-tenu de l'importance de diffusion inélastique et est effectivement plus sensible aux variations imposées sur les incertitudes des sections inélastiques.

TABLEAU III

Mesures Intégrales	Dev. standard Référence V_R %	Variation $\frac{V_M - V_R}{V_R}$ en % — Covariances * 2 pour : $\sigma_a, \sigma_i, \sigma_T$ (1)	$\sigma_a, \sigma_i, \sigma_i$	σ_a	σ_i	σ_T	Corrélation = 0 (2)
Na 1/3	3.9	21	97	0	0	97	- 36
Na 3/6	13.	0	105	0	0	97	- 40
Mn 1/3	5.4	35	98	0	0	98	- 35
Mn 3/6	12.6	<1%	97	0	0	97	- 40
Au 1/3	4.6	11	98	0	0	98	- 33
Au 3/6	15.2	0	97	0	0	97	- 34
S 1/2	23.7	100	100	0	100	3	- 17
S 2/4	53.1	101	100	0	98	2	- 51
Rh 1/3	13.8	100	100	0	0	100	- 51

(1) Dans cette colonne les variations de covariances ont été faites entre 14.7 MeV et 111 KeV alors qu'elles sont faites de 14.7 MeV à 0 pour les autres colonnes.

(2) Cette colonne contient le calcul des déviations standards avec des données de base de référence mais sans corrélation.

V_M Représente la valeur de la déviation standard avec modification des matrices de covariance.

V_R Représente la valeur de la déviation standard de référence.

La colonne N°7 possède les mêmes incertitudes sur les données de base que la référence mais n'a aucune corrélation en énergie : cela permet de se rendre compte de leur importance car l'incidence sur les valeurs intégrales est une forte diminution de la déviation standard allant de -17% à -51%.

On remarque la quasi linéarité des variations des incertitudes sur les données intégrales en fonction de celles imposées sur les données de base dans le cas d'une variation sur la somme des réactions ou même, soufre excepté, sur la section totale.

Ce dernier point nous permet par la suite de nous intéresser, lorsque nous en avons besoin, uniquement aux variations enregistrées sur la section totale et exceptionnellement à celles enregistrées sur les sections inélastiques.

Nous remarquons sur cet échantillonnage de mesure que les déviations standards sont vraiment très faibles en règle générale et ne permettent donc pas de corriger de forts écarts si ce n'est au détriment de la validité de l'ajustement comme nous allons le voir dans les paragraphes suivants.

6. EFFET DU NOMBRE D'EXPERIENCES

Parmi les 28 mesures du tableau, nous avons choisi 13 expériences dans la configuration HARMONIE de façon tout à fait arbitraire. Nous les avons associées par séries de 2, 3, 4, 5, 6, 8 ou 13 et nous avons regardé pour chaque série les variations par macrogroupe de la section totale du Na qui résulte de l'ajustement correspondant ainsi que de la valeur d'un test de validité χ^2_i.

Les résultats sont portés figures 2, 3 et 4 où la courbe R qui apparaît figures 2 et 3 est la limite maximale de variation don-

née actuellement par les estimateurs [2]. Cette courbe a aussi son symétrique en valeur positive.

Les ajustements des séries de 2 ou 3 expériences ne présentent aucune tendance particulière dans les variations des σ_T et sont en fait souvent contradictoires bien que les valeurs du χ^2_1 indiquent que la probabilité de l'ajustement comprise entre 5% et 55% reste valable.

A partir des séries de 4 et ce jusqu'à 13, on observe une même tendance : toutes les variations des $\Delta\sigma_T/\sigma_T$ des groupes d'énergie 1 à 4 sont négatives et celles du groupe 5 positives avec un fort maximum pour le groupe 3.

Les χ^2_1 par contre vont en diminuant et, pour 13 mesures, la probabilité d'ajustement est inférieure à 0.1% (figure 4).

Ces deux effets contradictoires montrent qu'il est important d'avoir un nombre suffisant d'expériences intégrales pour être sûr de la tendance obtenue mais il faut aussi, comme nous le verrons au paragraphe IX, que ces mesures soient compatibles pour avoir une probabilité d'ajustement suffisante.

7. EFFET DES INCERTITUDES SUR LES DONNEES INTEGRALES

Nous avons fait varier l'incertitude attribuée à chaque type d'expériences pour une série de 19 mesures (tableau IV).

Ces 19 mesures (tableau V) sont celles théoriquement compatibles entre elles (§ IX) choisies parmi l'ensemble des 28 données intégrales.

Nous avons regardé l'effet sur la validité de l'ajustement (χ^2_1), sur les écarts (E-C)/C ainsi que sur les corrections apportées aux sections totales du Na.

TABLEAU IV - VALEURS DES $\Delta E/E$ ATTRIBUEES AUX MESURES INTEGRALES

N° de série ——>	C1	C2	C3	C4
Incertitudes sur les mesures intégrales Mn, Au, Na, S	10 %	20 %	20 %	15%
Incertitudes sur les mesures intégrales du Rh	20 %	20 %	40 %	30%
Valeurs du χ^2_1 obtenues	< 0.5%	20 %	65 %	20%
Variation maximum des sections totales du Na	12.1%	8.5%	8.2%	9%

Les χ^2_1 dans ce tableau montrent que l'ajustement le plus probable est actuellement celui pour lequel nous attribuons les plus fortes incertitudes sur les mesures intégrales (série C3).

Dans ce cas, on observe aussi la plus faible des variations maximale sur les σ_T du Na.

Pour toutes ces séries, la figure 5 montre en détail que la réduction des écarts (E-C)/C est pratiquement identique. On observe bien sûr des résultats plus satisfaisants en fonction de la précision

ac ·rdée aux expériences. La figure 6 montre à quel prix par exemple l' ioration la plus conséquente obtenue avec la série C1 impose un ıriation sur les sections efficaces totales du Na d'une valeur do e à la valeur autorisée (courbe R).

Dans le cas de cet ajustement, on remarque aussi (figure 6) que la tendance générale de variation du groupe 4 est supérieure à la limite autorisée. Ce qui semble indiquer soit une erreur systématique de l'ensemble des expériences ou le besoin d'augmenter l'évaluation des marges d'erreur sur la section totale du Na entre 3 KeV et 8.31 eV.

Le détail (dans le découpage à 45 groupes PROPANE) de la variation imposée aux sections totales du Na est donnée figure 7 pour la série C3 dont la probabilité d'ajustement est la meilleure (65%). Il montre qu'effectivement dans cette plage nous débordons largement les covariances relatives fournies par ORNL [2].

La figure 8 montre que pour l'inélastique les variations imposées sont bien dans les limites permises.

L'utilisateur seul pourra dans ce cas juger de la validité des compromis qu'il est amené à faire entre l'intention de ramener au maximum les écarts (E-C)/C et ne pas dépasser les variations $\Delta\sigma/\sigma$ suggérées par les estimateurs.

8. EFFET DES AJUSTEMENTS SUCCESSIFS D'UN MEME CAS

Nous effectuons un premier calcul d'ajustement dont nous récupérons une nouvelle matrice de dispersion $B\tilde{y}$ des données de base etdes écarts "expériences-calcul" résiduels et nous les réinjectons comme données pour un nouvel ajustement.

Nous avons ainsi effectué 4 calculs successifs sur une série de 15 mesures HARMONIE-TAPIRO prises parmi les 19 mesures compatibles précédentes.

La figure 11 représente la variation globale (E-C)/C en fonction de l'itération :

$$[(E-C)/C]_{global} = \sum_{i=1,n} \sqrt{\frac{[(E-C)/C]_i^2}{n}}$$

L'optimum est obtenu en fait avec le premier calcul. C'est ce qui ressort des figures 9, 10 et 11 où les variations des valeurs (E-C)/C ainsi que celles des écarts imposés aux sections du Na sont fortes pour le premier calcul et continuent à varier faiblement pour les itérations suivantes.

Mais si l'on considère sur la figure 9 la somme des variations des $\Delta\sigma_T/\sigma_T$ correspondant à ce que l'on fait effectivement varier depuis le cas initial, on s'aperçoit que l'évolution de ces sections est largement au-delà de la limite permise par les estimateurs [2].

On obtient bien un ajustement qui semble meilleur mais avec des variations sur les données de base qui théoriquement ne sont pas acceptables.

Nous avons représenté en détail à 45 groupes l'effet de ces passages successifs (figure 12) sur la diagonale de la matrice de dispersion des sections totales du Na. Elles confirment bien la forte variation initiale suivie d'une faible évolution pour les cas suivants constatés plus haut.

9. ELIMINATION DES EXPERIENCES COMPATIBLES

Nous avons porté dans le tableau V les résultats de 3 séries d'ajustements :

C5 qui comprend l'ensemble des mesures qui sont à notre disposition
C4 qui comprend les 19 mesures utilisées dans les paragraphes précédents pour le test du choix des incertitudes expérimentales
C6 qui comprend 8 mesures de la série C4 plus une mesure dite "non compatible".

La colonne $(E-C_{J5})/C_{J5}$ résultat de l'ajustement de C5 montre que certaine de ces valeurs augmentent après le calcul : c'est le cas des mesures n° 3, 8, 9, 11, 15 à 19, 22.

Ces mesures sont supposées non compatibles et la série C4 est l'ajustement avec toutes les autres.

Cette élimination est certainement valable cas nous observons que la probabilité d'ajustement (χ^2_1) passe de 0.5% à 20% et que figure 13, les variations $\Delta\sigma_T/\sigma_T$ du sodium ont fortement diminuées.

Le résultat de la série C6 montre que l'effet d'une seule mesure incompatible se fait nettement sentir sur la probabilité d'ajustement qui retombe de 20% à 0.5%. Cela est par contre moins sensible sur les variations σ_T du Na qui gardent la même tendance bien qu'ayant des valeurs différentes.

On remarque (figure 13) avec la série C4, pratiquement retenue comme ajustement final, que les variations $\Delta\sigma_T/\sigma_T$ des macrogroupes 3 et 4 sont supérieures aux limites autorisées (courbe R) pourtant nous sommes loin de réduire à zéro les écarts expérience-calcul.

La colonne des déviations standards autorisées montre quelles sont effectivement trop faibles pour recouvrir les écarts (E-C)/C initiaux.

Nous avons d'ailleurs représenté figure 5 les déviations standards sous forme de barre d'erreur et nous nous apercevons que tous les ajustements obtenus, y compris celui de la série C4, vont au-delà de cette barre pour 13 mesures sur 19.

TABLEAU V - COMPARAISON AJUSTEMENT C4, C5, C6 ET EFFET DE LINEARITE

	N°	Mesur. Integ. (X)	$\frac{E-Cl_0}{Cl_0}$ %	Dev. stand (%)	$\frac{E-C_{j5}}{C_{j5}}$	$\frac{E-C_{j6}}{C_{j6}}$	$\frac{E-Cl_1}{Cl_1}$	$\frac{\Delta Cl}{Cl_0}$	$\frac{E-C_{j4}}{C_{j4}}$	$\frac{E-Cl_2}{Cl_2}$	$\frac{\Delta Cl}{Cl_0}$
H SCV	1	Na 1/3	-22.7	3.9	-15	-13.2	-14.8	7.	-13.5	-15.7	9.6
	2	Mn 1/3	-24.3	5.4	- 6	- 9.6	- 9.9	1.2	-10.4	-11.1	2.9
	3	Au 1/4	-27.6	8.6	- 4.6				- 5.9	- 9.4	12.6
	4	Au 1/3	-12.2	4.7	- 6.4	- 2.7	- 1.7	8.	- 2.2	- 1.7	4.
	5	S 1/2	-30.0	23.8	-18	- 7.3	-12.6	17.	- 8.8	-13.8	16.
	6	S 2/4	-38.5	53.3	-12.6	11.4	0.	30.	8.6	0.6	20.
	7	Rh 1/3	-22.8	13.8	+ 5.8	-14.1	-13.1	4.4	-17.7	-16.7	4.4
	8	Na 3/5	+20.0	7.9	+20.6						
	9	Na 3/6	+11.5	12.9	+13.2						
	10	Mn 3/6	-16.3	12.6	- 9.2				+ 7.1	+ 8.2	6.7
H ACV	11	Au 1/3	+ 9.5	4.6	+17.9	-19.4					
	12	Na 1/3	-16.3	3.8	- 7.0	- 6.5			- 6.9		
	13	Mn 1/3	-17.2	5.7	+ 2.1	- 2.			- 2.7		
	14	Mn 3/6	-13.8	12.7	- 7.1				+ 6.9		
	15	Na 3/6	+20.0	13.2	+21.5						
	16	Au 3/6	+10.0	15.3	10.7						
	17	S 1/2	+ 1.5	26.2	+13.9						
	18	S 2/4	- 6.8	55.8	+19.6						
	19	Rh 1/2	+ 6.0	7	+13.3						
T SCV	20	Na A/F	-33.9	3.7	-26.5				-22.6		
	21	Mn A/F	-47.3	6.1	-26.7				-27.5		
	22	S A/B	+ 2.5	5.7	+ 5.3						
	23	Rh A/D	-37.7	7.5	-29.6				-21.6		
T ACV	24	Na A/F	-33.7	4.8	-29.2				-21.6	-19.5	6.2
	25	Mn A/F	-45.3	6.1	-25.5				-25.6	-21.4	8.8
	26	Au A/F	-28.6	3.8	-21.8				-10.5	-12.6	7.3
	27	S A/B	-17.1	5.4	-14.4				-10.1	-13.8	17.5
	28	Rh A/D	-43.7	6.6	-34.9				-33.9	-23.6	23.5
		χ_1^2			<0.5%	<0.5%			20%		

Cl_0 Calcul ANISN avec sections σNa origine

Cl_1 Calcul ANISN avec sections σNa corrigées par ajustement C6

Cl_2 CALCUL ANISN avec sections σNa corrigées par ajustement C4

H = HARMONIE SCV = sans couverture

T = TAPIRO ACV = avec couverture

(X) voir définition des rapports tableau I.

10. CONTROLE DE LINEARITE

Le contrôle est fait à partir de deux ajustements différents le C6 et la C4 pour lesquels nous avons recalculé avec un calcul direct les valeurs des réponses intégrales avec les sections Na modifiées soit dans les configurations HARMONIE sans couverture, soit dans les configurations HARMONIE sans couverture et TAPIRO avec couverture.

Les colonnes du tableau V, $(E\text{-}Cl_1)/Cl_1$ et $(E\text{-}Cl_2)/Cl_2$ comparées aux valeurs de $(E\text{-}Cj_6)/Cj_6$ et $(E\text{-}Cj_4)/Cj_4$ montre le bon accord existant entre les calculs directs et les valeurs prévisionnelles (figure 14) du code CORDAJ calculées à partir des coefficients de sensibilité donc au premier ordre les valeurs :

$$\frac{\Delta Cl}{Cl_0} \text{ c'est à dire } \left(\frac{C_{CORDAJ} - C_{direct}}{Cl_0}\right)$$

sont comprises entre 1.2 et 30% et l'écart moyen des 19 mesures intégrales est de 10.9%. Cette valeur représente en quelque sorte une mesure des effets de non linéarité, qui restent donc assez limités.

On remarque donc que le recalcul direct des (E-C)/C ne remet pas en cause les tendances de l'ajustement.

11. CONCLUSION

Nous pouvons constater l'efficacité de cette méthode d'ajustement des données de base qui repose d'une part sur les sensibilités des mesures intégrales et d'autre part sur l'ensemble des matrices de covariances des erreurs sur les mesures intégrales et sur les données de base.

On remarque quand même que le résultat dépend pour une grande part de l'appréciation et du choix de l'utilisateur. S'il est relativement facile d'éliminer les expériences incompatibles dans certaines conditions, il est plus délicat de trouver le compromis intéressant entre le nombre d'expériences prises en compte dans l'ajustement, la valeur de χ^2_i acceptable ainsi que les variations des données de base que l'on peut considérer comme satisfaisantes.

Nous avons vu d'après les calculs effectués sur le nombre d'expériences qu'il était intéressant d'avoir un nombre suffisant d'expériences d'une part pour dégager les tendances des corrections effectuées (§ 6) et, d'autre part pour éliminer les mesures manifestement incompatibles (§ 9).

C'est à partir de cette étape que l'on doit faire un compromis entre les incertitudes sur les données de base et celles sur les mesures intégrales.

Manifestement les valeurs des incertitudes sur les données de base sont trop optimistes et l'on s'aperçoit compte tenu des valeurs des déviations standards qui s'en déduisent (tableau V), qu'il est difficile, voire impossible, de corriger totalement nos écarts (E-C)/C. On peut effectiver passer outre et imposer par une diminution des incertitudes sur les mesures (§ 5) une correction plus importante.

Cela est dangereux et n'est pas très satisfaisant. En effet, dans les valeurs des incertitudes sur les mesures intégrales fournies par les expérimentateurs, interviennent d'autres facteurs d'erreur que ceux dus aux données de base, ne serait-ce que les erreurs de positionnement de détecteurs, de statistique de comptage, de dérive d'installation, etc..., auxquelles on doit ajouter aussi les erreurs de méthode.

Il faut être prudent si l'on veut corriger artificiellement tous les écarts calcul-expérience. La méthode d'ajustements successifs que nous avons testé n'apporte pas de réponse à ce problème quisqu'en fait elle revient à imposer des variations $\delta\sigma/\sigma$ plus importantes : variations qui dépassent rapidement les limites permises au départ.

On remarque (§ 10) que l'efficacité de cette méthode est aussi apportée par la linéarité des résultats prévisionnels puisque ce que l'on pourrait appeler le taux de non linéarité se chiffre à 11%.

-oOo-

REFERENCES

[1] A. Gandini : "Nuclear data and integral measurements correlation for fast reactor, Part 1 : Statistical formulation", Rapport CNEN RT/FL(73)5,(1973).

[2] J.D. Drischler, C.R. Weisbin : "Compilation of multigroup cross-section covariance matrices of several important reactor materials", ORNL, 5318 (1979).

[3] J.C. Estiot, M. Salvatores, J.P. Trapp : "Basic nuclear data and the fast reactor shielding design formulaire PROPANE Do", International conference on nuclear cross-section for technology, Knoxville (22-26 Octobre 1979).

[4] J.C. Estiot, G. Palmiotti, M. Salvatores : "Le système de code SAMPO pour les analyses de sensibilité et de perturbation à différents ordres d'approximation", International Conference on nuclear cross-section for technology, Paris (27-29 Octobre 80).

[5] J.C. Estiot, M. Salvatores, J.P. Trapp, A. De Carli, V. rado : "Nuclear data for shielding calculation : Na cross-section adjustment using propagation experiments", International conference on nuclear cross-section for technology, Knoxville (22-26 Octobre 79).

[6] A. Mc Cracken : "The application of sensitivity analysis to the identification of data requirements", Proc. Spec. Meeting, OECD Vienne, (1977).

-oOo-

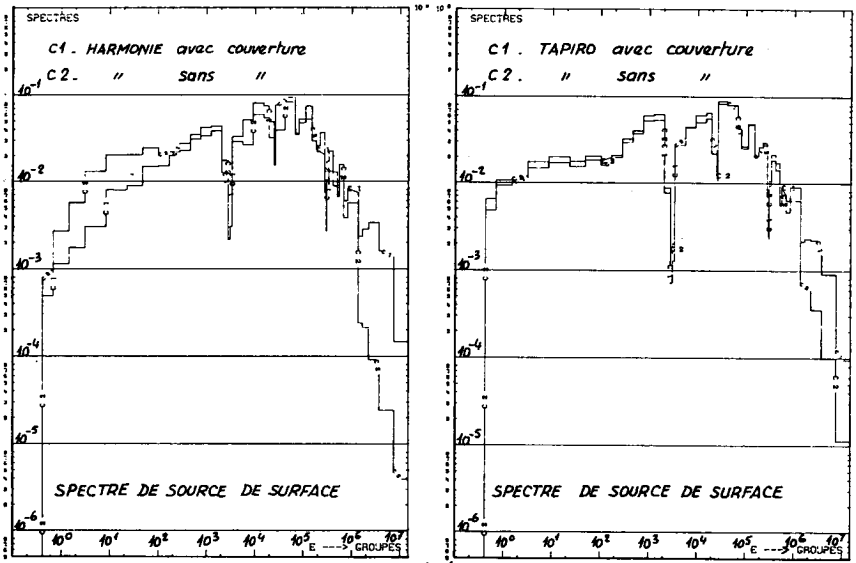

Fig.1

$\Delta\sigma_T/\sigma_T = f$ (Nombre d'expériences)

Figure 2

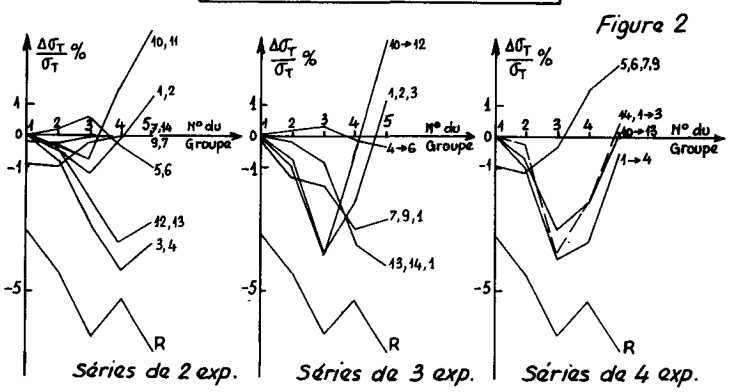

NOTA : les numéros 1 à 14 représentant les numéros des expériences de la série

Figure 3

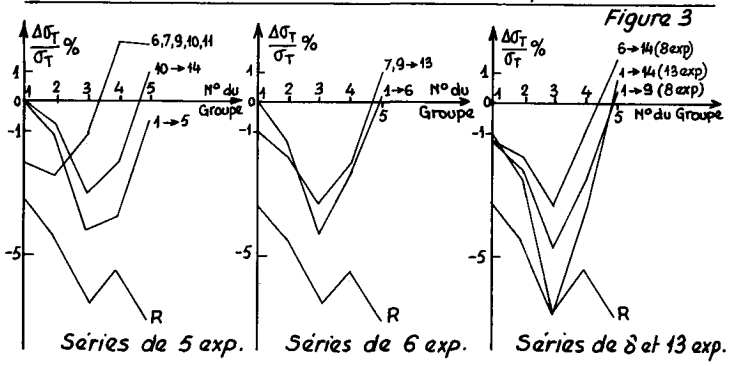

Fig. 4

VARIATION DU X_i^2 en FONCTION du NOMBRE de MESURES

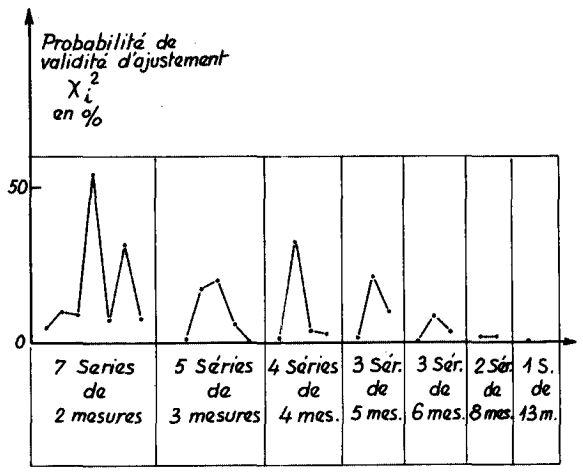

VARIATION des ECARTS (E-C)/C en FONCTION des INCERTITUDES EXPERIMENTALES ΔE/E

Fig. 5

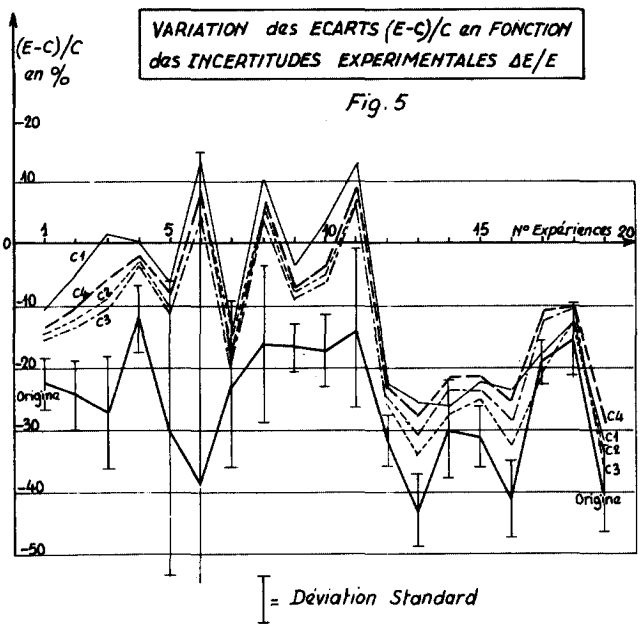

$\frac{\Delta\sigma_T}{\sigma_T} = f\,\frac{\Delta E}{E}$

Fig. 6

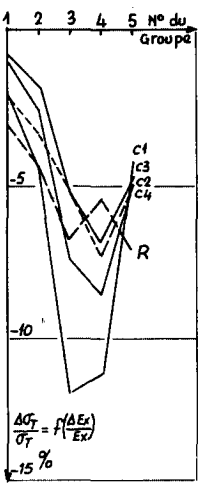

EFFET de l'AJUSTEMENT sur les DONNEES de BASE
SECTIONS TOTALES du Na à 45 groupes
—— = Covariances relatives origine
---- = Variations des sections imposées par l'ajustement $\Delta\sigma_T/\sigma_T$

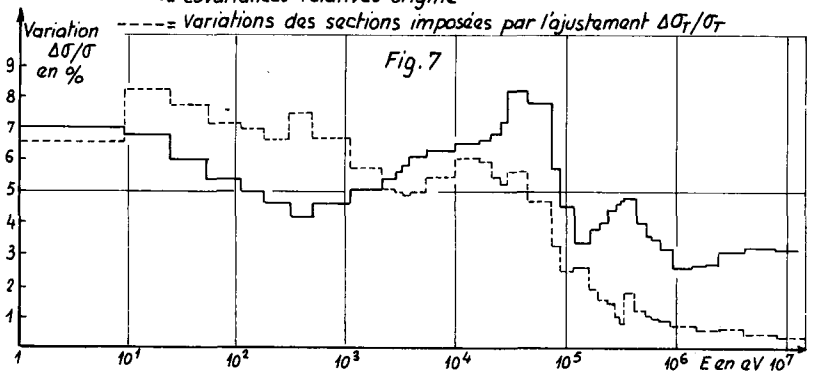

EFFET de l'AJUSTEMENT sur les DONNEES de BASE
SECTIONS INELASTIQUES du Na à 45 groupes
—— = Covariances relatives origine
---- = Variations des sections après ajustement $\Delta\sigma_{in}/\sigma_{in}$

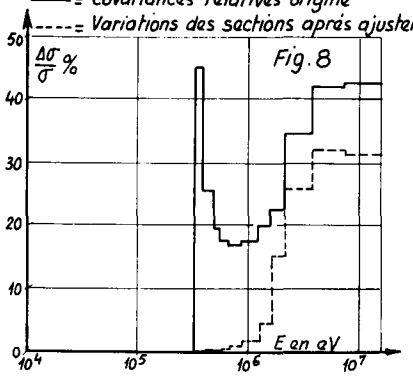

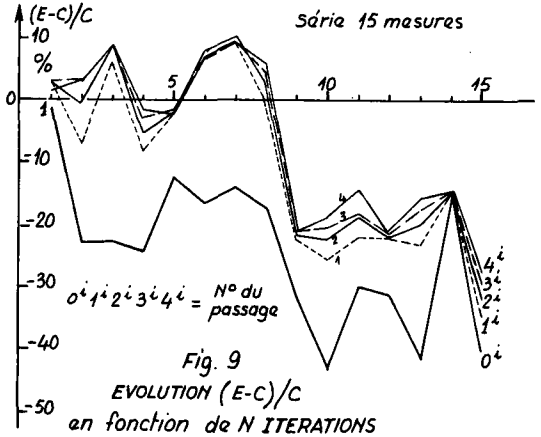

Fig. 9
EVOLUTION (E-C)/C
en fonction de N ITERATIONS

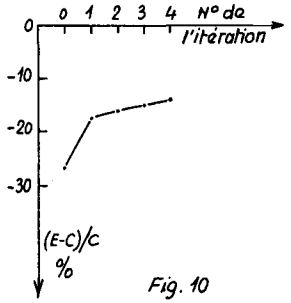

Fig. 10
EVOLUTION (E-C)/C GLOBAL
en fonction de N ITERATIONS

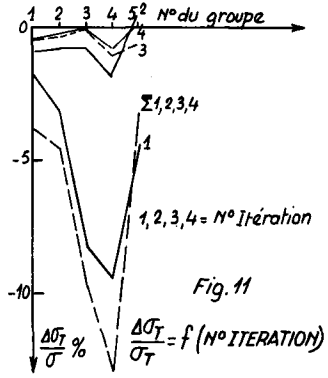

Fig. 11
$\frac{\Delta\sigma_T}{\sigma_T} = f$ (N° ITERATION)

EVOLUTION de la DISPERSION des DONNEES de BASE
avec l'ITERATION de l'AJUSTEMENT

——— Variation relative $\sqrt{COV < 1,1 >}$ origine
- - - - - - - " " " après ajustement initial
——— " " " après 4 itérations

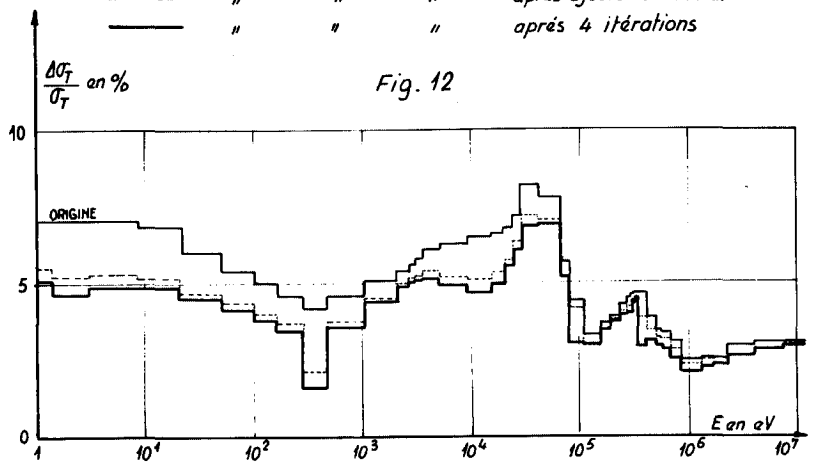

Fig. 12

COMPARAISON $\frac{\Delta\sigma_T}{\sigma_T}$
Séries C4, C5, C6

Fig. 13

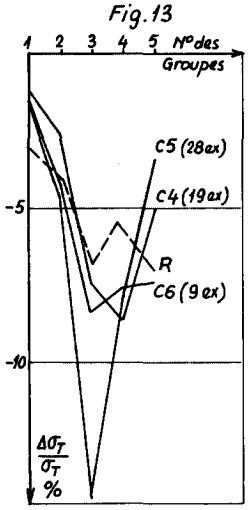

CONTROLE DE LA LINEARITE
DE L'AJUSTEMENT

× (E-C)/C cordoj série C4
\+ " " " C6
⊡ " Contrôle " C6
⊙ " " " C4
△ " Référence

Fig. 14

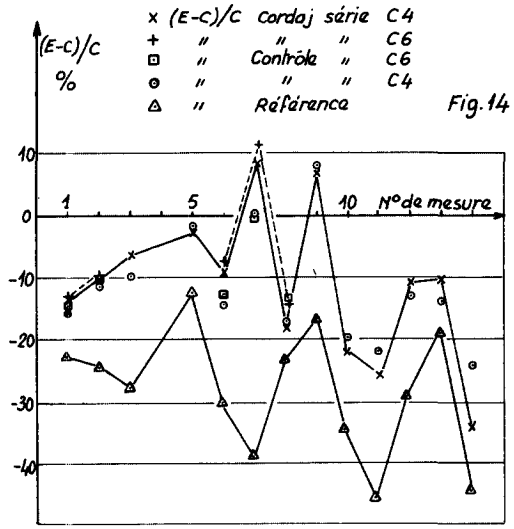

LIST OF PARTICIPANTS

LISTE DES PARTICIPANTS

AUSTRIA - AUTRICHE

KAMELANDER, G., Österreichische Studiengesellschaft für Atomenergie Sobieskigasse 21, 1090 Vienna

FRANCE

CAMOUS, B., Commissariat à l'Energie Atomique, Centre d'Etudes Nucléaires de Cadarache, B.P. No. 1, 13115 Saint Paul lez Durance

COLLIN, M., Commissariat à l'Energie Atomique, Centre d'Etudes Nucléaires de Bruyères-le-Châtel, B.P. No. 561, 92542 Montrouge

DEJONGHE, G., Commissariat à l'Energie Atomique, Centre d'Etudes Nucléaires de Saclay, B.P. No. 2, 91190 Gif-sur-Yvette

ESTIOT, J.C., Commissariat à l'Energie Atomique, Centre d'Etudes Nucléaires de Cadarache, B.P. No. 1, 13115 Saint Paul lez Durance

GONNORD, J., Commissariat à l'Energie Atomique, Centre d'Etudes Nucléaires de Saclay, B.P. No. 2, 91190 Gif-sur-Yvette

HAMMER, P., Commissariat à l'Energie Atomique, 29/33 rue de la Fédération, 75015 Paris

MAIRE, D., NOVATOME, 20 Avenue Edouard Herriot, 92350 Le Plessis Robinson

MARCIANO, J., NOVATOME, 20 Avenue Edouard Herriot, 92350 Le Plessis Robinson

NIMAL, J-C., Commissariat à l'Energie Atomique, Centre d'Etudes Nucléaires de Saclay, B.P. No. 2, 91190 Gif-sur-Yvette

PAQUIER, P., Commissariat à l'Energie Atomique, Centre d'Etudes de Limeil, B.P. No. 27, 94190 Villeneuve St. Georges

RECOLIN, J., Commissariat à l'Energie Atomique, Centre d'Etudes Nucléaires de Cadarache, B.P. No. 1, 13115 Saint Paul lez Durance

SALVATORES, M., Commissariat à l'Energie Atomique, Centre d'Etudes Nucléaires de Cadarache, B.P. No. 1, 13115 Saint Paul lez Durance

THEROND, P., Electricité de France, 1 Avenue du Géneral de Gaulle 92140 Clamart

TRAPP, J-P., Commissariat à l'Energie Atomique, Centre d'Etudes Nucléaires de Cadarache, B.P. No. 1, 13115 Saint Paul lez Durance

FEDERAL REPUBLIC OF GERMANY - REPUBLIQUE FEDERALE D'ALLEMAGNE

ERDMANN, W., INTERATOM, Postfach, 5060 Bergisch Gladbach 1

HEHN, G., Institut für Kernenergetik der Universität Stuttgart
Pfaffenwaldring 31, 7000 Stuttgart 80

KICHERER, G., Institut für Kernenergetik der Universität Stuttgart
Pfaffenwaldring 31, 7000 Stuttgart 80

SCHOLZ, A., Hochtemperatur-Reaktorbau GmbH, Gottlieb-Daimler-Str.8
6800 Mannheim 1

ITALY - ITALIE

DE CARLI, A., Comitato Nazionale per l'Energia Nucleare, CSN-Casaccia
00060 S. Maria di Galeria (Roma)

GANDINI, A., Comitato Nazionale per l'Energia Nucleare, CSN-Cassacia
00060 S. Maria di Galeria (Roma)

PALMIOTTI, G., NIRA, P.zza Carignano 2, 16128 Genova

JAPAN - JAPON

AN, S., Faculty of Engineering, University of Tokyo, 7-3-1 Hongo
Bunko-ku, Tokyo

OHTANI, N., Power Reactor and Nuclear Fuel Development Corporation
9-13, 1-chome, Akasaka, Minato-ku, Tokyo

SWITZERLAND - SUISSE

HERRNBERGER, V.R.D., Federal Institute for Reactor Research
5303 Würenlingen

UNITED KINGDOM - ROYAUME-UNI

BURN, K.W., 13 rue Hermel, 75018 Paris, France

BUTLER, J., United Kingdom Atomic Energy Authority, AEE Winfrith
Dorchester, Dorset DT2 8DH

GODDARD, A., Nuclear Power Section, Mechanical Engineering Department
Imperial College, London SW7 2AZ

KOOHI-FAYEGH, R., University of Birmingham, Dept. of Physics
B.P. No. 363, Birmingham B 15

McCRACKEN, A.K., United Kingdom Atomic Energy Authority, AEE Winfrith
Dorchester, Dorset DT2 8DH

SCOTT, M.C., University of Birmingham, Dept. of Physics, P.O. Box 363
Birmingham B 15

UNITED STATES - ETATS UNIS

GERSTL, S.A.W., Los Alamos Scientific Laboratory, Theoretical Division, MS-210, T-DOT, Los Alamos, N.M. 87545

ROUSSIN, R.W., Radiation Shielding Information Center, Oak Ridge National Laboratory, P.O. Box X, Oak Ridge, Tenn. 37830

COMMISSION OF THE EUROPEAN COMMUNITIES

COMMISSION DES COMMUNAUTES EUROPEENNES

MATTHES, W., Reactor Physics Dept., Euratom Joint Research Centre Ispra Establishment, C.P. No. 1, 21020 Ispra (Varese), Italy

PERLINI, G., Reactor Physics Dept., Euratom Joint Research Centre Ispra Establishment, C.P. No. 1, 21020 Ispra (Varese), Italy

RIEF, H., Reactor Physics Dept., Euratom Joint Research Centre Ispra Establishment, C.P. No. 1, 21020 Ispra (Varese), Italy

NUCLEAR ENERGY AGENCY OF THE OECD

AGENCE POUR L'ENERGIE NUCLEAIRE DE L'OCDE

L. Garcia de Viedma

A. Hasegawa

D. Johnson

E. Sartori

SOME NEW PUBLICATIONS OF NEA

QUELQUES NOUVELLES PUBLICATIONS DE L'AEN

ACTIVITY REPORTS

RAPPORTS D'ACTIVITÉ

Activity Reports of the OECD Nuclear Energy Agency (NEA)

- 7th Activity Report (1978)
- 8th Activity Report (1979)

Rapports d'activité de l'Agence de l'OCDE pour l'Énergie Nucléaire (AEN)

- 7e Rapport d'Activité (1978)
- 8e Rapport d'Activité (1979)

Free on request — Gratuits sur demande

Annual Reports of the OECD HALDEN Reactor Project

- 18th Annual Report (1977)
- 19th Annual Report (1978)

Rapports annuels du Projet OCDE de réacteurs de HALDEN

- 18e Rapport annuel (1977)
- 19e Rapport annuel (1978)

Free on request — Gratuits sur demande

• • •

NEA at a Glance

Coup d'œil sur l'AEN

Free on request — Gratuit sur demande

OECD Nuclear Energy Agency: Functions and Main Activities

Agence de l'OCDE pour l'Énergie Nucléaire : Rôle et principales activités

Free on request — Gratuit sur demande

Twentieth Anniversary of the OECD Nuclear Energy Agency

- Proceedings on the NEA Symposium on International Co-operation in the Nuclear Field: Perspectives and Prospects

Vingtième Anniversaire de l'Agence de l'OCDE pour l'Énergie Nucléaire

- Compte rendu du Symposium de l'AEN sur la coopération internationale dans le domaine nucléaire: bilan et perspectives

Free on request — Gratuit sur demande

SCIENTIFIC AND TECHNICAL PUBLICATIONS

PUBLICATIONS SCIENTIFIQUES ET TECHNIQUES

NUCLEAR FUEL CYCLE

LE CYCLE DU COMBUSTIBLE NUCLÉAIRE

Reprocessing of Spent Nuclear Fuels in OECD Countries (1977)

Retraitement du combustible nucléaire dans les pays de l'OCDE (1977)

£2.50 US$5.00 F20,00

Nuclear Fuel Cycle Requirements and Supply Considerations, Through the Long-Term (1978)

Besoins liés au cycle du combustible nucléaire et considérations sur l'approvisionnement à long terme (1978)

£4.30 US$8.75 F35,00

World Uranium Potential — An International Evaluation (1978)

Potentiel mondial en uranium — Une évaluation internationale (1978)

£7.80 US$16.00 F64.00

Uranium — Resources, Production and Demand (1979)

Uranium — ressources, production et demande (1979)

£8.70 US$19.50 F78,00

• • •

RADIATION PROTECTION

RADIOPROTECTION

Iodine-129
(Proceedings of an NEA Specialist Meeting, Paris, 1977)

Iode-129
(Compte rendu d'une réunion de spécialistes de l'AEN, Paris, 1977)

£3.40 US$7.00 F28,00

Recommendations for Ionization Chamber Smoke Detectors in Implementation of Radiation Protection Standards (1977)

Recommandations relatives aux détecteurs de fumée à chambre d'ionisation en application des normes de radioprotection (1977)

Free on request — Gratuit sur demande

Radon Monitoring
(Proceedings of the NEA Specialist Meeting, Paris, 1978)

Surveillance du radon
(Compte rendu d'une réunion de spécialistes de l'AEN, Paris, 1978)

£8.00 US16.50 F66,00

Management, Stabilisation and Environmental Impact of Uranium Mill Tailings (Proceedings of the Albuquerque Seminar, United States, 1978)

Gestion, stabilisation et incidence sur l'environnement des résidus de traitement de l'uranium
(Compte rendu du Séminaire d'Albuquerque, États-Unis, 1978)

£9.80 US$20.00 F80,00

Exposure to Radiation from the Natural Radioactivity in Building Materials
(Report by an NEA Group of Experts, 1979)

Exposition aux rayonnements due à la radioactivité naturelle des matériaux de construction
(Rapport établi par un Groupe d'experts de l'AEN, 1979)

Free on request — Gratuit sur demande

Marine Radioecology
(Proceedings of the Tokyo Seminar, 1979)

Radioécologie marine
(Compte rendu du Colloque de Tokyo, 1979)

£9.60 US$21.50 F86.00

Radiological Significance and Management of Tritium, Carbon-14, Krypton-85 and Iodine-129 arising from the Nuclear Fuel Cycle
(Report by an NEA Group of Experts, 1980)

Importance radiologique et gestion des radionucléides : tritium, carbone-14, krypton-85 et iode-129, produits au cours du cycle du combustible nucléaire
(Rapport établi par un Groupe d'experts de l'AEN, 1980)

£8.40 US$19.00 F76,00

• • •

RADIOACTIVE WASTE MANAGEMENT

GESTION DES DÉCHETS RADIOACTIFS

Objectives, Concepts and Strategies for the Management of Radioactive Waste Arising from Nuclear Power Programmes
(Report by an NEA Group of Experts, 1977)

Objectifs, concepts et stratégies en matière de gestion des déchets radioactifs résultant des programmes nucléaires de puissance
(Rapport établi par un Groupe d'experts de l'AEN, 1977)

£8.50 US$17.50 F70,00

Treatment, Conditioning and Storage of Solid Alpha-Bearing Waste and Cladding Hulls
(Proceedings of the NEA/IAEA Technical Seminar, Paris, 1977)

Traitement, conditionnement et stockage des déchets solides alpha et des coques de dégainage
(Compte rendu du Séminaire technique AEN/AIEA, Paris, 1977)

£7.30 US$15.00 F60,00

Storage of Spent Fuel Elements
(Proceedings of the Madrid Seminar, 1978)

Stockage des éléments combustibles irradiés (Compte rendu du Séminaire de Madrid, 1978)

£7.30 US$15.00 F60,00

In Situ Heating Experiments in Geological Formations
(Proceedings of the Ludvika Seminar, Sweden, 1978)

Expériences de dégagement de chaleur in situ dans les formations géologiques
(Compte rendu du Séminaire de Ludvika, Suède, 1978)

£8.00 US$16.50 F66,00

Migration of Long-lived Radionuclides in the Geosphere
(Proceedings of the Brussels Workshop, 1979)

Migration des radionucléides à vie longue dans la géosphère
(Compte rendu de la réunion de travail de Bruxelles, 1979)

£8.30 US$17.00 F68,00

Low-Flow, Low-Permeability Measurements in Largely Impermeable Rocks
(Proceedings of the Paris Workshop, 1979)

Mesures des faibles écoulements et des faibles perméabilités dans des roches relativement imperméables
(Compte rendu de la réunion de travail de Paris, 1979)

£7.80 US$16.00 64,00

On-Site Management of Power Reactor Wastes
(Proceedings of the Zurich Symposium, 1979)

Gestion des déchets en provenance des réacteurs de puissance sur le site de la centrale
(Compte rendu du Colloque de Zurich, 1979)

£11.00 US$22.50 F90,00

Recommended Operational Procedures for Sea Dumping of Radioactive Waste (1979)

Recommandations relatives aux procédures d'exécution des opérations d'immersion de déchets radioactifs en mer (1979)

Free on request — Gratuit sur demande

Guidelines for Sea Dumping Packages of Radioactive Waste
(Revised version, 1979)

Guide relatif aux conteneurs de déchets radioactifs destinés au rejet en mer
(Version révisée, 1979)

Free on request — Gratuit sur demande

Use of Argillaceous Materials for the Isolation of Radioactive Waste
(Proceedings of the Paris Workshop, 1979)

Utilisation des matériaux argileux pour l'isolement des déchets radioactifs
(Compte rendu de la Réunion de travail de Paris, 1979)

£7.60 US$17.00 F68,00

Review of the Continued Suitability of the Dumping Site for Radioactive Waste in the North-East Atlantic (1980)

Réévaluation de la validité du site d'immersion de déchets radioactifs dans la région nord-est de l'Atlantique (1980)

Free on request — Gratuit sur demande

Decommissioning Requirements in the Design of Nuclear Facilities
(Proceedings of the NEA Specialist Meeting, Paris, 1980)

Déclassement des installations nucléaires : exigences à prendre en compte au stade de la conception
(Compte rendu d'une réunion de spécialistes de l'AEN, Paris, 1980)

£7.80 $17.50 F70,00

Borehole and Shaft Plugging
(Proceedings of the Columbus Workshop, United States, 1980)
(in preparation)

Colmatage des forages et des puits
(Compte rendu de la réunion de travail de Columbus, États-Unis, 1980)
(en préparation)

£12.00 US$30.00 F120,00

• • •

SAFETY

Safety of Nuclear Ships
(Proceedings of the Hamburg Symposium, 1977)

£17.00 US$35.00 F140,00

Nuclear Aerosols in Reactor Safety
(A State-of-the-Art Report by a Group of Experts, 1979)

£8.30 US$18.75 F75,00

Plate Inspection Programme
(Report from the Plate Inspection Steering Committee – PISC – on the Ultrasonic Examination of Three Test Plates), 1980

£3.30 US$7.50 F30.00

Reference Seismic Ground Motions in Nuclear Safety Assessments
(A State-of-the-Art Report by a Group of Experts, 1980)

£7.00 $16.00 F64,00

SÛRETÉ

Sûreté des navires nucléaires
(Compte rendu du Symposium de Hambourg, 1977)

Les aérosols nucléaires dans la sûreté des réacteurs
(Rapport sur l'état des connaissances établi par un Groupe d'Experts, 1979)

Programme d'inspection des tôles
(Rapport du Comité de Direction sur l'inspection des tôles – PISC – sur l'examen par ultrasons de trois tôles d'essai au moyen de la procédure «PISC» basée sur le code ASME XI), 1980

Les mouvements sismiques de référence du sol dans l'évaluation de la sûreté des installations nucléaires
(Rapport sur l'état des connaissances établi par un Groupe d'experts, 1980)

• • •

SCIENTIFIC INFORMATION

Neutron Physics and Nuclear Data for Reactors and other Applied Purposes
(Proceedings of the Harwell International Conference, 1978)

£26.80 US$55.00 F220,00

Calculation of 3-Dimensional Rating Distributions in Operating Reactors
(Proceedings of the Paris Specialists' Meeting, 1979)

£9.60 US$21.50 F86.00

INFORMATION SCIENTIFIQUE

La physique neutronique et les données nucléaires pour les réacteurs et autres applications
(Compte rendu de la Conférence Internationale de Harwell, 1978)

Calcul des distributions tridimensionnelles de densité de puissance dans les réacteurs en cours d'exploitation
(Compte rendu de la Réunion de spécialistes de Paris, 1979)

LEGAL PUBLICATIONS

PUBLICATIONS JURIDIQUES

Convention on Third Party Liability in the Field of Nuclear Energy — incorporating the provisions of Additional Protocol of January 1964

Convention sur la responsabilité civile dans le domaine de l'énergie nucléaire — Texte incluant les dispositions du Protocole additionnel de janvier 1964

Nuclear Legislation, Analytical Study: "Nuclear Third Party Liability" (revised version, 1976)

Législations nucléaires, étude analytique: "Responsabilité civile nucléaire" (version révisée, 1976)

£6.00 US$12.50 F50,00

Nuclear Law Bulletin (Annual Subscription — two issues and supplements)

Bulletin de Droit Nucléaire (Abonnement annuel — deux numéros et suppléments)

£5.60 US$12.50 F50,00

Index of the first twenty five issues of the Nuclear Law Bulletin

Index des vingt-cinq premiers numéros du Bulletin de Droit Nucléaire

Free on request — Gratuit sur demande

Licensing Systems and Inspection of Nuclear Installations in NEA Member Countries (Revised version, 1980)

Régime d'autorisation et d'inspection des installations nucléaires dans les pays de l'AEN (Version révisée, 1980)

£7.60 US$19.00 F76,00

NEA Statute

Statuts de l'AEN

Free on request — Gratuit sur demande

• • •

OECD SALES AGENTS
DÉPOSITAIRES DES PUBLICATIONS DE L'OCDE

ARGENTINA – ARGENTINE
Carlos Hirsch S.R.L., Florida 165, 4° Piso (Galería Guemes)
1333 BUENOS AIRES, Tel. 33.1787.2391 y 30.7122

AUSTRALIA – AUSTRALIE
Australia and New Zealand Book Company Pty. Ltd.,
10 Aquatic Drive, French Forest 2086 (P.O.B. 450)
BROOKVALE, 2100. Tel. 452.4411

AUSTRIA – AUTRICHE
OECD Publications and Information Center
4 Simrockstrasse 5300 BONN. Tel. (0228) 21.60.45
Local Agent/Agent local :
Gerold and Co., Graben 31, WIEN 1. Tel. 52.22.35

BELGIUM – BELGIQUE
LCLS
35, avenue de Stalingrad, 1000 BRUXELLES. Tel. 02.512.89.74

BRAZIL – BRÉSIL
Mestre Jou S.A., Rua Guaipa 518,
Caixa Postal 24090, 05089 SAO PAULO 10. Tel. 261.1920
Rua Senador Dantas 19 s/205-6, RIO DE JANEIRO GB.
Tel. 232.07.32

CANADA
Renouf Publishing Company Limited,
2182 St. Catherine Street West,
MONTRÉAL, Quebec H3H 1M7. Tel. (514)937.3519
522 West Hasting,
VANCOUVER, B.C. V6B 1L6. Tel. (604) 687.3320

DENMARK – DANEMARK
Munksgaard Export and Subscription Service
35, Nørre Søgade
DK 1370 KØBENHAVN K. Tel. +45.1.12.85.70

FINLAND – FINLANDE
Akateeminen Kirjakauppa
Keskuskatu 1, 00100 HELSINKI 10. Tel. 65.11.22

FRANCE
Bureau des Publications de l'OCDE,
2 rue André-Pascal, 75775 PARIS CEDEX 16. Tel. (1) 524.81.67
Principal correspondant :
13602 AIX-EN-PROVENCE : Librairie de l'Université.
Tel. 26.18.08

GERMANY – ALLEMAGNE
OECD Publications and Information Center
4 Simrockstrasse 5300 BONN Tel. (0228) 21.60.45

GREECE – GRÈCE
Librairie Kauffmann, 28 rue du Stade,
ATHÈNES 132. Tel. 322.21.60

HONG-KONG
Government Information Services,
Sales and Publications Office, Baskerville House, 2nd floor,
13 Duddell Street, Central. Tel. 5.214375

ICELAND – ISLANDE
Snaebjörn Jönsson and Co., h.f.,
Hafnarstraeti 4 and 9, P.O.B. 1131, REYKJAVIK.
Tel. 13133/14281/11936

INDIA – INDE
Oxford Book and Stationery Co. :
NEW DELHI, Scindia House. Tel. 45896
CALCUTTA, 17 Park Street. Tel. 240832

INDONESIA – INDONÉSIE
PDIN-LIPI, P.O. Box 3065/JKT., JAKARTA, Tel. 583467

IRELAND – IRLANDE
TDC Publishers – Library Suppliers
12 North Frederick Street, DUBLIN 1 Tel. 744835-749677

ITALY – ITALIE
Libreria Commissionaria Sansoni :
Via Lamarmora 45, 50121 FIRENZE. Tel. 579751
Via Bartolini 29, 20155 MILANO. Tel. 365083
Sub-depositari :
Editrice e Libreria Herder,
Piazza Montecitorio 120, 00 186 ROMA. Tel. 6794628
Libreria Hoepli, Via Hoepli 5, 20121 MILANO. Tel. 865446
Libreria Lattes, Via Garibaldi 3, 10122 TORINO. Tel. 519274
La diffusione delle edizioni OCSE è inoltre assicurata dalle migliori librerie nelle città più importanti.

JAPAN – JAPON
OECD Publications and Information Center,
Landic Akasaka Bldg., 2-3-4 Akasaka,
Minato-ku, TOKYO 107 Tel. 586.2016

KOREA – CORÉE
Pan Korea Book Corporation,
P.O. Box n° 101 Kwangwhamun, SÉOUL. Tel. 72.7369

LEBANON – LIBAN
Documenta Scientifica/Redico,
Edison Building, Bliss Street, P.O. Box 5641, BEIRUT.
Tel. 354429 – 344425

MALAYSIA – MALAISIE
and/et **SINGAPORE - SINGAPOUR**
University of Malaysia Co-operative Bookshop Ltd.
P.O. Box 1127, Jalan Pantai Baru
KUALA LUMPUR. Tel. 51425, 54058, 54361

THE NETHERLANDS – PAYS-BAS
Staatsuitgeverij
Verzendboekhandel Chr. Plantijnstraat
S-GRAVENAGE. Tel. nr. 070.789911
Voor bestellingen: Tel. 070.789208

NEW ZEALAND – NOUVELLE-ZÉLANDE
Publications Section,
Government Printing Office,
WELLINGTON: Walter Street. Tel. 847.679
Mulgrave Street, Private Bag. Tel. 737.320
World Trade Building, Cubacade, Cuba Street. Tel. 849.572
AUCKLAND: Hannaford Burton Building,
Rutland Street, Private Bag. Tel. 32.919
CHRISTCHURCH: 159 Hereford Street, Private Bag. Tel. 797.142
HAMILTON: Alexandra Street, P.O. Box 857. Tel. 80.103
DUNEDIN: T & G Building, Princes Street, P.O. Box 1104.
Tel. 778.294

NORWAY – NORVÈGE
J.G. TANUM A/S Karl Johansgate 43
P.O. Box 1177 Sentrum OSLO 1. Tel. (02) 80.12.60

PAKISTAN
Mirza Book Agency, 65 Shahrah Quaid-E-Azam, LAHORE 3.
Tel. 66839

PHILIPPINES
National Book Store, Inc.
Library Services Division, P.O. Box 1934, MANILA.
Tel. Nos. 49.43.06 to 09, 40.53.45, 49.45.12

PORTUGAL
Livraria Portugal, Rua do Carmo 70-74,
1117 LISBOA CODEX. Tel. 360582/3

SPAIN – ESPAGNE
Mundi-Prensa Libros, S.A.
Castello 37, Apartado 1223, MADRID-1. Tel. 275.46.55
Libreria Bastinos, Pelayo 52, BARCELONA 1. Tel. 222.06.00

SWEDEN – SUÈDE
AB CE Fritzes Kungl Hovbokhandel,
Box 16 356, S 103 27 STH, Regeringsgatan 12,
DS STOCKHOLM. Tel. 08/23.89.00

SWITZERLAND – SUISSE
OECD Publications and Information Center
4 Simrockstrasse 5300 BONN. Tel. (0228) 21.60.45
Local Agents/Agents locaux
Librairie Payot, 6 rue Grenus, 1211 GENÈVE 11. Tel. 022.31.89.50
Freihofer A.G., Weinbergstr. 109, CH-8006 ZÜRICH.
Tel. 01.3624282

TAIWAN – FORMOSE
National Book Company,
84-5 Sing Sung South Rd, Sec. 3, TAIPEI 107. Tel. 321.0698

THAILAND – THAILANDE
Suksit Siam Co., Ltd., 1715 Rama IV Rd,
Samyan, BANGKOK 5. Tel. 2511630

UNITED KINGDOM – ROYAUME-UNI
H.M. Stationery Office, P.O.B. 569,
LONDON SE1 9NH. Tel. 01.928.6977, Ext. 410 or
49 High Holborn, LONDON WC1V 6 HB (personal callers)
Branches at: EDINBURGH, BIRMINGHAM, BRISTOL,
MANCHESTER, CARDIFF, BELFAST.

UNITED STATES OF AMERICA – ÉTATS-UNIS
OECD Publications and Information Center, Suite 1207,
1750 Pennsylvania Ave., N.W. WASHINGTON D.C.20006.
Tel. (202) 724.1857

VENEZUELA
Libreria del Este, Avda. F. Miranda 52, Edificio Galipan,
CARACAS 106. Tel. 32.23.01/33.26.04/33.24.73

YUGOSLAVIA – YOUGOSLAVIE
Jugoslovenska Knjiga, Terazije 27, P.O.B. 36, BEOGRAD.
Tel. 621.992

Les commandes provenant de pays où l'OCDE n'a pas encore désigné de dépositaire peuvent être adressées à :
OCDE, Bureau des Publications. 2, rue André-Pascal, 75775 PARIS CEDEX 16.

Orders and inquiries from countries where sales agents have not yet been appointed may be sent to:
OECD, Publications Office, 2 rue André-Pascal, 75775 PARIS CEDEX 16.

63562-1-1981

PUBLICATIONS DE L'OCDE, 2 rue André-Pascal, 75775 PARIS CEDEX 16 - N° 41 804 1981
IMPRIMÉ EN FRANCE
(2400 NS 66 81 02 3) ISBN 92-64-02118-3

2s 80. pdf

La conception de protections efficaces et économiques pour les réacteurs nucléaires dépend de la précision des ensembles de données nucléaires entrés dans les calculs. Ce compte rendu résume l'état actuel des techniques analytiques et expérimentales utilisées dans l'évaluation de tels besoins de données neutroniques.

(2400 NS 66 81 02 3) ISBN 92-64-2118-3